INTERNATIONAL CONFERENCE ON POWER, CONTROL AND SUSTAINABLE ENERGY SYSTEMS (ICPCSES-2022)

Dr. Venkatesh Boddapati
Dr. Prakash DB
Dr. P. Sanjeevikumar

River Publishers

International Conference on Power, Control and Sustainable Energy Systems (ICPCSES-2022)

Preface of the conference proceedings

ICPCSES-2022 is aimed at bringing out the innovative ideas of academicians, industry professionals, research scholars and students in Science and Engineering. Objective of the conference is to provide the platform to bridge the gap between industry and academia in the domain of Power Systems, Control Systems, Power Electronics, Renewable Energy and other interdisciplinary areas. This conference is also focusing on networking people with similar interests to have a collaborative work and to have better solutions to societal problems.

This book deals with the advanced topics of Power system engineering, Power electronics, Renewable Energy Technologies, Electric Vehicles and Smart Grid. This book is most suitable for an Undergraduate, postgraduate students who is interested in carrying out their research in above mentioned areas. Contents presented are also chosen according to the needs of industry-a right mix of modern and conventional concepts.

In the preparation of this book the editors received valuable help from several persons and would like to thank all of them. The editors wishes to record and appreciate all the authors for their contribution. Last but not the least, editors is grateful to the B.M.S College of Engineering, Bangalore, India for the support in preparation of this book and the patience and enthusiastic support provided by our family members during the preparation of this edited book. The Editors wishes to thank the support received from the publishers to bring out this book in a well manned way.

Keywords: Sustainable Power and Energy system, Power Electronics, Electric Drives, Electric Vehicles and Advances in Electronics systems.

Dr. P Sanjeevikumar, Dr.Venkatesh Boddapati and Dr.Prakash DB

Book Contents:

Article 1

PROFICIENT EVALUATION AND IMPLEMENTATION OF LSB BASED IMAGE STEGANOGRAPHY
by Deeksha Manjunath, Avani K V H, Rashmi Pai K and C.Gururaj

Article 2

IMPACT OF E-WASTE MANAGEMENT AND RECYCLING CHALLENGES: REVIEW
by Vyshnavi Gogula, Belwin Edward, W J Praiselin and Jacob Raglend I.

Article 3

A STUDY ON CONVERSION OF ICE VEHICLE TO EV
by Nishana B B, Puneeth G, Rahul Ganesh S, Vedanth Pandit B R, Raghunath M J and Sushma S R

Article 4

A STUDY OF PASSIVE CELL BALANCING AND STATE OF CHARGE ASSESSMENT USING COULOMB COUNTING METHOD
by Advaith Srinath, Syed Shoaib Hussaini, Nikshith K U, Shivaprasad G Indaragi, Venkatesh Boddapati and Prakash D B

Article 5

ADALINE LEAST MEAN SQUARE (ALMS) BASED MULTI-LEVEL INVERTER WITH PARTICLE SWARM OPTIMIZATION FOR PV SYSTEM
by Dr.B. Pragathi and Dr.B. Karunakar Rao

Article 6

CONTROL OF MICROGRID WITH HYBRID ENERGY STORAGE SYSTEM
by Suganthi.N and P. Usha

Article 7

DEVELOPMENT OF SMART SEMI-AUTONOMOUS WHEELCHAIR
by Chiraag A, Tejas B U, Vrishab Kushalappa, Tavishi Bansal and Prof. Asha S Patil

Article 8

COMPARATIVE ANALYSIS OF BIDIRECTIONAL BUCK/BOOST DC-DC CONVERTER AND INTERLEAVED BIDIRECTIONAL BUCK/BOOST DC-DC CONVERTER FOR EV APPLICATIONS
by Madhumitha G, Rajesh Uppara and Priya S

Article 9

COMPARITIVE ANALYSIS OF HIGH GAIN NON-ISOLATED CONVERTERS FOR DC MICROGRID
by Malathi.S.N and Dr. Rashmi

Article 10

ISLANDING DETECTION SCHEME FOR GRID-CONNECTED PV SYSTEM USING AI TECHNIQUE
by Ashok Valahoju, Shiva Rama Krishna Prasad L, B Kiran Kumar and B Pradeep Kumar

Article 11

ISLANDING DETECTION IN GRID CONNECTED WIND PLANT USING AI TECHNIQUE
by Srikanth Velpula, Ankathi Chandana and Ashok Valabhoju

Article 12

INVESTIGATIONS ON INFLUENCE OF GROUND IMPEDANCE ON THE INTERCONNECTED THREE PHASE FOUR WIRE BALANCED AND UNBALANCED DISTRIBUTION SYSTEM
by K Lokeswara Rao, A Usha and Raghunatha R

Article 13

DESIGN AND DEVELOPMENT OF CHARGING STATION FOR SWAPPABLE BATTERIES OF ELECTRIC VEHICLE
by B Sumedha Shenoy and Varsha M

Article 14

A DEEP LEARNING MODEL FOR THE PREDICTION OF REMAINING USEFUL LIFE OF LITHIUM-ION BATTERIES
by Manali Raman, V. Champa, Prema V and Priya Ranjan Mishra

Article 15

COMPARATIVE ANALYSIS OF POSITIVE BUCK BOOST CONVERTER WITH PID AND FUZZY LOGIC CONTROLLER
by Piyush Singh, P. Parthiban, R. Kalpana, S.Rambabu and M.Vijaya

Article 16

PV BASED SMART ENERGY EFFICIENT HYBRID MODEL FOR IRRIGATION USING SENSORLESS BLDC MOTOR
by Md Sagar Khan, Sujitha S, Kulshrestha Utkarsh Alok, Karthika M, L Ashwini B and Vivek Ranjan

Article 17

DESIGN AND IMPLEMENTATION OF A DUAL ACTIVE BRIDGE CONVERTER FOR BATTERY CHARGING APPLICATION
by Harikishan B Hanumannavar, Usha A and Priyaranjan Mishra

Article 18

MODELLING AND INVESTIGATION OF BEST PV ARRAY CONFIGURATION AND IMPLEMENTATION OF MPPT UNDER PARTIAL SHADING CONDITIONS
by Rajkumar Jukuri, B. Pradeep Kumar, V. Ashok Kumar, C. Subba Rami Reddy and V. Srikanth

Article 19

PV INTEGRATED DC-DC CONVERTER AND INVERTER TOPOLOGIES FOR GRID TIED/STANDALONE SYSTEM

by Pushpa K R and R S Geetha

Article 20

OPTIMAL DESIGN AND COMPARATIVE ANALYSIS OF DIFFERENT BI-DIRECTIONAL DC-DC CONVERTERS FOR ENERGY STORAGE APPLICATIONS

by Shubham Dongare, R S Geetha and Priyaranjan Mishra

Article 21

EXPLAINABLE MACHINE LEARNING FOR PREDICTING SOLAR POWER OUTPUT

by Pranav R, Shashank T K and Gururaja H S

Article 22

A NEW APPROACH FOR HYBRID ELECTRIC VEHICLES IN THE IMPLEMENTATION OF SWITCHED CAPACITOR VOLTAGE BOOST CONVERTER

by Sujitha S, Anitha A, Sushma M, Gagana C and Sushmitha T S

Article 23

TO STUDY THE BREAKDOWN VOLTAGE OF DIFFERENT SPACERS

by Sneha S Mallur, Sandya Kamashetty and C.Gururaj

Article 24

SURVEY ON ESTIMATION METHODS FOR EV BATTERY HEALTH USING ML TECHNIQUES

by Arya Jha, K Rahul Annamalai, C R Amrutha Varshini, Ayush Tiwari, K. Deepa, V. Sailaja

Article 25

DESIGN AND IMPLEMENTATION OF DUAL OUTPUT FORWARD CONVERTER TO POWER-UP DIGITAL UNIT FOR SPACE APPLICATION

by Nikhil Kumar, A.N. Nagashree, Santosh B L, Prakash G and B K Singh

Article 26

DESIGN AND IMPLEMENTATION OF 75W MAG-AMP CONTROLLED FORWARD CONVERTER FOR COMMUNICATION SYSTEM

by Kalpana N, Shubha Kulkarni, B K Singh, Santosh B L and Prakash G

Article 27

DEVELOPMENT AND SIMULATION OF 48V LI-ION BATTERY MANAGEMENT SYSTEM FOR ELECTRIC VEHICLES

by Guruprasad Naik G, R Harshavardhan Reddy and Dr. V Champa

Article 28

Performance Analysis of Boost and Interleaved Boost Converter with a novel switching technique
by Abhishek G A and R S Geetha

Article 29

SELECTION AND CONTINGENCY ANALYSIS OF EV CHARGING STATION ON 24-BUS IEEE SYSTEM
by Surbhi Aggarwal and Amit Kumar Singh

Article 30

DETECTION AND CLASSIFICATION OF ARRAY FAULTS IN PHOTOVOLTAIC SYSTEM USING WAVELET PACKET TRANSFORM
by M. Nivash, C. Kannan, S. Priyadharsini and V. Saravanan

Article 31

EFFECT, ANALYSIS AND ASSESSMENT OF ELECTRICITY USAGE PATTERN IN AN EDUCATIONAL INSTITUTE DURING COVID-19 PANDEMIC
by Shilpa Aralasurali Subramanya and A. N. Nagashree

Article 32

DESIGN AND IMPLEMENTATION OF FORWARD-BOOST HYBRID CONVERTER FOR SOLAR POWERED ELECTRIC VEHICLE CHARGING APPLICATIONS
by Rakesh B and Prakash D B

Article 33

INVESTIGATION AND ANALYSIS OF REAL TIME TRANSFORMER OIL IMAGES AT DIFFERENT TEMPERATURES USING GABOR TEXTURE FEATURES
by Maheshan C M and H Prasanna Kumar

Article 34

MODIFICATION OF ELECTRONIC WARFARE (EW) SUITE ON JAGUAR FIGHTER AIRCRAFT
by Sujitha S, Deepa V B, Vishnupriya G, Sankeerthini and Saranya S

Article 35

SMART IRRIGATION SYSTEM USING AGRIBOT

by Ahir Jay Satish, Gourav Kumar Patel, Pathak Krutarth Dhimant, Prajwal S C and Dipesh Kumar

Article 36

OPTIMAL LOCATION AND SIZING OF FACTS CONTROLLERS IN TRANSMISSION SYSTEM USING GENETIC ALGORITHM UNDER CONTINGENCY CONDITION

by Tanuja K.S, Dr.Shankaralingappa C. Byalihal and Dr.Prakash R

Article 37

DESIGN OF PARAMETERS OF BUCK CONVERTER INTEGRATED TO A HYBRID DC MICRO GRID USING GENETIC ALGORITHM

by M N Suneetha and C Lakshminarayana

Article 38

DESIGN, SIMULATION OF A SEPIC AND CUK CONVERTER FOR SOLAR POWERED ELECTRIC VEHICLE BATTERY CHARGING

by Ankush K M and Venkatesh Boddapati

Article 39

DESIGN, MODELLING AND SIMULATION OF TRADITIONAL DC - DC BOOST CONVERTER AND INTERLEAVED DC - DC BOOST CONVERTER

by Abhay P Badnur, Laksh C, Shrayan Karkun, Nishanth Madhava Navada and Divya S

Article 40

DESIGN AND IMPLEMENTATION OF TRIPLE OUTPUT FLYBACK CONVERTER WITH CURRENT MODE CONTROL FOR SPACE APPLICATIONS

by Shamanth Y, Usha A, Pradeep S, Nagaraju T K, B K Singh and Vinod Chippalkatti

Article 41

REVIEW OF STATE OF HEALTH MONITORING TECHNIQUES IN BATTERY MANAGEMENT SYSTEM

by R Sivapriyan, Sushmitha S V, C V Mohan and S Lavanraj

Article 42

DESIGN AND SIMULATION OF BACK TO BACK CONVERTER FOR BIFURCATED WINDING INDUCTION GENERATOR

by Manoj Kumar S and Prema V

Proficient Evaluation and Implementation of LSB Based Image Steganography

Deeksha Manjunath, Avani K V H, Rashmi Pai K and C.Gururaj

Abstract.

Abstract— Steganography is the craft of covering the way that correspondence is occurring by encasing information in different information. There are an assortment of transporter record types accessible, yet advanced photographs are the most utilized because of their pervasiveness on the Internet. There are a few distinctive steganographic procedures for concealing secret data in photos, some of which are more troublesome than others and all of which have their own qualities and shortcomings. The steganography strategy used for various applications has changed requirements. A few applications, for instance, may require total imperceptibility of the restricted data, while others might require the disguise of a greater mystery message. Picture Steganography is one such course of disguising data in a cover picture, which may be text, picture, or video.

Keywords- Image Steganography, Least Significant Bit, Data Hiding

1. INTRODUCTION

Image Steganography refers back to the procedure of hiding information inside an photograph file.The image chosen for this design is called the cover image, and the image taken later for steganography (data hiding) is called the steganographic image. It can be carried out in two major steps. In particular, it can be divided into an embedding phase, which hides information in the image (cover) using appropriate calculations and a mysterious key, and an extraction phase, where information is entered. It is extracted from the changed image. It uses a mysterious key to use the opposite calculation. When the stego picture is communicated, it could be plausible that the stego picture gets debased when a third individual captures this picture.

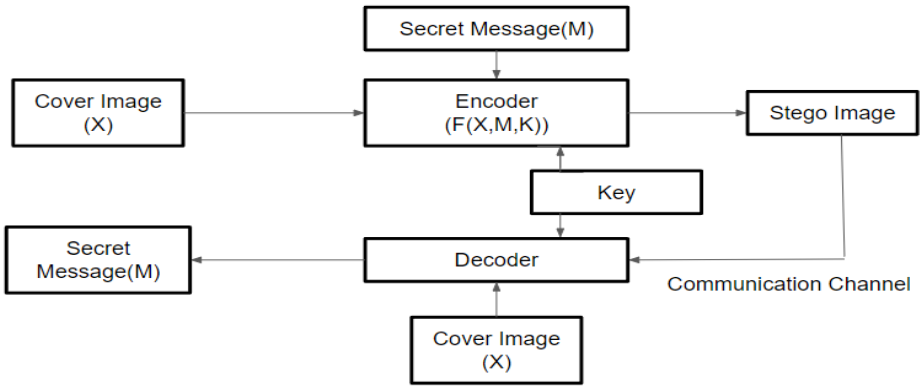

Fig 1: Block diagram of Image Steganography

The fundamental advances associated with picture steganography are displayed in the graph above. The mysterious message or information (X), the cover picture (M) and the mysterious key (K) picked are taken care of to the picture steganography calculation whose capacity is addressed as f(X,M,K). The result of this calculation is an adjusted picture containing the information (stowed away). This altered picture is then communicated to the collector who interprets the got picture with a vital K to separate the information that was covered up.[1]

During the plan of an information concealing framework or picture steganography calculation there are a couple of elements that must be thought of. The elements are subtlety, security, limit or payload, strength and implanting intricacy.

Imperceptibility is the ability of a related technology to transmit data without being seen by humans. If a third party intercepts the image file, the security service determines the resistance of the technology (to prevent third parties from tampering with the image). How much information that can be concealed in the cover picture by the calculation without rolling out the improvements perceptible is characterized by payload or limit. The capacity of the information that is concealed to stay unaltered in any event, when the stego picture is altered by activities like straight or non-direct separating, editing, honing or obscuring, pressure and so forth is characterized by Robustness of the calculation. Embedding complexity measures how complex the algorithm is.

2. BENEFITS AND DOWNSIDES OF LSB BASED IMAGE STEGANOGRAPHY

BENEFITS:

This strategy is exceptionally quick and effectively implementable contrasted with different methodologies of picture steganography.

The difference between information and encoded image is negligible.

Rather than implanting the data in just the LSB, we can insert the data in the last two LSBs, along these lines installing much bigger mystery messages.

This technique frames the establishment for other complex calculations.

DRAWBACKS:

LSB based encoding the information is frail as it tends to be handily decoded taking the LSBs of the picture and acquiring the mysterious message in its double structure.

This strategy is old and out of date and other better encryption techniques have been created.

While inserting the mysterious message in more than one LSB, the picture quality decreases relying upon the number of pixels that have changed.

3. IMAGE STEGANOGRAPHY AND ITS TYPES

Image steganography is classified into two categories: Spatial space information stowing away and Transform area information stowing away. Spatial area strategies use procedures dependent on basic controls which create spaces in the cover picture to conceal privileged information where changes can't be effectively distinguished. While in Transform space procedure [9], the pixel esteems in spatial area are changed over into recurrence space esteems by performing two layered changes [11]. The recurrence area esteems or coefficients changed by the restricted information are utilized to conceal the information. Most transform domain techniques are developed from spatial domain approaches.

Spatial domain image steganography can be classified into six categories as mentioned below[5].

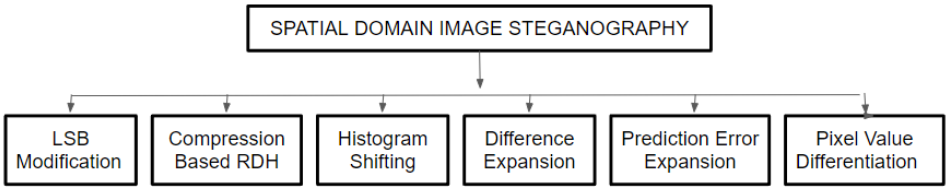

Fig 2: Types of Spatial Domain Image Steganography

LSB Modification: It is a method in which the least extended bit of each pixel in the image is replaced with the message bit intended to be hidden.

Compression based RDH (Reversible Data Hiding): This technique is performed on the bit planes of the cover image to create a gap to cover the data.

Histogram Shifting: This approximation is obtained by taking into account the histogram of the image. Adjusts all pixel values between the peak and null positions, creating enough space to hide the data.

Difference Expansion: This approach relies on the image's redundancy. The disparity between neighbouring pixels is increased, and the data is buried in the resulting space.

Pixel Value Differentiating: The difference between successive pixels in a block determines the number of bits of data to be buried (The cover image is divided into pixel blocks that do not overlap).[2]

Prediction Error Expansion: This approach combines differential expansion with histogram shifting.

Transform Domain Types:

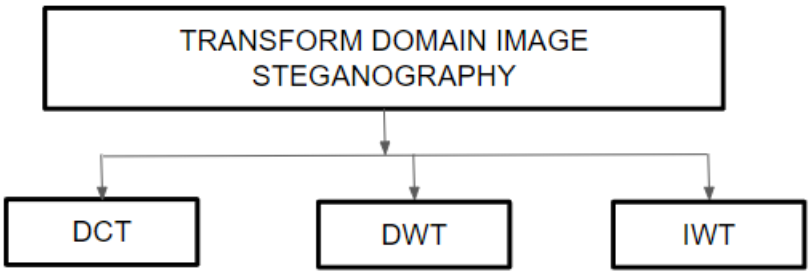

Fig 3: Classification of Transform Domain Types

DCT (Discrete Cosine Transform): DCT is an important aspect of image processing as it helps in JPEG compression. DCT transforms the spatial intensity of pixels into alternating current (AC) and direct current (DC) coefficients, which is the basis for this technology .

DWT (Discrete Wavelet Transform): It simultaneously provides image information in both the spatial and frequency domains [8] LSB or HS-based approaches can be used to implement DWT. Data bits are stored in the LSB position of the quantized coefficients of the DWT sub band when implemented using LSB. The coefficients of the histogram change based on the data bits when HS is used.

IWT (Integer Wavelet Transform): The lift system converts information about the pixels of the spatial domain into values in the frequency domain. The lifting strategy is based on computed averages and differences for pairings.

A combination of algorithms [10] can be used to design an algorithm appropriate for the application which depends on the factors described above.

4. LEAST SIGNIFICANT BIT

LSB strategy is a spatial area procedure as the calculation is applied straightforwardly on the spatial space pixel esteems. One of the principle reasons regarding the reason why we decided to perform information concealing utilizing LSB philosophy is a direct result of the speed of execution of this procedure. It's a lot quicker than a large portion of the other picture steganography strategies.

This technique depends on adjusting the last piece[6]. The last piece doesn't convey a ton of content and transforming it won't make a big deal about a distinction[7]. Since changing the last piece doesn't have a significant result it does regularly and consequently can be called as a high recurrence part

In this technique since just the most un-critical piece is adjusted, it is very helpless because of which an extra advance is performed – the crude information is encoded and afterward taken care of to the picture steganography calculation. This extra advance may be tedious however is a fundamental stage to work on the security of the privileged information. This technique is a simple to carry out strategy as it includes supplanting just the last piece of the multitude of pixels of the cover picture or a couple by the scrambled message bits.

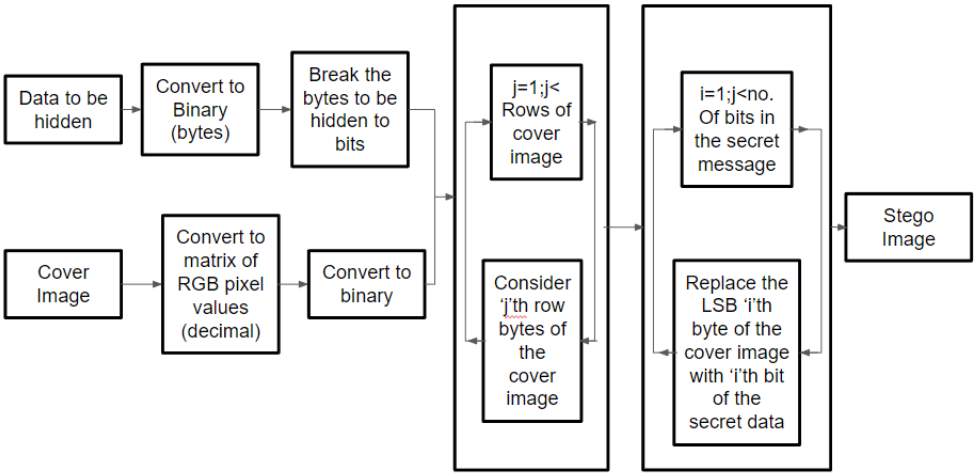

Fig 4: Block Diagram for LSB based Image Steganography

5. EVALUATION METRICS

Bit Error Rate (BER): This performance metric compares the two photos to see how big of a change there is by comparing the bits in the stego picture to the bits in the cover image in the received image

Bit error rate=BE/BC

BC – The total number of bits included inside the grayscale cover picture.

BE – The total amount of bits differing from that of the stego picture.

The bit error rate ranges from 0 to 1, with 0 indicating that the stego image is identical to the cover image and 1 indicating that the brightness of the stego image is significantly different from the cover image.

Mean Square error: Calculates the average squared difference between the estimated and actual values. In this case, the estimated picture is the stego image, while the real image is the cover image.

$$MSE = \frac{1}{n}\sum_{i=1}^{n}(Y_i - \hat{Y}_i)^2 \quad \text{(Eq.1)}$$

Peak Signal-to-noise ratio (PSNR): This ratio is used to compare the quality of an original and a compressed picture. The greater the PSNR, the higher the quality of the compressed or rebuilt image.[4]

$$PSNR = 10 \times log_{10}(\frac{I_{Cmax}^2}{MSE})\ dB$$

(Eq.2)

Icmax – The cover image's maximum pixel value

MSE – Mean square error

Histogram Analysis: A comparison of the stego image histogram and the cover image histogram is performed. If they are comparable, it indicates that the method utilised is effective.

Structural Similarity Index (SSIM): This approach is used to detect similarities between the cover picture and the stego image. As it assesses picture deterioration induced by image processing processes, this method is said to be perceptual.[3]

$$SSIM(I_c, I_s) = \frac{(2\mu_{I_c}\mu_{I_s} + k_1)(2\sigma_{I_cI_s} + k_2)}{(\mu_{I_c}^2 + \mu_{I_s}^2 + k_1)(\sigma_{I_c}^2 + \sigma_{I_s}^2 + k_2)}$$

(Eq.3)

6. RESULTS

A simple interactive interface (shown in fig 5) is created with 2 options:

1) to encode any text message to an image

2) to decode any text message from an image.

On choosing the option to encode, the user is asked to upload the text that has to be hidden and the image in which it is to be hidden (an example of this is shown in fig 5).

The decoding procedure can be performed by uploading the encoded image to obtain the original text message (shown fig 6)

```
--LSB Image Steganography--
1: Encode
2: Decode
1
Enter Source Image Path
rashmi.jpeg
```

```
Enter Message to Hide
Steganography is the practice of concealing a message wi
oncealment of information within computer files. In digi
coding inside of a transport layer, such as a document f
ographic transmission because of their large size. For e
e color of every hundredth pixel to correspond to a lett
cifically looking for it is unlikely to notice the chang
Enter Destination Image Path
rashmiencoded.png
Encoding...
Image Encoded Successfully
```

Fig 5: Encoding the hidden message into the Source Image

```
--LSB Image Steganography--
1: Encode
2: Decode
2
Enter Source Image Path
rashmiencoded.png
Decoding...
Hidden Message: Steganography is the practice of concealing a
y includes the concealment of information within computer file
e steganographic coding inside of a transport layer, such as a
ideal for steganographic transmission because of their large s
le and adjust the color of every hundredth pixel to correspond
e who is not specifically looking for it is unlikely to notice
```

Fig 6: Decoding the Source Image to access the concealed text

Below are the Mean Square Error (MSE) and Structural Similarity Index (SSIM) values.

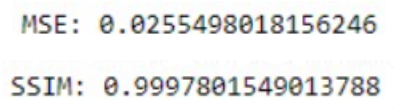

Fig 7: MSE and SSIM values

7. FUTURE SCOPE

Increased integration should be pursued while retaining anonymity. Using this technique, we can hide a text file the size of an image. Text files larger than images should be hidden. The secret key must be known to both the sender and the recipient. There are no keys on the lid, they must be prepared separately. You can create a system to secretly create and release these keys. If you need additional security, you can use the domain transfer technique. Steganography in combination with cryptography offers an incomparable technique to protect communication networks.

ACKNOWLEDGMENT

We wish to express our sincere acknowledgement to management, B.M.S. College of Engineering for sponsoring this work.

REFERENCES

[1] Mohammed A. Saleh, Image Steganography Techniques - A Review Paper, International Journal of Advanced Research in Computer and Communication Engineering, Vol. 7, Issue 9, September 2018. https://ijarcce.com/wp-content/uploads/2018/10/IJARCCE.2018.7910.pdf

[2] Hsien-Wen Tseng, Hui-Shih Leng, "A Steganographic Method Based on Pixel-Value Differencing and the Perfect Square Number", Journal of Applied Mathematics, vol. 2013, Article ID 189706, 8 pages, 2013. https://doi.org/10.1155/2013/189706

[3] Stoyanova V, Tasheva Zh, Research of the characteristics of a steganography algorithm based on LSB method of embedded information in images, International Scientific Journal "Machines. Technologies. Materials." https://stumejournals.com/journals/mtm/2015/7/65.full.pdf

[4] Priyandanu Filzasavitra, Tito Waluyo Purboyo and Randy Erfa Saputra, 2019. Analysis of Steganography on PNG Image using Least Significant Bit (LSB), Peak Signal to Noise Ratio (PSNR) and Mean Square Error (MSE), Journal of Engineering and Applied Sciences, Year : 2019 Volume: 14 Issue: 21 Page No. 7821 - 7827 DOI: 10.36478/jeasci.2019.7821.7827

[5] Ahmad Shaik, V. Thanikaiselvan and Rengarajan Amitharajan, 2017. Data Security Through Data Hiding in Images: A Review Journal of Artificial Intelligence,
Year: 2017 Volume: 10 Issue: 1 Page No.: 1-21 DOI: 10.3923/jai.2017.1.21

[6] [6] K. Thangadurai and G. Sudha Devi, "An analysis of LSB based image steganography techniques," 2014 International Conference on Computer Communication and Informatics, 2014, pp. 1-4, doi: 10.1109/ICCCI.2014.6921751

[7] Mamta Juneja, Parvinder S. Sandhu, and Ekta Walia,"Application of LSB Based Steganographic Technique for 8-bit Color Images, World Academy of Science, Engineering and Technology, 2009. 38. 427-429.

[8] Veena Nayak, Sushma P.Holla, AkshayaKumar K. M., C. Gururaj, "Automatic number plate recognition", International Journal of Advanced Trends in Computer Science and Engineering, Vol.9, No. 3, pp 3783 – 3787, ISSN 2278-3091, May – June 2020, DOI: 10.30534/ijatcse/2020/195932020

[9] C Gururaj, Satish Tunga, "AI based Feature Extraction through Content Based Image Retrieval",Journal of Computational and Theoretical Nanoscience, February 2020, volume 17, Issue 9-10, pp.4097-4101, ISSN: 1546-1955 (Print): EISSN: 1546-1963 (Online), DOI: 10.1166/jctn.2020.9018

[10] Maneesha K, Neha Shree, Pranav Datta R, Sindhu S K, C.Gururaj, "Real Time Face Detection Robot", 2nd IEEE International Conference on Recent Trends in Electronics, Information &Communication Technology (RTEICT-2017), ISBN: 978-1-5090-3704-9,19 th – 20 th May 2017 , pp 58-64, SVCE, Bengaluru. DOI: 10.1109/RTEICT.2017.8256558

[11] V Meghana, Manasa Suresh, S Sandhya, R Aparna, C Gururaj, "SoC implementation of network intrusion detection using counting bloom filter", IEEE International Conference on Recent Trends in Electronics, Information and Communication Technology (RTEICT-2016), ISBN: 978-1-5090-0774-5,20 th – 21 st May 2016 , pp 1846-1850, SVCE, Bengaluru. DOI: 10.1109 / RTEICT .2016.7808154

BIOGRAPHIES

Deeksha Manjunath is pursuing her Bachelor's degree in telecommunication engineering from B.M.S. College of Engineering. Her research areas include digital signal processing and image processing. She extends her interest in the field of machine learning and deep learning.

Avani K V H is pursuing her Bachelor's of Engineering undergraduate degree in Electronics and Telecommunication Engineering from B.M.S. College of Engineering, Bangalore. She will be graduating in 2022. Her areas of research include Image processing, Cryptography, Digital Electronics, Machine Learning and Deep Learning.

Rashmi Pai K is pursuing her Bachelor's of Engineering undergraduate degree in Electronics and Communication Engineering at B.M.S. College of Engineering. She is very interested in signal processing, digital and analogue electronics. She is also fascinated with image processing, machine learning, and blockchain.

Dr. C Gururaj received his B.E. degree in Electronics and Communication and MTech degree in Electronics, both from Visvesvaraya Technological University, Belagavi his PhD from Jain University, Bengaluru. He is currently working in the department of Electronics and Telecommunication Engineering, BMS College of Engineering, Bengaluru. He has more than 50 publications to his credit with high citations that are indexed in portals such as Scopus, Web of Science, Google scholar, Vidwan etc. He has received multiple awards and grants throughout his 18 years career. His areas of interest are Image Processing, VLSI Design, Machine Learning, Deep Learning, Artificial Intelligence and Engineering Education

Impact of E-Waste Management and Recycling Challenges: Review

Vyshnavi Gogula[1], Belwin Edward[2], W J Praiselin[3], Jacob Raglend I[4].
[1,2,3,4] School of Electrical Engineering, Vellore Institute of Technology Vellore, Tamil Nadu, India.

Abstract-Due to its economic potential, increasing commercial prospects, and possible contribution to the SDG (Sustainable Development Goals) 2030 target, urban mining of these metals has lately acquired favour. Due to transboundary imports and exports, it is the fastest increasing solid waste stream worldwide. There are several hazardous substances in the massive volume of electronic garbage that presents a significant problem. E-waste, or garbage made up of old electronics, is a problem for both people and the planet. The majority of industrialised nations now have E-waste handling infrastructures in place. Strangely, emerging countries have a lot of problems and no good solutions. Other issues that have an impact on the E-waste value chain in India include a lack of data inventory and treatment choices. To ensure the safety of the E-waste supply chain, improve social conditions, reduce negative effects on the environment, and promote long-term growth. Life cycle assessment, biotransformation, and the "4R" approach are all viable options as well. It is crucial to transform the underground recycling economy into a transparent market. Challenges in India's E-Waste Management and Recycling System. Addressing these challenges will ensure the health and safety of e-waste collectors, recyclers, and manufacturers. India has very few regulations governing the recycling of E-waste at the grass roots level.

1. Introduction

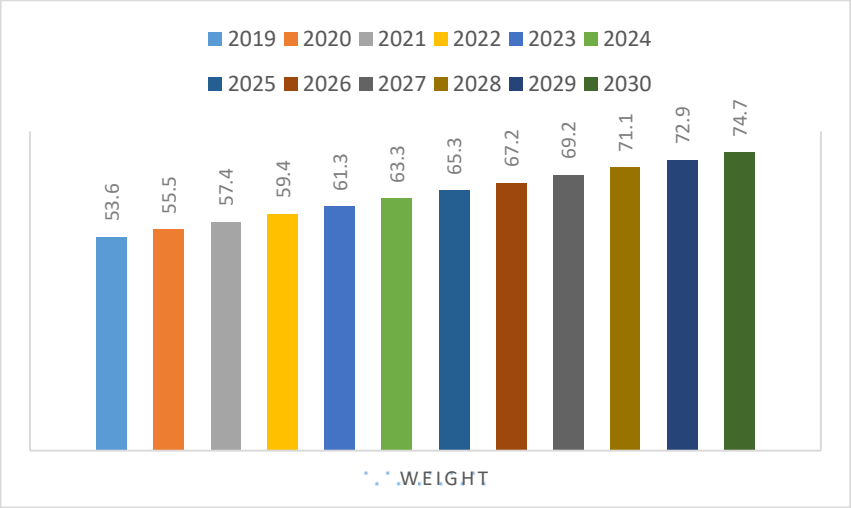

Fig. 1 WEEE generation between 2019 and 2030 [1]

WEEE, or "electronic waste," refers to unwanted electrical and electronic equipment (e-waste). E-waste encompasses a wide variety of electrical and digital gadgets, such as laptops, PDAs, video and audio devices (TVs, cameras), and more. The amount of electronic garbage produced every year has skyrocketed alongside the proliferation of IT equipment [1]. A considerable amount of electronic garbage is produced each year by a group of emerging and industrialised countries. Indian e-waste generation has increased from being one of the top five in 2018 to becoming the third largest in 2020 from being one of the top five [2].

In 2019, the world produced around 54 million metric tonnes of WEEE, up from 45 million metric tonnes in 2016 [3], with an average annual use of 7.3 kilogrammes per person. To get to 75 MT by 2030, annual growth in this generation rate is expected to be substantial. E-waste production was predicted to be 53.6 million metric tonnes in 2019, with just 17.4 percent of that total being recycled, according to the Global E-waste Monitor 2020 [4-5].

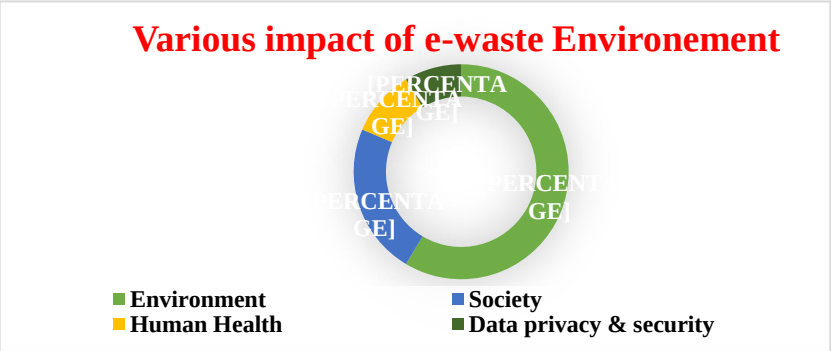

Fig. 2 various impacts of e-waste environment [6].

The risks to the privacy and security of electronic data held on these devices are considerable, and so are the environmental, health, and societal consequences of e-annual waste. Fig. 2. All of these issues stem from our current, ineffective, and contentious approach of dealing with e-waste. There is a growing need for effective e-waste management solutions due to the increasing volume of obsolete electronics.

1.1 Environment: The ecology could be endangered if e-waste isn't properly disposed of. Toxic chemicals discovered in electronic trash include heavy metals, chemical contaminants, and flame retardants. Negative environmental repercussions can be caused if e-waste is not properly handled. Heavy metals include cadmium, lead, nickel, and mercury. Cadmium can be found in a wide variety of electrical components, including switches, solder joints, and rechargeable batteries, to name just a few. Lead is used in batteries, electrical solders, and CRTs. In flat-screen televisions, circuit boards, switches and other components all contain mercury. Electronic equipment uses many heavy metals, such as barium, copper, and beryllium [7, 8-12]. They will pollute the

environment if these metals are put in landfills. When they are burned, they also release carbon dioxide into the environment." It is possible for animals to accumulate toxic compounds due to the slower metabolism of some metals. Foods such as milk, eggs, and other dairy products can cause amplification or bio magnification in the human body [13-15]. Animals are unable to consume trace elements and heavy metals in the air, soil, and river water. Some of the most prevalent semiconductor parts in electronic devices rely on the use of the trace elements bismuth (indium), antimony (antimony), and tungsten (tungsten). It was discovered that e-waste disposal sites in the Northern Vietnamese region were polluting the environment with significant concentrations of harmful compounds. Inorganic pollutants, such as polybrominated diphenyl ethers and polychlorinated biphenyls (PCBs), also endanger our ecology. PCBs are released into the environment through a variety of sources, including printing ink, hydraulic fluids, and capacitor dielectrics. Chemicals may also be released from wire and cable coatings that contain PVC components after burning [16, 17]. PCBs were outlawed in the 1980s, but the devastation they inflicted on the environment before that time is still visible. The use of these substances has resulted in pollution. Furthermore, environmentally toxic flame retardants like PBDEs and TPP are used. They're used in the plastic housing and foams of electronic gadgets like monitors. Furthermore, allowing them to penetrate the ecosystem has negative implications. Some of these plastic containers leave behind some non-burned particles, which may wash away due to rain and result in rivers. Discharges of harmful compounds into the environment harm the ecosystem in two ways: by polluting it or by causing hazardous molecules to build up. E-waste must be transported, disposed of, and recycled in a defined manner because of this.

1.2 Human Health: E-waste is among the most harmful types of household hazardous waste. Electronic waste contains a wide range of hazardous substances that can harm human health. You can either get sick from eating or working with harmful chemicals in e-waste, or you can get sick from being exposed to them while in the e-waste industry directly. Toxic metals such as cadmium and mercury damage children's cognitive and behavioural development, as well as their renal, bone, and reproductive systems; this has been demonstrated to be the case. E-waste and hair samples from people working in these industries were the most common sources of copper, antimony, and bismuth [18]. Many organs, including the liver, kidneys, thyroid, central nervous system, and reproductive system, are negatively impacted by the toxic substances included in e-organic waste. The presence of hazardous flame retardants in this trash is cause for alarm for human health. These factors have an effect on the growth of the fetus's immune system, hormone levels, thyroid, memory, learning, and behaviour. As one of the few dangerous substances that might potentially destroy Deoxyribonucleic acid (DNA), people who live near electronic waste disposal sites should take precautions to avoid exposure to hexavalent chrome. Dust and chemicals released during e-waste breakdown, renovation, reformation, recovery, and sorting may harm the health of recyclers. The release of all toxic chemicals from electronic waste poses a threat to human health [19].

1.3 Society: It's easy to ignore the harm that e-waste causes to the environment and to human health. In areas where illicit and informal e-waste operations are common, this component is more directly associated with the harm that these operations do to children and young adults. With the help of international agreements, Ghana is addressing the issue of e-waste management. Slum children and young men, on the other hand, are employed as cheap labour disassembling and recycling machinery because the area has long been regarded as a place to dispose of unwanted electronic devices. As a result, young people are becoming increasingly involved in illegal electronic trash transactions [20]. As health threats and environmental dangers become more serious, public health concerns are on the rise as well. As a result, social and economic conditions have shifted. As a result of decreased agricultural output, food insecurity and poverty have increased. Because of this, many of these workers have turned to crime. As the amount of e-waste grows, so do the number of unlawful e-waste trades and crimes. Health issues are often more strongly associated with e-social waste's impact in these situations.

1.4 Data privacy and security: Personal information, private information, and institutional data can all be stored on electronic devices such as computers and mobile phones. Data on this can both be deleted/formatted and disposed of, or it can be thrown away as is with no data remaining. A lot of people don't know that they can restore data from these storage devices. This sensitive information can be accessed by anyone with ulterior intents or business interests [21]. This is seen as a gold mine for cyber criminals. It is possible to use this information to impersonate, crack passwords, blackmail, gain access to credit and debit card numbers, and more. Disposal of e-waste raises issues of national security as well. Toxic information contained in electronic waste may be misused by criminal organisations if it is shipped to another nation for disposal. Malware-infected electrical components imported from foreign countries pose a threat to national security because they can reveal sensitive data about manufacturers. Some electronic devices' components can be copied and their data can be accessed by someone who are not authorised to do so when reverse engineering [22]. Because of this, when dealing with electronic waste, privacy and security are the most crucial issues to consider.

Table. 1 Efforts and regulations aimed at reducing electronic waste [23].

Initiatives	Key feature
Basal convention	In 1992, it was endorsed as a way to prevent hazardous waste from being exported from producing countries. The accord is supported by 172 countries, but the United States has not ratified the treaty.
Bamako convention	E-waste imports are to be regulated more strictly than in the Basel Convention. Since 1998, it has been used in African Union countries.
EU WEE Directive	All EU members embraced the system in 2007 and began taking back ten categories of

	electrical items as part of the system's takeback methodology.
Restriction of Hazardous Substances Directive (RoSH)	Restrictions on the use of hazardous compounds are part of the EU WEEE directive. Endorsed by a number of countries, including China and India.
Solving the E-waste Problem (StEP)	United Nations agencies began promoting the reuse of recycled components in 2007 as a means of cutting down on trash output.
5Rs (Report, Reduce, Reuse, Recycle and Recover)	Japan was the spark that lit the fire. Take steps to reduce the amount of electronic waste you produce. Allows remanufacturing and recycling to take place in another country.

Table 1 lists a slew of worldwide organisations and projects that have taken steps to ensure proper monitoring and recycling. These initiatives and organisations are working together to educate the public about the dangers of e-waste and find solutions to the problem.

2. Impact of e-Waste in climatic changes: A review

Deepali Sinha Khetriwal et al. [24] used data from two countries, Switzerland and India, to help readers understand the current practises for disposing of end-of-life appliances. This included details on how countries fund their appliance collection and recycling systems, as well as the social and environmental implications of these practises. The problem has been solved at last. The longevity of a recycling system depends on its capability of adjusting to upcoming shifts in trash quantity and quality. Despite existing in the shadow economy, market-based systems may be more flexible than ones based on an intergenerational contract. More quantitative indicators are needed, as this paper mainly gives a qualitative assessment of environmental and social aspects of e-waste recycling. G. Gaidajis et al. looked examined the things that make up e-waste, as well as the current and projected production of e-waste, the potential environmental challenges linked with their disposal, and management techniques. Furthermore, we learned that ill-handling of e-waste products contributes significantly to pollution in economically developing nations. S.B. Wath et al. [25] conducted a study with the intention of presenting the composition and categorization of e-waste, as well as global and Indian e-waste scenarios, prospects for reclaiming and reusing as well as recycling and recovering materials from e-waste, and environmental and occupational hazards associated with e-waste. Last but not least, more attention should be paid to recycling and recovery options at levels 2 and 3 of treatment systems in order to enhance e-waste treatment and management. Concurrently, the country needs the implementation of innovative programmes and best practises like ARF and EPR. Petheeswari Vetrivel [26] has written about the dangers that e-waste poses to the environment and to human health, as well as the three main ways to deal with it: recycling, reusing, and reducing. Peeranart Kiddee et al. [27] reviewed the toxic compounds found in discarded electronics, their possible

effects on the environment and human health, and the current treatment options available. Life Cycle Assessment (LCA), Material Flow Analysis (MFA), Multi Criteria Analysis (MCA), and Extended Producer Responsibility are only few of the methods created to deal with electronic waste (EPR). Mahesh C. Vats et al. [27, 28] analysed data to assess the current status of e-waste in India. In 2005, the country ranked 101 on the ESI (Environmental Sustainable Index), but only 66th in environmental governance; it has since been reported that the country's environmental governance could benefit from the infusion of FDI (Foreign Direct Investment) in the form of a PPP (People, Private Partnership) model for the treatment of electronic waste, since European countries possess the necessary technological know-how and India provides the necessary low-cost labour. Finally, we should be prepared with the most up-to-date infrastructure, awareness, and technology for e-waste treatment to face the new difficulties that the technological boom of the 21st century is predicted to bring. Opportunities worth millions of dollars can be swiftly unlocked by implementing 5R principles to reduce environmental loading in the country. According to Tansel et al. [29, 30], India and China face a double-edged sword in the shape of electronic trash, as they deal with both domestic production and illegal imports from wealthier countries. The cost of disposing of electronic trash has been shown to be somewhat attributable to its international transport.

Conclusion

Threats to the environment, human health, social welfare, and the privacy and security of personal data are just few of the many that electronic waste presents. Careful management of electronic trash is required to lessen its potentially harmful effects and the likelihood of illicit activity. E-waste must be managed and disposed of according to stringent laws and regulations. It's crucial to be knowledgeable about all aspects of e-waste, including the many crimes that could put people at risk from using it. In order to successfully recycle electronic waste over the long run, governments and regulatory agencies must provide the necessary infrastructure and encourage private sector engagement through financial support and other incentives. To stop the illegal dumping of electronics in the future, we need a mix of stricter laws, innovative technological solutions, and increased community accountability through education. It's possible that in the not-too-distant future, bio hydrometallurgy (i.e., bioleaching) strategies will play a pivotal role in metal recycling.

References

[1] Forti, V., Balde, C.P., Kuehr, R. and Bel, G., 2020. The Global E-waste Monitor 2020: Quantities, flows and the circular economy potential.

[2] India among top five nations in e-waste generation, says report, Financial Express, 04 June 2018, (2018).

[3]India third largest e-waste generator in the world, capacity limited to threat only few fourth of its waste. Times of India, 04 July 2020, (2020).

[4] Unger, N., Beigl, P. and Salhofer, S., 2017. Small waste electrical and electronic equipment–

from collection to secondary resource. *Österr Wasser-und Abfallw*.
[5]S. Mehta, The why and how of disposing electronic waste, Mongbay, 25 August 2020, (2020).
[6] Kapoor, N., Sulke, P.J. and Badiye, A., 2021. E-WASTE FORENSICS: AN OVERVIEW. Forensic Science International: Animals and Environments, p.100034.
[7]Sivaramanan, S., 2013. E-Waste Management, Disposal and Its Impacts on the Environment. Universal Journal of Environmental Research & Technology, 3(5).
[8] Hartwig, K. and MDes, A.D.P.D., 2016. DIGITAL WASTE & CYBER CRIME.
[9] A. Ashfaq, A. Khatoon, Environmental impacts and assessment of electronic waste management, Int. J. Curr. Microbiol. Appl. Sci. 3 (7) (2014) 772–779. ISSN: 2319- 7706.
[10] M.S. Sankhla, M. Kumari M, M. Nandan, S. Mohril, G.P. Singh, B. Chaturvedi, R. Kumar, Effect of electronic waste on environmental & human health – a review, IOSR J. Environ. Sci. Toxicol. Food Technol. 10 (9) (2016) 98–104, e-ISSN: 2319- 2402, p- ISSN: 2319-2399.
[11] J. Alghazo, O. Ouda, A. Elassanm, E-waste environmental and information security threat: GCC countries vulnerabilities, Euro-Mediterr. J. Environ. Integr. 3 (13) (2018) 13.
[12] B.S. Al-Anzi, A.A. Al-Burait, A. Thomas, C.S. Ong, Assessment and modeling of E-waste generation based on growth rate from different telecom companies in the State of Kuwait, Environ. Sci. Pollut. Res. 24 (35) (2017) 27160–27174.
[13] T. Sivakumar, G. Vijayaraghavan, A.V. Kumar, Global challenges in e-waste management: indian scenario, Int. J. Adv. Eng. Technol. 2 (4) (2011) 0976–3945 (E-ISSN).
[14] T. Udhayakumar T, Disposal methods of e-waste in India survey conducted in Chennai, Int. J. Appl. Environ. Sci. 12 (3) (2017) 505–512. ISSN 0973-6077.
[15] N.N. Ha, T. Agusa, K. Ramu, N.P. Tu, S. Murata, K.A. Bulbule, P. Parthasaraty, S. Takahashi, A. Subramanian, S. Tanabe, Contamination by trace elements at e-waste recycling sites in Bangalore, India, Chemosphere 76 (1) (2009) 9–15.
[16] N. Uchida, H. Matsukami H, M. Someya, N.M. Tue, L.H. Tuyen, P.H. Viet, S. Takahashi, S. Tanabe, G. Suzuki, Hazardous metals emissions from e-waste-processing sites in a village in northern Vietnam, Emerg. Contam. 4 (1) (2018) 11–21.
[17] J. Alghazo, O. Ouda, A. Elassanm, E-waste environmental and information security threat: GCC countries vulnerabilities, Euro-Mediterr. J. Environ. Integr. 3 (13) (2018) 13.
[18] P. Kiddee, R. Naidu R, M.H. Wong, Electronic waste management approaches: an overview, Waste Manag. 33 (2013) 1237–1250.
[19] K. Grant, F.C. Goldizen, P.D. Sly, M.N. Brune, M. Neira, M. Van de Berg, R. E. Norman, Health consequences of exposure to e-waste: a systematic review, Lancet Glob. Health 1 (6) (2013) e350–e361.
[20] A. Illes, Illegal shipment of e-waste from the EU: a case study on illegal e-waste export from the EU to China. A Study Compiled As Part of the EFFACE Project, IEEP,, London, 2015.
[21] Illicit trade in electrical and electronic waste (e-waste) from the world to the region. Transitional Organised Crime Treat Assessment- East Asia and the Pacific.
[22] Special Report. Recycling Electronic Waste. Initiative for Global Environmental Leadership (IGEL). Knowledge @ Whartone (2016).
[23] Thakur, P. and Kumar, S., 2021. Evaluation of e-waste status, management strategies, and legislations. International Journal of Environmental Science and Technology, pp.1-10.
[24] Sinha-Khetriwal, D., Kraeuchi, P. and Schwaninger, M., 2005. A comparison of electronic waste recycling in Switzerland and in India. Environmental Impact Assessment Review, 25(5), pp.492-504.

[25] Gaidajis, G., Angelakoglou, K. and Aktsoglou, D., 2010. E-waste: environmental problems and current management. Journal of Engineering Science and Technology Review, 3(1), pp.193-199.
[26] Wath, S.B., Dutt, P.S. and Chakrabarti, T., 2011. E-waste scenario in India, its management and implications. Environmental monitoring and assessment, 172(1), pp.249-262.
[27] Vetrivel, P., 2012. A Focus on E-Waste: Effects on Environment and Human Health. International Journal of Novel Trends In Pharmaceutical Sciences, 2(1), pp.47-51.
[28] Kiddee, P., Naidu, R. and Wong, M.H., 2013. Electronic waste management approaches: An overview. Waste management, 33(5), pp.1237-1250.
[29] Vats, M.C. and Singh, S.K., 2014. Status of e-waste in India-A review. transportation, 3(10).
[30] Tansel, B., 2017. From electronic consumer products to e-wastes: Global outlook, waste quantities, recycling challenges. Environment international, 98, pp.35-45.

Biographies

Gogula Vyshnavi was born in Andhra Pradesh, India, on January 24, 1994. She received her B.Tech degree in Electrical and Electronics Engineering from JNTU Anantapuramu in 2015. She received her M.Tech in Electrical Power System at the Department of Electrical and Electronic Engineering in Sree Vidyanikethan Engineering College, Andhra Pradesh, India. At present she is pursuing PhD in School of Electrical Engineering, VIT University, Tamil Nadu, and India. Her main research interest is power system protection, distributed generation, specifically detection and location faults in distribution system, high impedance faults, and E-waste management. Etc.,

Dr. J. Belwin Edward received his doctorate in Power Systems from Anna University in Chennai, India. Now, he works as a senior associate professor in the electrical engineering department at VIT in Vellore, India (an Institute of Eminence). He's presented over fifty of his works at various conferences and magazines. He has been in the academic field for over 18 years. His primary areas of study are home energy management, hybrid electric vehicles, power system optimization, and renewable energy systems.

W J Praiselin received a Bachelor of Engineering in Electrical and Electronics Engineering in 2013 from Udaya School of Engineering in Tamilnadu, India, and a Master of Engineering in Power Systems Engineering in 2015 from Francis Xavier Engineering College in Tamilnadu, India. She is a current Ph.D. student at VIT University in Vellore, India. Her areas of focus in academia are power systems, microgrid power quality

improvement, control operations, FACTS devices, and the integration of renewable energy sources.

Dr. I. Jacob Raglend, Ph.D., earned a first-class Bachelor of Science in Electrical Engineering from The Indian Engineering College in 2000 and a first-class Master of Science in Power Systems Engineering from Annamalai University in 2001. He earned his doctorate in 2007 from the Electrical and Electronics Engineering Department at the Indian Institute of Technology in Roorkee, India. Currently he is the head of the Electrical Engineering Department at Vellore Institute of Technology (VIT) in India and a professor there. He has written roughly 80 articles for peer-reviewed journals, another 65 for conferences both domestic and abroad, and 13 for collections of essays. Twelve students have earned their doctorates under his tutelage, and another six are now enrolled. Volunteering at National and International Conferences as a Technical and Advisory Member He has served as the publication chair for five different IEEE International conferences and the organising chair for two different conferences. At Noorul Islam University, I served as the Associate Project Director for a student group working on a Nano Satellite. To serve as a reviewer for the journals Journal of Applied Soft Computing, International Journal of Energy Sector Management, and International Journal of Electric Power and Energy Systems. Some of the topics he covered in his lectures included the fundamentals of electrical engineering, power systems, AI, and soft computing. Unit Commitment, Economic Dispatch, Smart Grid, Power System Restructuring and Deregulation, Renewable Energy Integration, Internet of Things Applications, Artificial Intelligence Applications to the Power System, and FACTS are all areas of study that pique his interest.

A Study On Conversion Of ICE Vehicle To EV

Nishana B B*, Puneeth G, Rahul Ganesh S, Vedanth Pandit B R, Raghunath M J and Sushma S R

Vidyavardhaka College of Engineering/ Electrical and Electronics Engineering Department, Mysuru, India

**Email: nishana.bb_ee@vvce.ac.in*

Abstract.

Due to the increase in oil prices and depletion oil resources, electric vehicles will undoubtedly be the next revolution in automobile industry. EVs generate zero emissions since they utilize power from batteries rather than fuels, making them eco-friendly. This shift towards electric vehicles will render the conventional mobility systems driven by internal combustion engine useless. Thus, there is an absolute necessity for converting IC engine vehicle to electric vehicle, as it will prevent the existing IC engine vehicles from being scrap.

Keywords. ***EV types, battery, motor, retrofitting, challenges.***

1. INTRODUCTION

Because there are more gasoline vehicles on the road, environmental pollution is increasing. Electric vehicles(EV) are extremely important in reducing pollution, and they are the best option when compared to regular automobiles. Due to environmental and economic considerations, electric vehicles have recently gained greater popularity than gasoline automobiles. With the improvement of battery and motor technology, EVs will become a viable alternative to petroleum automobiles[1]. EVs provide the following advantages over the conventional vehicles:

- No emissions: They do not emit any greenhouse gases from their exhaust. Furthermore, the process involved in manufacturing is more eco-friendly, regardless of the fact that manufacturing a battery has a negative influence on carbon emissions.

- Reduced complexity: Maintenance cost is less due to less number of components in an Electric Vehicle engine. There is no need for a cooling circuit, or a clutch, gearshift or any components to reduce noise in the engines. This makes them both simple and compact.

- Reliable: Since these vehicles have simpler and fewer components, they are less likely to break down. Furthermore, EVs are unaffected by engine explosions, vibrations, or gasoline corrosion, which cause wear and tear in conventional vehicles.

- Cheaper: In comparison to traditional combustion vehicles, the cost of the electricity required for the vehicle and it's maintenance costs are much lower. EV's seem to have a much lower energy cost per kilometer when compared to conventional vehicles.

- Comfort: Travel in an EV is more comfortable because there are no tremors or engine noise [2].

- Accessibility: EVs offers access to urban areas where other combustion vehicles are prohibited (e.g., low emissions zones). Electric vehicles are not subjected to same traffic restrictions as conventional vehicles in large cities, particularly when pollution levels are high.

2. CLASSIFICATION OF ELECTRIC VEHICLE

Electric vehicles can run purely on electricity or in combination with an IC engine. The most fundamental type of Electric vehicle is one that utilizes only batteries as its source of energy, but there are others that use various sources of energy. These are referred as hybrid electric vehicles (HEVs). Technical Committee 69 (Electric Road Cars) of the International Electrotechnical Commission proposed that the vehicles with two or more types of energy sources, converters or storage, can be classified as even if one of them provide electrical energy [2]. This specification allows for a wide range of HEV pairings, including battery and IC engine, battery and fuel cell, battery and capacitor, battery and flywheel, and so on. Therefore, both the general public and experts began to refer to vehicles with an electric motor and an IC engine as HEVs, battery and fuel cell vehicles as FCEVs and Capacitor and battery vehicles as ultra-capacitor-assisted EVs [2]. These terminologies have gained widespread acceptance, and EVs can now be classified as follows:

- Fuel Cell Electric Vehicle (FCEV)
- Hybrid Electric Vehicle (HEV)
- Plug-in Hybrid Electric Vehicle (PHEV)
- Battery Electric Vehicle (BEV)
- Extended range electric vehicle (ER-EV)

Fuel Cell Electric Vehicle (FCEV)

Fuel Cell Electric Vehicle are also known as Fuel Cell Vehicles (FCV). Fuel cells, which produce electricity through chemical reactions, are at the core of these vehicles [3]. Because hydrogen is the preferred fuel for this reaction, hydrogen fuel cell cars are sometimes termed as "hydrogen fuel cell vehicles." Fuel Cell Vehicles transport hydrogen in special high-pressure tanks, and oxygen, which is acquired from the surrounding air taken, is another ingredient in the process of power generation. The electricity generated from fuel cells, and this is utilized to power the electric motor, which drives the wheels. Excess energy is stored in battery or super capacitor storage systems [4].

Hybrid Electric Vehicle (HEV)

The electric motor and IC engine power the HEVs. The electric propulsion system is used by a HEV when the power demand is minimal. It has a considerable benefit in low speed conditions like cities. It also minimizes gasoline because the engine is turned off fully during standstill periods like traffic jams. This feature reduces greenhouse gas emissions as well. When more speed is necessary, the HEV shifts to the ICE. Both drive trains can boost performance by working together.

Plug-in Hybrid Electric Vehicle (PHEV)

The PHEV concept was developed in order to increase the range of HEVs that can run entirely on electricity [5]. Like a HEV, it has both an ICE and an electric powertrain, but the distinction is that the PHEV uses electric propulsion as the main driving force, necessitating a larger battery capacity than HEVs. PHEVs start in 'all electric' mode, run on electricity, and then call on the ICE for a boost or to charge up the battery pack when the batteries are low on charge. The ICE is employed to expand the range in this case. PHEVs have the ability to charge their batteries directly from the grid (but not possible in HEVs), as well as use regenerative braking. PHEVs have a lesser carbon footprint than HEVs because they may run on electricity for the most of the time. They also utilize less fuel, resulting in cheaper operating expenses.

Battery Electric Vehicle (BEV)

Battery Electric Vehicles are electric vehicles which rely exclusively on batteries to power the drivetrain. Battery Electric Vehicles must rely only on the stored energy in their battery packs; hence the range of these vehicles is directly proportional to the capacity of the battery. On a single charge, they can normally travel 100 to 250 kilometers [6], with top-tier models capable of travelling up to 500 kilometers [6]. Factors such as conditions and driving style, vehicle configurations, road conditions, weather, age, and battery type all influences the range. Charging of an exhausted battery pack takes longer than refueling a standard ICE car.

Extended-range electric vehicles (ER-EVs)

The ER-EVs vehicles are quite identical to BEVs. The difference is that the ER-EVs come with a backup combustion engine which is used to charge the vehicle's batteries if necessary. Unlike the engines found in HEVs and PHEVs, the engine here is utilized only for the charging of the battery and it is not connected to the wheels of the vehicle [7].

3. BATTERY

In an EV, the battery is the primary source of energy storage. In fact, it is considered as the driving force behind the electric vehicle's success [8]. There are various kinds of batteries. Batteries can be rechargeable and non-rechargeable. Below are the few main rechargeable batteries are mentioned.

Lead acid battery

The lead-acid battery which is the very first rechargeable battery ever made was developed in the year 1860 by Gaston Planté. Though used in electric vehicles they can also be seen in conventional automobiles. The electrolytes, as well as the positive and negative electrodes, are active materials in electrochemical charge/discharge. Diluted corrosive sulphuric acid acts an electrolyte. Sponge lead (Pb) serves as the negative electrode, while lead oxide serves as the positive electrode (PbO_2)[9].

Nickel cadmium battery

In 1899, Waldemar Jungner invented the basic Nickel cadmium battery. These are basically constructed of Nickel hydroxide as the positive electrode and Cadmium hydroxide as the negative electrode which are immersed in potassium hydroxide where the utilization of alkaline electrolyte was made [10]. During its time, Nickel cadmium became the most popular battery for portable electronic devices.

Nickel metal hydride battery

Instead of cadmium (Cd), an alloy which stores hydrogen is employed for negative electrodes. When researchers first started working on Nickel metal hydride, they discovered that it was unsuitable owing to metal hydride instabilities, therefore Nickel metal hydride was developed, which is primarily utilized in satellites. Nickel metal hydride was developed after the identification of new hydride alloys that gave superior stability and had a significantly higher specific energy. Other advantage it has over Nickel cadmium is that it is environmentally friendly, as it contains no hazardous metals [10].

Lithium ion battery

M Stanley Whittingham proposed lithium batteries while working for Exxon in the 1970s [11]. For anodes, he considered titanium sulphide and lithium metal. The positive electrode of present Li-ion batteries is of metal oxide, and the negative electrode is of carbon, with lithium salt used as the electrolyte which provides the required ions for the reversible electrochemical process between cathode and anode. The lightweight of lithium-ion

batteries' components, their internal resistance, high loading capacity, and high unloading and loading cycles are all advantages. The majority of electric vehicles and plug-in hybrids now use this sort of battery. Li-ion batteries should function within a reliable and safe operating range defined by voltage and temperature windows. Surpassing the limits of these windows would result in a rapid reduction in battery performance and may also pose a security risk.

Table 1: Comparison of different type of batteries [7]

	Lead acid	Nickel cadmium	Nickel metal hydride	Lithium ion
Energy density (Wh/L)	60-100	60-150	100-300	200-735
Temperature (° C)	-20 – 45	0 – 50	0 - 50	-20 – 60
Specific power (W/kg)	75-100	120-150	250-1000	350-3000
Specific energy(Wh/kg)	30-60	60-80	60-120	100-275

4. MOTORS

The propulsion system is at the heart of an electric vehicle [2], and the electric motor is at the center. Motor transforms battery's electrical energy into mechanical energy, allowing the vehicle to move. During regenerative action, motor serves as a generator, sending energy back to the source. Electric vehicle can possess varied numbers of motors depending on their needs. High efficiency, high torque, High power, wide speed range, dependability, robustness, affordable cost, small size and lower noise are among the requirements for an EV motor, according to references [12].

Brushed DC Motor

The stator of these motors is made of permanent magnets (PM), while the rotors feature brushes which power the stator. One of its advantages is its ability to deliver maximal torque at lower speeds. Its disadvantages include the huge structure, less efficiency, heat generated by the brushes, and the resulting loss in efficiency. Because the heat is generated in the rotor's center, it's also tough to remove. For such reasons Brushed DC motors are no longer incorporated in EVs [13]

Permanent Magnet Brushless DC Motor (BLDC)

This motor's rotor is built of PM, and an inverter provides an alternating current (AC) feed to the stator from a DC source. Due of the absence of rotor windings rotor copper losses in rotor does not take place, making it more efficient when compared to IM. It is also lighter, smaller, high efficiency in dissipating heat (from the stator), highly dependable, and has a better torque density and specific power [2].

Permanent Magnet Synchronous Motor (PMSM)

Permanent Magnet Synchronous Motor is one among the most advanced machines, which has the ability to function at various speeds without utilizing the gear system. This feature improves the compactness and efficiency of these motors. This setup is also ideal for in-wheel applications due to its ability of delivering great torque at lower speeds. PMSMs with an outside rotor are also viable to build without the use of rotor bearings. However, the one significant disadvantage of these machines occurs during in-wheel operations, when a large amount of iron is lost at high speeds, causing the system to become unstable [13].

Induction Motor(IM)

This is the most advanced of the several commutatorless motor driving schemes. To create Induction Motor drives which are able to address the needs of Electric Vehicle systems, vector control is useful. By torque control and decoupling field control, the field orientation control may make an Induction Motor behave as a separately excited Direct Current motor. The field orientation control can accomplish a range 3-5 times the base speed with the help of properly constructed Induction Motor [14], and the flux weakening extends the speed range while keeping the power constant over the base speed [15].

Switched Reluctance Motor (SRM)

Recently the Switched Reluctance Motor is popular due it's tolerance of fault which is mainly because its phases are not coupled with each other. It has a different power stage when compared with the motors mentioned so far. In the style of flyback circuit every phase winding are connected [7].

In-wheel and direct drive motor

Direct drive lowers the losses in drive train's mechanical parts. Motor is directly attached to the shaft, eliminating the need for a transmission, clutch, or gearbox. Recently, a researcher [15] has advocated for an in-wheel motor. In-wheel motor spins the rotor inside out and is linked to the rim and tyre of the wheel. It does not possess drive shaft or gearbox. Wheel-hub motor is another name for the motor. Its key advantage is that each wheel may be controlled independently. Each wheel spins at its own pace and in any direction. As a result, parallel barking is simple to produce. The technology can readily deploy the anti-lock braking system. It has been demonstrated that it can effectively avoid spinout. The structure of the entire vehicle is substantially simpler.

5. REVIEW ON CONVERSION PROCESS TO EV

[16] proposed the process of converting the conventional vehicle to electric vehicle. The process can be divided into 3 parts. First step is to dismantle the mechanical systems, second step is to install the electrical components and the third step is to install power system. The main constitutive elements like motors, energy storage and charging systems were also presented. Also it was suggested that the conversion will save the environment from pollution and also prevent the ice vehicles from going scrap.

[17] here the experimental setup for the process of retrofitting is presented. They retrofitted a four wheeler ic engine vehicle to electric vehicle. They also gave the motor parameters calculation and suggested that the motor specifications should be more than sufficient to replace the engine of the vehicle. They used BLDC motor and lithium polymer based battery pack was selected. Even the BLDC motor simulation results were provided. The operational cost comparison showed that EV is more cost effective than the IC engine vehicle.

[18] here a project of conversion of ICE to EV was presented. The process of conversion and also the conversion cost benefit ratio was presented. The main task of any conversion process is the selection of appropriate vehicle which should have lowest weight, simple construction and more space in the engine area. Therefore, the conversion was done on Opel Kadett C from 1978.

[19] here scooter with engine capacity of 80cc petrol internal combustion engine is converted to hybrid vehicle where the front wheel gets an electric hub motor. It is converted to a two-wheel drive scooter with the internal combustion engine which powers the rear wheel and the electric motor powers the front wheel. Simulation results and also the calculations for savings were presented. The results showed that hybrid scooter can run at a higher torque than the EVs and in case of emergency it can be operated in engine mode.

[20] proposed the conversion of the four-stroke gasoline powered bike into electric vehicle and selection of required components was done with the help of calculations. Here lithium ion battery and BLDC motor was used. Step by step process of assembling the components and the test results were provided. With the project's implementation it was seen that there was cost reduction and with the help of the components the range and speed for the vehicle can be obtained.

[21] presented the conversion of an IC Engine vehicle into an EV. Both the batteries charging power converters and the power train were developed for the process of conversion. The power train comprises of 3-phase inverter with space vector modulation and Field Oriented Control. The main components assembly of the EV was also presented.

[22] presented the conversion of the fuel based garbage vehicle to electric vehicle. The conversion process was done by replacing the existing parts like internal combustion engine, fuel tank, exhaust system, radiator, tailpipe etc., with induction motor and battery power train. The conversion process also helped in reducing the driver's efforts. It also describes the electric powered vehicle has a numerous benefits over conventional one.

[23] here the development of electric vehicle from internal combustion vehicle is shown. The cost of operation of an electric vehicle and an internal combustion vehicle is compared and it was seen that the electric vehicle has less operating costs. The components needed and design for the conversion is also provided.

[24] here an IC engine powered Mercedes Benz Class A 190 was converted into Electric vehicle. The materials required and the methods are also discussed. The results indicated that the conversion is feasible with the operating costs being low for the converted vehicle and this operating cost can be reduced by PVs to generate electricity.

[25] here a system for conversion of ICEV to BEV is shown. The total cost of ownership of the EV and the economic benefits of the BEV over the EV is presented. The working of the electric car and different components are explained.

6. SAFETY CHALLENGES

Electrical risks are a serious concern, given the massive quantity of electrical energy that may be stored in batteries and the use of high voltage (HV) cables [26]. As a result, if a defect occurs, a high-energy release could occur, potentially posing a safety danger, and because the battery cannot be turned off, there is always an electrical risk [26]. Other dangers include chemicals, which could be released as a result of battery technology, and collisions, which could puncture the battery or damage high-voltage wires, perhaps resulting in a fire [26]. The weight distribution of a vehicle will change if the IC Engine

and exhaust system are replaced with the electric drive train, which will be studied and analyzed in the design and testing stages before manufacturing a new EV. However, in the case of an electric conversion, the vehicle was not designed to carry an electric drive train from the start, and thus, if not taken into account, it may affect the loads on the chassis, potentially causing structural damage in the future, as well as affecting dynamic handling and braking [27]. Another factor to consider is user safety during maintenance, with appropriate protection offered to users who might perform basic maintenance tasks, while vehicle technicians and repair staff must be sufficiently trained to assure complete safety while adjusting and changing parts [28]. Testing of the insulation resistance and the leakage current controller function, also the verification of battery status, should all be included in routine maintenance [28].As a result, these safety concerns emphasize some of the aspects why electric retrofitting must be conducted in a suitable standards, largely to avoid major failures.

7. CONCLUSION

Electric retrofits do have potential to assist in the transition to zero-emission vehicles, reducing the transportation sector's considerable contribution to GHG emissions. By embracing the re-use notion of a circular economy, transforming current vehicles could reduce the number of well-functioning vehicles going to scrap as a result of the purchase of new EVs. Furthermore, EV technology might be embraced at a moderate pace, eliminating the requirement to build and promote a large number of EVs in the near future. Thus there is an increasing need for converting existing combustion engine vehicles to electric vehicle. In this paper, we have discussed about the types of electric vehicles, different battery types used and also the different motors used. Here we have also discussed about conversion process and also the safety challenges that are faced in conversion process.

8. REFERENCES

[1] Ching-Ming Lai, Yu-Huei Chang, Ming-Hua Hsieh, Yuan-Chih Lin ”Development of a Bidirectional DC/DC Converter with Dual-Battery Energy Storage for Hybrid Electric Vehicle System,” IEEE Trans. Vehicular Technology., vol. 67, no.23, Feb 2018.

[2] Chan, C.C. The state of the art of electric, hybrid, and fuel cell vehicles. Proc. IEEE 2007, 95, 704–718.

[3] Fuad Un-Noor, Sanjeevikumar Padmanaban, Lucian Mihet-Popa, Mohammad Nurunnabi Mollah and Eklas Hossain, “A Comprehensive Study of Key Electric Vehicle (EV) Components, Technologies, Challenges, Impacts, and Future Direction of Development”, Energies 2017, 10, 1217;

[4] Miller, J.F.; Webster, C.E.; Tummillo, A.F.; DeLuca, W.H. “Testing and evaluation of batteries for a fuel cell powered hybrid bus”, the Energy Conversion Engineering Conference, Honolulu, HI, USA, 27 July–1 August 1997; Volume 2, pp. 894–898.

[5] Gao, Y.; Ehsani, M. Design and control methodology of plug-in hybrid electric vehicles. IEEE Trans. Ind. Electron. 2010, 57, 633–640.

[6] Grunditz, E.A.; Thiringer, T. Performance Analysis of Current BEVs Based on a Comprehensive Review of Specifications. IEEE Trans. Transp. Electr. 2016, 2, 270–289.

[7] Julio A. Sanguesa, Vicente Torres-Sanz, Piedad Garrido, Francisco J. Martinez, Johann M. Marquez-Barja, “A Review on Electric Vehicles: Technologies and Challenges”, Smart Cities 2021, 4, 372–404.

[8] Pruthvija B, K P Lakshmi, “Review on Battery Technology and its Challenges”, International Journal of Scientific & Engineering Research Volume 11, Issue 9, September-2020

[9] Cheng, K.W.E.. “Recent development on electric vehicles,” 3rd International Conference on Power Electronics Systems and Applications, PESA. 1 – 5, 2009

[10] Pruthvija B, K P Lakshmi, “Review on Battery Technology and its Challenges”, International Journal of Scientific & Engineering Research Volume 11, Issue 9, September-2020, 1706-1713.
[11] Lu, L.; Han, X.; Li, J.; Hua, J.; Ouyang, M, “A review on the key issues for lithium-ion battery management in electric vehicles”, J. Power Sources, 2013, 226, 272–288.
[12] Rajashekara, K, “Present status and future trends in electric vehicle propulsion technologies”, IEEE J. Emerg. Sel. Top. Power Electron. 2013, 1, 3–10.
[13] Jose, C.P. Meikandasivam, S, “A Review on the Trends and Developments in Hybrid Electric Vehicles”, Innovative Design and Development Practices in Aerospace and Automotive Engineering; Springer: Singapore, 2017; pp. 211–229.
[14] Yamada, K.; Watanabe, K.; Kodama, T.; Matsuda, I.; Kobayashi, T, “An efficiency maximizing induction motor drive system for transmissionless electric vehicle”, Proceedings of the 13th International Electric Vehicle Symposium, Osaka, Japan, 13–16 Octobor 1996; Volume II, pp. 529–536.
[15] K.W.E Cheng, “Recent Development on Electric Vehicles”, 3rd International Conference on Power Electronics Systems and Applications, 2003.
[16] K. S. Sathish Kumar, Franklin Xavier. A, Avinash. R, Muthupitchiya. P, Jerrin K Abraham.:“Conversion of an IC Engine Vehicle into Electric Vehicle”, International Journal of Engineering Research & Technology (IJERT), Vol. 7, Issue 06, pp. 4-7, Special Issue - 2019
[17] Ashish Rajeshwar Kulkarni, Sudhanshu Singh, Krishan Kant, Hemant Bharti.:“Experimental Electric Retrofitting of an ICE Vehicle with Simulation and Cost Analysis”, International Journal of Innovative Technology and Exploring Engineering (IJITEE), Vol. 9, Issue-9S, pp 45-50, July 2020.
[18] Mario Vraziu , Damir Vuljaj, Arsen Pavasoviu, Hrvoje Paukoviu.:“Study of a vehicle conversion from internal combustion engine to electric drive”, IEEE International Energy Conference (ENERGYCON), pp. 1544-1548, May 2014.
[19] Najmuddin Jamadar, Suhani Jamadar, Abhilasha Kumbhar, Shital Tanvandkar, Manali Patil, Sourabh Zagde, “Retrofitting of Existing Scooter into Hybrid Electric Scooter”, Journal of Automation and Automobile Engineering Vol. 4, Issue-2, pp 6-13,
[20] S.Vasanthaseelan, D.S. Dharun, S.Sreerag, R.Gokul.:“Conversion Of IC Engine Vehicle To Electric Vehicle”, International Research Journal of Engineering and Technology (IRJET), Vol. 6, Issue 03, pp. 3325-3330, Mar 2019.
[21] Delfim Pedrosa, Vítor Monteiro, Henrique Gonçalves, Júlio S. Martins, João L. Afonso. “A Case Study on the Conversion of an Internal Combustion Engine Vehicle into an Electric Vehicle”, IEEE Vehicle Power and Propulsion Conference, pp. 1-5, Oct 2014.
[22] Kapil Shrivastava, Ram Bansal, Himanshu Jain, Nimil Doshi, Niraj Soni And Nikita Soni, “Conversion Of Conventional Vehicle Into An Electric Vehicle”, Advances and Applications in Mathematical Sciences, Vol 20, Issue 1, pp. 15-24, Nov 2020.
[23] li Eydgahi, Edward Lee Long, “Converting an Internal Combustion Engine Vehicle to an Electric Vehicle”, Proceedings of ASEE Annual Conference, Vancouver, Canada, June 2011.
[24] Jardel Eugenio da Silva, Jair Urbanetz, “Converting a Conventional Vehicle into an Electric Vehicle (EV)”, Brazilian Archives of Biology and Technology, Vol 62, Jan 2019.
[25] Nachiket Chavan, Varun Rathor, “Transition Of Icev To Ev: Process And Efficiency”, International Journal of Engineering Applied Sciences and Technology (IJEAST), Vol. 5, Issue 3, pp. 402-408, Jul 2020.
[26] Freschi, F.; Mitolo, M.; Tommasini, R. Electrical Safety of Plug-In Electric Vehicles: Shielding the Public from Shock. IEEE Ind. Appl. Mag. 2018, 24, 58–63.
[27] Zakrzewicz, W.; Sys, E.; Mrowicki, A.; Siczek, K.; Kubiak, P. Safety Issues for Electric and Hybrid Vehicles; IEEE: Kielce, Poland, 2020.
[28] Robbie Watts, Aritra Ghosh, Justin Hinshelwood, “Exploring the Potential for Electric Retrofit Regulations and an Accreditation Scheme for the UK”,Electronics2021,10,31

Biographies

Nishana B B completed the bachelor's degree in Electrical and Electronics Engineering from VTU in 2022.

Puneeth G completed the bachelor's degree in Electrical and Electronics Engineering from VTU in 2022.

Rahul Ganesh S completed the bachelor's degree in Electrical and Electronics Engineering from VTU in 2022.

Vedanth Pandit B R completed the bachelor's degree in Electrical and Electronics Engineering from VTU in 2022.

Raghunath M J received the bachelor's degree in Electrical and Electronics Engineering from VTU, the master's degree in Computer Application in Industrial Drives from VTU. He is currently working as Assistant Professor in department of Electrical and Electronics Engineering, Vidyavardhaka College of Engineering, Mysuru.

Sushma S R received the bachelor's degree in Electrical and Electronics Engineering from VTU, the master's degree in Computer Application in Industrial Drives from VTU. She is currently working as Assistant Professor in department of Electrical and Electronics Engineering, Vidyavardhaka College of Engineering, Mysuru.

A Study of Passive Cell Balancing and State of Charge Assessment Using Coulomb Counting Method

Advaith Srinath, Syed Shoaib Hussaini, Nikshith K U, Shivaprasad G Indaragi,
*Venkatesh Boddapati and Prakash D B
B.M.S College Of Engineering, Bangalore-560019.
*Corresponding Author- *venkateshb.eee@bmsce.ac.in*

Abstract.

Cell balancing and State Of Charge (SOC) assessment are important aspects of electric vehicle (EV) battery management systems. Cell balancing makes sure that all of the cells in a battery pack are at the same level of charge, which contributes to the battery packs overall longevity and performance. SOC estimation, on the other hand, is the process of determining the current state of charge of the battery pack. This information is used to predict the remaining range of the EV and to prevent overcharging or over-discharging of the battery pack. Both cell balancing and SOC estimation are typically accomplished through the use of sophisticated software algorithms and hardware sensors. These algorithms and sensors must be able to accurately measure the temperature, current, and voltage of each cell in the battery pack to provide accurate and reliable cell balancing and SOC estimates.

1. INTRODUCTION

Renewable energy system development has increased as a result of rising crude oil prices and greater environmental consciousness around the world. Because of their superior performance and low environmental impact, batteries are among the most alluring energy storage technologies. The industry currently uses several different battery kinds. Li-ion batteries provide the benefits of high cell voltage, low pollution, low discharge rate, and high-power density. Batteries are frequently utilized in industrial applications, hybrid electric cars, and mobile gadgets [1-12].

1.1 SOC Estimation

The Coulomb counting method is a technique for estimating the State of Charge (SOC) of a battery. It is based on measuring the charge flowing into and out of the battery and integrating this overtime to give the total charge that has been stored or discharged. The basic idea is that the net charge that has flowed into the battery since it was last fully charged is equal to the SOC of the battery.

To implement Coulomb counting, a current sensor is needed to measure the current flowing into and out of the battery, and a discrete-time integrator is used to perform

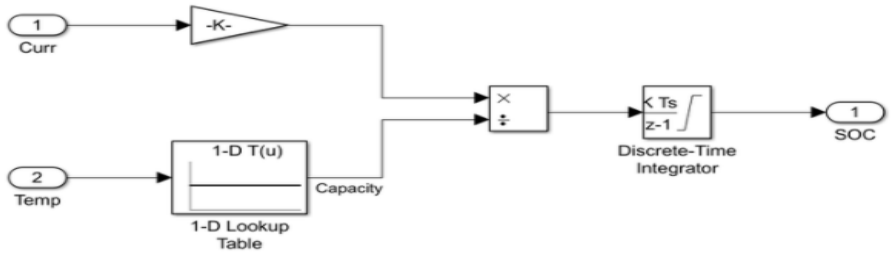

Figure 1.1

the integration of the current over time. The battery is connected in series with the current sensor, which periodically detects the current going into or out of the battery. The integrator then integrates this current overtime to give the total charge that has been stored or discharged. The SOC is then calculated as the total charge stored divided by the total capacity of the battery.

1.2 Cell balancing

It is nearly impossible to produce two identical cells with the exact same capacity, and this results in a variation in the battery's terminal voltage. When consistent current is given to or removed from all of the cells, this also results in overcharging of cells with higher SOC during the charging cycle and complete discharge of cells with lower SOC during the discharge cycle. Cell balance is the method we employ to get rid of this issue.

Cell balancing's primary goals are to maintain a constant voltage across the battery, achieve higher rates of discharge from cells with higher SOC than other cells during the discharge cycle, and achieve higher rates of charging from cells with lower SOC than other cells during the charging cycle. In other words, to achieve the same voltage level, cells with greater SOC should charge cells with lower SOC.

In parallel operation, the voltage across the parallel combination of batteries remains constant, while current is distributed among the batteries in proportion to their capacity. This concept is used to balance the cells, so the cells in the battery are arranged in parallel.

Implementing cell balancing allows us to provide a longer battery life while also increasing battery efficiency.

Figure 1.2

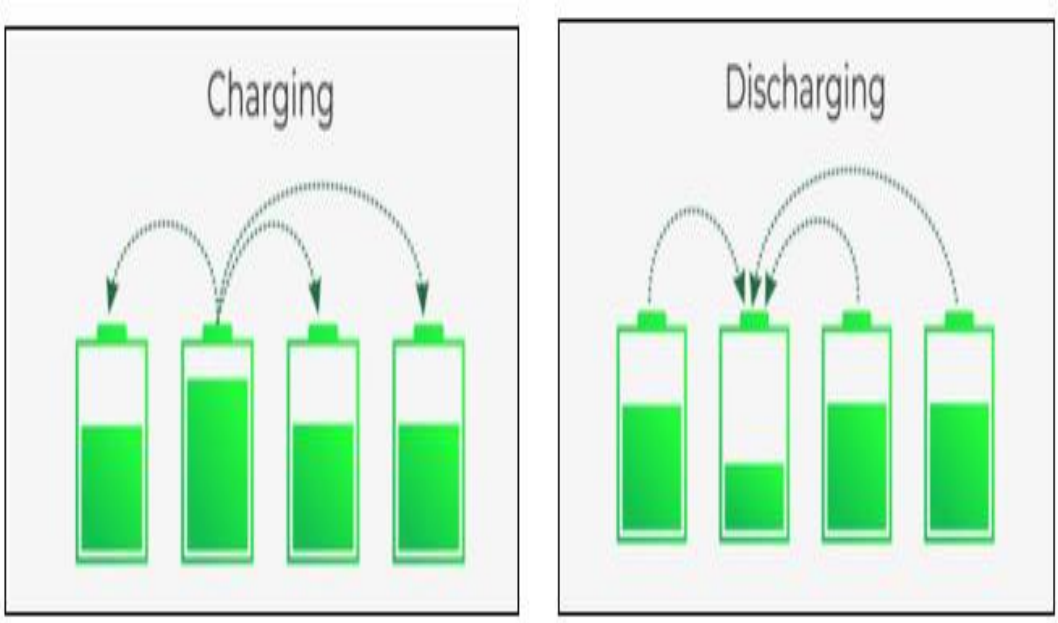

2. SIMULATION ANALYSIS

2.1 Simulation of SOC Estimation

Table 2.1 shows the specifications of the lithium-ion battery used in simulation 2.1.

Parameter	Value	Unit
Nominal Voltage	48	Volts
Rated Capacity	50	Ah
Capacity at Nominal Voltage	45.21	Ah
Cut-off Voltage	36	Volts
Fully Charged Voltage	55.87	Volts
Nominal Discharge Current	21.73	Amp
Internal Resistance	0.0096	Ohms

The following figure 2.1 shows the Simulink model of SOC estimation in a simulated vehicle.

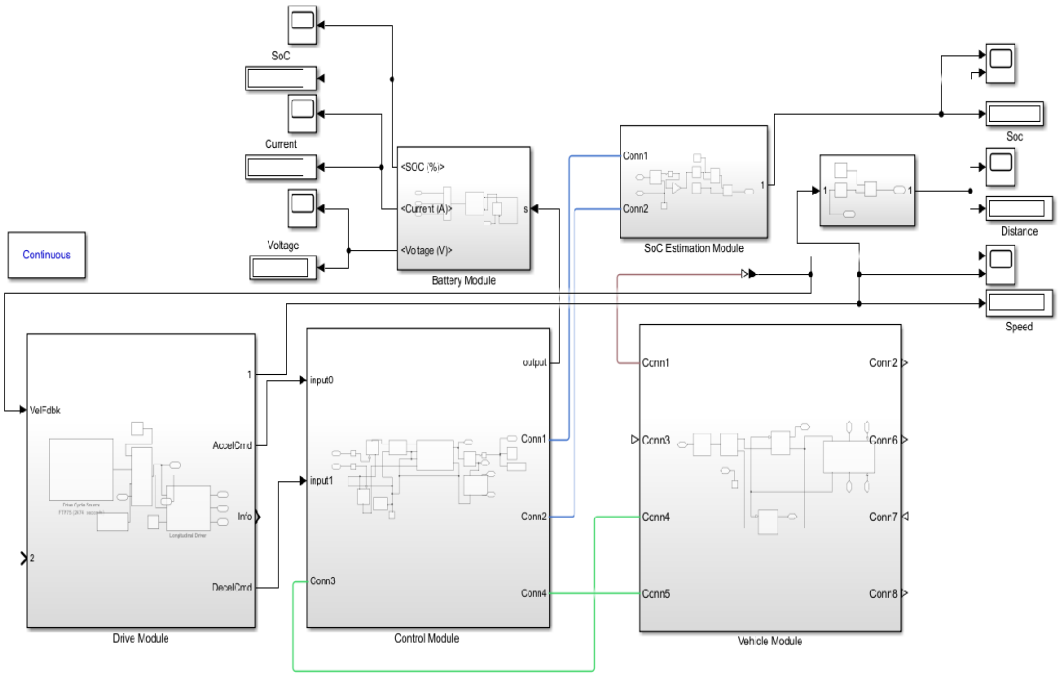

Figure 2.1

SOC estimation using the Coulomb counting method is discussed in this simulation. A virtual vehicle has been simulated using a built-in drive cycle function from Matlab. The initial SOC is assumed to be 90%.

2.1.1 Sub-systems

Drive Module

The drive module (figure 2.1.1) consists of a simulated driver with a built-in drive cycle source which creates a system to show the real-time variation in velocity and how it affects the SOC of the battery.

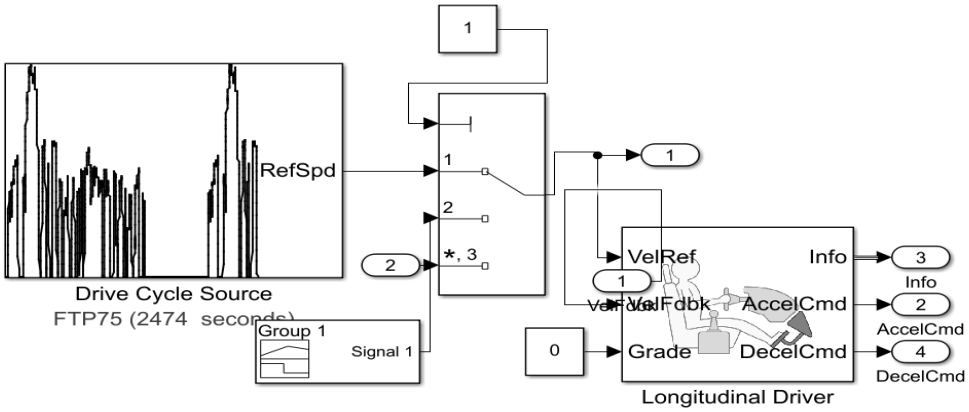

Figure 2.1.1

Control Module

This system consists of a PWM generator and H-bridge which helps in generating a pulse waveform from the velocity variation in the drive module, to help us analyze the electrical part of the circuit.

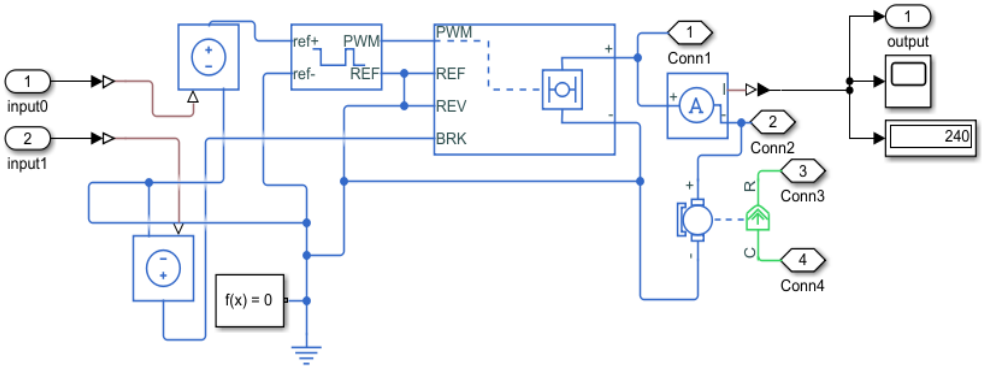

Figure 2.1.2

Vehicle Module

This system shows the layout of the vehicle consisting of a gear system, wheels, and the vehicle body.

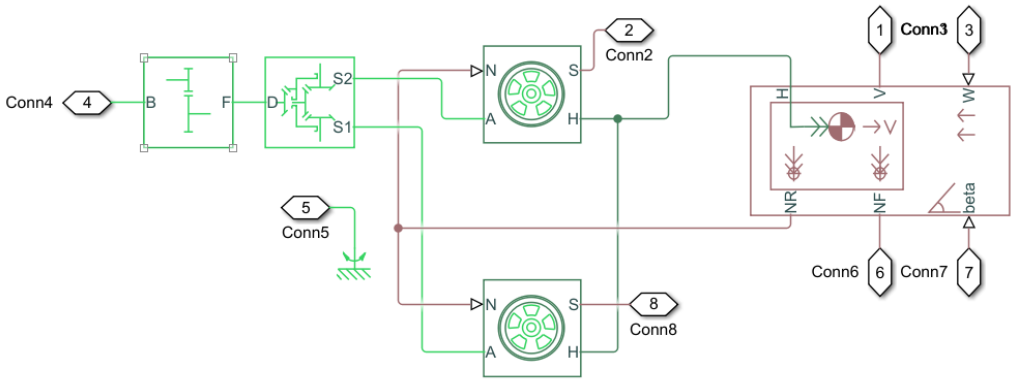

Figure 2.1.3

Battery Module

Figure 2.1.4 shows the connections to the battery and the measurement of SOC from it.

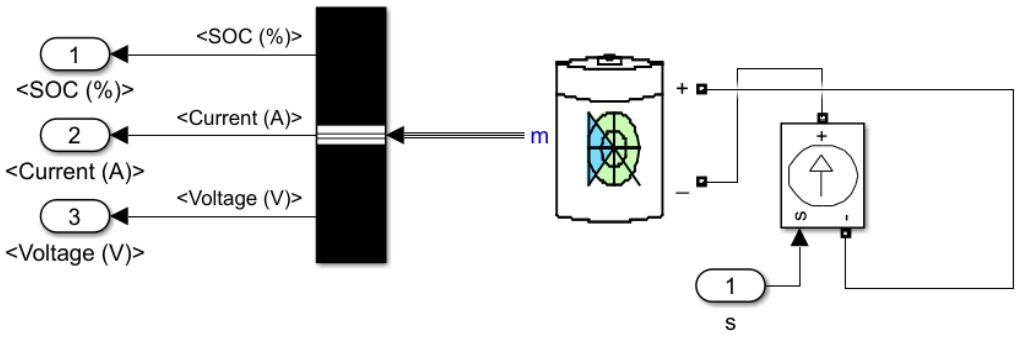

Figure 2.1.4

2.1.2 Result and Analysis

This division converses the simulation outcomes obtained in MATLAB. Here, in figure 2.1.5 the variation of SOC through the ideal method and the SOC using Coulomb counting method is observed. The difference in the plots is due to the lack of inaccuracy reduction methods which is to be addressed.

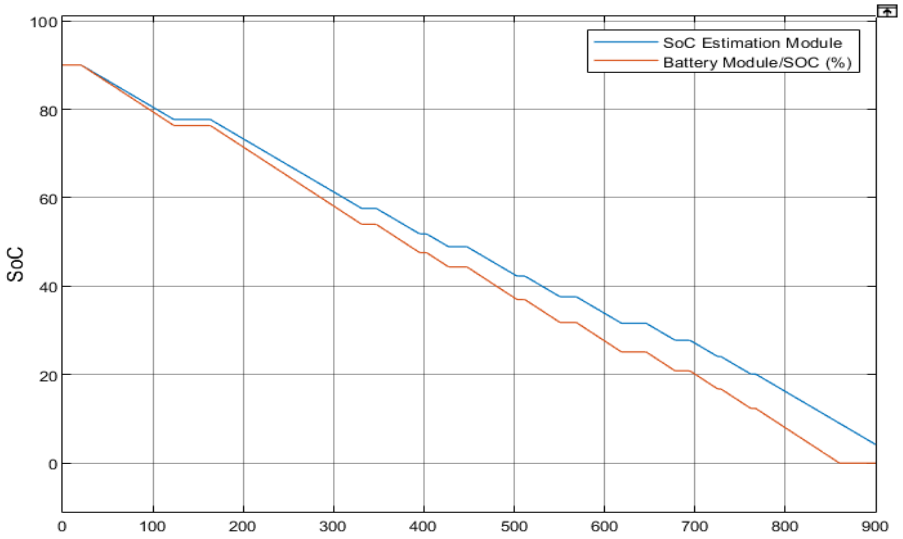

Figure 2.1.5

The graph for current and voltage variation is shown in figure 2.1.6

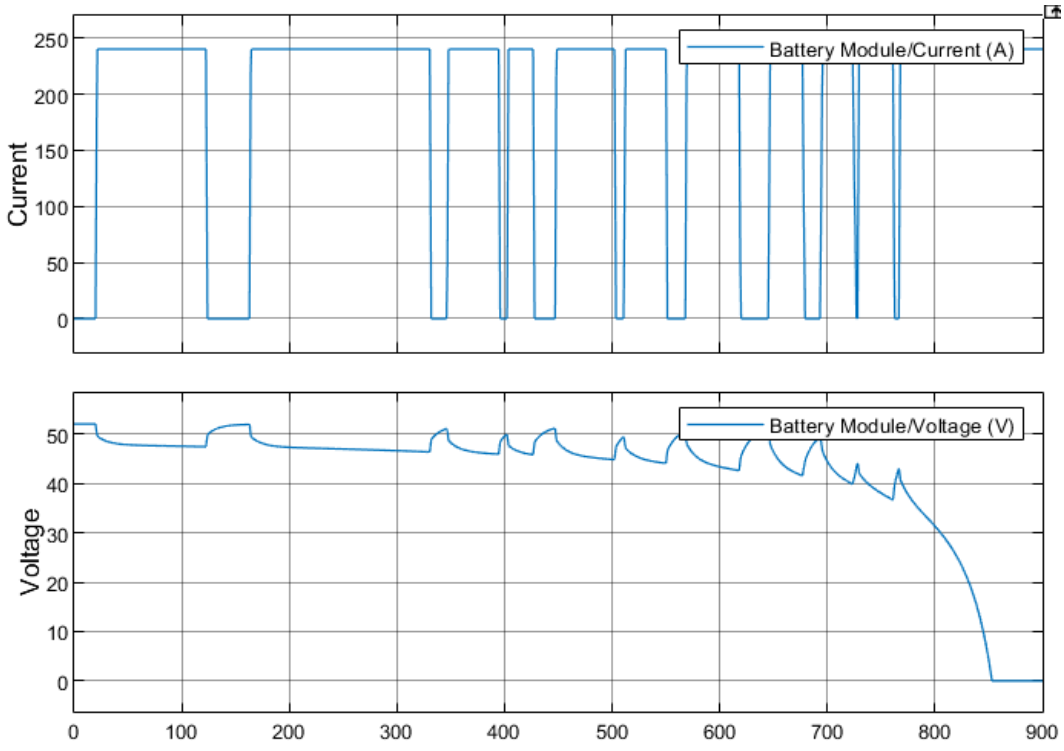

Figure 2.1.6

2.2 Simulation of Cell Balancing

A simulation was carried out for cell balancing of three lithium-ion cells. Figure 2.2.1 shows the Simulink model for passive cell balancing technique. Three lithium-ion cells are connected in series wherein each cell is connected to an IGBT switch along with series resistor.

For simulation, imbalance in SOC is taken as 85%, 80% and 75% for cell 1, cell 2 and cell 3 respectively. The SOC of each cell is given as input to the controller. Controller compares the SOC of cells, and based on the algorithm, output is generated. This output from the controller is given as input to IGBT gate signal.

Table 2.1 shows the specifications of the lithium-ion battery used in the simulation 2.1.

Parameter	Value	Unit
Nominal Voltage	48	Volts
Rated Capacity	50	Ah
Capacity at Nominal Voltage	45.21	Ah
Cut-off Voltage	36	Volts
Fully Charged Voltage	55.87	Volts
Nominal Discharge Current	21.73	Amp
Internal Resistance	0.0096	Ohms

Table 2.1

Figure 2.2.1

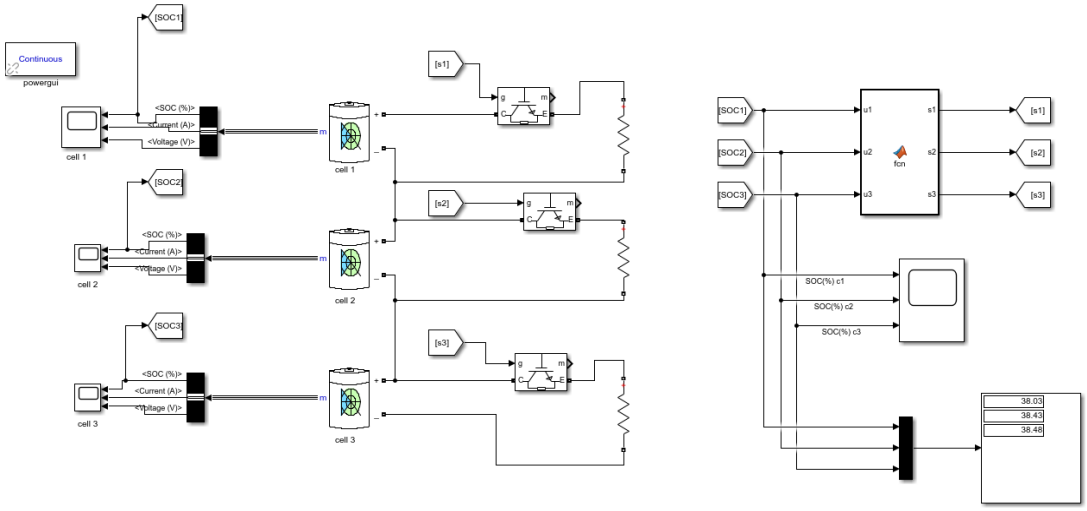

and Analysis

Figure 2.2.2 shows graph of SOC of three cells vs time. It has been observed that cells with higher SOC dissipate energy through series resistor and after certain time, SOC of cells will be equal, that is cells are balanced.

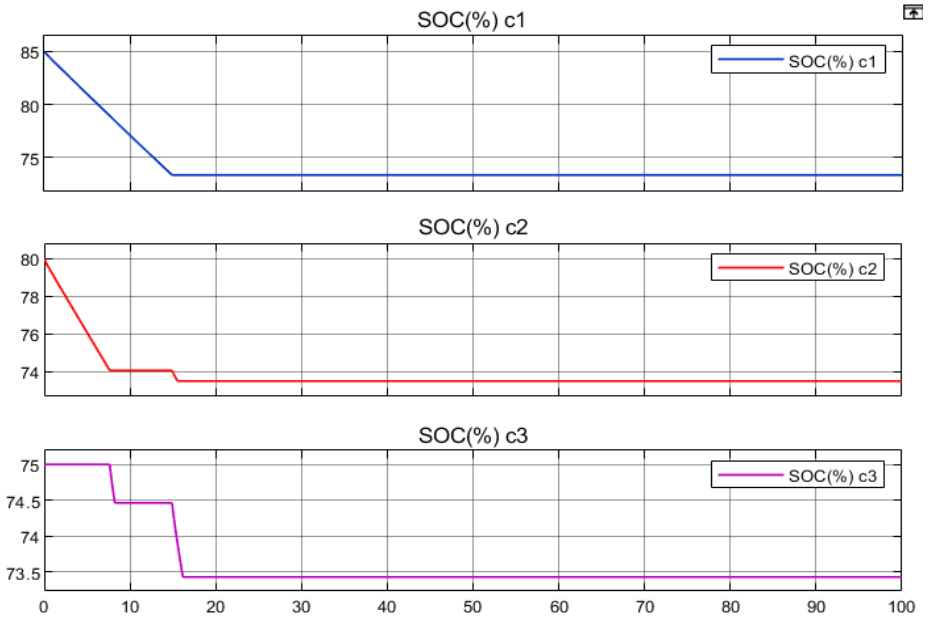

Figure 2.2.2

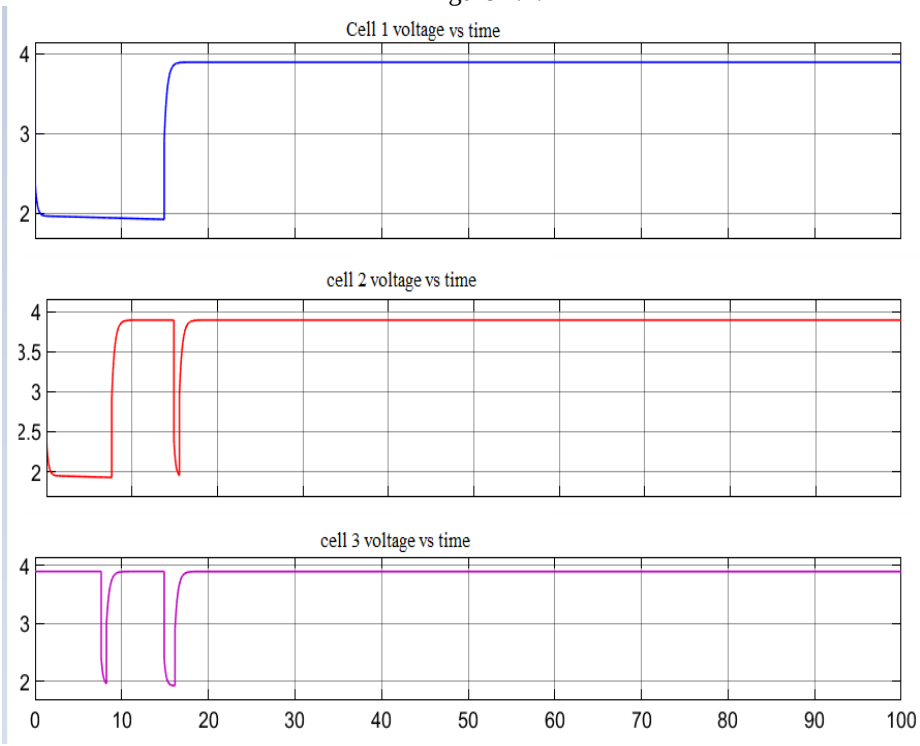

Figure 2.2.3

Figure 2.2.3 shows the graph voltage of three cells vs time. It has been observed that voltage of all the three cells is equal when cells are balanced.

3. CONCLUSIONS

Cell balancing and State of Charge (SOC) estimation are critical components of electric vehicle battery management systems. Cell balancing confirms that all cells in a battery pack are in the same state of charge, which helps to extend the battery pack's overall lifespan and performance. SOC estimation refers to the process of determining the current state of charge of the battery pack, which is used to predict the EV's remaining range and prevent overcharging or over-discharging of the battery pack.

Overall, cell balancing and SOC estimation are critical to EV battery performance and longevity. Additional research is required to increase the accuracy, reliability, and effectiveness of these techniques, as well as to optimize their integration into an EV's overall battery management system.

REFERENCES

[1] M.A. Hannan, M. M. Hoque, A. Hussain, Y. Yusof and P. J. Ker, "State-of-the-Art and Energy Management system of Lithium-Ion Batteries in Electric Vehicle Applications: Issues and Recommendations," in IEEE Access, IR pp. 19362-19378.

[2]. Wen-Yeau Chang, "The State of Charge Estimating Methods for Battery: A Review", Department of Electrical Engineering, St. John's University, 499, Sec. 4, Tam King Road, Tamsui District, New Taipei City 25135, Taiwan.

[3]. Jiale Xie*, Jiachen Ma** and Kun Bai***," Enhanced Coulomb Counting Method for State-of-Charge Estimation of Lithium-ion Batteries based on Peukert's Law and Coulombic Efficiency", *, **School of Astronautics, Harbin Institute of Technology, Harbin, China and *State Grid Jibei Electric Power Co. Ltd., Maintenance Branch, Beijing, China.

[4]. Chen, Chen, Ka Lok Man, T. O. Ting, Lei Chi-Un, Tomas Krilavičius, T. T. Jeong, J. K. Seon, Sheng-Uei Guan, and Prudence WH Wong. "Design and realization of a smart battery management system." in Engineers and computer scientists: 2012 IMECS: proceedings of the international Multiconference, 2012, 14-16 March, 2012 Hong Kong. Vol. 2, pp. 1173-1176. Newswood Limited.

[5]. Changhao Piao,1,2 ZhaoguangWang,1 Ju Cao,1 Wei Zhang,2 and Sheng Lu1. "Lithium-Ion Battery Cell-Balancing Algorithm for Battery Management System Based on Real-Time Outlier Detection." Institute of Pattern Recognition and Applications, Chong Qing University of Posts and Telecommunications, Chongqing 400065, China Mechanical Engineering, INHA University, Incheon 400072, Republic of Korea.

[6]. Ines Baccouche*, ** ‡, Sabeur Jemmali*, Asma Mlayah*, Bilal Manai***, Najoua Essoukri Ben Amara* "Implementation of an Improved Coulomb-Counting Algorithm Based on a Piecewise SOC-OCV Relationship for SOC Estimation of Li-Ion Battery" LATIS-Laboratory of Advanced Technology and Intelligent Systems, ENISo, Sousse University, 4002 Sousse, Tunisia.

[7]. "A Review of Coulomb Counting Methods for State of Charge Estimation in Lithium-Ion Batteries" by Y. Zhang et al.

[8]. J. Kim et al "Passive Cell Balancing in Lithium-Ion Battery Packs for Electric Vehicles".

[9]. Sun et al "An Overview of State of Charge Estimation Techniques for Lithium-Ion Batteries in Electric Vehicles" by C.

[10] Venkatesh Boddapati, S Arul Daniel "Design and Feasibility Analysis of Hybrid Energy-Based Electric_Vehicle Charging Station". Distributed Generation & Alternative Energy Journal. 41–72-41–72.

[11] Venkatesh Boddapati, A Rakesh Kumar, DB Prakash, S Arul Daniel," Design and Feasibility Analysis of a Solar PV and Biomass-based Electric Vehicle Charging Station for Metropolitan Cities (India). Distributed Generation & Alternative Energy Journal. 793–818-793–818. 2022/2/18.

[12] Venkatesh Boddapati, A Rakesh Kumar, S Arul Daniel, Sanjeevikumar Padmanaban. Design and prospective assessment of a hybrid energy-based electric vehicle charging station." Sustainable Energy Technologies and Assessments.53:2022: 102389.

ADALINE LEAST MEAN SQUARE (ALMS) BASED MULTI-LEVEL INVERTER WITH PARTICLE SWARM OPTIMIZATION FOR PV SYSTEM

Dr.B. Pragathi[1], Dr.B. Karunakar Rao[2]

[1]*Associate Professor, Electronics and Communication Engineering, MIC College of Technology, drbpragathi@mictech.ac.in*

[2]*Associate Professor, Electronics and Electrical Engineering, MIC College of Technology, karunakarphdau@gmail.com*

Abstract.

This paper deals with a three-phase, four-wire multi-level inverter, based photovoltaic (PV) system with a lower total harmonic distortion (THD) to increase the system's stability and reliability. The active power filter plays a vital role in the compensation of power quality issues and maintaining the total harmonic distortion level within the IEEE-519 standards. The proposed method develops the active power filter with a voltage source converter (VSC) which is controlled by the Adaline-least mean square algorithm(ALMS) with the hysteresis current controller (HCC). The proposed method is compared with the recursive least mean algorithm (RLS) and found lower THD levels. The ALMS algorithm maintains the constant DC capacitor voltage level thereby compensating for the power quality issues under varying load conditions. The partial swarm optimization (PSO) MPPT technique is used to maintain constant and extract maximum power from the PV panels. The performance of the PSO-based multi-level inverter with the ALMS algorithm is developed and validated by using MATLAB/SIMULINK with reduced THD levels under unbalanced load conditions.

Keywords: PSO-MPPT, Adaline-based LMS, multi-level inverter, recursive least square, total harmonic distortion, power quality.

1. INTRODUCTION

The best source of energy that can be produced is the renewable energy source for clean and sustainable energy [1]. Power from natural sources such as solar, wind. The energy from the non-replenishing sources can be harvested and given to the power grids via an inverter that is connected to the grid. The energy produced by solar panels and other renewable forms of energy is DC in nature. The function of an inverter is to alter a DC input source voltage to a symmetrical AC output voltage in desired amplitude and frequency with a minimal amount of harmonics [2] However, inverters produce an alternative square wave at the output, thus increasing the THD of the waveform. The output generated from the inverter must a sinusoidal wave with a reduced amount of THD also output frequency should match with line frequency. The output sinusoidal with the lowest distortion is achieved in inverters by using high switching frequency along with various other Pulse Width Modulation (PMW) techniques [3,4]. There are many advancements in the development of the Multi-Level Inverter (MLI) to improve the power quality that most energy obtained can be effectively put to use. Deterioration of Power Quality, because of harmonics, happens in distribution systems and electric transmission

due to the loads. These are generally caused by non-linear load usage. In the past few years the nearest solution we can obtain multi-level inverter-based APF which injects the compensating current into the power distributing system, improving power quality, can control and regulate electrical disturbances [5.-7] MLIs are used in large numbers in energy storage systems. Circuit topology, control techniques of MLI have been developed significantly in recent days. With MLI, the current harmonic compensation is effective for high power quality [8,9]. Various MLI configurations have been discussed in this area. In [10,11], the MLI they have minimized the number of switches that can be used. In [12.13] half-bridge cascaded multi-level inverter-based SAPF the authors presented providing the equal output voltage with a lower number of semiconductor switches in comparison with different MLI topologies that generate the same amount of output voltage. Among all MLI topologies, the [14] has implemented a hybrid multi-level inverter that generates the required output voltage from a combination of Level generation, polarity generation. Moreover, it provides a reduced number of component utilization in implementation by implementing alternate phase opposition disposition, carrier overlapping, and sinusoidal PWM techniques. In [15,16] the author is clear in working on a three-phase system using a multi-level inverter by supplying the compensating current to reduce TDH percentage below 5% as per IEEE for unbalanced load cases. However, the authors have used an artificial neural network [17], a recursive least square (RLS), A-LMS algorithms that are simple, robust, and linear in the computation are verified. A HILBAPF (H-bridge interleaved buck-type active power filter) [18] for linear and non-linear loads. This has been observed to be capable of balancing the capacitor voltages can exclude interfacing transformer.

In the proposed system the Adaline least mean square (ALMS) based multi-level inverter with particle swarm optimization MPPT algorithm for a PV system is developed. The ALMS algorithm is used to control the switching operation of the multi-level inverter to compensate for the power quality issues in the grid-connected PV system under nonlinear load conditions.

2. PROPOSED SYSTEM CONFIGURATION

The development of the proposed three-phase, four-wire module with optimum performance and lower THD level is shown in Fig.1(a). The system is a combination of a solar PV panel, DC-DC converter, a DC bus capacitor, interfacing inductors, and three-leg VSC. The PSO-MPPT technique is used to extract maximum PV power. The ALMS algorithm is used to maintain constant DC capacitor voltage and provides the functionality of an active power filter of harmonics elimination, and reactive power compensation. The model of the multi-level inverter is shown in Fig.1(b).

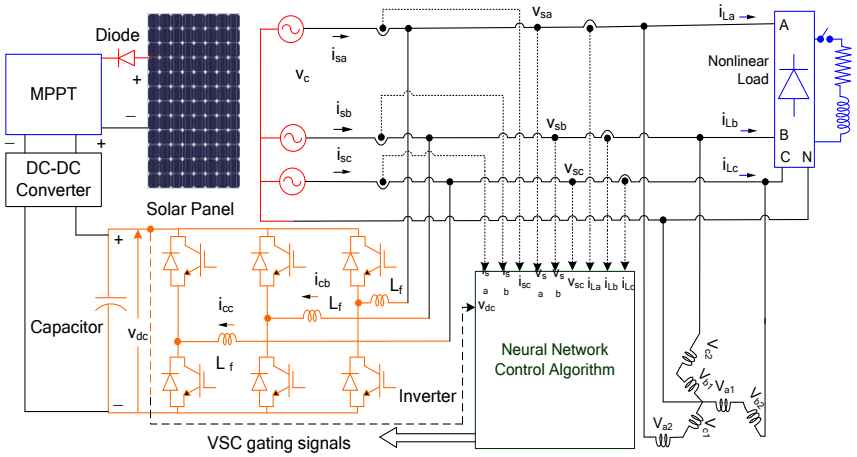

Fig.1(a) Proposed three-phase, four-wire PV system using ALMS algorithm

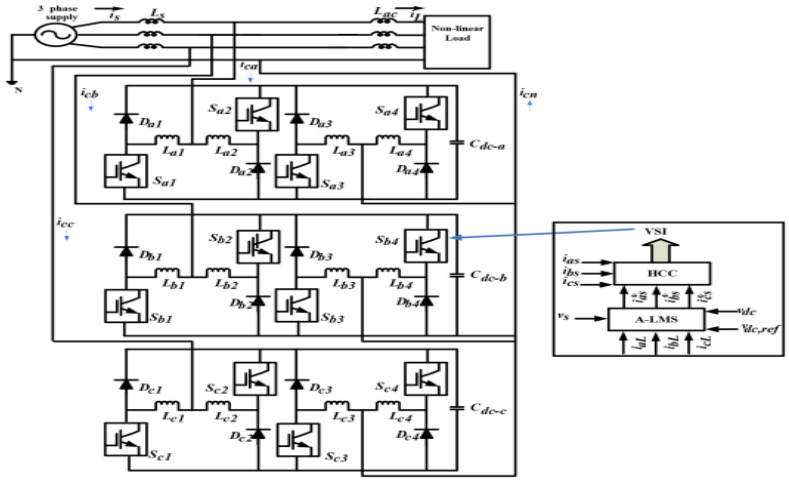

Fig.1(b) Multi-level inverter using ALMS algorithm

3. CONTROL ALGORITHMS

The fundamental source current is generated by injecting or absorbing the filter current by an active power filter which is in phase opposition with the harmonic components. The efficiency and reliability are improved by the control algorithms RLS and ALMS algorithms for multi-level voltage source converter (VSC), PSO-MPPT for PV panels.

Particle swarm optimization (PSO) MPPT technique:

The PSO-MPPT algorithm is used to extract the maximum power from the PV panels by updating the voltage and current values of the PV panels at different intervals of time. The PSO-MPPT is used to find the optimal solutions by increasing the speed of the tracking. The PSO-MPPT technique is shown in Fig.2.

RLS Algorithm

The recursive least mean square (RLS) algorithm is used to compensate for the reactive power and reduce the total harmonic distortion (THD) level in the system. Under the balanced load condition, the source active power is equal to the load active power and there is no current flow through the multi-level inverter. Under unbalanced load conditions, the DC capacitor voltage causes the power difference between source and load currents. To maintain a constant DC capacitor voltage, the RLS algorithm is used to control the voltage source converter (VSC) section as shown in Fig.3.

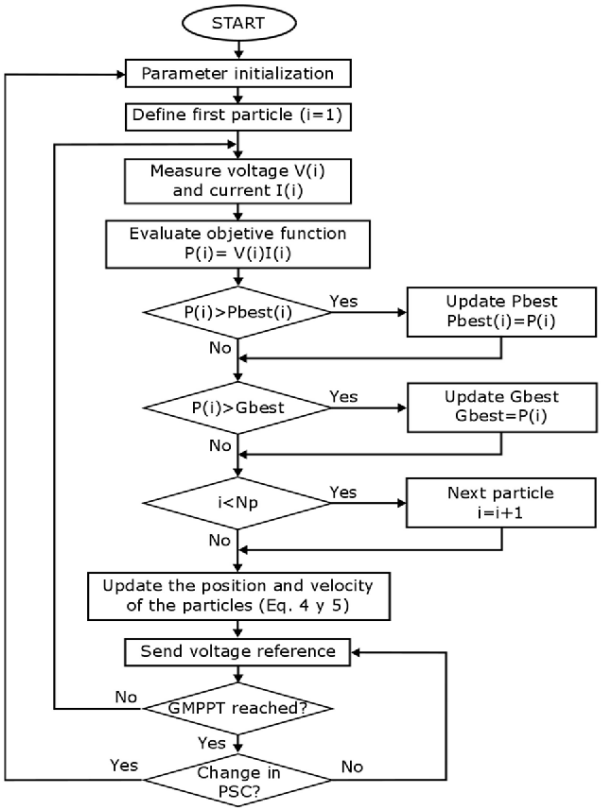

Fig.2 Particle swarm optimization MPPT technique

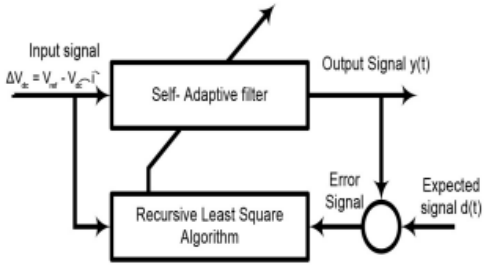

Fig.3 Recursive least mean square algorithm

The instantaneous current for each phase is given as

$$I_x(t) = I_{ax}(t) + I_{nx}(t) \quad (1)$$

Where $I_{ax}(t)$ Is the active current given as

$$I_{ax}(t) = A_x V_x(t) \quad (2)$$

The active parameter is given as

$$A_x = A_{ax} + A_{dc} \quad (3)$$

Where A_{dc} is given as

$$A_{dc} = P_{dc}(i)/V_x^2 \quad (4)$$

$$P_{dc}(i) = \left[\left(V_{ref} + V(i)\right)^2 - V_{ref}^2\right] * {}^{C}/_{2} \quad (5)$$

Adaline least mean square algorithm (ALMS):

This proposed ALMS algorithm as shown in Fig.4 is developed by combining two techniques, the Adaline and LMS algorithm. The weights in Adaline are updated using the LMS algorithm. The proposed algorithm is used to calculate the reference current components for the multi-level inverter and the convergence rate depends on the fixed step-size parameter.

The weight equation for active and reactive components are for single phase x at time t is given as

$$w_{Ax}(k+1) = w_{Ax}(t) + \mu e_x(t) u_{Ax}(t) \quad (6)$$

$$e_x(t) = \{i_x(k) - i^*_{AX}\} \quad (7)$$

$$w_{Qx}(k+1) = w_{Qx}(t) + \mu e_{Qx}(t) u_{Qx}(t) \quad (8)$$

$$e_{Qx}(t) = \{i_x(k) - i^*_{Qx}\} \quad (9)$$

Where e_x(t), is the error output of the reference current and load at phase x. and (μ) is the convergence factor which varies between 0.01 to 1.0. It is taken as 0.2 for the proposed multilevel ALMS system.

PI controller for active and reactive components is given as

$$w_{lA}(t) = w_{lA}(k\text{-}1) + k_{pA}\{v_{eA}(t) - v_{eA}(k\text{-}1)\} + k_{iA} v_{eA}(t) \quad (10)$$

Where $v_{eA}(t) = v^*_{refA}(t) - v_{DCA}(t)$ (11)

$$w_{lQ}(t) = w_{lQ}(k\text{-}1) + k_{pQ}\{v_{eQ}(t) - v_{eQ}(k\text{-}1)\} + k_{iQ} v_{eQ}(t) \quad (12)$$

Where $v_{eQ}(t) = v^*_{refQ}(t) - v_{DCQ}(t)$ (13)

The reference currents for active and reactive components for phase 'x' are estimated as

$$i^*_{xA} = w_{xA}(t)\, u_{xA}(t) \quad (14)$$

$$i^*_{xQ} = w_{xQ}(t)\, u_{xQ}(t) \quad (15)$$

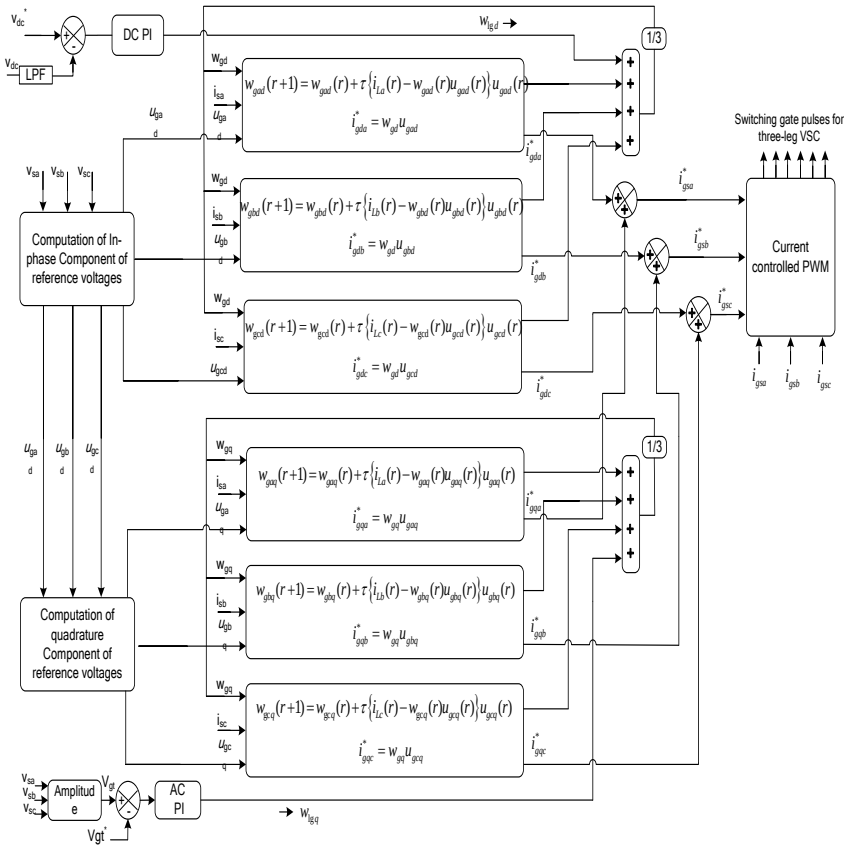

Fig.4 Adaline least mean square algorithm for three-phase multi-level inverter

4. RESULTS AND DISCUSSION

The Adaline least mean square based multi-level inverter PV system is developed and simulated in MATLAB/SIMULINK. The proposed system under balanced and varying load conditions with different control algorithms is analyzed with lower THD levels. The performance of the proposed model is analyzed with the recursive least square (RLS) and Adaline least mean square (ALMS) under varying load conditions. During nonlinear load conditions, the load current is distorted thereby increase in the THD level. The performance of the grid-connected single level inverter for the load current with the THD level of 38.97% under unbalanced load conditions and load current with the THD level of 28.53% is shown in Fig.5.

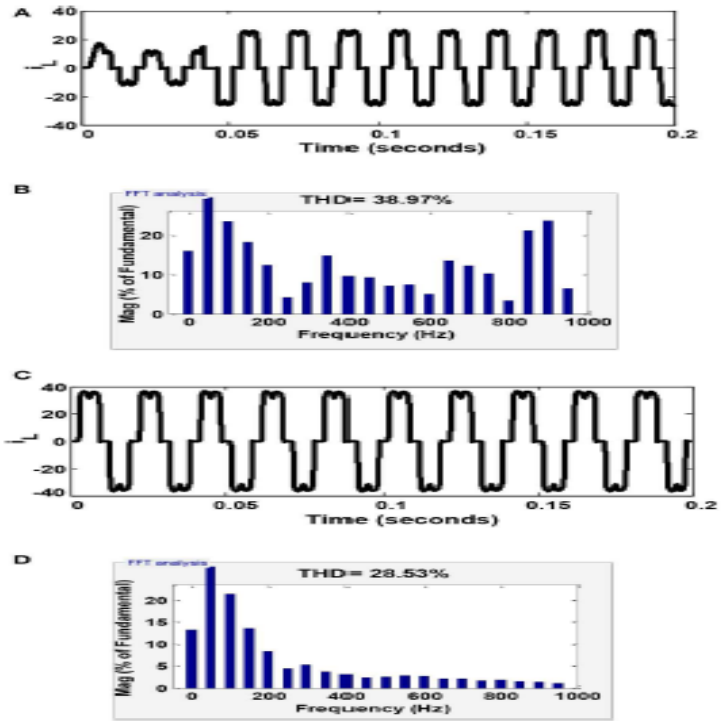

Fig.5 (A) Load current under unbalanced load conditions (B) THD level of load current under unbalanced load condition (C) Load current under balanced load conditions (D) THD level of load current under balanced load conditions

Balanced load condition

The performance of the multi-level inverter with recursive least mean square (RLS) algorithm is shown in Fig.5. The RLS algorithm is used for controlling the multi-level inverter thereby reducing the THD level. It is observed from Fig.6, that the THD level under balanced load conditions for the load current is reduced to 1.75%.

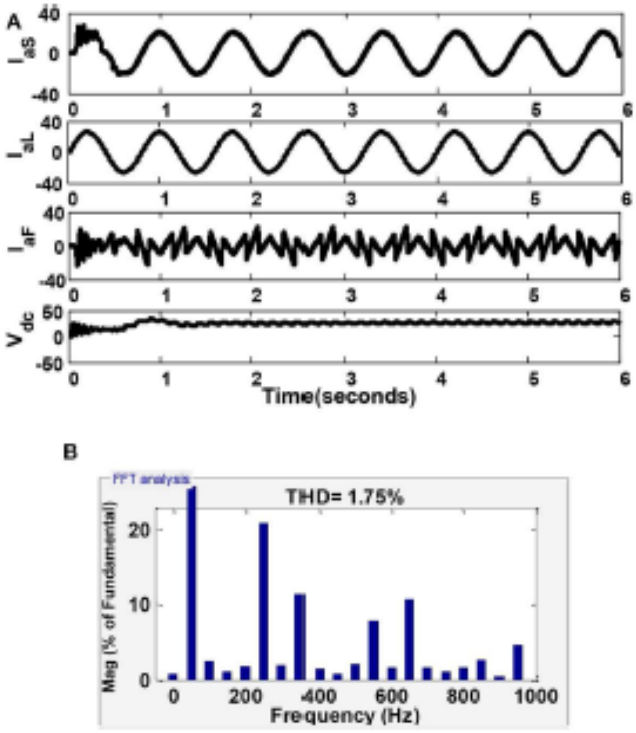

Fig.6 (A) Load current, source current, and V_{dc} (B) THD level

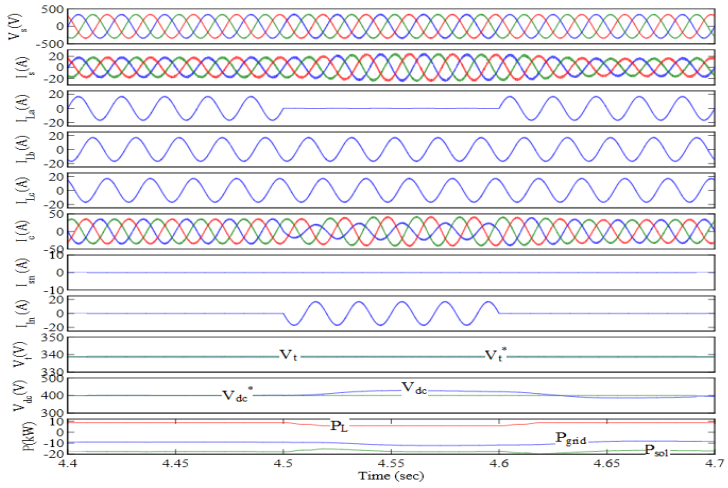

Fig.7 THD level for load current using ALMS multi-level inverter for linear loads

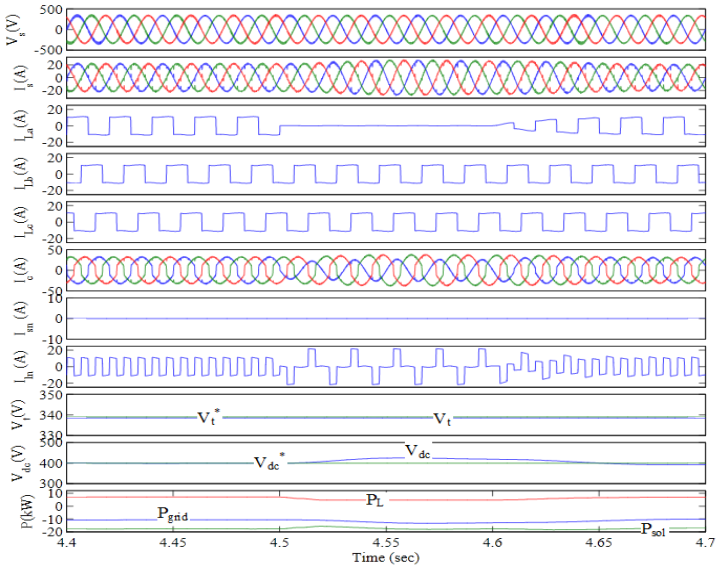

Fig.8 THD level for load current using ALMS multi-level inverter for non-linear loads

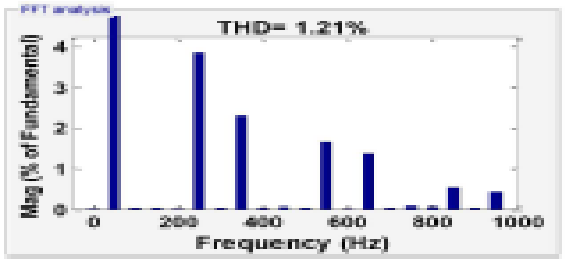

Fig.9, where the THD level is reduced to 1.21%,

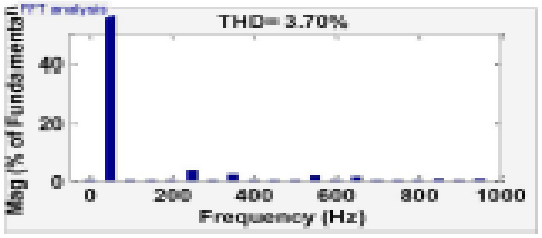

Fig.10 THD level for load current under nonlinear load conditions

The performance of the Adaline least mean square multi-level inverter under linear load conditions is shown in Fig.7, and the performance of the Adaline least mean square multi-level inverter under non-linear load conditions is shown in Fig.8. The performance of three-phase source current, load current, solar power, grid power, DC capacitor voltage are shown in Fig.7 and Fig.8. At time 4.5s, one of the phases is disconnected and the ALMS algorithm compensates for the fluctuations in the load current thereby maintaining constant DC voltage across the capacitor. The THD level for the load current using ALMS under linear loads is shown in Fig.9, where the THD level is reduced to 1.21%, and the THD

level for load current under nonlinear load conditions is shown in Fig.10, where the THD level is reduced to 3.70%.

5. CONCLUSION

The proposed Adaline least mean square multi-level inverter with particle swarm optimization for PV system is implemented. The proposed system is compared with the conventional single level inverter and multi-level inverter with recursive least mean square (RLS) algorithm. The proposed ALMS algorithm has compensated for the power quality issues in the system under non-linear load conditions. The THD level of the three-phase multi-level inverter is reduced compared to the RLS multi-level inverter. The ALMS has maintained constant DC capacitor voltage under varying load conditions. The maximum solar power is extracted by the use of the particle swarm optimization-MPPT technique. The proposed model is developed and simulated in MATLAB/SIMULINK and found satisfactory results under varying load conditions.

6. REFERENCES

1. Ali, J. S. M., and Krishnaswamy, V. (2018). An assessment of recent multilevel inverter topologies with reduced power electronics components for renewable applications. Renew. Sustain. Energy Rev. 82, 3379–3399. doi: 10.1016/j.rser.2017.10.052.
2. Chilipi, R., Al Sayari, N., Al Hosani, K., and Beig, A. R. (2016). Control scheme for grid-tied distributed generation inverter under unbalanced and distorted utility conditions with power quality ancillary services. IET Renew. Power Gen. 10, 140–149. doi: 10.1049/iet-rpg.2015.0095.
3. B. Pragathi, Fazal Noor pasha, V. Rajagopal, “Power quality improvement for grid interconnected solar PV system using neural network control algorithm”, Int. J. Power and Energy Conversion- Inderscience, Vol. 9, No. 2, 2018
4. Das, S. R., Ray, P. K., and Mohanty, A. (2017). Improvement in power quality using hybrid power filters based on RLS algorithm. Energy Proc. 138, 723–728. doi: 10.1016/j.egypro.2017.10.207
5. Ertl, H., Kolar, J. W., and Zach, F. C. (2002). A novel multicell DC-AC converter for applications in renewable energy systems. IEEE Trans. Ind. Electron. 49, 1048–1057. doi: 10.1109/TIE.2002.803212.
6. Gupta, K. K., Ranjan, A., Bhatnagar, P., Sahu, L. K., and Jain, S. (2015). Multilevel inverter topologies with reduced device count: a review. IEEE Trans. Power Electron. 31, 135–151. doi: 10.1109/TPEL.2015.2405012
7. Hoon, Y., Radzi, M. A. M., Hassan, M. K., and Wahab, N. I. A. (2016). A simplified synchronous reference frame for indirect current controlled threelevel inverter-based shunt active power filters. J. Power Electron. 16, 1964–1980.doi: 10.6113/JPE.2016.16.5.1964.
8. Bellamkonda, Pragathi & Poonia, Ramesh & Polaiah, Bojja & Nayak, Deepak. (2021). Evaluation and Analysis of Soft Computing Techniques for Grid Connected Photo Voltaic System to Enhance Power Quality Issues. Journal of Electrical Engineering & Technology. 16. 10.1007/s42835-021-00720-w.

9. Karasani, R. R., Borghate, V. B., Meshram, P. M., Suryawanshi, H. M., and Sabyasachi, S. (2016). A three-phase hybrid cascaded modular multilevel inverter for renewable energy environment. IEEE Trans. Power Electron. 32,1070–1087. doi: 10.1109/TPEL.2016.2542519.
10. Hachani, K., Mahi, D., and Kouzou, A. (2017). Shunt active power filtering based on the pq theory control. Electrotehn. Electron. Automat. 65, 85–89.
11. B. Pragathi, Deepak Kumar Nayak, Ramesh Chandra Poonia, "Solar PV system-frequencyadaptive disturbance observer control algorithm for compensating harmonics and frequency disturbance", Journal of interdisciplinary mathematics-Taylor and Francis, Vol. 23 (2020), No. 2, pp.573–581.
12. Lei, Y., Barth, C., Qin, S., Liu, W. C., Moon, I., Stillwell, A., et al. (2017). A 2-kW single-phase seven-level flying capacitor multilevel inverter with an active energy buffer. IEEE Trans. Power Electron. 32, 8570–8581. doi: 10.1109/TPEL.2017.2650140.
13. Babu, T. S., Priya, K., Maheswaran, D., Sathish Kumara, K., and Rajasekar, N. (2015). Selective voltage harmonic elimination in PWM inverter using bacterial foraging algorithm. Swarm Evol. Comput. 20, 74–81. doi: 10.1016/j.swevo.2014.11.002
14. Gangui, Y., Jigang, L., Gang, M. U., Yu, L., Yang, L., and Wei, S. (2012). Research on modular multilevel converter uitable for direct-drive wind power system. Energy Proc. 17, 1497–1506. doi: 10.1016/j.egypro.2012.02.272.
15. Merabet, L., Saad, S., Abdeslam, D. O., and Merckle, J. (2017). Direct neural method for harmonic currents estimation using adaptive linear element. Electr.Power Syst. Res. 152, 61–70. doi: 10.1016/j.epsr.2017.06.018.
16. Pratheesh, K. J., Jagadanand, G., and Ramchand, R. (2017). A generalizedswitch-matrix-based space vector modulation technique using the nearest level modulation concept for neutral-point-clamped multilevel inverters. IEEE Trans. Ind. Electron. 65, 4542–4552. doi: 10.1109/TIE.2017.2772172
17. Ozdemir, E., Ozdemir, S., Tolbert, L. M., and Ozpineci, B. (2008). "Fundamental frequency modulated multilevel inverter for three-phase stand-alone photovoltaic application," in 2008 Twenty-Third Annual IEEE Applied Power Electronics Conference and Exposition (Austin, TX: IEEE), 148–153.
18. Panda, A. K., and Patel, R. (2014). PI and fuzzy-controlled 3-phase 4-wire interleaved buck active power filter with shoot-through elimination for power quality improvement using RTDS hardware. Int. J. Emerg. Electr. Power Syst.15, 177–194. doi: 10.1515/ijeeps-2013-0104.

Control of Microgrid with Hybrid Energy Storage System

Suganthi.N, P. Usha
Dayananda Sagar College of Engineering,
suganthin-eee@dayanandasagar.edu,pu1968@yahoo.co.in

Abstract.

This paper proposes the energy management system for DC side of the microgrid which consists of PV system, wind energy system, along with hybrid energy storage system consist of battery and supercapacitor. Solar and wind systems are implemented with maximum power point control to extract maximum power. To improve the power output and to manage its intermittent nature of these sources hybrid energy storage devices is implemented with appropriate control strategy . Hybrid energy storage system with high energy density and high-power density is implemented to reduce the fluctuation in DC link voltage and to maintain power balance in DC microgrid. The control strategy proposed fulfills the need of transient power and average power requirements of the load. The proposed DC microgrid is realized in MATLAB Simulink and the performance of the system is verified for different cases.

Keywords. Wind, Solar, PV, Energy, Storage, battery, super capacitor.

1. INTRODUCTION

In the current scenario as power demand is increasing and fossil fuel is getting depleted need for alternate energy sources and also distributed generation-based grid is increasing.[1] Renewable energy sources are the promising solution for these energy needs. Among the several renewable energy sources wind and Solar are the prominent sources as it available in plenty and it is a clean energy. Microgrids with wind and solar are evolving. [2] To handle the variable nature these sources and to increase the penetration of these devices in to main grid energy storage devices are required. Battery is the most commonly used energy storage system [3]. Some loads such as refrigerator, Air conditioner, require high starting current and sizing the battery for such requirements proved to be costly.[4] In situations such as sudden load change /generation change to handle the momentary as well as regular current requirements combination of high power and high energy density devices are required [5]. Most commonly used combinations are flywheel and battery, battery and supercapacitor, fuel cell -flywheel, pumped hydro-battery and etc. [6]-[7] However, battery -super capacitor is an effective solution, as flywheel suffers with rotor failure, pumped hydro system requires large area, fuel cell responds slowly to fast load variations.[8]. In microgrid with hybrid energy storage devices such as battery and supercapacitor meeting the load demand by maintainingthe SOCs of the storage devices is challenging. Therefore, designing a control strategy for energy management plays a important role in the continuous, stable and reliable operation of the microgrid. In [9]-[11] an energy management system is proposed with battery as the storage device. In these system DC link voltage rating and Battery voltage rating should be kept same. Any load /generation disturbances must be buffered by the battery. This places high stresses on the battery and also this reduces the life cycle of it. [12]. A perfect storing system in a DC microgrid must be able to supply together high-power density and energy density needs to manage the circumstances such generation, load, and climate changes. By applying battery and supercapacitor (SC) hybrid combination battery life time, reduction in battery size,

reduction in cost of the battery can be achieved. Several types of control approaches been reported in the literature for energy management Model predictive control, neural networks, decision tree, fuzzy logic and etc [13]-[17] However, these methods involve large data storage requirements and extensive computations. And the disadvantage of the Model predictive Controller method is itrequires large mathematical computations.

Potential development in battery life time is quantified in [18]-[19] In[20] advantages of addition SC to battery storage system in wind energy conversion systems is been verified. The basic concept of all the above-mentioned energy management strategies is that battery provides a low frequency current requirement and transient current component is handled by super capacitor momentarily and the battery slow response is not compensated. This proposed paper is based on dividing average current requirement and high frequency current requirement for generating reference current for battery and SC. The battery error component is utilized to generate current reference for supercapacitor along with high frequency current component to compensate the slow response of the battery, to achieve faster voltage regulation.

2. DC MICROGRID ARCHITECTURE

The DC micro grid considered contains of PV power generation system, wind energy system (WES) along with battery and ultra-capacitor Hybrid Energy Storage System (HESS) is shown in Fig.2.1. In the represented Microgrid system, Photo Voltaic with the boost converter implemented with MPPT controller utilizing peturb&obseve algorithm to increase the output power of the PV system. The output pulses from MPPT controller are supplied to the boost converter that is linked to DC bus. WES consists of wind turbine coupled with PMSG generator. The AC power generated from WES system is converted into DC power using AC -DC converter. HESS is employed to handle the transient as well as the regular load necessities. The energy storage devices super capacitor and battery is parallelly attached to DC bus via bi-directional DC-DC boost-buck converter. A DC-AC converter is employed to convert DC power from the PV, battery and SC to AC power and supply to ACload and is represented in Fig.2.1. Proposed system constitutes the DC microgrid.

2.1. Wind Energy Conversion System

In the wind turbine wind's dynamic energy is changed into mechanical energy and is given in equation (2.1) below

$$P_W = \frac{1}{2}\rho\pi r^2 C_p(\lambda,\beta)V^3 \quad (2.1)$$

Where Cp is the co-efficient of power (Betz), ρ is density of air in kg/m^3, V is the velocity of wind in m/s, r is the length of the blade in m. Equation (2.2) gives the wind turbine's aerodynamic torque.[22]

$$T_W = \frac{P_W}{\omega} \quad (2.2)$$

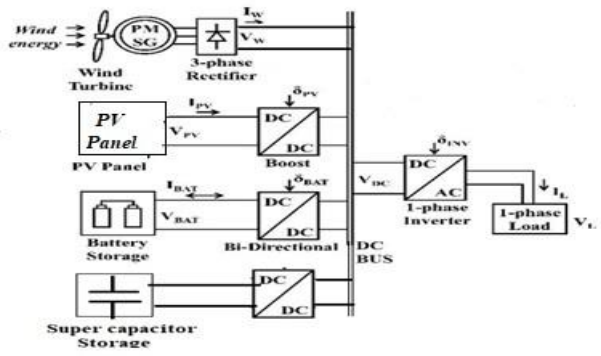

Figure 2.1. Configuration of Hybrid Energy sources with HESS

Where ω is the rotor speed in radians per second. The generated mechanical energy is changed in to electrical energy in Permanent Magnet Synchronous Generator. The diode rectifier converts the three-phase AC voltage of the PMSG into DC voltage.

2.2. PV System Model

The single -diode equivalent circuit of PV cell is shown in the Fig:2. This cell can be symbolized as an ideal Photovoltaic cell with a diode connected parallel to the current source.[23]. To prevent the reverse power flow, the bypass diode is used.

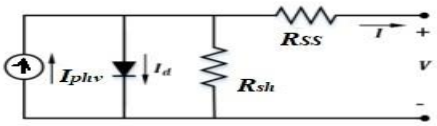

Fig:2.2 Equivalent circuit of PV cell[23]

$$I_{pvv} = I_{phv} - I_d \quad (2.2.1)$$

and Current of diode ($\boldsymbol{I_d}$) is represented in idyllic form as follow

$$I_d = I_0(e^{\frac{qVocpv}{ypK_pT_p}} - 1) \quad (2.2.2)$$

$$Ipvv = Iphv - I_0(e^{\frac{qVocpv}{ypK_pT_p}} - 1) \quad (2.2.3)$$

Where I_d, $Iphv$, V_{oc}, q, ηp, and T_p denote the current (diode), Photo current, output potential of PV, total Charge, factor of ideality, Boltzmann constant and temperature in Kelvin accordingly. Shunt resistance (Rsh) is negligible as it has less effect on I-V features of the Photovoltaic cell. Therefore equation (2.2.1) can be simplified to (2.2.3). Detailed specifications of the model is given in the table (2.2.1) below and the model used is WAAREEEnergiesWU-120. Boost converter design is similar to that reported in [7].

S.No	Solar cell Details		
	Constraints	Symbol	Value
1	Highest power	Pmm	120W
2	Highest voltage	Vmm_P	17.1V
3	Highest current	Immp	7.1A
4	Short circuit current	Ishh	8A
5	Open circuit Voltage	V_{open}	21 V

Table 2.2.1 Details of PV System

Wind Energy system Details			
S.No	Parameter	Variable	Value
1.	Base rotational speed	ω	1.2pu
2.	Maximum power atbase speed	Pw	0.85 pu
3.	Nominal output power	Pout	1Kw
4.	Wind turbine rated Velocity	V	12m/s
5	Turbine radius	R	1.1m

Table2.2.2 Details of WECS

The boost converter is realized with MPPT control implemented with P&O algorithm. There various types of MPPT algorithm [24] stated in the literature. Amid various types, Perturb and Observe procedure is simple to employ, and is used to increase the photovoltaic system

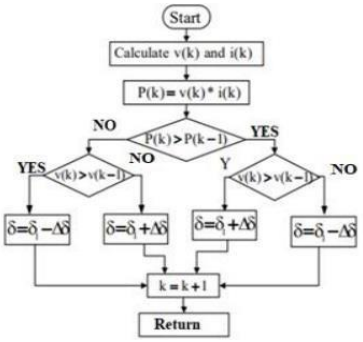

Fig.2.2.1.P&OMPPTAlgorithm

Systems	Storage system Requirement
Battery	Li-ion-24 V,14Ah
SC	32V,29F
Two-way DC-DC converter	L_{bat}=0.03mH, Lsc=0.352mH, C=400µF, Vo=50v, R=5Ω, f=16KHZ
gains for controller of HESS	Kbp=0.004, Kbi=0.9, Kscp=0.55, Ksci=16800, Kppv=1.58, Kiiv=4097.

Table.2.3.1Storage system

power output and also to rise the system effectiveness of the photovoltaic system.[25]. The P&O algorithm flow chart is presented in Fig.2.2.1. This algorithm is used to give pulse input to the boost converter. This algorithm disturbs the voltage and relative change in power is calculated and is compared with previous power value. The operating point will be traced towards MPP if the power change is positive and away from MPP if the change in power is negative. This process will be repeated until maximum peak is obtained.[26]

2.3. Battery &super capacitor Modeling

In the DC microgrid system Li -ion battery model obtainable in MATLAB /Simulink 2018 is been considered. Equivalent circuit of the Li-ion is shown in Fig.2.3.1. The Battery model represents the different variations of battery and its features. Battery is modelled as current source with some inbuilt resistance, according to the SOC level of the battery charges and discharges.

When battery works in charging mode battery voltage rises and when it works in discharging mode the current rises.

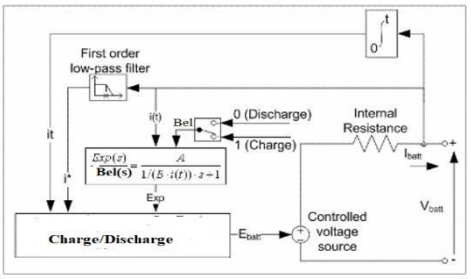

Fig.2.3.1 Battery Model [27]

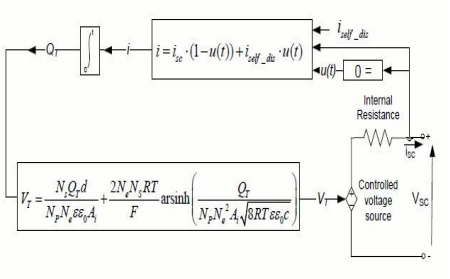

Fig2.3.2 Supercapacitor model [28]

The DC microgrid system also utilizes Stern -Tafel model of the ultra-capacitor which is obtainable in Simulink (Mat lab) is depicted in Fig.2.3.2. It is established as the voltage source that can be controlled with inbuilt resistance. The ultra-capacitor model performance depends on the numerous constraints such as ultra-capacitor's inbuilt resistance, ultra-capacitor rated capacitance and net stored charge.

2.4. DC Microgrid System with Two-way Converter control

In the presented DC microgrid, energy storage devices ultra-capacitor and battery are linked to the DC bus parallel to each other using individual two-way converters which can transfer the power in both directions. Depending on the switching pulses received from the energy management control system the converters of the battery and ultra-capacitor either discharges(supplies) or charges(absorbs) power depending on the power flow direction. Converter construction is depicted along with microgrid system simulation in Fig.2.4.1. In case of boost mode, the switches SW-bb1 and SW_SCC1 is switch to on condition and in buck mode SW-bb2 and SW_SCC2 is switch to on condition.

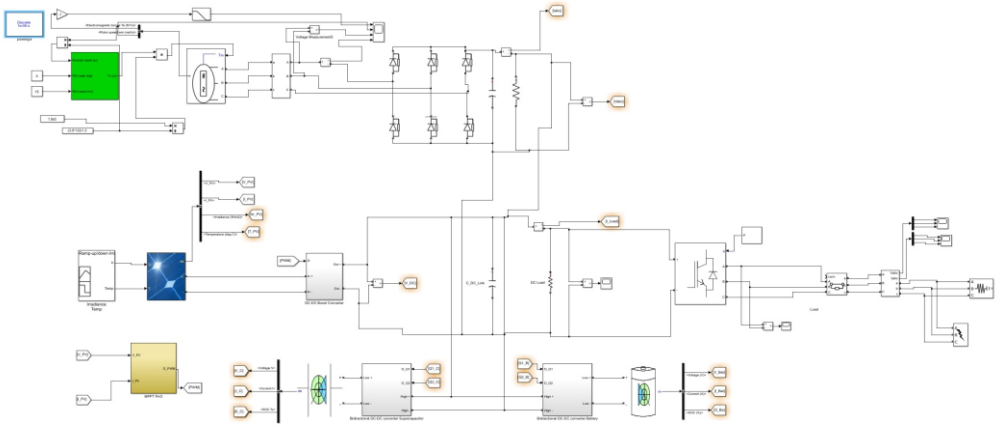

Fig.2.4.1. Simulation circuit of DC Microgrid with HESS

3. ENERGY MANAGEMENT ALGORITHM

In this proposed energy management algorithm basically works on the net current required from storage devices which is obtained from the feeding difference between DC bus voltage and actual available voltage to Proportional Integral controller. PI regulator 's output current signal is further split into high frequency current component and average current component using filter controller. The average current component is obtained as follows

$$I_{B\,av} = F(I_{Tot}) \qquad (3.1)$$

$$I_{Berr} = I_{B\,av} - I_{Bat} \qquad (3.2)$$

This obtained average current component ($I_{B\,av}$) is compared with the available battery currentI_{Bat}, and the error signal (I_{Berr})obtained as in equation (3.2) is supplied to the PI regulator to produce duty ratio. Then duty ratio is converted in to switching pulses by means of pulse width modulator (PWM), using these signals the switches SW1 and SW2 are operated. The transient current necessities (II_{Hf}) are attained from the net current necessities(I_{Tot})by deducting the low frequency current requirement ($I_{B\,av}$) as follows

$$I_{Hf} = I_{Tot} - I_{B\,av}. \qquad (3.3)$$

In order to compensate the slow response of the battery, and to compensate uncompensated($Punc$) power by the battery for first few seconds uncompensated power is calculated as follows,

$$Punc = (I_{B\,av} - I_{Bat})\,V_b \qquad (3.4)$$

Where V_b is the voltage of the battery. The current reference given to the super capacitor includes the uncompensated current component of the battery and high frequency current component. In the equation 3.5 second part represents the uncompensated current of the battery.

$$I_{SCRef} = I_{Hf} + (I_{B\,av} - I_{Bat})\,\frac{Vb}{Vsc} \qquad (3.5)$$

The reference current for the supercapacitor is obtained by subtracting actual supercapacitor from current obtained from equation (3.5) and the variance obtained is provided to PI regulator to produce duty ratio and the switching pulses are generated from PWM and is given to the supercapacitor bi-directional converter switches (SW3&SW4) as shown in the figure 2.4.1. In order to maintain the constant DC link voltage, super capacitor and battery will either act boost/discharge mode or in buck /charge mode. Energy management strategy is shown in figure.3.1.

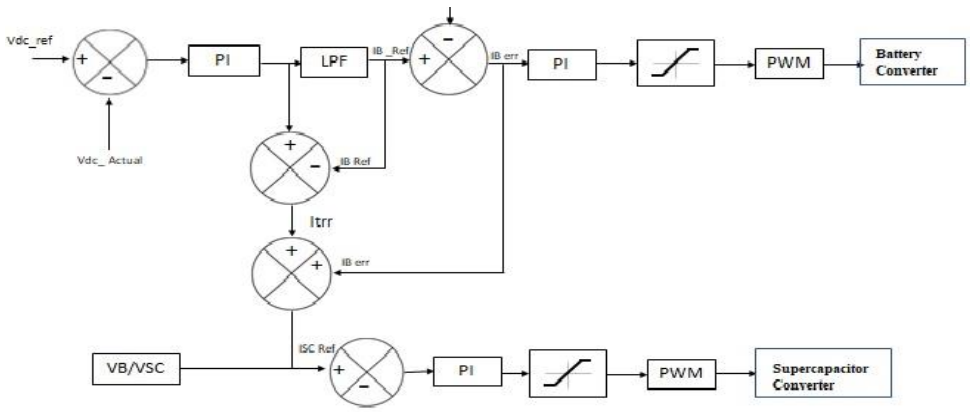

Fig.3.1 Energy Management Strategy of DC Microgrid

4. SIMULATION AND ANALYSIS

The DC microgrid system is analyzed for load variation and generation variation and the results of two cases are discussed below

4.1 Case1: Load Variation

To analyze the load variation, generated power is kept constant, and load is varied as from 1500W to 2000W at 0.25 sec. Before 0.25 sec power from is wind power 1300Wand solar power is 1000W which is more than the load requirement, and the extra power is been absorbed by battery(700W) upto 0.25 sec as shown in figure4.1, sudden rise in load power at 0.25 sec is momentarily satisfied by super capacitor and average power requirement is satisfied by battery. It is also verified that the DC link voltage is kept constant(50V) regardless of load change as observed in figure4.2

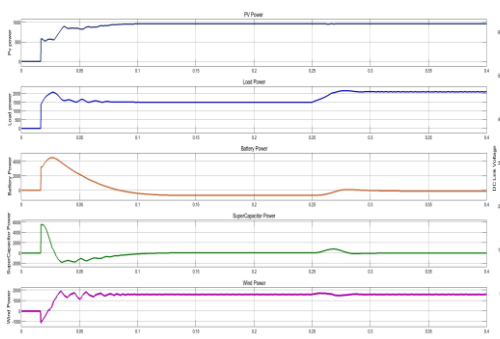

Fig4.1 Power response for load variation

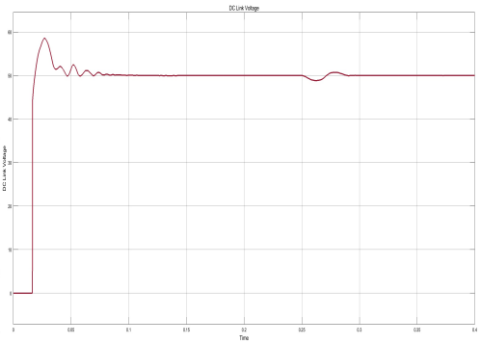

Fig4.2DC Link Voltage

Case4.2: Variation in Generated Power

DC microgrid is analyzed for variation in generation by keeping load power requirement constant at 1500W. In this case wind power generation is kept at 1000W and PV power is varied by varying irradiance. At starting power generation from PV system is 500W and it increase to 1000W at 0.2. Upto 0.2 sec the power generation from PV and wind systems is equal to the load demand of 1500W. After 0.2 sec PV power is increased to 1000W, now power generation form PV and wind is more than the load requirement. The extra power of 500W is absorbed by supercapacitor momentarily for few microseconds followed by battery as shown in figure 4.3 And also from figure 4.4, it is verified that DC link voltage is sustained constant regardless of generation deviation.

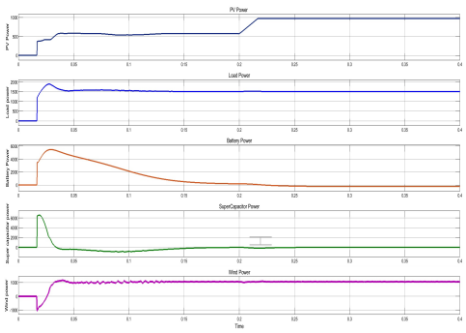

Fig 4.3 Response to PV generation variation

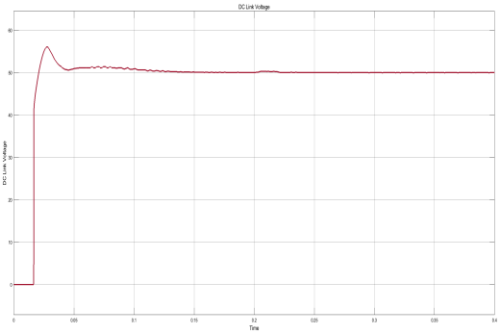

Fig 4.4 DC link Voltage

Similarly when wind velocity is changed at 0.2 sec, the wind power generation changes from 1000w to 500W along with variation in solar irradiance introduced at 0.2 sec from 1000W/m^2 to 400w/m^2, due to this total power generation becomes less than the load demand of 1500W. Momentary power deficit of 600w is supplied by the super capacitor for 0.008 sec followed by the battery as shown in figure 4.5.Form the figure 4.6 ,it is clear that DC link voltage remains constant irrespective of generated power variation. All simulation results are tabulated and presented in table4.1 below

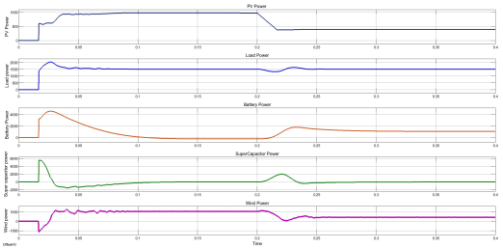

Fig 4.5 Response to PV&Wind generation variation

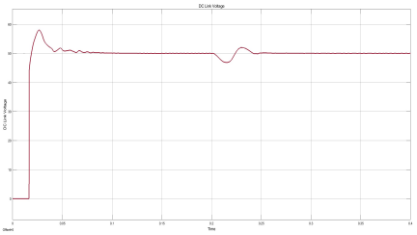

Fig 4.6 DC link Voltage

Different Scenarios	DC link voltage Variation		
	Overshoot	Steady state - time	Disturbance recovery time
Load Variation	58V	0.007 sec	0.004 sec
PV Generation Variation	55V	0.006 sec	0.001sec
PV &Wind Generation Variation	58V	0.007	0.004 sec

Table4.1 Summary of Simulation and Analysis results

5. CONCLUSION

Hybrid Energy Storage system along with two renewable energy sources are effectively utilized in the presented energy management control strategy. The main goal of the proposed energy management algorithm is to sustain thedc link voltage constant irrespective of load changes and the generation variation. The proposed system is simulated and analyzed and is also verified that dc link voltage is sustained at constant value irrespective of change in wind velocity, variation in irradiance and load variation and also the stability of the system is maintained.

6. REFERENCES

[1] Punna, Srinivas & Manthati, Udaya. (2020). Optimum design and analysis of a dynamic energy management scheme for HESS in renewable power generation applications. SN Applied Sciences. 2. 10.1007/s42452-020-2313-3.

[2] S. Kotra and M. K. Mishra, "Design and Stability Analysis of DC Microgrid With Hybrid Energy Storage System," in IEEE Transactions on Sustainable Energy, vol. 10, no. 3, pp. 1603-1612, July 2019, doi: 10.1109/TSTE.2019.2891255.

[3] S. Augustine, M. K. Mishra and N. Lakshminarasamma, "A Unified Control Scheme for a Standalone Solar-PV Low Voltage DC Microgrid System With HESS," in IEEE Journal of Emerging and Selected Topics in Power Electronics, vol. 8, no. 2, pp. 1351-1360, June 2020, doi: 10.1109/JESTPE.2019.2916421.

[4] D. Das, M. J. Hossain, S. Mishra and B. Singh, "Bidirectional Power Sharing of Modular DABs to Improve Voltage Stability in DC Microgrids," in IEEE Transactions on Industry Applications, vol. 58, no. 2, pp. 2369-2377, March-April 2022, doi: 10.1109/TIA.2022. 3144653..

[5] Suganthi.N, Dr.P. Usha, **"**Overview of Micro grid Controllers and Energy Storage Systems", 6th International E-Conference on Latest Trends in Science, Engineering and Technology (ICLTSET'20) on April 13,2020.

[6] Sangeeta Modi, Dr.P. Usha published paper on "Mathematical Modelling, Simulation and Analysis of Microgrid: A Pre-requisite for Devising a Controller" GIS Science Journal, ISSN NO : 1869-9391, Dec.2021, Vol.8, issue12, page no.433-461.

[7] Suganthi. N and P. Usha, "Modeling and Analysis of Dynamic Energy Management of DC Microgrid Using HESS," 2021 5th International Conference on Electronics, Communication and Aerospace Technology (ICECA), 2021, pp. 23-29, doi: 10.1109/ICECA52323.2021.9676105

[8] K. Kevin, S. Modi and P. Usha, "Micro Grid: An Energy Efficient Approach for Modern Power System," 2019 IEEE International Conference on Distributed Computing, VLSI, Electrical Circuits and Robotics (DISCOVER), Manipal, India, 2019, pp. 1-5

[9] A. K. Podder, O. Chakraborty, S. Islam, N. Manoj Kumar and H. H. Alhelou, "Control Strategies of Different Hybrid Energy Storage Systems for Electric Vehicles Applications," in IEEE Access, vol. 9, pp. 51865-51895, 2021, doi: 10.1109/ACCESS.2021.3069593.

[10] M. Rezkallah et al., "Coordinated Control Strategy for Hybrid off-Grid System Based on Variable Speed Diesel Generator," in IEEE Transactions on Industry Applications, vol. 58, no. 4, pp. 4411-4423, July-Aug. 2022, doi: 10.1109/TIA.2022.3174825.

[11] Sangeeta Modi, Ashish Anand and P. Usha, "Microgrid Control: A Comparative Study on Control Strategies for Controlling the Circulating Current", IEEE International Conference on Communication, Control and Intelligent Systems (CCIS), pp 339-343, Nov. 2015.

[12] Nikhil Korada, Mahesh K. Mishra," Grid Adaptive Power Management Strategy for an Integrated Micro grid with Hybrid Energy Storage", IEEE Transactions on Industrial Electronics, 64(4),2017, pp. 2884-2892. (Journal).

[13] Z. Zhu, F. Xiao, Z. Huang, J. Liu, P. Chen and Q. Ren, "Bidirectional Power Control Strategy for Super Capacitor Energy Storage System Based on MMC DC-DC Converter," in IEEE Access, vol. 10, pp. 53225-53233, 2022, doi: 10.1109/ACCESS.2022. 3175207..

[14] D. Sun, H. Long, K. Zhou, Y. Lv, J. Zheng and Q. Chen, "Research on SCESS-DFIG DC Bus Voltage Fluctuation Suppression Strategy for Frequency Inertia Regulation of Power Grid," in IEEE Access, vol. 8, pp. 173933-173948, 2020, doi: 10.1109/ACCESS.2020. 3025292..

[15] C. Serrano-Canalejo et al, "Energy management system design and economic feasibility evaluation for a hybrid wind power/pumped hydroelectric power plant," in IEEE Latin America Transactions, vol. 17, no. 10, pp. 1686-1693, October 2019, doi: 10.1109/TLA.2019. 8986447..

[16] Aws saleh et al, Modeling, Control, and Simulation of a New Topology of Flywheel Energy Storage Systems in Microgrid", IEEE access, Vol.7, Nov 2019. (journal).

[17] Rishi Kant Sharma et al,"Dynamic Power Management and Control of a PV PEM Fuel-Cell-Based Standalone ac/dc Microgrid Using Hybrid Energy Storage" IEEE Transactions on Industry Applications Vol. 54(1), pp.526-538,2018.

[18] P. Mathew, S. Madi Chetty and S. Mishra, "A Multilevel Distributed Hybrid Control Scheme for Islanded DC Microgrids," in IEEE Systems Journal, vol. 13, no. 4, pp. 4200-4207, Dec. 2019, doi: 10.1109/JSYST.2019.2896927.

[19] I. A. Ibrahim, M. J. Hossain, B. C. Duck and C. J. Fell, "An Adaptive Wind-Driven Optimization Algorithm for Extracting the Parameters of a Single-Diode PV Cell Model," in IEEE Transactions on Sustainable Energy, vol. 11, no. 2, pp. 1054-1066,April 2020R.

[20] Timbus, A et al., "Evaluation of Current Controllers for Distributed Power Generation Systems." IEEE Transactions on Power Electronics, 24(3), 654–664,2009. doi:10.1109/tpel.2009.2012527.

[21] Mohannad Jabbar Mnati et al.," Review Different Types of MPPT Techniques for Photovoltaic Systems", International Conference on Sustainable Energy and Environment Sensing (SEES 2018).

[22] Tremblay, O.; Dessaint, L.-A. Experimental Validation of a Battery Dynamic Model for EV Applications. // World Electric Vehicle Journal, 3, (2009), pp. 289-298.

[23] Henry Miniguano et al.," A General Parameter Identification Procedure Used for the Comparative Study of Supercapacitors Models", Energies Journal,12,1776.

[24] M.H.Nehrir,C.Wang et al.,"A Review of Hybrid Renewable /Alternative Energy Systems for Electric Power Generation:Configuration,control,and Applications",IEEE Trans.Sustain.Energy,Vol.2,no.4.pp392-403,Oct2011.

[25] S. Singh, S. Manna, M. I. Hasan Mansoori and A. K. Akella, "Implementation of Perturb & Observe MPPT Technique using Boost converter in PV System," 2020 International Conference on Computational Intelligence for Smart Power System and Sustainable Energy (CISPSSE), 2020, pp. 1-4.

[26] S. R. Pendem and S. Mikkili, "Assessment of Cross-coupling Effects in PV String-integrated-converters with P&O MPPT Algorithm Under Various Partial Shading Patterns," in CSEE journal of power and Energy Systems, Vol.8,no.4 pp. 1013-1028, July 2022.

[27] https://www.mathworks.com/help/physmod/sps/ powersys /ref/ battery.html.

[28] https://www.mathworks.com/help/physmod/sps/powersys/ref/supercapacitor.html

[29] Y. S. Perdana et al," Direct Connection of Super capacitor-Battery Hybrid Storage System to the Grid-tied Photovoltaic System", IEEE Transactions on Sustainable Energy,Vol.10(3), pp.1370 - 1379, 2019.

Development of Smart Semi-Autonomous Wheelchair

Chiraag A[1], Tejas BU[2], Vrishab Kushalappa[3], Tavishi Bansal[4] and Prof. Asha S Patil[5]

[1,2,3,4] *Final year students, Department of Electrical & Electronics Engineering, PES University, Bangalore*

[5] *Professor & project guide, Department of Electrical & Electronics Engineering, PES University, Bangalore*

Abstract.

This research paper focuses on the development of a semi-autonomous smart wheelchair based on the line follower ideology [4,7], to assist the physically challenged, mainly in interior spaces. In this paper the different modes of operation, overall hardware and software architecture along with communication protocols have been discussed. For people having disabilities or the elderly, requirement of mobility support could restrict their independence, on account of third-party reliance. Hence, a cost effective, reliable, autonomous system has been developed to tackle this issue. The system has three main modes, the autonomous line follower mode, remote web control mode and the manual mode. In the manual mode, the user can either make use of the touchscreen GUI application or voice commands to manoeuvre the wheelchair.

1. INTRODUCTION

The US Access Board, Washington, DC, in 2015, reported that the percentage of operators using powered wheelchairs was 48% and manual chairs was 50% [1]. This abnormality could be explained by the hefty price tags the powered wheelchairs have. Hence, this project not only aims at devising a semi-autonomous wheelchair but also to keep the costs as low as possible.

For handicap individuals, a manual wheelchair using brute strength could work well to an extent. But those with crippled legs/hands will not find it feasible to operate a manual wheelchair and instead would have to rely on another person [2]. This is rather an inconvenience for both the parties and hence, a power operated wheelchair is the best solution. Adding onto this issue, disorders like gait are estimated to increase from 10 % for the population aged 60–69 years and more than 60 % for people over 80 years [3]. In most cases, the conventional joystick operation could also prove to be a difficult task for the disabled and falls out of favour. The simple solution as discussed in this paper is to develop an autonomous powered wheelchair which would drastically ease the operation and improve independence of the disabled.

This paper is organized into the following sections. Section II describes, Implementation and System configuration, Section III, IV & V describe the three modes of operation while Section VI & VII, deals with conclusion and future prospects respectively.

2. IMPLEMENTATION AND SYSTEM CONFIGURATION

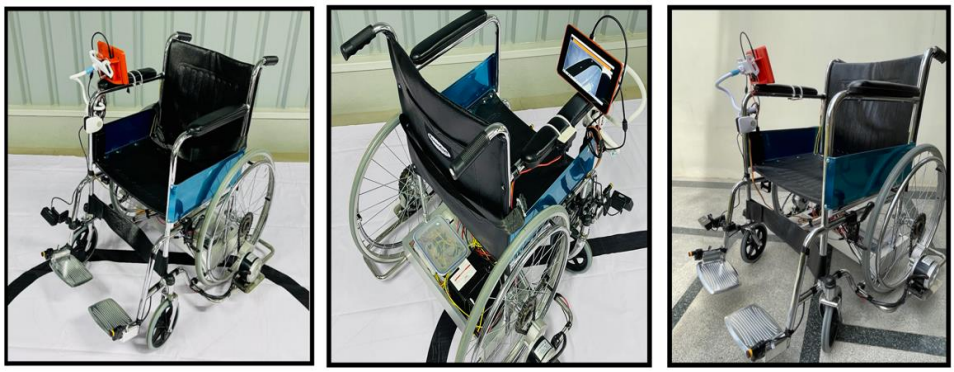

Figure 2.1. Final product: Semi-Autonomous Smart Wheelchair (left to right: wheelchair on track, top-view with active touchscreen interface, front-view)

A differential drive setup is used in converting a manual wheelchair to an electric wheelchair. Two PMDC motors are attached to the rear wheels of the wheelchair, using a chain drive setup. Custom fabrication was done on the manual wheelchair to host this system. Mild steel is used to extend the platforms on the outer sides of either wheels. A plate is provided on both the sides for the motor to be placed onto. Arc welding is used to attach the framework to the chassis of the manual wheelchair, as evident from Fig. 2.1. Motors are placed just below the sprocket attachment. This design philosophy is followed to help facilitate the forward/backward motion of the wheelchair and avoid chain slips and loss of torque or power transmission.

Fig. 2.3, shows the block diagram of the system. It mainly consists of Raspberry Pi as the heart, for computer vision [5]. Interfaced with it via I2C protocols, is the 7-inch Raspberry Pi touchscreen, which serves as the control panel and display unit for our wheelchair. A webcam with inbuilt microphone is connected to the Raspberry Pi using USB, for detecting the predefined black line, and for remote video streaming [6]. This whole setup is powered by a 10,000mah power bank. The Arduino UNO serves as the slave microcontroller and performs motor manipulation operations based on the commands received from the master, Raspberry Pi [5]. It is interfaced to the Pi via 3.3V to 5V logic level converter and makes use of UART communication protocols. The UNO is connected to a dual channel 12A Sabertooth motor controller, which is setup to be used in simplified serial mode via UART protocols.

The motor controller is connected to two 24V 250 W PMDC motors which are hooked onto the rear wheels of our wheelchair to work as a differential drive setup. To the Arduino, two optical sensors are interfaced and are mounted on either side at the front of our wheelchair to detect obstacles and come to a halt until the obstacle is removed. A buzzer is interfaced to the Arduino to go ON, when an obstacle is in the path of traversal [5]. This whole setup is powered by two 12V 12AH lead acid batteries connected in series to provide a combined energy capacity of 24AH and voltage of 24V.

MODEL	SPECS	V	NO LOAD		RATED LOAD				
			SPEED RPM	CURRENT A	TORQUE N.M.	SPEED RPM	CURRENT A	P-OUT W	EFFICIENT η
1016Z2	250W24V	24	434± 5%	≤1.8	6.65± 5%	357±5%	≤13.7	250	≥76%

Figure 2.2. 250W 24V PMDC Motor Specification

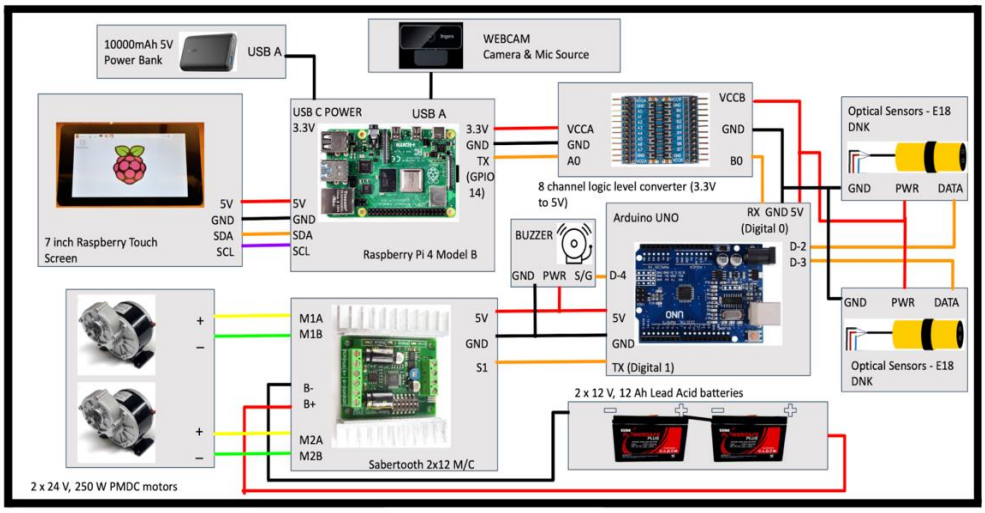

Figure 2.3. System Block Diagram

2.1. UART Communication Protocols

The choice of communication protocols that was selected to establish between Raspberry pi and the Arduino UNO was UART. The reason being, this kind of communication requires less no. of wires, it's a 2-way communication and there's no assigned master-slave components as such, as this is a multi-master way of communication. The communication protocols in serial mode of operation of the Sabertooth motor controller and the Arduino UNO were fixed to use UART protocols. The UART protocol is

established in this way, Raspberry Pi to Arduino UNO to Sabertooth Motor controller in this direction only.

In this system, the assigned GPIO or digital RX and TX pins on Raspberry Pi and Arduino UNO are made use of. To configure these pins Software serial is used on Arduino. The connections between these components can be understood more clearly from the above block diagram.

2.2. System Flowchart

Fig. 2.4 shows the flowchart of the full operation and modes of the wheelchair. The system basically has three modes, autonomous mode, web-controlled mode and the manual mode.

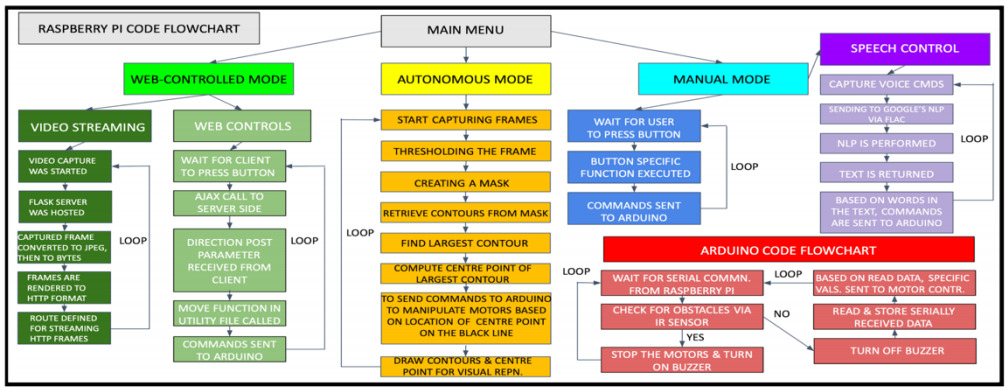

Figure 2.4. System Flowchart

3. AUTONOMOUS LINE FOLLOWER MODE

To achieve line follower capabilities, computer vision using OpenCV library was utilized. On the frames received from the webcam, thresholding and masking are applied to only detect the dark/black line or a track over a light background. The frames are converted to grayscale since we are only looking for the black path. Noise is eliminated using Gaussian blur. In the thresholding process, a pixel below 65 turns white and anything above turns black. After which contours are retrieved from the frame using the masked image. Now, to avoid errors of drawing contours around another black object, only the contour with the largest area will be selected, which is obviously going to be the track and next, the center point of this track is found and based on the position of this centre point on the original frame, wheelchair will be turned right/left or will move forward. This is the ideology behind our line follower algorithm. This system can be put to use in interior spaces, where a predefined track can be laid down precisely and a controlled environment can be created to control the errors that could occur.

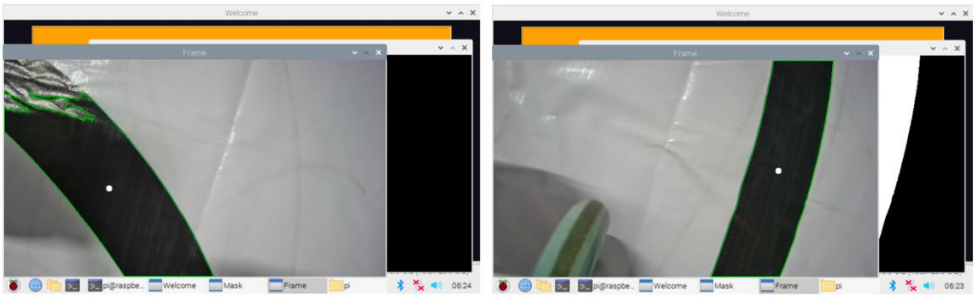

Figure 3.2. Black line contour detection (left to right: *case a and case b*)

As it can be seen from *case a* in Fig. 3.1, the center point is located on the left part of the frame, which is less than the 300-pixel range and thus, the wheelchair will be turned in the left direction, and the path to be traced is also a left curve.

As it can be seen from *case b* in Fig. 3.1, the center point is located on the right part of the frame, which exceeds the 320-pixel range and thus, the wheelchair will be aligned in the right direction, since the path to be traced is curved right.

Hence, the main goal of this algorithm is to align the system along the center point of the largest detected contour. The algorithm is constantly checking for the center point of the contour and is highly sensitive. This sensitivity can be relaxed to make the system work smoother, depending on the precision of the line follower algorithm. Altering the range of pixel values can also increase the lenience of the system. In our case, preference is given to sensitivity, precision and accuracy of the algorithm and the system constantly tries to adjust the wheelchair orientation and position.

4. WEB-CONTROLLED MODE & REMOTE VIDEO STREAMING

In this mode, the wheelchair can be controlled remotely from any internet enabled device using the IP address of the Raspberry Pi. To assist the user, real-time video streaming of 180^0 forward vision of the wheelchair is made available. This mode requires the system to be connected to internet. Currently, the system works on Wi-Fi, however, this restricts the wheelchair to be operated in interior spaces with Wi-Fi provision. Provision of cellular connection to the system would expand the range to outdoors as well.

4.1. Web Controls

The webpage for the GUI controls is developed using HTML, PHP & JavaScript. This page can be accessed using the URL, via any internet enabled device, from anywhere in the world. When a user presses on a direction button, a specific function is called and a

letter specific to each button is passed as a parameter to the function. Then, this function makes an AJAX call in the background, and sends the direction value to the backend.

The interface for the web controls using apache web server was developed successfully as shown int Fig. 4.1. The wheelchair can be controlled using the GUI web page. The corresponding blackened communications were set up using AJAX calls. Hence, now making use of the Raspberry Pi's IP address, the wheelchair can be manoeuvred easily and remotely. It can be seen in the above figure, the webpage is being accessed by the Raspberry Pi's IP address i.e., 192.168.1.8. This way using these four buttons, the wheelchair, can be controlled remotely via the internet.

Figure 4.3. GUI controls on webpage

4.2. Remote Video Streaming

The programming was done on python & HTML. The motion JPEG frames are broadcasted over HTTP protocols, onto the Flask mini framework. This means, this broadcast can be visible from any web browser. This is called through context path, in which the frames are uploaded to the HTML page, from where it can be accessed anywhere.

4.3. Voice Control System

Speech command system was made possible using the speech_recognition module for python along with Google's web speech API. This method, takes the voice input from the mic, and then uploads the same to Google's cloud NLP, and then retrieves the processed words, which represent output of the input voice command as text, which we can use to our own benefit. The voice control system will make use of the simplest method of Speech-to-text API conversion i.e., synchronous recognition request. This method can process commands with maximum data of one minute. A synchronous request is sent to the Google web speech API, which basically blocks the user from giving any more voice commands, which is a safety feature to avoid unambiguous control of the wheelchair. On an average of 2 seconds, the speech to text processing is performed.

5. GUI APPLICATION AND MANUAL MODE

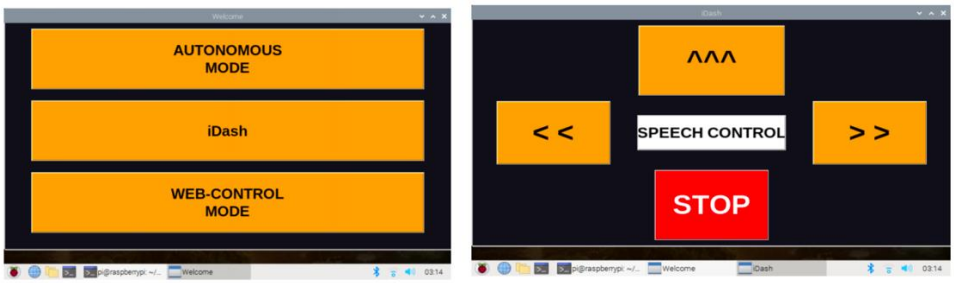

Figure 5.4. Graphic User Interface (left to right: Home Screen and Manual Mode Screen)

5.1. GUI Application

The graphic user application was developed in python2 making use of the Tkinter library, which basically, brings in GUI features to python programming language. A menu-based approach was adopted to develop this application. Using the Tkinter library, buttons, window and different colours were applied to the application to give it a colourful and fresh look. The user interaction with the wheelchair was made to feel easy and convenient.

5.2. Manual Mode

In the manual mode, the patient or the user can control the wheelchair by touch-based commands through the touch control panel. For this too, a GUI python program is created, which is executed, when the manual mode button is pressed. Similar to the controls, seen on the web control mode, even in this mode, there are four buttons to control the motion of the wheelchair, namely, forward, left, right and stop buttons.

The voice control system can also be activated, from the button here. Basically, when the control buttons are pressed, a specific byte of value corresponding to each button is sent to the Arduino UNO using UART protocols. Say, for example, when the forward button is pressed, character '1', is sent as serial communications, and when right, left or stop buttons are pressed, then the Raspberry Pi, starts sending, '2', '3' and '4' byte size values at 38400 baud rates, to the Arduino. The baud rate is chosen to be 38400, since the Arduino has to communicate with the motor controller using UART protocols itself, and we make use of standard RX & TX pins for this setup. Based on the values received, the Arduino performs the desired action, either to move, turn left or right or stop the wheelchair, by again sending motor values to the motor controller, via UART protocols, which manipulate the motors.

6. CONCLUSION

According to the methodology plan, a smart semi-autonomous wheelchair is developed, with three modes, Autonomous mode, Web-controlled mode and Manual mode. The wheelchair can autonomously commute on its own in a controller environment, making use of a predefined path. It can also be controlled manually by the user or by the internet, and as a use case, proves to be helpful for the hospital staff to control a patient remotely, in case of any mishaps. Through remote video streaming, the wheelchair can be monitored in terms of its position and orientation in an environment. The patient can also give voice commands, which is a convenient feature, to control the wheelchair. A safe speed of 4kph can be achieved and the system can support a total weight of 100kg, inclusive of the wheelchair weight.

The core functionality of serving as an automated wheelchair relies on Computer Vision. High accuracy with less processing overhead was achieved by choosing an optimal frame rate, 18 fps through trial and error. The developed codebase assures safety from bugs and software crashes. The attached infrared sensors avoid obstacles and safeguards the patient from potential collisions. Concluding, an autonomous wheelchair in a controlled environment with smart features like voice controls, remote control over the web with video streaming and touchscreen UI has been developed to cater to the needs of many.

7. FUTURE PROSPECTS

Further research on this project would focus on making the system fully autonomous. ROS using Simultaneous Localisation and Mapping Algorithms could be used to achieve this. In this, the idea is to map an environment, in different ambient conditions before hand, and with this database in hand, to help the wheelchair commute from one point to another inside this environment, avoiding obstacles. The LiDAR sensor could be used to achieve such a system, to map and help the wheelchair to navigate on its own. As of now, only obstacle detection is developed. As an extension of this section, obstacle avoidance could also be developed making use of computer vision.

8. REFERENCES

[1] Shubham Pandey, Shubham Chandewar, Krishnamoorthy A, “Smart Assisted Vehicle for Disabled/Elderly Using Raspberry Pi”, Vol. 6, No. 2, July 2017, pp. 82~87, ISSN: 2089-4864, DOI: 10.11591/ijres.v6.i2.pp82-87, 2017

[2] G. Bourhis, K. Moumen, P. Pino, S. Rohmer and A. Pruski, “Assisted navigation for a powered wheelchair. Systems Engineering in the Service of Humans”,

Proceedings of the IEEE International Conference on Systems, Man and Cybernetics, France, pp. 553–558, 1993.

[3] W. Pirker and R. Katzenschlager, "Gait disorders in adults and the elderly, A clinical guide," Wien Klin Wochenschr., vol. 129, no. doi: 10.1007/s00508-016-1096-4, p. 81–95, 2016.

[4] A. Parsad, "Line Following Robot,"Dept. Elex. & Comm. Eng., Visvesvaraya Technological University, Banglore, India, 2005.

[5] Ayush Wattal, Ashutosh Ojha, Manoj Kumar. “Obstacle Detection for Visually Impaired Using Raspberry Pi and Ultrasonic Sensors”. National Conference on Product Design (NCPD 2016), July 2016.

[6] Matsumoto, O., Komoriya, K., Hatase, T., Yuki, T., & Goto, S. (2008). Intelligent Wheelchair Robot "TAO Aicle". Service Robot Applications. doi:10.5772/6064

[7] Bajestani, S.E.M., Vosoughinia, A., “Technical Report of Building a Line Follower Robot” International Conference on Electronics and Information Engineering (ICEIE 2010), vol 1, pp v1-1 v1-5, 2010.

[8] Development and Applications of Line Following Robot Based Health Care Management System Deepak Punetha, Neeraj Kumar, Vartika Mehta, International Journal of Advanced Research in Computer Engineering & Technology (IJARCET), Volume 2, Issue 8, August 2013 p2446-2450

Biographies

Chiraag A received their bachelor's degree in Electrical & Electronics Engineering and Minor Degree in Computer Science from PES University, Bangalore in 2022. He has interned at Deloitte USI as a Full Stack Web Development intern. He is currently working as a Full Stack Software Engineer at Byju’s Think & Learn Pvt. Ltd. His interests are web development, system software development including embedded systems.

Tejas BU received their bachelor's degree in Electrical & Electronics Engineering from PES University, Bangalore in 2022. He has interned at Continental Automotive as a Software Testing intern. He is currently working as a Software Development Engineer at IBM. His interests are data science, machine learning & artificial intelligence.

Vrishab Kushalappa received their bachelor's degree in Electrical & Electronics Engineering from PES University, Bangalore in 2022. He has interned at ABB and Toyota Kirloskar Motor Pvt. Ltd. He is currently working as an Associate Software Engineer at Harman Connected Services, Product Development division. His interests are embedded systems, system software development etc…

Tavishi Bansal received their bachelor's degree in Electrical & Electronics Engineering from PES University, Bangalore in 2022. She has interned at Delta X Automotive as an Embedded Engineer intern. She is currently working as an Analyst at Deloitte USI. Her interests are embedded systems, VLSI etc…

Mrs Asha. S. Patil has obtained MTech from VTU and pursuing Ph.D. at PES University. She is currently working as an Assistant Professor in PES University, Bangalore. She has published 4 papers in conference proceedings. Her areas of interest are VLSI, Microcontrollers, Data Communication, etc.

Comparative Analysis of Bidirectional Buck/Boost DC-DC Converter and Interleaved Bidirectional Buck/Boost DC-DC Converter for EV applications

Madhumitha G, Rajesh Uppara and Priya S

Dept of Electrical & Electronics Engineering, Siddaganga Institute of Technology, Tumkur, Karnataka, India
Email : madhumithagangadhar@gmail.com ; rajeshu@sit.ac.in ; priyas@sit.ac.in

Abstract.

Electric vehicles are getting massive popularity considering their enhanced performance and inexpensive maintenance. The efficacy of electric vehicles is determined by how well energy repository devices and power electronics converters are interfaced. In the case of Evs, DC-DC converters are crucial. In EVs, Bidirectional converters are employed since power management is vital. Bidirectional converters allow the power flow in both directions. In terms of higher efficiency, current reduction, and voltage ripple, an Interleaved Bidirectional DC-DC converter outperforms a Bidirectional DC-DC converter. This manuscript proposes a comparison of the "Bidirectional Buck/Boost DC-DC converter" with the "Interleaved Bidirectional Buck/Boost DC-DC converter". Matlab is used to predict the behavior of both converters.

Keywords. Electric Vehicles, Bidirectional converter, Interleaved Bidirectional converter

1. INTRODUCTION

Electric vehicles have gained in popularity over the last decade as a result of more ecologically friendly power sources, minimal maintenance, and the lack of a gasoline supply. The power electronics converter serves as the primary link between the source and the load. Electric vehicles typically feature a "Bidirectional DC-DC converter" in the middle of the "source" and "battery" [1] [2]. In Electric Vehicles, the usage of energy repository devices like Batteries & Supercapacitors is a must. Many Bidirectional DC-DC converters have been proposed for the automotive electrical system, however, the Buck/Boost converter with two switches and one inductor stands out because of its simple circuit and inexpensive cost. Power flow is unidirectional in a traditional Buck/Boost converter, however, power can move in both directions with a "Bidirectional DC-DC converter". [4]. "Bidirectional DC-DC converters" are adopted mainly to escalate and deescalate voltage levels with power flow in either forward or reverse directions. [2]. To step up the voltage Boost converter is employed and to step down the voltage Buck converter is employed [8]. During regenerative braking, the bidirectional DC-DC converter allows electricity to flow backward into a storage device. Bidirectional converters are beneficial over unidirectional DC-DC converters because of this functionality. Interleaved is a technique employed to reduce the size of the inductor and capacitor and also to excel the converter's efficiency, & reduction in both voltage & current ripple & switching losses.

2. BIDIRECTIONAL BUCK/BOOST DC-DC CONVERTER

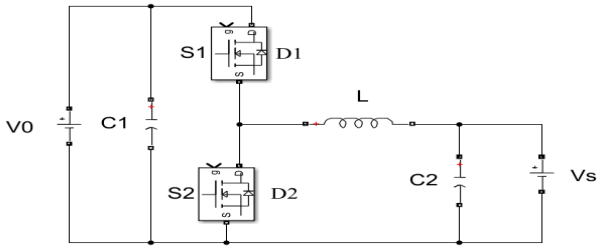

Figure 2.1. Schematic diagram of a Conventional Bidirectional DC-DC converter

A “Bidirectional Buck/Boost DC-DC Converter” comes under a “Non-isolated converter” and this converter consists of two switches, 1 inductor, and 2 capacitors which are shown schematically in Figure 2.1. The converter has 2 operating modes i.e., Forward and Backward. In Forward mode, the electricity flows from the low voltage level such as the battery to the high voltage level side, and in this approach, the converter performs as a “Boost converter” [5][6]. At the time of regenerative braking, the electricity flows back to the low voltage level side to rejuvenate the battery & the converter performs as a “Buck converter”.

2.1 Boost mode

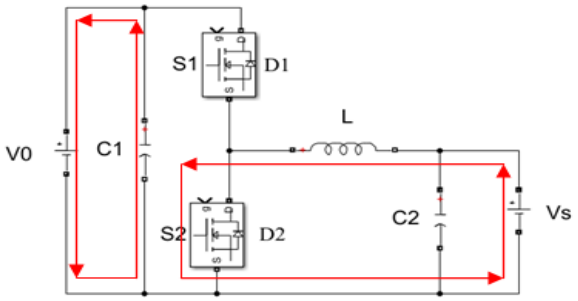

Figure 2.1.1. When S2 is ON

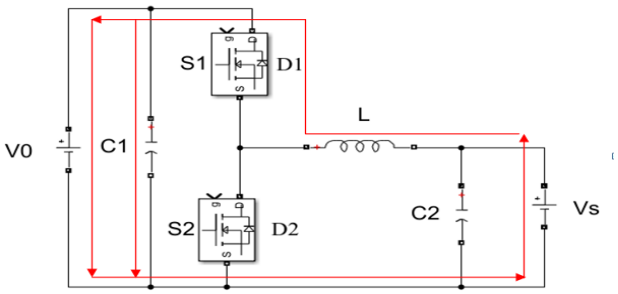

Figure 2.1.2.when D1 is forward biased

Figure 2.1.1 shows how current is flowing when S2 is ON & S1 is OFF. Inductor charges & the current will increase linearly. Figure 2.1.2 is when diode D1 is ON, S1 & S2 are OFF and diode D2 is reverse biased. The energy accumulated in the inductor will start discharging through diode D1. In this mode, the energy from the source and inductor will be fed to the load, thus there will be a step up in voltage level.

2.2 Buck mode

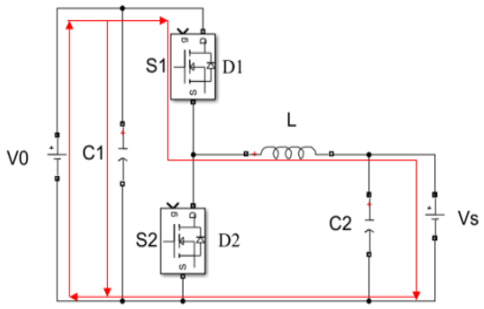

Figure 2.2.1. when S1 is ON

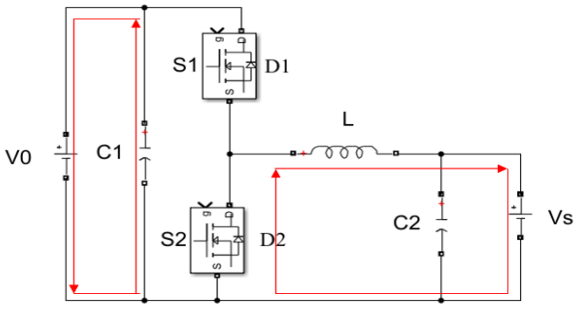

Figure 2.2.2.when D2 is forward biased

Figure 2.2.1 shows how current is flowing when S1 is ON, S2 is OFF & both the diodes D1 & D2 are reverse biased. The energy stored in the inductor will discharge in a negative slope. Figure 2.2.2 shows when diode D2 is ON, D1 is reverse biased & S1 and S2 are OFF. During regenerative braking, this mode of operation is employed to charge the battery.

2.3 Converter Design Calculations

The output voltage for the Bidirectional Buck/Boost converter is obtained by (2.3.1)

$$Vo = \frac{Vs}{(1-D)} \tag{2.3.1}$$

Inductor ripple current & Voltage ripple can be calculated by using (2.3.2) & (2.3.3)

$$\Delta Il = \frac{VsD}{Lf} \tag{2.3.2}$$

$$\Delta Vc = \frac{VsD}{8Lf^2C} \tag{2.3.3}$$

Inductor and Capacitor values can be calculated using (2.3.4) & (2.3.5)

$$L = \frac{VsDR}{2fVo} \tag{2.3.4}$$

$$C = \frac{DVs}{16Lf^2V0} \tag{2.3.5}$$

Where V_o - output voltage, Vs - input voltage, D - duty ratio, f - switching frequency, L - Inductor, R - equivalent resistance & C - capacitor.

3. INTERLEAVED BIDIRECTIONAL BUCK/BOOST DC-DC CONVERTER

The interleaved approach was introduced to reduce the size of filtering components. An interleaved converter is a parallel arrangement of 2 or more converters having a phase shift of 360°/n [7]. Figure 3.1 depicts the schematic diagram of a 2-phase interleaved bidirectional dc-dc converter. Switches operate at 180°, resulting in 180-degree out-of-phase inductor currents [3]. The sum of inductor currents, which has a slight peak-to-peak variation and a frequency double that of lone inductor currents, is the incoming current to filter capacitor C1 and load. Current splits into parallel pathways, resulting in lower conduction losses with fewer switches. This Interleaved Bidirectional converter will also operate in two modes i.e., Forward & Backward mode. In forward mode, the converter performs as “Boost converter” & in backward mode the converter performs as “Buck converter”.

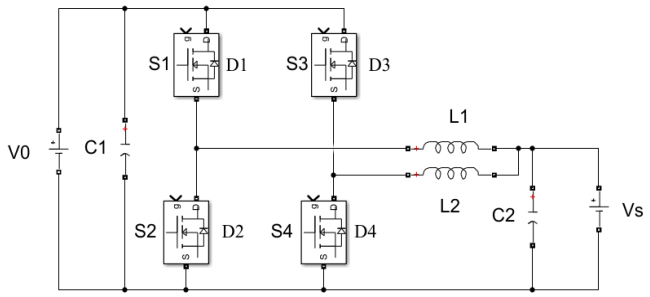

Figure 3.1. Schematic diagram of Interleaved Bidirectional dc-dc converter

3.1 Boost mode of operation (Forward mode)

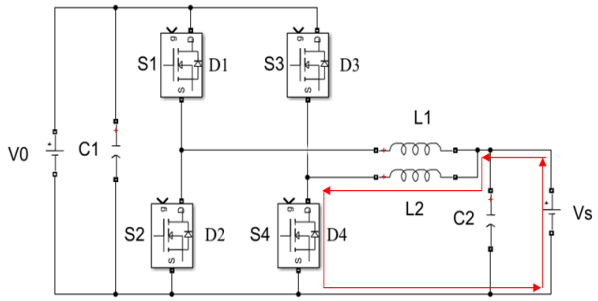

Figure 3.1.1.when S4 is ON

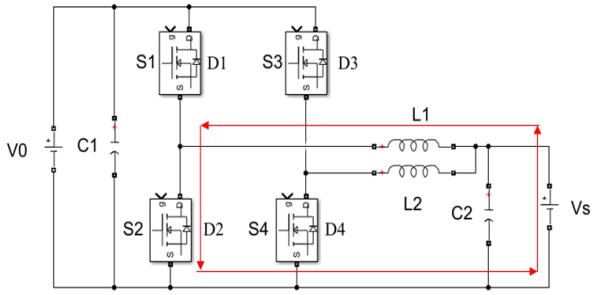

Figure 3.1.2.when S2 is ON

In this mode, S2 & S4 are ON and S1& S3 are OFF. D2 & D4 are reverse biased D1 & D3 are forward biased. The current inductors L1 & L2 increase linearly. To deliver electricity to the load, the battery discharges.

3.2 Buck mode of operation (Backward mode)

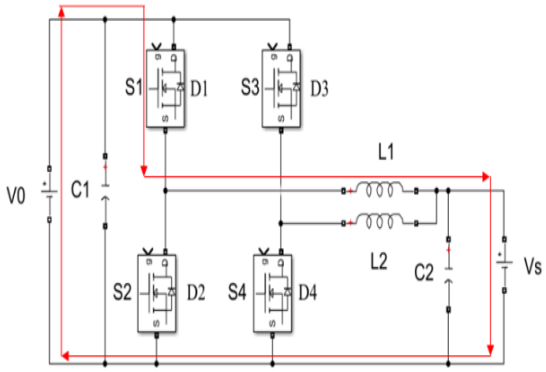

Figure 3.2.1. when S1 is ON

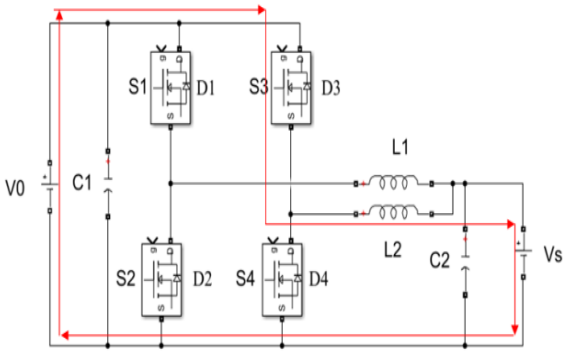

Figure 3.2.2.when S4 is ON

In this mode, S1 and S4 are ON and S2 & S3 are OFF. D1 & D4 are reverse biased and D2 & D3 are forward biased. The power flow is reversed from the load to charge the battery. The

inductor current will turn negative as the power flow reverses. The battery is charged from the load during regenerative braking in this mode.

3.3 Converter Design Calculations

The output voltage for Interleaved Bidirectional Buck-Boost converter is obtained by (3.3.1)

$$Vo = \frac{Vs}{(1-D)} \tag{3.3.1}$$

Inductor ripple current & Voltage ripple can be calculated by using (3.3.2) & (3.3.3)

$$\Delta Il = \frac{(Vs-Vo)(1-D)}{L(2f)} \tag{3.3.2}$$

$$\Delta Vc = \frac{VsD}{32Lf^2C} \tag{3.3.3}$$

Inductor and Capacitor values can be calculated using (3.3.4) & (3.3.5)

$$L = \frac{DR}{4f} \tag{3.3.4}$$

$$C = \frac{VsD}{32Lf^2Vo} \tag{3.3.5}$$

Where V_o - output voltage, Vs - the input voltage, D - duty ratio, f - switching frequency, L - Inductor, R - equivalent resistance, and C - capacitor.

4. SIMULATION MODEL AND SIMULATION RESULT OF BIDIRECTIONAL BUCK/BOOST DC-DC CONVERTER

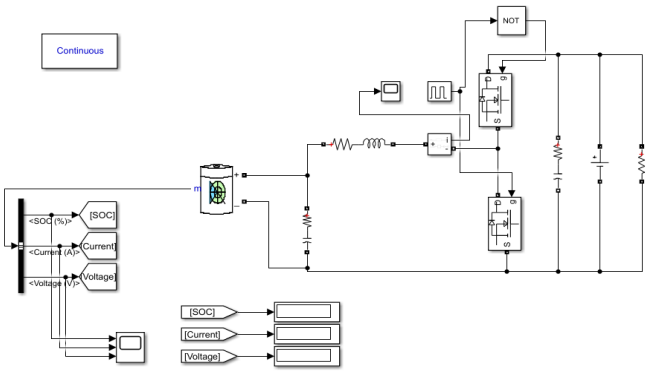

Figure 4.1.Simulation model of Bidirectional converter

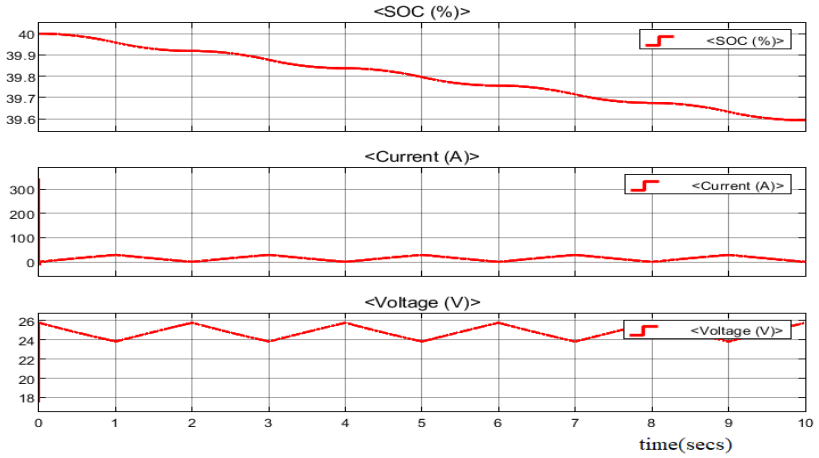

Figure 4.1.2.Simulation results of discharging mode
With SOC – 39.59%, Current – 3.527e-5A, Voltage – 25.76V

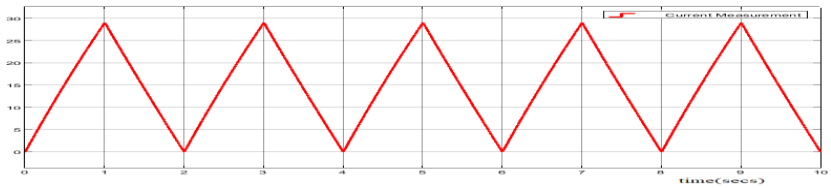

Figure 4.1.3. Inductor current ripple of L (Boost mode)

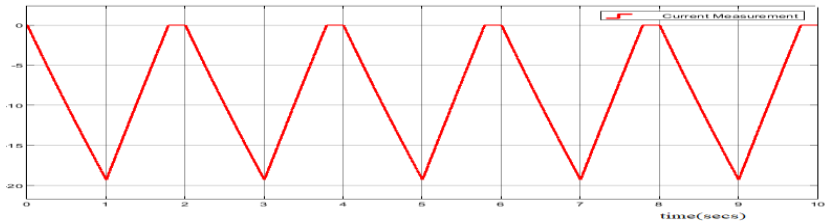

Figure 4.1.4. Inductor current ripple of L (Buck mode)

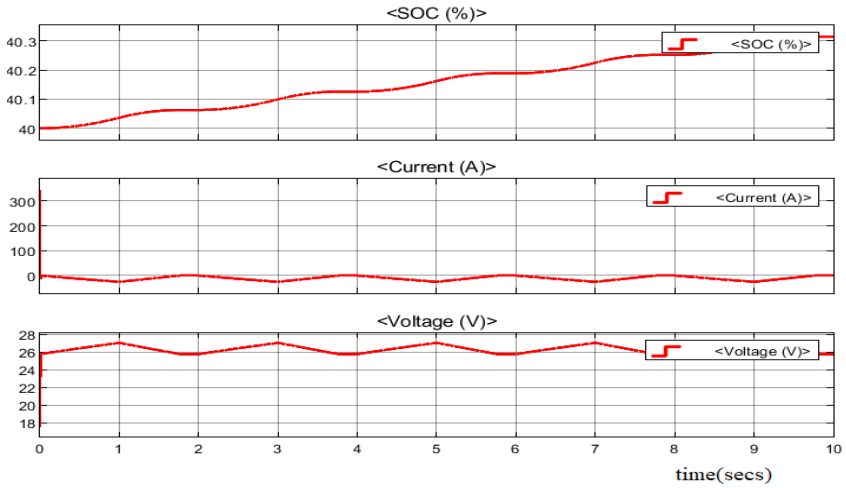

Figure 4.1.5.Simulation results of charging mode
With SOC – 40.31%, Current – 3.542e-5A, Voltage – 25.77V

5. SIMULATION MODEL AND SIMULATION RESULTS OF INTERLEAVED BIDIRECTIONAL BUCK/BOOST DC-DC CONVERTER

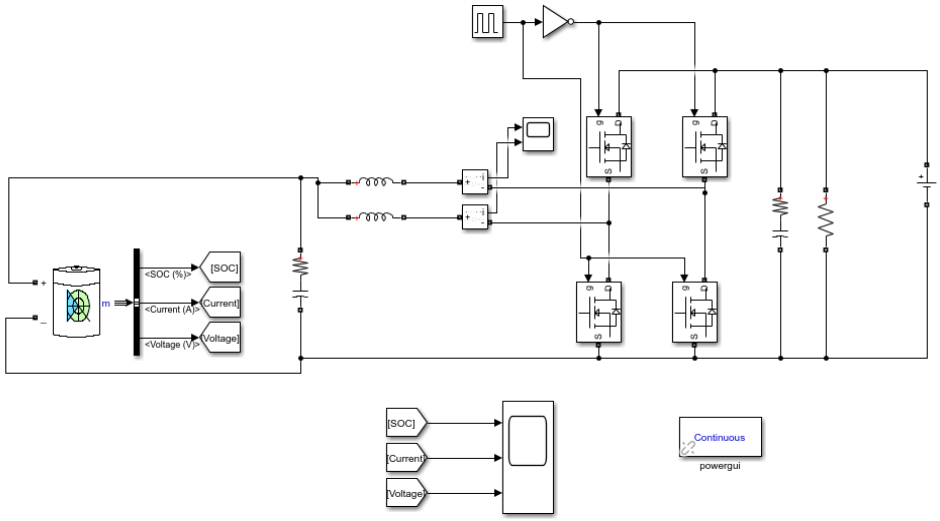

Figure 5.1.Simulation model of Interleaved Bidirectional converter

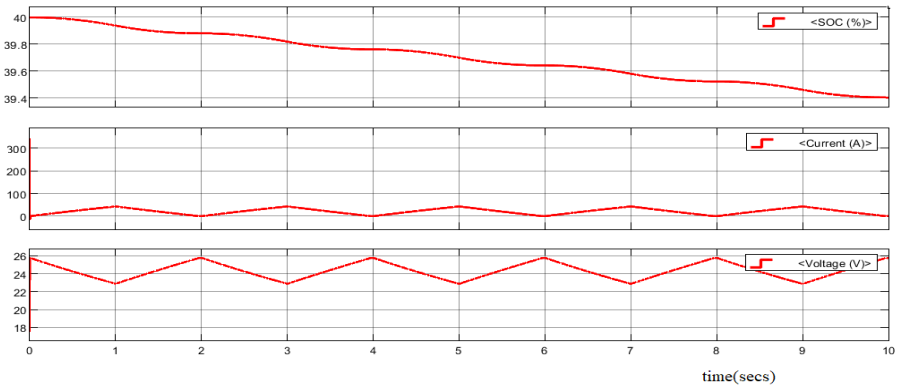

Figure 5.1.2. Simulation results of discharging mode
With SOC – 39.4%, Current – 7.046e-5A, Voltage – 25.76V

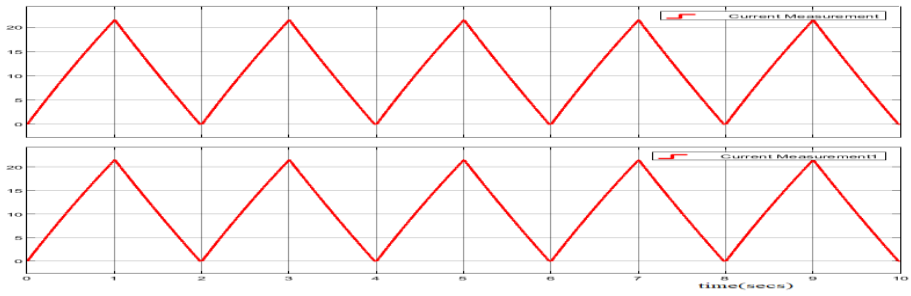

Figure 5.1.3. Inductor current ripple of L1 & L2 (Boost mode)

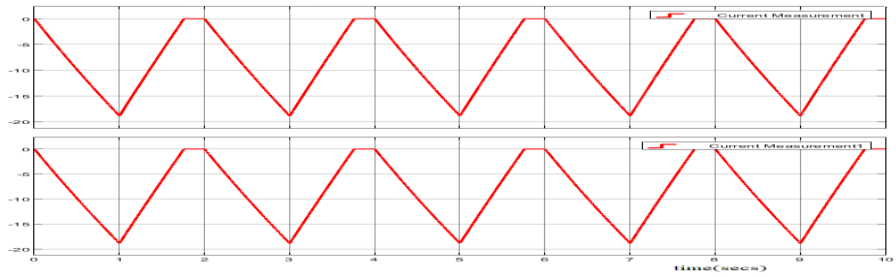

Figure 5.1.4. Inductor current ripple of L1 & L2 (Buck mode)

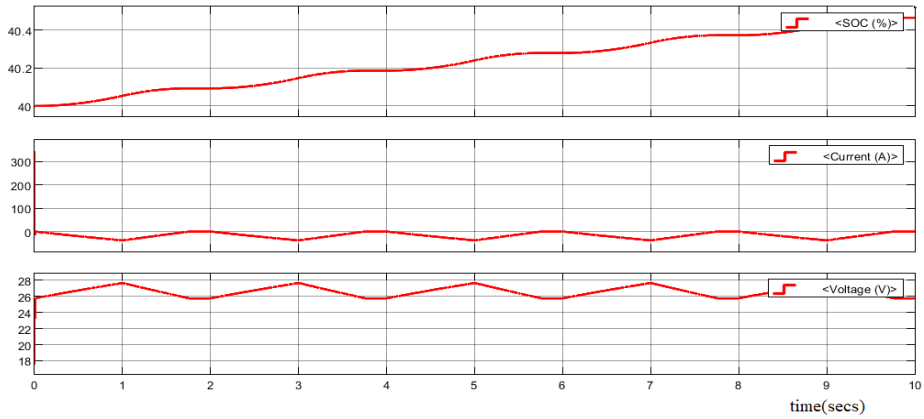

Figure 5.1.5. Simulation results of charging mode
With SOC – 40.37%, Current – 7.059e-5A, Voltage – 25.77V

5. COMPARISON BETWEEN BIDIRECTIONAL AND INTERLEAVED CONVERTER

Parameters	Bidirectional Buck-Boost	Interleaved Bidirectional Buck-Boost
Input Voltage	24V	24V
No of switches	2	4
Inductor	1	2
Voltage stress	48.02V	48V
Current stress	25.2	18.8
Current Ripple	9.65	9.35

Table 6.1.Comparison table of Bidirectional and Interleaved Bidirectional DC-DC converter

7. CONCLUSION

The comparison of a “Bidirectional Buck/Boost converter” and an “Interleaved Bidirectional Buck/Boost converter” is presented in this manuscript. Through mathematical analysis and simulation results, these two converters are analyzed. The voltage ripple and current ripple are reduced by using interleaved technique thus increasing efficiency & switching losses are also reduced, whereas in bidirectional dc/dc converter voltage ripple & current ripple are more. By using interleaved technique current and voltage stresses are also reduced. The “Interleaved Bidirectional DC-DC Converter” is highly suitable for an EV application, as per simulated results.

8. REFERENCES

[1] Viswanatha V, Venkata Siva Reddy R, "Microcontroller based bidirectional buck-boost converter for photo-voltaic power plant", Journal of Electrical Systems and Information Technology 5(2018).

[2] Akash Pathak, Vikas Sahu, "Review & Study of Bidirectional of DC-DC Converter Topologies for Electric Vehicle Application", International Journal of Science, Engineering and Technology 2015.

[3] Akshay Chandekar, Jobin Joseph, Jonathan Fernandes, Emmanuel Raj, "Design and Simulation of Two-Phase Interleaved Bidirectional DC to DC Converter", International Journal of Advance Research in Science and Engineering, March 2018.

[4] Ahmed M. Omara, M. Sleptsov, "Bidirectional Interleaved DC/DC Converter for Electric Vehicle Application", IFOST-2016: Mechatronics, Electrical Engineering, and Power Electronics.

[5] Deepak Ravi, Bandi Mallikarjuna Reddy, Shimi S.L, Paulson Samuel," Bidirectional dc to dc Converters: An Overview of Various Topologies, Switching Schemes and Control Techniques**",** International Journal of Engineering & Technology 2018.

[6] Kostiantyn Tytelmaier, Oleksandr Husev, Oleksandr Veligorskyi, Roman Yershov, "A Review of Non-Isolated Bidirectional DC-DC Converters for Energy Storage Systems", International Young Scientists Forum on Applied Physics and Engineering 2016.

[7] Rodnei Regis de Melo, Fernando Lessa Tofoli, Sergio Daher, Fernando Luiz Marcelo Antunes, "Interleaved bidirectional DC–DC converter for electric vehicle applications based on multiple energy storage devices", Springer-Verlag GmbH Germany, part of Springer Nature 2020.

[8] Yun Zhang, Yongping Gao, Jing Li, Mark Sumner**,** "Interleaved Switched-Capacitor Bidirectional DC-DC Converter with Wide Voltage-Gain Range for Energy Storage Systems", IEEE Transactions on Power Electronics 2017.

[9] Seema Jadhav, Neha Devdas, Shakila Nisar, Vaibhav Bajpai, "Bidirectional DC-DC converter in Solar PV System for Battery Charging Application**",** 2018 International Conference on Smart City and Emerging Technology (ICSCET)**.**

COMPARITIVE ANALYSIS OF HIGH GAIN NON-ISOLATEDCONVERTERS FOR DC MICROGRID

Malathi.S.N and Dr. Rashmi

Siddaganga Institute of Technology, Tumakuru, Karnataka, India
snmalathi014@gmail.com and rash_mysore@sit.ac.in

Abstract.

DC microgrids are becoming most popular because of easier interconnection of non-conventional energy sources like photovoltaic array, batteries and fuel cells. It is obvious fact that the output voltage generated by these sources are low, therefore it is necessary to overcome this drawback by selecting a suitable DC-DC converter with high gain and works effectively. Further, the different types of non-isolated DC-DCconverter with high gain is proposed by avoiding a technique of voltage multiplier cell. The converters consist of certain number of switches which operates in different duty ratio. The simulation work is carried out using PSIM software tool and analysis is carried out for different conditions.

Keywords. DC Microgrid, Non-isolated Converters High Gain Converter, Photovoltaic Array, Batteries and Fuel Cells.

1. Introduction

DC Microgrid methodology is tremendously increasing its importance due to the local power generation. The voltage produced by DC power sources like DC generators, solar panels, batteries and fuel cells are quite low[2.5]. Therefore, it is necessary to use high gain efficient DC-DC converters in order to match the requirements of DC loads. Recently the high gain converters are widely used in various fields like battery charging system and uninterrupted power supplies in addition to renewable energy field[1.2].

In order to increase the DC input voltage, the conventional method is using of boost converter. Even though the boost converter increases input voltage, the switching stress is very high. Therefore, it is necessary to use high rating switches[2.3]. Also, the duty cycle requirement is very high which increases additional losses like power dissipation. Several isolated converters produce high gain but because of presence of transformer these become bulky and costly.

To achieve high voltage gain, the non-isolated DC-DC converters are used which reduces switching stress, size and cost.

In this paper, the different types of non-isolated high gain converters are analyzed with modes of operation. These converters are designed for some output voltage by selecting some input voltage and switching frequency. The parameters like duty cycle requirement, gain factor, inductors, capacitor, voltage stress and current stress are compared with conventional boost converter.

2. Proposed converters

2.1. Boost converter

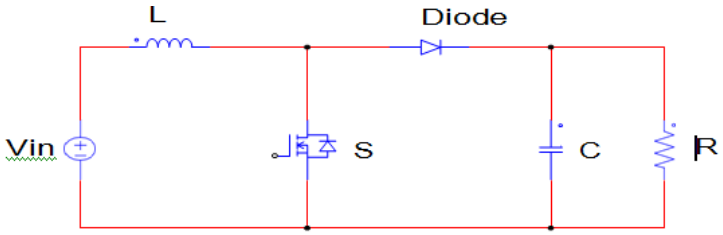

Figure 2.1. Circuit of Conventional Boost Converter

The circuit topology of step-up DC-DC converter is as shown above [2]. It consists of input voltage source Vin , inductor L, capacitor C , MOSFET, diode and load resistor R. It can be operated in two modes. In the first mode, the MOSFET switch is ON, therefore diode is reverse biased. The equivalent circuit is as shown in fig. 2.2.

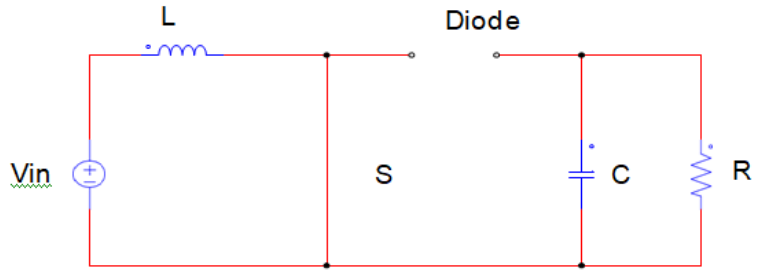

Figure 2.2. Equivalent Circuit of Conventional Boost Converter when Switch S is closed

Further in the next mode, the MOSFET switch will be OFF therefore the inductor current forces diode to operate.The equivalent circuit is as shown below:

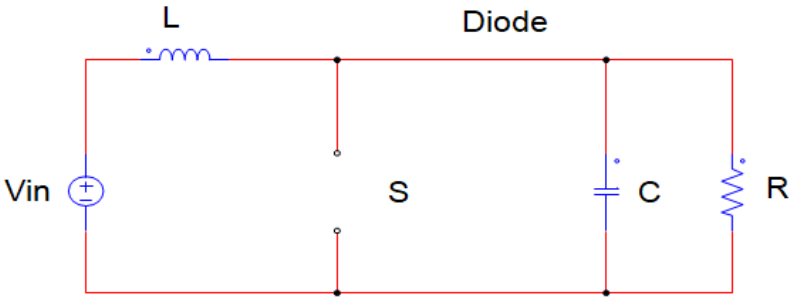

Figure 2.3. Equivalent Circuit of Conventional Boost Converter when Switch S is opened

2.2. *Non-isolated converter 1*

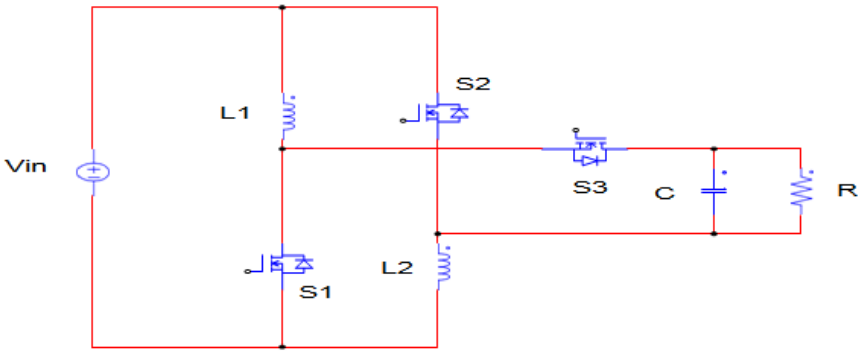

Figure 2.4. Circuit Diagram of Non-isolated Converter 1

The circuit topology of non-isolated converter 1 is as shown in fig.2.4. It consists of an input voltage source Vin, a pair of inductors L_1 and L_2 with equal values, capacitor C and three MOSFET switches (S_1, S_2 and S_3) [3.5].

In the first mode, the switches S_1 and S_2 will be ON, the equivalent circuit is as shown below. Here both the inductors are connected in parallel and it is equal to input voltage. The capacitor is connected across load resistor and starts discharging

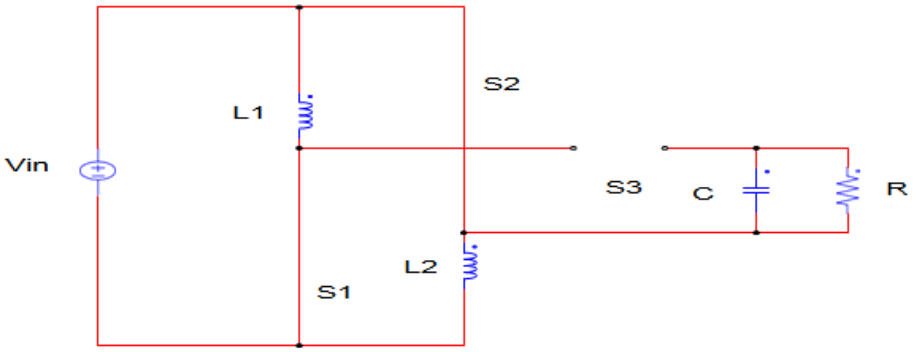

Figure 2.5. Equivalent Circuit when S_1 and S_2 are Closed

In the second mode, the switches S_1 and S_2 will be OFF, S_3 will be ON. The equivalent circuit is as shown in fig.2.5.The input voltage is obtained across load terminals via switches S_3. The capacitor starts charging.

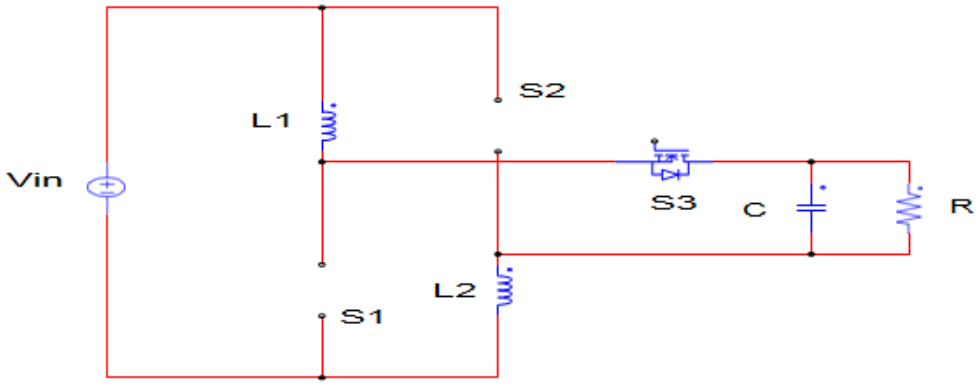

Figure 2.6. Equivalent Circuit when S_3 is Closed

2.3. *Non-isolated Converter 2*

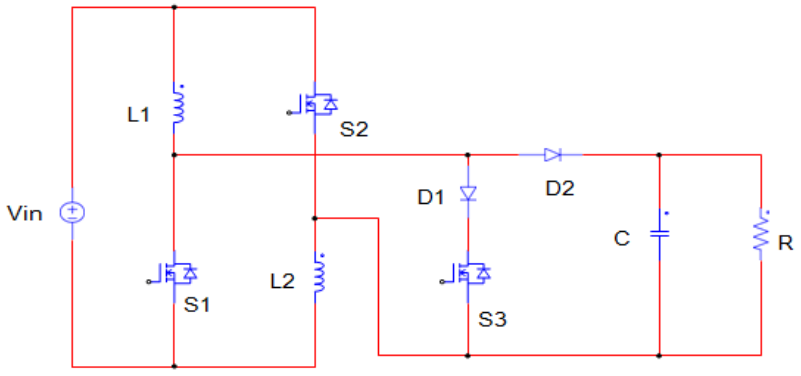

Figure 2.7. Circuit Diagram of Non-isolated Converter 2

It is also similar to non-isolated converter 1. Further, it includes input voltage source V_{in}, a pair of inductors L_1 and L2, Capacitor C, three MOSFET switches S_1, S_2 and S_3 and diodes D_1 and D_2. This can be operated in three mode.In the first mode the switches S_1 and S_2 will be ON and S_3 will be OFF[5.6]. Here both the inductors are connected in parallel and having equal values. The voltage across both the inductors will be same as input voltage. The capacitor connected across load resistor and starts discharging. The diodes are reverse biased [3.6].

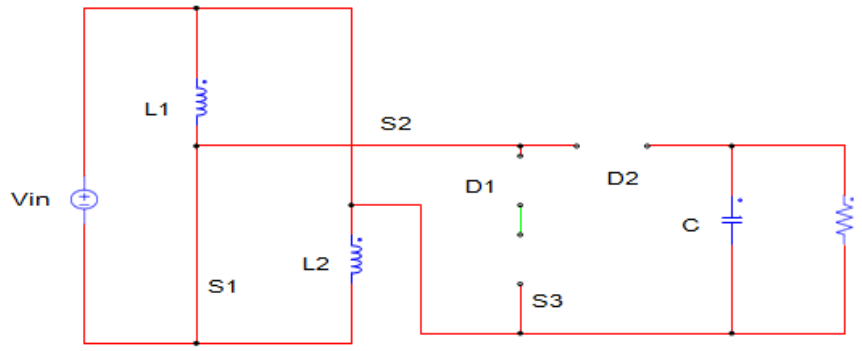

Figure 2.8. Equivalent Circuit when S_1 and S_2 are ON and S_3 is OFF

In the second mode the switches S_1 and S_2 will be OFF and S_3 will be ON. Hence the diode D_1 is forward biased and D_2 is reverse biased as shown in equivalent circuit below. The capacitor is connected across load resistor R and startsdischarging.

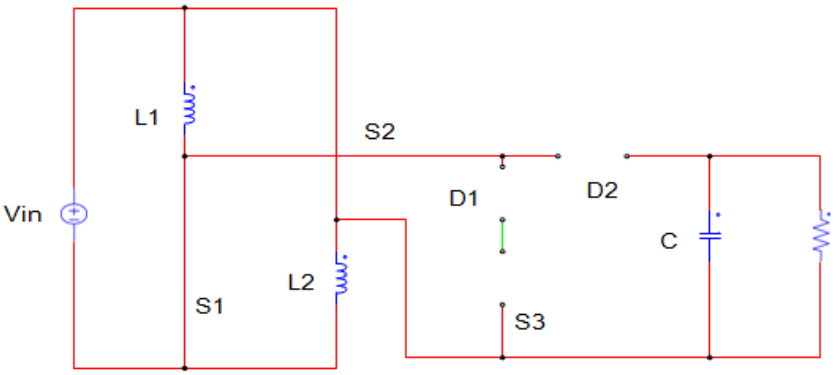

Figure 2.9. Equivalent Circuit when S_1 and S_2 are OFF and S_3 is ON

In the third mode, all the switches will be OFF, the diode D_1 is reverse biased and diode D_2 is forward biased as shown in Fig.2.9. The input voltage is obtained across load terminals through diode D_2. The capacitor starts charging during this mode[2].

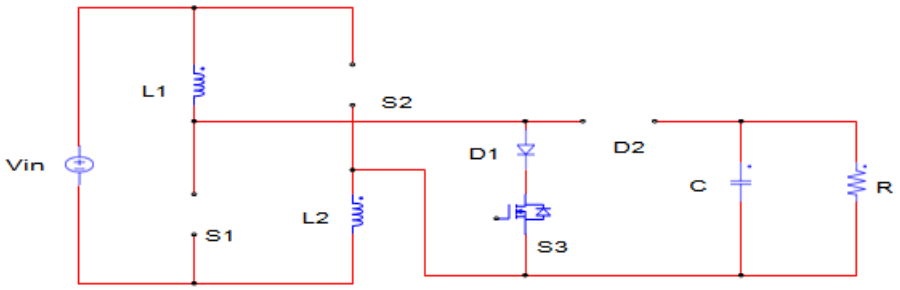

Figure 2.10. Equivalent Circuit when S_1,S_2 and S_3 will be OFF

3. Results and discussions

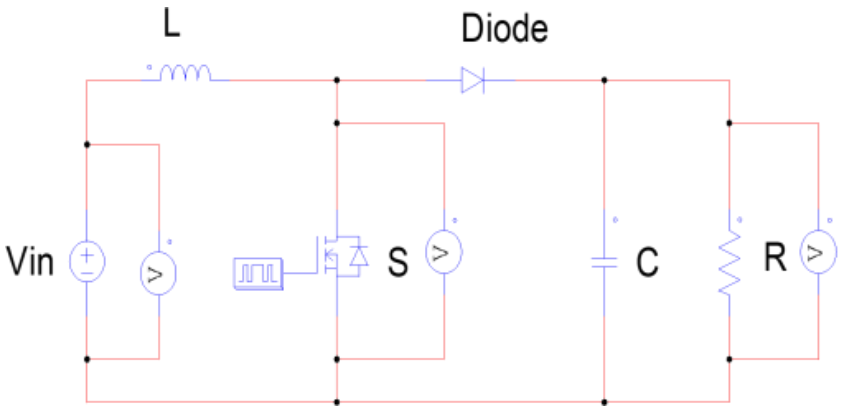

Conventional boost converter

Figure 3.1. Simulation Model of Conventional Boost Converter

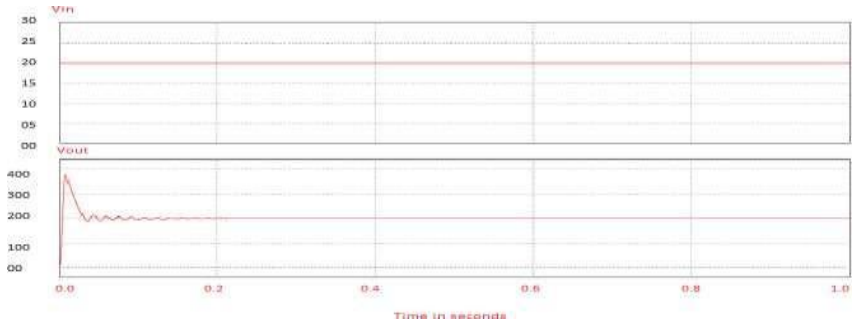

Figure 3.2. Input and Output Voltage Waveform of Boost Converter

The Fig. 3.2 shows waveforms of input and output voltage of conventional Boost converter with input as 20V andoutput as 200V [2]

Figure 3.3. Simulation of conventional Boost Converter (SWITCH WAVEFORMS)

The Fig 3.3 shows waveforms of switch current and voltage of conventional Boost converter.The switching currentis 5A and voltage across the switch is 200V which is equal to output voltage.

Simulation Model of Non-isolated Converter 1

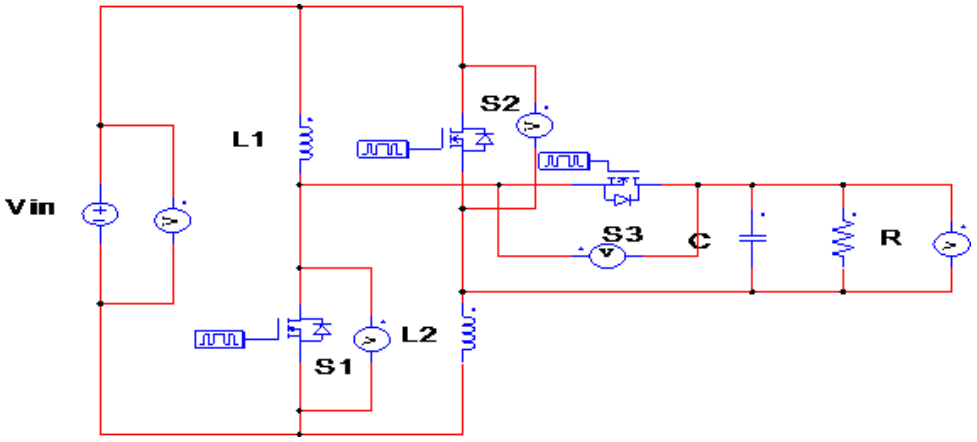

Figure 3.4 Simulation model of non-isolated converter 1

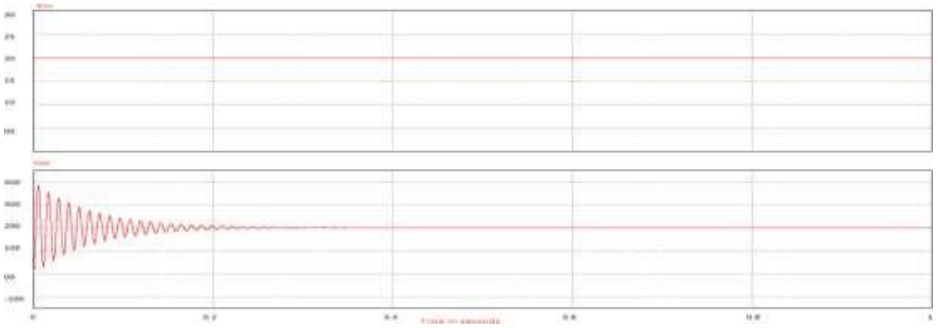

Figure 3.5. Simulation Results of Non-isolated Converter 1

The Fig.3.5 shows waveforms of i/p and o/p voltage of proposed DC-DC converter withinput as 20V and output as200V.

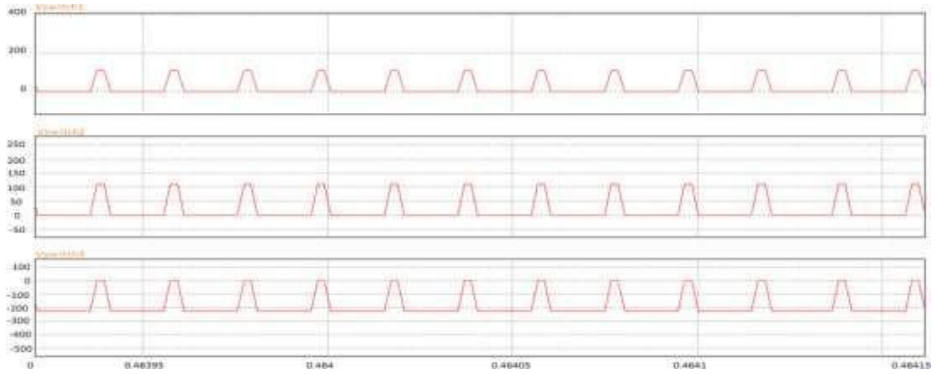

Figure 3.6. Simulation Results of Non-isolated Converter 1(Voltage Stress)

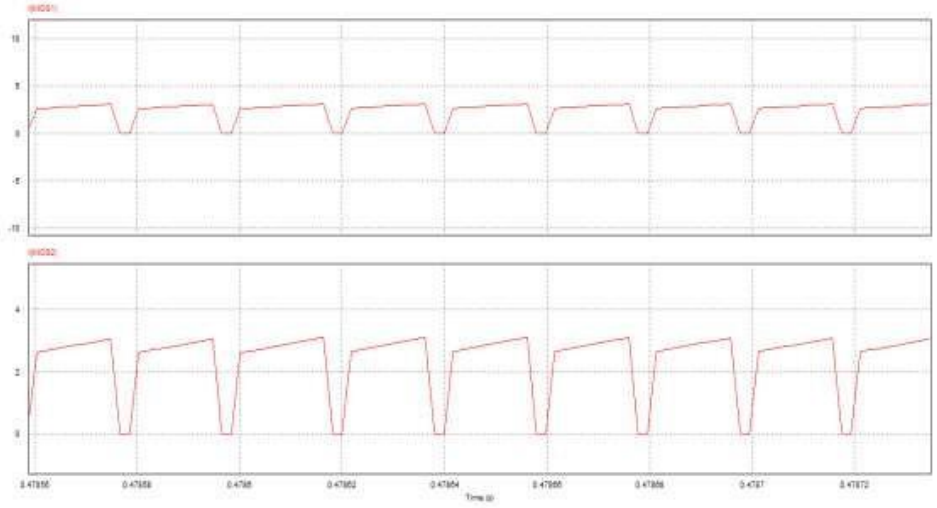

The Figure 3.7. Simulation Results of Non-isolated Converter 1(Current Stress)

Simulation Model of Non-isolated Converter 2

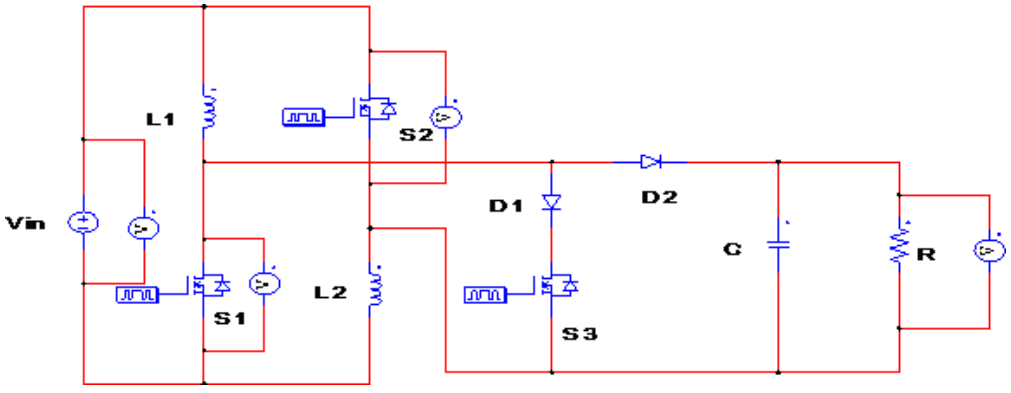

Figure 3.8. Simulation Circuit Model of Non-isolated Converter 2

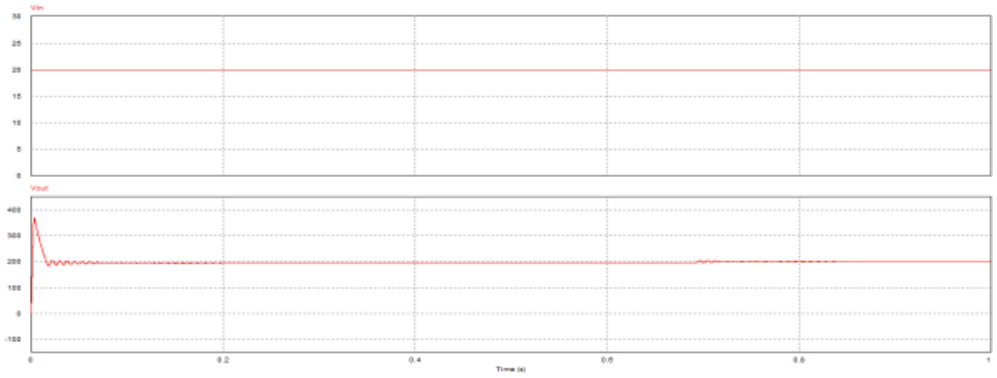

Figure 3.9. Simulation Results of Non-isolated Converter 2 (i/p and o/p Voltage)

The Fig.3.9 shows waveforms of input and output voltage of proposed converter 2 with i/p as 20V and o/p as200V.

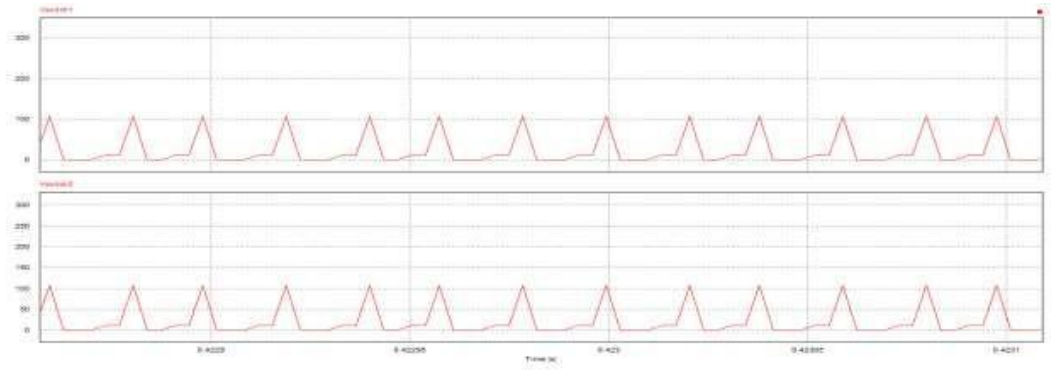

Figure 3.10 Simulation of Non-isolated Converter 2(Voltage Stress)

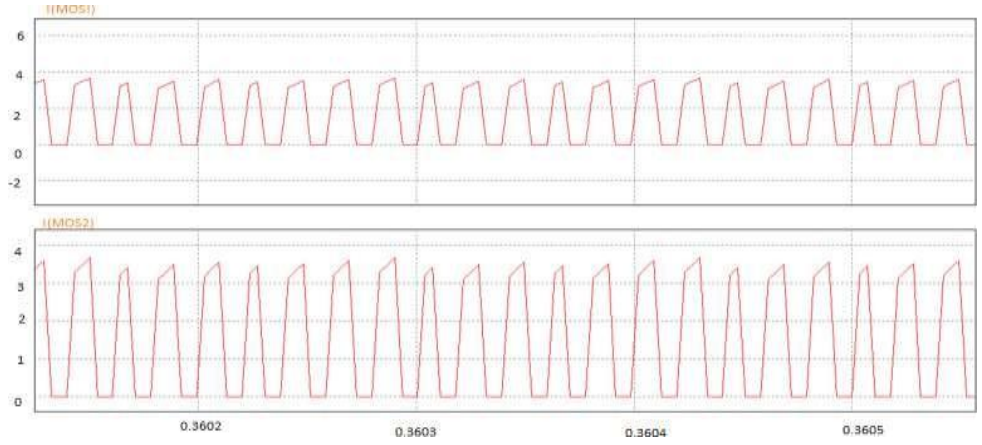

Figure 3.11 Simulation of Non-isolated Converter 2(Current Stress)

The Fig.3.10 and 3.11 shows the waveforms of switch voltage and current of proposed DC-DC converter 2. Theswitching current is 3.5A and voltage across the switch is 100V which is equal to half of o/p voltage [2].

4. Comparison of conventional boost converter, non-isolated converter 1 and non-isolated converter 2

In the present study, the distinct converters for DC micro grid are simulated using PSIM. The input voltage is taken as 20V and output voltage is designed for 200V with a switching frequency of 50kHz.The various parameters of different converters is as given below [1.2]:

SI NO.	Parameter	Conventional Boost Converter	Non-isolated Converter 1	Non-isolated Converter 2
1	Input Voltage	20	20	20
2	Output Voltage	200	200	200
3	Switching Frequency (KHz)	50	50	50
4	Duty Cycle	0.9	0.818 1	0.5
5	Gain Factor	1/(1-D)	(1+D)/(1-D)	$(1+D_1)/(1-D_1-D_2)$
6	Inductor (in µH)	720	650	360
7	Capacitor (in µF)	90	82	50
8	Voltage across Switch (in volts)	200	100	100
9	Current stress in Switch (in Amps)	5	3.5	3.5

5. Conclusion

In this paper, various types of DC-DC converters are analyzed and represented to obtain maximum possible voltagegain.

From the simulation results it is observed that,

- The conventional DC-DC boost converter is designed 200V output from 20V input. Here the duty cycle required is 0.9 to achieve required voltage. The voltage and current stress is also high and becomes bulky due to large values of passive elements like inductors and capacitor.

- Because of the above drawbacks, the non-isolated converter 1 is designed for the same output 200V from 20V. Here it is observed that duty cycle requirement reduces. Comparatively the size of passive elements also reduces. The voltage & current stress reduces to some extent.

- The non-isolated converter 2 is also designed for same output 200V from 20V. It is observed the duty cycle requirement still reduces and stress also reduces.

- Because of this the conventional boost converter has limited application. The non-isolated converter 1 can be used for standalone applications. The non-isolated converter can be used for high power applications because of low switching stress.

6. REFERENCES

[1] M. Lakshmi and S. Hemamalini, "Non-isolated High Gain DC–DC Converter for DC Microgrids," in IEEETransactions on Industrial Electronics, vol. 65, no. 2, pp. 1205-1212, Feb. 2018.

[2] K.V. Suresh, K.U. Vinayaka, N.V. Jyothi. “Chapter16 Comparitive analysis of high gain transformer less DC-DCConverter for DC microgrid”, Springer Science and Business media LLC-2022.

[3] Fernando Lessa Tofoli and D. C. Pereira and W. J. de Paula and Demercil de Souza Oliveira,“Survey on non-isolated high-voltage step-up dc–dc topologies based on the boost converter,” Iet Power Electronics 2015.

[4] S. Khan, A. Mahmood, M. Tariq, M. Zaid, I. Khan and S. Rahman, "Improved Dual Switch Non-Isolated High Gain Boost Converter for DC microgrid Application," 2021 IEEE Texas Power and Energy Conference (TPEC), 2021.

[5] S. Singh, S. Ghosh, S. Sathiyamurthy, N. Tewari, M. J and V. T. Sreedevi, "Performance Evaluation of a High Gain DC-DC Converter for DC Microgrid Applications," 2020 IEEE Region 10 Symposium (TENSYMP), 2020, pp.

[6] Srivastava, Shivam and Chattopadhyay, Oiheek and Athikkal, Sivaprasad and Majumdar, Indeevar and Peter, Joseph, A Non Isolated High Gain DC-DC Converter for DC Microgrid Application (May 4, 2020). International Journal of Electrical Engineering and Technology, 11(2), 2020.

[7] Pandey, A., Pattnaik, S. (2022). Single Switch Non-isolated High-Gain Converter with Reduced Voltage Stress.In: Gupta, A.R., Roy, N.K., Parida, S.K. (eds) Power Electronics and High Voltage in Smart Grid. Lecture Notesin Electrical Engineering, vol 817. Springer, Singapore.

Biographies

Malathi S N, received the bachelor's degree in Electrical and Electronics Engineering VTU in 2012, pursuing the Master's degree in Power Electronics from Siddaganga Institute of Technology.

Dr. Rashmi, working as professor and Head in the Department of Electrical & Electronics Engineering, SIT, Tumkur, having total of 23 years of teaching experience, published 17 research papers in international journals, presented 25 numbers of research papers in national and international conferences. She is guiding 3 Ph.D. students and has guided 15 number of M.Tech. Projects and guided 30 UG projects.

.

Islanding Detection Scheme for Grid-Connected PV System Using AI Technique

Ashok Valabhoju*, Shiva Rama Krishna Prasad L, B Kiran Kumar,

B Pradeep Kumar

Kakatiya Institute of Technology & Science Warangal, Telangana, India-506015

*ashokjntuk@gmail.com, shivalingabathini@gmail.com , bkk.it@kitsw.ac.in, pradeep301327@gmail.com

Abstract.

In recent days, the solar photovoltaic (PV) system is one of the utmost renewable energy systems in the existing power system which will improve grid dependability. There is an adverse effect on the PV system on the grid, when the main grid power supply to the local/remote loads is interrupted and then there is a percentage of the load is supplied through the PV system. This paper presents the detection of the islanding state using the DWT-ANN approach. The voltage signals and current signals at the point of common coupling (PCC) bus and load bus are considered to detect the condition. Simulation study has been performed using MATLAB / Simulink software, and the results indicate that the proposed DWT – ANN based scheme is reliable.

Keywords. Photo Voltaic (PV) System, Artificial Neural Network Method (ANN), Islanding detection.

1. INTRODUCTION

Distributed generation (DG) connections such as solar plants, wind turbines, fuel cells, etc., to a system that has greatly increased the demand for clean energy is increasingly found. A few problems arose before the DG became part of the most important grid [1].

The unintentional discovery of an island in a connected DG grid is one of the biggest challenges that event events can be relied upon. It explained, "A situation in which a specific component system includes both distributed power resources (DER), and loads that remain dynamic while separated from the rest of the system in use" [2]. Unexpectedly, existing on the islanding causes serious problems, including:

- Maintenance of power and frequency range within acceptable limits of normal standards,
- Supplying loads in DG units will create threats on the line of personnel safety, as well,

- DG unit reset is out of phase which results in immediate reset. Therefore, in the most important energy system to find the occurrence of an islanding.

The means of finding an island are broadly divided into 2 types namely remote islanding scheme and local islanding scheme. Additionally local methods, distinguishing between active and passive: Passive routes have a lot of uninspected territory (NDZ) and depend on the unfavourable situation to identify the island. Effective methods have low NDZ [3], apart from that it causes addition of harmonics.

2. POWER SYSTEM EXPLANATION

This proposed scheme, must classify or discriminate islanding conditions with non-islanding conditions in order to obtain reliable islanding conditions. Non-island conditions such as faults [1] etc.

It has been recorded the desired three-phase voltages and currents on the grid bus and PV bus distinctively each/every simulation event. Generated for each case a data set of 50 cases each and a total of 200 cases of data set from PV bus and also at grid bus under fault condition, and islanding condition separately. These 200 cases of dataset have been processed through lowpass filter to reduce the noise from electrical signals, and are Extracted feature by DWT. Input dataset has been trained with corresponding targets using DWT-ANN modules. So, then the DWT-ANN modules have been designed based on Levenberg-Marquardt (LM) algorithm to reduce learning error.

3. FAULT DETECTION SCHEME FOR GRID-TIED PV SYSTEM

There is different type of faults like LG, LLG, LLLG, LLL, open-circuit etc. Assumed LG's fault for this proposed approach to discriminate faults and islanding conditions. To produce 50 sets of data by changing the fault inception time and by varying islanding situations in the power system network. For each and every case such as islanding situation or/and fault situation, measured voltage and current signals at the PV bus and grid bus. Fig.1. shows the voltage and current signals on the grid bus (B120) and Fig.2. shows current voltages and signals on PV bus (B25) at fault condition at 1.25 seconds respectively.

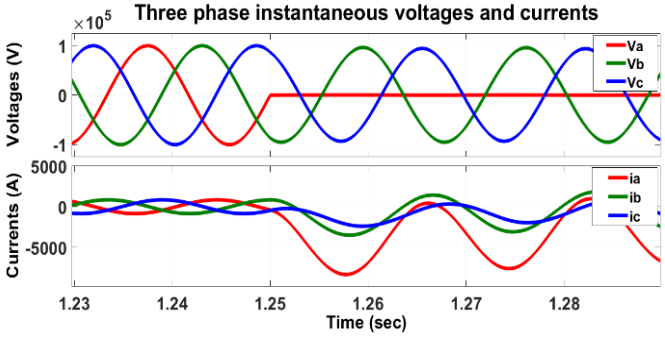

Fig.1. 3-phase signals at fault inception time-1.25sec at Grid bus (B120): (a). voltage waveform (b). current waveform

The LG fault has been applied between phase A and the ground which is the reason why the phase A power becomes zero and the current phase A raises its peak to at the grid bus after the fault shown in Fig. 1. In the PV bus, the three-phase voltage and current signals are replaced by the amplitude of the voltage signals decreases and the magnitude of the current signals increases as shown in Fig.2.

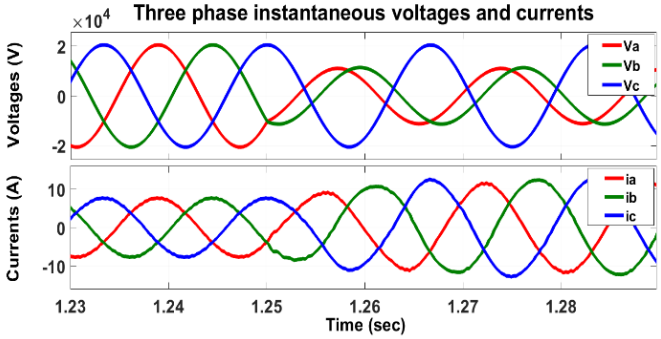

Fig.2. 3-phase signals at fault inception time-1.25sec at PV bus (B25): a) voltage waveform b) current waveform

4. ISLANDING DETECTION SCHEME FOR GRID-CONNECTED SOLAR PV SYSTEM

There are different methods to identify an islanding condition in which is an effective and passive method [4]. Functional methods are Sandia frequency shift [5], Active slip frequency [6], Active Frequency Drift [7-8], DG voltage variation [9], and a mixed analysis method with current d injection -axis [10]. The passive islanding method is proposed in [11]. In this proposed scheme a grid side power turned off in the system using a circuit breaker, and produced 50 cases of dataset by changing the switching times of the circuit breaker. For each/every islanding case, measured the electrical voltage and current signals at the PV bus and grid bus. Fig.3. shows the voltage and current signals on the grid bus (B120), and Fig.4. shows the electric current and current signals on the PV (B25) bus during the island's first 1.25 seconds consecutive.

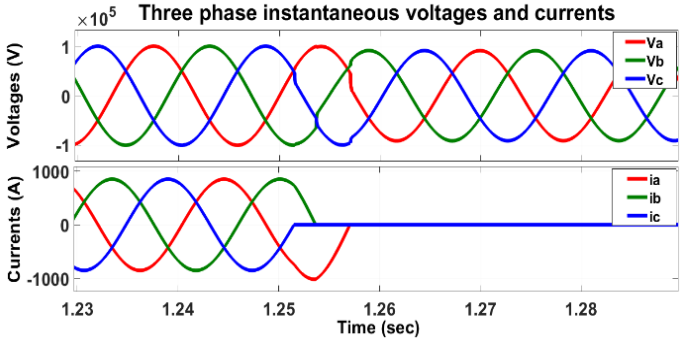

Fig.3. 3-phase signals at islanding situation with inception time -1.25sec at Grid bus (B120): a) voltage waveform b) current waveform

The grid disconnection to the PV system has been done by using the circuit breaker and noticed that the magnitude of the three-phase voltage signals decreased and the current three-phase signals became zero on the grid bus respectively shown in Fig.3. In the PV bus, the three voltage and current signals are altered as shown in Fig.4.

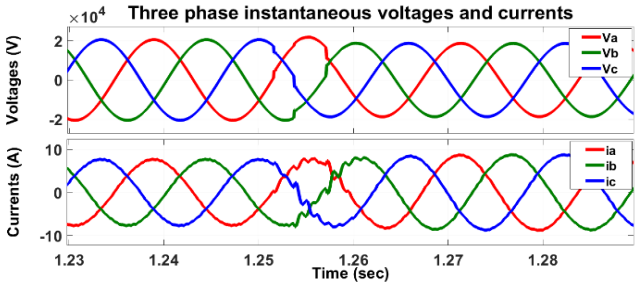

Fig.4. 3-phase signals at islanding situation with inception time-1.25sec at PV bus (B25): (a) voltage waveform (b) current waveform

5. PROPOSE DWT-ANN SCHEME

This proposed model consists of a DG (PV system), grid and conventional loads are connected with different type of loads in the power system network. Fig.5. shows a grid-connected SPV system block diagram where voltage/current signals are recorded at PCC. If any alteration or disruption occurs, and then it has been detected by the DWT-ANN module. Then, it should detect the islanding situation, and issues a trip signal to the circuit breaker to avoid damage caused by disturbance in the PV system and local loads.

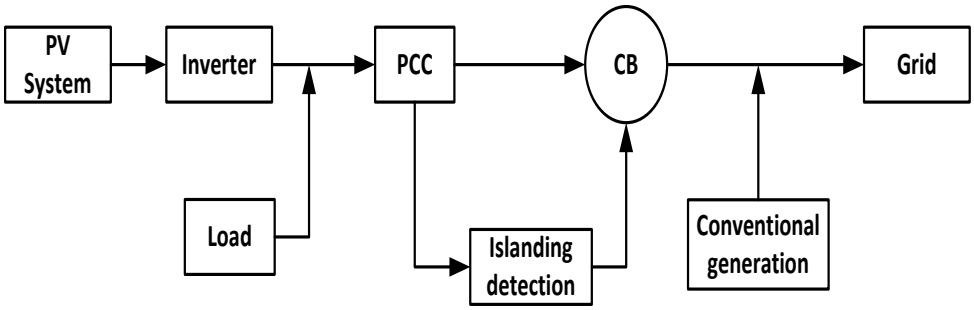

Fig.5. Block diagram of Grid-connected SPV system

6. DWT-ANN FOR THE GRID-CONNECTED SOLAR PV SYSTEM

The DWT-ANN has been trained using the feedforward network with Levenberg – Marquardt (LM) [12] with the input data set consisting of 200 cases. This dataset is also processed thereby considering a 2-cycle data window in which 1-cycle samples of the pre-fault and/or pre-islanding, and additionally 1-cycle samples of the post-fault and/or post-islanding situations. However, the standard deviation [13-14] of 2-cycle data window of three-phase voltage/current signals, at grid bus and PV bus for fault, and islanding situations of power system network have been taken as an input to train DWT-ANN module, and also considered the target vector '0' for fault scenario, and '1' for the islanding scenario during the training, testing, and validation cases with training of 70%, testing and validation of 15% of dataset considered respectively.

Fig.6. demonstrates the flow diagram of the proposed DWT-ANN approach. Total cases of 200 simulated and three voltages/current signals are recorded, and further, it is processed with the help of lowpass filter to eliminate the noise in the signals. Then after voltage/current signals have been pre-processed using DWT to extract features. An input dataset used to train/test DWT-ANN to detect the islanding condition. Numerous constraints have been used to produce input datasets for training/testing as reported in Table.1. The constraints particularly inception time, type of fault and islanding scheme, number of cases for islanding, and fault at the grid bus and PV bus are used for the training and testing of DWT-ANN modules.

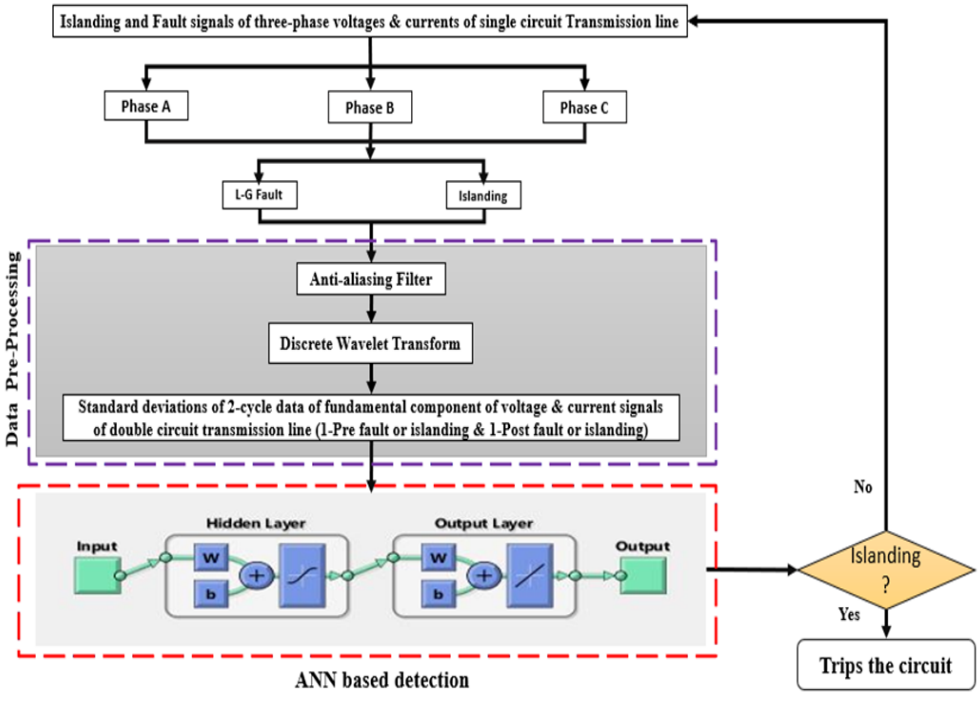

Fig.6. Flowchart of the Proposed ANN model

7. SIMULATION RESULTS

Subsequently designed the proposed DWT-ANN modules using the Levenberg – Marquardt (LM) algorithm in MATLAB software. Fig.7. shows a Simulink diagram of the PV system connected to the Grid.

The MATLAB code is used to train DWT-ANN which continues to use parameters such as performance goal, validation checks, number of neurons, number of layers in hidden layer, number of epochs (iterations) [15]. The training constraints which are reported to train the DWT-ANN network and recorded the (mean square error) MSE minimum. Performance of DWT-ANN module exhibits good response for the islanding detection.

For DWT-ANN module having one layer with 6 neurons, one outer layer with 6 neurons and one hidden layer with a different number of neurons that has provided to the feed-forward network at different situations. The DWT-ANN Feed-forward network has trained in the various architectures shown in Table.2 and its performance during training/testing with Epochs and MSE are illustrated in Fig.7.

From the performance graphs, can yield the best case by considering at training/testing and validation, where case 2 is the best possible one because of its 3 training patterns (i.e., training, testing and validation) that justifies the detection of islanding situations properly.

Table.1 Fault & islanding situations considered to produce the datasets for training & testing

S. No	Condition	Parameters	Training & Testing data
1	Fault	Fault type	AG
		Fault resistance	0.001
		Fault inception time	0.9-1.88 (in steps of 0.02)
		Voltage and Current signals recorded	At PV bus & Grid bus
		Total no. of cases	Training cases =70, Testing cases =30, Total no. of cases = 100
2	Islanding	Islanding type	Passive
		Islanding resistance	0.01
		Islanding inception time	0.9-1.88 (in steps of 0.02)
		Voltage and Current signals recorded	At PV bus & Grid bus
		Total no. of cases	Training cases =70, Testing cases =30, Total no. of cases = 100

Table.2. Training architecture of different cases of Feed forward ANN

Cases	1	2	3	4
Size of Input Dataset	6×200	6×200	6×200	6×200
Size of Architecture	6-15-6	6-20-6	6-25-6	6-30-6
No. of Epochs	975	192	446	391
Performance Goal	9.85e-5	9.98e-6	0.00199	0.00496
Training time(sec)	24	4	19	16
Mutation	2e-7	1e-5	5e-6	0.0001
Validation Checks	931	176	275	319

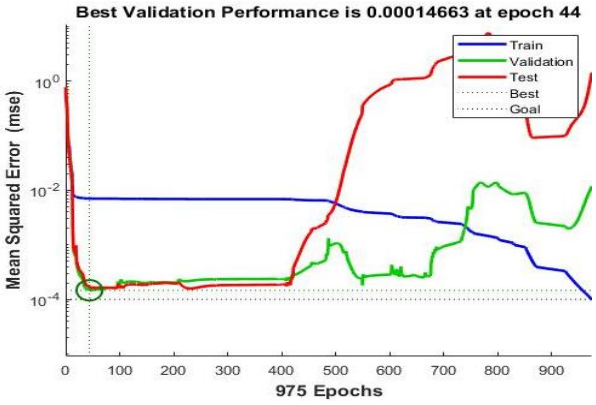

(a)

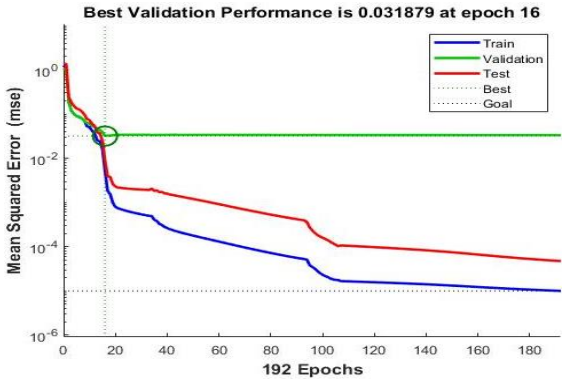

(b)

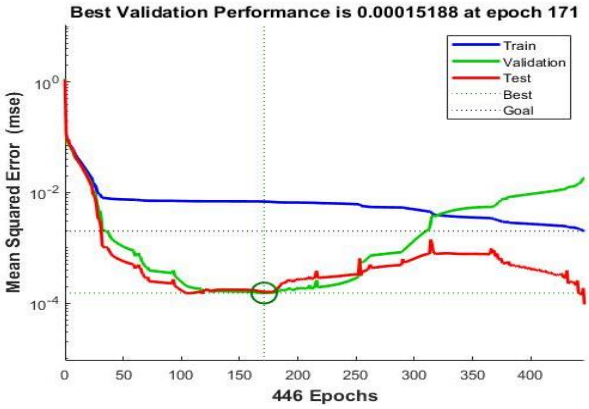

(c)

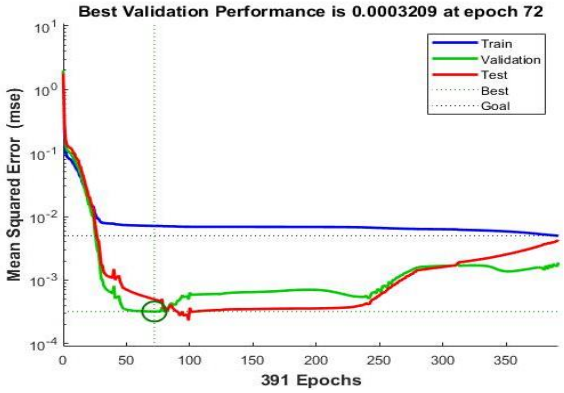

(d)

Fig.7. Performance Validation curves during ANN between Epochs and MSE (a) case 1 (b) case 2 (c) case 3 (d) case 4

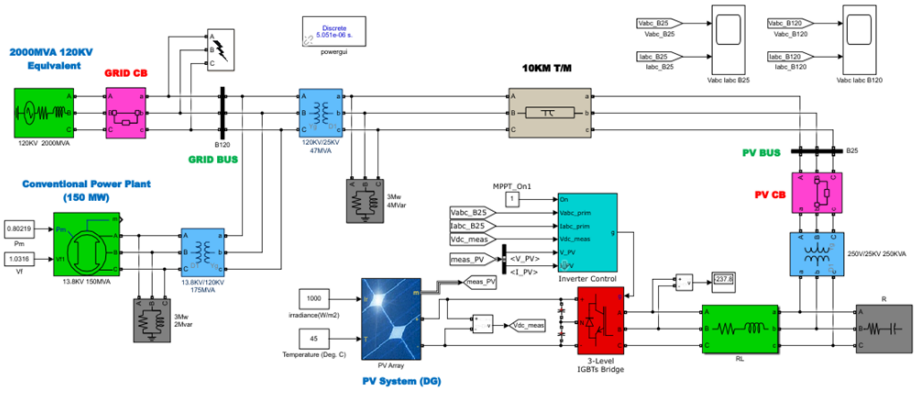

Fig.8. MATLAB Simulink diagram of Grid-Tied PV System

8. CONCLUSION

In this paper, proposed a DWT-ANN based islanding detection scheme by considering its current three-phase signals. The main purpose of DWT-ANN is that trained topology can be used in an effort to improve the performance and speed of the island detection system. To get the MSE is small, and the minimum MSE case should be given an additional process to get the system to get an accurate and quick response to finding an island situation reliably.

9. REFERENCES

[1] R. Nale, "A Transient Component Based Approach for Islanding Detection in Distributed Generation," IEEE Transactions on Sustainable Energy,2019.

[2]. Ruchita Nale and Monalisa Biswal, "Comparative Assessment of Passive Islanding Detection Techniques for Microgrid," 2017 International Conference on Innovations in information Embedded and Communication Systems.

[3]. Bokka Krishna Chaitanya, Anamika Yadav, Senior Member, IEEE and Mohammad Pazoki., "Reliable Islanding Detection Scheme for Distributed Generation based on Pattern-Recognition," IEEE Transactions on Industrial Informatics.

[4]. Tirta Samuel Mehang, Dedet Candra Riawan and Vita Lystianingrum B. Putri, "Islanding Detection in Grid-Connected Distributed Photovoltaic Generation Using Artificial Neural Network," 2018 International Seminar on Intelligent Technology and Its Applications.

[5]. A. Y. Hatata, E.-H. Abd-Raboh, and B. E. Sedhom, "Proposed Sandia frequency shift for anti-islanding detection method based on artificial immune system," Alex. Eng. J., vol. 57, no. 1, pp. 235–245, Mar. 2018.

[6]. P. K. Ganivada and P. Jena, "An Active Slip Frequency Based Islanding Detection Technique for Grid Tied Inverter," in IEEE Transactions on Industrial Informatics. doi: 10.1109/TII.2019.2949009.

[7]. J. Stevens and G. Ginn, "Development and testing of approach to anti-islanding in utility-interconnected photovoltaic systems," 2000.

[8]. Y. Jung, J. Choi, B. Yu, J. So, G. Yu, and J. Choi, "A Novel Active Frequency Drift Method of Islanding Prevention for the grid connected Photovoltaic Inverter", 2005, pp. 1915–1921.

[9]. Khalil El-Arroudi, Géza Joós, Innocent Kamwa and Donald T. McGillis, "Intelligent-Based Approach to Islanding Detection in Distributed Generation," IEEE Transactions on Power Delivery, Vol. 22, No. 2, April 2007.

[10]. S. Murugesan and V. Murali, "Hybrid Analyzing Technique Based Active Islanding Detection for Multiple DGs," IEEE Trans. Ind. Inform, vol. 15, no. 3, pp. 1311-1320, March 2019.

[11]. F. Wang and Z. Mi, "Passive Islanding Detection Method for Grid Connected PV System," 2009, pp. 409–412.

[12]. V. Ashok, Yadav Anamika, C. C. Anthony, K. K. Yadav and U. K. Yadav, "An Intelligent Fault Location Algorithm for Double Circuit Transmission Line Based on DFT-ANN Approach," G. Panda et al. (eds.), Microelectronics, Electromagnetics and Telecommunications, Lecture Notes in Electrical Engineering 521Springer Nature Singapore Pte Ltd. 2019.

[13]. V. Ashok, and Anamika Yadav, “A Protection Scheme for Cross-Country Faults and Transforming Faults in Dual-Circuit Transmission Line Using Real-Time Digital Simulator: A Case Study of Chhattisgarh State Transmission Utility,” Iranian Journal of Science and Technology, Transactions of Electrical Engineering.

[14]. Ashok, V., Yadav, A. A Protection Scheme for Cross-Country Faults and Transforming Faults in Dual-Circuit Transmission Line Using Real-Time Digital Simulator: A Case Study of Chhattisgarh State Transmission Utility. Iran J Sci Technol Trans Electr Eng 43, 941–967 (2019).

[15]. Valabhoju, Ashok, Yadav, A., Pazoki, M., & El-Sehiemy, R.A. (2021). Optimized ensemble of regression tree-based location of evolving faults in dual-circuit line. Neural Comput. Appl., 33, 8795-8820.

Islanding Detection in Grid Connected Wind Plant Using AI Technique

Srikanth Velpula, Ankathi Chandana, Ashok Valabhoju*

Kakatiya Institute of Technology & Science, Warangal-506015, India,

** ashokjntuk@gmail.com*

Abstract.

This paper introduces an ingenious scheme of island detection in a dispersed generation. The discovery of Islanding in distribution generation is one of the most important aspects of a defensive aspect. Islanding is insensible for security of the system as it may cause damage to personnel and equipment in the system due to the improper islanding in the distributed generation system. Islanding detection is needed whenever there is a sudden disconnection of wind power plant and fault. The system operates through the current control mode, in normal or stable mode. The system switches to the power control mode after sitting down. In the proposed work has made using the MATLAB / Simulink software**.**

Keywords. Wind turbine (PV) System, Artificial Neural Network Method (ANN), Voltage, Current, islanding, Levenberg–Marquardt (LM) algorithm and DWT–ANN.

1. INTRODUCTION

Modern day use of distribution production increases distribution production and worse with benefits. Islanding is one such problem. The termination of a local distributed generation (DG) system is termed as an islanding, unintended termination is termed as an unplanned islanding. Islanding can be an error in the main distribution system, due to power disturbance for a short period of time DG is cut off from the main grid.

There are many ways to find an island in a distributed generation system. Local and remote routes practical and idle local routes. In terms of power generation and frequency it is supplied to the PCC and compared to the threshold value while effectively the external interference is injected into the PCC. The reversal of the operating path is an invisible surface. It has low power quality.

Unintended islanding cause main problems which include:

a) Voltage & frequency within tolerable limits.

b) By supplying loads in DG system will risks to monitor staff safety, and

c) The closure of the DG system is out of phase which results in a rapid re-closure. Therefore, in the most important energy system to find the occurrence of an islanding condition.

The means of finding an island are broadly divided into 2 types namely remote and local. Auxiliary local methods, distinguishing between active and passive:

1) Passive routes have a lot of undiscovered area (NDZ) and depend on the unattainable condition to identify the island's population.

2) Effective methods have low NDZ, apart from that it will create a harmonic issue in current.

In this paper a systematic literature review has been carried out thereby considering previous research articles to understand the technical challenges. A recurrent neural network-based islanding protection scheme by using generator speed change has been reported [1]. A review of various islanding detection schemes for renewable based DG system has reported in [2-4]. New ANN-based technique for islanding detection of DG based power network was illustrated in [5] and Deep learning based hybrid scheme for islanding detection in DG system is demonstrated in [6]. Islanding detection based on ANN and novel S-transform for DG system has been explicated in [7] and an Islanding detection method for Inverter-Based DG in Microgrid network has been reported in [8]. In view of the above literature it has been concluded that the importance of identification of islanding condition in a distributed power system network is very significant where grid-connected wind power generation makes system more complex.

2. SYSTEM DESCRIPTION

In this paper, authors have taken the islanding inaction and the mistakes of non-existing on the islanding situation as a research interest. A classification of islanding and non-islanding conditions for islanding acquisition was made. Island and faults are given in a grid connected wind plant at different parameters. The 3-phase voltage and current signals are recorded from the side of the grid and PCC by changing the different parameters. The data sets are simulated from the grid side on the PCC are supplied as an input to ANN after reducing the undesirable noise from the signals. The algorithm used to study the training process by ANN is the Levenberg Marquardt (LM) algorithm.

3. FAULT IN GRID-CONNECTED WIND PLANT

The short circuit fault has been applied at the grid side with a total of 50 fault cases and recorded voltage & current signals on the grid bus (B120) and (wind plant). Fig.1-2 illustrations the voltages and current signals at bus B120 and B25 respectively.

The L-G fault, which is applied phase-A to ground, as shown in Fig.1. The three phases of instantaneous voltage and current signals at the wind turbine bus (B25) are changed, with the amplitude of voltage signals decreasing and the magnitude of current signals increasing, as shown in Fig.2.

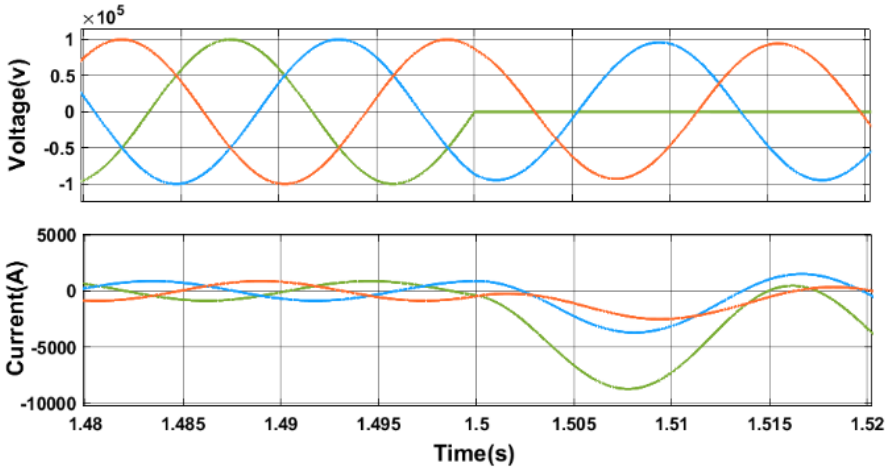

Figure 1 3-phase signals at fault inception time 1.5s at Grid bus (B120):

(a) voltage waveform (b) current waveform,

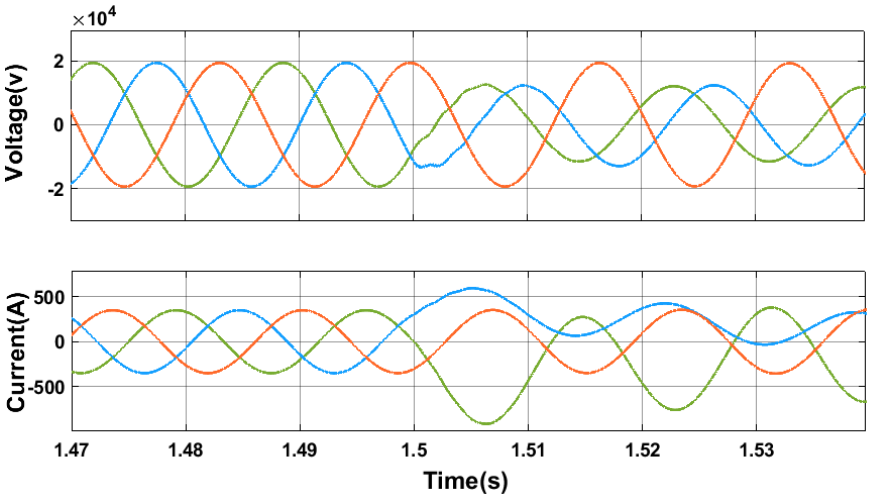

Figure 2 3-phase signals at fault inception time-1.25s at Wind turbine bus (B25): (a) voltage waveform (b) current waveform,

4. ISLANDING CONDITION IN A GRID-CONNECTED WIND PLANT

Grid disconnection is provided using a breaker and a total of 50 cases of Islanding conditions are recorded on the grid bus and wind plant bus. Measure the voltage and current signals on the side of the grid and at the wind plant. Fig.3-4 demonstrations the voltage/current signals of the side grid B120 and wind plant bus B25 respectively.

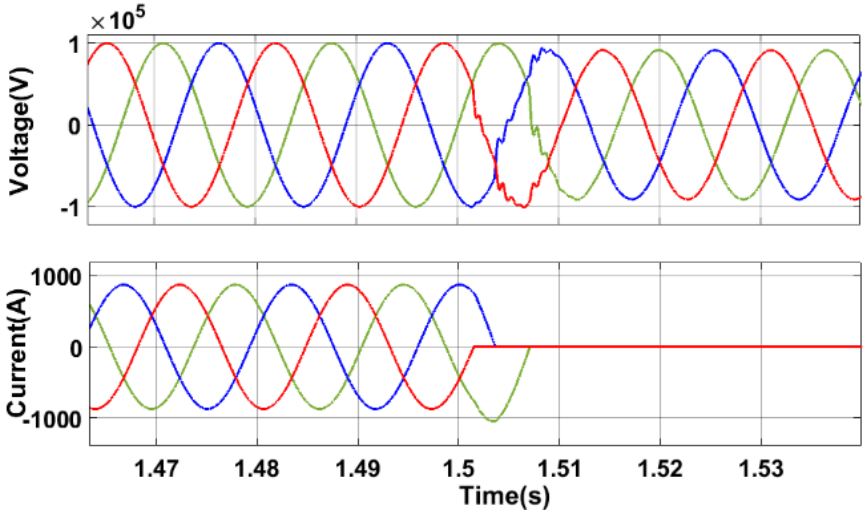

Figure 3 3-phase signals at islanding inception time-1.5s at Grid bus (B120): (a) voltage waveform (b) current waveform

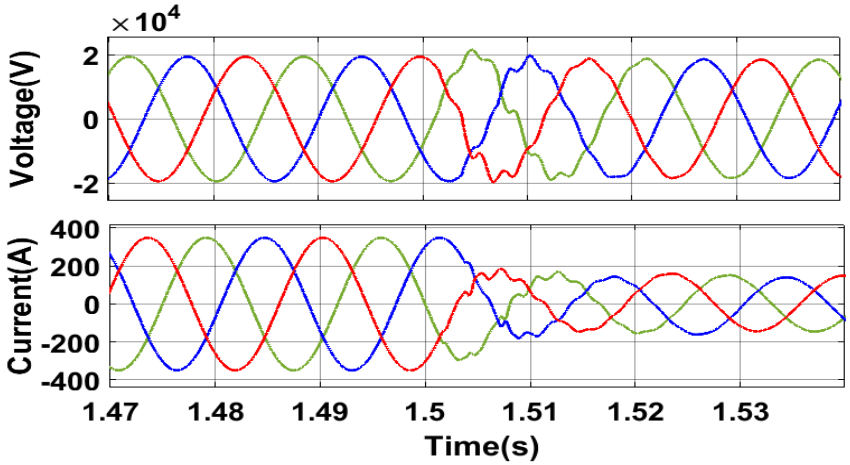

Figure 4 3-phase signals at islanding inception time-1.5s at PV bus (B25): (a) voltage waveform (b) current waveform

5. PROPOSED METHODOLOGY

The proposed MATLAB/Simulink model consists of a wind plant, grid and existing power plants with different loads connected and a transmission cable. Fig.5 shows a single line diagram of the connected wind plant when voltage and currents are measured at PCC.

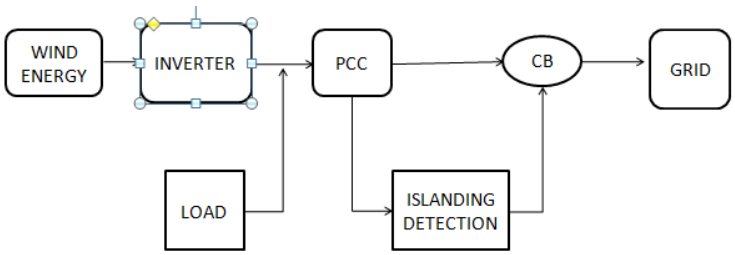

Figure 5 Single line diagram of Grid-connected wind plant

It must be separated the electrical signals from the wind plant and the grid on the PCC, and in the event of any deviation, they should be returned to ANN, and identify the islanding status and issues a trip signal to the breaker to isolate the wind plant to avoid damage with local loads caused by disturbance.

6. ANN FOR GRID-CONNECTED WIND PLANT

A multi-layered neural network is used for the island wind turbine detection. The multi-layered neural network contains output, input and encryption layers that require algorithm training to minimalize the error using the LM-algorithm. Discrete wavelet transform is employed to eliminate noise. These databases are then processed through a DWT-ANN processor to remove noise from the current 3-phase and voltage signals to read the model as quickly and accurately as possible. Then, from all the voltage and current signal on the Wind turbine bus and the Grid bus, we must take samples of two cycle data (single-cycle or pre-islanding data, and one single-cycle data- fault or post-landing).

Finally, the standard deviation of the two-cycle data of current and voltage signals on the grid bus and wind plant bus during fault, as well as islanding situation are used to design input data set to train DWT-ANN. module, and provide the target output at '0 'if incorrect, and '1' when connected to the ANN feed network to the ANN feed supply provided 70 percent training, 15 percent testing, and 10 percent verification -15. Typical data diversion of two three-phase current and voltage signals on bus120 and bus25 with error modes and single-line circuit islands used to design a data set input training DWT-ANN module. Various parameters have been used to generate input / output data set for training and testing as noted in Table.1.

Parameters in particular start time, type of error and islanding method used, number of data sets or cases of island residency, and error Grid bus and wind turbine we used for training and testing using the ANN feed-forward network we have. is done throughout the project to acquire an island Grid-connected wind turbine via ANN.

Table.1 Parameters variation considered to generate the datasets for training & testing

S.no	Condition	Parameter	Training and Testing data
1	Fault	Fault type	AG
		Fault resistance	**0.001**
		Fault inception time	0.9-1.88
		Voltage signal and current signals measured	At grid bus and wind turbine
		Total no.of cases	Training cases -70,testin-30 Total no.of cases 100
2	Inception	Islanding type	Passive
		Islanding resistance	0.01
		Islanding inception time	0.9-1.88
		Voltage and current signals measured	At grid bus and wind turbine
		Total no.of cases	Training cases -70,testing-30 Total no.of cases 100

7. MODELLING & SIMULATION

After that, we constructed the proposed ANN model with feedforward network utilizing the Levenberg–Marquardt (LM) method with DWT-ANN processor to remove noise from the signals, which we did using MATLAB Simulink. The Grid-connected wind turbine system is depicted in Fig.6.

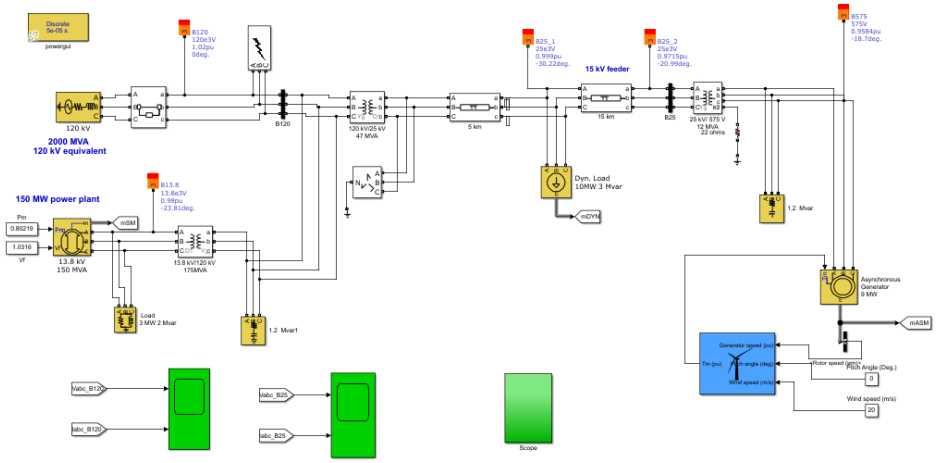

Figure 7. MATLAB Simulink diagram of Grid-connected wind plant

ANN is trained using the MATLAB code, which includes parameters such as performance goal, conversion, verification check, number of layers hidden in the feedforward network, and number of epochs. Provide some parameter values in the code and trained the network, check the MSE performance for each variation where the MSE is the lowest, and then apply those values to the ANN Feed Transfer Network to find the islanding condition to respond quickly and accurately. In the ANN feedforward network, there is a single layer with six neurons, a single outgoing layer with six neurons, and a hidden layer with a different number of neurons that are provided to the feed network in a variety of conditions. ANN network. The ANN Feed-forward network training structure is shown in Table.2, and the curves to ensure their performance during ANN between Epochs and MSE are set out in Fig.7.

Table.2. Training architecture of different cases of Feed forward ANN

Cases	1	2	3	4
size of input dataset	6×200	6×200	6×200	6×200
Size of architecture	6-20-6	6-20-6	6-30-6	6-35-6
No.of epochs	10,000	11,000	15,000	20,000
Performance goal	10e-51	10e-01	10e-9	10e-11

By looking at training curves, tests, and performance confirmation curves, we can determine the best case. Case 2 is advanced because its three curves (training, testing,

and validation) will meet in one place that satisfies the island's living conditions whenever a descent is possible in the system.

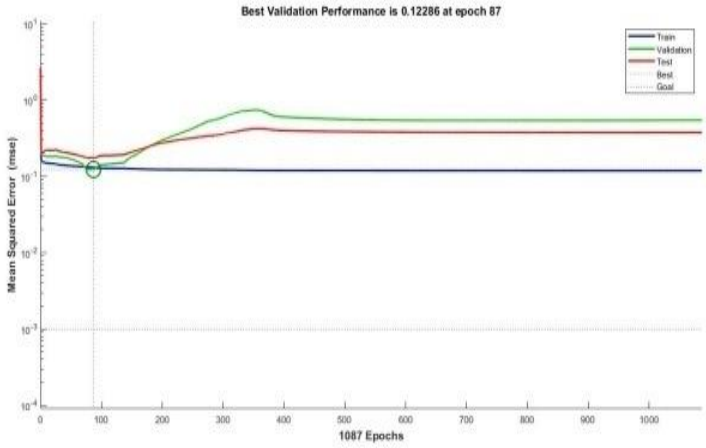

(a)

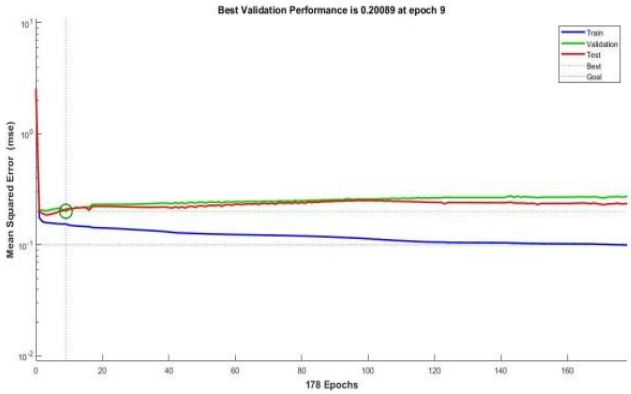

(b)

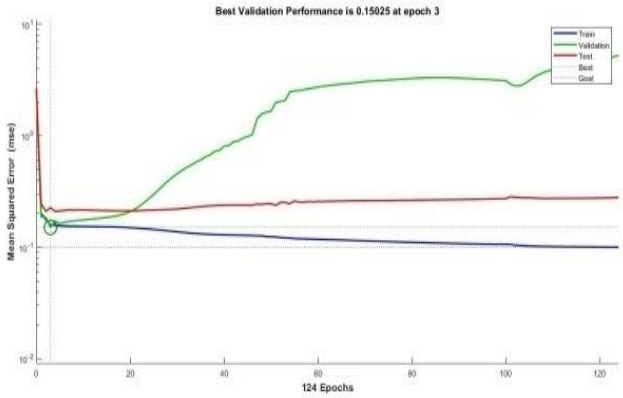

(c)

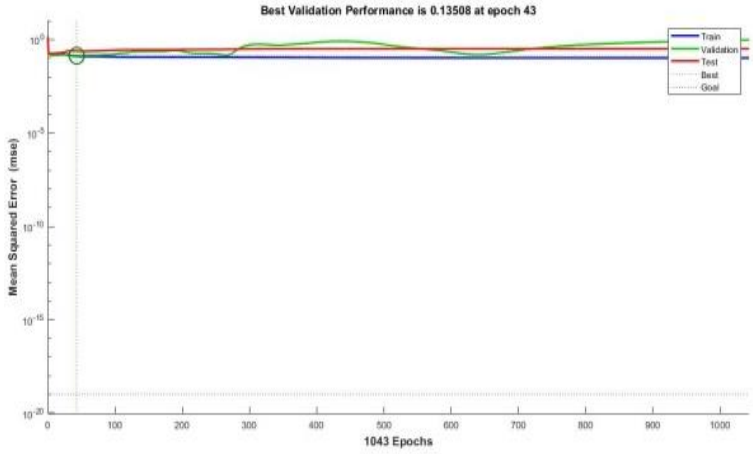

(d)

Figure 7. Performance Validation curves during ANN using different size of architectures: (a) case-1(6-20-6), (b) case-2 (6-25-6) (c) case-3 (6-30-6), (d) case-4 (6-35-6)

8. CONCLUSION

This paper is based on the detection of an islanding of wind plant using the ANN method. Electrical power and current side grid and PCC signals at different inception times are provided as input to the DWT-ANN module and are trained by the Levenberg-Marquardt algorithm with 100 instances of ANN training data sets. Testing / training and verification is done to improve the performance of proposed method.

9. REFERENCES

[1]. Mehmet Bayrak, “Recurrent artificial Neural network-based island protection by using generator speed deviation” (Sakarya University, Electrical-Electronics

Engineering Department, Sakarya, Turkey.rences), Scientific Research and Essay Vol.4 (4), pp. 212-216, April, 2009

[2]. Aziah Khamis, Hussain Shareef, ErdalBizkevelci, and Tamer Khatib, “A review of islanding detection techniques for renewable distributed generation system” in Renewable and Sustainable Energy Reviews, Volume 28, December 2013, Pages 483-493,

[3]. P. Mahat, Z. Chen and B. Bak-Jensen, "Review of islanding detection methods for distributed generation," 2008 Third International Conference on Electric Utility Deregulation and Restructuring and Power Technologies, 2008, pp. 2743-2748,

[4]. R. S. Kunte and W. Gao, "Comparison and review of islanding detection techniques for distributed energy resources," 2008 40th North American Power Symposium, 2008, pp. 1-8.

[5]. V. L. Merlin, R. C. Santos, A. P. Grilo, J. C. M. Vieira, D. V. Coury, and M. Oleskovicz, “A new artificial neural network based method for islanding detection of distributed generators”, Int. J. Electr. Power Energy Syst., vol. 75, pp. 139-151, Feb. 2016.

[6]. Xiangrui Kong, Xiaoyuan Xu, Zheng Yan,Sijie Chen, Huoming Yang, Dong Han, “Deep learning hybrid method for islanding detection in distributed generation”, in Applied Energy, Volume 210, 15 January 2018, Pages 776-785.

[7]. T. S. Menezes, D. V. Coury and R. A. S. Fernandes, “Islanding Detection Based on Artificial Neural Network and S-transform for Distributed Generators”, 2019 IEEE Milan PowerTech, 2019, pp.1-6,

[8]. Karimi, M.; Farshad, M.; Hong, Q.; Laaksonen, H.; Kauhaniemi, K. “An Islanding Detection Technique for Inverter-Based Distributed Generation in Microgrids”. Energies, 2021, 14(1), 130.

Investigations on Influence of Ground Impedance on the Interconnected Three phase Four wire Balanced and Unbalanced Distribution System

K Lokeswara Rao[1], A Usha[2], Raghunatha R[3]

[1]School of Technology, GITAM Bengaluru, lokehch85@gmail.com
[2]Professor, B.M.S.C.E Bangalore, usha.eee@bmsce.ac.in
[3]Rtd Professor, BNMIT, Bengalore, powerapps@gmail.com

Abstract.

Numerous generating stations are connected in synchronism with different loads through LV and HV transmission lines at multiple stages in the power system (PS) network. These power generating stations and loads are balanced and unbalanced types: Single-phase and Three-phase, AC and DC, overhead and underground cables. The neutral point of generators, transformers, etc., is grounded at multiple points to serve the protection and safety of the PS components. Resistance of earth is affected by various parameters like type of soil, temperature, and moisture content in the ground clearly says that earth resistance is not constant or zero. Various research studies considered a balanced power generating system and loads, assumed zero neutral currents in load flow studies. This article considers the effect of ground Impedance on a three-phase transmission line and refined mathematical relations to transform voltage, current and power equations in sequence domine. To examine the influence of ground Impedance on the Three-phase transmission line an experimental setup was prepared in the laboratory and observed the effect of ground Impedance on the neutral current.

Keywords: Ground Impedance, Unbalanced loads, Transformation matrix (D).

1. INTRODUCTION

The use of electrical energy to run various electrical and electronic appliances for multiple purposes is a part of day-to-day activities to lead human life comfortable. In the early day's power was generated centrally with the help of various available sources to meet the required load demand. Consumption of energy in domestic and industrial needs created a massive demand for power production. Multiple reasons (lack of fossil fuels, global warming, cost of power production, latest technologies in power production) influence power production centrally (in MW) and locally (in KW) to meet the excess load demand. These days' various power plants (conventional, non-conventional, few KW to MW) and loads (AC, DC, Single Phase and Three Phase) operate in synchronism. The dynamic nature of power plants (PV, wind) and loads (switching ON/OFF large industrial loads, faults) introduces power quality (PQ) issues. Researchers proposed various mitigation techniques to address these PQ issues (centrally and locally), but the PQ in the PS network is a big challenge to researchers. Various research studies assumed the effect of earth resistance is negligible, but Earth resistance is one reason that influences the PQ issues, which cannot be considered zero [1].

In paper [4,12] proposed Primary control to maintain constant output voltage, reduction in THD, uniform power distribution, secondary control to compensate reactive power and maintain frequency within limits. A primary layer consisting of a multi-loop control scheme makes use of the orthogonal signal generation technique to transform output phase voltages (Van, Vbn, Vcn) to αβ frame and αβ frame to d-q frame with the help of park transformation. The LV system self, mutual admittance expressed in 4x4 matrix.

In paper [5] a PV distribution network with 4-wire medium and low voltage configuration with merged neutral return grounded at multiple points impedance matrix considered. The admittance matrix obtained from Carson's line equation, the mismatch between specified and calculated current at each node/bus overcome using NR load flow studies applied to radial and ring distribution networks.

PS components are higher in rating, bulk in size and costlier. These components are provided with primary and secondary protection schemes to protect them. These protective schemes sense the fault quickly, select the fault's location, and disconnect faulted phase/feeder. A protective scheme selectivity, sensitivity, and speed depend on the current at faulted phase. Ground resistance at fault location impacts the operating fault current of protective systems. The impact of ground resistance is higher during lighting because Lighting currents are at a high current magnitude, and frequency ranges from few Hz to kHz [8].

Paper [11] presents backwards current sweep, forward voltage sweep methods to minimise neutral current in 3 phase 4 wire multi grounded system with a ground return. The Kron reduction technique is applied to reduce the load flow problem, which eliminates a grounding resistance effect that is not realistic.

Line to Ground (LG) fault frequently occurs in the EHV line, which causes a massive amount of primary current flow through the fault path to the ground. The faulted phase is open-circuited with the help of a single-pole tripping mechanism. Even though faulted phase opened within the time interval, electrostatic and electromagnetic coupling between healthy phases causes a small secondary arc between contacts. Ground resistance at the fault location of phases is one more reason which influences the secondary arc during tripping between contact terminals of a faulted phase. The external line to ground faults causes zero-sequence current (ZSC) passing through the power transformer leading to differential protection false tripping because of the weak grounding of the neutral source [6,10].

The Monopolar HV-DC system inserts many amps of DC into the ground through the ground electrode. The current inseminates within the ground media and returns to the power line due to the current flow into the environment, a rise in ground potential through the ground electrode. Because of differences in earth's surface potentials in different substations, the flow of DC through the neural grounding transformer and the transmission lines. The DC that flows through the windings of transformers has driven transformers into half-cycle saturation (i.e., dc bias), which can increase the hotspot, harmonic generation, reactive power absorption, audible noise, and vibration of transformers [2,7].

2. THREE PHASE FOUR WIRE DISTRIBUTION SYSTEM MODEL

Many PS algorithms assumed a three-phase four wired network in distribution systems to evaluate PS parameters considering the balance distribution system and loads. The neutral voltage and current equations are eliminated by assuming zero neutral voltages. Given IEEE standards [1], stating that voltage drop across neutral and ground not be zero under an unbalanced system.

The proposed article, to understand the influence of ground Impedance on a three-phase four-wire unbalance Distribution line with its self and mutual impedance reference to ground considered [3]. Figure 2.1 shows a three-phase four-wire star connected distribution system.

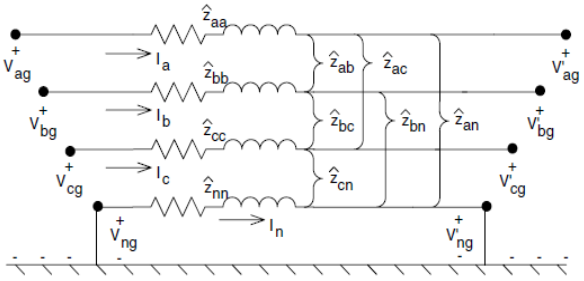

Figure 2.1 Three phase four wire star connected Distribution system

The voltage equation for the network shown in figure 2.1 is written as

$$\begin{bmatrix} V_a \\ V_b \\ V_c \\ V_n \end{bmatrix} = \begin{bmatrix} Z_{aa} & Z_{ab} & Z_{ac} & Z_{an} \\ Z_{ba} & Z_{bb} & Z_{bc} & Z_{bn} \\ Z_{ca} & Z_{cb} & Z_{cc} & Z_{cn} \\ Z_{na} & Z_{nb} & Z_{nc} & Z_{nn} \end{bmatrix} \begin{bmatrix} I_a \\ I_b \\ I_c \\ I_n \end{bmatrix} + \begin{bmatrix} V_a{}' \\ V_b{}' \\ V_c{}' \\ V_n{}' \end{bmatrix} \tag{2.1}$$

Equation (2.1) also written as

$$\begin{bmatrix} [V_{abc}] \\ [V_{ng}] \end{bmatrix} = \begin{bmatrix} [Z_{ij}] & [Z_{in}] \\ [Z_{nj}] & [Z_{nn}] \end{bmatrix} * \begin{bmatrix} [I_{abc}] \\ [I_n] \end{bmatrix} + \begin{bmatrix} [V'_{abc}] \\ [V'_{ng}] \end{bmatrix} \tag{2.2}$$

Because the neutral is grounded, the voltages Vng and V'$_{ng}$ are equal to zero. Applying Kron's reduction technique, the final phase impedance matrix becomes

$$[V_{abc}] = [Z_{abc}][I_{abc}] + [V_{abc}{}'] \tag{2.3}$$

Considering impedance between neutral and ground the effect of ground impedance in Figure 2.1 is modified as shown in Figure 2.2.

The effect of ground impedance is equally distributed half considered at sending end and another half considered at receiving end. We know that in an unbalanced system-neutral current is not equal to zero($I_n \neq 0$). The voltage equation for the three-phase four-wire system represented as the equation (2.4).

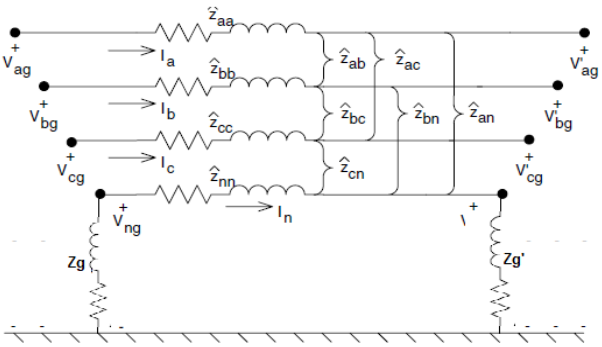

Figure 2.2 Modified Three phase four wire Distribution system

$$\begin{bmatrix} V_a \\ V_b \\ V_c \\ V_n \end{bmatrix} = \begin{bmatrix} Z_{aa} & Z_{ab}Z_{ac} & Z_{an} \\ Z_{ba} & Z_{bb}Z_{bc} & Z_{bn} \\ Z_{ca} & Z_{cb}Z_{cc} & Z_{cn} \\ Z_{na} & Z_{nb}Z_{nc} & Z_{nn} \end{bmatrix} \begin{bmatrix} I_a \\ I_b \\ I_c \\ I_n \end{bmatrix} + \begin{bmatrix} V_a{}' \\ V_b{}' \\ V_c{}' \\ V_n{}' \end{bmatrix} \tag{2.4}$$

$$[V_{abcn}] = [Z_{abcn}][I_{abcn}] + [V_{abcn}{}'] \tag{2.5}$$

$$V_n = Z_g I_n = Z_{nn} I_n + V_n{}' \tag{2.6}$$

$$\therefore V_n{}' = Z_g{}' I_n \tag{2.7}$$

The ground impedance

$$Z_g = Z_g{}' = \frac{1}{2}\ ground\ impedance\ from\ sending\ end\ to\ receiving\ end$$

3. HARDWARE IMPLEMENTATION

The experimental setup is established in the laboratory to evaluate the voltage drop, current flow in neutral during unbalanced system due to the effect of ground Impedance. In the first experimental setup, a 3 KVA star connected alternator is driven by a 5 HP DC shunt motor. The output of a 3 KVA alternator is connected to the primary side of a 3 phase (Y-Y) connected transformer. An ammeter connected in series with the line for the measurement of current (I_1) flow in the R-phase. Further, an ammeter connected to measure current I_2 through the neutral point of an alternator out put through the rheostat, also an ammeter is connected in series through a rheostat to measure the effect of earth resistance (R_1), current flow on the secondary side of a transformer.

4. RESULTS AND DISCUSSION

Figure 3.1 (a) shows a circuit diagram of an Unbalanced Load on R-Phase of the Transformer secondary, and Figure 3.1 (b) shows Laboratory setup for an Unbalanced Load on R-Phase of the Transformer secondary. The results observed from the experimental setup are given in Table-1. From Table-1, it is observed that due to the effect of earth resistance (R_1), there is a change in transformer primary neutral current (I_2) and also secondary voltage (V_R).

Rating & Specifications:

Alternator : 3KVA, 3-Ø 415V, 50Hz
Transformer : 3-Ø 0-415V, 50Hz Y-Y connected
Transmission line Rheostat: 360Ω/1.2A
Resistive Load : 400Ω/2A (R,Y,B phases), 18Ω/5A (for neutral)
Inductive Load : 3 Phase, 415V, 10A

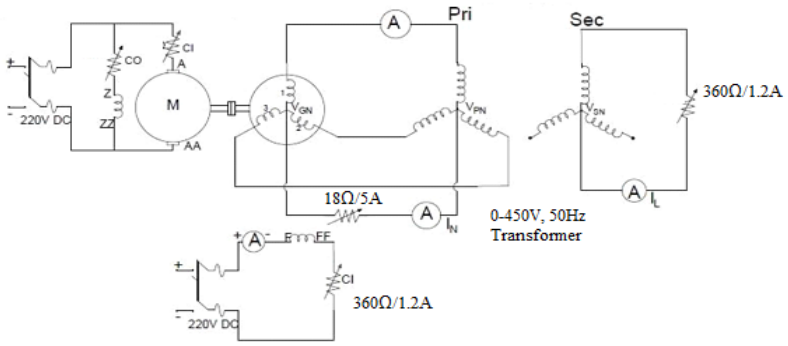

Figure 3.1 (a) Experimental setup for Unbalanced Load on Phase-A of Transformer secondary

Figure 3.1 (b) Laboratory setup for Unbalanced Load on Phase-A of Transformer secondary

Where, the different electrical parameters for Figure 3.1 (a) are defined as follows

R_1= Resistance at generator & Transformer primary Neutral
I_1= Neutral Current flow through Generator & transformer primary
I_2= R-phase current at generator side
R_2= change in ground Impedance at R phase of transformer secondary
I_3= Current flow in R-Phase of a Transformer secondary
V_R = Voltage across R-Phase at Secondary side of a Transformer

Table-1: System Voltage & Current During both transmission, Loads, are balanced with the effect of change in earth resistance

Generator side			Transformer side		
R_1 (Ohms)	I_1 (A)	I_2 (A)	R_2 (Ohms)	I_3 (A)	V_R (Volts)
0	1.4	2.22	17.8	0.66	240
6.7	1.4	2.2	17.8	0.65	238
9.5	1.4	2.18	17.8	0.64	236

12.9	1.4	2.16	17.8	0.64	233
16.5	1.4	2.12	17.8	0.63	231
18	1.4	2.12	17.8	0.63	229

In the second experimental setup, Figure 3.2 (a) illustrates three identical rheostats that are used to implement an unbalanced distribution. Three variable rheostats with inductive load are connected in series to form RL load. A variable rheostat is considered between the common neutral of an alternator and RL load. These two experimental setups are shown in Figure 3.1 &Figure 3.2 are implemented to observe the neutral voltage across an alternator neutral and three-phase RL load, connected series with ground Impedance.

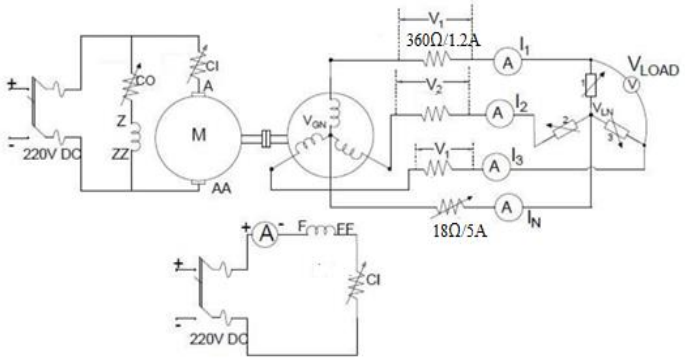

Figure 3.2 (a) Experimental setup for Three Phase Four wire with Unbalanced Transmission and RL Load.

Figure 3.2 (b) Laboratory setup for Three Phase Four wire with Unbalanced Transmission and RL Load.

Where the different electrical parameters for Figure 3.2 (a) are defined as follows:

I_R = Current flow in R-Phase in Amp's
I_Y = Current flow in Y-Phase in Amp's
I_B = Current flow in B-Phase in Amp's
I_{NG} = Current flow in Neutral conductor in Amp's
V_{NG} = Voltage drop across Ground rheostat
R_{GE} = Ground Impedance in Ohms

The experimental results obtained from the Figure-3.2 are tabulated in Table-2,3,4 and 5. It is observed from Table-2 that a rise in neutral voltage (V_{NG}) and an increase in neutral current (I_{NG}) due to the effect of ground Impedance (R_{GE}) during both transmission and loads are balanced.Further it is observed from Table 3,4 and 5 that the rise in neutral

voltage and flow of neutral current during various unbalanced conditions (between Transmission line and Load) with the affect of ground impedance.

Table-2: System Voltage &Current during Balanced transmission & Balanced Load

I_R (A)	I_Y (A)	I_B (A)	I_{NG} (A)	V_{NG} (V)	R_{GE} (Ω)
0.25	0.25	0.23	0	0.021	4
0.25	0.25	0.23	0	0.024	4.6
0.25	0.25	0.23	0.01	0.057	5.2
0.25	0.25	0.23	0.01	0.088	6.1
0.25	0.25	0.23	0.01	0.124	7.4
0.25	0.25	0.23	0.02	0.172	8.9
0.25	0.25	0.23	0.02	0.236	9.7
0.25	0.25	0.23	0.02	0.284	10.8
0.25	0.25	0.23	0.02	0.338	11.9
0.25	0.25	0.23	0.03	0.391	13.1
0.25	0.25	0.23	0.03	0.446	14.4
0.25	0.25	0.23	0.03	0.511	16.2
0.25	0.25	0.23	0.03	0.576	17.5
0.25	0.25	0.23	0.03	0.63	18

Table-3: System Voltage & Current during Unbalance in transmission & Balanced Load

I_R (A)	I_Y (A)	I_B (A)	I_{NG} (A)	V_{NG} (V)	R_{GE} (Ω)
0.25	0.25	0.24	0.01	0.23	2.4
0.28	0.24	0.23	0.04	0.24	2.4
0.3	0.24	0.22	0.065	0.24	2.4
0.3	0.25	0.22	0.07	0.24	2.4
0.31	0.26	0.22	0.08	0.25	2.4
0.31	0.28	0.22	0.08	0.25	2.4
0.31	0.29	0.24	0.07	0.26	2.4
0.31	0.29	0.25	0.05	0.26	2.4
0.31	0.29	0.26	0.04	0.25	2.4

Table-4: System Voltage & Current during Balanced transmission & Unbalanced Load

I_R (A)	I_Y (A)	I_B (A)	I_{NG} (A)	V_{NG} (V)	R_{GE} (Ω)
0.28	0.25	0.22	0.07	0.24	2.4
0.32	0.25	0.23	0.12	0.25	2.4
0.36	0.26	0.3	0.22	0.26	2.4
0.37	0.32	0.22	0.21	0.27	2.4
0.37	0.34	0.25	0.15	0.28	2.4
0.36	0.34	0.32	0.02	0.28	2.4

Table-5: System Voltage & Current during Unbalance in transmission & Unbalanced Load

I_R (A)	I_Y (A)	I_B (A)	I_{NG} (A)	V_{NG} (V)	R_{GE} (Ω)
0.28	0.25	0.22	0.1	0.24	2.4
0.32	0.25	0.23	0.12	0.25	2.4

0.35	0.25	0.23	0.21	0.26	2.4
0.36	0.25	0.23	0.24	0.27	2.4
0.36	0.26	0.23	0.22	0.26	2.4
0.37	0.28	0.22	0.22	0.27	2.4
0.37	0.32	0.22	0.21	0.27	2.4
0.37	0.34	0.22	0.23	0.28	2.4
0.37	0.34	0.25	0.15	0.28	2.4
0.36	0.34	0.27	0.12	0.27	2.4
0.36	0.34	0.32	0.02	0.28	2.4
0.35	0.34	0.31	0.08	0.36	2.4

5. TRANSFORMATION OF EXISTING THREE PHASE SYMMETRICAL MODEL TO THREE PHASE FOUR WIRE MODEL

Existing PS models assume a balanced system 3-Φ network, and these models are effectively established. In the proposed model, the Three-phase Four-wire system along with a consolidated solutions for balanced and unbalanced system analysis having with categorical neutral voltage representation. Extending many of the presently available three phase symmetrical component models become necessary to equivalent three phase four wire models.

It is convenient to represent the system parameters during unbalance in sequence domine and also support to calculate self & mutual impedance of each line with the available line sequence parameters.

$$\begin{bmatrix} V_a \\ V_b \\ V_c \\ V_n \end{bmatrix} = \begin{bmatrix} 1 & 1 & 1 & 0 \\ 1 & a^2 & a & 0 \\ 1 & a & a^2 & 0 \\ 3 & 0 & 0 & x \end{bmatrix} \begin{bmatrix} V_0 \\ V_1 \\ V_2 \\ 0 \end{bmatrix} \tag{4.1}$$

$$\therefore V_n = V_a + V_b + V_c = 3V_{a0} \tag{4.2}$$

$$\therefore D = \begin{bmatrix} 1 & 1 & 1 & 0 \\ 1 & a^2 & a & 0 \\ 1 & a & a^2 & 0 \\ 3 & 0 & 0 & x \end{bmatrix}$$

$$[V_{abcn}] = [D] * [V_{012x}] \tag{4.3}$$

Similarly current equation written as

$$[I_{abcn}] = [D] * [I_{012x}] \tag{4.4}$$

$$[I_{abcn}] = [V_{abcn}] * [Z_{abcn}]^{-1}$$

Or

$$[I_{abcn}] = [V_{abcn}] * [Y_{abcn}] \tag{4.5}$$

Substituting equation (4.3) & (4.4) in (4.5)

$$[D] * [I_{012x}] = [D] * [V_{012x}] * [Y_{abcn}] \tag{4.6}$$

$$[I_{012x}] = [D] * [Y_{abcn}] * [D]^{-1} * [V_{012x}] \tag{4.7}$$

$$\therefore [D] * [Y_{abcn}] * [D]^{-1} = [Y_{012x}]$$

$$[I_{012x}] = [Y_{012x}] * [V_{012x}] \tag{4.8}$$

The equation 4.1 does not affect the original symmetrical component equations. With the assist of a new transformation matrix ‘D’, it can be converted to any conventional Three phase distribution system component impedance model to equivalent three phase four wire system.

6. CONCLUSION

All the generating stations, distributed sources and loads are interconnected through transmission and distribution systems. All the components are effectively grounded with various methods to provide additional protections. Earth resistance depends on the type of soil, moisture present, temperature and mineral content; this resistance affects the performance of equipment and components. However, the practical approach offers some small current to ground, and it provides a considerable amount of voltage drop. In this work, the entire PS symmetrical components (012) convert into (012x) without affecting existing system components. In future scope, the proposed novel technique will be applied to both balanced and unbalanced distribution systems with or without grid-connected systems to evaluate the effect of ground impedance and improve the protection of individual components and Power Systems.

REFERANCES

[1] "81-2012 - IEEE Guide for Measuring Earth Resistivity, Ground Impedance, and Earth Surface Potentials of a Grounding System" 28 Dec. 2012.

[2] Nian Yu , ZhikunCai , Ruiheng Li , Qiang Zhang, Lei Gao, and Zhibo Sun "Calculation of Earth Surface Potential and Neutral Current Caused by HVDC Considering Three-Dimensional Complex Soil Structure" IEEE Transactions on Electromagnetic Compatibility · March 2021.

[3] Raghunath R.,Muralidhara V.,Thukaram D.,K. Lokeswara Rao"Experimental Validation and Review of Neutral Voltage Modeling for Unbalanced System Analysis" 2018 15th IEEE India Council International Conference (INDICON), March 2020.

[4] AmirrezaNaderipour, Zulkurnain Abdul-Malek, Vigna K. Ramachandaramurthy, Akhtar Kalam, Mohammad Reza Miveh "Hierarchical control strategy for a three-phase 4-wire microgrid under unbalanced and nonlinear load conditions" ISA Transactions, Volume 94, Pages 352-369, November 2019.

[5] Obaidur Rahman, Kashem M. Muttaqi and Danny Sutanto "Time Series Variations of the Neutral-to-Ground Potential in a 4-Wire LV Network under Unbalanced Allocation of Rooftop Solar PV and Mitigation using Energy Storage" 2019 IEEE Power & Energy Society General Meeting (PESGM), 2019.

[6] Ahmed Maged Ismail, Hany Elghazaly, Ahmed Mohamed Emam "Elimination of Zero Sequence Currents Effect on Differential Protection For Power Transformers Connected to Power Grid" 2019 21st International Middle East Power Systems Conference (MEPCON), Tanta University, Egypt.

[7] Z. Pan et al., "Potential compensation method for restraining the DC bias of transformers during HVDC monopolar operation," IEEE Trans. Power Del., vol. 31, no. 1, pp. 103–111, Feb. 2016.

[8] AnggoroB.a ,Yutadhia. R.E.b, "The Grounding Impedance Characteristics of Grid Configuration", Procedia Technology Vol 11, pp 1156 – 1162, 2013.

[9] G. Ahmadi and S.M. Shahrtash "Neutral to Earth Voltage Reduction Methods in Three-Phase Four Wire Distribution Systems" 2009 International Conference on Electrical and Electronics Engineering - ELECO 2009

[10] Wei Shi, Fan Li, Yanhua Han, and Yunge L "The effect of ground resistance on secondary arc current on an EHV transmission line", IEEE Transactions on Power Delivery, Vol: 20, Issue: 2, pp 15202-1506, April 2005.

[11] Rade M. Ciric, Antonio PadilhaFeltrin and Luis F. Ochoa “Power Flow in Four-Wire Distribution Networks—General Approach’ IEEE TRANSACTIONS ON POWER SYSTEMS , VOL. 18, NO. 4, NOVEMBER 2003

[12] Paulo A. N. Garcia, Jose Luiz R. Pereira, Sandoval Carneiro, Vander M. da Costa, Nelson Martins “Three-Phase Power Flow Calculations Using the Current Injection Method” IEEE TRANSACTIONS ON POWER SYSTEMS, VOL. 15, NO. 2, pp 508-514, MAY 2000.

Biographies

Mr. K.Lokeswara Rao received his B.Tech degree in Electrical and Electronics Engineering from India in 2007 and the PG. Degree in power and energy system from NITK in 2009, where he is currently pursuing a PhD in BMSCE, Bengaluru. His research interest is power quality, Distributed generation.

Dr Usha A has an experience of about 30 years of both teaching and research. She received PhD degree from the University of Mysore. Currently, She is a Professor with DEEE, BMSCE Bangalore, VTU. She guided Five Research Scholars in various domains. His research interests include Smart sensors, Power electronics and Microgrid.

Raghunath Ramaswamy Retired professor, DEEE, BNMIT. He received his PhD from IISc Bengaluru and Master's in power systems from Mysore University, and He has served in the Consulting Industry for nearly 30 years. His research interest includes Energy management systems, optimization in power systems, power system protection, control, and stability.

Design and Development of Charging Station for Swappable Batteries of Electric Vehicle

B Sumedha Shenoy **Varsha M**
Dept. of Electrical and Electronics, BMS College of Engineering, Bangalore, Karnataka,
sumedha.ee18@bmsce.ac.in, varsha.ee18@bmsce.ac.in

Abstract.

Petroleum and oil resources across the globe are deteriorating at a high rate due to a significant reliance on it, being a primary source of fuel for automobiles. Electric Vehicles (EVs) are one of the immediate alternatives that have been implemented. Development of EVs is heavily reliant on Battery design, its charging infrastructure, Motor drives and Power Electronics. One of the most important aspects is the charging station infrastructure and its design that should accommodate the changing scenario, and the same is discussed in this paper. The designed charging system is an AC charging system consisting of a two-stage converter which provides a regulated DC Voltage supply to the swappable EV Battery. The designed system consists of a single-phase diode bridge rectifier, a boost converter and a buck converter. The boost converter is mainly used to incorporate Active power factor correction in the circuit. The proposed work involves a current controller for Power factor correction.

Keywords. Electric vehicle, Charging stations, swappable battery, active power factor correction, uncontrolled rectifier.

1. INTRODUCTION

Electric cars are growing more appealing every year in comparison to automobiles with Internal Combustion Engines (ICE) due to a number of advantages namely less pollution, lower transportation costs and less petroleum consumption.[1] Manufacturers and researchers have paid close attention to the development of electric vehicles (EV), which relies on the development of charging stations with higher efficiency and improved power factor [1].

In many applications, fast-charging stations have two conversion stages: an input AC to DC rectifier and an output DC to DC converter. The DC-to-DC converter regulates the Charging Station's (CS) output voltage and current [1]. The battery receives this regulated output voltage via a relay, which disconnects the battery from the main supply when it is fully charged.

A swappable battery charging station was proposed to solve the problem of charging time and the urgent need to charge a vehicle. A vehicle's discharged battery or battery pack can be immediately swapped for a fully charged one, eliminating the time spent in waiting for the vehicle's battery to charge. [2]

When it comes to establishing a swappable battery charging station, there are a number of obstacles to overcome. One of the primary challenges that may be overcome is the design of a battery pack in such a way that it can be simply and quickly detached from cars and reattached in a short amount of time. Another issue is the battery packs' brand compatibility. [2]

Electric vehicle batteries can be charged using either a single phase or three phase power supply. EV chargers are linked to this system due to the widespread availability of single-phase supply outlets.

These EV chargers behave like non-linear loads due to the presence of power electronic converters. An EV charger's nonlinear feature might cause harmonics in the current and influence the system's voltage profile. Non-linear voltage loss can be caused by high non-linear loads, resulting in distorted voltage waveforms.[3]

In this paper, the EV battery charging station with power factor correction was designed, simulated, and described. Plecs, a software tool for system-level simulations of electrical circuits developed by Plexim, was used to simulate the EV charger. It is specifically built for modeling of Power electronic circuits but can be employed for any other electrical circuit applications.

2. CHARGING STATION DESIGN DETAILS

The block diagram of the proposed EV Battery charging station is shown in Fig 1.1

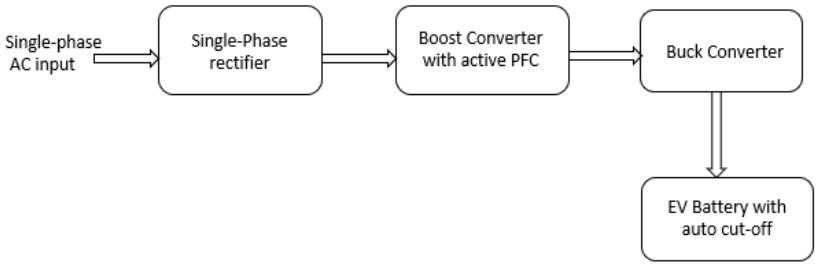

Fig.1.1 Block diagram of the charging system

The requirements for the proposed charging station design are shown in Table 1.

TABLE 1 - Requirements

Sl.No	Parameters	Values
1.	Input Voltage	220V AC
2.	Output Voltage	54.6V DC
3.	Output Current	6A
4.	Battery specifications	48V, 24Ah Li-ion Battery suitable for an e-bike
5.	Other requirements	Battery Protection circuit, heat sinks

The proposed EV Battery Charging Station consists of four stages as shown in Fig. 1 namely

1. Rectification
2. Power factor Correction using Boost Converter

3. Higher to lower voltage conversion using DC-DC Buck Converter
4. Auto cutoff using a Relay

The Rectification is accomplished by a single phase uncontrolled full wave rectifier which produces a pulsating output waveform having an average value given by the equation (2.1) below.[8]

$V_{avg} = 2*V_{max}/\pi = 0.637*V_{max}$ (2.1)

where,

V_{avg}= Output Voltage of rectifier

V_{max}= Peak of input AC Voltage

In this work, a single-phase supply of 220V having an amplitude of 311.12V is connected in series with an inductor of 100 uH. It is meant for current smoothing and the output has been fed to the uncontrolled full wave rectifier for conversion of AC to DC Voltage.

The relative phase difference between the voltage and current signals fed to a load is known as Power factor. The phase difference should be kept to a minimum so that the maximum amount of power delivered to the load is usable power which is nothing but real power. The block diagram showing the Power Factor Correction mechanism is shown in Fig 2.1 The Boost converter Inductor Current and rectifier output voltage is sensed using a sense resistor. The voltage is given a gain and the output of it is multiplied with reference Inductor current. The current controller compares this with the actual inductor current, and the controller output is fed to the boost converter switch, which switches such that the current drawn by the inductor and the rectified DC voltage are in phase with each other.

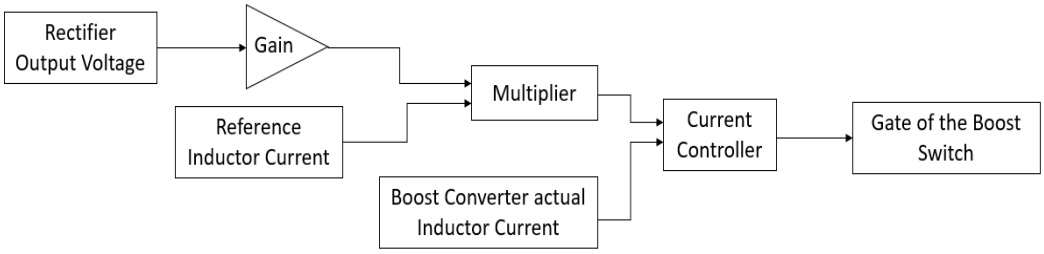

Fig. 2.1 Block diagram of Power Factor Correction mechanism

The output of the Power factor correction boost Converter is connected through a filter capacitor to a buck converter which is used to step down the voltage to 54.6V required for the Battery. The switching frequency of the buck MOSFET Switch is set as 500 kHz. The load is a resistor across which the output voltage and current has been measured. All the semiconductor switches used in the circuit have been provided with heat sinks to make sure the switches operate at optimal temperature conditions.

The design equations for the proposed buck converter are as follows: [9]

Duty cycle $D = V_{out}/V_{in}$ (2.2)

Where, V_{out} = Output Voltage

V_{in} = Input Voltage

ΔIL= 5% of Iout (2.3)
Where, Iout = Output Current
ΔIL = Inductor current ripple

L= (Vout*(1-D))/(Fsw*ΔIL) (2.4)
Where, L = Inductance
Vout = Output Voltage
D = Duty Cycle
Fsw = Switching Frequency

TABLE 2 - Specifications of Buck Converter

Sl No.	Parameter	Value
1	Input Voltage (Vin)	690V
2	Output Voltage (Vout)	54.6V
3	Output Current (Iout)	6A
4	Switching Frequency (Fsw)	500 kHz
5	Inductor Current Ripple (ΔIL)	5% of Iout=0.3A
6	Duty Cycle (D)	0.08
7	Inductor(L)	334μH

To limit the input voltage to the load, the relay is used for auto cut-off of the battery. The relay will be in on state if the input signal surpasses the upper threshold and if the input falls below the lower threshold, it will be in off-state. Input levels between the thresholds have no effect on the relay.

3. SIMULATION MODEL

The simulation model of the charging station developed using Plecs Software is shown in Fig 3.1

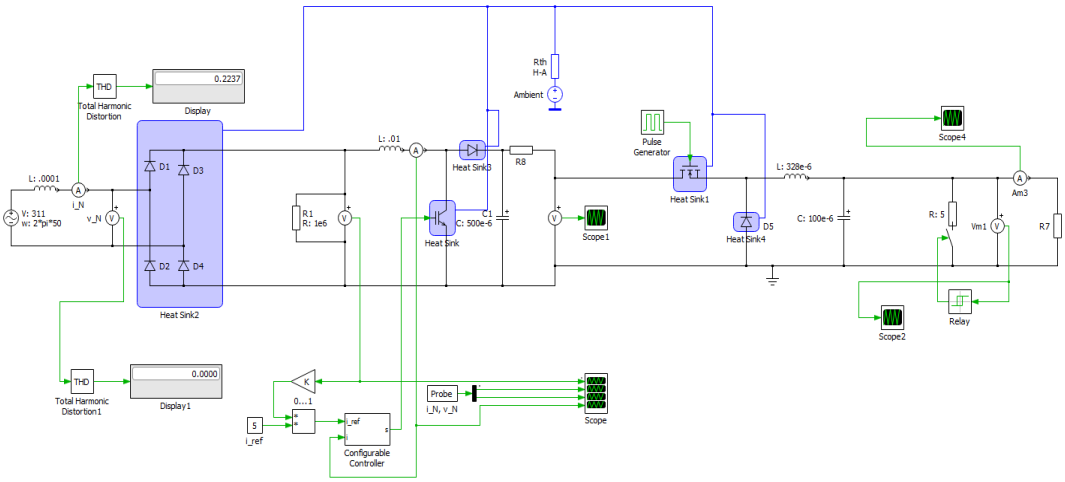

Fig 3.1 Simulation Model of the proposed charging station in Plecs

In the simulation model, the single phase 220V RMS AC Supply is given as input to the single-phase diode rectifier. The output of the rectifier is connected to a Power factor correction boost converter whose IGBT switch is controlled by a Configurable Controller. The output of PFC Boost Converter is connected to a buck converter which steps down the voltage as per the battery voltage and current requirement. The output of the boost converter is connected to the relay which cuts off the battery from the supply when the battery is fully charged. In the simulation, a load resistance is connected instead of a battery to validate the designed system and the working of the current controller.

The Simulation model of the current controller is shown in Fig 3.2

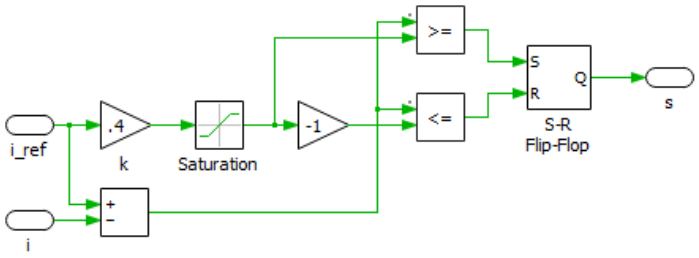

Fig 3.2 Configurable controller scheme

The output of the configurable controller is used to drive the IGBT of the Boost Converter for achieving power factor correction. The inductor current in the boost converter is compared with a reference current and given to the SR Flip Flop. The state of the SR Flip Flop is decided by the error in the inductor current compared to reference current. The output of the SR Flip Flop is given to the IGBT switch of the PFC Boost Converter of the proposed charging station.

4. RESULTS

The input and output waveforms of the single-phase diode bridge rectifier without power factor correction is shown in Fig.5.1 The mains current and voltage refer to input AC supply which are not in phase with each other which leads to non-unity power factor. Also, it can be observed that the mains current waveform is peaky in nature and not sinusoidal.

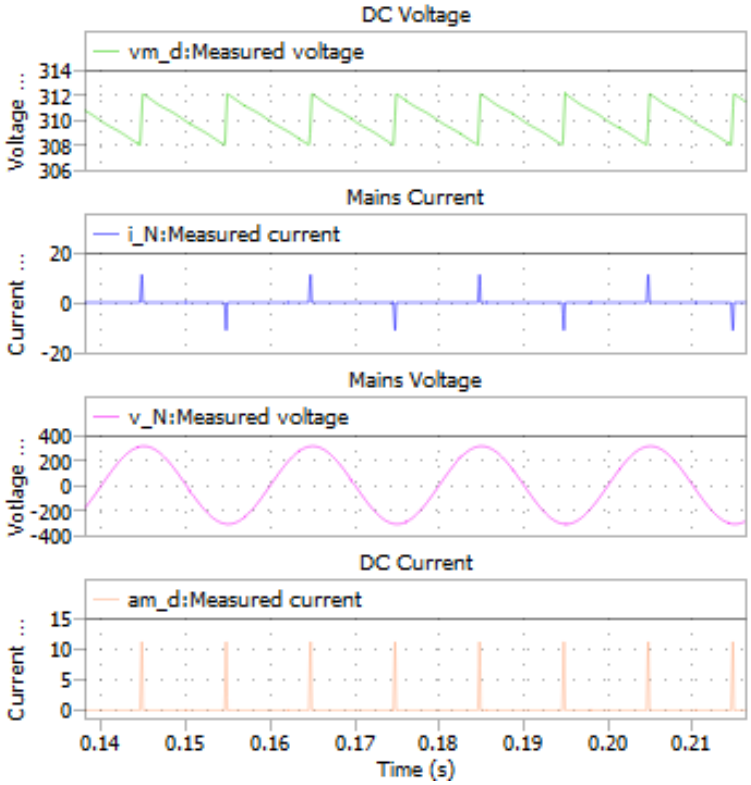

Fig.5.1 Measured voltages and currents without PFC

The input and output waveforms of the single-phase diode bridge rectifier with power factor correction as explained in the previous sections is shown in Fig.5.2 It can be observed that the mains voltage and current are in phase with each other and the mains current waveform is sinusoidal.

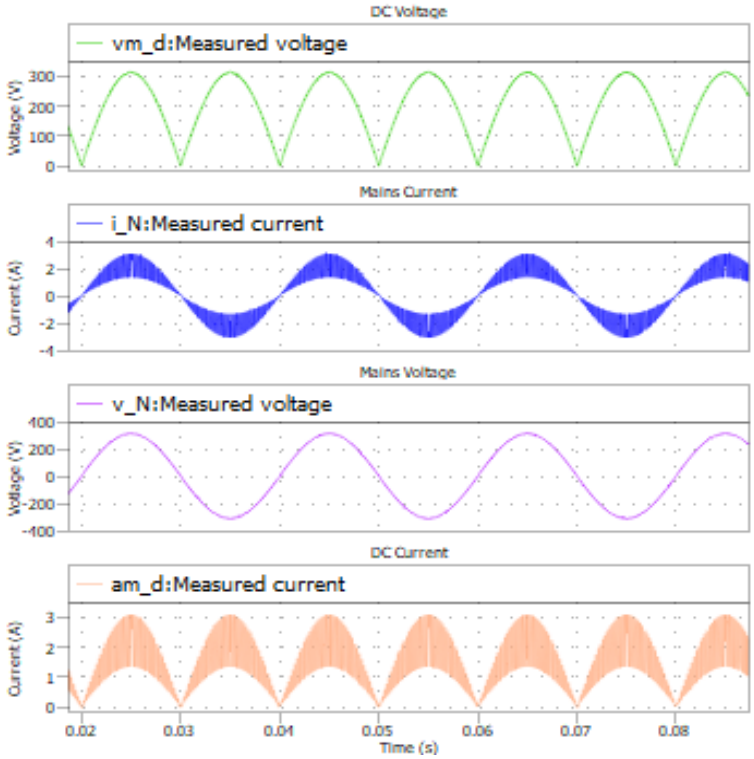

Fig.5.2 Measured voltages and currents with Active PFC

The output voltage waveform of the PFC Boost Converter is shown in Fig.5.3 It can be observed that the voltage has been rectified and has been boosted depending on the gate pulses given by the current controller to the IGBT Switch of the Boost Converter.

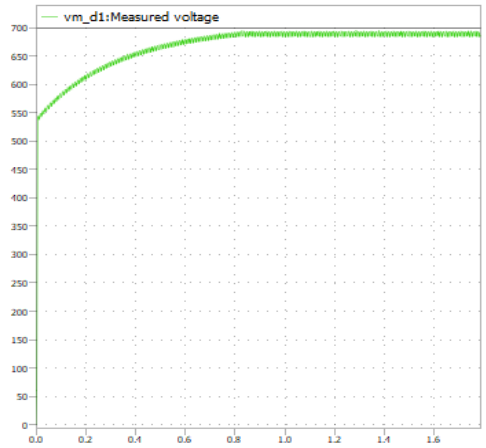

Fig.5.3 Measured voltage after boost converter and PFC

The output voltage and current waveforms of the buck converter is shown in Fig.5.4 and Fig.5.5 This steady DC voltage is fed as input to the EV Battery through a relay which is meant for auto cut-off. The

duty ratio of the Buck converter switch was fixed based on the output voltage requirement and input voltage fed.

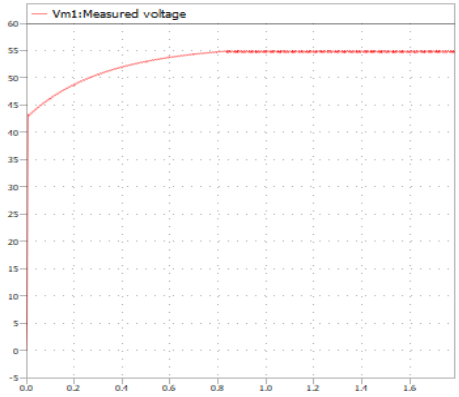

Fig.5.4 Measured voltage across the load

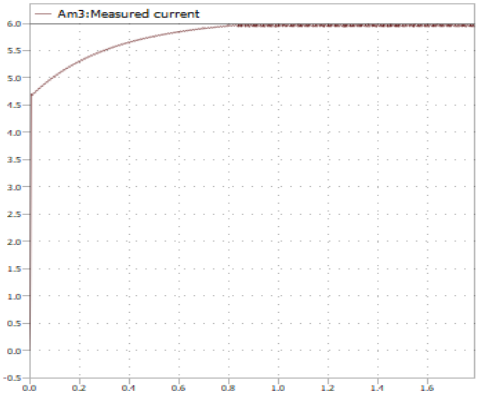

Fig.5.5 Measured current through the load

5. CONCLUSION

In this paper, the design of a charging station for EV swappable batteries is described. It was designed considering the requirements of the swappable Li ion battery for an e-bike. The proposed circuit design is simulated and verified using an open-source software called Plecs. The working of the current controller for Power Factor Correction and the designed system was validated by connecting a resistive load in the simulation. The results obtained from the simulation clearly shows that the incorporation of the Power factor Correction circuit reduces the amount of Reactive Power drawn from the AC Supply thereby reducing the Power losses and increasing the Power factor of the system. Hence the Power Factor Correction plays an important role in increasing the overall efficiency of the EV Charging Station.

6. ACKNOWLEDGMENT

We would like to thank Krushabh Prajapati and Dhruv Singh, co-founders of RedEvQ startup, for giving us the opportunity to intern in their startup and help in designing the charging station for the given requirement. It was indeed a great learning experience. Special regards and thanks to our professor, Dr. R.S Geetha for guiding and encouraging us to make this research paper possible.

7. REFERENCES

[1] “Efficiency Analysis of Charging Station for Electric Vehicles Using the Active Rectifier in Microgrid System” by Zhemerov, G., Plakhtii, O., & Mashura, A 2020 IEEE 4th International Conference on Intelligent Energy and Power Systems (IEPS).

[2] "Electric Vehicle Charging Station Challenges and Opportunities: A Future Perspective", Pareek, S., Sujil, A., Ratra, S., & Kumar, R. 2020 International Conference on Emerging Trends in Communication, Control and Computing (ICONC3).

[3] “Analysis of the Impact of Electric Vehicle Charging Station on Power Quality Issues” by Ashish Kumar Karmaker, Sujit Roy, Md. Raju Ahmed, 2019 International Conference on Electrical, Computer and Communication Engineering (ECCE), 7-9 February, 2019.
[4] "Design, simulation and analysis of a fast charging station for electric vehicles" by Mohd Khalid,Furkan Ahmad,Bijya Ketan Panigrahi, 4th July 2021.
[5] "A Comprehensive Review on Developments in Electric Vehicle Charging Station Infrastructure and Present Scenario of India" by Shubham Mishra,Shrey Verma, Subhankar Chowdhury ,Ambar Gaur ,Subhashree Mohapatra,Gaurav Dwivedi and Puneet Verma, 23rd Feb 2021, IEEE Access.
[6] "Power Electronics Converters for an Electric Vehicle Fast Charging Station with Energy Storage System and Renewable Energy Sources" by J. G. Pinto, Vitor Monteiro, Bruno Exposto, Luis A. M. Barros, Tiago J. C. Sousa, L. F. C. Monteiro and João L. Afon, 21st Nov 2019, EAI.EU.
[7] "Power factor correction (PFC) circuit basics" by Texas Instruments.
[8] "Rectification of a single-phase supply" by Electronics tutorials.
[9] “Buck Converter Design” by Infineon technologies

Biographies

B Sumedha Shenoy has completed Bachelor’s Degree in Electrical and Electronics Engineering from B.M.S College of Engineering, 2018-2022. Currently working in Schneider Electric, R&D India in the field of Electromechanics and Energy management.

Varsha M completed her Bachelor’s in Electrical and Electronics Engineering from B.M.S College of Engineering, Bangalore in 2022. She is currently working as Electrical Engineer 1 at Lam Research, India in the area of power distribution system design.

A Deep Learning Model for the Prediction of Remaining Useful Life of Lithium-Ion Batteries

Manali Raman[1], V. Champa[1], Prema V[1] and Priya Ranjan Mishra[2]*
[1]Dept. of EEE, BMS College of Engineering, Bangalore, India
[2]BelBird Technologies Private Limited, Bangalore, India
**manalir@bmsce.ac.in*

Abstract.

Accurate state of Health (SOH) and remaining useful life (RUL) prediction is the key to ensure safety and reliability of Lithium-Ion Batteries (LIBs). Recent advances in deep learning algorithms have led to data-driven estimation approaches with improved accuracy. This paper employs data-driven technique for SOH prediction by utilizing multiple battery datasets that are multivariate time series (MTS) that are packed with dynamical information of the battery ageing system. In this paper, authors have proposed a hybrid method, namely the CNN-LSTM model, which improves the prediction accuracy by exploiting advantages of both Convolutional Neural Network (CNN) and Long Short-Term Memory (LSTM) methods, for the prediction of SOH and RUL of the LIBs. A comparison against relevant deep learning forecasting algorithms is carried out by utilizing various statistical indicators like the MAE, MAPE and RMSE, to numerically evaluate the prediction results. The proposed hybrid estimation approach outperforms other relevant deep learning techniques. Authors have validated the results experimentally by utilizing multiple NASA battery datasets at different temperatures.

Keywords. Convolutional Neural Network, CNN-LSTM network, Deep Neural Network, Long-short term memory network, State of Health Estimation and Remaining Useful Life estimation of batteries

1. INTRODUCTION

The rapid endorsement of electric vehicles (EVs) has led to significant rise in the demand of LIBs [1]. In the meantime, EV batteries have started to reach their end-of-life condition and it is expected to observe an exponential growth of these retired EV batteries in the nearing decades. Consequently, the world would be in risk from potential waste of retired EV LIBs. Bloomberg New Energy Finance predicts that the incremental addition of the retired EV batteries can show up at 185.5 GWh/year in capacity by 2025 [2]. A second study estimates the cumulative retired EV batteries capacity could hit approximately 1000 GWh by 2030 [3]. IDTechEX predicts that the total amount of EV batteries retiring from vehicles will reach 7.8 million tonnes per year by 2040 [4]. These retired EV batteries can either be reutilized for a second life in stationary applications or it can be recycled to procure the raw materials.

Theoretically, recycling is marginal sustainable measure taken in circular economy and therefore, recycling should be the final step, only in the case when batteries are not utilizable anymore. Hence, before recycling retired EV batteries, they should be taken into consideration for remanufacturing or repurposing for second life. The LIBs retired from EVs retain 70-80% of their initial capacity unlike the batteries used in consumer

electronics [5]. These retired EV batteries are ineffective for EV service as decline in battery capacity limits the driving range. But these retired EV batteries, with lower SOH, can still meet the requirements of less demanding stationary applications like energy storage [6]. Therefore, second life becomes an attractive option for retired EV batteries having LFP chemistry.

However, estimating SOH is complex because numerous internal and external factors causing degradation of batteries are involved in calculation. Estimates of capacity and power degradation of ageing battery could reasonably estimate SOH [7]. SOH prediction methods are categorized into experimental methods and adaptive battery methods. Experimental techniques include model-based measurements and direct measurements. Merits of these experimental techniques are lesser computational power and easier Battery Management System (BMS) implementation [8]. Demerits like lower accuracy and time consuming make these methods less popular. Alternatively, adaptive methods like Kalman Filters need high computational effort and integration to BMS is difficult [9]. Recent method of combining electrochemical and mathematical models yields better results at cost of increased complexity and computational resources [10].

The data-driven method being the state-of-the-art method can be utilized if data from the battery's previous life can be gained. These methods are asserted to be more powerful as statistical and machine learning approaches are incorporated, without depending on complete understanding of the various degradation mechanisms like solid electrolyte interphase formation, dendrite formation, lithium plating, physical changes like particle cracking and fragmentation. Considering these aspects, data-driven approaches have an edge over conventional SOH estimation methods, as data-driven methods use historical data for prediction and do not need understanding of complex physical, chemical and mathematical models of LIBs capacity degradation. Hence, authors have considered data driven methods for estimating SOH of ageing LIBs. Data driven approaches are machine learning techniques, evolutionary algorithms, artificial neural network and deep neural networks. Various researchers have proposed different data driven methods for RUL prediction of LIBs, like recurrent neural network [11], LSTM [11], support vector machine [12], etc. LSTM models and CNNs are widely accepted, efficacious and established deep learning methods [13]. [14]-[16] are the recent research papers which have employed CNN-LSTM technique to estimate RUL of LIBs. The essential ideology supporting the implementation of CNN and LSTM techniques on time-series forecasting is the ability of LSTM networks to proficiently apprehend sequence pattern information of long sequential data owing to their distinct architecture design which constitutes internal memory. Whereas CNN networks can efficiently filter the noise of sequential data and can draw significant features of multivariate time series data. Standard CNNs are suitable for addressing spatial autocorrelation data, and LSTM models are tailored to deal with temporal correlations. Therefore, authors have proposed a deep learning network which exploits the merits of both LSTM and CNN techniques to enhance the SOH and RUL prediction performance of ageing LIBs. Authors have employed multiple battery datasets at different temperatures that are multivariate time series for SOH and RUL estimation, which are unlikely to be seen in available literatures.

The paper is organized in following manner: Section 1 presents a brief survey of retired EV lithium-ion batteries and its current literatures concerning the second life application

various data-driven techniques in SOH and RUL prediction of ageing LIBs. Section 2 describes the details of the proposed CNN-LSTM deep learning technique. Section 3 discusses the data of ageing lithium-ion battery. Section 4 presents results obtained and related discussions. Section 5 summarizes the findings of the research undertaken.

2. PROPOSED MODEL

The primary idea of the proposed model is to effectively integrate the merits of the two established and efficient deep leaning techniques namely CNN and LSTM.

2.1. Convolutional and pooling layers

These layers are particularly made for data pre-processing; hence it filters noises from input data and extract input features i.e., important information which is usually utilized as an input for next network layer [17]. These convolutional layers perform convolution operation on convolution kernels and input data generate some feature values. This necessitates that input to be organised in matrix form, as CNN was essentially developed to extract features of image. Convolution kernel can be thought of as a small window containing coefficient values in matrix for (for comparison with the input matrix). This tiny window performs convolution operation on every patch met by the specified window across the input matrix as the window slides over the input data. The resulting convolved matrix corresponds to a feature value. By employing various convolution kernels on the input datasets, several corresponding features are developed. These convolved features are better than the actual features of the input datasets and hence, the model performance is improved. The convolutional layers are generally accompanied by a nonlinear activation function to introduce some amount of non-linearity. These layers are then followed pooling layers to decrease dimensionality of feature maps. Consequently, the pooling layer provides matrices which comprehend the convolved features. The pooling operation assists in making the system more robust

2.2. LSTM layers

LSTM models are specialized recurrent neural networks (RNNs) that learn the long-term dependencies by employing feedback connections [18]. Conventional RNNs are feed forward neural networks, and its lack of memory causes underperformance on long temporal sequences and time-series problems. RNNs use recurring connections on their hidden layers to obtain information from time-series sequential data and attain short term memory. However, RNNs are inefficient in learning long-term dependencies of sequential data as it’s affected by vanishing gradient problem. LSTM resolves this issue by learning long term dependencies by managing controlled flow of information by storing important data on memory cells and deleting insignificant information.

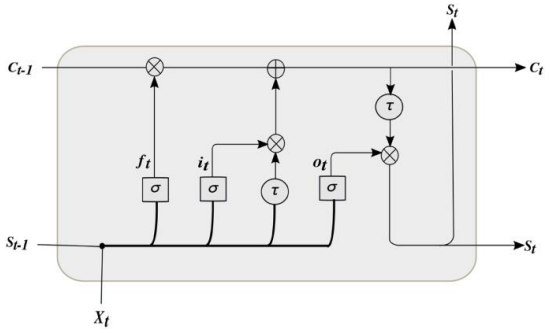

Fig. 1: LSTM block andf_t, i_t, o_t are forget, input and output gates respectively

As exhibited in Fig. 1 the LSTM cell is comprised of different gates, which are input gate, output gate, forget gate and self-recurrent neuron. The inter activeness among various memory units are controlled by these gates. The input gate checks if the input data can change memory cell's state or not. The output gate manages the modification of other memory cells' state. In contrast the forget gate can decide to discard or retain its past information. Various gates, cell states, hidden states and outputs can be represented as follows:

$$f_t = \sigma(X_t U^f + S_{t-1} W^f + b_f) \quad (1)$$
$$i_t = \sigma(X_t U^i + S_{t-1} W^i + b_i) \quad (2)$$
$$o_t = \sigma(X_t U^o + S_{t-1} W^o + b_0) \quad (3)$$
$$C_t^{\sim} = \tanh(X_t U^c + S_{t-1} W^c + b_c) \quad (4)$$
$$C_t = C_{t-1} \otimes f_t \oplus i_t \otimes C_t^{\sim} \quad (5)$$
$$S_t = o_t \otimes tanh C_t \quad (6)$$

where(U^f , U^i, U^o , U^c),(b_f , b_i, b_0, b_c) and (W^f, W^i , W^o, W^c) are input weights, biases and recurrent weights respectively. C_t, X_t and S_t and are cell, input and hidden states respectively at time step t. While at time step t − 1, C_{t-1} and S_{t-1} are cell state and hidden respectively. $\otimes$, σ, $\oplus$ and are pointwise multiplication, sigmoid activation and pointwise addition respectively.

2.3. CNN–LSTM model

The objective of the research undertaken is to attain RUL prediction with improved accuracy and acceptable execution time by combining CNN and LSTM. CNN-LSTM is employed for multivariate time series ageing Li-ion batteries datasets for prediction of the RUL. The architecture of CNN-LSTM comprising its building blocks is as shown in Fig. 2. The CNNLSTM model exploits the usefulness and merits of both CNN model and LSTM model. Here both spatial and temporal features are extracted. The interrelations within present inputs are the spatial features and these are extracted by CNNs. Whereas LSTM bring out the correlations between present SOH and previous inputs which can be understood as the temporal (time domain) features. By recursive execution of the input vectors processing, the LSTM networks become better at treatment of time-series information [19].

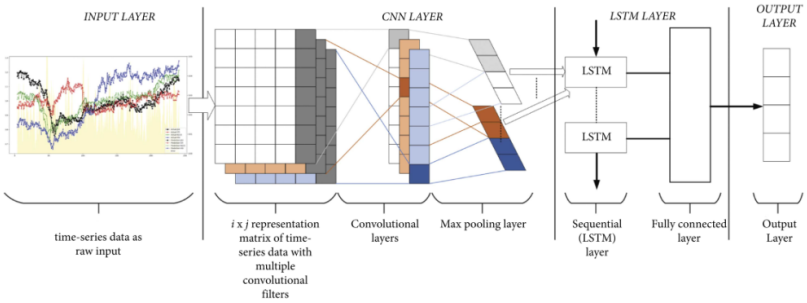

Fig. 2: Proposed architecture of CNN-LSTM network

3. DATASETS

The experimental datasets are considered by extracting different batteries of NASA Prognostics Centre of Excellence Battery ageing datasets that consists of aging data for LIBs [20]. All the LIBs were examined through 3 distinct operational processes namely: charge, discharge and impedance. For all the LIBs, charging was carried out at a constant current (CC) mode at 1.5A till the LIB voltage hit 4.2V, following this a constant voltage (CV) mode was carried out until the charging current decreased to 20mA. A set of four LIBs (# 05, 06, 07 and 18) were run at room temperature (24 deg C), another set of four LIBs (# 29, 30, 31 and 32) were run at elevated ambient temperature (43 deg C) and yet another set of four LIBs (# 53 - 56) were run at reduced temperature of 4 deg C. Table I illustrates the information about LIBs used.

Table I: Experimental Dataset, Comprising 3 Groups of Cells at Different Temperature

File Name	Included Cell	Discharge	Temperature Cycled	Cycled until
Battery Aging ARCFY08Q4	Three cells numbering #05 and #6	Discharge was conducted with CC level of 2A till LIB voltage dropped to 2.7V and 2.5V for batteries #05 and #06 respectively	24 deg C	30% fade
Battery Aging ARC 25-44	Three cells numbering #29 and #30	Discharge was conducted with CC level of 4A till LIB voltage dropped to 2.0Vand 2.2V for batteries #29 and #30 respectively	43 deg C	30% fade
Battery Aging ARC 53 54 55 56	Three cells numbering #55 and #56	Discharge was conducted at fixed load current of 2A and distinct stop voltages 2.5V and 2.7V for batteries #55 and #56 respectively	4 deg C	30% fade

Sustained charge discharge cycles caused accelerated aging of LIBs. These experiments were discontinued when LIBs reached 30% fade in rated capacity which is End-of- Life (EOL) criteria. Fig. 3 depicts capacity degradation over time for all the LIBs considered for testing and implementation. By data pre-processing, authors can obtain the datasets of particular LIBs. These datasets constitute the fields like impedance, charge and discharge. Among these fields, authors have selected the discharge data as discharge datasets are more relevant in case of capacity degradation. In discharge datasets we have considered all relevant features like cycle number, battery capacity (Ahr), terminal battery voltage, battery current, battery temperature, load current, voltage under load. These parameters are

highly reliable, and they characterize the actual performance and degradation LIBs accurately under different cell aging conditions.

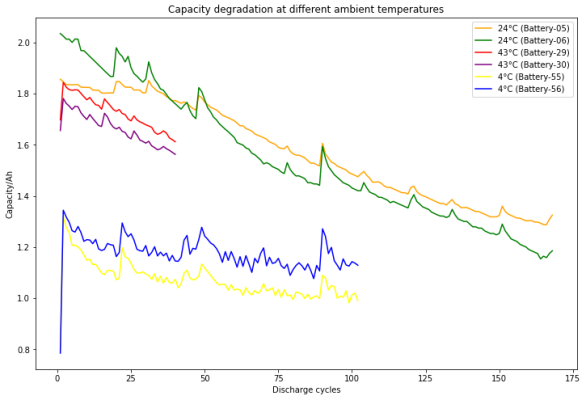

Fig. 3: Capacity Degradation over Charge/Discharge Cycles

4. RESULTS AND DISCUSSIONS

This section summarizes SOH and RUL estimation methods and various performance metrics that are adopted for the comparisons and validation. Further, we evaluate the effectiveness of the proposed CNN–LSTM model in comparison with the state-of-the-art methods namely LSTM and CNN.

4.1. SOH and RUL Estimation

In literature, there are various definitions for battery SOH. For understanding, we used the SOH [%] , which can be defined as:

$$SOH(\%) = \frac{C_{bat}}{C_{nom}} * 100\ [\%] \tag{7}$$

Where: SOH [%] is the battery SOH, C_{bat} is the current LIB capacity and C_{nom} is the LIB nominal capacity. RUL is stated as the length of remaining charge/discharge cycles to reach the threshold of failure of the LIBs. Threshold of failure can be considered as the EOL of LIBs when the remaining output capacity hits to 70–80% of the nominal output capacity of LIB. This is established as:

$$RUL = T_{EOL} - T_{CC} \tag{8}$$

T_{EOL} is the cycle number at which output capacity hits the failure threshold i.e. EOL and T_{CC} is the current capacity's cycle number.

4.2. Performance Measures

Besides, evaluation of RUL prediction performance, we have used the mean absolute error (MAE), mean absolute percentage error (MAPE), and the root mean square error (RMSE) as performance metrics for SOH estimation:

$$MAE = \frac{1}{n}\sum_{1}^{n} |C_k - C_k^{\wedge}| \tag{9}$$

$$MAPE = \frac{100}{n}\sum_{k}^{n} \frac{|C_k - C_k^{\wedge}|}{C_k} \tag{10}$$

$$RMSE(\%) = \sqrt{\frac{1}{n}\sum_{k}^{n}(C_k - C_k^{\wedge})^2} \tag{11}$$

Where k is the cycle number, $C_k^{\wedge}$ is estimated LIB capacity, C_k is the true capacity of LIB and n is total number of cycles. The MAE measures how close the predictions are to the corresponding true observations without sign consideration. MAE is insensitive to outliers as it gives less weight to outliers. MAPE is closer to MAE, but it is normalized by true observation. RMSE refers to Root of MSE which is a combination measurement of variance and bias of the prediction. The unit is brought back to actual unit by RMSE and makes model accuracy interpretation is made easier. When these indicators are close to zero, then it can be stated that capacity prediction accuracy is higher.

4.3. Experimental Results

The code was implemented in Python by using open-source distribution for programming namely Anaconda 3.0. The deep learning models were developed using Keras library [21] with Tensorflow 2.0 as backend. All the models (LSTM, CNN and CNNLSTM) were trained for maximum of 500 epochs with early stopping. Adaptive moment estimation (ADAM) is used as optimizer and the batch size used was 72. The activation function employed is rectified linear unit (ReLU) and the loss function is mean-squared loss.

We have adopted multi battery datasets for SOH estimation. Since training and testing datasets should have similar operational profiles, therefore one battery from each temperature group is considered for training and other battery is utilized for testing. For batteries at 24 deg C, #05 is used for training the model and #06 is employed for testing. For batteries at 43 deg C, #29 is employed for training and #30 is utilized for validating the model. Similarly for batteries at 4 deg C, #55 is adopted for training the models and #56 is used for testing. Various performance metrics results are displayed in Table II.

Table II: SOH Estimation Results for Various Batteries

Battery	Model	MAE	MAPE	RMSE
B0006	LSTM	0.115316	0.076345	0.12709
	CNN	0.0872128	0.058788	0.098374
	CNNLSTM	**0.080202**	**0.054259**	**0.089557**
B0030	LSTM	0.059344	0.034233	0.06207
	CNN	0.058901	0.034158	0.059317
	CNNLSTM	**0.051973**	**0.030214**	**0.052244**
B0056	LSTM	0.043546	0.036565	0.050271
	CNN	0.031195	0.026098	0.037071
	CNNLSTM	**0.027973**	**0.023428**	**0.033831**

Fig. 4a, 4b and 4c show the prediction results for batteries at 24 deg C, 43 deg C and 4 deg C respectively. Battery #30 at 43 deg C has a smaller number of cycles than batteries at 24 deg C during capacity degradation. It can be evidently seen that it's challenging to forecast with the battery datasets. Despite that, the CNN-LSTM algorithm achieved better results in comparison of simpler LSTM and CNN networks. Further, RUL errors at 80% capacity degrade for #06 is 2, -8 and -1 cycles for LSTM, CNN and CNN-LSTM networks respectively. For other batteries, as per given datasets capacity degrade does not reach 80%, which can be observed in Fig. 4b and Fig. 4c. Hence, it is seen that RUL is significantly less for CNN-LSTM technique. The aforesaid experiments declare that the proposed CNN-LSTM based algorithm has effectively captured the dynamic features of LIBs with efficient learning.

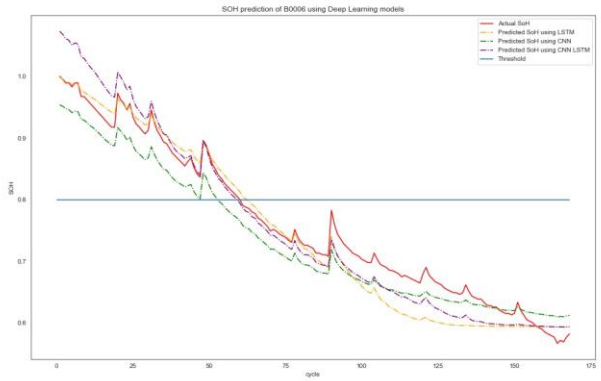

a.

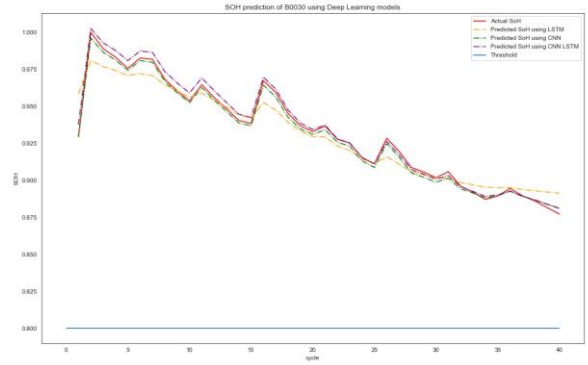

b.

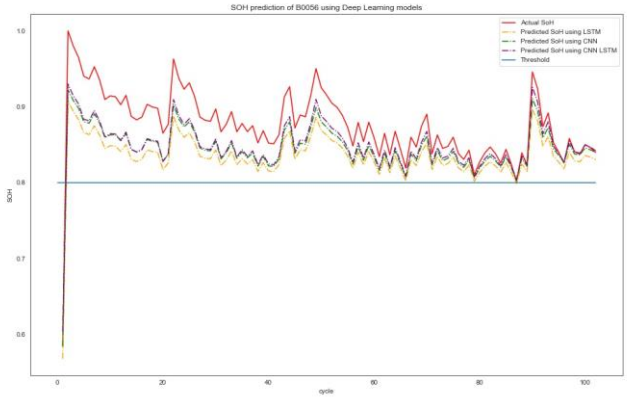

c.

Fig. 4: SOH Estimation Results for Battery (a.) #6, (b.) #30 and (c.) #56

The proposed methods, particularly CNN-LSTM has improved estimation performance with significant prediction accuracy. MAPE of CNNLSTM is 0.05, 0.03 and 0.02 for batteries #06, #30 and #56 respectively. Hence it is observed that improved values are obtained

5. CONCLUSION

In the research undertaken, authors have presented multi battery SOH prediction method based on state-of-the-art CNNLSTM neural networks. The proposed deep learning framework has been implemented and tested on different LIBs dataset, for three different temperature ranges (24 deg C, 43 deg C, and 4 deg C). The estimation performance of the proposed method has been assessed using various performance metrics. Comparisons performed against different relevant deep neural networks CNN and LSTM show the superior performances of the CNN-LSTM. The estimation errors of the hybrid CNNLSTM method are lesser than the ones obtained with the single deep learning algorithm. Hence, CNN-LSTM-based estimation method is a very suitable candidate for multi battery SOH and RUL prediction.

6. REFERENCES

[1] Gavin Harper, Roberto Sommerville, Emma Kendrick, Laura Driscoll, Peter Slater, Rustam Stolkin, Allan Walton, Paul Christensen, Oliver Heidrich, Simon Lambert, et al, 'Recycling lithium-ion batteries from electric vehicles', Nature, 575(7781), pp. 75–86, 2019.

[2] David Stringer and Jie Ma, 'Where 3 million electric vehicle batteries will go when they retire', Bloomberg Business week, 27, 2018.

[3] Gerard Reid and Javier Julve, 'Second life-batteries as flexible storage for renewables energies', Bundesverband Erneuerbare Energies EV (BEE), 2016.

[4] Dr Na Jiao Dr Alex Holland, 'End-of-life electric vehicle batteries: Recycling or second-life?', http://https://www.idtechex.com/de/research-article/end-of-life-electric-vehicle-batteries-recycling-or-second-life/20900/, Online; accessed 11-June-2020.

[5] Yang Hua, Sida Zhou, Yi Huang, Xinhua Liu, Heping Ling, Xinan Zhou, Cheng Zhang, and Shichun Yang, 'Sustainable value chain of retired lithium-ion batteries for electric vehicles', Journal of Power Sources, 478:228753, 2020.

[6] Eklas Hossain, Darren Murtaugh, Jaisen Mody, Hossain Mansur Resalat Faruque, Md Samiul Haque Sunny, and Naeem Mohammad, 'A comprehensive review on second-life batteries: Current state, manufacturing considerations, applications, impacts, barriers & potential solutions, business strategies, and policies', IEEE Access, 7, pp. 73215–73252, 2019.

[7] MS Hossain Lipu, MA Hannan, Aini Hussain, MM Hoque, Pin J Ker, MH Md Saad, and Afida Ayob, 'A review of state of health and remaining useful life estimation methods for lithium-ion battery in electric vehicles: Challenges and recommendations', Journal of cleaner production, 205, pp.115–133, 2018.

[8] Youlang Zhang, Yan Li, Yibin Tao, Jilei Ye, Aiqiang Pan, Xinzhou Li, Qiangqiang Liao, and Zhiqin Wang, 'Performance assessment of retired ev battery modules for echelon use', Energy, 193:116555, 2020.

[9] Gregory L Plett, ‘Extended kalman filtering for battery management systems of lipb-based hev battery packs: Part 1. Background’, Journal of Power sources, 134(2), pp. 252–261, 2004.

[10] Wladislaw Waag, Christian Fleischer, and Dirk Uwe Sauer, ‘Critical review of the methods for monitoring of lithium-ion batteries in electric and hybrid vehicles’, Journal of Power Sources, 258, pp. 321–339, 2014.

[11] Yongzhi Zhang, Rui Xiong, Hongwen He, and Michael G Pecht, ‘Long short-term memory recurrent neural network for remaining useful life prediction of lithium-ion batteries’, IEEE Transactions on Vehicular Technology, 67(7), pp. 5695–5705, 2018.

[12] X Hu, J Jiang, D Cao, and B Egardt, ‘Battery health prognosis for electric vehicles using sample entropy and sparse bayesian predictive modeling’, IEEE Transactions on Industrial Electronics, 2015.

[13] Hassan Ismail Fawaz, Germain Forestier, Jonathan Weber, Lhassane Idoumghar, and Pierre-Alain Muller, ‘Deep learning for time series classification: a review’, Data mining and knowledge discovery, 33(4): pp. 917– 963, 2019.

[14] B. Zraibi, C. Okar, H. Chaoui and M. Mansouri, "Remaining Useful Life Assessment for Lithium-Ion Batteries Using CNN-LSTM-DNN Hybrid Method," in IEEE Transactions on Vehicular Technology, vol. 70, no. 5, pp. 4252-4261, May 2021, doi: 10.1109/TVT.2021.3071622.

[15] A. Rastegarpanah, Y. Wang and R. Stolkin, "Predicting the Remaining Life of Lithium-ion Batteries Using a CNN-LSTM Model," 2022 8th International Conference on Mechatronics and Robotics Engineering (ICMRE), 2022, pp. 73-78, doi: 10.1109/ICMRE54455.2022.9734081.

[16] Yassine Toughzaoui, Safieh Bamati Toosi, Hicham Chaoui, Hasna Louahlia, Raffaele Petrone, Stéphane Le Masson, Hamid Gualous, “State of health estimation and remaining useful life assessment of lithium-ion batteries: A comparative study”, Journal of Energy Storage, vol. 51, 2022, 104520, doi:10.1016/j.est.2022.104520.

[17] Waseem Rawat and Zenghui Wang, ‘Deep convolutional neural networks for image classification: A comprehensive review’, Neural computation, 29(9), pp. 2352–2449, 2017.

[18] Sepp Hochreiter and J¨urgen Schmidhuber, ‘Long short-term memory’, Neural computation, 9(8), pp. 1735–1780, 1997.

[19] Aniruddha Ghosh and Tony Veale, ‘Fracking sarcasm using neural network’, In Proceedings of the 7th workshop on computational approaches to subjectivity, sentiment and social media analysis, pp. 161–169, 2016.

[20] B Saha and K Goebel, ‘Battery data set. NASA ames prognostics data repository’, NASA ames research center. moffett field, ca, USA, 2007.

[21] Antonio Gulli and Sujit Pal, ‘Deep learning with Keras’, Packt Publishing Ltd, 2017.

Comparative Analysis of Positive Buck Boost Converter with PID and Fuzzy Logic Controller

Piyush Singh[1,*], P. Parthiban[1], R. Kalpana[1], S.Rambabu[2], M.Vijaya[2]

[1]Department of Electrical & Electronics Engineering – National institute of technology Karnataka, surathkal India-575025

[2]NSTL Visakhapatnam India

[*]Email id – piyushsingh210196@gmail.com

Abstract.

This paper presents the closed loop working and analysis of PBB converter. Implementation of closed loop is performed with both PID and Fuzzy logic controller separately, the results are verified with simulations. Obtained performances are further compared on the basis of settling time, overshoots & Output deviations. It requires small signal analysis done by small signal linearization or state space averaging method. Both gives the similar transfer function of converter after which compensator is designed for obtaining the desired output. Instead of modelling, FLC is implemented according to system behaviour.

Keywords. Positive buck boost (PBB), fuzzy logic controller (FLC), state space averaging, small signal modelling, right half plane (RHP), pulse width modulation (PWM), proportional–integral–derivative controller (PID)

1. INTRODUCTION

There's a major difference between the textbook's simple inverting buck-boost converter, which produces a negative output voltage, and real-world buck-boost applications, which requires a positive output voltage, when it comes to buck-boost converter design. Thus, the PBB converter topology as shown in Figure 2.1 is used to obtain the positive output voltage, which is nothing more than the cascading of buck and boost converters, which by default produces positive output voltage and can also be used as a Bi-directional converter with minor changes, which is widely used in the renewable energy sector [1] and in electric vehicle (EVs) [2] applications. SEPIC, Zeta and Flyback topologies also have positive output voltage but are avoided because of their complexity in structure, RHP zero and fourth-order system, which makes closed loop control techniques challenging. In this paper our aim is to achieve smooth transition from one mode to another mode automatically when input supply is varying between below and above the reference output voltage.

This paper is divided into five sections, the second section discusses the working analysis of PBB converter, third section describes about closed loop operation with single PID controller and fuzzy logic controller, the fourth section presents simulation results with discussions, which is followed by conclusion in the fifth section.

2. POSITIVE BUCK BOOST CONVERTER WORKING

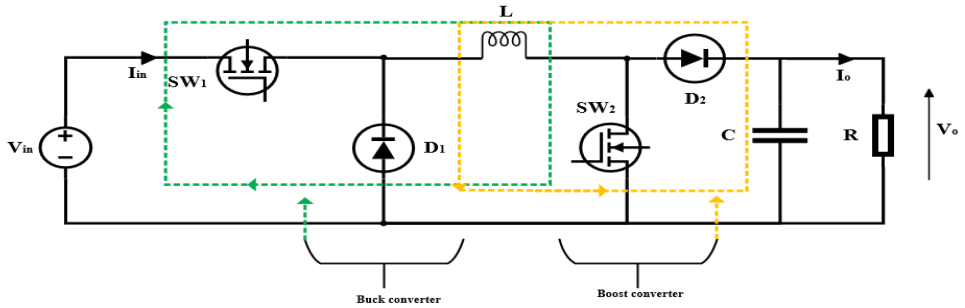

Figure 2.1 Positive buck boost converter

2.1. Buck mode

In this mode switch (sw_1) is given controlled PWM and (sw_2) is kept open as shown in Figure 2.2 thus behaving exactly as conventional buck converter and both charging and discharging mode is performed according to given duty cycle to (sw_1).When input voltage is same as reference output voltage switch (sw_1) is continuously ON. [3]

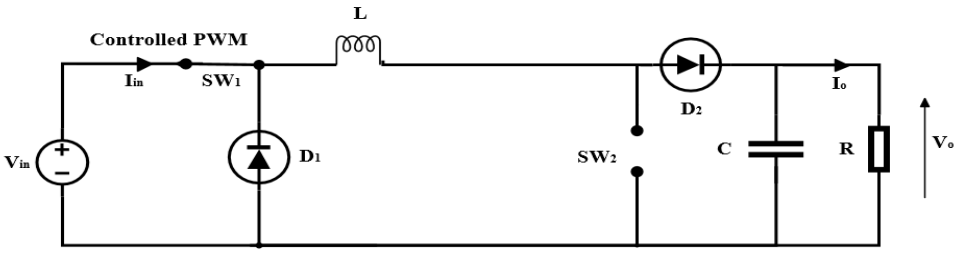

Figure 2.2 Buck mode

2.2. Boost mode

In this mode switch (sw_1) is continuously ON to provide path for the circuit and (sw_2) is given controlled PWM to make boost mode operation successful as shown in the Figure 2.3. Thus it can be operated as standalone boost converter with all conventional equations valid.

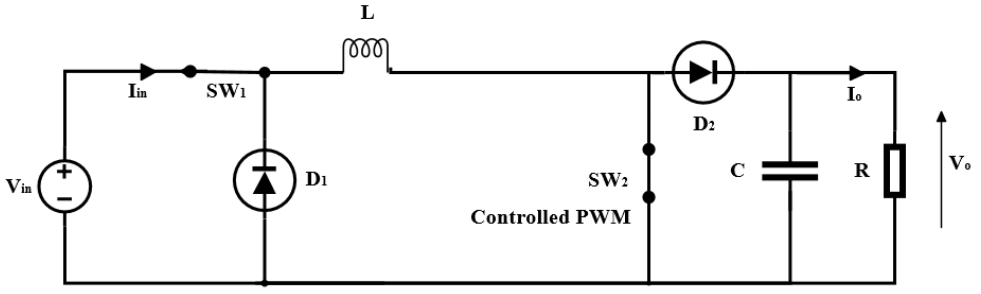

Figure 2.3 Boost mode

2.3. Buck-boost mode

In this mode of operation both the switches are given controlled PWM so that it performs both buck and the boost operations simultaneously without inverting the output voltage and giving positive output voltage as depicted in Figure 2.4. The issue with this mode of operation is that both the switches (sw_1) and (sw_2) are operating at the same time which will create high turn- on and turn-off losses. Also these losses would be high as power ratings and switching frequency of the converter is increased so this mode of operation is avoided. Instead separate buck and boost mode is performed when buck-boost operation is required.

Although controlling of both the switches for separate modes in PBB converter makes it challenging as compared to conventional buck-boost converter where only one switch needs to be controlled for closed loop operation. But due its certain advantages it is used over conventional converter according to applications.

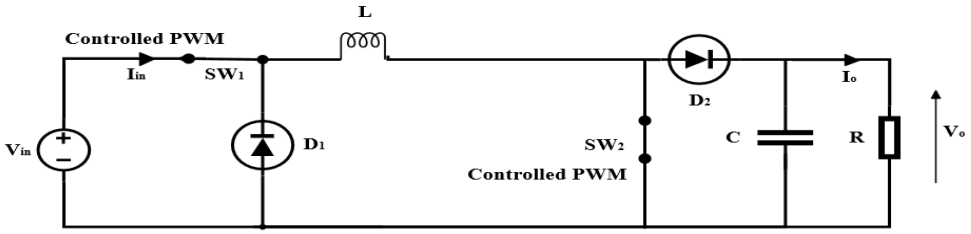

Figure 2.4 Buck boost mode

2.4. Selection of inductor

Since PBB converter is capable of operating in different modes, selection and design of inductor value is very crucial and it should works in continuous conduction for all the modes. Equations 2.1 & 2.2 are used for inductor calculation as shown below. [4] [5]

Boost inductor

$$\mathbf{L} > \frac{\mathbf{V_{in,min}^2} * \left(\mathbf{V_o} - \mathbf{V_{in,min}}\right)}{\mathbf{f_{sw}} * \mathbf{0.3} * \mathbf{I_o} * \mathbf{V_o^2}} \qquad \mathbf{2.1}$$

Buck inductor

$$\mathbf{L} > \frac{\mathbf{V_o} * \left(\mathbf{V_{in,max}} - \mathbf{V_o}\right)}{\mathbf{0.3} * \mathbf{f_{sw}} * \mathbf{V_{in,max}} * \mathbf{I_o}} \qquad \mathbf{2.2}$$

Where $\mathbf{f}_{sw}$ is switching frequency of MOSFET

From above two equations the higher inductor value obtained is chosen so that it satisfies working in all the modes. In practice slight variations are acceptable from ideal calculations.

Table 1 Switching pattern of MOSFETs

Modes	**Switch (sw_1)**	**Switch (sw_2)**
Buck	PWM	Always off
Boost	Always on	PWM
Buck–boost	PWM	PWM

3. CONTROL METHODS OF CONVERTER

3.1. PID controller

To obtain the desired output values with stability in close loop operation the feedback path needs to be designed and in this case PID controller is used. For tuning of controller, transfer function of converter is needed which is obtained by small signal modelling. The converter can be switched between two states: ON and OFF. During turn-on, the State Space representation can be written as given in equations 3.1 to 3.4 and shown in Figure 3.1. [6]

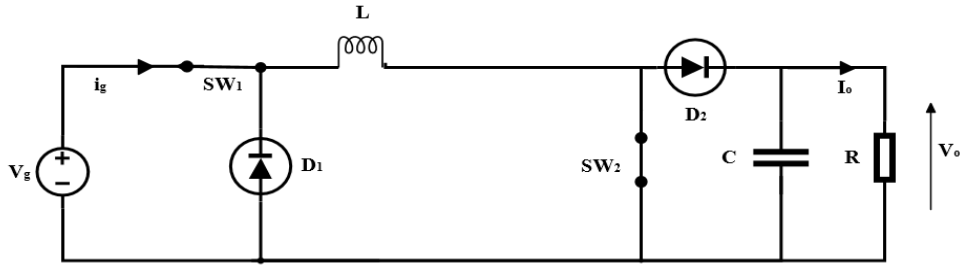

Figure 3.1 During turn on mode

$$\frac{dx(t)}{dt} = A_1 x(t) + B_1 u(t) \quad \textbf{3.1}$$

$$y(t) = C_1 x(t) + D_1 u(t) \quad \textbf{3.2}$$

From equations 3.1 and Figure 3.1, obtained relations are shown below

$$\begin{bmatrix} \frac{di(t)}{dt} \\ \frac{dv(t)}{dt} \end{bmatrix} = \begin{bmatrix} -R_{on}/L & 0 \\ 0 & -1/RC \end{bmatrix} \begin{bmatrix} i(t) \\ v(t) \end{bmatrix} + \begin{bmatrix} 1 & 0 \\ 0 & 0 \end{bmatrix} \begin{bmatrix} v_g \\ v_D \end{bmatrix} \quad \textbf{3.3}$$

$$\begin{bmatrix} i_g \end{bmatrix} = \begin{bmatrix} 1 & 0 \end{bmatrix} \begin{bmatrix} i(t) \\ v(t) \end{bmatrix} + \begin{bmatrix} 0 & 0 \end{bmatrix} \begin{bmatrix} v_g \\ v_D \end{bmatrix} \quad \textbf{3.4}$$

$$\frac{dx(t)}{dt} = A_2 x(t) + B_2 u(t) \quad \textbf{3.5}$$

$$y(t) = C_2 x(t) + D_2 u(t) \quad \textbf{3.6}$$

From equation 3.5 and Figure 3.2 during turn-off of both switches equations 3.7 &3.8 are obtained.

$$\begin{bmatrix} \frac{di(t)}{dt} \\ \frac{dv(t)}{dt} \end{bmatrix} = \begin{bmatrix} 0 & {}^{1}/_{L} \\ {}^{-1}/_{C} & {}^{-1}/_{RC} \end{bmatrix} \begin{bmatrix} i(t) \\ v(t) \end{bmatrix} + \begin{bmatrix} 0 & -1 \\ 0 & 0 \end{bmatrix} \begin{bmatrix} v_g \\ v_D \end{bmatrix} \quad \textbf{3.7}$$

$$[i_g] = [0 \quad 0] \begin{bmatrix} i(t) \\ v(t) \end{bmatrix} + [0 \quad 0] \begin{bmatrix} v_g \\ v_D \end{bmatrix} \quad \textbf{3.8}$$

The small signal model obtained is shown in Figure 3.3 and transfer function derived is given below in equation 3.9. It has a RHP zero making it unstable and difficult to control. Thus proper compensator is required for desired performance and stable operation.

$$\boldsymbol{G_{vd} = \frac{V_{out}}{DD'} \left\{ \frac{\left(1 - \frac{s}{D'^2 V_{out}/DLI_O}\right)}{1 + \frac{s}{D'^2 R/L} + \frac{s^2}{D'^2/LC}} \right\}} \quad \textbf{3.9}$$

Where $D' = 1 - D$

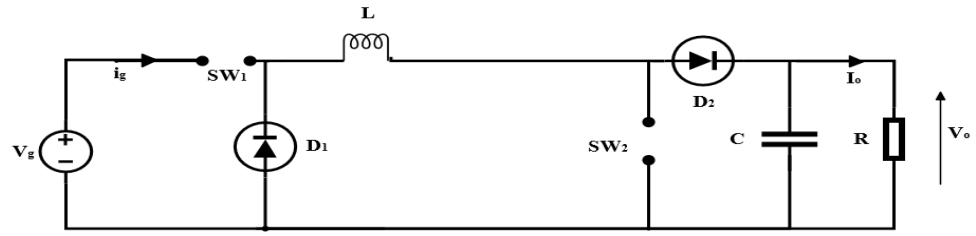

Figure 3.2 During turn off mode

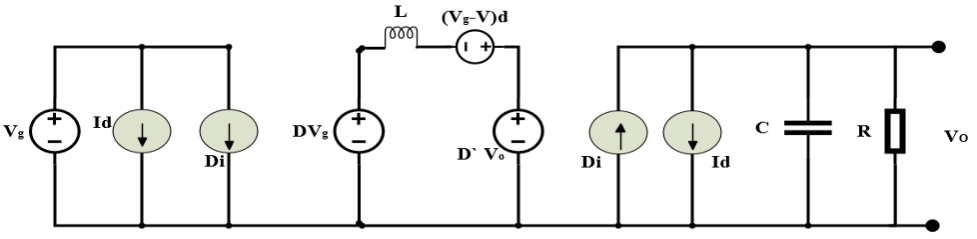

Figure 3.3 Small signal model

3.2. Fuzzy logic controller (FLC)

The fuzzy logic controller is a heuristic approach that relies on human expertise rather than being an expert system in and of itself. Fuzzification, Rule base and Defuzzification are the three steps. This sort of controller is commonly employed in non-linear systems and is now gaining popularity in the renewable energy sector with proper knowledge and working of system. This controller can be designed without requiring any mathematical

relations which brings it in huge demand. The major portion of the controller is the rule base block, which generates fuzzy rules between input and output. There is two input to FLC error e(x) and change in error Δe(x) and output is duty cycle d(x) as shown in equations 3.10 to 3.12. The rule base for all 2nd order converter is as follows. "If the ERROR in the output voltage is a BIG POSITIVE quantity & the CHANGE IN ERROR is a BIG POSITIVE quantity, the DUTY CYCLE must be reduced by a large amount, resulting in a BIG NEGATIVE perturbation in the duty cycle." Table 2 shows the fuzzy logic rules [7]

$$\boldsymbol{e(x) = v_o - v_{ref}} \quad \textbf{3.10}$$

$$\boldsymbol{\Delta e(x) = e(x) - e(x-1)} \quad \textbf{3.11}$$

$$\boldsymbol{d(x) = d(x-1) + \Delta d} \quad \textbf{3.12}$$

Table 2 Fuzzy Logic Rules

Error /ΔError	**NB**	**NS**	**ZE**	**PS**	**PB**
NB	PB	PB	PB	PS	PS
NS	PB	PS	PS	PS	ZE
ZE	PS	PS	ZE	NS	NS
PS	ZE	NS	NS	NS	NB
PB	NS	NB	NB	NB	NB

4. SIMULATION RESULT AND DISCUSSIONS

Simulation results of both the control techniques are shown below one by one where the input voltage is varying between (250-600) volts as shown in Figure 4.2. Closed loop operation is achieved to obtain constant output voltage of 300 v with constant load.

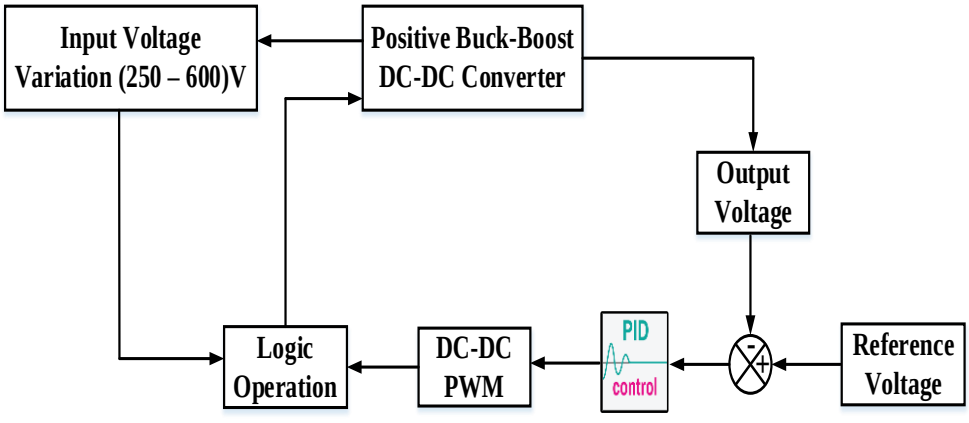

Figure 4.1 Block diagram of Closed loop PBB converter with PID controller

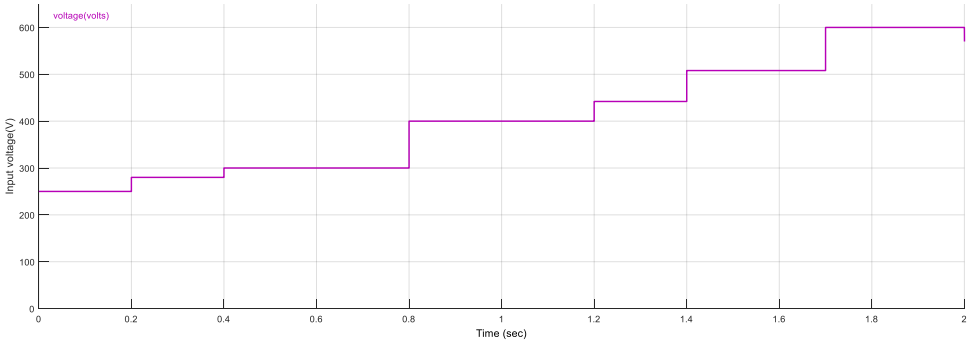

Figure 4.2 Input voltage

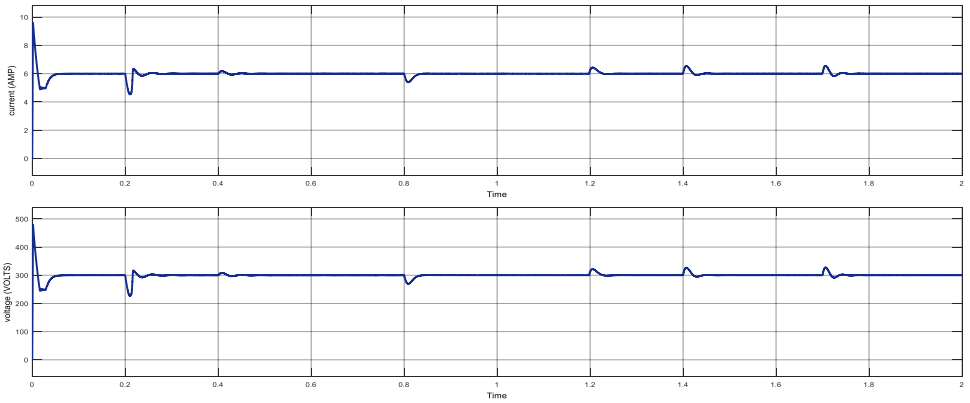

Figure 4.3 Output current & voltage with PID controller

A combination of logic gates are used for mode selection of converter as shown in Figure 4.1.Whenever input voltage variation occurs below and above reference voltage automatically there is smooth transition from buck mode to boost and vice-versa. Here design of controller value is of importance it should be such that it works for all the modes instead of working for just single mode. “Type-3 compensator” **[8]** is also suggested in literature to obtain desired results. From (250- 300) volts the circuit is working as boost converter to step up the voltage to 300 volts and for rest from (300-600) volts it works as buck converter to step down the voltage. The constant output voltage of 300 volts is obtained & transient conditions are as shown in Figure 4.3.

In FLC, the sensed output is compared with given desired reference and error is generated. It is good practice to keep membership function values in the range of [-1 to 1] and other segments (NB,NS,ZE,PS,PB) is scaled accordingly. The error obtained is multiplied with some constant gain factor and used as one input to fuzzy controller the other input of which is change in error as mentioned in Figure 4.4. The working of FLC is according to the rules we provided the output of which is scaled by some gain factor. The obtained result is given as duty cycle to the gate of MOSFETs. Tuning of gain values of various blocks is a sensitive work and needs to be done carefully. Setting up of wrong values may outperform the controller despite of correct logic used in fuzzy rule base. As in previous section for smooth buck to boost mode transition combination of logic gates is used instead of that fuzzy logic based switch can also be implemented. [9] According to the requirements, fuzzy sets can be 3 or 7, resulting in 9 or 49 control rules. The complexity of

the system will increase as additional fuzzy sets are added, although efficiency may improve. The major function of a fuzzy logic controller is to provide a rule basis, and this is accomplished by analysing the behaviour of the system rather than modelling it, which makes it attractive in the renewable energy industry. Because modelling of any system is a challenging endeavour.

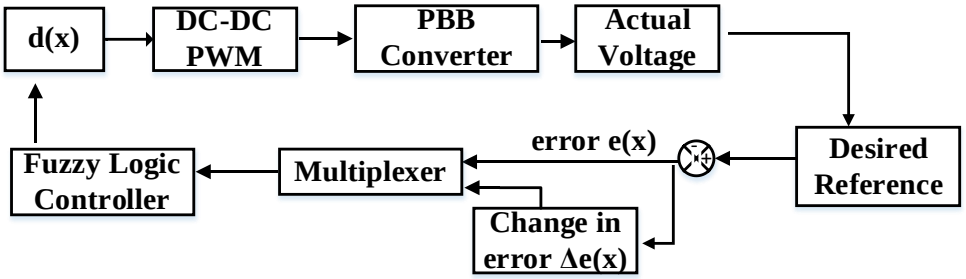

Figure 4.4 Block diagram of Closed loop PBB converter with FLC controller

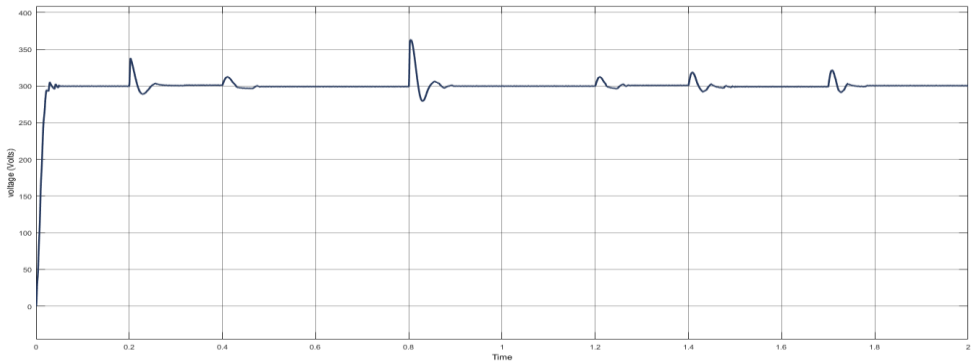

Figure 4.5 Output voltage of PBB with FLC

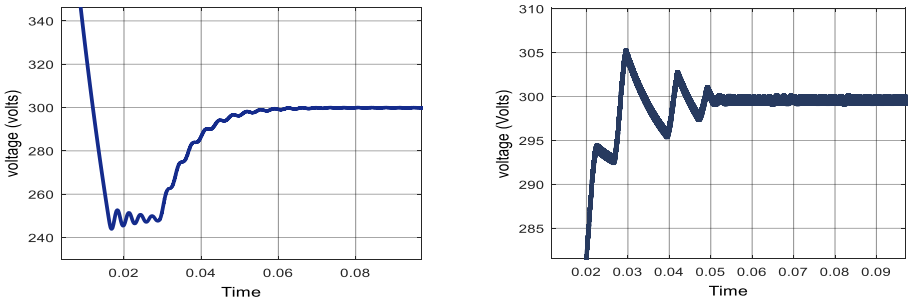

(a) (b)

Figure 4.6 Initial transients with different controllers (a) PID (b) FLC

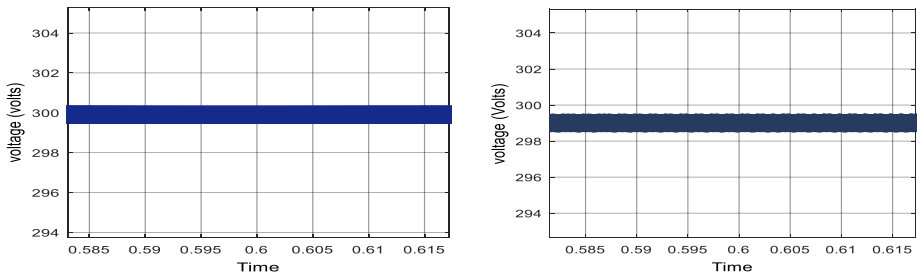

(a) (b)

Figure 4.7 Output voltage deviations (a) PID (b) FLC

CONCLUSION

For same circuit parameters and input variations the initial transients in PID is much higher as compared to FLC as shown in Figures 4.6. During every input variation the overshoots & undershoots are much higher in FLC as compared to PID shown in Figure 4.5. FLC is taking more settling time compared to PID to achieve desired output also the later one achieves perfect output whereas FLC shows slight variations of (1-2) volts as shown in Figure 4.7. Also with extensively performed simulations it is verified that FLC alone can't be implemented for smooth transitioning between separate modes of operation of converter whereas it can easily be done with proper tuned PID controller. It can be operated in all the three modes independently that is buck, boost & buck-boost. If implementing single FLC in PBB then it can only be implemented in third mode buck-boost mode when same duty cycle is given to both the switches at the same time. But this mode is avoided in PBB converter working as losses are increased due to both switches working at a time and most important the beauty of this converter for operating independently in all the three modes is lost.

5. REFERENCES

[1] Y. S. Joel, . H. V. Saikumar and S. S. R. Patange, "Design & performance analysis of Fuzzy based MPPT control using two-switch non inverting Buck-Boost converter," in *International Conference on Electrical Power and Energy Systems (ICEPES)(pp. 414-419)*, 2016.

[2] A. Hajizadeh, "Fuzzy/StatFeedback Control of a Non-Inverting Buck-Boost Converter for Fuel Cell Electric Vehicles," *Iranica Journal of Energy & Environment,* vol. 5, no. 1, pp. 34-41, 2014.

[3] V. Viswanatha and R. V. S. Reddy, "Modeling, simulation and analisis of noninverting buck-boost converter using PSIM," in *International Conference on Circuits, Controls, Communications and Computing (I4C), (pp. 1-5),* 2016.

[4] V. Choudhary, . T. Hegarty and D. Pace, "Under the hood of a noninverting buck-boost converter," Power Supply Design Seminar,Texas Instruments, Rep. SLUP346, (2016).

[5] J. Hagedorn, "Basic calculations of a 4 switch buck-boost power stage," Texas Instruments, Rep. SLVA535B, Dallas, Texas, USA, (2018).

[6] . R. W. Erickson and D. Maksimovic, Fundamentals of power electronics, Springer Science & Business Media, 2007.

[7] . S. K. Gadari, P. Kumar, K. Mishra, A. R. Bhowmik and A. K. Chakraborty, "Detailed analysis of Fuzzy Logic Controller for Second order DC-DC Converters," in *8th International Conference on Power Systems (ICPS) (pp. 1-6). IEEE.*, (2019, December).

[8] . A. K. Chauhan, . V. R. Vakacharla, A. K. Verma and S. K. Singh, "Multiple PMSG fed Non-inverting buck-boost converter for HEVs," in *IEEE 6th International Conference on Power Systems (ICPS) (pp. 1-6). IEEE.*, (2016).

[9] O. N. Almasi, V. Fereshtehpoor, M. H. Khooban and . F. Blaabjerg, "Analysis, control and design of a non-inverting buck-boost converter: A bump-less two-level T–S fuzzy PI control," *ISA transactions*, vol. 67, pp. 515-527, (2017).

Biographies

Piyush Singh received his B.Tech in Electrical Engineering from Kamla Nehru Institute of Technology (KNIT), Sultanpur, India in the year 2019. Currently, He is working towards M.Tech (Research) degree in Power & Energy Systems, Department of Electrical & Electronics Engineering from National Institute of Technology Karnataka (NITK) Surathkal, India. His research interests are Power Electronics in EV applications, DC-DC Converter topologies and their control techniques.

P.Partiban Currently, He is working as Associate Professor in Department of Electrical & Electronics Engineering National Institute of Technology Karnataka (NITK) Surathkal, India. His research area includes Power Electronics & Drives.

R. Kalpana Currently, She is working as Assistant Professor in Department of Electrical & Electronics Engineering National Institute of Technology Karnataka (NITK) Surathkal, India. Her research area includes Power Electronics & Drives.

S.Rambabu is working as scientist in NSTL Visakhapatnam. His research area includes Power Electronics & Drives.

M.Vijaya is working as scientist in NSTL Visakhapatnam. His research area includes Power Electronics & Drives.

PV based Smart Energy Efficient Hybrid Model for Irrigation using Sensorless BLDC Motor

Md Sagar Khan, Sujitha S, Kulshrestha Utkarsh Alok, Karthika M, L Ashwini B, Vivek Ranjan

Department of Electrical & Electronics Engineering,

New Horizon College of Engineering, Bangalore. Karnataka, India-560103

Abstract.

At present, in the farming world there are many problems, one among them is irrigation. The existing solar pumps used for irrigation operates using Induction Motor which have certain flaws i.e., they are less efficient, they also have water wastage issue, this pumps also requires more current which results in increase of the electricity bill and also there is noise problem in the existing structure. So, to overcome these issues the proposed system is introduced with Sensorless Brushless Direct Current (SLBLDC) motor so that the efficiency can be increased. In the proposed system the concept of tank for the storage and usage of water whenever required is introduced to get rid of water wastage problem. The given system is not only solar based but also it is smart and automatic for irrigation on the agriculture field. This system is a hybrid model which can work on solar power or can also operate using direct single-phase Alternating Current (AC) supply.

Keywords. Arduino, Battery, MPPT, Pump, RTC Module, Sensorless BLDC motor, Solar Panel, Solenoid Valve, Tank, Water Level Indicator.

1. INTRODUCTION

India is an agricultural country, which is also known as the global agricultural powerhouse. In India around 17-18% to country's GDP comes from agriculture. As per the records approximately 50% of total personnel of India works in agricultural sector. Report says that due to poor management around 70% of irrigation water is wasted. As the country is progressing towards new and advanced technologies the traditional way i.e., at a fixed time the water will be provided for farmers and at that duration only farmer have to make use of that water with the help of plough cut design on the farming land is reducing and farmers are using their individual pumps for irrigating water in their farmlands. As country is taking several steps towards smart systems there is also advancement in the technology of irrigation system from past few years. Now a days the motor used in pumps for irrigation purpose is Induction motor or Synchronous motor [1]-[6]. But due to recent advancement of Brushless Direct Current (BLDC) motors they are replacing Induction motor or Synchronous motor in the water pumps. So, in simple words, the BLDC is taking over Induction motor or Synchronous motor in pumps [1]. As because the fact is known that BLDC motors are more efficient than the Induction or Synchronous motor [1]. SLBLDC motor is Sensorless BLDC motor, as compared to the sensored BLDC motor this motor is light weight, less complicated, less expensive, less noisy and less prone to failure also its high-speed performance is excellent [3] [4]. So, the initiated model is introduced with SLBLDC motor.

The proposed system is a novel smart energy efficient irrigation system using hybrid SLBLDC motor which is integrated with several types of technologies embedded in one unique block. This energy efficient model is introduced with the concept of off-peak, on-peak, valley filling, load shifting terminologies by using timers, relays etc [3]-[5]. The

performance of the motor is based on the water level indicator connected to tank and also the timings provided to turn on/off the motor [7]. The term Hybrid in the proposed model is suggested because of the use of hybrid source with the motor i.e., the motor can operate using solar power or also the motor can start with the help of direct single-phase AC supply [5]. This hybrid model is also used to achieve energy conservant and energy efficient model.

2. PROPOSED SYSTEM

This hybrid model is an energy efficient model which is proposed to save electrical energy and to do the water irrigation in the agricultural field as well as this model is also useful for household usage [5]-[8]. This model is an automatic control system for solar PV pump applications.

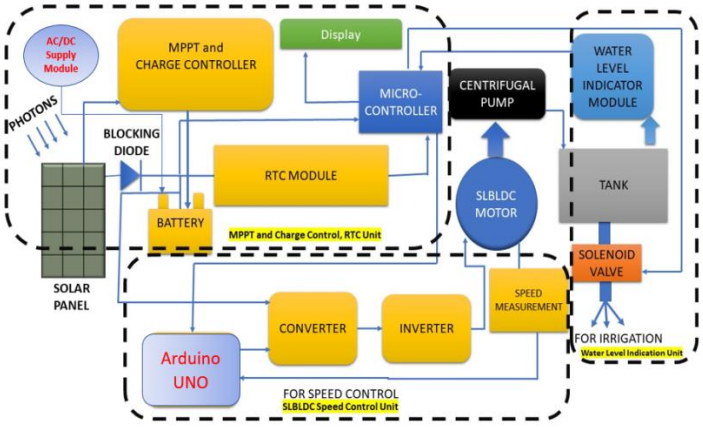

Figure 1. Proposed Block Diagram

This smart system does all the work automatically. A Real Time Clock (RTC) module is introduced in this system to control the indication of water level, which means the tank is empty i.e., without water the motor will start by itself as introduced by the water level indicator module and when the water is up to the mark in the tank than automatically the motor will stop filling the tank with water and the signal will be sent to the timer to on the valve, the valve used here is solenoid valve to prevent water wastage the valve will be started at a particular time and for a fixed interval to irrigate water in the agricultural field by itself. Fig. 1 depicts the block representation of the proposed model [8].

2.1. MPPT and Charge Control, RTC Unit:

The charging of the battery is done with the help of solar panel. After the battery is charged, the stored energy is used to power on or run the SLBLDC motor the SLBLDC motor is also given an option to run on the single-phase AC supply. Since there can be two supplies given as per the requirement so the motor is called hybrid SLBLDC motor [4]. At the specific time that is set in the RTC module unit the motor runs accordingly as required with Solar charge battery or with single-phase AC supply [8]-[10]. The RTC module provides real time and the model is started as per the time which is required to run the system [6]. The Maximum Power Point Tracking (MPPT) is an efficient tracking technique used to track point of maximum sunlight fall on the solar panel with the help of certain MPPT algorithm

set. The microcontroller used is Arduino Uno which is used for the controlling of MPPT and Charge Control and RTC Unit this is depicted in Figure 1.

2.2. SLBLDC Control Unit:

In this part of the SLBLDC control unit here the action performed is the speed control of SLBLDC motor. This system proposes a PI controller with the help of Arduino Uno to control the working in this section as seen in Figure 1. Basically, this section is for the speed control of the SLBLDC motor. In this the actual speed is tally with the reference speed and the error produces a pulse called gate pulse for the converter [1][4]. This speed control of SLBLDC motor is useful for the motor to run at the desired rate so that the proper use of the SLBLDC can be avail in this application.

2.3. Water Level Indication Unit:

This unit is used to indicate the condition of the water tank in this application model. It helps to indicate whether the tank is empty or full. When the water level indicator unit indicates the tank is full as per the convenient the signal is sent to the controller in this case it is Arduino Uno and also the signal from the RTC module is also taken and as per the desired timing set in the RTC module the Arduino Uno as per the signals starts irrigating water with the help of Solenoid valve [8]. And after the duration is over which is provided in the Arduino Uno the irrigation will stop i.e., the solenoid valve will stop. As per the condition of the tank provided by the water level indicator the tank starts to fill itself again automatically if the tank is empty or with less water [6]-[8]. The water level indicator will send signal to the Arduino Uno regarding the condition of the tank weather the tank is full or empty or partially full and according to that signal or indication the Arduino Uno will take the decision whether to start the motor and pump set-up to fill the tank or no actions are required if the is full or up to the mark.

The signal from the RTC module is send to the microcontroller on the other hand the water level indicator also senses the condition of the tank and accordingly sends the signal to the microcontroller [6]-[8]. After getting both the signals the microcontroller decides whether to on the SLBLDC motor or not. The process is done automatically as per the instructions set in the microcontroller. Table I. shows the condition of the motor at different stages.

TABLE I. State of SLBLDC motor/Pump at different signals

SI.No.	***Water level indicator signal***	***RTC module signal***	***Condition of SLBLDC motor/Pump***
1.	Tank empty	At set time	Motor on, pump on filling of tank starts
2.	Tank full	When set time over	Motor off, pump off, filling of tank stops

Due to the water wastage problem in the agricultural field with the help of the timer and the water level indicator the solenoid valve for the purpose of irrigation is switched on/off automatically as per the requirement set [6]-[8]. TABLE II. Shows the condition of the solenoid valve at different stages.

TABLE II. State of Solenoid valve at different signals

SI.No.	***Water level***	***RTC module signal***	***Condition of Solenoid Valve***

	indicator signal		
1.	Tank full	At set time	Solenoid valve opens for irrigation
2.	Tank empty	When set time over	Solenoid valve stops

The energy from the battery which is connected to solar panel provides supply to the converter and from the converter the supply goes to the inverter, inverter converts DC supply to AC and thus the motor starts [1] [2].

After that the supply starts the motor and the centrifugal pump connected to the motor will also start doing its work simultaneously for the duration of time set in the RTC module and the pump will start storing the water in the tank [5]-[8]. And after the duration set in the RTC module the pump stops filling water in the tank.

The proposed system is smart real time energy efficient and water preserving system with the joint venture of several types of technology embedded in one single unit. The best advantage of this smart system is the unique and advance approach of irrigation in the agricultural field.

3. SIMULATION OF PROPOSED SYSTEM

The simulation of the proposed system was carried out successfully on a simulation platform named as on ProteusProfessional 8. The entire system as per the block diagram is divided into three different simulation model.

A. MPPT and Charge Control, RTC Unit
B. SLBLDC Control Unit
C. Water Level Indication Unit

3.1. MPPT and Charge Control:

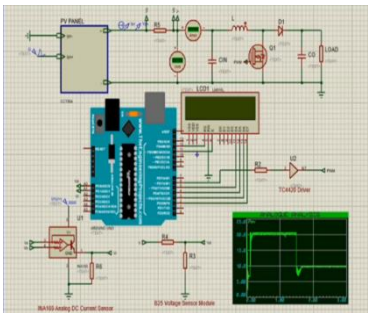

Figure 3.1. MPPT and Charge Control, RTC Unit

The MPPT and Charge Control, RTC Unit which is shown in Figure 3.1. is a part in which the specific algorithm is set as required to obtain the maximum efficiency from the solar panel it is use to set the solar panel at a point where the maximum solar light falls on the panel to store maximum energy in the battery to supply it to the required area [5]-[8]. To keep the track of the battery and to charge the battery charge control is used. The RTC unit is for the real time control of the SLBLDC motor and for the irrigation purpose in the agricultural field.

3.2. SLBLDC Control Unit:

This SLBLDC control unit shown in Fig. 4 is for the speed control of the Sensorless BLDC motor. Here for speed control of Sensorless BLDC motor PI controller unit is used with the help of microcontroller Arduino Uno in this case [2]. The microcontroller is given the pulse by comparing the actual speed and the reference speed and according to the error the Arduino Uno sets the speed of the Sensorless BLDC motor.

3.3. Water Level Indication Unit:

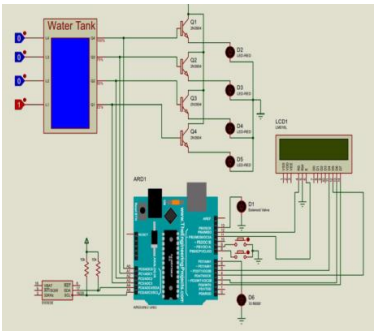

Figure3.3. Water Level Indication Unit

The water level indicator shown in Figure 3.3. is for the indication of the level of water available in the tank. The LED's connected in the water level indicator shows the level of water and the RTC module gives information of the time set in the module. Also, the solenoid valve is connected for the irrigation purpose as per the signal send by the water level indicator the microcontroller (Arduino Uno) switches on/off the solenoid valve as required for irrigation.

4. SIMULATED OUTPUT OF THE PROPOSED SYSTEM

The simulated output of the proposed system is given through the software named as Proteus Professional 8 which is as follows

4.1. Output of MPPT and Charge Control:

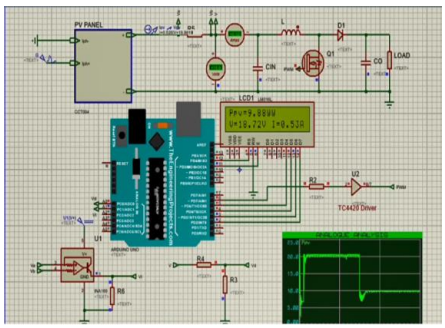

Figure4.1. Output of MPPT and Charge Control

Figure 4.1. shows the output of MPPT and charge control. The LED screen shows the Ppv(t) value and also the current and voltage measured by current sensor and voltage sensor respectively is shown by the LED successfully. The graph in the output shows the Ppv(t) curve.

4.2. Output of SLBLDC Control Unit:

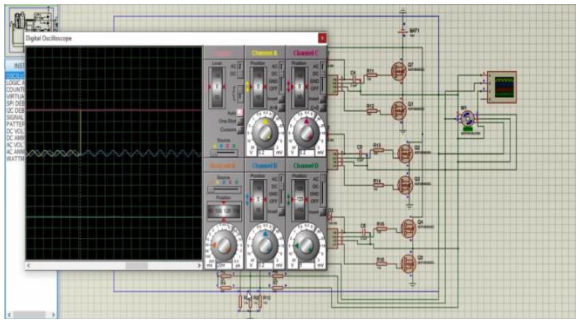

Figure 4.2. Output of SLBLDC Control Unit

The output of the SLBLDC control unit is shown by the Figure 4.2. Here the graph in the digital oscilloscope shows the working of the sensor less BLDC motor. The controller used for speed control is PI controller in which the microcontroller part is changed by Arduino Uno.

4.3. Output of Water Level Indication Unit:

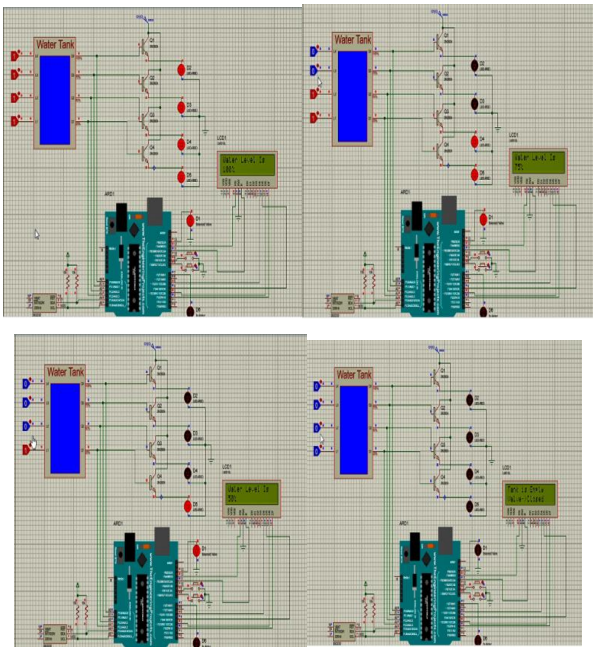

Figure 4.3. Output of Water level indicator at different phases of water in a tank

The output of water level indicator at different phases of water filled in the tank is shown by Figure 4.3. In this Figure 4.3. it is shown the working of water level indicator. When the tank is full the LED will show the message “Water Level Is 100%” and all the LEDs will glow at once. When the water level decreases i.e., when two LEDs glow the message shown is “Water Level Is 75%”. When only one LED glow “Water Level Is 50%” is shown by the LED panel. And when the tank is fully empty no LEDs will glow and the message will come is “Tank Is Empty Valve-> Closed” and the solenoid valve will stop irrigation in the field. The whole process will take place vice-versa when required.

The signal from RTC module and water level indicator module helps the Arduino Uno to decide when to irrigate the field or when to open the motor to fill the tank with water.

5. RESULTS AND DISCUSSIONS

When the time comes as set in the RTC module, it sends signal to the microcontroller (Arduino Uno) and the signal is then sent to sensorless BLDC motor. And accordingly, when the conditions are meet the motor starts.

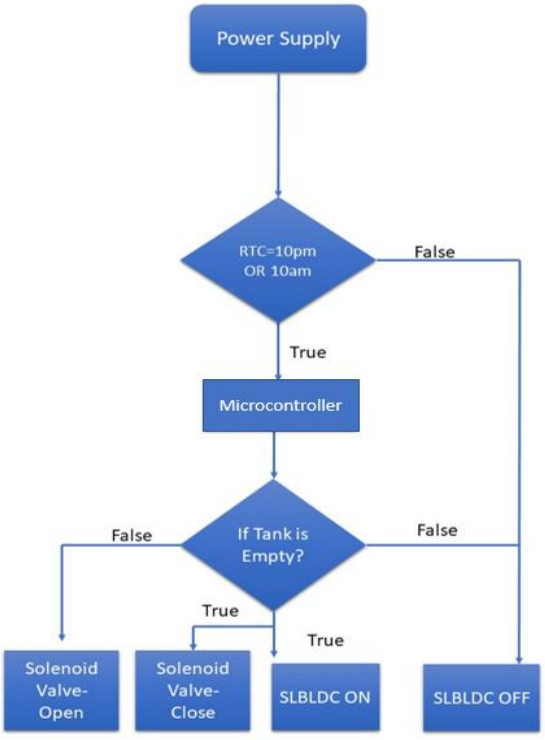

Figure 5.1. Flow Chart of Proposed Model

After getting the supply the motor starts and the centrifugal pump connected to the motor will also start doing its function simultaneously during that interval of time which is set in the RTC module and the water will get stored or irrigate through solenoid valve in the tank

or in the agricultural field respectively. And if the duration that is set in the module is over the tank stops filling or the irrigation stops in the agricultural field as shown in Fig. 6.

The proposed system is simulated, tested and the results are analyzed in Proteus Professional 8 software. A 24V, 100W solar panel is used for the supply of energy to the 24V, 250W sensorless BLDC motor. A RTC module is used to send the signal to the microcontroller (Arduino Uno) and the signal from the water level indicator is utilize to operate the sensorless BLDCmotor so that the tank can be filled according to the requirement and also the water can be irrigated through solenoid valve in the agricultural field.

Table III. Status of Switches and LED in tank

Switches/Transistor state	***LED***	***Water level of the tank***
All transistors are OFF	All LEDs OFF	No water inside the tank
Two transistors are ON and Two transistors are OFF	Two LEDs are ON and Two LEDs are OFF	Water tank is partially filled with water
All transistors are ON	All LEDs ON	Water tank is completely filled with water

Table III. gives the information about the condition of the tank with the help of switches/transistors and LEDs

6. CONCLUSION

The model proposes a system which uses water as per the requirement in a smart and efficient manner. The motor in the proposed system will start at the night time or at the time which is required by the farmers so to fill the tank at that time mostly at night time. This will reduce the electricity bill since the load is operated during off-peak time and hence if more electricity consumed also the electricity bill will be less as compared to morning time as morning time is the on-peak time when the load is operated even for a short time also the electricity bill will come more. In this way this system is more convenient and efficient as compared to other conventional systems.

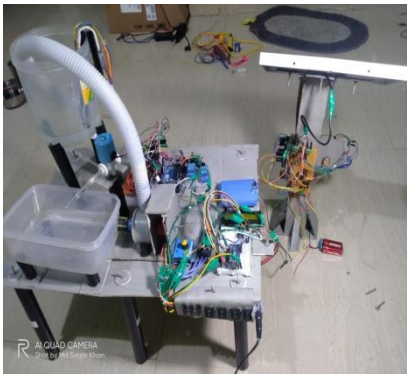

7. FUTURE SCOPES

This system can be made more intelligent by introducing the concept of IoT. More than two sources can also be introduced in future, more sensors, Bluetooth modules, Node MCU, etc. can be introduced, so that one can sit at home and control all the functions from his home sitting at one place. Speed control method for BLDC motor with the help of PIC microcontroller using python, Arduino using python, etc. can also be introduced. Complete integration with Python is only possible using Raspberry pi.Using Raspberry pi the entire system can be connected to cloud. So that the entire system can be operated through internet. Internet operation will make the entire system to be controlled from anywhere in the World.

8. REFERENCES

[1] State of the Art on Permanent Magnet Brushless DC Motor Drives Bhim Singh* and Sanjeev Singh† †* Electrical Engineering Department, Indian Institute of Technology, Delhi, New Delhi, India

[2] R. Shanmugasundaram, C. Ganesh, A. Singaravelan, B. Gunapriya, and B. Adhavan, "High-Performance ANFIS-Based Controller for BLDC Motor Drive," in *Ubiquitous Intelligent Systems*, Springer, Singapore, 2022, pp. 435–449.

[3] R.Mohan Das, E.Chandira Sekaran "A Cloud System Model Employing Random Space Vector Pulse width Modulation for Noise Reduction in VSI fed Induction Motor" Cluster Computing, Springer, ISSN:1386-7857 (Print) 1573-7543 Online), Published Online : 23.02.2018. February 2018.

[4] Karthika M, "Review on Torque Ripple Reduction Techniques of BLDC Motor," *IEEE*, pp. 1092–1096, 2020

[5] Comprehensive review on solar, wind and hybrid wind-PV water pumping systems-an electrical engineering perspective Sachin Angadi;Udaykumar R Yaragatti;Yellasiri Suresh;Angadi B Raju CPSS Transactions on Power Electronics and Applications Year: 2021 | Volume: 6, Issue: 1

[6] Simulated Design and Implementation of Solar based Water Pumping System Vijay Ravindran;RamPrakash Ponraj;R PRAVEEN;K Praveenkumar;P Ravichandran;T Sivaramakrishnan 2021 2nd International Conference for Emerging Technology (INCET) Year: 2021

[7] Sujitha S. and Venkatesh, C. " Design and Comparison of PV Switched Reluctance Motor drives Using Asymmetric Bridge Converter and Buck Boost Converter", Australian Journal of Basic Applied Sciences, ISSN: 1991-8178, Vol.08, No. 06 , 2014.

[8] S.Sujitha, Venkatesh. C, "Stand alone Hybrid Driven Switched reluctance motor using H Bridge Converter", International Journal of Applied Engineering and Research, ISSN:0973-4562, 2015

[9] Sujitha. S;Vinoth Kumar K;Shiva R V;Sagar Kulkarni;Ponnappa M M,"An implementation of soft computing approach of smart control for induction motor using ANFIS,"2022 4th International Conference on Smart Systems and Inventive Technology (ICSSIT 2022),2022

[10] Comparative study on Water Max A 64 DC pump performances based Photovoltaic Pumping System design to select the optimum heads in arid area Azzedine Boutelhig;Yahia Bakelli 2012 24th International Conference on Microelectronics (ICM) Year: 2012

[11] Solar powered automated water pumping system for eco-friendly irrigation Rajesh Kannan Megalingam;Vamsy Vivek Gedela 2017 International Conference on Inventive Computing and Informatics (ICICI) Year: 2017
[12] Peak Current Detection Starting based Position Sensorless Control of BLDC Motor Drive for PV Array Fed Irrigation Pump Aryadip Sen;Bhim Singh 2019 IEEE International Conference on Environment and Electrical Engineering and 2019 IEEE Industrial and Commercial Power Systems Europe (EEEIC / I&CPS Europe) Year: 2019
[13] Peak Current Detection Starting Based Position Sensorless Control of BLDC Motor Drive for PV Array Fed Irrigation Pump Aryadip Sen;Bhim Singh IEEE Transactions on Industry Applications Year: 2021 | Volume: 57, Issue: 3
[14] Vinoth Kumar K; S Sujitha; B Stalin; ,"Execution of smart electric vehicle charging station driven by RE technology using soft computing approach," 2021 Innovations in Power and Advanced Computing Technologies (i-PACT), 2021, pp. 1-5, doi: 10.1109/i-PACT52855.2021.9696545.
[15] Sujitha. S;Vinoth Kumar. K;Vinodha. K;Josh F T;Venkatesh. B, "Experimental Setup of Smart E-Vehicle Charging Station using IOT Technology," 2021 IEEE International Conference on Mobile Networks and Wireless Communications (ICMNWC), 2021, pp. 1-4, doi: 10.1109/ICMNWC52512.2021.9688523.
[16] S.Sujitha, Dr. Srinivasa G, Design and Performance of High Frequency Temperature Compensated Crystal Oscillator, Journal of Advanced Research in Dynamical and Control Systems, ISSN: 1943-023X, 2019
[17] Srinivasa G , S.Sujitha, “Spanning Trees of a Triangle Snake Graph by BFS and DFS Algorithms, International Journal of Innovative Technology and Exploring Engineering (IJITEE) ISSN: 2278-3075, Volume-8 Issue-8 June, 2019
[18] G. Srinivasa, S.Sujitha, “ Study on characteristics of a tadpole Graph”, Journal of Adv Research in Dynamical & Control Systems, Vol. 11, 06-Special Issue, 2019
[19] Comparative study on Water Max A 64 DC pump performances based Photovoltaic Pumping System design to select the optimum heads in arid area Azzedine Boutelhig;Yahia Bakelli 2012 24th International Conference on Microelectronics (ICM) Year: 2012
[20] Solar powered automated water pumping system for eco-friendly irrigation Rajesh Kannan Megalingam;Vamsy Vivek Gedela 2017 International Conference on Inventive Computing and Informatics (ICICI) Year: 2017
[21] Peak Current Detection Starting based Position Sensorless Control of BLDC Motor Drive for PV Array Fed Irrigation Pump Aryadip Sen;Bhim Singh 2019 IEEE International Conference on Environment and Electrical Engineering and 2019 IEEE Industrial and Commercial Power Systems Europe (EEEIC / I&CPS Europe) Year: 2019
[22] Peak Current Detection Starting Based Position Sensorless Control of BLDC Motor Drive for PV Array Fed Irrigation Pump Aryadip Sen;Bhim Singh IEEE Transactions on Industry Applications Year: 2021 | Volume: 57, Issue: 3

Design and Implementation of a Dual Active Bridge Converter for Battery Charging Application

Harikishan B Hanumannavar[1], Usha A[1],

Priyaranjan Mishra[2]

[1]*Department of EEE, BMSCE, Bengaluru, India*

[2]*Belbird Technologies Pvt. Ltd. Bengaluru, India*

Email: harikishan.epe20@bmsce.ac.in

Abstract

This work focuses on the design and implementation of a Dual active bridge converter for battery charging application as well as comparative study of different semi-conductor devices for Dual active bridge converters. The proposed converter is designed and realized for the given specifications using suitable equations. The converter operates at a switching frequency of 50KHz. The phase shift control technique is employed for closed-loop control of converter which is necessary to maintain the output voltage and current constant to charge the battery. The parameters of Silicon carbide (SiC) and Gallium nitritide (GaN) MOSFETs are considered for the comparative study of different semi-conductor devices. In this work, MATLAB Simulink software is used to simulate the converter. Also, experimental results of the converter for the required output are illustrated in this paper.

Keywords. Dual active bridge converter, Sic and GaN MOSFET, Bi-Directional converter.

1. INTRODUCTION

The rise in electricity demand, environmental concerns, and discrepancy in energy generation, modern hybrid technology for conversion of renewable energy sources have attracted more attention. It is the job of the bidirectional DC/DC converter to act as an interface between the many forms of renewable energy, such as fuel cells or photovoltaic (PV) arrays, and the various forms of energy storage, such as batteries and super capacitors [1,2]. They're used in a variety of applications, including hybrid cars, distribution networks, electric aircraft, and uninterruptible power supplies (UPS).

Isolated and non-isolated are the two categories of bidirectional DC/DC converters. In this work, a Dual active bridge converter with an isolated topology is selected. In this converter the power transfer will take place in both the directions [3,4]. This converter has a wide variety of advantages over other converters such as improved efficiency, isolation in the circuit, ability to operate at high frequencies and reliability [5].

The converter is operated at 50% duty cycle. The PWM pulses are phase shifted by some degree so that there is no zero voltage switching. The control strategy employed in this converter is phase shift control method [6]. The constant output voltage and current can be obtained by varying the phase of the PWM pulses of the secondary side bridge circuit. This study indicates that the dual active bridge converter is proposed for battery charging applications, such as those using Li-ion batteries [7]. Modern technology semiconductor devices such as SiC MOSFET are proposed, the efficiency of the converter is increased significantly. MATLAB Simulink software is effectively used to carry out simulation and analysis of the system, also necessary waveforms are observed and recorded in this work.

2. OPERATION AND DESIGN PROCEDURE

2.1. Block Diagram and Methodology

Figure 2.1 shows the block representation for the proposed converter along with controller. The proposed converter operation is similar to that of a typical Dual active bridge converter circuit.

A DC source is given as an input to the dual active bridge converter. The output of the dual active bridge converter is connected to the battery. In this work, the topology is used for battery charging applications. The output of converter is connected to the battery so; in this application, the output current should be maintained constant to charge the battery. The controlled output current is a function of input DC voltage. The controller detects the variation in the output current and maintains a constant output current constant by varying the phase of the secondary side of the bridge with respect to the primary side of the bridge circuit.

The DC input given to the circuit is 300V. The switches used in the converter circuit are MOSFET which operate at a frequency of 50KHz. The duty cycle considered is 50 percent.

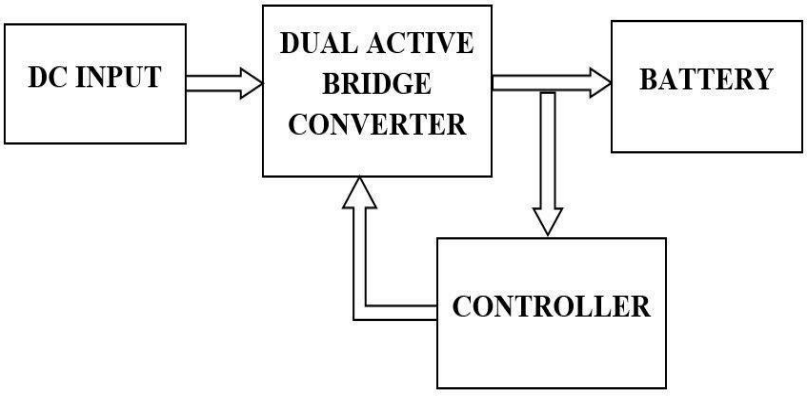

Figure 2.1. Block Diagram for the proposed converter

2.2. Dual Active Bridge Converter

The dual active bridge converter circuit consists of eight MOSFET switches, a high-frequency transformer, an energy transfer element which is an inductor, and dc-link capacitors for bi-directional, controllable, high-power dc-to-dc converter. Simply put, the converter is a standard full-bridge with a programmable rectifier. Due to the symmetry of the primary and secondary bridges, this converter can regulate power flow in both directions. [9,10].

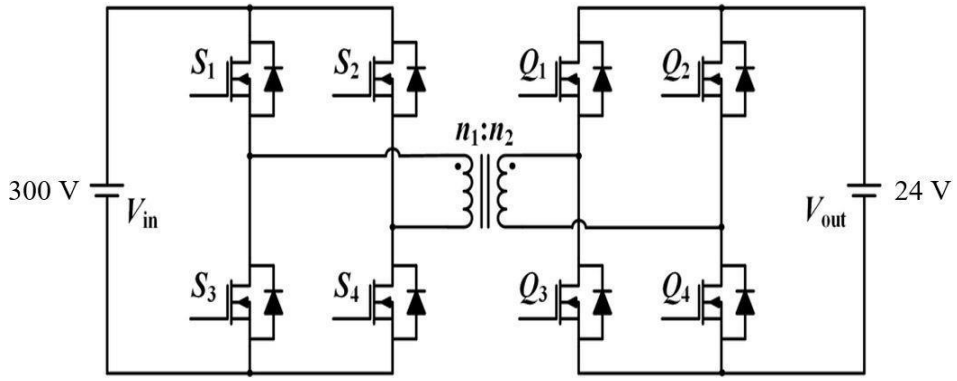

Figure 2.2. Schematic for Dual active bridge converter

The converter is comprised of two bridges: the primary bridge and the secondary bridge. The primary side bridge circuit functions as an inverter, while the secondary side bridge circuit functions as a rectifier. The isolation of the circuit is provided by the high-frequency transformer, which is connected to both bridges.

In a dual-active bridge converter, both the primary and secondary bridges are simultaneously controlled. All switches operate at a duty cycle of 50 percent. The diagonal switches turn on and off simultaneously, resulting in a square wave at the output of each bridge.

In the figure 2.3 the switching waveform of a conventional dual active bridge converter is depicted. S1, S2, S3 and S4 are the switches for the primary side circuit of dual active bridge converter. Q1, Q2, Q3 and Q4 are switches for the secondary side circuit of the dual active bridge converter. At a time four switches are turned ON. The switches operate in four intervals which is as follows. S1, S2, Q2 and Q3 are triggered in the first interval. In second interval S1, S4, Q1 and Q4 are triggered. In the third interval S2, S3, Q1 and Q4 are triggered. In the fourth interval Q2, Q3, S2 and S3 are triggered. There is a phase difference between the triggering of pulses from primary to secondary side [11,12]. The phase difference is usually maintained in the range 0 degree to 30 degrees.

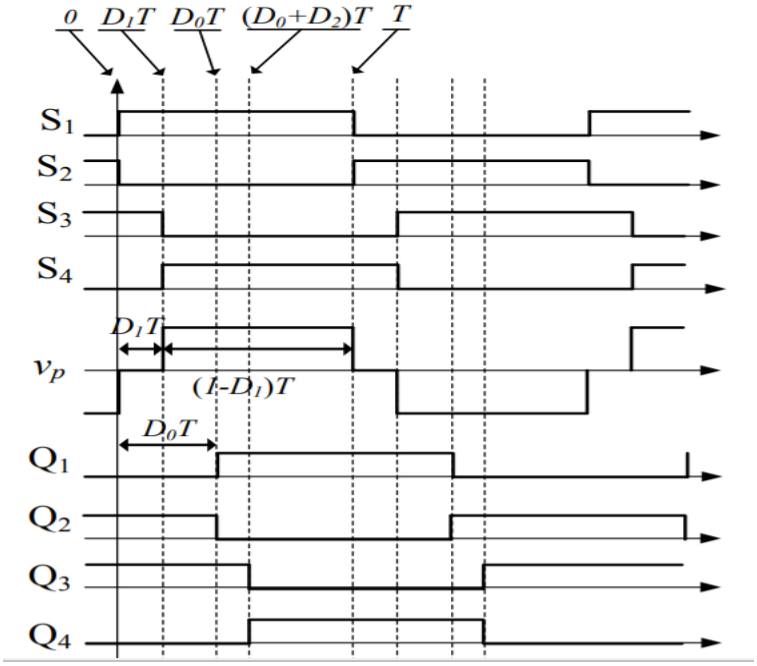

Figure 2.3. Switching waveforms for Dual active bridge converter

3. CONVERTER DESIGN

3.1. Converter Specification

- Input voltage range : 300 V
- Switching Frequency : 50 kHz
- Output Voltage : 24V
- Output Current : 10A
- Current Ripple : 20%
- Voltage Ripple : 1%

Abbreviations:

V_i	: Input voltage	f_s	: Switching frequency
V_o	: Output Voltage	V_L	: Voltage across the inductor
D	: Duty Cycle	I_{ripple}	: Window factor
V_{ripple}	: Voltage Ripple	T_s	: Switching Time
C	: Capacitance	B_{max}	: Maximum permeability
A_c	: Area of cross section		

3.2. Calculation

$$Turns\ Ratio\ (n) = \frac{N_s}{N_p} = 0.1 \tag{3.1}$$

$$V_L = V_i \frac{N_s}{N_p} - V_o \tag{3.2}$$

$$V_L = 6V \tag{3.3}$$

$$D = \frac{1}{2} \times \frac{24}{30} = 0.4 \tag{3.4}$$

$$I_{rippl} = 0.2A \tag{3.5}$$

$$L = \frac{V_L\ D\ T_s}{I_{ripple}} = 24\mu H \tag{3.6}$$

$$V_{ripple} = 1\%\ of\ 24 = 0.24V \tag{3.7}$$

$$C = \frac{I_{ripple}\ D\ T_s}{V_{ripple}} = 66.67\mu F \tag{3.8}$$

3.3. Transformer design

For the operation below 500 KHz core material with permeability of 2000 to 2500 is selected. High frequency transformers favour ferrite cores due to their high resistance to high current, low eddy current losses, and high permeability.

Core shape selected is EE core and Area of cross section is 1.54 cm^2.

$$N_p = \frac{V_i \times 10^8}{4 \times f \times B_{max} \times A_c} = 29 \tag{3.9}$$

$$\frac{N_p}{N_s} = \frac{V_p}{V_s} \tag{3.10}$$

$$N_s = 7 \tag{3.11}$$

In this work, winding the transformer, wire used is 19SWG copper wire which has an area of cross section of 1.016mm and current carrying capacity of 3.2A.

3.4. Closed loop control

The phase shift modulation approach is used to build closed loop control for the dual active bridge converter. The duty cycle of the primary side of a Dual Active bridge converter is phase-shifted in reference to the secondary side in phase shift modulation. The output voltage and current are regulated as needed by varying the phase shift angle [13].

In this work, a digital controller is used for closed loop control. A Matlab function block is implemented in Matlab Simulink in which the programme is written to control the output voltage and current of dual active bridge converter. By changing the PI controller to a discrete PI controller, the programme is developed. The Matlab function block detects the output current, and if the output current varies, the Matlab function block adjusts the phase of the secondary side of the bridge until the current reaches the desired value.

4. SIMULATION, HARDWARE IMPLEMENTATION AND RESULTS

4.1. Simulation and Results

Simulation for the dual active bridge converter circuit is carried out using Matlab Simulink software. The simulation circuit for dual active bridge converter and switching waveforms for the dual active bridge converter are illustrated in Fig. 4.1 and Fig. 4.2 respectively.

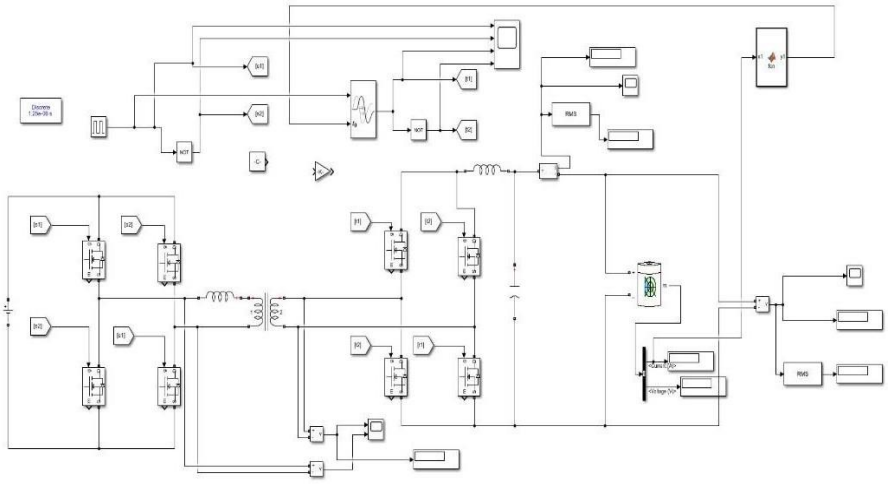

Figure 4.1. Simulation model for the closed loop control

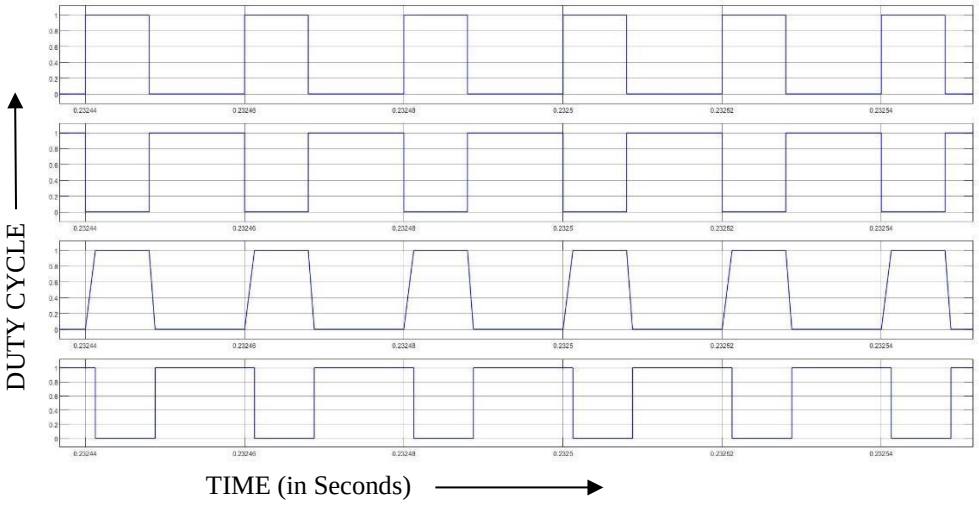

Figure 4.2. Switching waveforms for the dual active bridge converter

The Fig. 4.3 depicts the graph for variation in input voltage in reference to the output current for battery charging. The input voltage ranges between 260V and 360V, so that the output current remains constant at 10A.

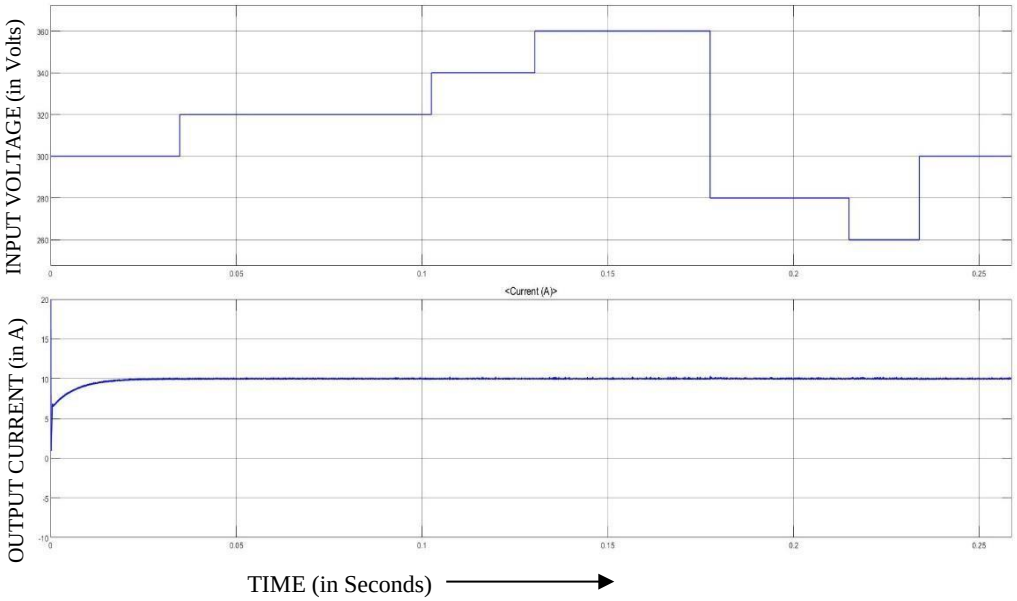

Figure 4.3. Input voltage variation vs Output current for battery charging

4.2. Comparative analysis of semiconductor devices

The comparison is made between (Silicon carbide) SiC MOSFET and (Gallium nitride) GaN MOSFET. The Resistance between drain and source (Rdson) parameter of the MOSFET is considered from the datasheet. In Matlab Simulink, the Rdson parameter is altered in the MOSFET parameter section, and the resulting parameter change are analysed and recorded in the table 4.1. It is observed from the table 4.1 that SiC MOSFET is comparatively exhibits better performance tha GaN MOSFET switch.

Table 4.1. Comparison between SiC and GaN MOSFET

PARAMETER	SiC MOSFET	GaN MOSFET
Rds in Ω	0.107 Ω	0.190 Ω
Output Voltage (V_o)	22.35 V	18.04 V
Output current (I_o)	8.93 A	7.183 A

4.3. Hardware Implementation

In this work, PWM pulses for the dual active bridge converter are generated using the TMS320F28335 digital signal processor. The processor's enhanced pulse width modulation (epwm) pins are responsible for generating the pulses. The MOSFET employed in the converter is a PSM20N50CT with Vds=500V and Id=20A current carrying capacity. A driver IC, TC4420, which is a non-inverting type MOSFET driver IC, is selected for the efficient switching of the MOSFET switch. In this work, the duty cycle considered is 50 percent for testing purpose.

Complimentary PWM pulses are generated having a duty cycle of 50% for the primary side bridge circuit as illustrated in the Figure 4.4.

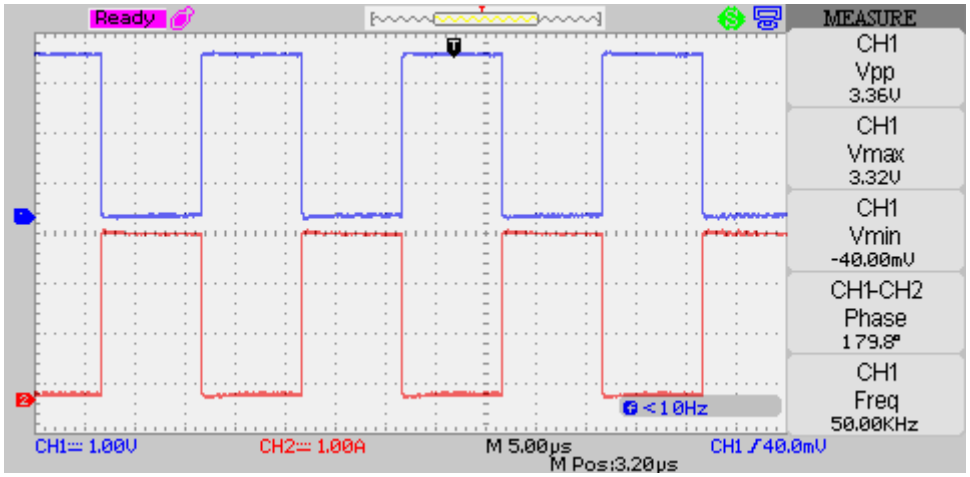

Figure 4.4. Complimentary PWM pulse generated with a duty cycle of 50%.

The phase shifted PWM pulses with a phase shift of 30 degrees are generated for the secondary side of the bridge circuit as illustrated in Figure 4.5.

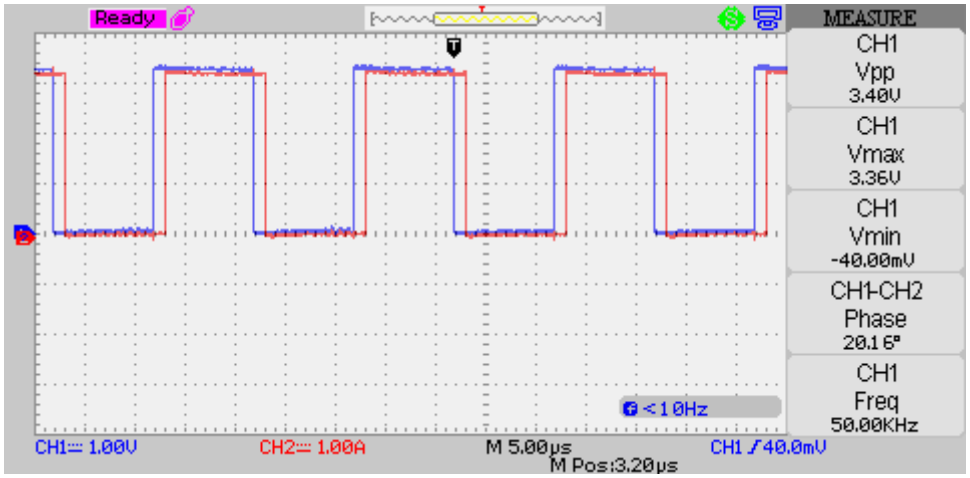

Figure 4.5. 30° Phase shifted PWM pulses.

The hardware setup for testing the driver IC TC4420 for the MOSFET switch is effectively implemented out and presented in Figure 4.6.

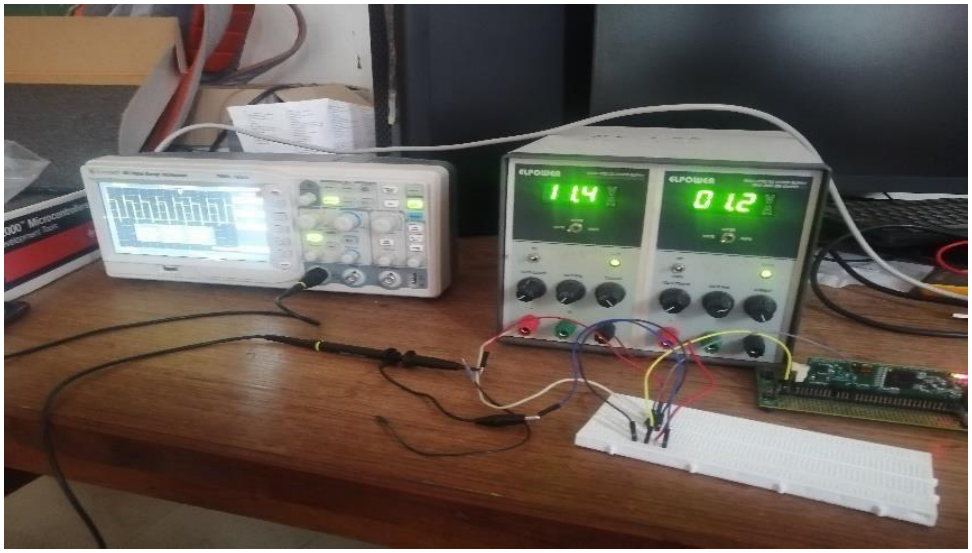

Figure 4.6. Experimental setup for MOSFET driver testing

5. CONCLUSION

Dual active bridge converter for battery charging application is designed and simulated using MATLAB Simulink software. Simulation model also provides a closed loop control for the Dual active bridge converter which maintains the output current constant at 10A. Further the comparative study between different power semiconductor devices (Sic and GaN) has been carried out using the MATLAB Simulink software. Also in this work, the PWM pulses are effectively generated using TMS320F28335 digital signal processor. At present work is carried out using PSM20N50CT MOSFET switches and hardware implementation of the same is performed. However, GaN and SiC MOSFET switches are a bit expensive and it is proposed as future work. Further the parameters in the simulation study for the GaN and SiC switching devices are very much limited. Hence limited comparative study between SiC and GaN switches is carried out.

6. REFERENCES

[1] D. Costinett, R. Zane and D. Maksimovic, "Discrete time modeling of output disturbances in the dual active bridge converter," 2014 IEEE Applied Power Electronics Conference and Exposition - APEC 2014.

[2] Dongzhi Wang, Weige Zhang and Jingxin Li, "PWM plus phase shift control strategy for dual-active-bridge DC-DC converter in electric vehicle charging/discharging system," 2014 IEEE Conference and Expo Transportation Electrification Asia-Pacific (ITEC Asia-Pacific), 2014.
[3] V. Karthikeyan and R. Gupta, "Closed-loop control of isolated dual active bridge converter using dual phase shift modulation," IECON 2015 - 41st Annual Conference of the IEEE Industrial Electronics Society, 2015.
[4] S. Hazra et al., "High Switching Performance of 1700-V, 50-A SiC Power MOSFET Over Si IGBT/BiMOSFET for Advanced Power Conversion Applications," in IEEE Transactions on Power Electronics, vol. 31, no. 7, pp. 4742-4754, July 2016.
[5] M. S. Ullah Khan, A. I. Maswood, H. D. Tafti, M. M. Roomi and M. Tariq, "Control of bidirectional DC/DC converter for back to back NPC-based wind turbine system under grid faults," 2016 4th International Conference on the Development in the in Renewable Energy Technology (ICDRET), 2016.
[6] Anping Tong et al., "Power flow and inductor current analysis of PWM control for Dual Active Bridge converter," 2016 IEEE 8th International Power Electronics and Motion Control Conference (IPEMC-ECCE Asia), 2016.
[7] M. Ishigaki, J. Shin and E. M. Dede, "A Novel Soft Switching Bidirectional DC–DC Converter Using Magnetic and Capacitive Hybrid Power Transfer," in IEEE Transactions on Power Electronics, vol. 32, no. 9, pp. 6961-6970, Sept. 2017.
[8] A.Vazquez, A.Rodriguez, M.R.Rogina and D.G.Lamar, "Different Modular Techniques Applied in a Synchronous Boost Converter With SiC MOSFETs to Obtain High Efficiency at Light Load and Low Current Ripple," in IEEE Transactions on Industrial Electronics, vol. 64, no. 10, pp. 8373-8382, Oct. 2017.
[9] F. Yazdani and M. Zolghadri, "Design of dual active bridge isolated bi-directional DC converter based on current stress optimization," 2017 8th Power Electronics, Drive Systems & Technologies Conference (PEDSTC), 2017.
[10] D. Mahajan and S. Khandelwal, "Impact of p-GaN layer Doping on Switching Performance of Enhancement Mode GaN Devices," 2018 IEEE 19th Workshop on Control and Modeling for Power Electronics (COMPEL), 2018.
[11] G. Brando, A. Del Pizzo and S. Meo, "Model-Reference Adaptive Control of a Dual Active Bridge dc-dc Converter for Aircraft Applications," 2018 International Symposium on Power Electronics, Electrical Drives, Automation and Motion (SPEEDAM), 2018.
[12] C. Peng et al., "SiC MOSFET switching characteristic optimization and application in battery charging/discharging," 2019 IEEE 10th International Symposium on Power Electronics for Distributed Generation Systems (PEDG), 2019.
[13] A. Platon, S. Oprea, A. Florescu and S. G. Rosu, "Simple and Digital Implementation of PI Controller Used in Voltage-Mode Control," 2018 10th International Conference on Electronics, Computers and Artificial Intelligence (ECAI), 2018.
[14] F. D. Esteban, F. M. Serra and C. H. De Angelo, "Control of a DC-DC Dual Active Bridge Converter in DC Microgrids Applications," in IEEE Latin America Transactions, vol. 19, no. 8, pp. 1261-1269, Aug. 2021.

Modelling and Investigation of Best PV Array Configuration and Implementation of MPPT Under Partial Shading Conditions

Rajkumar Jukuri[1], B. Pradeep Kumar[1], V. Ashok Kumar[1], C. Subba Rami Reddy[2], V. Srikanth[1]

1. Kakatiya Institute of Technology and Science, Warangal

2, B V Raju Institute of Technology, Narsapur,

nanirajkumar7569@gmail.com, pradeep301327@gmail.com, va.eee@kitsw.ac.in, csubbaramireddy2020@gmail.com

Abstract.

In practical, majority of the photovoltaic (PV) modules are possessing inbuilt bypass diodes for avoiding hotspot formation under partial shading conditions. However, on account of the activation of bypass diodes, multiple peaks will occur on the characteristics of PV array. The traditional maximum power point tracking (MPPT) algorithms decline to track the global peak and settles at the local peak, thereby resulting in huge power loss. Thus, this paper investigates the influence of partial shading on different PV array configurations (like , total-cross tied, series-parallel, honey-comb, series) under distinct shading patterns (such as wide and short, narrow and short, wide and long, narrow and long, and diagonal). Further, best suitable PV array configuration is identified by comparing the array losses and global peak position is discussed under various shading patterns. Apart from this, traditional P&O algorithm is implemented in MATLAB to extract the Maximum Power Point (MPP) amongst the best PV array configuration.

Keywords. PV Module, Power-Voltage Characteristics, Photovoltaic (PV) array configurations, Partial Shading patterns, MPPT, P&O algorithm.

1. INTRODUCTION

On considering recent times, there is a drastic upsurge in the global photovoltaic (PV) installations owing to the growing emphasis on reducing global warming, natural abundance of solar irradiance, easy scalability, flexibility and low maintenance costs. Apart from these encouraging aspects, PV output power mainly depends upon the environmental conditions such as irradiation, load profile, temperature and moving clouds [1]. Further, due to non-linear characteristics of PV, Power-Voltage curve exhibits a unique Maximum Power Point (MPP), at which peak power is extracted. This MPP operating will never remain constant and varies considerably with respect to environmental conditions. For extracting the peak power under varying environmental conditions, a Maximum Power Point Tracking (MPPT) scheme is commonly adopted [2], which requires power electronic interfaces such as DC/AC inverters or DC/DC converters.

Depending on the current and voltage required by the system load, series-parallel connections of individual PV modules are usually adopted. A “string” refers to a set of series-connected PV modules. Under normal operating conditions, each module in a string receives the same amount of irradiance, and the PV characteristics of the string resembles that of the single module, with the voltage increased by as many times as the number of series modules and the current being the same. In such cases, the P-V curve of that string exhibits single peak [3].

However, as the PV modules are installed in outdoor, due to the shadow originated by nearby objects such as, poles, trees, or bird droppings, clouds, buildings and dirt etc, these modules receive unequal levels of irradiance/mismatch in the irradiance values, and this phenomenon is called to be as partial shading[4]. Under partial shading systems, shaded module turns reverse biased and leads to considerable heat dissipation known as hotspot. To avert the hotspot formation, bypass diodes are connected in antiparallel with each PV module to safely bypass the shaded module. However, under partial shading conditions, due to the activation of these bypass diodes, the string P-V characteristic exhibits multiple peaks, with several Local MPPs (LMPPs) and also drastically affects the PV output power [5]. Under certain partial shading conditions, traditional MPPT algorithms fails to track the global peak and settles on a local MPP, thereby results in huge power loss. It has been proclaimed that, reduction in output power by applying improper MPPT technique might be up to 70% under partially shaded conditions. This power loss may vary from one configuration to another, shading pattern, shading intensity and number of modules having shading [6].

Patel et al [7] inspected the effect of shading on series-parallel array configuration under distinct shading patterns is enclosed. While in [8][9], presented the performance comparison among various array configurations such as Total Cross-tied, Series-parallel, Honey-comb, Series and identified TCT as the best array configuration. In another study [10], devised a MATLAB program to analyse the shading patterns effect on various array configurations. By comparing all the configurations under various shading pattern, the best configuration is then investigated and P&O algorithm is applied for the tracking of maximum power point.

The rest of the paper is explicated as follows- section II-PV module modelling in MATLAB/simulink, PV array configurations and shading patterns (wide & short, diagonal, wide & long, narrow & short and narrow & long,), Section III- presented the P-V characteristics of distinct array configurations under distinct shading patterns and implementation of P&O algorithm on the best configuration is discussed, flowed by conclusion in Section IV. Thus, to investigate the performance of array configuration paper investigates on identifying the best PV array configuration positioning of global peak and performance

2. VARIOUS PV ARRAY CONFIGURATIONS, SHADING PATTERNS

2.1. PV Module Modelling

In a PV module, many PV cells are connected in series. A single diode model described in Fig.2.2 [12] is considered for modelling the 250 Wp PV module and its datasheet parameters are mentioned in the Table 1. For modelling the PV module, the

unknown parameters such as shunt resistance, diode ideality factor, reverse saturation current, photon current and series resistance are demonstrated by using the Lambert function [11]. The PV module's I-V characteristics are illustrated by the following equation.

$$Ipv = Iph - Io * \left[e^{\left(\frac{Vpv + Ipv * Rs}{Ns * \left(\frac{Kb.\eta.t}{q} \right)} \right)} - 1 \right] - \frac{Vpv + Ipv * Rs}{Rsh} \qquad (2.\ 1)$$

The above equation is simulated in MATLAB/simulink and is mentioned in Figure 2.2. For obtaining the I-V characteristics, a capacitor is connected across the load (described in Figure 2.2.), which act as a variable load. At distinct irradiance and temperature values, P-V curves and I-V curves are plotted and is illustrated in Figure 2.1.

Table 1. Specifications for PV Module and various Array Configurations

	PV Module	**SeriesArray Configuration**	**Series-Parallel / Honey-Comb/TCT Array Configurations**
Peak Power	250 Watts	6250 Watts	6250 Watts
Voltage At Max Power (V_{mp})	30.72 Volts	768 Volts	153.6 Volts
Current At Max Power (I_{mp})	8.14 Amps	8.14 Amps	40.7 Amperes
Open Circuit Voltage (V_{oc})	37.82 Volts	945 Volts	189 Volts
Short Circuit Current (I_{sc})	8.633 Amps	8.63 Amps	43.15 Amps

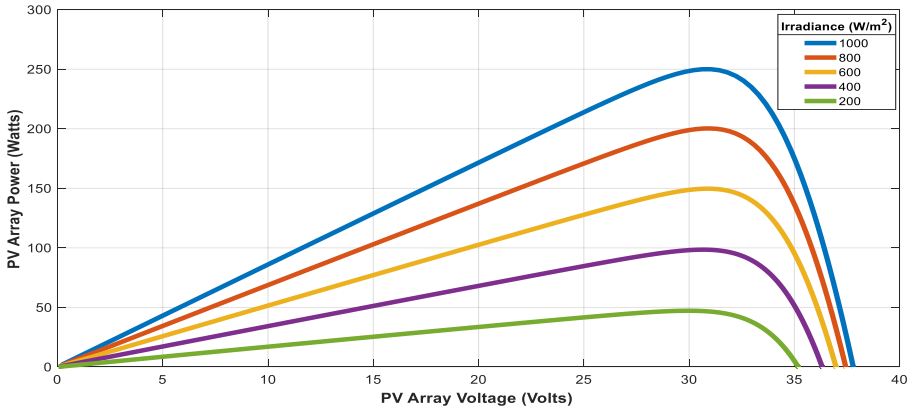

Figure 2.1 PV Module's Characteristics at 200 W/m^2, 400 W/m^2 , 600 W/m^2 800 W/m^2 and 1000 W/m^2

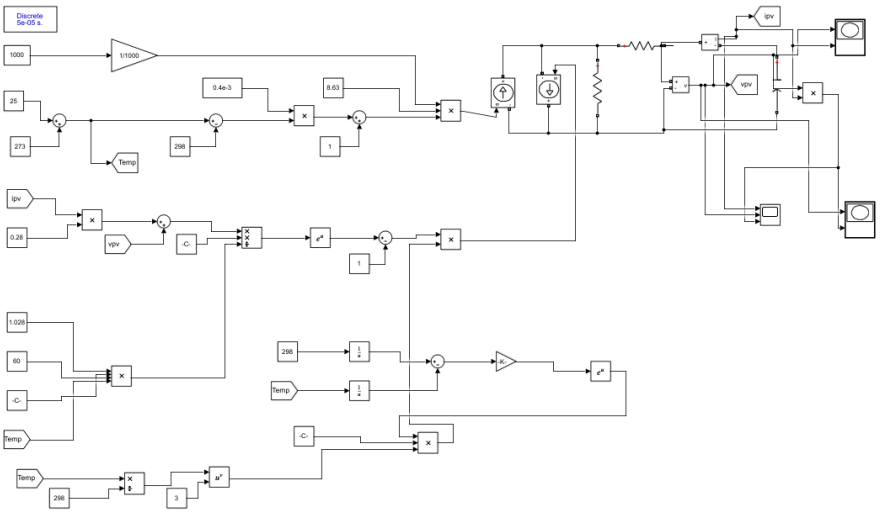

Figure. 2.2. PV Module Simulation diagram

2.2. PV Array configurations

Few number of the PV Modules are connected in a particular pattern to achieve the required voltage, current and power ratings. The various array configurations considered for the investigation are - i) Series, ii) Series-parallel, iii) Honey-Comb (H-C), iv) Total Cross-tied (TCT).

The figure 2.3(a). shows a 5x5 Series PV Array configuration. In this, Series PV Array configuration is formed by connecting all the 25 PV modules in series. In this configuration, module current is considered to be the array current, and the sum of the individual PV module voltages connected in series is considered as the array voltage. The product of the array current and voltage is calculated as the array power.

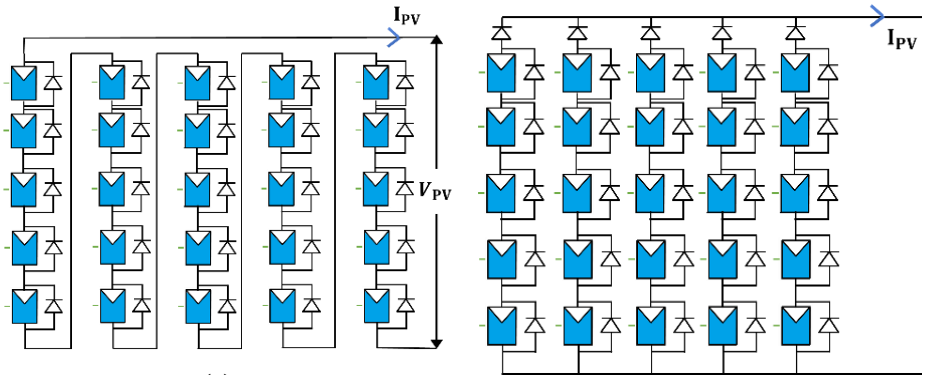

(a) (b)

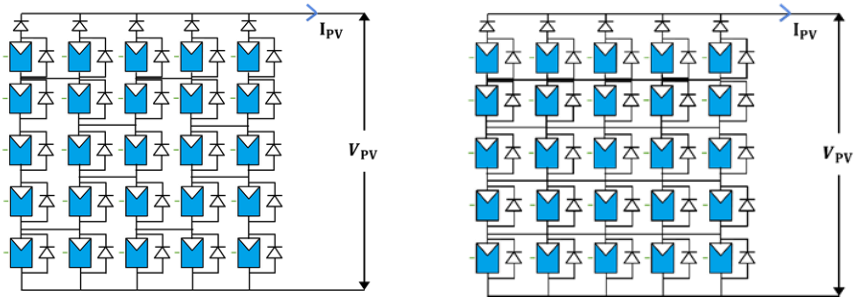

(c) (d)

Figure 2.3. Series PV Array Configurations (a) 5 x 5 Series, (b) 5 x 5 Series-Parallel, (c) 5 x 5 Honey-Comb (d) 5 x 5 TCT

The figure 2.3(b). shows 5x5 Series-parallel PV Array configuration and its specifications mentioned in Table 1. To meet the output current and voltage requirement, to form a string, photovoltaic modules are connected in series, and these are connected in parallel then after. This arrangement is that the most typically used since it's straightforward to line up and has no redundant connections.

The figure 2.3(c). shows 5 x 5 Honey-comb PV Array configuration and its ratings are tabulated in Table 1. Photovoltaic modules are connected in such a way as shown in the figure 2.3(c). to replicate the obtain the output current and voltage.

The figure 2.3(d). shows 5 x 5 TCT PV Array configuration and its specifications are mentioned in Table 1. Photovoltaic modules are cross tied to each other to secure the required output current and voltage. In this case, each row's voltage is the same, and the sum of the voltages across each row is same. The current in each column is the same.

A blocking diode to connected to each string to avoid the circulating currents among the strings under equal irradiance conditions and to resist the current flow from battery/grid to photovoltaic panel.

2.3. Shading Patterns

For investigating the PV array performance and positioning of global peak, five shading patterns are considered namely; under wide & short, diagonal, wide & long, narrow & short and narrow & long.

	S1	S2	S3	S4	S5
R1	300	300	1000	1000	1000
R2	500	500	1000	1000	1000
R3	700	700	1000	1000	1000
R4	1000	1000	1000	1000	1000
R5	1000	1000	1000	1000	1000

(i)

	S1	S2	S3	S4	S5
R1	300	300	500	500	1000
R2	300	300	500	500	1000
R3	700	700	700	700	1000
R4	1000	1000	1000	1000	1000
R5	1000	1000	1000	1000	1000

(ii)

	S1	S2	S3	S4	S5
R1	300	300	1000	1000	1000
R2	500	500	1000	1000	1000
R3	500	500	1000	1000	1000
R4	500	700	1000	1000	1000
R5	700	700	1000	1000	1000

(iii)

	S1	S2	S3	S4	S5
R1	300	300	500	500	1000
R2	300	300	500	500	1000
R3	300	300	500	500	1000
R4	700	700	900	900	1000
R5	700	700	900	900	1000

(iv)

	S1	S2	S3	S4	S5
R1	300	1000	1000	1000	1000
R2	1000	400	1000	1000	1000
R3	1000	1000	500	1000	1000
R4	1000	1000	1000	700	1000
R5	1000	1000	1000	1000	900

(v)

Figure 2.4. Pictorial illustration of module level irradiance in a PV array under Various shading pattern, (i) Narrow & Short, (ii) Wide & Short, (iii) Narrow & Long, (iv) Wide & Long, (v) Diagonal

2.3.1. Narrow & Short Shading Pattern

In narrow and short shading condition, out of five strings (narrow by comparing alongside the width of the PV array), only two strings are shaded and the three modules are shaded per string (short by comparing alongside the string's length), thus this shading type is considered to as narrow and short shading condition as illustrated in the Figure 2.4(i).

2.3.2.Wide and Short Shading Pattern

In such pattern of shading, out of five strings four are shaded (wide by comparing alongside the PV array's width) and there are three number of shaded modules per string is described in Figure 2.4(ii).

2.3.3. Narrow & Long Shading Pattern

In this shading pattern, shading is confines to only two strings (narrow, say) and in these strings, each and every modules in that string are shaded to different irradiance values (long, say), illustrated in Figure 2.4(iii).

2.3.4.Wide & Long Shading Pattern

Out of five strings, the four strings of the photovoltaic array are shaded and each and every module of these strings are to be shaded, and noted to as wide and long shading condition.

2.3.5. Diagonal Shading Pattern

In a Photovoltaic array, the five diagonally placed PV modules are subjected to different solar irradiance levels. The different levels of solar irradiance on diagonally positioned PV modules are set to be as 900 Watts/m^2, 700 Watts/m^2, 500 Watts/m^2, 400 Watts/m^2 and 300 Watts/m^2 respectively and is depicted in Figure. 2.4(v).

Under shading condition, irradiance at some of the modules are changed according to the type of pattern and the remaining are left at an irradiance of 1000 Watts/m^2.

3. SIMULATION RESULTS AND DISCUSSION

In this chapter, each array configuration (i.e., TCT, Honey-Comb, Series-Parallel and Series) is simulated under various partial shading pattern (i.e., Diagonal, Narrow & Short, Wide and Long, Wide & Short, Narrow and Long,) and their respective P-V curves are plotted. These P-V curves are compared and the best configuration is determined based on the computation of mismatch losses and global peak position.

3.1. Performance Analysis of Photovoltaic Array Configurations under various Partial Shading Conditions (PSCs).

In this section, it describes about the performance of TCT, Honey-Comb, Series-Parallel and Series photovoltaic array configurations under normal and PSC's is to be selected as the best photovoltaic array configuration that which furnishes the better performance overall. The performance of photovoltaic array configuration is examined with respect to maximum power and the mismatching losses.

3.1.1. Series PV Array Configuration

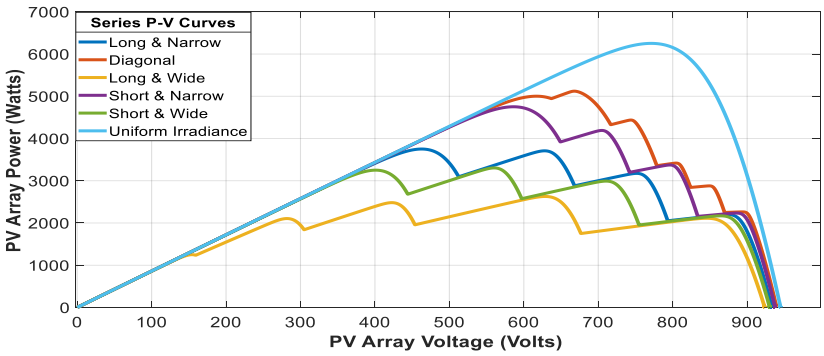

Figure 3.1. P-V Curves of Series PV Array Configuration under uniform and PSCs

The simulation is carried out for Series photovoltaic array configuration under uniform irradiance and partial shading conditions like wide & short, diagonal, wide & long, narrow & short and narrow & long, and the respective P-V curves are plotted in figure 3.1. The Series photovoltaic array configuration gives maximum power of 6250.48 Watts at uniform irradiance. Under partial shading condition, series PV array configuration generates a peak power of 5120.8 Watts under diagonal shading pattern, 4742.8 Watts – under narrow and short, 3708.55 Watts- narrow and long, 3295.81 Watts- Wide and short and 2627.16 Watts -wide and long patterns as referred to the Figure 3.2.

3.1.2. Series - Parallel PV Array Configuration

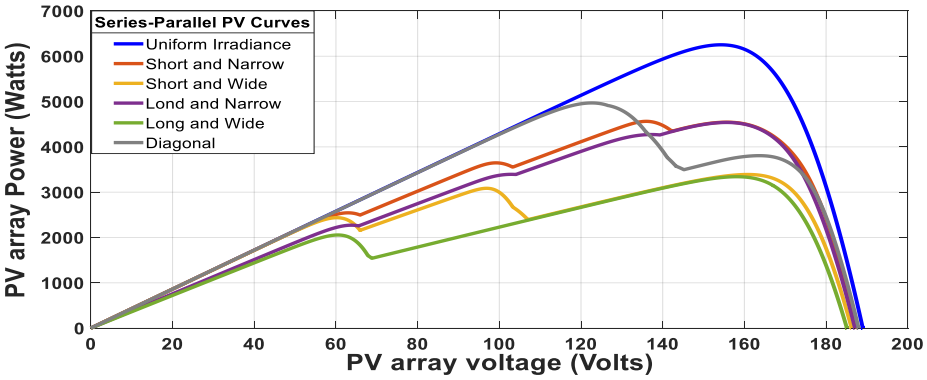

Figure 3.2. P-V Curves of Series-Parallel photovoltaic Array Configuration under uniform and PSCs

The simulation is carried out for Series-Parallel photovoltaic array configuration under uniform irradiance and PSC's like wide & short, diagonal, wide & long, narrow & short and narrow & long. The P-V curves of each condition are plotted as depicted in the figure 3.2. The Series - Parallel photovoltaic array configuration gives maximum power of 6249.4 Watts at uniform irradiance. At diagonal shading condition, the Series - Parallel photovoltaic array gives the maximum power of 4996.95 Watts followed narrow and short (4683.7 Watts), narrow and long (3973.12 Watts), wide and short (3325.56 Watts) and then by wide and long (3092.7 Watts) as referred to the Figure 3.2.

3.1.3. HONEY-COMB PV Array Configuration

The simulation is carried out for Honey-Comb PV array configuration under uniform irradiance and PSC's like wide & short, diagonal, wide & long, narrow & short and narrow & long. The P-V curves of each condition are plotted as shown in figure 3.3. The HC photovoltaic array configuration gives maximum power of 6248.9 Watts at uniform irradiance. At diagonal shading condition Series PV array gives the maximum power of 4855.9 Watts followed by narrow and short (4825.22 Watts), narrow and long (4637.28 Watts), wide and long (3462.38 Watts) and wide and short (3336.91 Watts) as referred to the Figure 3.3.

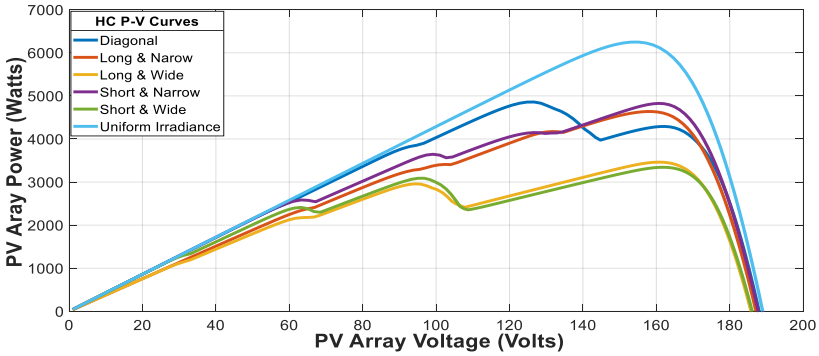

Figure 3.3. P-V Curves of HC PV Array Configuration under uniform and PSCs

3.1.4. TCT PV Array Configuration

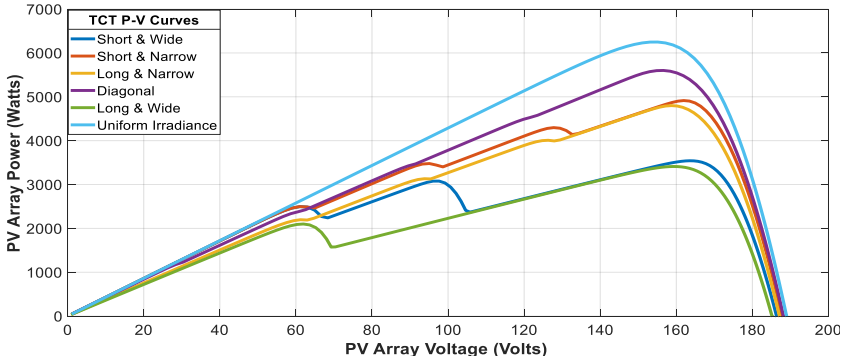

Figure 3.4. P-V Curves of TCT PV Array Configuration under uniform and PSCs

The simulation is carried out for TCT photovoltaic array configuration under uniform irradiance and PSC's like wide & short, diagonal, wide & long, narrow & short and narrow & long. The P-V curves of each condition are plotted as depicted in Figure.3.4. The maximum power in each shading condition is noted and compared with each other as shown in the fig.3.4 . The Series photovoltaic array configuration gives maximum power of 6248.9 Watts at uniform irradiance. At diagonal shading condition Series photovoltaic array gives the maximum power of 5596.82 Watts followed by short and narrow (4914.31 Watts), long and narrow (4790.31 Watts), Short and Wide (3538.12 Watts) and long and wide (3408.35 Watts).

3.2. Comparison of photovoltaic Array Configurations under various PSC's.

After plotting all the P-V characteristics, the maximum powers are compared for each and every array configuration under each shading pattern. By referring the data from Figure 3.5., it can be observed that under wide & short, diagonal, wide & long, narrow & short and narrow & long, TCT gives the maximum power and low losses as taken from the Table 2, and chosen as the best configuration for all the shading patterns except Long & Wide (L&W) as Honey-Comb provides the max power and lowest losses than TCT,

although the difference between the losses between TCT and Honey-Comb for Wide & Long is neglected. By overall consideration from the Figure 3.5. and Table 2, TCT is spotted as the best configuration.

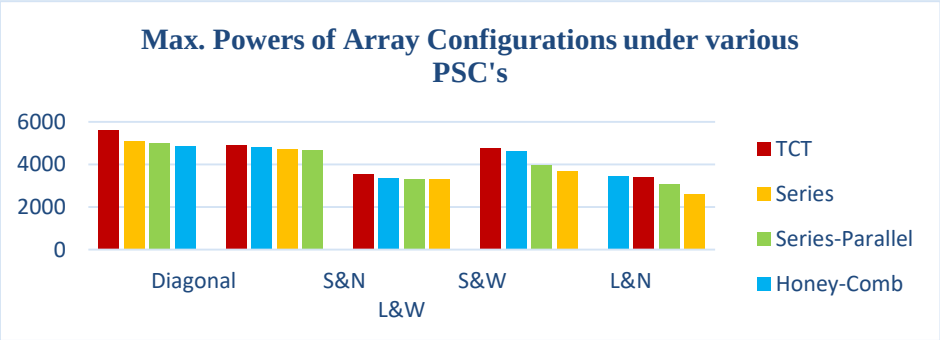

Figure 3.5. Max. Powers chart of distinct PV Array Configuration under various PSCs

Table 2. Losses in PV Array Configuration under various PSC's

	Diagonal	**Short & Narrow**	**Short & Wide**	**Long & Narrow**	**Long & Wide**
TCT	**652.08**	**4914.31**	**2710.78**	**1458.59**	**2830.55**
Honey - Comb	**1392.97**	**1423.68**	**2911.99**	**1611.62**	**2786.52**
Series & Parallel	**1252.45**	**1565.7**	**2923.84**	**2276.28**	**3156.7**
Series	**1129.68**	**1507.68**	**2954.67**	**2541.93**	**3623.32**

3.3. Implementation P&O algorithm for TCT by changing irradiance.

To track the maximum power point in a photovoltaic system, P&O algorithm is most generally used MPPT algorithm as it is easy and due to its flexibility. As TCT PV array configuration is found as the best configuration, P&O algorithm is applied to it and can be observed that from 6 to 8 seconds, the irradiance is uniform and is 1000 Watts/m^2. Accordingly, the power is also uniform and is about 6250 Watts. As there is a slant decrease and increase in irradiance from 8 to 10 seconds, the power also declined and then inclined respectively along with irradiance. A sudden change in irradiance from 1000 Watts/m^2 to 500 Watts/m^2 at 12th second resulting in power to sudden decrease from 6250 watts to 3125 watts is also tracked by the P&O algorithm as demonstrated in the Figure 3.5.

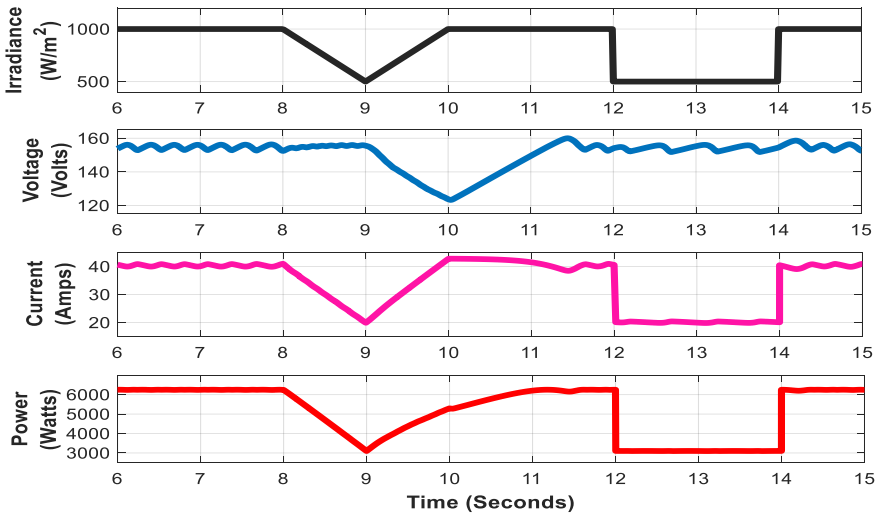

Figure 3.5. PV Voltage, Current, Power waveforms of TCT array configuration under constant irradiance, sudden and slow changing irradiance conditions.

4. CONCLUSION

By simulating various photovoltaic array configurations under distinct partial shading patterns, the best suitable configuration (i.e., Series, Series-Parallel, Honey-Comb, TCT) is identified as TCT based on the array losses. Furthermore, in the TCT PV array characteristics, the global peak is always located near to open circuit voltage, irrespective of the shading pattern. Hence, global maximum power point trackers are not required for tracking the global peak positions for TCT configuration and is required for other configurations, since global peak position may or may not be located near to the open circuit voltage for particular shading pattern (i.e., wide & short, diagonal, wide & long, narrow & short and narrow & long). As investigated on the whole, it is found that TCT is the best of all configurations considering various shading patterns. Furthermore P&O algorithm is implemented for the best confirmation (TCT) to track the maximum power point (MPP) by changing various irradiance which replicates the shading.

5. REFERENCES

[1] M. A. G. de Brito, L. Galotto, L. P. Sampaio, G. d. A. e Melo and C. A. Canesin, "Evaluation of the Main MPPT Techniques for Photovoltaic Applications," in *IEEE Transactions on Industrial Electronics*, vol. 60, no. 3, pp. 1156-1167, March 2013, doi: 10.1109/TIE.2012.2198036.

[2] Jain, S. and Agarwal, V. (2007) A single- stage grid connected inverter topology for solar PV system with maximum power point tracking, IEEE Trans. Power Electron., 22, 1928-1940.

[3] C. Manickam, G. P. Raman, G. R. Raman, S. I. Ganesan and N. Chilakapati, "Fireworks Enriched P&O Algorithm for GMPPT and Detection of Partial Shading in PV Systems," in *IEEE Transactions on Power Electronics*, vol. 32, no. 6, pp. 4432-4443, June 2017, doi: 10.1109/TPEL.2016.2604279.

[4] H. Patel and V. Agarwal, "MATLAB-Based Modeling to Study the Effects of Partial Shading on PV Array Characteristics," in IEEE Transactions on Energy Conversion, vol. 23, no. 1, pp. 302-310, March 2008, doi: 10.1109/TEC.2007.914308.

[5] B. Pradeep Kumar, G. Saravana Ilango, M. Jaya Bharatha Reddy and C. Nagamani, "Online Fault Detection and Diagnosis in Photovoltaic Systems Using Wavelet Packets," IEEE Journal of Photovoltaics, vol. 8, no. 1, pp. 257-265, Jan. 2018.

[6] Balasubramanian, I. R., Ganesan, S.I. and Chilakapati, N, "Impact of partial shading on the output power of PV systems under partial shading conditions", IET Power Electron., 7, 657-666, 2014.

[7] H. Patel and V. Agarwal, "MATLAB-Based Modeling to Study the Effects of Partial Shading on PV Array Characteristics," in IEEE Transactions on Energy Conversion, vol. 23, no. 1, pp. 302-310, March 2008, doi: 10.1109/TEC.2007.914308.

[8] Belhachat, F., and C. Larbes. "Modeling, analysis and comparison of solar photovoltaic array configurations under partial shading conditions." Solar Energy 120 (2015): 399-418.

[9] Pendem, Suneel Raju, and Suresh Mikkili. "Modeling, simulation and performance analysis of solar PV array configurations (Series, Series–Parallel and Honey-Comb) to extract maximum power under Partial Shading Conditions." Energy Reports 4 (2018): 274-287.

[10] Ramaprabha, R. and Mathur, B.L.," A comprehensive review and analysis of solar photovoltaic array configurations under partial shaded conditions", International Journal of Photoenergy, 2012.

[11] Femia N., Petrone G., Spagnuolo G. et al.: ' Power electronics and control techniques for maximum energy harvesting in photovoltaic systems' (CRS Press/Taylor and Francis, Oxfordshire, UK, 2013).

[12] B. Pradeep Kumar, M. Nitheesh kumar, M. Chakkarapani, G. Saravana Ilango, C. Nagamani, " Estimation of PV Module Degradation Through Extraction of I-V Curve at Inverter Pre-Startup Condition," submitted to IET Renewable Power Generation (accepted for publication in Jan 2021).

PV integrated DC-DC converter and Inverter topologies for grid tied/standalone system

PUSHPA K R[1] **R S GEETHA[2]**

[1]*Research Scholar, Electrical & Electronics Department, VTU, B.M.S.C.E, pushpakr@pes.edu*
[2]*Professor, Electrical & Electronics Department, B.M.S.C.E, rsgeetha.eee@bmsce.ac.in*

Abstract.

In this paper comparative analysis of various PV integrated power converter topologies used for improving performance and efficiency of a PV converter- Inverter system is analysed. Analysis and design are carried out for varying irradiation for fixed load. The power conversion and efficiency in various inverter topologies namely centralized, string, power optimizer and micro inverter topologies is simulated and analysed.

Keywords. ***Photo Voltaic (PV) converter-Inverter system, power converter.***

1. INTRODUCTION

The converter topology plays an important role in deciding the PV system cost. Cost of Balance of System (BoS) components in PV system can be reduced by reducing the price of inverter, boosting its efficiency [1]. With the implementation of panel level DC-DC converters, the maximum available power can be extracted from each panel regardless of any mismatch caused by partial shading [2]. Shading and mismatch in PV panel characteristics affects energy production and its impact depends on PV architecture. Under uneven shading conditions, converter topology used in a PV system plays a significant role in extracting energy [3]. PV system can have centralized, string, power optimizer or micro inverter architecture.

In central inverter topology only one large inverter is connected to series or parallel connected DC-DC converter which receives power from PV panels. In string inverter topology each string has its dedicated inverter and are connected in parallel to supply load. In Micro inverter topology each panel has its own dedicated inverter [1][2][3]. In the central inverter topology, series connected PV panels forming strings are paralleled to obtain the desired output power. In string configuration all PV strings has same voltage. With string configuration all the panels are not utilized effectively as the voltage required to obtain maximum power point tracking by each panel is not same [4]. In central inverter topology PV panels are connected to common array in series – parallel configuration which in turn is connected to a single DC-DC converter and then to a large inverter as shown in Figure 1. In string inverter topology each string has its own dedicated DC-DC converter and an inverter which are paralleled to supply load as shown in Figure 2.

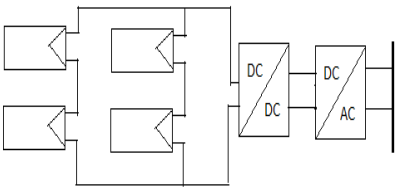

Figure 1. Centralized Inverter topology

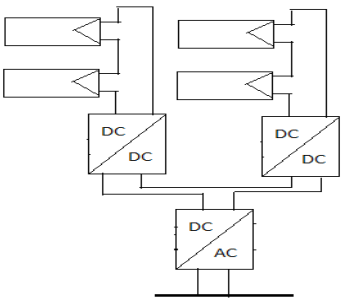

Figure 2. String Inverter topology

Non-isolated module level DC-DC converters can be connected in series to create a high voltage string. Buck, boost, buck-boost and Cuk converters are used for cascading. In power optimizer topology each module has its own DC-DC converter. The outputs of these converters are connected in series to boost string voltage as shown in Figure 3. Micro-inverters power conversion efficiencies are above 90% with power ranges between 100–250 W [5-6]. In micro inverter topology each PV panel has its dedicated DC-DC converter and an inverter which in turn are paralleled to supply load as shown in Figure 4.

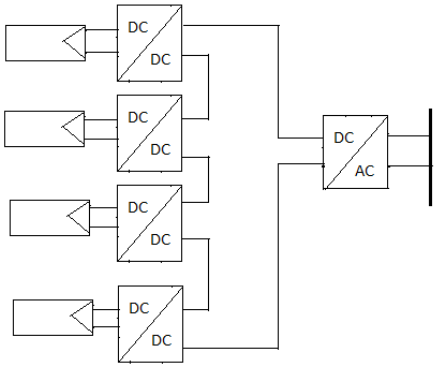

Figure 3. Power optimizer topology

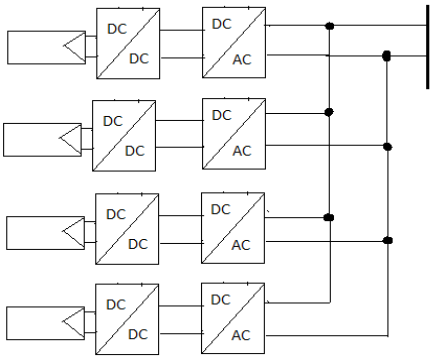

Figure 4. Micro Inverter topology

In this paper analysis is carried out for series and parallel connected DC–DC converter topologies along with inverter to obtain high current-low voltage or high voltage-low current output. In addition, a comprehensive analysis of the converter and inverter efficiency with varying irradiation for a specific load is addressed.

2. DESIGN SPECIFICATIONS

In this work, the analysis of PV system with centralized, string, power optimizer and micro inverter topologies are carried out with 213W panel. In all the four-configuration panel is operated at a temperature of 25^0C at different irradiation (1000W/m^2 and 700W/m^2). Design and analysis are carried out for 426W resistive load with the PV panel specification as shown in Table1. Filter components L and C of boost converter is designed for 10%

ripple voltage and current at a frequency of 30 KHz using equation 1 and 2 is shown in Table 2.

$$\Delta I = \frac{V_{IN}D}{f_S L} \quad (1)$$

$$\Delta V_c = \frac{I_0 D}{f_S C} \quad (2)$$

Open circuit voltage V_{oc}	36.3V
Short circuit current I_{sc}	7.84A
Maximum voltage V_{max}	29V
Maximum current I_{max}	7.35A

Table 1:
PV Panel specification

Topology	V_{in} V	V_{out} V	L mH	C uF	D	P W
Centralized	58	120	3	4.62	0.516	426
String	29	60	1.4	10.17	0.516	213
Power optimizer	29	60	1.4	10.17	0.516	213
Micro	29	120	4.12	3.73	0.758	213

Table 2:
Boost converter specification

For the panel integrated DC-DC boost converter as shown in Figure 5, output power for varying irradiation with and without MPPT is shown in Table 3. PV panel P-V and I-V characteristics is shown in Figure 6.

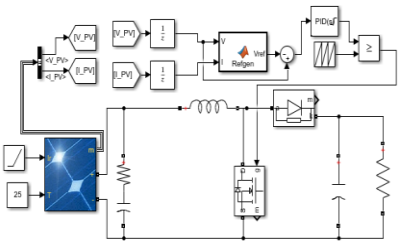

Figure 5. Boost converter characteristics

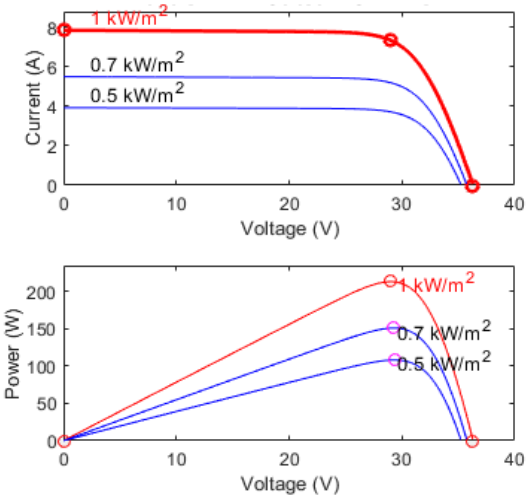

Figure 6. PV panel I-V and P-V

Table 3:
PV output for varying irradiation

Irradiation W/m^2	Without MPPT		With MPPT	
	P_{out}(W)	$R_{load}(\Omega)$	P_{out}(W)	$R_{load}(\Omega)$
1000	210.9	16.9	212.4	4
700	143	28.73	145.2	6.8
500	105.7	33.8	108	8

Single phase H bridge inverter shown in Figure 7 is operated at 1KHz switching frequency with specifications as shown in Table 4. To obtain sine wave output, an LC filter is designed using equations 3 and 4 [9].

$$\boldsymbol{L = \frac{V_{dc}}{4f_s \Delta I_0}} \quad (3)$$

$$\boldsymbol{C = \frac{\Delta I_0}{8f_s \Delta V_0}} \quad (4)$$

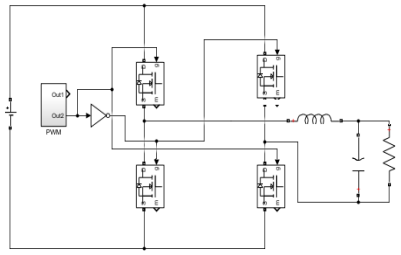

Figure 7. Single phase H bridge inverter

Table 4:
Inverter specification

Power W	V_{out}(rms)	I_0(rms)	R_{load} Ω
426	120/√2	5.02	16.9
213	120/√2	2.51	33.8

The PWM and sine wave output obtained for 426W single phase inverter is shown in Figure 8 and 9.

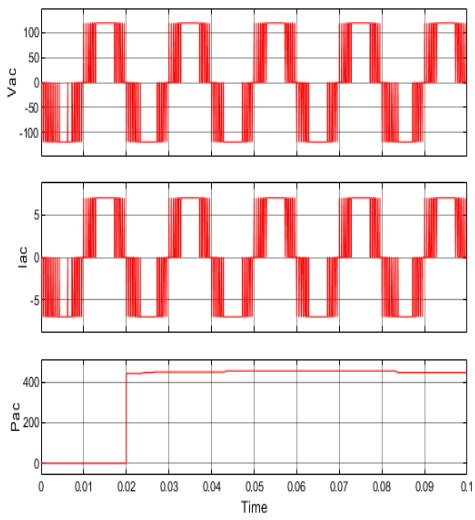

Figure 8. PWM output

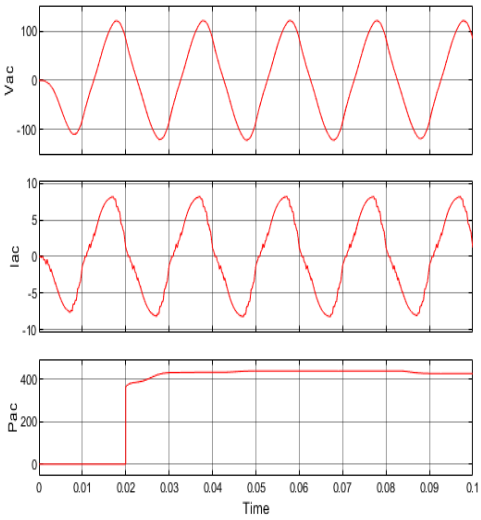

Figure 9. Sine wave output

3. CONVERTER AND INVERTER TOPOLOGIES

3.1 Centralized Inverter topology

In centralized topology panels are connected in series to increase string voltage and is then given to DC-DC converter and to inverter. Each panel can supply maximum power of 213W.Due to series connection of panel maximum output voltage of 58V is obtained for the chosen specifications. This voltage is boosted to 120V using boost converter to feed a load of 426W.The output power obtained from boost converter shown in Figure 10 that is fed from series connected panels is shown in Figure 11.

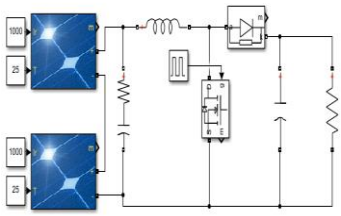

Figure 10. Series connected PV panels fed

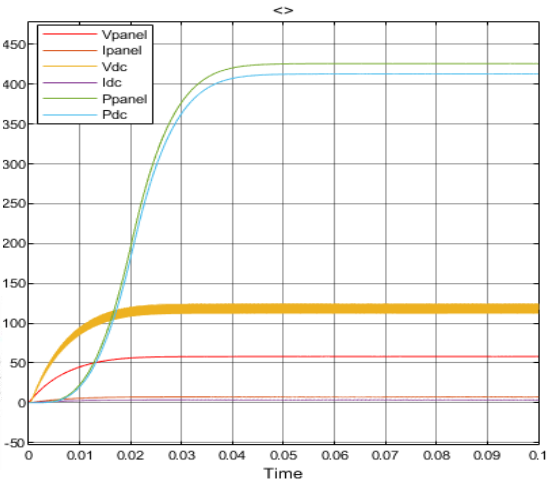

Figure 11. Power output of boost converter from series connected PV panels

Centralized inverter topology for 426W capacity is shown in Figure 12. Output of DC-DC converter is given to H bridge inverter to obtain ac output. Voltage, current and power output from this topology is shown in Figure 13. It is observed that the ac voltage and currents have high transients since the same designed values as shown in Table 3 are used. However, it can be reduced by fine tuning L and C values.

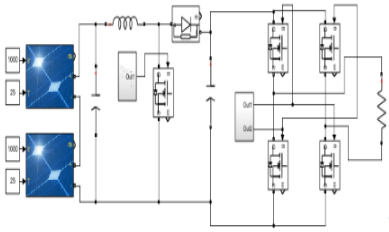

Figure 12. Centralized Inverter topology from

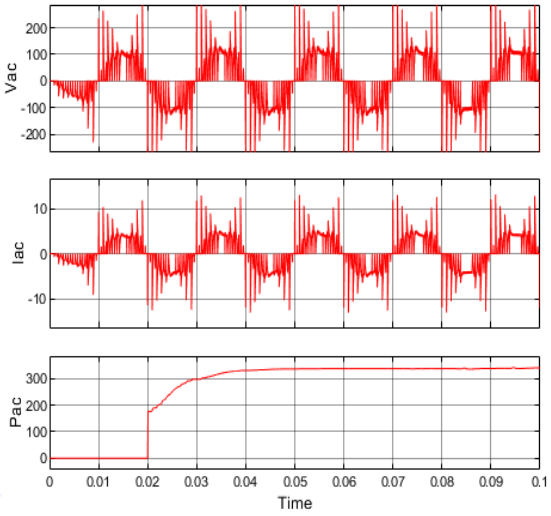

Figure 13. Ac voltage, current and power Centralized inverter topology

3.2 String Inverter topology

In this topology each string has its own DC-DC converter. Output of DC- DC converters are connected in parallel as shown in Figure 14. With parallel connected DC-DC converter,426W output power obtained is shown in Figure 15.

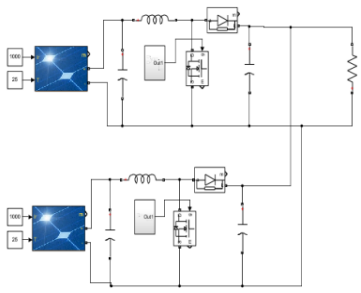

Figure 14. Parallel DC-DC converter

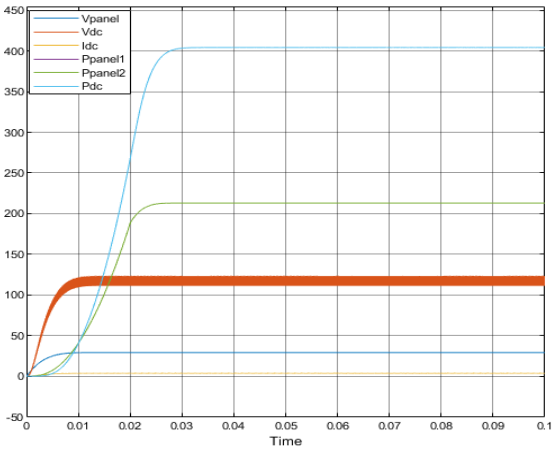

Figure 15. Power output from parallel connected boost converter

String inverter topology for 426W capacity is shown in Figure 16. Output of DC-DC converter is given to H bridge inverter to obtain ac output. Voltage, current and power output from this topology is shown in Figure 17

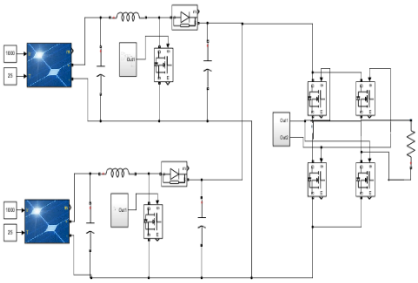

Figure 16. String Inverter topology

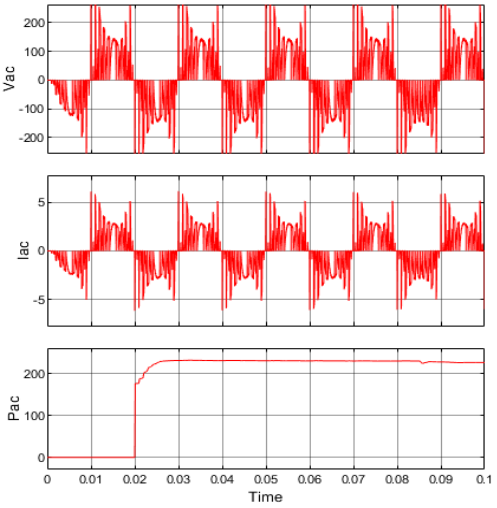

Figure 17. Ac voltage, current and power from string inverter topology

3.3. Power optimizer

In this topology DC-DC boost converters are connected in series as shown in Figure 18. To overcome problems of short circuit diodes are connected across output of each converter. Series connection of converters increases output voltage and hence the output power. With series connected DC-DC converter 426W output power obtained is shown in Figure 19.

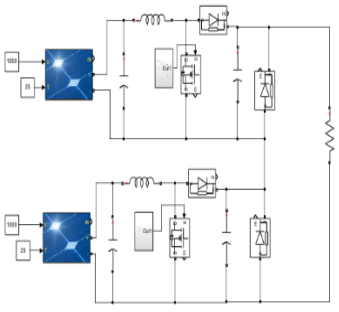

Figure 18. Series DC-DC converters

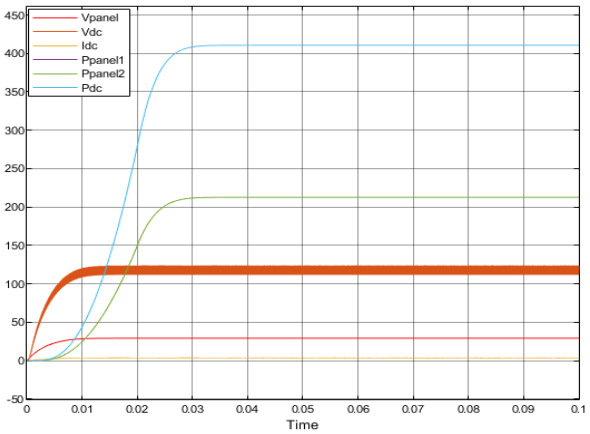

Figure 19. Power output from series connected boost converter

Each panel can supply a maximum power of 213W. Total output wattage is 426W Input to each DC-DC converter is from 213W PV panel. Output voltage 29V obtained from each

panel is boosted to a higher voltage of 60V. Output of these boost converters are series connected to obtain 120V DC to feed the load. Figure 20 shows series connected DC-DC converter connected to an inverter feeding resistive load. Voltage, current and power output from this topology is shown in Figure 21.

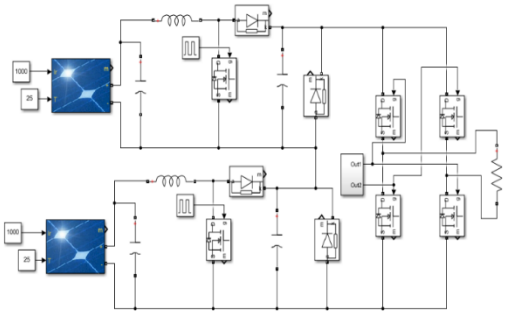

Figure 20. Power optimizer topology

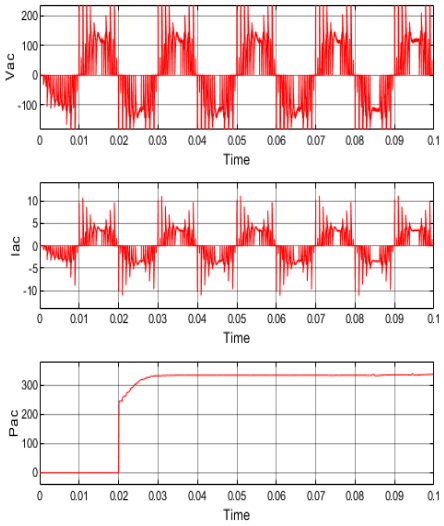

Figure 21. AC Voltage, current and power output from power optimizer

3.4. Micro inverter topology

In micro inverter configuration each PV panel has its own DC-DC converter and an inverter. Later inverters ouput is connected in parallel to supply the load as shown in Figure 22 .Each inverter has its own control. Power output from each 213W DC-DC converter is shown in Figure 23.

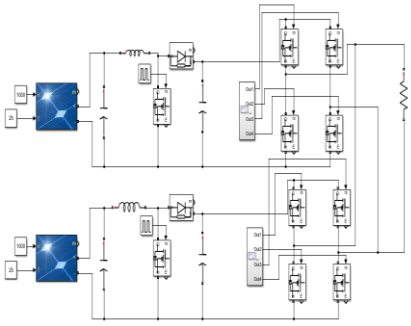

Figure 22. Micro inverter topology

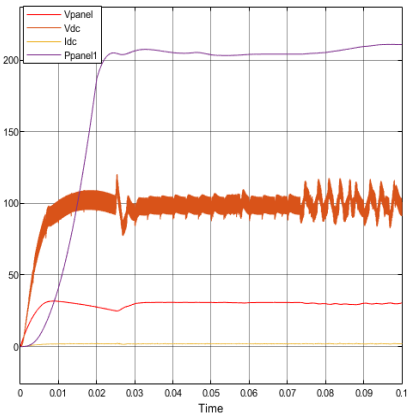

Figure 23. Power output from each DC-DC converter

4. RESULTS AND DISCUSSIONS

This section discusses efficiency of converter, inverter as well as overall PV converter inverter system efficiency for centralized,string,power optimizer and micro inverter topologies. Power output at each stage with conversion efficiency is shown in Table 5 and 6 for varying irradiation at constant temperature .Power output from PV panel with varying irradiation is analysed.

Table 5 :
$Panel_1$ =1000W/m^2,25^{0}C $Panel_2$ =1000W/m^2,25^{0}C

Type	$\mathbf{P_{panel}}$	$\mathbf{P_{dc}}$	$\mathbf{P_{ac}}$	$\%\eta_{con}$	$\%\eta_{Inv}$	$\%\eta_{overall}$
Centralized	306.4	297.5	269.1	97	90.45	87.8
String	253.4	236.9	193.1	93.48	81.5	76.2
Power optimizer	313.2	299	268.8	95.4	89.89	85.82
Micro	391	350.6	350	89.66	100	89.51

Table 6:
$Panel_1$ =1000W/m^2,25^{0}C $Panel_2$=700W/m^2,25^{0}C

Type	$\mathbf{P_{panel1}}$	$\mathbf{P_{panel2}}$	$\mathbf{P_{pane1}}$	P_{ac}	$\%\eta_{overall}$
Centralized	177.4	-23.33	153	134.7	87.4
String	108.5	75.48	183.98	139.8	75.98
Power Optimizer	203.6	37.82	241.42	193.4	80.10
Micro Inverter	98.82	65.35	164.17	138	84.05

From results it is observed that with constant and varying irradiation condition micro inverter topology has improved efficiency compared to other topologies for the same specification of load. Also, it is observed that module level topologies power optimizer and micro inverter have better efficiency compared to centralized and string topologies.

5. CONCLUSION

In this work comparision and performance evaluation of centralized , string, power optimizer and micro inverter topologies for a standalone system is carried out. Effect of irradiation on power generated from panel and power conversion efficiency of the entire PV system under those conditions are simulated and analysed .It is observed from simulation results , power output from panel under varying irradiation condition is maximum in micro inverter topology compared to centralized, string and power optimizer topologies.

6. REFERENCES

[1] Sebastian Strache, Ralf Wunderlich and Stefan Heinen "A Comprehensive, Quantitative Comparison of Inverter Architectures for Various PV Systems cells and Irradiance Profiles" IEEE transactions on sustainable energy, vol. 5, no. 3, july 2014

[2] Matthias Kasper, Dominik Bortis, and Johann W. Kolar, "Classification and Comparative Evaluation of PV Panel- Integrated DC–DC Converter Concepts" IEEE transactions on power electronics, vol. 29, no. 5, may 2014

[3] Huiying Zheng, Shuhui Li, Rajab Challoo , Julio Proano Shading and bypass diode impacts to energy extraction of PV rays under different converter configurations" ELSEVIER Renewable Energy, 2014

[4] Mouhoub Birane, Cherif Larbes, Ali Cheknane "Comparative study and performance evaluation of central and distributed topologies of photovoltaic system" ELSEVIER, International journal of hydrogen energy ,2016

[5] Hadeed Ahmed Sher, Khaled E. Addoweesh "Micro- inverters — Promising solutions in solar photovoltaics" ELSEVIER, Energy for Sustainable Development 68(2014) 58-66

[6] G. R. Walker P. C. Sernia, "Cascaded DC-DC Converter Connection of Photovoltaic Modules" IEEE.

[7] Leonardo Callegaro, Mihai Ciobotaru, John E. Fletcher and Pablo cuna Rios Daniel J. Pagano "Design of Cascaded Control Loop Solar Power Optimizer Based on a Buck-Boost Converter" ,2016 IEEE

[8] L Hassaine,E Olias,J Quintero,V Salas "Overview of power inverter topologies and control structures for grid connected photovoltaic systems" Renewable and Sustainable Energy Reviews,Elsevier,December 2013

[9] K R Pushpa and R S Geetha, "Mathematical model and analysis of PV Converter-Inverter System", IOP Conf.Series: Material Science and Engineering,2021

Biographies

Pushpa K R is currently working as a Assistant Professor in the Department of Electrical and Electronics Engineering, PES University. Obtained MTech from VTU. Her research areas include power converters and control, power quality analysis.

Geetha R S is presently working as a Professor in the Department of Electrical and Electronics Engineering at B.M.S.C.E. Obtained Ph.D. from VTU, Belagavi for the work carried out in the area of "Voltage Source Converter based DC systems". Guided several projects in the area of Power Electronics Converters, HVDC systems, power quality, power converter controls, various topologies of Multilevel converters and renewable energy systems. She is a member and also secretary of IEEE-SSIT professional body (2019 till date). She has more than 25 conference / journal publications.

Optimal Design and Comparative Analysis of Different Bi-Directional DC-DC Converters for Energy Storage Applications

Shubham Dongare[1], R S Geetha[1], Priyaranjan Mishra[2]

[1]*Department of EEE, BMSCE, Bengaluru, India*

[2]*Belbird Technologies Pvt Ltd, Bengaluru*

Email: shubham.epe20@bmsce.ac.in

Abstract

Bi-Directional DC-DC converters are widely used in many applications where two way power flow is required that is in forward and reverse direction. In this paper design and comprehensive analysis is carried out for Non-Isolated Bi-Directional Buck-Boost Converter and Isolated Dual Active Bridge DC-DC Converter, for same power rating and operating frequency. Detailed qualitative and quantitative comparison is carried out in terms of efficiency, number of components used and size. This comparison analysis helps to choose an appropriate topology for the specific application. The paper also discusses the novel method to switch the MOSFETs in Bi-Directional Buck-Boost converter and Dual Active Bridge converter. Furthermore, as an application of these converters, the concept of Bi- directionality charge and discharge of battery in one cycle is shown using MATLAB/SIMULINK software.

Keywords. Batteries, Bi-Directional, DC-DC Converters, Efficiency, SoC (State of Charge)

1. INTRODUCTION

One of the solution for the ongoing environmental problems such as depletion of non-renewable energy resources is to use electric vehicle (EV) for transportation [1]. Hence, Energy Storage Systems (ESSs) are gaining importance in real world applications [2]. Energy storage systems such as batteries and super capacitors are used in many emerging technologies.

Many emerging applications require energy to be transferred in both the directions. In the recent past, one of the important research area in the Power Electronics field is the design and implementation of Bi-Directional DC-DC converters. It is known that in Bi-Directional converters, power flows in both direction whereas in unidirectional power flows in one direction. Hence Bi-Directional DC-DC converters are used in many applications such as electric vehicles (EVs), Hybrid Electric Vehicle (HEVs), Uninterruptable power supplies (UPS), and renewable energy sources [3]. By integrating Bi-Directional DC-DC Converter in between the DC bus and Energy storage system the power wastage can be significantly reduced and also efficiency and reliability of overall

system can be improved. One of the applications of Bi-Directional DC-DC converter in Electric Vehicle power train is shown in Fig 1.

DC-DC Converters are classified into two categories: Non-Isolated and Isolated Topologies. The Non – Isolated Bi-Directional converter has advantages like less complex circuit and design, less component count and simple control [3]. However isolation is not present between input and output. Isolated Bi-Directional DC-DC converter have high voltage gain ratio conversion factors and therefore used in high power applications. Isolated topologies provide good stability and reliability. However the circuit is more complex with high frequency transformer. The components counts is more that increases the overall size and weight of the converter.

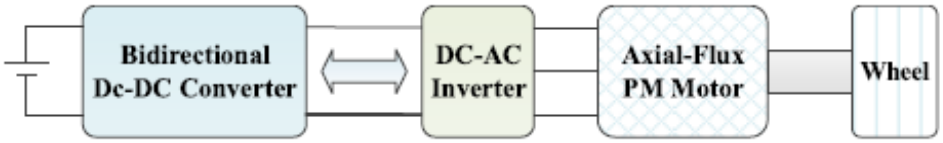

Fig.1 Use of Bi-Directional DC-DC Converter in EVs [3]

2. OPERATION AND DESIGN PROCEDURE

2.1. Bi-Directional Buck-Boost Converter

The Bi-Directional Buck-Boost topology which is Non – Isolated DC-DC converter is shown in Fig.2. Q1 and Q2 are two power stage MOSFETs and both will operate in complimentary fashion. In buck mode Q1 will be on and Q2 will be off and will operate as per duty cycle and in boost mode Q2 will be on and Q1 will be off. To avoid short circuit across the DC bus a small dead time will be provided between two MOSFETs [4]. This topology does not has transformer and hence used for low power application and also it has high efficiency.

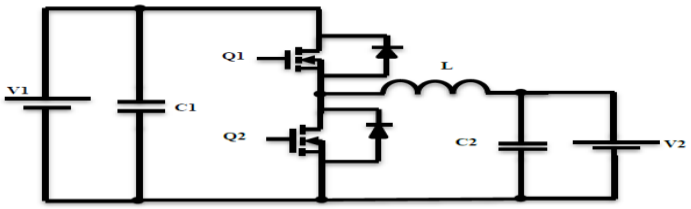

Fig.2 Bi-Directional Buck-Boost Converter [4]

2.2. Specifications and Design

Table 1: Specifications of Bi-Directional Buck-Boost converter

Parameter	Symbol	Value	Unit
Input Voltage	Vin	300	V
Output Current	Io	10	A
Switching Frequency	f	50 k	Hz
Output Voltage	Vo	24	V
Duty Cycle	D	50 %	-
Inductor	L	240 µ	H
Capacitor	C	416.67 µ	F

$$L = \frac{Vo*(1-D)}{\Delta I_l * f_s} = 240\ \mu H;\ \Delta I_l = 10\ \%\ of\ total\ output\ current \quad (1)$$

$$C = \frac{Io*D}{\Delta V_o * f_s} = 416.67\ \mu F;\ \Delta V_o = 1\ \%\ of\ total\ output\ voltage \quad (2)$$

2.3. Dual-Active Bridge DC-DC Converter

Fig.3 shows Dual Active Bridge converter which is an isolated Bi-Directional DC-DC converter. It consists of H–bridge inverter on the primary side. The DC input is fed to the inverter which gives the AC output of high frequency square pulses at the primary side of the transformer. The AC signal is then converted into DC using secondary side rectifier. The Secondary side MOSFETs are operated in Phase shift manner, since transformer provides a phase shift of 180 degrees [5], [6] and [7].

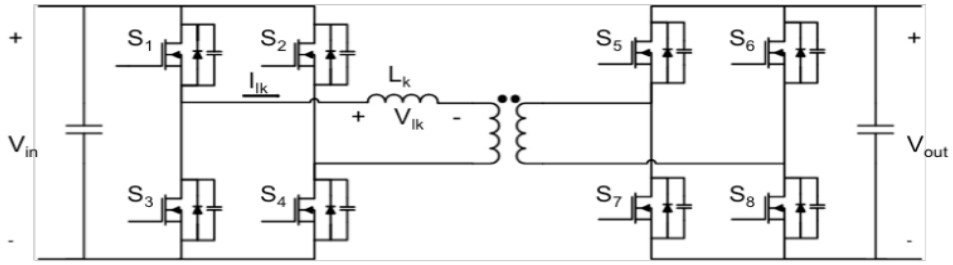

Fig.3 Isolated Dual Active Bridge DC-DC Converter [8]

2.4. Specifications and Design

Table 2: Specifications of Dual Active Bridge converter

Parameter	Symbol	Value	Unit
Input Voltage	Vin	300	V
Output Current	Io	10	A
Switching Frequency	f	50 k	Hz
Output Voltage	Vo	24	V
Duty Cycle	D	40 %	-
Inductor	L	24 µ	H
Capacitor	C	66.67 µ	F

$$L = \frac{Vl*D}{\Delta I_l * f_s} = 24\ \mu H;\ \Delta I_l = 20\ \%\ of\ total\ output\ current \quad (3)$$

$$C = \frac{Il*D}{\Delta V_o * f_s} = 66.67\ \mu F;\ \Delta V_o = 1\ \%\ of\ total\ output\ voltage \quad (4)$$

In this paper the simulation is carried out for both topologies of Bi-Directional DC-DC converter and the efficiency analysis is also carried out for same specifications.

3. SIMULATION RESULTS AND COMPARISON

3.1. Bi-Directional Buck-Boost Converter

To compare both non-isolated and isolated topologies, same specifications are considered and the simulation model is built in MATLAB/ Simulink. Li- Ion battery of 24V is used as storage device. The Initial SoC of the battery is considered to be 70% and the rated capacity of 10 Ah. The switching technique is described in the following sections

The Simulink model of non-isolated bi-directional buck-boost converter is shown in Fig.4

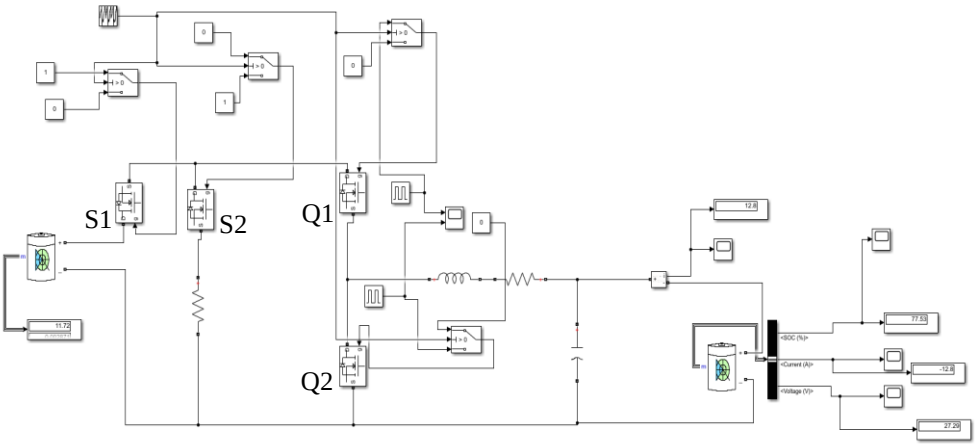

Fig.4 Bi-Directional Buck-Boost converter

By using two control stage MOSFETs S1 and S2 as shown in Fig.4. Both S1 and S2 switches are operated in such a manner that S1 will be enabled only during charging of the battery and S2 will be disabled, S2 will be enabled during discharging of the battery, and S1 will disabled. These S1 and S2 switches are enabled and disabled with high (1) and low (0) signal using two switches. In repeating sequence block corresponding output values are set, for respective time values. Discharging of the battery happens through the resistor which is connected across the input DC bus. Two power stage MOSFETs Q1 and Q2 are operated in complimentary manner. Initial SoC of the battery is set at 70%, and duty cycle set for the two power stage MOSFETs Q1 and Q2, the SoC of battery is increased from 70% to 75%. From Fig. 5 it can be seen that the battery is in charging mode up to 60 seconds and after that battery is in discharging mode up to 115 seconds. This is achieved by using the two control switches in the input section. During charging mode battery voltage was increased from 24 V to around 27 V and while battery is in discharge mode battery voltage is around 25 V. The transition can be seen in Fig. 6 at the point of discharging the battery. Similarly battery current during charging and discharging is shown in Fig.7

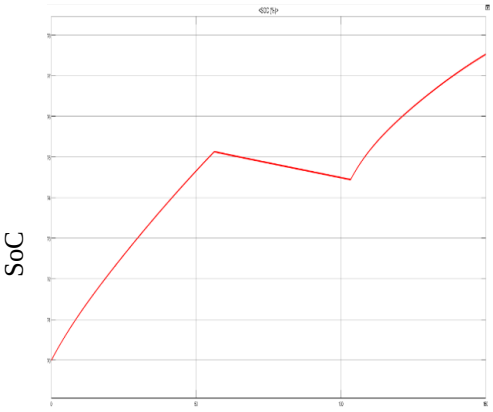

Fig.5 SoC of battery (charge-discharge-charge pattern)

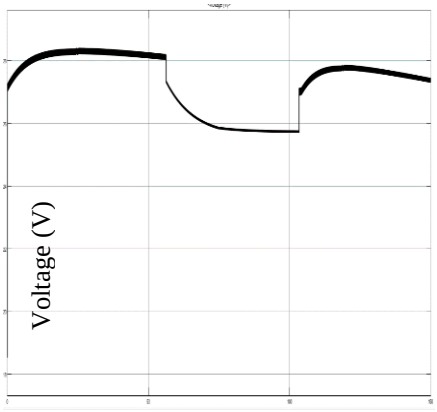

Fig. 6 Output Voltage

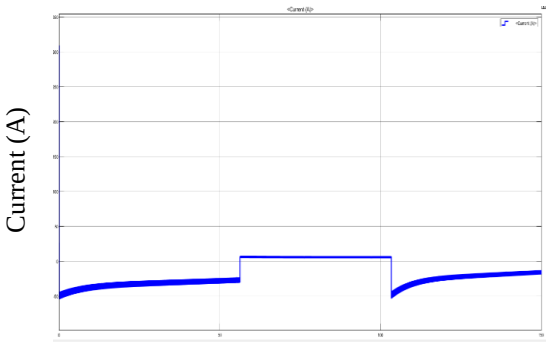

Fig.7 Output Current

3.2. Dual- Active Bridge Converter

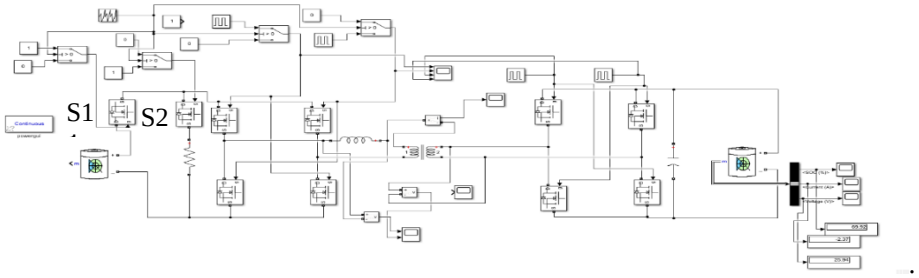

Fig.8 Dual Active Bridge

By using two control switches S1 and S2 as shown in Fig.8 in the input section. These two switches are controlled in such a way that when S1 is enabled battery starts charging and S2 is disabled, by providing the high (1) and low (0) signal to the two MOSFETs. Similarly when S2 is enabled battery discharges through the resistor and S1 is disabled. In this topology also initial SoC of the battery was set at 70 and by using two control switches S1 and S2, the charge-discharge-charge pattern is achieved, since current through the battery is positive as well as negative. We can say that power is flowing in both direction that is from source to load and vice versa. Respective SoC, Voltage and Current waveforms as shown in Fig 9, 10 and 11.

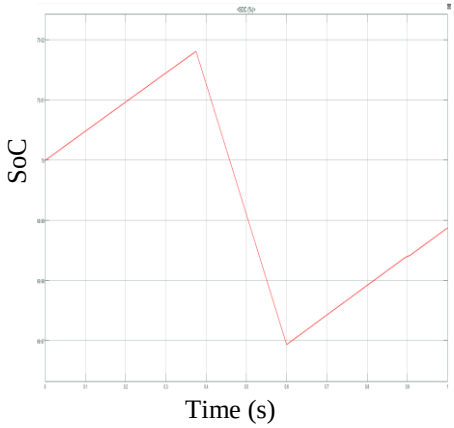

Fig.9 SoC of battery (charge-discharge-charge pattern

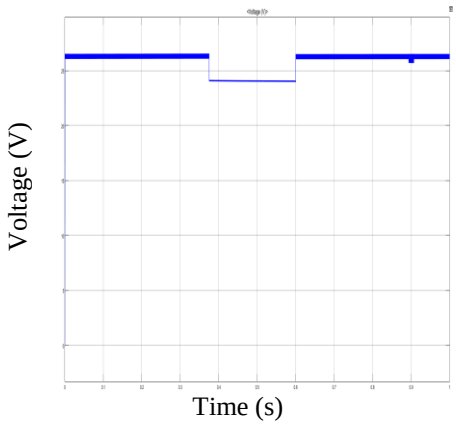

Fig.10 Output Voltage

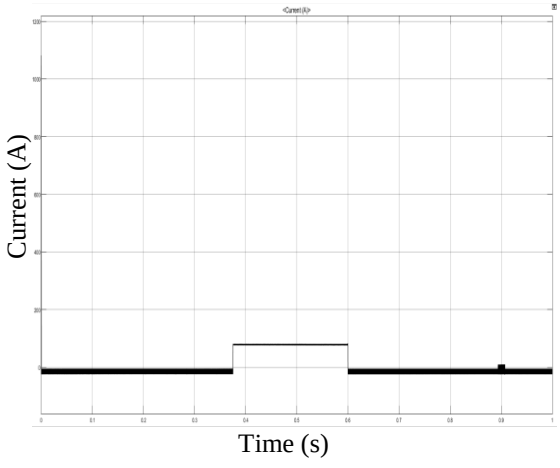

Fig.11 Output Current

4. EFFICIENCY CALCULATION COMPARISONS

Losses occurring in the converter are represented, from equation 3 to 10 [9].

4.1. Bi-Directional Buck - Boost Converter

1. $The\ inductor\ power\ loss\ P_L = \frac{rIo^2}{(1-D)^2}$ = 0.178 W (5)

r = equivalent series resistance of inductor; D= Duty Cycle; Io = Output Current

2. $Power\ Loss\ in\ MOSFETs\ during\ charging\ and\ discahrging\ mode$

$$P_{MOS} = \frac{D.r_{DS.}Io^2}{(1-D)^2} \quad (6)$$

$r_{DS.}$= Drain to source resistance of MOSFET, 45 mOhm [10]

$P_{charging}$ = 8.89 W

$P_{discharging}$ = 0.72 W

3. $The\ Capacitor\ Power\ loss\ P_{Cap} = \frac{D*r_C*Io^2}{1-D}$ = 0.033 W (7)

$P_{Total} = P_L + P_{MOS} + P_{Cap} + P_{Other\ losses}$

= 0.178+8.89+0.72+0.033+1

= 10.821 W

Other losses implies MOSFET switching losses, quiescent current losses etc.

Efficiency = $\frac{Po}{Po+P_{Total}} = \frac{24*10}{24*10+10.821} = 95.6\ \%$ (8)

4.2. Dual-Active Bridge Converter

1. $The\ inductor\ power\ loss\ P_L = \frac{rIo^2}{(1-D)^2}$ = 0.4 W (9)

r = equivalent series resistance value of inductor

2. $Power\ Loss\ in\ MOSFETs\ during\ charging\ and\ discahrging\ mode$

$$P_{MOS} = \frac{D.r_{DS.}Io^2}{(1-D)^2} \quad (10)$$

$P_{charging}$ = 5.76 W

$P_{discharging}$ = 16.64 W

3. *The Capacitor Power loss* $P_{Cap} = \frac{D*r_C*Io^2}{1-D}$ = 0.1 W (11)

$P_{Total} = P_L + P_{MOS} + P_{Cap} + P_{Other\ losses}$

= 0.4+5.76+16.64+0.1+4

= 26.9 W

Other losses implies MOSFET switching losses, quiescent current losses and Transformer magnetic losses etc.

Efficiency = $\frac{Po}{Po+P_{Total}} = \frac{24*10}{24*10+26.9} = 89.9\ \%$ (12)

Table 3: Qualitative and Quantitative Comparison table

Parameters	Bi-Directional Buck-Boost	Dual-Active Bridge
Input Voltage (V)	300	300
Output Voltage (V)	24	24
Inductor Value (µH)	240	24
Output Current (A)	10	10
Output Power (W)	240	240
Efficiency (η)	95.6	89.9
Components count	Less	More
High Gain Voltage Ratio Application	Not Recommended	Recommended
Size of overall converter	Less	More

5. CONCLUSION

This paper mainly focuses on the comparison of Isolated and Non – Isolated DC-DC converters with same specifications in terms of efficiency, components counts and size of the converter and charge-discharge of battery in one time period. From simulations it is found that bi-directional buck-boost converter has an efficiency of 95.6 % whereas dual active bridge dc-dc converter has an efficiency of 89.9 %, which is slightly less due to losses in the transformer and more components count. However, Dual-Active Bridge DC-DC converters can be used in applications with high voltage gain ratio.

6. REFERENCES

[1] “Idris Azizi and Hammoud Radjeai, “A Bidirectional DC-DC Converter fed DC Motor for Electric Vehicle Application,” Conference paper. December 2015 978-1-4673-6673-1/15 ©2015.

[2] “Nguyen Anh Dung, Hsin-Che Hsieh, Jing-Yuan Lin, Huang-Jen Chiu, Jih-Sheng Lai, “Design of Bi-directional DC-DC Converter for Energy Storage System in High Power Application,” IEEE 978-1-7281-3153-5/19 ©2019.

[3] “Saman A. Gorji, Hosein G. Sahebi, Mehran Ektesabi and Ahmad B. Rad, “Topologies and Control Schemes of Bidirectional DC-DC Power Converters an Overview,” Special Selection On Advanced Energy Storage Technologies And Their Applications Volume 7, 2019.

[4] “Deepak Ravi, Bnadi Mallikarjuna Reddy, Shimi S.L. 3, Paulson Samuel, “Bidirectional DC to DC Converters: An Overview of Various Topologies, Switching Schemes and Control Techniques,” Internal Journal of Engineering & Technology ©2018.

[5] "Teja Vineet Mhatre, Vishal Dake, "Design and operation of 20KW Bidirectional DC-DC Converter and Comparison of different topologies”. 2019 2nd International Conference on Intelligent Computing, Instrument and Control Technologies (ICICICT).”

[6] F. Krismer "Modelling and Optimization of Bidirectional Dual Active Bridge DC-DC Converter Topologies", A dissertation submitted to ETH ZURICH for the degree of Doctor of Sciences2010

[7] “Kenny George University of Arkansas, Fayetteville Design and Control of a Bidirectional Dual Active Bridge DC-DC Converter to Interface Solar, Battery Storage, and Grid-Tied age, and Grid-Tied Inverters,” University of Arkansas, F ersity of Arkansas, Fayetteville ScholarWorks@UARK.

[8] Biao Zhao; Qiang Song; Wenhua Liu; Yandong Sun, "Overview of Dual-Active-Bridge Isolated Bidirectional DC–DC Converter for High-Frequency-Link Power- Conversion System," in Power Electronics, IEEE Transactions on , vol.29, no.8, pp.4091-4106, Aug. 2014

[9] “Haroutuon A. Haitil, Ali Kadhim Abdul Abbas Khalid A. Abbas, “DC/DC Buck-Boost Converter Efficiency and Power Dissipation Calculation at Operating Points Not included in the Datasheet,” Journal of Multidisciplinary Engineering Science and Technology (JMEST) Vol. 6 Issue 6, June- 2019

[10] “Application Note 600V CoolMOS™ C7 Design Guide.

Explainable Machine Learning for Predicting Solar Power Output

Pranav R

Student, Department of EEE
B.M.S. College of Engineering
Bangalore, India
pranav.ee18@bmsce.ac.in
shashanktk.me19@bmsce.ac.in

Shashank T K

Student, Department of ME
B.M.S. College of Engineering
Bangalore, India

Gururaja H S

Assistant Professor, Department of ISE,
B.M.S. College of Engineering
Bangalore, India
gururajhs.ise@bmsce.ac.in

Abstract.

In an everlasting effort to move away from fossil fuels, solar photovoltaic power has emerged as one of the most promising environmentally friendly, renewable power sources in the ongoing endeavor to move away from fossil fuels. However, lack of understanding optimum solar panel positioning would result in less optimal power output from the panels. This research provides a Machine Learning method for estimating solar panel power production. Three state-of-the-art tree based algorithms namely, LightGBM, XGBoost and Random Forests are considered in this study to predict the solar power output using historical data. Machine Learning algorithms, although extremely powerful, suffer from the "black-box" problem which is a condition where a user cannot explain the predictions of ML algorithms. The issue has been addressed in this paper using SHAP Explainable AI. Model explainability is extremely critical in determining which variables or features played the most important roles in models prediction. In this paper, model explainability helps understand which features are most important in predicting Solar Power Output. This helps industries set up solar panels in such a way that maximum electrical power can be extracted from the panels.

Keywords. Solar Power, Machine Learning, Explainable AI, SHAP Xai.

1. INTRODUCTION

Artificial Intelligence is turning out to be increasingly significant in deeply shaping our day to day routines. Moreover, as AI-based arrangements [1,2,3] multiply in fields like loaning, law enforcement, medical services, and schooling, the individual and expert outcomes of AI are wide-running. Because AI models assume such an overwhelming part in different spaces, there is rising stress over possible predisposition in these models, as well as a necessity for model interpretability. Model logic is also critical for building trust and reception of AI frameworks in high-stakes areas requiring unwavering quality and security, such as medical services and robotized transportation, as well as basic modern

applications with significant monetary implications, such as predictive maintenance, regular asset investigation, and environmental change displaying.

Deep learning has contributed a substantial amount to artificial intelligence's recent progress. Deep learning algorithms, as proven in [4,5], outperformed traditional machine learning methods significantly. Deep Neural Networks (DNNs) on the other hand, are bad at describing their inference processes and final outcomes, and both developers and consumers consider them as a black box.

Solar energy, in its various structures, sunlight based heat, sun powered photovoltaic, sunlight based warm power, and solar oriented fuels gives humanity a perfect, environment well disposed, extremely plentiful, and endless energy asset. Sun oriented power is the transformation of daylight into power, either straightforwardly through Photovoltaic (PV) boards or by implication through Concentrated Solar Panels (CSP). Starting from the beginning, research has been led to create a modest, non-exhausting, and clean sun powered energy framework with long haul benefits. Therefore, the study in [6] inspects the advancement of sun oriented power age innovative work since its initiation. The existing and future problems associated in the creation of quality and reliable solar power technologies for future applications are also highlighted.

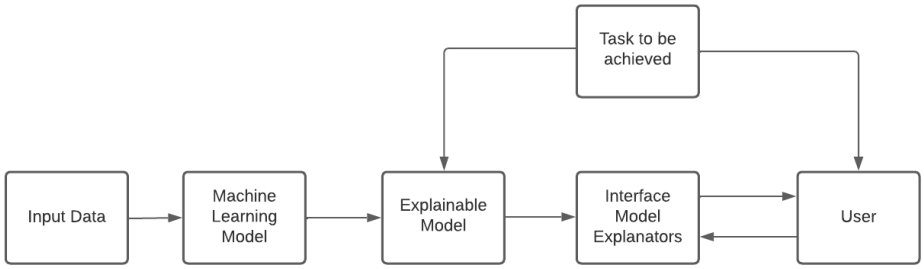

Figure 1. Explainable AI Architecture

Explainable AI is a collection of tools and frameworks that can aid in the understanding and interpretation of machine learning predictions. Figure 1. Represents the working of Explainable AI model for predicting the solar power output generation.

2. LITERATURE REVIEW

One study examines how to expect sunlight based photovoltaic (PV) energy utilizing Explainable AI (XAI) instruments like ELI5, SHAP and LIME, which can assist with the reception of XAI methods for shrewd lattice applications [8]. Understanding the internal functions of an AI-based forecast model can give knowledge into the field of use. Such information can assist with improving sun based PV forecasting models and distinguish significant qualities.

For short-term solar power prediction, [9] presents a least-square (LS) SVM-based model (SPP). The model accounts for variables such as wind speed, relative humidity, and sky cover, and provides verifiable information on air transmissivity in an original two-layered (2D) structure. The model's output is projected environmental transmissivity, which is then

converted to solar oriented electricity based on the scope of the site and the time of day. Utilizing data from the NSRDB, which stands for **National Solar Radiation Database**, virtual simulations are performed to endorse the proposed model. The outcomes propose that the suggested model not simply just beats a reference autoregressive (AR) model concerning assumption accuracy, but moreover defeats a RBFNN, which is short for Radial Basis Function Neural Network - based model.

One of the barriers to their widespread use in power networks is the random character of solar energy supplies. Using meteorological data is the most feasible technique to forecast this renewable energy source. However, such information is frequently presented in a subjective configuration that can't be utilized with regular quantitative methodologies however can be demonstrated with fuzzy logic. Study [10] proposes type-1 and stretch sort 2 Takagi-Sugeno-Kang (TSK) fluffy frameworks for the demonstrating and expectation of sun based power plants. Type-2 TSK models with type2 predecessors and fresh outcomes supply the optimum presentation in light of the sun-powered plant information.

The research [11] proposes a method for forecasting generation of solar power based on the least absolute shrinkage and selection operator (LASSO). The model compares the proposed system to two example schemes using three real-world datasets. Using three real-world datasets, the model compares the proposed system to two sample plans (schemes). The work has additionally found that the algorithm based on LASSO accomplishes altogether higher accuracy than current techniques, while utilizing fundamentally less preparation information and being vigorous to inconsistency data of interest in the preparation information. Its variable determination capacity additionally gives an advantageous tradeoff among intricacy and accuracy, all of which join to make the proposed LASSO-based approach an exceptionally serious answer for forecasting solar power generation.

The study [12] tackles the issue of projecting renewable energy in the short term. Renewable energy sources' stochastic character affects power system arranging methods, influencing the reliability and security of force supply for extreme clients. Utilizing retroactive metering information and open source climate data offered by meteorological types of assistance, the creators propose an ML approach for effective day-ahead anticipating. The challenge of feature identification and acceptable error measures is addressed in this study. The user interface was built and tested on a genuine solar power plant in the Russian Federation's southern region in order to ensure effective testing.

Tree based State of the art models like LightGBM, XGBoost and Random Forests are being used in research work for many classification and regression problems nowadays. Study [13] proposed a LightGBM model to predict customer loyalty in the finance industry. It was found that LightGBM model performed better than XGBoost model in terms of RMSE score. A different study used LightGBM for Sales Forecasting. It was found that LightGBM outperformed classical methods like SVM and Logistic regression [14]. Another study used Random Forests and XGBoost algorithms to predict a student’s behavior [15]. Model explainability is an important aspect to tackle the black-box problem of ML models. A particular study used SHAP method to explain reinforcement learning for power system frequency control [16]. In [17], SHAP and LIME explainable models were used to explain ML algorithms for identifying failure in a network of microwaves. Another study [18] implemented Dalex Xai for interpreting algorithms used for predicting credit defaulters. This paper focuses on implementing the SHAP model explainability.

3. METHODOLOGY

3.1. Random Forests

Random Forests is a decision tree-based ensemble machine learning model. It contains an implicit decision system, thus it can handle a variety of data restrictions without removing a few for reduced dimensionality [19]. The marginal function for a given classifier's group $d_1(a)$, $d_2(a)$ ….. $d_k(a)$ and the training set drawn aimlessly from the dispersion of the arbitrary vector B, A is characterized as shown :

$$mg(A,B) = av_k I(h_k(A) = B) - max\ jA\ av_k I(h_k(A) = j) \tag{3.1.1}$$

where *I(·)* is the indicator function. The generalization error is given by:

$$PE^* = P_{A,B}(mg(A,B) < 0) \tag{3.1.2}$$

3.2. XGBoost

XGBoost is a supervised learning algorithm based on ensemble trees. Numerous classification projects in different fields are being applied using this model [20]. Many Kaggle competitions that are won nowadays, use XGBoost. Crediting to its astounding performance, XGBoost opens door to a lot of research opportunities.
It targets enhancing a cost objective function made out of a loss function (*l*) and a regularization term (δ):

$$\mathrm{F}(\theta) = \sum_{i=1}^{n} l(y_i, \hat{y}_i) + \sum_{k=1}^{K} \delta(f_k) \tag{3.2.1}$$

Where fk is a specific tree from the ensemble group trees, n is the number of cases in the preparation set, K is the number of trees to be provided, and is the predictive value. The term "regularization" is defined as follows:

$$\delta(f_t) = \gamma T + \frac{1}{2}\left[\alpha \sum_{j=1}^{T} | r_j | + \lambda \sum_{j=1}^{T} r_j^2\right] \tag{3.2.2}$$

Where γ is loss reduction factor, λ is regularization term and r is weight corresponding to a tree leaf.

3.3. LightGBM

LGBM additionally uses continuous feature histogram binning, which provides even greater speed than classic gradient boosting. Binding numeric values reduces the amount of split points in decision trees and eliminates the necessity for sorting methods, which are always computationally intensive. Light GBM builds trees upward, but other computations

build trees equally, implying that Light GBM builds trees not level by level but rather leaf by leaf. It will grow the leaf that has the most delta-loss. While growing a similar leaf, leaf-wise calculations can restrict more loss than level-wise calculations [21].

3.4. SHapley Additive exPlanations (SHAP)

SHAP is a visualization tool that can be utilized to interpret the result of an AI/ML model to make it more reasonable. It can be used in making sense of any model's forecast by processing each variable's commitment to the prediction can be utilized. It combines a number of tools, including lime, SHAPley sample values, DeepLift, QII, and others. SHAPley values are one of the essential components of the SHAP tool since it allows SHAP to correlate optimal credit allocation with local explanations. The Figure represents the Pipeline of post hoc explainable tool SHAP [7].

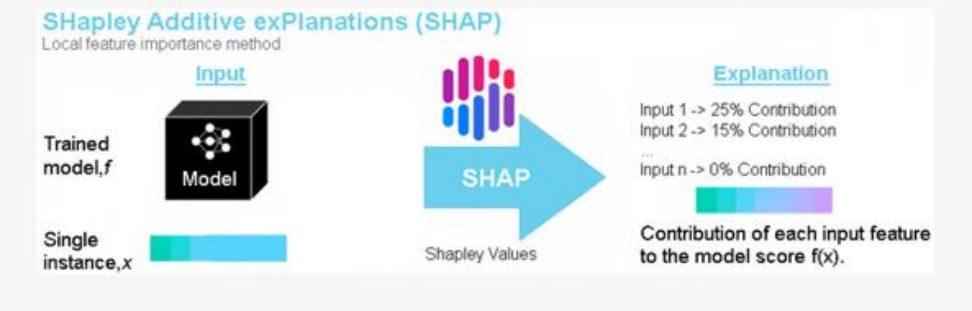

Figure 3.4. Visual of SHAP Explainable model

4. RESULTS AND DISCUSSION

4.1. Data analysis and pre-processing

The dataset used for this study was taken from Kaggle. It has 21045 training examples consisting of weather data and power output acquired for 14 months. The dataset was analyzed and checked for missing values. The categorical variables were handled using Label Encoder. The dataset was split in the ratio 8:2(80% training and 20% testing) and was standardized using sklearn's StandardScaler.

4.2. Model evaluation

Models	Metrics		
	RMSE	MAE	R2 Score
LightGBM	4.029	2.632	0.681
XGBoost	4.134	2.639	0.664
Random Forests	4.150	2.833	0.661

For evaluating the models, the paper considers the following metrics:

Mean Absolute Error:

The Mean Absolute Error (MAE) is a regression model evaluation statistic. The difference between the true value and the anticipated value for each instance is the prediction error.

$$mae = \left(\sum_{i=1}^{n} abs\left(yi - \lambda(\text{xi})\right) \right) \div \text{n} \tag{4.2.1}$$

R2 score:

R-squared (R2) is a factual measure that evaluates how much variety made sense of by an independent variable or factors in a relapse model for a dependent variable

$$R^2 = 1 - \frac{\sum(y - \hat{y}_i)^2}{\sum(y - \bar{y}_i)^2} \tag{4.2.2}$$

Root Mean Squared Error:

Having a solitary number to quantify a model's exhibition is unquestionably valuable in AI, whether it's during preparing, cross-validation, or checking after organization. One of the most frequently involved estimations for this is root mean square mistake. It's a straightforward scoring decide that is additionally viable with a few of the most pervasive measurable presumptions.

$$RMSE = \sqrt{\frac{\sum_{i=1}^{N}(y - \hat{y}_i)^2}{N}} \tag{4.2.3}$$

By considering all the parametric evaluation results, the results of each model is depicted in Fig 4.2. It can be seen that the LightGBM performed best on this dataset in terms of all the considered metrics followed by XGboost with Random Forest not too far behind.

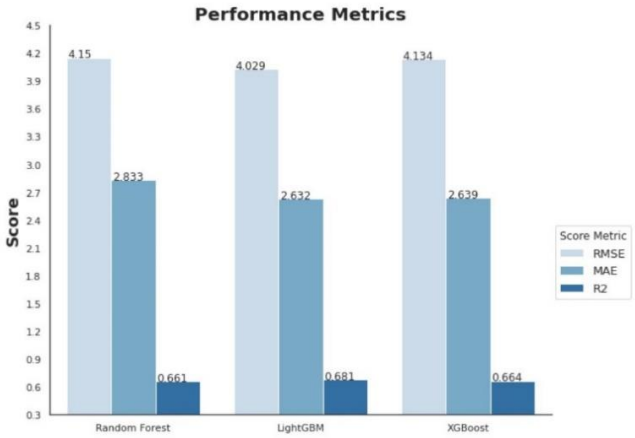

Figure 4.2. Bar Plot of performance metrics of the models

4.3. Model Explainability

4.3.1. Light Gradient Boosted Machine (LGBM):

The bee swarm plot depicts the overall performance of the model and discusses the features that led to model prediction. As can be seen, according to LGBM, the ambient temperature was the most crucial feature. Lower ambient temperatures (blue color) do not help the panels produce a good quantity of electricity production. For a single instance, the bar plot provides a good interpretation of features that contribute to model prediction. It should come as no surprise that the most essential feature was the ambient temperature.
The bee swarm plot depicts the overall performance of the model and discusses the features that led to model prediction. As can be seen, according to LGBM, the ambient temperature was the most crucial feature. Lower ambient temperatures (blue color) do not help the panels produce a good quantity of electricity production. For a single instance, the bar plot provides a good interpretation of features that contribute to model prediction. It should come as no surprise that the most essential feature was the ambient temperature.

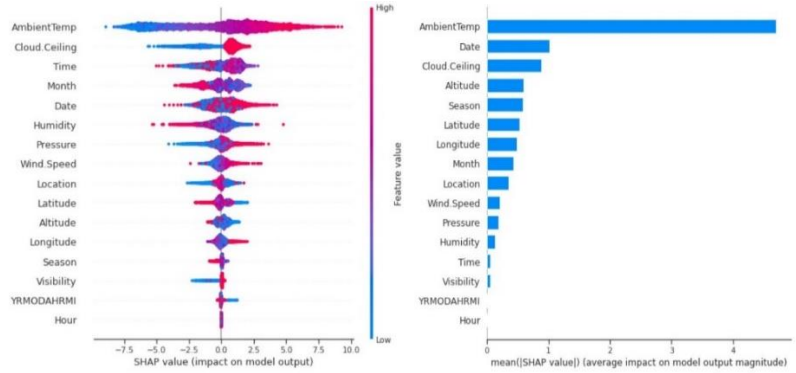

(a) (b)

Figure 4.3.1. (a) Bee-Swarm plot for global interpretability. (b) Bar plot for local interpretability for LGBM model.

4.3.2. Extreme Gradient Boosting (XGBoost):

Tree boosting is a popular and successful machine learning technique. It additionally remembers data for store access designs, information compression, and sharing to assist with building a versatile tree boosting framework. XGBoost grows past billions of illustrations utilizing impressively less assets than earlier frameworks by coordinating these thoughts.

We can note that the XGBoost and LightGBM were dependent on similar features for model prediction. However, it is important to note that XGBoost gave more importance to Latitude than Wind speed and Location in contrast to the LGBM model.

It is interesting to note that when a single instance is considered, the same features, in the same order contributed for both XGBoost and LGBM models. This comes as no surprise as XGBoost and LGBM are always in fierce competition with each other and a single instance is just not enough to decide which features take precedence in model prediction.

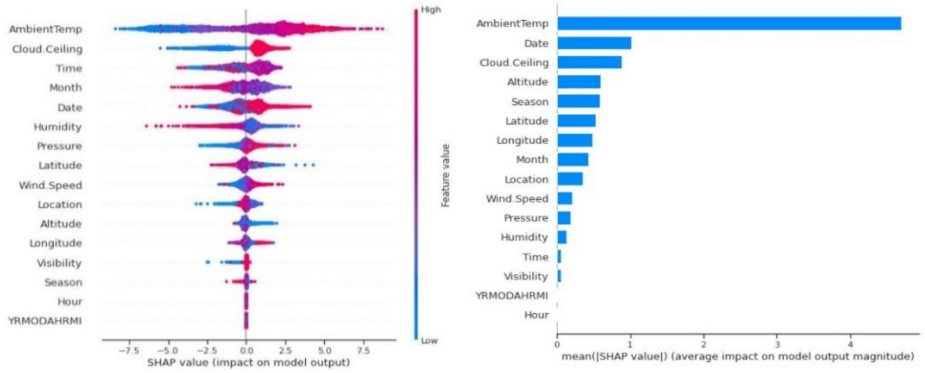

(a) (b)

Figure 4.3.2. (a) Bee Swarm plot. (b) Bar plot for XGBoost Model

4.3.3. Random Forests (RF)

It is no surprise that ambient temperature is the most important factor in random forests as well when the entire range of training examples is considered. Month and date, rather than time, take primacy. According to Random Forest, the hours of the day and the season have risen up the table and are now deemed fairly essential in comparison to altitude and visibility.

However, when a single instance is considered, date ends up as a significant feature after Ambient temperature for model prediction. Season and WindSpeed are also considered important which was not seen in LGBM or XGBoost. Another point to note is that, Humidity, which was a fairly important feature for model prediction in LGBM and XGBoost, has plummeted to the bottom. This can be attributed to Random Forests missing the key features of the data by a decent margin as it is the worst performing model of the three considered models.

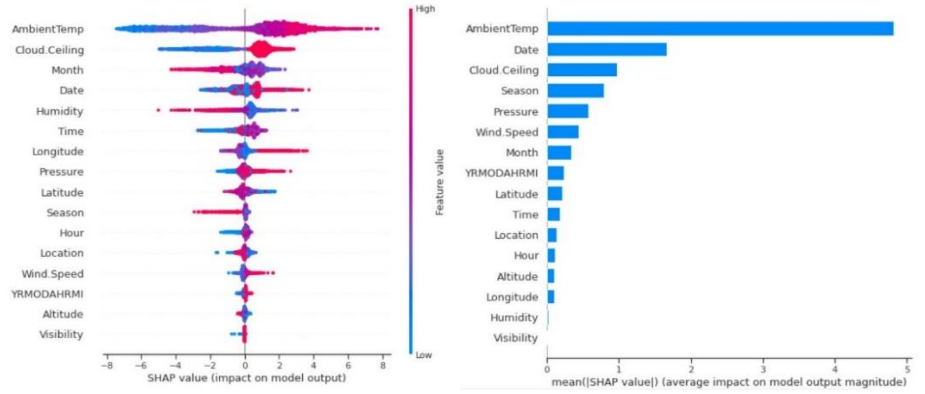

(a) (b)

Figure 4.3.3. (a) Bee-Swarm plot for global interpretability. (b) Bar plot for local interpretability for LGBM model.

5. CONCLUSION AND FUTURE SCOPE

Based on input characteristics such as solar PV panel's temperature, ambient temperature, solar flux, relative humidity and time of the day, tree based ML methods such as Random forest, XGBoost, and LGBM, which support non-linearity, were explored to predict PV power. Regardless of the high performance of the suggested ML techniques, other factors such as the size of the solar PV panel, dust, and wind can have a significant impact on solar PV output.

With the help of SHAP Explainable AI, the features that most impacted for model prediction was interpreted, thus tackling the black-box issue of ML algorithms. Going forward, this research can be implemented with hybrid and stacked ensemble models to achieve better results. A comparative analysis of different XAI models can be done to visualize the behavioural aspects of different models. Explainable AI is a hot topic now and provides ubiquitous opportunities to conduct research.

6. REFERENCES

[1] Gade, K., Geyik, SC, Kenthapadi, K., Mithal, V., and Taly, A. (July 2019). Descriptive AI in the industry. Minutes of ACM SIGKDD International Conference on Understanding Discovery and Real Mining

[2] Samek - W. - Montavon - G. - Vedaldi - A. - Hansen - L. K, & Müller, K.R. (Edit). (2019). Descriptive AI: Explanation of in-depth research, explanation, and visualization (Volume 11700). Springer Nature.

[3] Xu, F., Uszkoreit, H., Du, Y., Fan, W., Zhao, D., and Zhu, J. (October 2019).

[4] Holzinger, A. (2018, August). From studying gadget to descriptive AI. In 2018 an international series on virtual intelligence of buildings and equipment (DISA) (pages 55-66). IEEE.

[5] Tjoa, E., & Guan, C. (2020). Survey on descriptive ingenuity (xai): Focus on xai science. Implementation of IEEE on neural networks and learning structures, 32 (11), 4793-4813.

[6] Singh, G.K. (2013). Photovoltaic power generation technology using PV (photovoltaic power generation) technology: a review. Power, 53, 113.

[7] Knapič S, Malhi A, Saluja R, Främling K. Descriptive AI for web decision-making in the field of medicine. Machine learning and extracting information. 2021; 3 (3): 740770. https://doi.org/10.3390/make3030037

[8] Kuzlu, M., Cali, U., Sharma, V., & Güler, Ö (2020). Use descriptive artificial intelligence tools to get PV technology prediction details. Access IEEE, 8, 187814187823.

[9] Zeng, J., and Qiao, W. (2013). Short-term forecast of sunset using assist vector gadgets. Renewable Energy, 52, 118127.

[10] Jafarzadeh, S., Fadali, M.S., and Evrenosoglu, C.Y. (2012). Solar intensity forecast using C Type2TSK programming language model

IEEE Transactions on Sustainable Energy, 4 (2), 333339.

[11] Tang N, Mao S, Wang Y, and Nelms R M (2018). Predicting solar intensity technology with a LASSO-based holistic approach. IEEE Journal of Online Objects

[12] Khalyasmaa, A.、 Eroshenko S. A.、 Chakravarthy T. P.、 Gas、 V

G., Bollu S. K. Y., Caire, R., ... & Karrolla、 S. (2019 年 10 Predictability of Renewable Energy Production Based on the Random Deforestation Model. 2019 International MultiConference in Engineering, Computer and data Sciences (SIBIRCON) (p.07800785) .IEEE.

[13] M.R. Machado, S. Karray unddassi. T. de Sousa, LightGBM: A Good Way to Develop a Consumer Decision Predictability in the Financial Industry, 14th International Conference on Applied Science and Education (ICCSE), 2019, S ...

[14] T. Deng 、 Y 8-Zhao 、 S.Wang 、 H。 Yu, "Sales Forecast Supports LightGBM", IEEE 2021 International Conference on Consumer Electronics and Computer Engineering (ICCE), 2021, S. 383386, doi: 101109 / ICCECE51280.2021.934244.

[15] H. T. T. Nguyen, L. H. Chen, V.S.Saravanarajan、 H.Q Pham, Student Behavior Predicting Using XG Boost and Random Forest Classification Algorithms, New Trends in 2021 Industry 4.0 (ETI 4.0), 2021, S. 15,

[16] K. Zhang, P. Xu und J. Zhang, "Descriptive AI in Deep-Based Learning Models: SHAP Techniques Used for Institutional Emergency Management", 2020 IEEE 4th Conference on Energy Internet and Energy System Integration (EI2), 2020, S. 711716.

[17] O. Ayoub, F Musumeci, F. Ezzeddine, C. Passera, and M. Tornatore, "Using Explained Computer Diagnostics Computer in Microwave Networks," 2022, 2022, 25 Cloud Conference, Internet, and Network Innovation. (ICIN), 2022, p. .4855, doi: 10.1109 / ICIN53892.2022.9758095

[18] Tanmay Srinath, H.S. Gururaja, Descriptive Machine in Automated Credit Card Identification, Land Reform Processes, 2022, ISSN 2666285X

[19] Brayman, Leo "Zufällige Wälder" Machine Learning 45.1 (2001): 532.

[20] I. L. Cherif no-A. Kortebi, "Using the eXtreme Gradient Boosting (XGBoost) Machine Learning Algorithm for Home Network Traffic Classification", 2019 Wireless Days (WD)), 2019, S. 16.

[21] Machado, Marcos Roberto, Salma Karray, and Ivaldo Tributino de Sousa. "LightGBM: An effective way to grow a decision tree to predict customer loyalty in the financial industry." 14th International Conference on Computer Science and Education (ICCSE) 2019. IEEE, 2019.

A New Approach For Hybrid Electric Vehicles In The Implementation of Switched Capacitor Voltage Boost Converter

Sujitha S[1], Anitha A[2], Sushma M[3], Gagana C[4], Sushmitha T S[5]

[1]Associate Professor,[2] Assistant Professor, Department of Electrical & Electronics Engineering, New Horizon College of Engineering, Bangalore.

[3,4,5] Student, Department of Electrical & Electronics Engineering, New Horizon College of Engineering, Bangalore.

Abstract.

Electric car demand is now growing significantly due to the decline of fossil fuels and environmental sustainability. One of the most serious challenges with electric vehicles is the lack of charging infrastructure. In an ideal world, EV adoption would be predicated on how quickly EVs outperform internal combustion engines in terms of availability and cost. In the final phase, the drive train is among the most popular essential units for converting power. The updated powertrain is smaller, has a faster dynamic speed/torque, and uses energy from a battery more efficiently. A two-position voltage source is found in the vast majority of today's electric automobiles. Inverters with or without boost stages are employed because of their dependability. As a result, the voltage across the dc-link is a device that allows you to connect two devices together must be greater than the voltage across the dc or ac input. The escalating charge Equalization speed is an issue when battery cells are connected in series. It's similar to when you're trying to isolate a single is analogous to when a cell in a series connection dies, lowering the voltage of the entire series connection. To avoid a short circuit with other non-faulty series rows of cells, the complete series row of batteries must be removed from the dc-link in this situation.

1. INTRODUCTION

As energy efficiency becomes increasingly significant, high efficiency and power viscosity are becoming more relevant while constructing power converters. The operations of smart cities are moving from generalities to development. One of the smart metropolis operations that are now gaining popularity is smart transportation. Electric vehicles (EVs) are one of the most important components of smart transportation systems. Due to their implicit contribution to declining dependency on fossil energies and hothouse gas emigrations, electric vehicles are gaining in popularity. Nonetheless, the massive expansion of EV charging stations poses significant obstacles to the industry.

Furthermore, nonsupervisory pressures to minimize civic pollution, CO2 emissions, and major city noise have made plug-in electric automobiles a very appealing alternative to internal combustion.

The two main types of electric car battery chargers are on-board and off-board chargers (EVBC). In charging stations, off-the-shelf EVBCs are used, resulting in higher power consumption. The battery is one of the most important factors, as it has a direct impact on EV performance. Advances in charging uniformity, charge, and discharge techniques have led to the use of many coffers in the development of a revolutionary lithium-ion battery that exceeds current lithium-ion batteries.

Battery chargers are supposed to be effective and dependable enough to supply high power viscosity despite their modest size and weight. In electric car battery chargers for power factor adjustment, a boost converter step is used

Interleaving is also advised for various charger topologies to reduce current ripple and inductor size. Depending on the power input capability between the vehicle and the electric power grid, electric vehicle (EV) chargers are classed as unidirectional or bidirectional. Unidirectional EV chargers offer decreased system complexity, lighter circuit elements, and a short footprint, but they cannot provide additional or reactive services. Complex smart grid operations will require electrical support in the future to maintain the power system, load balancing is important. Bi-directional electric car chargers allow power to flow in both directions between the power grid and the vehicle.

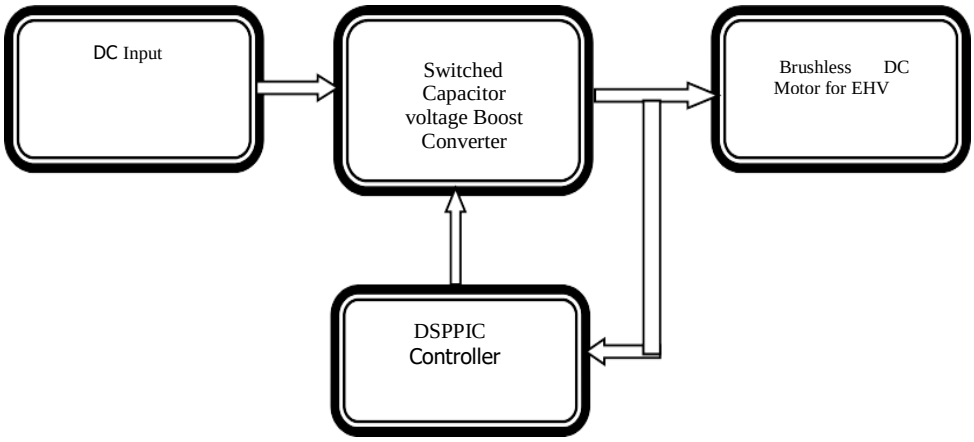

Fig.1 Block Diagram

2. METHODOLOGY

Switch-mode electronics are used in DC to DC converters to change one DC voltage state to another. These circuits convert by applying a DC voltage for a length of time across an inductor or converter, then switching off the voltage and allowing the stored energy to be transferred to the voltage output in a planned manner. This conversion procedure is more energy-efficient than

direct voltage conversion, which must disperse unwanted energy. This efficiency aids in extending a product's handling time in a battery-operated device.

Isolated DC-DC converters convert a DC power source to a DC power source between the input and output, making it possible for a differential in the input-output ground capability of hundreds or thousands of volts.

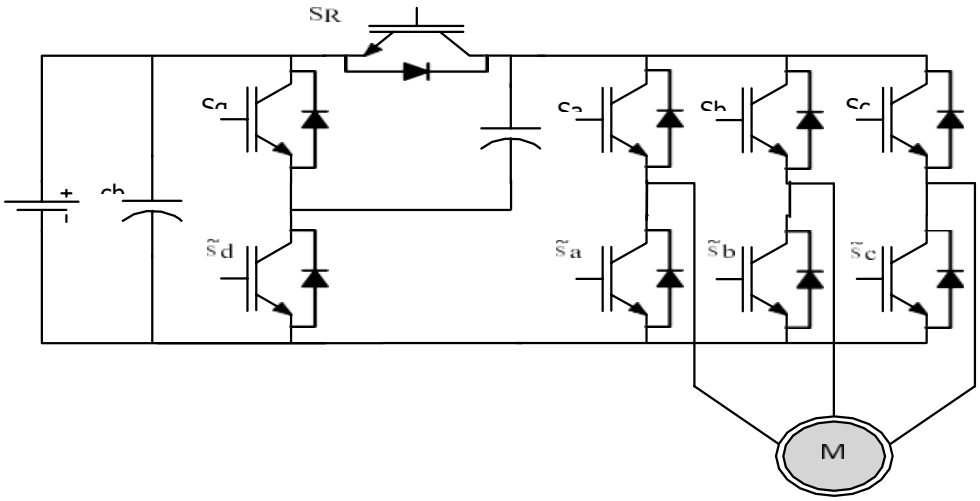

Fig.2.Circuit diagram for switch mode DC to DC converter

Because all conversion losses are exhibited by voltage drop associated with non-zero load current via the output impedance, the converter achieves a perfect voltage conversion from dc to ac rate at rest conditions. The resistive output impedance accounts for Losses due to capacitor charging and discharging, as well as losses due to resistive conduction. The model can include short-circuiting current and parasitic capacitors to the base in addition to gate-drive losses. The provision of a comprehensive framework for analysis and planning is our primary objective.

Two asymptotic output impedance limitations are the slow and quick switching limits. The impedance of the slow switching limit is computed using absolute conductive interconnects and impulsive charge transfers between the input and output sources, as well as between the condenser and the input and output sources. Once the fast-switching limit is achieved, the capacitors effectively operate as fixed voltage sources due to the resistances associated with switches, and capacitors. Although the impedance is related to the switching frequency, Financial Services has a piecewise constant current inflow pattern that is frequency independent. In Ideal capacitors, resistive switches, and resistive switches are used exclusively in two-phase converters.

An inverter is a type of power electronic equipment that converts energy from one form to another at the required frequency and voltage, such as from DC to AC. The source of supply as

well as the accompanying topology in the power circuit can be used to classify this. As a result, they are either categorized as voltage source inverters or CSI inverter's current source inverters.

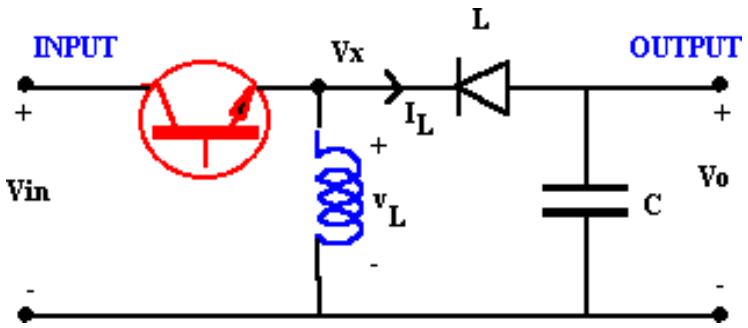

Fig.3.Buck-boostconverter

To convert DC EMF to three-phase AC electricity, a three-phase repealer is used. Applications required a lot of power and changing frequency as the transmission of HVDC energy is typically used but in a single-phase network, just one current is out of phase with each other repealed, and power is transmitted using one current.

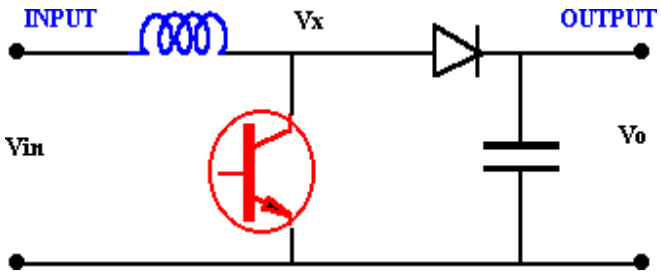

Fig .4. Buck Boost

In the inductor n the ON state, current flows via the diode, yielding Vx = Vo, while in the OFF state, current flows through the inductor. The inductor current is considered to be flowing at all times for the sake of this analysis (non stop conduction). For the average current to remain constant, the voltage across the inductor and the normal must be zero stable.

$(V_{in})\ t_{on}+ (\ _n - V_0)\ t_{off} = 0$

It is possible to rearrange this as $\frac{V_o}{V_{in}} = \frac{T}{T_{off}} = \frac{1}{1-D}$

Also the power balance ensures Io(1 D)I in a circuit with no losses

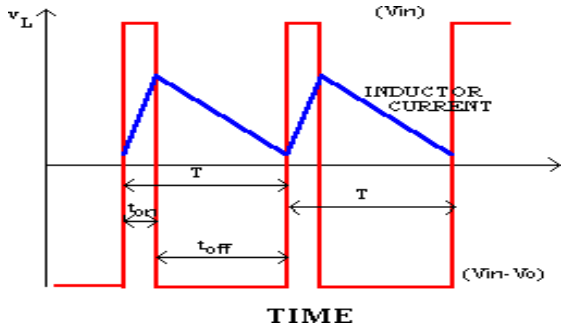

Fig.5.wave form

Because the duty rate "D" is between 0 and 1, the output voltage must be constant higher in magnitude than the input voltage. A sensory reversal in the output voltage is indicated by the negative sign.

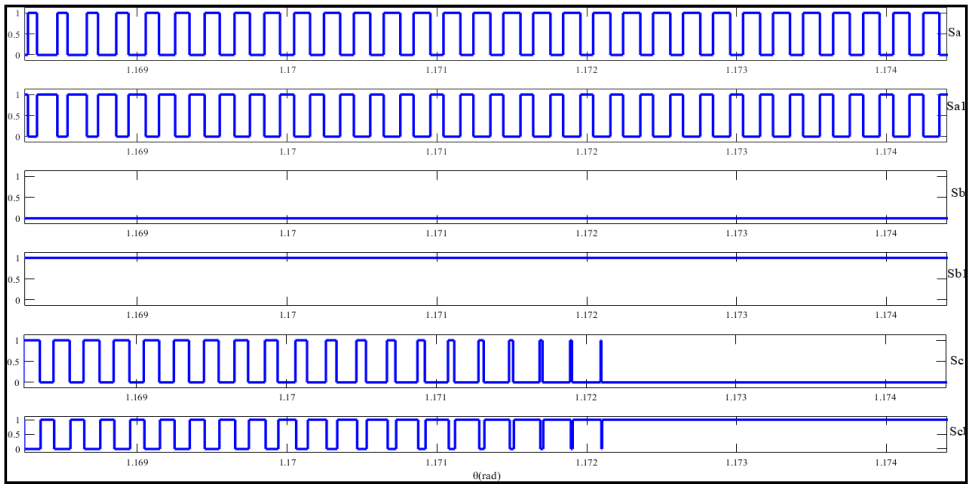

Fig .6.GatePulses

3. SIMULATION RESULT

The PMBLDCM drive is made up of mathematical equations that simulate different features of the PMBLDCM drive with the PFC converter. These component models are used to provide a full model of the proposed PFC drive.

This is a method of producing DC-link voltage as a reference that is original a PMBLDCM's specified reference speed.

The voltage regulator is a proportional and integral (PI) regulator that monitors the error voltage between the reference voltage and the detected voltage at the DC link and provides a control signal based on the PI regulator's proportional and integral earnings.

To create the PFC converter's switching signal MOSFET, the PWM regulator amplifies the current mistake by comparing it to the tooth carrier waveform, which has a set.

It depicts the indicated motor winding resistance/phase and stands for discrimination driver (d/ dt), currents, and flux linkage in comparable stages, neutral phase reverse electromotive force of the permanent magnet brushless dc motor. Ls is another indicator (self-inductance).Mutual inductance is a term used to describe the relationship between two is represented by the letter M. As measured by motor angular speed, torque is defined as produced electromagnetic torque. Tl is the load torque, and J is the number of poles B as a metric of disunion and moment of inertia.

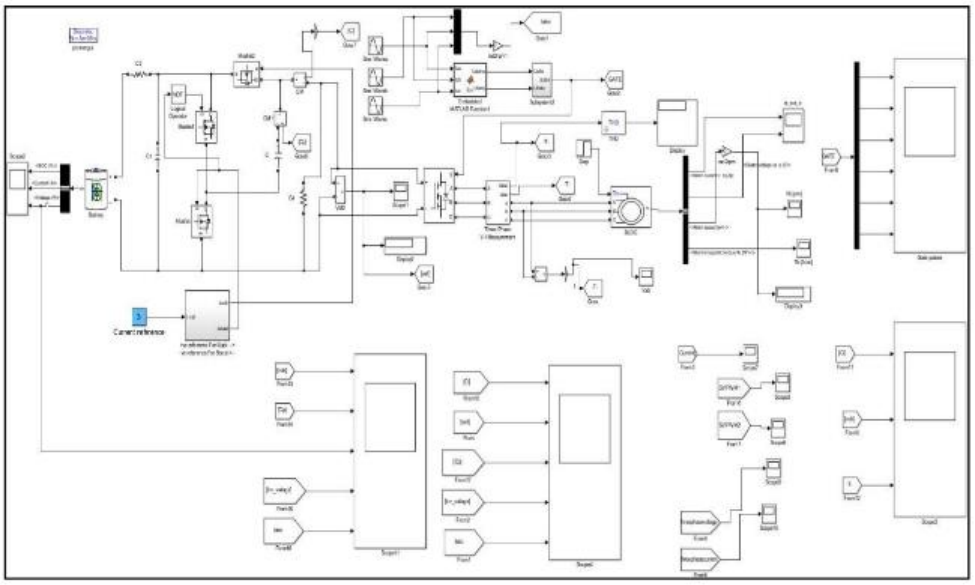

Fig.7.SimulationCircuit

The figure shows the simulation results for one fundamental cycle. The voltage drop v max is greatest in the capacitor voltage v cap. This fact lends credence to the logical interpretation of the highest voltage decrease in the sector.

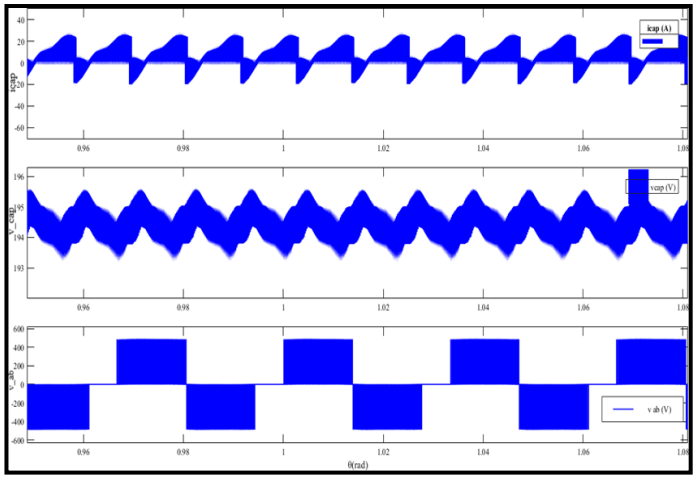

Fig.8.Simulation results

The current charging limit behaviour simulation data from one basic cycle are used to demonstrate the basic cycle. Across the capacitance, the drop in voltage V ca is the instantaneous voltage drop across the capacitance.

The reference signals are depicted in Figure as A varies Mi is the highest, ranging from 0 to 0.75.The figure shows a simplified control diagram. The waveform of reference can be constructed in a look-up table for sine with minimal computing effort.

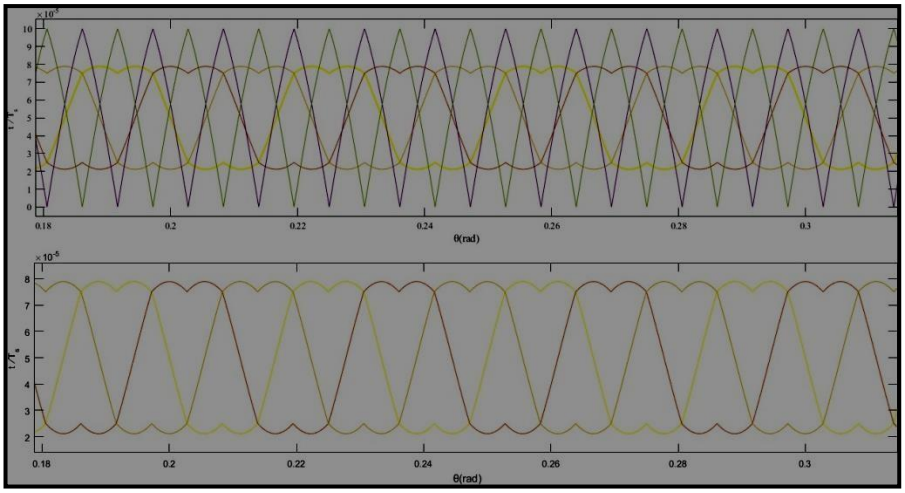

Fig .9. Waveforms of Reference

The inverter switches are subjected to voltage stress equal to that experienced by inverters in self-restraining mode. The voltage stress across the switches in an original SC converter system is just 100V, whereas the dc-link voltage is 200 V. When the inverter is running in the ravenous region, the emf stress is limited to 400 V. The switches' emf stress was cut in half. What it was in the operational range of the SC converter. PWM operation with a low modulation indicator, on the other hand, results in the most extensive harmonious deformation (THD). By working in a self-restraining mode, the converter maintains its advanced state in the direct area when compared to an original fixed dc-link inverter system. THD can be reduced by as much as 60%.According to the testing results, the SC converter's efficiency is less than three over its full operating range. Laminated copper strips could be used instead of wire to further reduce loop inductance.

4. CONCLUSION

Electric vehicles are gaining popularity as a result of their important role in decreasing CO2 emissions, reducing noise pollution, avoiding excessive energy prices, and providing consumers with more efficient and environmentally friendly Electric vehicles. Different types of converters used in electric vehicles are discussed in this study. For charging batteries from DC grids, many DC-DC converters are employed. Different types of converters are utilized for battery charging depending on the demand for electric vehicles.

This design introduces a novel power motor with switching capacitors for converting dc to ac and ac to dc. The SC motor uses a capacitor circuit with a switched capacitor that is connected to the power supply and the primary motor circuit, allowing it to perform tasks that the standard VSI cannot .One of these notable aspects is the doubling of the direct modulation region's area.

To enhance voltage, the SC motor avoids the need for a large and expensive inductor. Rather, it generates voltage rise purely through capacitors, allowing for larger power viscosity .Analytically, the minimum charging current and the capacitor's maximum voltage drop are determined. The logical conclusions give a detailed description understanding of the style fundamentals that influence the current of charging gestures, enabling faster operation.

By raising or bucking voltage, the SC motor can increase power density while lowering element count and saving money. The control system for a low-cost GC micro-inverter with MPPT employed in solar operations is proposed in this study. To test the suggested system and reduce simulation times, a macro-model is proposed. Experimental results have confirmed the AM and circuit utilized for inverter simulations.

5. REFERENCES

[1] State of the Art on Permanent Magnet Brushless DC Motor Drives Bhim Singh* and Sanjeev Singh† †* Electrical Engineering Department, Indian Institute of Technology, Delhi, New Delhi, India

[2] Sujitha S. and Venkatesh, C. " Design and Comparison of PV Switched Reluctance Motor drives Using Asymmetric Bridge Converter and Buck

Boost Converter", Australian Journal of Basic Applied Sciences, ISSN: 1991-8178, Vol.08, No. 06 , 2014.

[3] S.Sujitha, Venkatesh. C, "Stand alone Hybrid Driven Switched reluctance motor using H Bridge Converter", International Journal of Applied Engineering and Research, ISSN:0973-4562, 2015

[4] Sujitha. S;Vinoth Kumar K;Shiva R V;Sagar Kulkarni;Ponnappa M M,"An implementation of soft computing approach of smart control for induction motor using ANFIS,"2022 4th International Conference on Smart Systems and Inventive Technology (ICSSIT 2022),2022

[5] Vinoth Kumar K; S Sujitha; B Stalin; ,"Execution of smart electric vehicle charging station driven by RE technology using soft computing approach," 2021 Innovations in Power and Advanced Computing Technologies (i-PACT), 2021, pp. 1-5, doi: 10.1109/i-PACT52855.2021.9696545.

[6] Sujitha.S;Vinoth Kumar. K;Vinodha. K;Josh F T;Venkatesh. B, "Experimental Setup of Smart E-Vehicle Charging Station using IOT Technology," 2021 IEEE International Conference on Mobile Networks and Wireless Communications (ICMNWC), 2021, pp. 1-4, doi: 10.1109/ICMNWC52512.2021.9688523.

[7] S.Sujitha, Dr. Srinivasa G, Design and Performance of High Frequency Temperature Compensated Crystal Oscillator, Journal of Advanced Research in Dynamical and Control Systems, ISSN: 1943-023X, 2019

[8] Srinivasa G , S.Sujitha, "Spanning Trees of a Triangle Snake Graph by BFS and DFS Algorithms, International Journal of Innovative Technology and Exploring Engineering (IJITEE) ISSN: 2278-3075, Volume-8 Issue-8 June, 2019

To Study the Breakdown Voltage of Different Spacers

Sneha S Mallur[1]*, Sandya Kamashetty[1], C.Gururaj[2]
[1]PG student , [2]Faculty, BMS College of Engineering, Bengaluru, India
*snehasm.epe21@bmsce.ac.in

ABSTRACT

The aim of this thesis work is to find the effect of breakdown voltage on solid insulation material (spacers) Polymethyl methacrylate (PMMA), Polytetrafluoroethylene (PTFE), Polypropylene (PP) and Polyvinyl chloride (PVC). In electrical power system HV power equipment is mainly affected by breakdown voltage. This over voltage is mainly caused by lightning strokes which helps to determine the safe clearance required for proper insulation level. To avoid this problem in HV power equipment, plane-plane and point-plane gap method is considered as one of standard methods. The plane-plane and point-plane gap method is not complex and accuracy is acceptable. The knowledge of the BDV of different solid insulating materials of different composite materials with various electrode configurations and thickness of spacers helps us to determine the insulation type and their strength in order to protect the equipment so that it works efficiently and to avoid failure.

1. INTRODUCTION

Over the past few years, many researches are done on BDV. Recent trend is towards introducing high voltage transmission lines with gas insulated systems, the existing spacers are inadequate to withstand such high voltages. There are many merits and demerits for this issue. One of the benefits is to produce HV for laser printer and cathode ray tube televisions, which has similarities to auto ignition for the spark plug to start the engine. The spark over can be seen if a HV transmission line is not properly installed at actual gap. The spacer materials will have variation in breakdown strength based on operating condition of system such as applied voltage and pressure of air/gas insulation. It can be harmful to human and can cause sparking. So, the technology is important and must be designed for safety. Also, there is a need for better solid dielectrics with good breakdown strength which reduce the size of high voltage equipment [1] [3].

Rapid development over recent years in the power sector has given the opportunity to electrical engineers to protect the electrical equipment for reliable operation. Therefore, it is important for today's engineers to know different types of solid insulations and their properties to reduce the cost applications also keeping in mind safety considerations. Degradation of insulation of solid insulating material is one of the main problems of high voltage engineering. HV power equipment are mainly subjected to spark over voltage caused by lightning strokes and switching action. The plane-plane and point-plane electrode configurations are commonly used for this purpose.

In this research high voltage laboratory is used for measuring BDV. The application of spacer can increase the BDV [4]. For this purpose, four kinds of spacers namely Polymethyl methacrylate (PMMA), Polytetrafluoroethylene (PTFE), Polypropylene (PP), Polyvinyl chloride (PVC) with diameters of 25 mm, in two different high-voltage electrode configuration plane-plane and plane-point are investigated under normal temperature and pressure [5] [6]. These two electrode configurations are tested by using different spacer thickness with 5mm, 10mm, 15mm, 17.5mm and 20 mm. The effect of

parameters such as electrode spacing and spacer material on BDV are determined for applied DC and 50 Hz AC voltages.

2. METHODOLOGY

The impact of spacer on BDV enhancement will be found for both DC and AC voltages are applied. Hence, four kinds of spacers namely Polymethyl methacrylate (PMMA), Polytetrafluoroethylene (PTFE), Polypropylene (PP), Polyvinyl chloride (PVC) with diameters of 25 mm in two different high-voltage electrode configuration plane-plane and point-plane are investigated [2]. This two electrodes configuration are tested by using different spacer length with 5mm, 10mm, 15mm, 17.5mm, 20 mm. The influence of different parameters such as gap between electrodes, uniform and non-uniform field electrodes and spacer materials on BDV will be investigated for applied DC and 50 Hz AC voltages. Various real time applications can be observed with respect to this research [7] [8] [9].

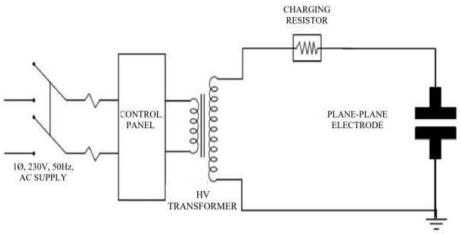

Figure 2.1 Circuit for the measurement of BDV under HVAC using plane-plane electrode

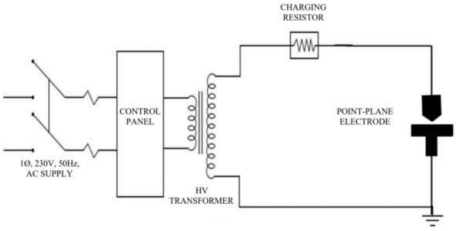

Figure 2.2 Circuit for measuring BDV under HVA Causing point-plane electrode

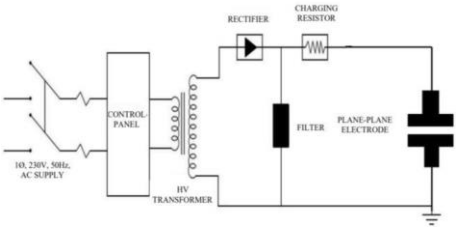

Figure 2.3 Circuit for measuring BDV under HVDC using plane-plane electrode

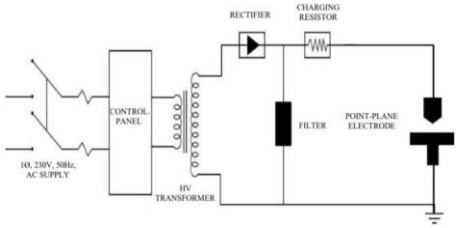

Figure 2.4 Circuit for measurement of BDV under HVDC using point-plane electrode

The circuit diagram for experiments to determine the breakdown voltages for different electrode configurations is shown in Figure 2.1, Figure 2.2 for AC and Figure 2.3, Figure 2.4 for DC. The electrodes are vertically arranged. The lower electrode which is above the ground plane is grounded where as the top electrode is connected with HV connector. The used plane electrode has a diameter of 50 cm and the electrode is made of Aluminium with nickel coating and air acts as an insulating medium between two electrodes. The ac source used is 100 kV (RMS). An input voltage of 230 V ac is given to a step-up transformer. The secondary output of transformer is fed to the test object. The HV electrode is energized from the 50 Hz transformer with a power rating of 5kVA with a transformation ratio of 230V/100kV. The input voltage to the transformer can be in increased or decreased as per requirements of the experiments in steps of 1kV/sec. Required dc voltage can be obtained after passing the output voltage through a rectifier unit and a filter capacitor to reduce ripple. A charging resistor is used

to control the current in the circuit. There is provision for tripping of electricalcircuit at the instant of breakdown. In addition, 100 kV ac and 140 kV dc breakdown equipment's were used for experiments requiring higher voltages. The test voltages are applied through the filter unit to isolate the noise of the transformer from the measuring circuit and current limiting device for protection in case of complete breakdown and prevent the high frequency current to the high voltage lead.

2.1 Control desk

To control and operate HVAC/HVDC test equipment control desk is used. The control panel consists of all the measuring instruments including the safety controlling switch such as mains switch, control switch (key), voltmeter, primary ON, secondary ON, primary OFF, secondary OFF, voltage regulation increase and decrease button, circuit breaker. All equipment under test is controlled by control panel. The desk contains operating and signal elements for the control circuit of the test equipment for warning and safety. It is fabricated of steel and stands on 4 wheels. The control panel displays the breakdown voltage at that particular gap distance between the electrodes.

2.2 Test setup

To conduct the breakdown test between the different electrode configurations, all the measuring instrument is referred to the test setup in the voltage laboratory. Experimental test setup is connected by using the circuit diagram.

2.3 Electrode arrangement

The types of electrode configurations for measuring HV are sphere-sphere, sphere-plane, rod-rod, rod-plane, point-point, point-plane and plane-plane. In this study two electrode configuration (plane-plane and point-plane) were used for the experimental study of different gap. The electrode is made of aluminium material and air acts as an insulating medium between these electrodes. Before the experiment is conducted, the two electrodes are cleaned to remove the dust particles residing over the surface. The behaviour of electric field is based on the nature of electrode configuration (uniform and non-uniform). Uniform electric field using plane-plane and non-uniform electric field using point-plane is produced as we apply the high voltage between the electrodes. The merits of plane–plane electrode arrangement is not influenced by polarity effect. However, there are many disadvantages such as very precise mechanical finish to the electrode is required, careful parallel alignment of the two electrodes and influence of dust brings in erratic breakdown of the gap. This is much more serious in these gaps as compared to sphere gaps as the highly stressed electrode areas become much larger. Hence, uniform field gap is generally not used for HV measurements. The electrode geometries used are 50 mm diameter Plane electrodes and 10 mm (60^o cone) Point electrode.

2.4 Different spacer materials used for study

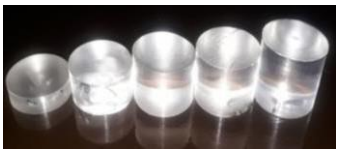

Figure2.5 PMMA spacer

Figure2.6 PTFE spacer

Figure2.7 PVC spacer

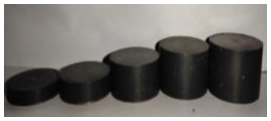

Figure2.8 PP spacer

Spacers are commonly used in air, oil and SF6 insulated systems both for mechanical support and insulation. The spacers are always weak links in the gas, solid and composite insulation systems and the breakdown is invariably by surface flashover across the spacer. Four cylindrical spacers made from PMMA, PTFE, PP and PVC materials are used for the investigation. Spacers of various lengths namely 5, 10, 15, 17.5 and 20 mm of diameter 25 mm are used for these experiments. Care is taken to see that spacer-electrode contact is firm so that there is no air gap between the two. It is possible to mount the spacers of different sizes by altering the electrode spacing. The photograph of the spacer materials used is shown in Figure 2.5, Figure 2.6, Figure 2.7and Figure

2.8. These materials are thoroughly cleaned. A clean and dry cloth is used for cleaning the surface. Thus, only clean and dry spacers and electrodes are used and they are handled with special surgical gloves to avoid direct contact with hands. These materials have good dielectric properties but their structural differences (spacer length) and dielectric constant make them give different results.

2.4 Spark over on spacer

Figure 2.9 Spark over on surface of spacer between electrodes.

A spark gap shown in Figure 2.9 shows the arrangement of two conducting electrodes separated by a gap normally filled with gas e.g., air, designed voltage difference between the conductors exceeds the gap's breakdown voltage, a spark forms drastically reducing its electrical resistance. Invariably, the breakdown observed with cylindrical spacers occurs on the surface along its length.

2.6 Precaution

1. The equipment must be grounded firmly.
2. The electrodes must be cleaned properly before fixing to the vessel.
3. Do not touch the equipment without grounding it with the discharge rod.
4. Before switch ON the supply, make sure the electrodes are properly aligned.

2.7 Standard operating procedure for measuring breakdown voltage

1. Install plane-plane/point-plane electrode at Measuring Spark Gap vessel and properly close the vessel cap. Make the electrodes properly aligned and zero

adjustment.

2. Now insert the spacer and adjust the gap between the electrodes by controlling the motor speed connected to the gear box of the movable electrode. (5mm, 10mm, 15mm, 17.5mm, 20mm)
3. Connections are made as per the circuit diagram for the required measurement of HVAC/HVDC breakdown.
4. For HVAC breakdown measurement the output terminal of the HV transformer is connected to the plane-plane/point- plane electrode through charging resistor. For HVDC breakdown measurement the output terminal of the HV transformer is connected to the plane-plane/point-plane electrode through silicon rectifier, filter and charging resistor. The other end of the supply is grounded.
5. After connections take discharge rod from the contact and keep at the corner and properly close the door.
6. Switch ON the mains switch (power supply).
7. Switch on the control switch (key) in control panel.
8. Switch ON the mains switch button at control panel (Green), observe the indication of mains ON.
9. Decrease 'voltage Regulation' to set primary to zero.
10. Press the 'Primary' ON button (GREEN) and the earthing switch stick will be down.
11. Press the 'Secondary' ON button (GREEN), the red light on the fence will glow. Slowly push the 'Voltage regulation' increase button and high voltage is applied between the electrodes until the spark over occurs.
12. Note down the readings of breakdown voltage.
13. Under HVAC breakdown, secondary will automatically turn off. Under HVDC breakdown, after breakdown occur decrease the 'Voltage regulation' and turn off both 'secondary' and then 'primary' OFF buttons (RED).
14. Switch OFF the main switch and wait for minimum 3 minutes.
15. Repeat the steps 8 to 14 to take average readings and for different values of spacer length adjustment.

3. RESULTS AND ANALYSIS

As previously mentioned, the main aim of this research is to observe the state of various solid spacer materials under the effect of breakdown voltage. In order to understand the effect of breakdown of solid spacers PVC, PP, PMMA and PTFE, experiments were carried out and data was obtained for different electrode configurations namely Plane-Plane and Point-Plane configurations with spacers length of 5mm, 10mm, 15mm, 17.5mm and 20 mm. These experiments were carried out to determine the BDV under AC, DC for comparison. The results obtained in the course of study are presented in the form of tables and graphs to highlight the various aspects of the study.

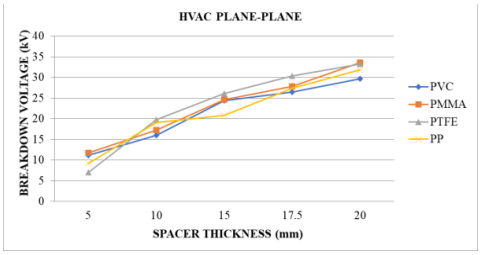

Figure 3.1 Variation of BDV of spacers with thickness using plane to plane electrode configuration under HVAC

Table 3.1 shows breakdown voltage with thickness of spacers using plane-plane electrode configuration under HVAC. Figure 3.1 shows the graph for variation of BDV with the thickness of the material for all spacers namely PVC, PMMA, PTFE and PP. The graph it shows that as the thickness of the spacer increases, the breakdown voltage increases. PP has the breakdown voltage lower than the PTFE and PMMA while PVC has the least breakdown voltage among the all.

Table 3.2 shows breakdown voltage with thickness of spacers using plane-plane electrode configuration under HVDC. Figure 3.2 shows the graph of variation for the breakdown voltage with the thickness of the material for all spacers namely PVC, PMMA, PTFE and PP. The graph shows that as the thickness of the spacer increases there is a considerable increase in its breakdown voltage. PMMA has higher breakdown voltage among the all. breakdown voltage with the thickness of the material for all spacers namely PVC, PMMA.

Table 3.3 shows breakdown voltage with thickness of spacers using point-plane electrode configuration under HVAC. Table 3.4 shows breakdown voltage with thickness of spacers using point-plane electrode configuration under HVDC. The graph shows variation for the breakdown voltage with the thickness of the material for all spacers namely PVC, PMMA, PTFE and PP. The graph shows that as the thickness of the spacer increases there is a considerable increase in its breakdown voltage. PP has the BDV lower than the PTFE and PMMA while PMMA has higher breakdown voltage among the all.

Table 3.5 shows breakdown voltage with thickness of PMMA using plane-plane electrode configuration under HVAC and HVDC. Figure 15 shows the variation graph of the breakdown voltage with thickness of PMMA under HVAC and HVDC. The graph depicts that PMMA is better insulating material at HVAC plane-plane electrode configuration.

Table 3.6 shows breakdown voltage with thickness of PMMA using point-plane electrode configuration under HVAC and HVDC. Figure 3.6 shows the comparison graph of the breakdown voltage with thickness of PMMA under HVAC and HVDC. The curve depicts that PMMA is better insulating material at HVDC point-plane electrode configuration. It is observed for all the cases that there is change in the BDV. It is observed that the spacers dielectric constant also has influence on observed result. On analyzing the graphs, as thickness of the material increases, the breakdown voltage for various spacers increases.

Table 3.1 Breakdown voltage of spacers using plane-plane electrode configuration under HVAC

Type of electrode configuration	Sl. No	Spacer Thickness (mm)	HVAC Breakdown Voltage (kV) Of Spacers			
			PVC	PMMA	PTFE	PP
PLANE-PLANE	1	5	11.19	11.76	7.012	9.23
	2	10	16	17.33	19.83	19.08
	3	15	24.35	24.64	26.16	20.81
	4	17.5	26.43	27.86	30.37	27.4
	5	20	29.73	33.58	33.28	31.91

Table 3.2 BV of spacers using plane-plane electrode configuration under HVDC

Type of electrode configuration	Sl. No	Spacer Thickness (mm)	HVAC Breakdown Voltage (kV) Of Spacers			
			PVC	PMMA	PTFE	PP
PLANE-PLANE	1	5	8.68	9.032	8.995	8.143
	2	10	12.68	17.36	13.45	16.08
	3	15	20.92	22.81	18.55	19.81
	4	17.5	23.88	23.52	22.57	20.4
	5	20	25.04	25.6	28.14	24.7

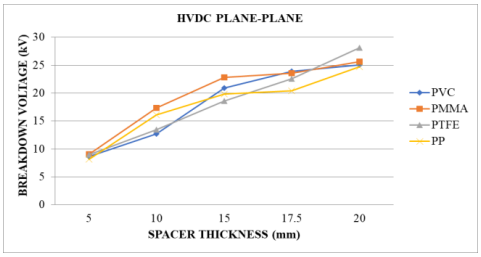

Figure 3.2 Variation of BDV of spacers with thickness using plane-plane electrode configuration under HVDC

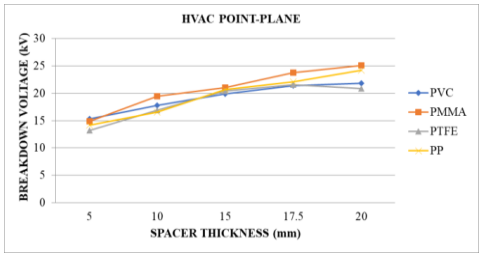

Figure 3.3 Variation of BDV of spacers with thickness using point-plane electrode configuration under HVAC

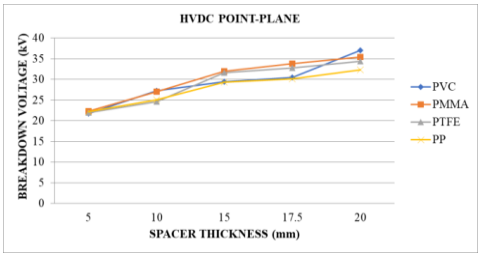

Figure 3.4 Variation of BDV of spacers with thickness using point-plane electrode configuration under HVDC

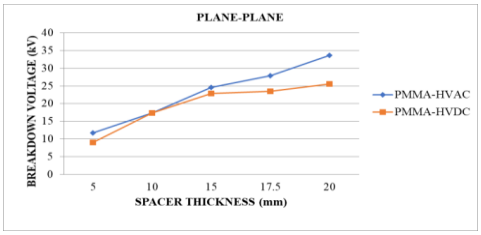

Figure 3.5 Variation of BDV with thickness of PMMA spacer under HVAC and HVDC plane-plane electrode configuration

Table 3.5 Breakdown voltage of PMMA using plane-plane electrode configuration under HVAC and HVDC

Type of electrode configuration	Spacer	Sl. No	Spacer Thickness (mm)	Breakdown Voltage (kV)	
				HVAC	HVDC
PLANE-PLANE	PMMA	1	5	11.7	9.03
		2	10	17.3	17.3
		3	15	24.6	22.8
		4	17.5	27.6	23.5
		5	20	33.5	25.6

Table 3.6 Breakdown voltage of PMMA using point-plane electrode configuration under HVAC and HVDC

Type of electrode configuration	Spacer	Sl. No	Spacer Thickness (mm)	Breakdown Voltage (kV)	
				HVAC	HVDC
POINT-PLANE	PMMA	1	5	14.88	22.29
		2	10	19.49	27.04
		3	15	21.087	31.985
		4	17.5	23.74	33.85
		5	20	25.057	35.46

4. CONCLUSIONS

Configurations have been investigated in this work. The plane-plane and point-plane electrode configuration are commonly used for this purpose. The effects of different parameters such as inter-electrode spacing, thickness of the spacer and dielectric materials on the breakdown voltage are investigated for applied 50 Hz AC and DC voltages. Hence the finding BDV of various insulating material provides major area of interest to the HV engineers and in particular to the high voltage engineers. Therefore, there is a possibility of developing solid insulating materials with excellent breakdown strength. It is observed for all the cases that there is change in the BDV. It is observed that the spacers dielectric constant also has influence on observed result. On analysing the graphs, as thickness of the material increases, the BDV for various spacers increases. It is also observed that PMMA has the higher breakdown voltage among the all spacers.

REFERENCES

[1] L. Wadhwa, “High Voltage Engineering”, published by New Age International (P) Limited,2nd edition 2007M.Young, The Technical Writer’s Handbook. Mill Valley, CA: University Science, 1989

[2] Comparative study on various dielectricbarriers and their effect on breakdown voltage", Elham Foruzan , Amir A.S. Akmal, Kaveh Niayesh, Jeremy Lin, Desh Deepak Sharma, Department of Electrical and Computer Engineering, University of Nebraska-Lincoln, Lincoln, NE 68588, USA.

[3] M.S. Naidu and V. Kamaraju, "High Voltage Engineering", published by Tata McGraw-Hill 5th edition, 2013

[4] Some Factors Affecting the Breakdown Strength of Solid Dielectrics", by R. Sarathi, Indian Institute of Technology Madras, Department of Electrical Engineering Chennai, India.

[5] Comparative Study of DC and Lightning Impulse Breakdown Voltages of Air gaps with and without Spacers", Dr. K.L.Ratnakar 1, Dr.B. Rajesh Kamath 1, Dr. J. Sunderarajan 2, 1 Professor and Research scholar of Sri Siddhartha Academy of Higher Education, 2 Professors of Electrical and Electronics Engineering of Sri Siddhartha Institute of Technology, Tumakuru

[6] DC Breakdown Voltage of Solid Dielectric Barrier under Non-Uniform Electric Field", Phloymuk N1, Pruksanubal A1, Tanthanuch N2, 1 Electrical and Computer Engineering, King Mongkut's University of Technology North Bangkok,Bangkok, Thailand, 2 Electrical and Computer Engineering, Thammasat University Pathumthani, Thailand

[7] Lavanya K.N., Ramyashree D, Nischitha B.R., T.Asha, C.Gururaj, "Gesture Controlled Robot",IEEE International Conference on Electrical, Electronics, Communication, Computer and Optimization Techniques, ISBN: 978-1-5386-2361-9/17, 15th -16th December 2017, pp 465-469, GSSSIETW, Mysuru

[8] Maneesha K, Neha Shree, Pranav Datta R, Sindhu S K, C.Gururaj, "Real Time Face Detection Robot", 2nd IEEE International Conference on Recent Trends in Electronics, Information & Communication Technology, ISBN: 978-1-5090-3704-9,19th – 20th May 2017 , pp 58-64, SVCE, Bengaluru

[9] Lavanya K.N., Ramyashree D, Nischitha B.R., T.Asha, C.Gururaj, "Vision Interfaced Warfield Robot with Wireless Video Transmission",IEEE International Conference on Trends in Electronics and Informatics, ISBN: 978-1-5386-3570-, 11th -12th May 2018, pp 833-838, SCAD College of Engineering and Technology, Tirunelveli, Tamilnadu

Survey on Estimation Methods for EV Battery Health using ML Techniques

Arya Jha, K Rahul Annamalai, C R Amrutha Varshini, Ayush Tiwari, K. Deepa, V. Sailaja

Department of Electrical and Electronics Engineering, Amrita School of Engineering, Bengaluru, Amrita Vishwa Vidyapeetham, India, aryajha0512@gmail.com, k_deepa@blr.amrita.edu, v_sailaja@blr.amrita.edu

Abstract.

Battery management system (BMS) is one of the vital components of an electric vehicle's battery. In BMS, input parameters are extracted from the main system and data related to the same is fed to the algorithm. State of Health and the State of Charge, abbreviated as SoH and SoC, respectively, are two crucial factors from which the life, reliability, efficiency, and safety of a battery are indicated. When dealing with a large dataset, Machine Learning (ML) approaches are utilized to make these factors' predicted value relatively precise to the real value. The result ensues from the past information as well as the present information, which is called the training for the ML technique. This paper compares the various ML methods based on the parameters as accuracy, training dataset, requirement, complexity, and temperature. It suggests LSTM as the appropriate method for the estimation of SoH and SoC of the battery.

Keywords. State of Health (SoH), Long Short-Term Memory (LSTM), State of Charge (SoC), Machine Learning (ML).

1. INTRODUCTION

The solution to the growing concern regarding the environment revolves around minimizing the use of non-renewable resources and increasing the efficiency of renewable resources, making them more economical [4]. One of the sectors which affect the environment by about 23-25% is the transportation industry. To minimize this percentage, electric vehicles (EVs) were introduced, and they are a boon to this industry [2, 15]. The demand for EVs is increasing day by day, seeing the advantages of high energy, power density and long lifespan[31]. In electric vehicles, batteries are used in the place of fuels which decreases the emission of carbon dioxide. [26] As the battery is a chemical energy storage source, for efficient working of a battery, it is important to know the behaviour of battery parameters like voltage, current, and temperature[30]. Battery management system (BMS) of an EV battery has a significant role in predicting the parameters related to battery health accurately [5]. BMS's role in battery includes protecting the battery, preventing over-discharge, improving the battery parameters, allowing applications to make rational control strategies to save energy and estimating of SoC and SoH of the battery. Both the parameters enable the study of the performance of battery ageing as the battery goes through several cycles [3, 29]. Here, one process means the completion of the loop of one-time charging and discharging of the battery. In this work, large amounts of data inputs are taken under consideration for predicting SoH. Therefore, this paper emphasizes more on the analysis of different Machine

Learning (ML) methods that are used for the prediction of SoH. For the precise and accurate estimation of SoH, different machine learning methods like Feedforward neural network (FNN), Support vector machine (SVM), Backpropagation Neural Network BP(NN), Radial Basis Function (RBF- NN), Extreme Learning Machine (ELM) , Recurrent Neural Network (RNN), Long Short-Term Memory (LSTM) and Gated Recurrent Unit (GRU) are compared based on training speed, memory cell, efficiency, etc. The procedure of formulation for respective ML methods has been described and demonstrated with block diagrams of operation and working. Also, the comparison has been made featuring the most appropriate method to use for SoH estimation as the conclusion.

2. SYSTEM DESCRIPTION

2.1. State of Health (SoH)

SoH of an EV battery suggests the functionality of the battery at the cell or pack level. It illustrates the ratio of maximum available capacity denoted by C_P that is used to the nominal rated capacity C_N that was not used as shown in Equation (1)[1, 27]. In simple terms, the number of times the battery can be charged and discharged is specified by the SoH of the battery.

$$\text{SoH (\%)} = \frac{C_P}{C_N} \text{ x } 100 \quad (1)$$

However, SoH is an indicator that requires details of health-related parameters such as ageing, history etc. Therefore, evaluating the SoH accurately increases the battery's life and avoids performance degradation [14]. Based on the analysis and working of the system, there are different models to forecast SoH precisely. There are many model-based SoH prediction methods-model-based, data-driven methods, hybrid methods and other methods that include such as SoC etc.

2.2. ML methods for SoH estimation

Different ML methods are categorised as in Figure 1 and discussed based on memory unit use, speed, training parameter and performance[1-7].

2.2.1. FNN 2.2.2. SVM 2.2.3. BP-NN 2.2.4. RBF-NN

2.2.5. ELM 2.2.6. RNN 2.2.6.1. LSTM 2.2.6.2. GRU

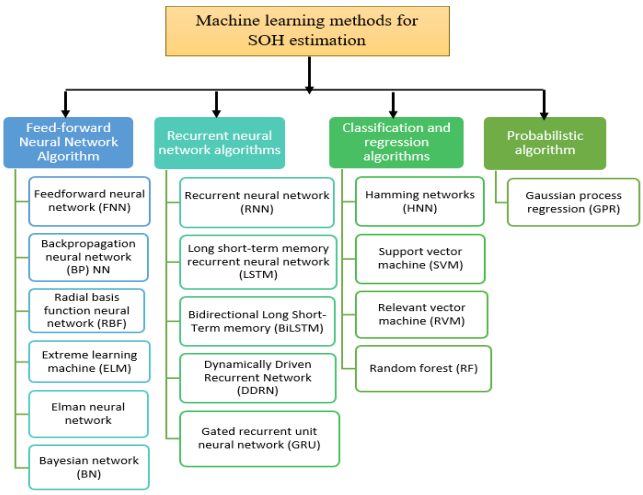

Figure 1. Machine learning methods for SOH estimation [1,4]

2.2.1. Feedforward Neural Network (FNN)

A Neural Network comprises input layers with input neurons in it, followed by several intermediate hidden layers to finally give an output [1, 12]. For this model to be understood, a k- means algorithm approach has been taken where the data has been extracted, which is based on the battery's parameters like current, voltage and temperature from 10 drive cycle so that more subregions could be detected and taken into consideration. A total of 44 datasets were created - 11 each for each of the temperatures 10 deg, 25 deg, 45 deg and 60 deg and with this, a point cloud distribution based is created. Here each sub-region is taken as input for this method, which is around 80, which means 80 inputs with 80 hidden layers of nodes giving a single output. Here the nodes are neurons that activate themselves to receive data from the previous set of information layers, and links that are used for mapping purposes are the weights.

This neural network aims to balance the weight links to achieve accuracy with minor modelling error, i.e., overfitting [7]. When this is compared with SVM models, it has been observed that the first showed commendable results than SVM models. But this model has some disadvantages like adjustment to variations from cell to cell in a pack and updating that in histogram from time to time. The calculation for FNN can be done by following (2) [28]:

$$a_n = f(\mu_n)$$

$$\mu_n = \sum p_{nm} q_m$$

$$f(\mu) = \frac{1}{1 + exp(-\mu)}$$

$$U = \frac{1}{2}(a_0 - a_{0r})^2$$

$$p_{nm}{}^{(j+1)} = p_{nm}{}^{(j)} - \beta \left(\frac{\partial F}{\partial q_{mn}}\right)^{j} \quad (2)$$

p_{nm}= weight coefficient a_n = output

μ_n = nth neuron potential f(μ) = transfer function

U = object function β = learning rate

a_0 and a_{0r} = output neuron's computed and required activities

2.2.2. Support Vector Machine (SVM)

Earlier, SVM was created for the problems related to classification and is further being used for solving the regression problem in a method known as Support Vector Regression, abbreviated as SVR [5]. Data which are not linearly separable, like battery environmental conditions and internal parameters, are solved by this ML technique. Steps involved in modelling SVM models are extraction, data processing, optimal SVM parameters searching, data training, data prediction, etc. The kernel function is invoked in the new feature space for the transformation of the initial input space into a high-dimensional feature space [1].

$$min_{m,c} = \frac{1}{2}\alpha^{T'}\alpha$$

$$q_n - \alpha \cdot a_n - c \leq \mu$$

$$\alpha \cdot a_n + c - q_n \leq \mu$$

$$f(a) = \sum_{n=1}^{N}(\beta_n - \beta *_n) K(a, a_n) + b \quad (3)$$

Following the mapping of the vector to a higher dimension, two parallel hyperplanes are determined, dividing the data on either side of the hyperplane. The formulae to be followed for the related problem are given in (3), where,

μ = toleration deviation α and c = found from Lagrange multipliers $\beta_n and\ \beta *_n$

f(a) = approximation function

2.2.3. Backpropagation Neural Network BP(NN)

Backpropagation NN BP(NN) is a multilayer feedforward NN in the traditional sense, which has an input layer, hidden layers (few), and an output layer [24]. In directed learning algorithms, the error back propagation algorithm is commonly used [16]. In case if accuracy is not attained between the expected and predicted value, propagation takes place and error propagates back from the output layer [1-2, 9, 25]. Under this method, threshold and weight are adjusted to get the convergence of error between expected output and network output until accuracy is met [1]. Stepwise formulation for BP(NN) in given in (4-8).

$$Bp_k = \sum_{j=0}^{n} a_{k,j}x_j + \emptyset\phi_{k,j} \quad (4)$$

n = number of neurons i to n = input neuron number range

$a_{k,j}$= weight of i and n range $\emptyset\phi_{k,j}$ = neuron threshold

$$b_k = f(Bp_k) \tag{5}$$

f(B_{pk}) = sigmoid function which is represented as an activation function.

In the below equation, S = α × s, where take alpha to be compression of the activation function and the other terms are considered just like the above equation.

$$f(Bp_k) = \frac{1}{1+e^{-S}} \tag{6}$$

$$Bp_m = \sum_{j=0}^{n} c_{jm} y_j + \emptyset\phi_{jm} \tag{7}$$

$$d_f = f(Bp_m) \tag{8}$$

2.2.4. Radial Basis Function (RBF) NN

For the hidden layer in RBF, the activation function is nonlinear and hence RBF can be used for any nonlinear function [27]. It provides faster convergence as compared to other methods, including Backpropagation neural network [19-21, 11]. The formulation for RBF selection has been given in (9), (10)[1].

$$e_i = \delta\,(x, y_i, z_i) = \sum_{i=1}^{n} exp\left(\frac{-||x-y_i||^2}{2{z_i}^2}\right) \tag{9}$$

$$\mathrm{E} = (\sum_{\mathrm{i}=1}^{\infty} \mathrm{m_i}\ \mathrm{n_i}\ ) + \mathrm{B_2} \tag{10}$$

Here, e(i) is taken as a nonlinear Gaussian function, y = average and z = standard deviation, which results in the output function given in (9), (10).

2.2.5. Extreme Learning Machine (ELM)

ELM proves to be most effective in clustering, classification, regression, and feature learning application areas [22].The features of ELM include the use of generalized theory for optimization. Moreover, the linear independence of random hidden neurons has been demonstrated by ELM, and it can be applied to almost any nonlinear piecewise continuous function. It exhibits the linear independence of random hidden neurons and expands to kernels and a higher degree of mapping of hidden instances. It also shows how, in the ELM framework, hidden node data autonomous parameters may be used to link ridge rectification, system stability, theoretically based neural network creation, maximum margin, and network optimization requirements. [8, 17]. The given set of equations (11) gives the step calculation for ELM.

$$\sum_{n=1}^{N} \boldsymbol{\delta}_n k(P_n \bullet X_i + b_n) = q_{n\,,}\ i = 1, \ldots, M$$

$$\| q_n - h_n \| = 0$$

$$\sum_{n=1}^{N} \boldsymbol{\delta}_n k(P_n \bullet X_i + b_n) = h_{n\,,}\ i = 1, \ldots, M$$

$$J\delta = \mathrm{H}$$

J (P_1,… P_R, b_1,… b_R, Y_1,… Y_M)

$$= \begin{bmatrix} k(p_1 \cdot x_1 + b_1) & \cdot & \cdot & \cdot & k(p_1 \cdot x_1 + b_R) \\ \cdot & \cdot & \cdot & \cdot & \cdot \\ \cdot & \cdot & \cdot & \cdot & \cdot \\ \cdot & \cdot & \cdot & \cdot & \cdot \\ k(p_1 \cdot x_M + b_1) & \cdot & \cdot & \cdot & k(p_1 \cdot x_M + b_R) \end{bmatrix}_{M \times R}$$

$$\delta = J^{\dagger} H \tag{11}$$

Here, X= Input from collected sample

h = Label vector corresponding to training sample

M = Total samples N = Number of hidden nodes

k(x) = Activation function of hidden layer P = Hidden layer's input weight

δ = Output weight J= Hidden layer output matrix

2.2.6. Recurrent Neural Network (RNN)

RNN, is an appropriate ML technique for the short-term sequence as it follows a close loop for data passing where the past information is used [1, 4]. The disadvantage of this method is gradient vanishing while training the data. This is occurring because only for a certain time limit does RNN possesses past information. The actually hidden layer of RNN includes the current information with the recursion of time, resulting in information loss [6, 14]. This way, it draws a limit to the RNN structure resulting in the disadvantage of gradient vanishing. Calculation of RNN has been demonstrated in (12).

$$t_h = \gamma(W_i \times A_t + H_W \times t_{h-1} + S) \tag{12}$$

t_h = hidden layer activations in time t ( ) = activation function

A_t = input vector W_i = weight of the input vector

H_w = weight of hidden layer activations S = bias

2.2.6.1. Long Short-Term Memory (LSTM)

LSTM is one of the types of Recurrent Neural network (RNN) [3]. Moreover, the improved learning of the Long short-term memory is that it works on the shortcomings of traditional RNN, such as gradient vanishing. LSTM is considered over RNN because of the difference in the number of states. In RNN, only one state exists, whereas in LSTM, four states are present in one cycle. In this method, huge data is fed to train the models using sequences which keep track of persistent unit state and is used for decision making the task of whether to retain or store the information for further operation or to be forgotten. The computation procedure of LSTM has been given in (13).

Here n, I, O, and m denote the forget, input, output gates and memory cells, respectively[1].

b = forget gate bias W_o, W_i = last step output and input weight

α = activation function tanh = tan hyperbolic function

P_{in} and P_{on-1} = Input and output of instantaneous step

P_n= Internal variable of LSTM

$$f_n = \alpha(b_f + P_{in}W_{if} + P_{on-1}W_{of})$$

$$i_n = \alpha(b_i + P_{in}W_{ii} + P_{on-1}W_{oi})$$

$$g_n = \tanh(b_g + P_{in}W_{ig} + P_{on-1}W_{og})$$

$$m_n = m_{n-1}f_n + g_n i_n$$

$$O = \alpha(b_o + P_{in}W_{io} + P_{on-1}W_{oo})$$

$$P_{on} = \tanh(p_n) \times O \quad (13)$$

i. Explanation of battery system

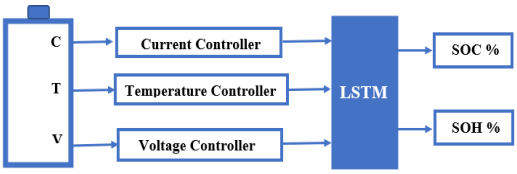

Figure 2. Battery system block diagram

For SoH estimation of the battery using the appropriate ML technique, that is, LSTM, huge data should be provided to trace the continuous change in parameter and to extract the approximately near value of actual SoH of the battery. For the more precise and accurate value of SoH, readings are taken for a longer duration which decreases the extent of the error. As shown in Figure.2, current, voltage, and temperature have been taken as the variable parameters, which have been traced against time to give the resultant SoH of the battery following feeding the input data of I, V, T to LSTM for training and data interpretation.

ii. Working of LSTM

LSTM layer has been shown in Figure.3 [2], where the input data layer at instantaneous step time n and hidden layer at n-1 step time are denoted as α_n and h_{n-1}, respectively; Input, output, forget gates and memory cells are given by i_t, O_t, f_n, and M_k, respectively. It suggests that in a closed-loop, information is passed in a neural network in a recurrent pattern where the output or intermediate state can be used as an input[13]. As LSTM involves long sequential data and uses past information, it makes SoH estimation easy [9, 18]. It stores the data and transfers the past or previous and current state data, which is used in the future state and acts as feedback [3] friendly algorithm using memory cell m_n.

The forget gate f_n decides on the information and how much of it will be useful and needed from m_{n-1} and should be passed to the next step. The input gate decides on the amount of information that should be passed to the memory cell, and the output gate O_n is responsible for the amount of information available that should be computed in the memory cell and will be counted in the output denoted by h_n.

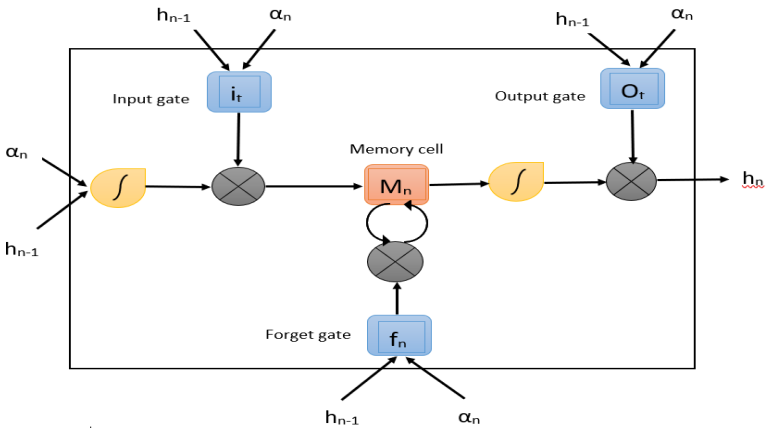

Figure 3. Block diagram for LSTM working

Working of LSTM has been illustrated in Figure.3[2] as well as Workflow of estimation of SoH involving the step of feeding input (Voltage, Current, Temperature), LSTM operation, and output extraction has been shown in Figure.4 [2].

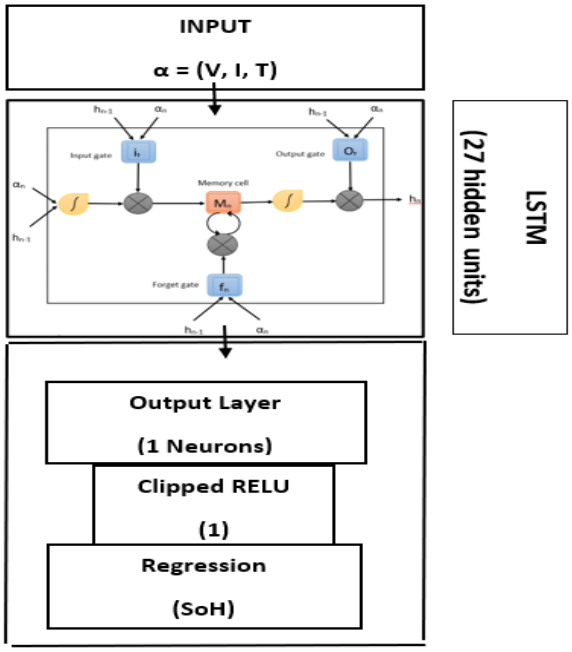

Figure 4. Estimation structure of LSTM for SoH

2.2.6.2. Gated Recurrent Unit

Based on gate control, RNN has been extended to a Gated recurrent unit (GRU), where it shares most of the features of LSTM NN [13, 23]. Integration happens to the input and forgetting gates of LSTM into an update gate. The structure of GRU is simpler as compared to LSTM. Moreover, training speed and prediction efficiency are higher. The two gates, the update gate and reset gate, determine the amount of previous information that should be passed and the amount of information that should be neglected or eliminated, respectively. Taking vast amounts of data under consideration for the inputs Voltage (V), Current (I) and Temperature (T), GRU does not give accuracy as much as LSTM NN [4]. Following are the equations involved in the computation of GRU (14) [18]:

$$a_t = \alpha(y_t W^a + H^a n_{t-1} + s_z)$$

$$q_t = \alpha\left(y_t W^q + H^q n_{t-1} + s_q\right)$$

$$n'_t = \tanh(q_t \times n_{t-1} H + y_t W + s)$$

$$n_t = a_t \times n_{t-1} + (1 - a_t) \times n'_t \quad (14)$$

W^a, W^q, W = corresponding input vector weight matrices

H^a, H^q, H = previous time step weight matrices

s_q, s_a, s = biases

α = logistics sigmoid function

q_t = reset gate

a_t = update gate

n'_t = candidate hidden layer

3. COMPARISON OF ML METHODS

In Table 1, various ML methods have been listed and compared. Given the advantages and disadvantages, which demonstrate that LSTM and GRU are appropriate methods for the estimation of the precise and accurate value of SoH. All the methods listed are used for nonlinear data analysis, but BP-NN and RBF-NN lack efficiency, whereas, in ELM and RNN, problems of data training and gradient vanishing are encountered, respectively.

Methods	Features/ Advantages	Disadvantages
BP-NN [1]	• Multilayer feedforward NN • Comprises of - the input layer, an output layer followed by a few hidden layers • Backpropagation of error and correction weight • Until the error is reduced to the accepted limit signal, forward propagation and error backpropagation takes place	• Complexity due to net layers as the number is not fixed for the initial step • Working efficiency is less
RBF-NN [1]	• Faster convergence • Nonlinear activation function for hidden layer (usually) • Good performance	• Less operating efficiency • Easily falls into local optimality
ELM [1, 18]	• Faster training speed while ensuring the estimation accuracy • Time of parameter optimization is reduced • Better prediction accuracy, faster calculation speed	• Batch-based algorithm • During the training phase, all the training data is needed to implement training and testing rather than updating the arrival of new data.
Elman-NN	• Embedded one-step delay mechanism • Global stability, time-varying ability • Dynamic modelling • Fast approaching speed	• Easily falls into local optimality • Slow training operation
RNN [1, 4, 7, 10]	• The impact of temperature is taken into consideration • Sequence data processing with varying length • Presence of parameter sharing • Does not operate on fixed-length input • Recurrent connection possible • Self-feedback present	• No spatial relationship • The range of context information is limited • The problem of gradient vanishing. • Battery ageing happens under high temperatures • Implementation of constant charging/discharging for creating the dataset

LSTM **[1-6, 10]**	• Consists of a memory cell multilayer framework • Effect of temperature is taken under consideration • Maintains a persistent unit state as well as allows one to choose which information should be preserved and which should be forgotten. • Gives support to the real-world driving platform because of the practical EV environment. • Tracks for a longer time with accuracy	• Complexity in training execution • Difficulty in the acceleration of training • I/V pattern is needed for the account of battery degradation (the difference is there depending upon the battery chemistry)
GURU **[1]**	• Based on the gate control • Input and Forgetting gates (of LSTM) get integrated into an update gate • Simpler structure than LSTM • When compared to LSTM, its training and prediction efficiency is higher • Has fewer parameters	• Possibility of the uncertainty of battery deterioration and overfitting • Accuracy is less as compared to LSTM for a greater number of data • Sensitive to a Kernel function • Higher computational cost compared to LSTM

Table 1. ML method comparison

4. CONCLUSION

In this paper, different ML techniques have been discussed with advantages and disadvantages. The performance and accurate estimation of SoH have been analyzed by comparing the methods. The main focus of this paper is the accurate estimation of SoH, which has been seen in the LSTM method. In LSTM, a huge amount of data has been trained, which dominates the advantages of GRU. Although GRU is easy to modify, faster to train and does not need memory units, or fewer training parameters, LSTM is more accurate compared to GRU when a longer sequence is used and is more accurate too. LSTM also rectifies the problem of gradient vanishing.

5. REFERENCES

[1] Shu, Xing & Shen, Shiquan & Shen, Jiangwei & Zhang, Yuanjian & Li, Guang & Chen, Zheng & Liu, Yonggang. State of Health Prediction of Lithium-Ion Batteries Based on Machine Learning: Advances and Perspectives. iScience, .2021.

[2] C. Vidal, P. Malysz, P. Kollmeyer and A. Emadi, "Machine Learning Applied to Electrified Vehicle

[3] Battery State of Charge and State of Health Estimation: State-of-the-Art," in IEEE Access, vol. 8, pp. 52796-52814, 2020.

[4] T. G. T. A. Bandara, J. C. Á. Antón, M. González, D. Anseána and J. C. Viera, "State of Health Estimation using Machine Learning for Li-ion battery on Electric

Vehicles," 2021 IEEE Vehicle Power and Propulsion Conference (VPPC), 2021, pp. 1-4.

[5] Venugopal, P.; T., V. State-of-Health Estimation of Li-ion Batteries in Electric Vehicles Using IndRNN under Variable Load Condition. Energies 2019, 12, 4338.

[6] X. Feng et al., "Online State-of-Health Estimation for Li-Ion Battery Using Partial Charging Segment Based on Support Vector Machine," in IEEE Transactions on Vehicular Technology, vol. 68, no. 9, pp. 8583-8592, Sept. 2019.

[7] Y. Wu, Q. Xue, J. Shen, Z. Lei, Z. Chen and Y. Liu, "State of Health Estimation for Lithium-Ion Batteries Based on Healthy Features and Long Short-Term Memory," in IEEE Access, vol. 8, pp. 28533-28547, 2020.

[8] M. Naguib, P. Kollmeyer, C. Vidal and A. Emadi, "Accurate Surface Temperature Estimation of Lithium-Ion Batteries Using Feedforward and Recurrent Artificial Neural Networks," 2021 IEEE Transportation Electrification Conference & Expo (ITEC), 2021, pp. 52-57.

[9] A. Densmore and M. Hanif, "Modeling the condition of lithium-ion batteries using the extreme learning machine," 2016 IEEE PES PowerAfrica, 2016, pp. 184-188.

[10] T. Duraisamy and D. Kaliyaperumal, "Machine Learning-Based Optimal Cell Balancing Mechanism for Electric Vehicle Battery Management System," in IEEE Access, vol. 9, pp. 132846-132861, 2021.

[11] N. Khan, F. U. M. Ullah, Afnan, A. Ullah, M. Y. Lee and S. W. Baik, "Batteries State of Health Estimation via Efficient Neural Networks With Multiple Channel Charging Profiles," in IEEE Access, vol. 9, pp. 7797-7813, 2021.

[12] L. Mao, H. Hu, J. Chen, J. Zhao, K. Qu and L. Jiang, "Online State of Health Estimation Method for Lithium-ion Battery Based on CEEMDAN for Feature Analysis and RBF Neural Network," in IEEE Journal of Emerging and Selected Topics in Power Electronics.

[13] N. Junhuathon, G. Sakunphaisal and K. Chayakulkheeree, "Li-ion Battery Aging Estimation Using Particle Swarm Optimization Based Feedforward Neural Network," 2020 International Conference on Power, Energy and Innovations (ICPEI), 2020, pp. 73-76.

[14] Ardiansyah, Y. Kim and D. Choi, "LSTM-based Multi-Step SOC Forecasting of Battery Energy Storage in Grid Ancillary Services," 2021 IEEE International Conference on Communications, Control, and Computing Technologies for Smart Grids (SmartGridComm), 2021, pp. 276-281.

[15] S. Basmati and H. Chaoui, "Lithium-Ion Batteries Long Horizon Health Prognostic Using Machine Learning," in IEEE Transactions on Energy Conversion, vol. 37, no. 2, pp. 1176-1186, June 2022.

[16] T. Duraisamy and Dr K. Deepa, "Adaptive passive balancing in battery management system for e-mobility", International Journal of Energy Research, vol. 45, pp. 10752-10764, 2021.

[17] P. Wang and X. Li, "Estimation and Prediction on State of Health of Electric Vehicle Battery Based on BP Neural Network," 2021 IEEE 3rd International Conference on Frontiers Technology of Information and Computer (ICFTIC), 2021, pp. 729-732.

[18] B. Deng, X. Zhang, W. Gong and D. Shang, "An Overview of Extreme Learning Machine," 2019 4th International Conference on Control, Robotics and Cybernetics (CRC), 2019, pp. 189-195.

[19] Tan, S.-W.; Huang, S.-W.; Hsieh, Y.-Z.; Lin, S.-S. The Estimation Life Cycle of Lithium-Ion Battery Based on Deep Learning Network and Genetic Algorithm. Energies 2021, 14, 4423.

[20] Sherstinsky, A., “Fundamentals of Recurrent Neural Network (RNN) and Long Short-Term Memory (LSTM) network”, Physica D Nonlinear Phenomena, vol. 404, 2020.

[21] Dash, Ch & Behera, Ajit Kumar & Dehuri, Satchidananda & Cho, Sung-Bae. (2016). Radial basis functions neural networks: A state-of-the-art topical survey. Open Computer Science. 6. 10.1515/comp-2016-0005.

[22] Bors, Adrian. (2001). Introduction of the Radial Basis Function (RBF) Networks.

[23] Pande, Shubhangi & Rathore, Neeraj & Purohit, Anuradha. (2021). A Survey and Analysis of Extreme Machine Learning Models and Its Techniques. 10.21203/rs.3.rs-599856/v1.

[24] Mateus, B.C.; Mendes, M.; Farinha, J.T.; Assis, R.; Cardoso, A.M. Comparing LSTM and GRU Models to Predict the Condition of a Pulp Paper Press. Energies 2021, 14, 6958.

[25] S. C. Ng, S. H. Leung and A. Luk, "A generalized backpropagation algorithm for faster convergence," Proceedings of International Conference on Neural Networks (ICNN'96), 1996, pp. 409-413 vol.1.

[26] Hecht-Nielsen, "Theory of the backpropagation neural network," International 1989 Joint Conference on Neural Networks, 1989, pp. 593-605 vol.1.

[27] Poornesh, Kavuri, Kuzhivila Pannickottu Nivya and K. Sireesha. “A Comparative study on Electric Vehicle and Internal Combustion Engine Vehicles.” 2020 International Conference on Smart Electronics and Communication (ICOSEC) (2020): 1179-1183.

[28] J. Zhou, Z. He, M. Gao and Y. Liu, "Battery state of health estimation using the generalized regression neural network," 2015 8th International Congress on Image and Signal Processing (CISP), 2015, pp. 1396-1400.

[29] Dong C, Jin B, Li D. Predicting the heating value of MSW with a feedforward neural network. Waste Manag. 2003;23(2):103-6.

[30] Thiruvonasundari, D. and Deepa, K. “Adaptive Passive Balancing in Battery Management System for e –Mobility “, International Journal of Energy Research, Wiley Publication, vol.45, Issue.7, 2021, pp.10752 – pp. 10764.

[31] K. M. Sai Lakshmi and S. V., "Resonant converter-based PV battery charger for EV applications," 2019 2nd International Conference on Power and Embedded Drive Control (ICPEDC), 2019, pp. 219-224.

Biographies

Arya Jha is pursuing the bachelor's degree in Electrical and Electronics Engineering from Amrita School of Engineering, Bengaluru, member of IEEE student branch, EXICOM member of IEEE PES and IAS joint student branch chapter Bangalore section and pursued a certification course on Data Science with applied python as well as headed Bangalore section ambassadors for PES Day 2022 and served as CSAC Ambassador for Online course category. Her area of interest involves e-mobility, Data Science, and Renewable energy technologies.

K Rahul Annamalai is pursuing the bachelor's degree in Electrical and Electronics Engineering from Amrita School of Engineering, Bengaluru and member of IEEE student branch and an EXICOM of IEEE PES and IAS and pursued a certification course on python basics, His area of interests are e-mobility, Automobile, Renewable energy technologies and power electronics.

C R Amrutha Varshini is pursuing the bachelor’s degree in Electrical and Electronics Engineering from Amrita School of Engineering, Bengaluru, member of IEEE student branch, EXICOM member of IEEE sensors, IEEE PES and IAS and pursued a certification course on Data Science with applied python. Her area of interests are Electric Vehicles(BMS), Embedded Systems and Data Science.

Ayush Tiwari is pursuing the bachelor's degree in Electrical and Electronics Engineering from Amrita School of Engineering, Bengaluru and pursued a certification course on Data Science with applied python. His area of interests are Electric Vehicles(EV),Power Electronics and Renewable Energy Technologies.

Dr. K. Deepa graduated from Alagappa Chettiar college of engineering and Technology, T.N, India in 1998. She obtained M.Tech degree from Anna University, Guindy campus, T.N, India in 2005. She received Doctoral degree from Jawaharlal Nehru Technological University, Anantapur, A.P, India in 2017. Currently she is working as Associate professor in Electrical and Electronics Engineering Department, Amrita School of Engineering, Amrita Vishwa Vidyapeetham University, Bangalore, Karnataka, India. She has 23+ years of teaching experience. She is a life Member of IETE and ISTE, India and a senior member of IEEE. She has authored two textbooks on "Electrical Machines" and "Control Systems". She has published 35+ international journal paper, 60+ papers in international conference and 6 papers in national conference. 20+ M.Tech Degrees were awarded under her guidance. She is the advisor for the IEEE-PES & IAS student branch joint chapter and advisor for IEEE WIE in Amrita School of Engineering, Bengaluru from 2015. She is also Secretary for 2021 and 2022 IEEE PELS Bangalore chapter. She ahs received the outstanding Exofficio- 2021 award for her incredible volunteering in IEEE PELS Bangalore section. Her areas of interests include Power electronics, Renewable energy technologies and Control Engineering.

V.Sailaja received the bachelor's degree in Electrical and Electronics Engineering from JNTU college of Engineering, Hyderabad in 2001, the master’s degree in Power Electronis and Industrial drives from JNTU college of Engineering, Hyderabad in 2007 and currently pursuing philosophy of doctorate degree from Visvesvaraya Technological University. V.Sailaja is Assistant professor, Department of Electrical and Electronics, Amrita School of Engineering, Bangalore. Her area of interest are power quality, power electronic applications in electrical drives, battery management systems , smart grid , hybrid power systems.

DESIGN AND IMPLEMENTATION OF DUAL OUTPUT FORWARD CONVERTER TO POWER-UP DIGITAL UNIT FOR SPACE APPLICATION

Nikhil Kumar[1], A.N. Nagashree[2], Santosh B L[3], Prakash G[4], B K Singh[5]

[1]*M.Tech PE, Dept of EEE, BMSCE Bengaluru. nikhil.epe20@bmsce.ac.in*
[2]*Associate Professor and Head, Dept of EE,BMSCE. annagashree.eee@bmsce.ac.in*
[3]*Assistant Manager ,Centum Electronics Ltd, santoshbl@centumelctronics.com*
[4] *Engineer, Centum Electronics Ltd, prakashg@ centumelctronics.com*
[5]*Director, Centum Electronics Ltd.*

Abstract.

In recent years, DC-DC converters find many applications in low to medium power range. The isolated converters are used in medium power application since they provide isolation between input and output and protection from input side faults.This paper presents application of isolated DC-DC converter to power-up digital unit subsystem for space mission. The proposed converter is designed to operate at switching frequency of 140 kHz which reduces the size of magnetic components. The proposed topology uses a voltage feed forward control technique to adjust duty cycle for an input variation. It has a built in EMI filters to mitigate noise that emerge from surrounding components and vice versa. Meeting cross regulation is a challenging task and this is achieved by maintaining secondary feedback circuit in stable region. A prototype model is developed having Hybrid Micro Circuits (HMC) which reduces the size of the converter. It is aimed to achieve converter efficiency greater than 65%.

Keywords: DC-DC Converter, Forward Converter, Feed Forward, Mag-amp, LCD(Lossless) Snubber, UC2525 PWM controller.

1. INTRODUCTION

Nowadays, DC- DC converters are used in a range of applications from consumer electronics and telecommunications to industrial, medical and space. For space mission application, the most important requirements are high reliability and light weight design rather than conversion efficiency[1]. Though other topologies like full bridge, half Bridge and push pull DC-DC converters are capable of high efficiency but their reliability is low due to high side switch structure. Hence single switch forward converter with tertiary winding as demagnetizing or reset winding is used, as the converter is best suitable for low to medium power applications with high output currents. However, in single switch forward converter, reset winding is unable to put off leakage inductance spike, which may cause stress on the MOSFET switch. Therefore, this core has to be reset completely using an RCD snubber circuit consisting of resistor, capacitor and a diode. When the switch turns on the capacitor charges through diode and when the switch turns off it discharges stored energy into resistor. But the drawback of this method is, it decreases the efficiency

due to losses in the resistor [2]. To overcome this, LCD or lossless snubber is used as an alternative to RCD snubber which is non-dissipative in nature. It gives protection against dv/dt as well as di/dt. It is a challenging task to achieve good load regulation while designing the converter. So magnetic-amplifiers (Mag-amp) are used as post regulators on secondary side to maintain load regulation within the specification. The feedback control circuits for each output are used to achieve precise regulation of output voltages.

2. SPECIFICATIONS AND BLOCK DIAGRAM

The Forward Converter specifications are shown in Table 1

Table I. Forward Converter Specification

Parameters	Specification
Input Voltage	24V(min),36V(nom),42.5V(max)
Output-1	5.5V/12A
Output-2	5V/2A
Switching Frequency	140±5kHz
Efficiency	>65%
Output Power	76W
Ripple	<30mVp-p
Line Regulations	<±1%
Load Regulations	<±2%

The detailed block diagram of the proposed converter is shown in Fig 1. On the input side it has an EMI filter to reduce noise. Inrush current limiter circuit, limits the input current on application of ON command with 100% load to less than the twice of input current. Current sense circuit protects the converter from over current or short circuit current. It uses N-channel MOSFET as a switch and duty of this switch is controlled using voltage feed forward control method. The bias turns on the input side is used to provide a constant supply to the ICs. The outputs on the secondary side are rectified and filtered using diode rectifier and output filter circuits. To achieve good load regulation, mag-amp is used as post regulators. The maximum voltage requirement by digital unit is 6.6V, therefore over voltage protection circuit is designed with opto-coupler to limit output voltage to 120% of actual output.

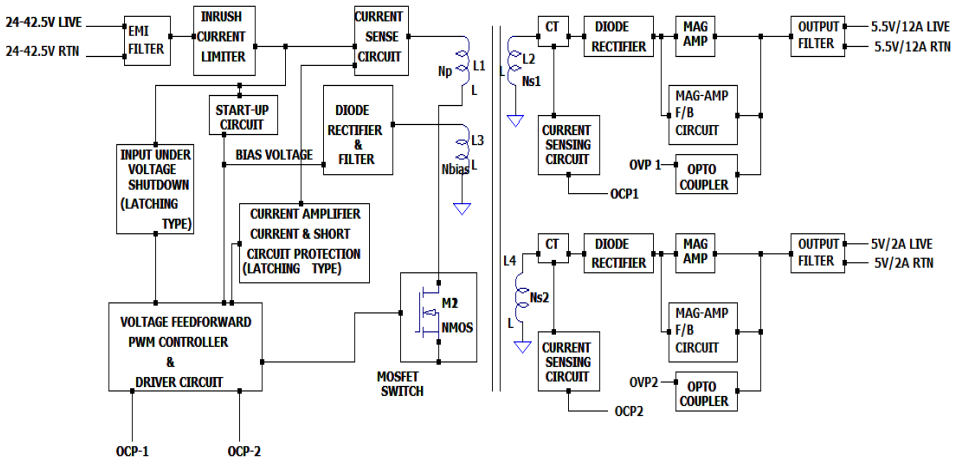

Fig 1. Block Diagram of the proposed converter

3. DESIGN PROCEDURE

In this section design of a) transformer b) criteria for selecting MOSFET switch c) snubber circuit selection d) output filter design e) mag-amp design have been explained. To make converter efficient, optimal selection of components are required.

3.1. Transformer Design

The area product calculation is used for selecting the transformer core. The optimum design is finally decided by the smaller size and lower power dissipation of transformer [3]

$$A_p = \frac{\sqrt{\text{Dmax}} \cdot P_{out} \cdot (1+\frac{1}{\eta})}{K_w \cdot J \cdot 10^{-6} F_{sw} \cdot \text{Bm}} \quad (1)$$

$$A_p = \frac{\sqrt{0.4} \cdot 76 \cdot (1+\frac{1}{0.65})}{0.35 \cdot 6 \cdot 10^{-6}\ 140.10^3 \cdot 0.2}$$

$$= 4150.17\ mm^4.$$

Where,

i) K_w : Window factor. ii) J: Current density A/mm^2. iii) F_{sw} : Switching frequency Hz. iv) D_{max} :Maximum duty cycle. v) **η**: Efficiency. vi) B_m: Maximum flux density T

An appropriate core will be selected which must have area product greater than the calculated Ap and better power handling capacity. From the ferrite core catalogue, selected **POT** core is **OR43019UG** which is having $\mathbf{A_L}$**=6680nH/1000**Turns.

Primary turns are calculated from equation (2)

$$N_p = \frac{V_{in} \cdot \text{Dmax}}{B_m \cdot A_C \cdot 10^{-6} \cdot F_{sw}} \quad (2)$$

To know secondary turns, turns ratio to be calculated using formula (3)

$$\text{Tratio} = \frac{Np}{Ns} = \frac{Vout+Vd*Dmax}{Dmax*Vin(\min)} \quad (3)$$

Where,

i) Vd : Diode drop. ii)$Vin_{(min)}$: Minimum input voltage

Hence,

$$Ns = Tratio* Np \quad (4)$$

3.2. MOSFET SELECTION

Parameters to be considered for selection of MOSFET are drain to source voltage(V_{DS}), gate to source voltage(V_{GSth}) required to turn it on, continuous drain current(I_{Dmax}), drain to source ON resistance (R_{DS}(on)), input capacitances(C_{iss}) and output capacitances(C_{oss}). The stress on the MOSFET is calculated using equation (5) and suitable MOSFET is selected, which can withstand this stress.

$$V_{peak\text{-}MOSFET} = V_{in\text{-}max}\left(1+\frac{Npri}{Nreset}\right) \quad (5)$$

IRHM57260 is selected which has V_{DS} = 200V, $R_{DS(on)}$= 49mohm, I_{Dmax}=35A and $V_{GS(th)max}$=4V.

3.3. SNUBBER DESIGN

Parasitic inductances and resistances are associated with voltage spikes and current spikes. These will introduce electrical stresses on the switching devices. Hence snubbers are necessary to limit switching transients like dv/dt and di/dt and it also helps in lowering EMI by reducing ringing noise, that occurring due to leakage inductance of transformer. Lossless snubber (LCD snubber) is selected for recovering the leakage power loss from the MOSFET. It reduces switching off loss in mosfet. Lossless snubber contains two diodes, one inductor (Lsnubber) and one capacitor (Csnubber) (LCD). The suitable core for inductor is selected by calculating area product as shown in equation (6)

$$A_P = \frac{\text{Lsnubber} * Iout^2 * (1+\frac{K}{2})}{Kw*Bm*J*10^{-6}} = 16.411\text{mm}^4 \quad (6)$$

Where,

i) B_m : Max flux density. ii) K : Fill factor.

The selected core is **C055291A2 with A_L = 32nH/T^2**.

3.4. VOLTAGE FEED FORWARD CONTROL

In the conventional voltage feedback technique, the output voltage is compared with the reference wave and pulse width modulation is performed by comparing error signal with the constant ramp waveform. Though feedback technique is easier to design and analyse, the response is slow in regulating the duty cycle due to changes in input line voltage.

Hence voltage feed forward control is used to achieve fast dynamic response. In this control technique saw tooth wave is generated using RC network and this wave is compared with output of error amplifier which is taken as reference wave as shown in Fig 2 & 3. Hence duty ratio adjusted according to changes in input voltage[4].

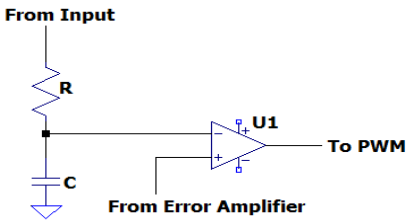

Fig 2. Duty cycle control using saw tooth and reference signal

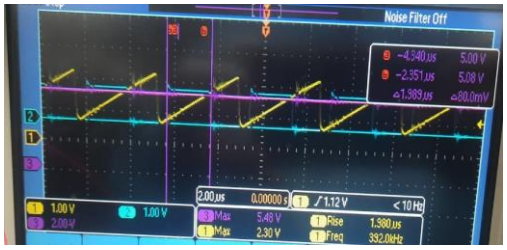

Fig.3 Duty cycles generated comparing saw tooth wave with output of error amplifier.

3.5. MAG-AMP DESIGN

A mag amp is a coil of wire wound on a core with a relatively square B-H characteristic [4]-[5]. This gives the coil two operating modes. When unsaturated, it does not allow current to flow and when saturated, it allows current to flow with zero voltage drop. The first task in design of mag amp is selection of proper core.

Core size is selected based on following area product method

$$A_p = \frac{Ax*A*}{\Delta B*K} 10^8 \ \ cm^4 \qquad (7)$$

Where,

i) ΔB : Flux excursion T ii) Ax : Wire area(One Conductor) in mm^2. iii) A: Required withstand area V-sec.

Selected core is **6-L2016-W763, Nanocrystalline Vitroperm 500Z, Square Loop Core**

3.6. OUTPUT FILTER DESIGN

The transformer's secondary voltage is rectified and filtered suitably to get the desired quality of output voltage waveform. The diode selected for rectification should have fast switching action and less reverse recovery time. Hence a suitable schottky diode is selected. The filter inductor and capacitor values need to be chosen optimally to arrive at a cost-effective, less bulky power supply. The filter capacitor merely supplies the ripple (ac) current of switching frequency. It has linear relation between the output voltage and the switch duty ratio, the inductor current is desired to be continuous. The L and C values are designed using following equations.

$$L = \frac{Vo*(1-Dmin)*Ts}{\Delta iL} \ H \qquad (8)$$

From above equation L1 = 12.1µH and L2 = 18µH are calculated values for master and slave outputs respectively.

$$C = \frac{1-Dmin}{8*L*Fsw^2*\delta Vo} \quad F \qquad (9)$$

Similarly C1 = 940µF and C2 = 470µF are the filter capacitances.

4. EXPERIMENTAL RESULTS

The Fig 4 a & b shows experimental set up and top view of the forward converter. The converter is powered up using DC voltage source and output is connected to an electronic load which measures the output voltage and load current. To measure ripple in the outputs a digital storage oscilloscope(DSO) is connected.

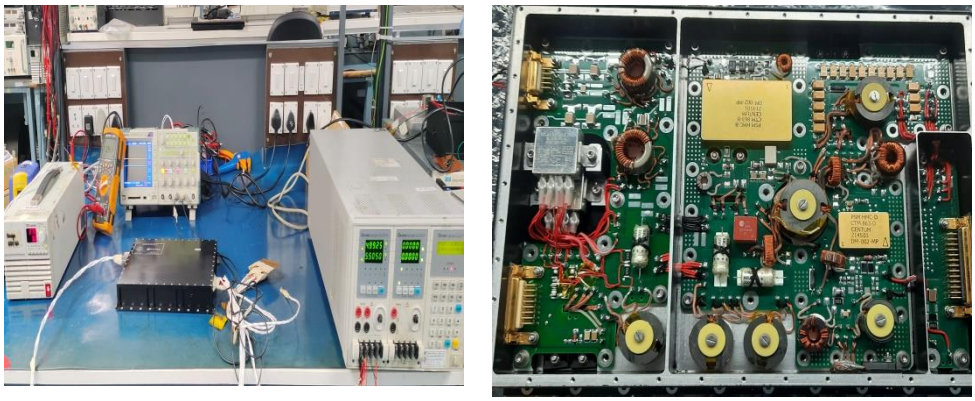

a b

Fig 4 a) Experimental Setup b) Top view of the forward converter.

The test results of the experimental prototype are shown in Table II, Table III, Table IV, Table V, Table VI and Table VII.

Table II. Outputs at full load(100%) condition

The measured outputs at full load condition are near to specified values and an efficiency greater than 65% is achieved.

V_{in} (V)	I_{in} (A)	V_{01} (V)	I_{o1} (A)	V_{02} (V)	I_{o2} (A)
24	4.653	5.468	12	4.971	2
36	3.111	5.472	12	4.974	2
42.5	2.656	5.547	12	4.98	2

Table III. Outputs at min load(10%) condition

Outputs at min load condition are measured and these values are nearly equal to the specified values since drop is less.

V_{in} (V)	I_{in} (A)	V_{01} (V)	I_{o2} (A)	V_{02} (V)	I_{o2} (A)
24	0.694	5.515	1.2	4.994	0.2
36	0.512	5.516	1.2	4.993	0.2
42.5	0.457	5.516	1.2	4.995	0.2

Table IV. Efficiency at different input voltages and full load

From table IV it can be seen that converter is designed to achieve efficiency greater than 65%.

Input Voltage(V)	Input Power(W)	Output Power(W)	Efficiency (%)
24	111.672	75.558	67.66
36	111.996	75.612	67.51
42.5	112.880	76.524	67.79

Table V. Line Regulation

With the use of feed-forward control method a line regulation <1% is achieved on both the outputs and it's shown in table IV.

	Line Regulation (%)	
Load	5.5V/12	5V/2A
100%	0.0144	0.0018
10%	0.0001	0.0002

Table VI. Load Regulation

The changes in the output voltage due to change in load current is less than the specified value (<±2%) and this is achieved by using post regulators mag-amps.

V_{in} (V)	Load Regulation (%)	
	5.5V/12A	5V/2A
24	0.0852	0.0046
36	0.0081	0.0038
42.5	0.0056	0.0003

Table VII. Ripple voltages in mV_{P-P}

The ripple is measured at full load condition for both the outputs and this value is less than the specified value($30mV_{p-p}$).

V_{in} (V)	5.5V	5V
24	18.8	13.6
36	13.2	20.8
42.5	20.4	14

The output ripple waveform at full load and maximum input voltage is shown in Fig 5. The ripple content in the first output is $18.8mV_{p-p}$ and in the second output is $13.6mV_{p-p}$, implying that the performance of the converter is improved with the use of output filter by limiting ripple value less than the specified value($30mV_{p-p}$).

For load transient response, the output-1 is kept at min load and output-2 load is varied from 50% to 100% and corresponding overshoot and undershoot are measured and these values are less than the specified value 275mV(5%) which is shown in below figure 6.

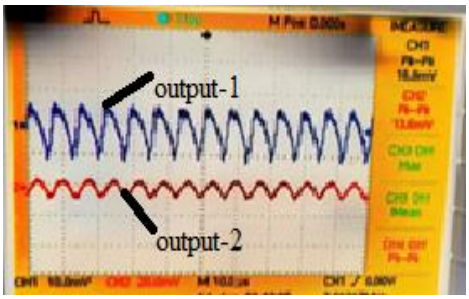

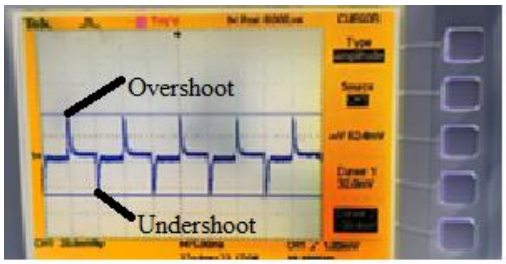

Fig.6 Load transient of output-2 at 36V

Fig 5 Output ripple waveform at full load and maximum input voltage(42.5V)

Output-1:5.5V/12A with Ripple =18.8mV

Output-2: 5V/2A with Ripple =13.6mV

input

Overshoot = 32mV ; Undershoot =30.4mV

Fig 7 shows the gate voltage and drain voltage values measured at nominal input voltage(36V). It can be seen that, the converter is operating at a specified frequency of 140kHz with a duty ratio of about 29.866%. With the use of LCD snubber, the spikes in the drain voltage(V_{DS}) are reduced and MOSFET can operate safely.

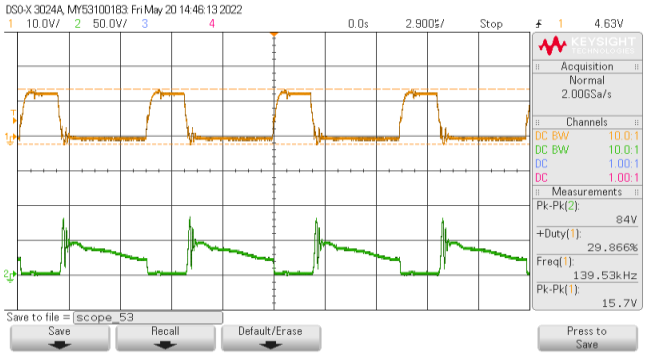

Fig 7. ■ Gate voltage and ■ Drain voltage(V_{DS}) at 36V input

7. CONCLUSION

The prototype model of the converter is designed and tested for all the selected specifications. Mag-amp regulation method gives better load regulation to regulate individual outputs. The voltage feed forward control method helps in meeting line regulation (< ±1%) as it gives fast dynamic response.

Acknowledgment

Authors are thankful to the Management, BMS Educational Trust, Principal and Vice Principal, BMS College of Engineering and Centum Electronics Ltd. for their continuous support.

REFERENCES

1] N. Lee, J. -Y. Lee, Y. -J. Cheon, S. -K. Han and G. -W. Moon, **"A High-Power-Density Converter With a Continuous Input Current Waveform for Satellite Power Applications,"** in IEEE Transactions on Industrial Electronics, vol. 67, no. 2, pp. 1024-1035, Feb. 2020, doi: 10.1109/TIE.2019.2898584

2] A. Bhat, K. U. Rao, Praveen P K, B. K. Singh and V. Chippalkatti, **"Multiple output forward DC-DC converter with regenerative snubber for space application,"** 2016 Biennial International Conference on Power and Energy Systems: Towards Sustainable Energy (PESTSE), 2016, pp. 1-5, doi: 10.1109/PESTSE.2016.7516487.

3] I. Shirsi, A. N. Nagashree, P. kumar Kulkarni, B. Singh, V. Chippalkatti and T. Kanthimathinathan, **"Self-resonant reset forward converter with dual-outputs for military application,"** 2012 IEEE International Conference on Power Electronics, Drives and Energy Systems (PEDES), 2012, pp. 1-6, doi: 10.1109/PEDES.2012.6484425.

4] A. Bhat, K. U. Rao, Praveen P K, B. K. Singh and V. Chippalkatti**,** "**Multiple output forward DC-DC converter with Mag-amp post regulators and voltage feedforward control for space application,"** 2016 Biennial International Conference on Power and Energy Systems: Towards Sustainable Energy (PESTSE), 2016, pp. 1-6, doi: 10.1109/PESTSE.2016.7516488.

5] Youhao Xi and P. K. Jain, **"A forward converter topology with independently and precisely regulated multiple outputs,"** in IEEE Transactions on Power Electronics, vol. 18, no. 2, pp. 648-658, March 2003, doi: 10.1109/TPEL.2003.809348..

6] N. Lee, T. -Y. Kim, J. -Y. Lee, S. -K. Han, T. -J. Chung and J. -D. Choi, "**Improved EMI noise performance by the reduced input ripple of the Satellite converter**," 2019 European Space Power Conference (ESPC), 2019, pp. 1-5, doi: 10.1109/ESPC.2019.8932057.

7] A. I. Pressman, **Switching Power Supply Design**. New York: McGrawHill, 1991, pp. 381–412**.**

Design and Implementation of 75W Mag-Amp Controlled Forward Converter for Communication System

Kalpana N[1], Shubha Kulkarni[2], B K Singh[3], Santosh B L[4], Prakash G[5]

[1] M.Tech, Dept of EEE, DSCE, kalpana.nmurthy@gmail.com
[2] Associate Professor, Dept of EEE, DSCE, shubha-eee@dayanandasagar.edu
[5] Engineer, Centum Electronics Ltd, prakashg@centumelectrnics.com

Abstract.

The application of DC-DC converter is booming in the field of power electronics design applications in this era. This paper elaborates the usage of forward converter with reset winding. The Magnetic-amplifiers(Mag-Amp) are used as a post regulator for the dual output to maintain the right output voltage and to maintain lesser ripple. Voltage feed forward has been implemented to improve the converter performance against fast changing input voltage. It is used to comply this converter for military standard. Basic design procedure and all the specifications are covered in this paper. The paper is focused on design and hardware implementation of voltage mode controlled dual output converter. The proposed converter delivers output of 6V/12A (output1) and 6V/0.5A (output2) and operates at switching frequency of 140 kHz. Voltage feed forward technique is implemented using UC2525 Pulse Width Modulation controlled circuit (PWM IC). It is aimed to achieve converter efficiency greater than 68%.

.

Keywords: DC-DC converter, Magnetic Amplifier, Voltage feed forward control, Forward converter, LCD Snubber, UC2525 PWM controller.

.

1. INTRODUCTION

In SMPS applications, forward converter topology has been used for low power applications ie.,100W to 200W. It's use can be found in military, aero-space, renewable energy, space application, automotive industries [1]. It is important to have high reliability than the efficiency for space missions. Single switch forward converter is implemented in this paper. It operates for an input DC voltage of 24V- 42.5V giving a dual output voltage of 6V/12A and 6V/0.5A. An inrush current limiter circuit is being placed at the input side to protect converter from high magnitude current when power supply is plugged in. The converter has a built in EMI filter to mitigate noise which is reaching converter as well as coming out of converter. Voltage feed-forward control technique is used to achieve good line regulation which gives an instantaneous response to the changes in the input voltage thereby adjusting the duty cycle. The voltage spikes on MOSFET are caused due to leakage inductance. An LCD (Inductor, Capacitor, Diode) snubber is used to protect the circuit against spikes [2].

2. SPECIFICATIONS AND BLOCK DIAGRAM

Table I Specification of the forward converter

Parameter	Specification
Input voltage	24V(min),36V(nom),42.5V(max)
Outputs	6V/12A, 6V/0.5A
Efficiency	≥ 68%
Line regulation	<1%
Load regulation	<2%
Operating frequency	140 ± 5kHz
Ripple Voltage	<30mV$_{p-p}$ (5%)
D_{max}	35%
D_{min}	20%

The Fig 1 represents the basic circuit diagram of the dc-dc converter and Fig 2 shows the complete block diagram of the mag-amp controlled forward converter, which includes EMI filter to mitigate noise coming from the converter as well as to the converter. Inrush current limiter circuit, limits the input current on application of ON command with 100% load to less than the twice of input current. Current sense circuit protects converter from over current or short circuit current. The duty cycle of the switch is controlled using voltage feed forward technique, Start-up circuit provides power supply to the IC's. PWM controller turns ON and initiates GATE pulses at switching frequency of 145±5 kHz.to primary side of MOSFET. The rectifier circuit and output filters are used to get the rectified output voltage with ripple less than 30mV$_{p-p}$. To achieve the load regulation less than 2% mag-amps are used as post regulators. Over voltage protection circuit does not allow output voltage to exceed 120% of the actual output.

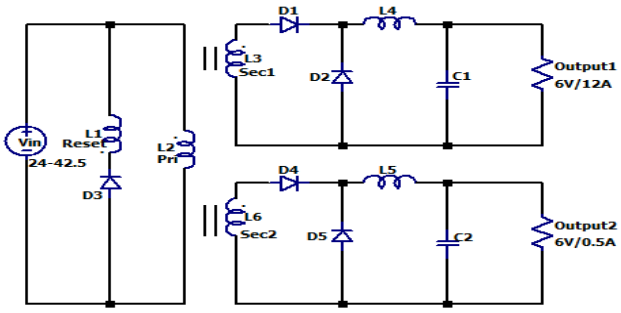

Fig 1. Basic Circuit of the forward converter

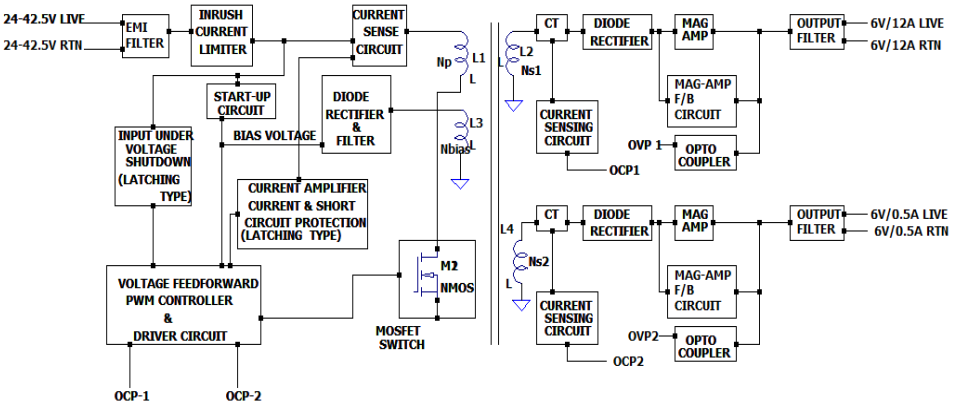

Fig 2. Block Diagram of the forward converter

3. DESIGN PROCEDURE

The above specifications are used in designing prototype model of the converter. In this section a) design of transformer, b) criteria for MOSFET selection and snubber design, d) mag-amp design and e) output filter design are explained

3.1. Voltage Feed Forward

Variations in input voltage affect the overall performance of the circuit through duty cycle variations. In order to avoid that there must be a loop which corrects the duty cycle, so that even though there is a change in the input voltage the output voltage is not affected [3]-[4]. The voltage feed forward mode of PWM control is used which adjusts the duty ratio according to the changes in the input voltage. This type of feed forward technique uses RC network to generate saw tooth waveform using input voltage which is shown in the Fig 2 & 3. As the input goes high or doubles, the slope of the comparator will also doubles which causes the duty cycle will immediately be halved. This type of duty cycle correction is very much important for circuit in order to wait for an error amplifier to detect the error in the output voltage.

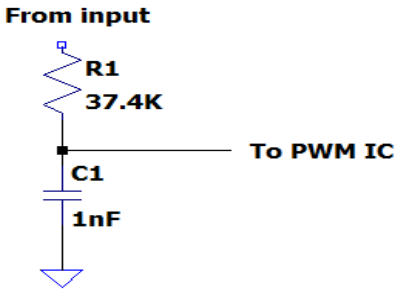

Fig.2 RC network for saw tooth wave generation.

Fig.3 Saw tooth wave generated using RC network

3.2. Transformer Design

For designing transformer area product must be calculated. Usually, a core is selected based on the area product method and it's calculated using equation (1).[4]-[5]

In a forward converter area product is given by:

$$A_P = \frac{\sqrt{D}\,.P_{out}.\left(1+\frac{1}{Eff}\right)}{K_w\,.\,J.\,10^{-6}\,B_m\,.Fsw} \quad (1)$$

A_p = Area product of the core (mm^4); K_w = Window factor ; Pout = Output power (W)
J = Current density (A/mm^2): D_{max} = Maximum Duty cycle; B_m = Maximum flux density (T) ; F_{sw} = Switching frequency (Hz).

For ferrite core Kw = 0.35, Bm= 0.12T, J=6A/mm^2

$$A_p = \frac{\sqrt{0.4}.75.(1+\frac{1}{0.65})}{0.3.6.10^{-6}\,.0.12.140.10^{3.}} = 3378.67\ mm^4$$

Referring to the ferrite core catalogue, an appropriate core is selected which has area product greater than the calculated value and better power handling capacity at converter operating frequency. Therefore, the selected POT core is **OR43019UG** which is having an **A_L=6680nH/1000Turns**.

3.3. MOSFET Selection and Snubber Design

Parameters to be considered for selection of MOSFET are drain to source voltage(V_{DS}), gate to source voltage(V_{GSth}) required to turn it on, continuous drain current(I_{Dmax}), drain to source ON resistance (R_{DS}(on)), input capacitances(C_{iss}) and output capacitances(C_{oss}). The stress on the MOSFET is calculated using equation (2)

$$V_{peak\text{-}MOSFET} = V_{in\text{-}max}\left(1+\frac{Npri}{Nreset}\right) \quad (2)$$

IRHM57260 is selected which has V_{DS} = 200V, $R_{DS\ (on)}$= 49mΩ, I_{Dmax} =35A and $V_{GS(th)}$=2V.

Leakage inductance and resistance causes spikes in voltage and current. This introduces electrical stress on the switching device. So therefore, an LCD snubber is designed to protect switch against these spikes. It consists of two diodes, inductor and capacitor. Based on area product calculation, the core is selected for inductor [5].

$$A_P = \frac{Lsnubber * Iout^2 * (1+\frac{K}{2})}{Kw*Bm*J*10^{-6}} \quad (3)$$

Selected core is **C055291A2** with **$N_{snubber}$ = 7T**.

3.4. Mag-amp Design

Mag-amp is a controlled switch which uses an inductive element [5]. It has a square BH curve characteristic. Basically, it operates in two different modes they are saturated and unsaturated. When it operates in a saturated mode, at that time leakage impedance will be

less, producing current to flow through it with less or no voltage drop. But when it operates in unsaturated mode, core makes coil to operate as a high inductance, capable of supporting high voltage with minimum or zero current flow. One of the significances of mag-amp is that load current doesn't determine the reset, but the reset is determined by the core and number of turns as mag-amp is inductive element.

There are additional requirements for selecting the core material, they are [6]

- Regulator output voltage.
- Maximum output current,
- Input voltage waveform including limits for both voltage amplitude and pulse width
- The maximum volt-seconds called the "withstand Area"

The core size is decided by area product method as

$A_p = \frac{Ax*A*10\text{^}8}{\Delta B*K}$ cm^4 (4)

A_x = Wire Area (One Conductor) (mm^2); ΔB = Flux excursion (T)

K= Fill factor ; A= Required withstand area (V-sec)

Selected core is **P/N 6-L2016-W763, square loop core.**

The purpose of designing a control loop is to provide good regulation of the output voltage, not only from a DC standpoint, but in the transient case as well.

3.5. Output filter Design

An output filter basically consists of Inductor (L) as well as Capacitor (C). By assuming optimum ripple values for inductor current and output voltage for L & C respectively we can design the output filter [4].

$L = \frac{Vo*(1-Dmin)*Ts}{\Delta iL}$ H (5)

$C = \frac{1-Dmin}{8*L*Fsw^2*\Delta Vo}$ F (6)

Therefore,

L1 = $8.1*10^{-6}$ H; C1 = $846*10^{-6}$ for the filter elements of 6V/12A &

L2= $18*10^{-6}$ H; C2= $376*10^{-6}$F for the filter elements of 6V/0.5A.

4. PRACTICAL ASPECTS AND TEST RESULTS

The Fig 4 & 5 shows top view and experimental set up of the forward converter. The converter is powered up using DC voltage source and output is connected to an electronic load which measures the output voltage and load current. To measure ripple in the outputs a digital storage oscilloscope(DSO) is connected.

Fig 4 Top view of the converter

Fig 5 Overall hardware setup of the converter module

Test results of the proposed forward converter are shown in Table I, Table II, Table III, Table IV and Table V.

Table I .Input and output parameter measurement at full load (100%)

Input Voltages(V)	**Input Current(A)**	**Output parameters**		**Ripple Voltage (mVp-p)**	
		O/P-1 (6V/12A)	O/P-2 (6V/0.5A)	O/P-1 (6V/12A)	O/P-2 (6V/0.5A)
24	4.498	5.974	6.029	12.4	6
36	3.001	5.984	6.031	14.4	6
42.5	2.567	5.987	6.027	14	6

Table II. Output parameter measurement at min load (10%)

Input Voltages(V)	Output parameters		Ripple Voltage (mVp-p)	
	O/P-1 (6V/1.2A)	O/P-2 (6V/0.05A)	O/P-1 (6V/1.2A)	O/P-2 (6V/0.05A)
24	5.999	6.03	9.6	4
36	5.998	6.032	10.4	3.6
42.5	5.998	6.031	10.8	4

Table III. Efficiency at different input voltages are shown.

Input Voltage (V)	Output Power (W)	Input Power (W)	Efficiency (%)
24V	74.7025	107.952	69.19
36V	74.8235	108.036	68.98
42.5	74.8575	109.097	68.61

Table IV. Shows line regulation at max and min load condition

Load	Line Regulation (%)	
	6V/12	6V/0.5A
100%	0.0021	-0.0033
10%	-0.0001	0.0001

Table V. Shows load regulation at different input voltages

V_{in} (V)	Load Regulation (%)	
	6V/12A	6V/0.5A
24	0.234	0.017
36	0.084	0.033
42.5	0.017	0.033

5. WAVEFORMS

The Fig 5 shows inrush current waveform at an input voltage of 42.5V. The maximum inrush current is 4.24A, which lasts for duration of 5.8msec and the time taken to reach maximum value is about 2.181msec.

The sudden or sharp changes happening on the power line due to abrupt changes in the load or power supply is known as turn on transient. Fig 6, shows turn on transient waveform at 24V input. It reaches steady state output voltage value of 6V in 4msec.

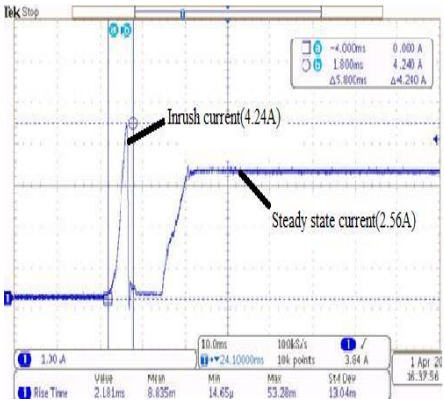

Fig 5 Inrush Current at maximum input voltage (42.5V) and duration of inrush is 5.80msec

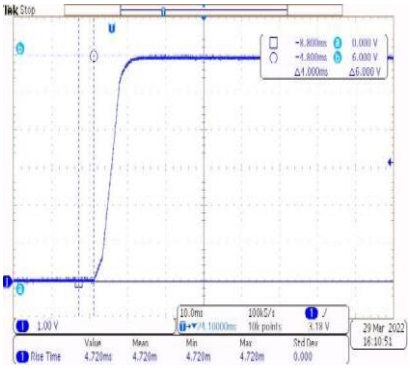

Fig 6 Turn on transient at minimum input voltage (24V)

The ripple voltage waveforms of the dual outputs at 36V input and full load condition is shown in Fig 7. The channel-1 denotes ripple output voltage of 6V/12A and channel-2 denotes ripple output voltage of 6V/0.5A. The measured ripple output voltage is less than the specified value ($30mV_{p-p}$). The ripple in the outputs is reduced using LC filter.

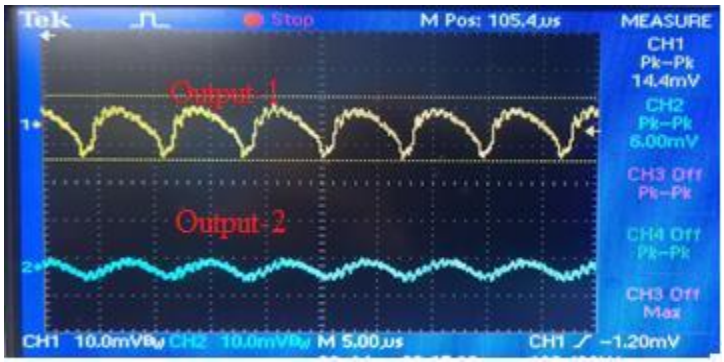

Fig 7 Ripple at full load condition .Output 1-14.4mV; Output 2-6mV

The transient response of the output voltage due to load fluctuation is known as load transient. Fig 8 & Fig 9 shows the load transient response of the outputs 1 and 2. The measured values are less than the specified value of 300mV(5%).

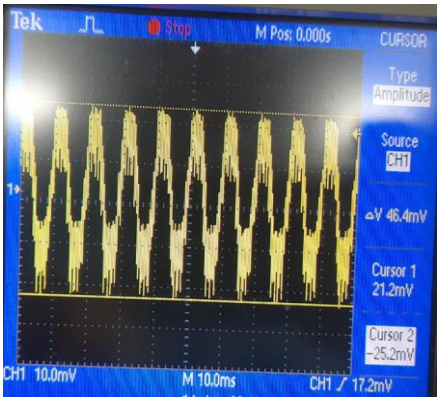

Fig 8 Load Transient of output 1

Overshoot = 21.2mV ; Undershoot = 25.2mV

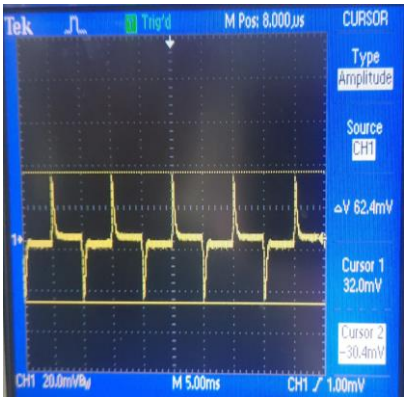

Fig 9 Load Transient of Output 2

Overshoot = 32.0mV ; Undershoot = 30.4mV

CONCLUSION

The converter is tested satisfactorily for all the specifications mentioned. The mag-amp is used as post regulator, which helps in maintaining good load regulation. The results show that, line regulation within the specification is achieved using voltage feed forward control technique. Feedback circuit on each output regulates the output voltages within the limit. Overall, all the necessary conditions are met and the converter underwent all the tests for the proposed application.

ACKNOWLEDGEMENT

Authors are thankful to the Management, Principal and Vice Principal, Dayananda Sagar College of Engineering and Centum Electronics Ltd. for their continuous support.

REFERENCES

[1] Youhao Xi and P. K. Jain, "**A forward converter topology with independently and precisely regulated multiple outputs**," in IEEE Transactions on Power Electronics, vol. 18, no. 2, pp. 648-658, March 2003, DOI:: 10.1109/TPEL.2003.809348.

[2] N. Lee, J. -Y. Lee, Y. -J. Cheon, S. -K. Han and G. -W. Moon, **"A High-Power-Density Converter with a Continuous Input Current Waveform for Satellite Power Applications,"** in IEEE Transactions on Industrial Electronics, vol. 67, no. 2, pp. 1024-1035, Feb. 2020, DOI: 10.1109/TIE.2019.2898584

[3] A.I. Pressman, **Switching Power Supply Design**. New York: McGraw-Hill, 1991, pp. 381–412

[4] Bhat, K. U. Rao, Praveen P K, B. K. Singh and V. Chippalkatti, "**Multiple output forward DC-DC converter with Mag-amp post regulators and voltage feedforward control for space application,**" 2016 Biennial International Conference on Power and

Energy Systems: Towards Sustainable Energy (PESTSE), 2016, pp. 1-6, DOI: 10.1109/PESTSE.2016.7516488.

[5] N. L, L. Venkatesha and N. J, **"Design and Implementation of a Separate Control Driven High Current Synchronous Rectified Forward Converter with Non-Dissipative Snubber Reset,"** 2019 Global Conference for Advancement in Technology (GCAT), 2019, pp. 1-6, DOI: 10.1109/GCAT47503.2019.8978437.

[6] **Magnetic amplifier control for simple, low cost, secondary regulation** by Bob Mammano.

Development and Simulation of 48V Li-ion Battery management system for Electric vehicles

Guruprasad Naik G[1], R Harshavardhan Reddy[2], Dr. V Champa[3]

[1]*Department of EEE, BMSCE, Bengaluru, India*

[2]*Senior design Engineer, Rohm semiconductor India, Bengaluru, India*

[3]*Associate professor, Department of EEE, BMSCE, Bengaluru, India*

Email: guruprasad.epe20@bmsce.ac.in

Abstract.

Battery Management Systems (BMS) are being utilized in many commercial systems to use the battery efficiently and estimate battery state to enhance the life of battery and limit it entering destructive state. For this purpose, some very important monitoring techniques are employed to monitor the state of charge of battery, temperature and current. The proposed project, Battery management system for battery powered Electric Vehicles (EV) evaluates the battery performance like temperature, charging/discharging current, State of Charge (SOC) and other battery parameters. The system supports 16 Series cell battery pack of voltage up to 48V.

Keywords— Battery management system, Cell balancing, fault detection, state of charge, state of health, Analog Front End (AFE).

1. INTRODUCTION

Automobiles exhaust is one of the key contributors for air pollution in the atmosphere. The main agenda of the electric vehicles, concerns about air pollution caused by petroleum vehicles exhaust emissions. Electric vehicles are the future of transportation and are equipped with batteries and can be re-charged with electricity. The batteries supply the energy required for the electric motors to propel the vehicle forward using a series of propulsive electric motors. Plug-in Hybrid Electric Vehicles (PHEVs), Hybrid Electric Cars (HEVs), and Battery Electric Vehicles (BEVs) are the three primary types of electric vehicles (EVs) categorised by the degree to which electricity is used as a source of energy. The interest in EV batteries can be traced back to the mid-19th century when the first EV came into existence. The most prevalent electrical energy storage device for EVs is batteries.

The lithium ion batteries are very sensitive in nature as they should not be over charged, over discharged and should not be operated at high temperature. So, these batteries should be monitored to make it to operate in specified working environment. In electric vehicles, a battery management system (BMS) monitors the battery's operation and status, as well as to protect the battery. So, BMS can be used for smart battery management and maintenance. For electric vehicle batteries, BMS needs to monitor battery status to avoid over-charging and over-discharging of the battery, estimate SOC and SOH to prolong battery life.

2. LITERATURE SURVEY

The architecture of BMS has 3 main components i.e., the BMS IC and Microcontroller (8 bit/16bit) and battery pack [1]. BMS senses the cell parameters like, voltage and current measurement, cell balancing during charging and discharging, Over Voltage, Under Voltage, Over Current.

Type Energy	Efficiency (%)	Energy Density (Wh/kg)	Power Density (W/kg)	Cycle life (Cycles)	Self-discharge
Lead-acid	70 - 80	20 – 35	25	200 – 2000	Low
Ni-Cd	60 – 90	40 – 60	140 – 180	500 – 2000	Low
NI-MH	50 – 80	60 – 80	220	3000	High
Li-ion	70 – 85	100 – 200	360	More than 2000	Medium
Li-polymer	80-90	200	250 – 1000	More than 1200	Medium
LFP	90	325	260	More than 1200	Negligible
Fuel Cell	50 - 80	250 - 350	800 – 1200	More than 2000	Negligible
Super Capacitors	95	0.3 – 0.5	2500	More than 30 000	high

Table 1: Battery characteristics.

The table 1 shows the characteristics of various battery chemistries [6] and Li-ion batteries are widely utilized in applications such as electric automobiles and electric bicycles because of their high energy density, low discharge rate, high cell voltage, and lack of memory effect. Furthermore, the SOC and internal impedance of the battery cells constantly vary. This means that if the weak cell reaches the protection limit while the remaining cells in the series continue to power the system, the battery pack will no longer be usable. This will reduce the battery pack's capacity and efficiency.

Individual battery cells are combined to form a pack in this article, which presents a unique battery management method. As a result, each battery is individually monitored in order to increase the Li-ion battery pack's dependability and capacity. Due to their high energy density, high charging and discharging efficiency, and other qualities, lithium batteries are increasingly being preferred over lead acid batteries by electric bicycle manufacturers [6]. The battery management system can continuously monitor the voltage, current, temperature, energy storage, and Health of the battery pack, as well as communicate data to the Application end user.

3. BATTERY MANAGEMENT SYSTEM

Battery management system is an efficacious electronic system that monitors the single cell and whole pack, connected in series and parallel combination and loaded with algorithms to protect the cells and battery pack from being operated outside its safe operating region and monitoring its state, cell balancing, reporting that data, calculating data, controlling its operation depending on real-time parameters.

Parameters calculated are:

▪ **SOC (State of Charge):** The ratio of remaining charge in the battery to the total charge/ maximum charge of the battery is defined as the **State of Charge**. This algorithm is used to estimate the percentage of the battery charge available for the usage. This can be calculated by monitoring the cell voltage, coulomb counting, by estimating depth of

discharge (DOD) and Kalman filter method. SOC estimation depends on types of electrolytes used in battery, operating condition, internal resistance (increases with aging), Battery aging, temperature change. SOC can be estimated by equation mentioned below.

$$\textbf{SOC} = \frac{\text{capacity remaining}}{\text{total capacity}} = \text{SOC}(t_0)\text{-}(\int \frac{I(t)}{Capacity} dt)$$

▪ **SOH (State of Health):** The ratio of present battery capacity to the total charge/ battery capacity at beginning is defined as the **State of Health**. The health of the battery depends on the environment which pack being used and its aging. The conditions that are affecting the battery health should be monitored and rectified to enhance the battery life. SOH can be estimated by equation mentioned below.

$$\textbf{SOH} = \frac{\text{present total capacity}}{\text{capacity at beginning}}$$

▪ **SOE** (**State of Envelope**): It is the operating area with respect to voltage, current and temperature boundary. This helps detecting fault, which helps to increase the battery life and hence the health of the battery maintained well.

• **Safety and fault management:** It is related to SOE, which defines the algorithms like SOA (Safe operating area), operating area within voltage, current and temperature limits.

Other operations of the battery management system are to provide Cell balancing, estimating the DOD, limiting C-rate, preventing thermal run away, as these may affect the performance.

4. PROPOSED METHOD

Usually a BMS consists of Battery pack, BMS IC, MCU and switches connected to load [2][3][6]. Fig 1 shows the block diagram of the Battery management system and it consists of the battery pack connected to the battery management IC (ML5238 by LAPIS) through discharging resistors. On the low side of pack, FETs for the charging and discharging are connected.

The microcontroller (ML62Q1367) monitors the battery parameters continuously and makes sure that battery is operating in safe operating area. The load and charger are connected at same terminal but the BMS IC decides whether it has to charge/discharge the battery.

ML5238 (BMS IC) is an Analog Front End IC for 16 series Lithium Ion battery pack protection system [8]. ML5238 has built-in SPI communication feature and provides functionalities like of cell voltage monitoring, cell balancing, charge/discharge current monitoring function, and it can detect over charge, over current and over discharge. This also provides built-in short current detecting function which can turn off the external charge/discharge MOS-FET without external MCU.

ML62Q1367 (MCU) is 16-bit RISC CPU microcontroller [7], which can operate at 16 MHz clock frequency, supports SPI communication and is chosen as the controller for the system.

MCU monitors the BMS IC continuously to monitor the battery parameters [9].

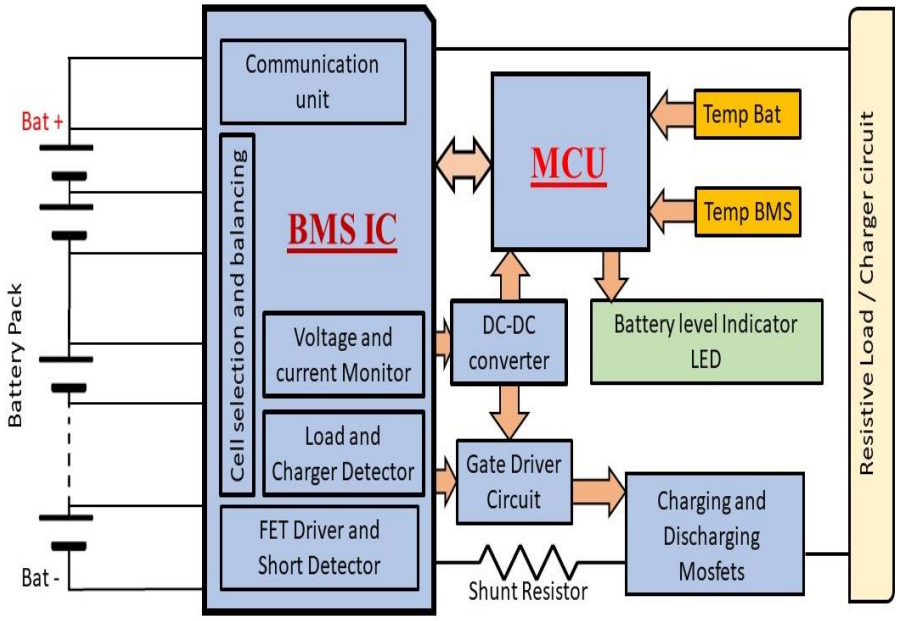

Fig 1: Block Diagram of BMS.

BMS IC monitors the voltage of each cell in the battery pack and estimates the battery pack voltage and current flowing in and out of the battery pack and outputs to the MCU. The MCU retrieves the voltage and current parameters from the BMS IC and estimates the lowest cell voltage in the battery pack. The MCU writes into the BMS IC to perform the cell balancing for high voltage cell, to make charge equal throughout the pack. MCU reads the voltage of cells from the BMS IC and estimates the SOC of the battery pack. Communication between the MCU and BMS IC happens by SPI protocol.

MCU retrieves the status of load and charger connection from the BMS IC. Depending on our requirement and the battery voltage level, MCU makes the BMS IC to generate gate signal for the FET's by considering whether it has to charge or discharge. Also, the MCU performs the temperature monitoring of the entire system including the battery pack.

Buck regulator IC, BD9G341AEFJ, brings down the battery pack voltage to the level required for the operation of Gate diver IC - BD2310G, which generates the gate pulses for

Charging and Discharging MOSFETs. The output from the buck converter is also used for generating 5V using Low Dropout Regulator (LDO - BD433M2FP3).

Fig 2 represents the flowchart of the Battery management system for method proposed, which also shows the firmware [5] operation sequence.

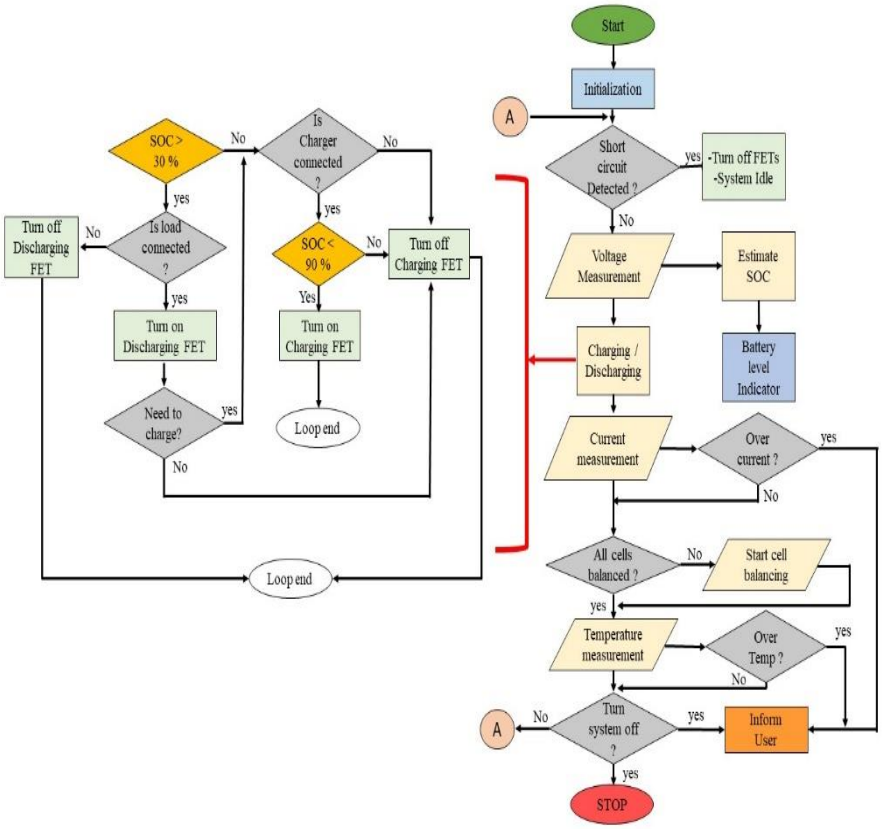

Fig 2: Flowchart of firmware for BMS

5. HARDWARE

The hardware circuitry consists of two boards: A Digital board (low voltage board) and a power board (high current board). In fig 3, The digital board (left side board) includes cell monitoring, discharging resistors, AFE BMS IC, DC-DC converter, the microcontroller and the gate driver circuit. The power board (right side board) includes the charging and discharging Mosfets and current sensing resistors.

In fig 3, Section 1 shows the cell monitoring section and the discharging resistors for the cell balancing. Battery pack of 16 series cells is connected for battery monitoring through the discharging resistors to consume 130mA (200 mA - max) current while cell

balancing. Section 2 shows the BMS IC, where cells to be monitored are connected. Section 3 shows the gate driver for driving the charging and discharging FETs. Section 4 shows the DC-DC step down converter to drop battery pack voltage to the voltage level for the gate driver and for the MCU power up and Section 5 shows the MCU used for controlling the BMS IC with the set of algorithms written into it.

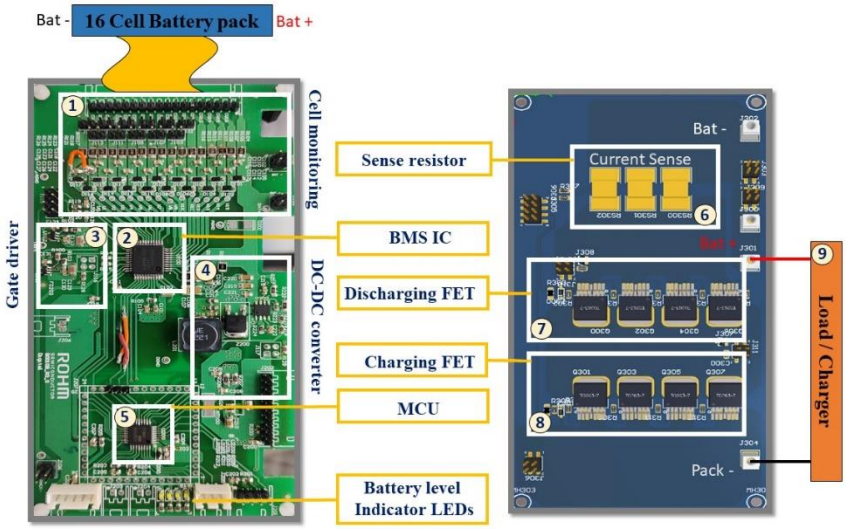

Fig 3: Hardware rig-up of BMS using ML5238.

Metal clad copper PCB board of 115µ thickness is used for the power application section of the BMS, which has high current carrying capability up to 200 A. Section 6, shows the current sensing resistors connected in parallel. Here, 5Ω is used as current sensing resistor, as testing is carried out to sense the low current [4]. Section 7 and 8, shows the MOSFET used for the charging and discharging. The Mosfets used can handle up to 100V voltage and 200A current. section 9, shows the load/charger connected to the power board.

6. SIMULATION

Simulation circuit is designed for the 48V BMS in MATLAB Simulink. The circuit can perform real-time monitoring of battery cell voltage, cell balancing and charging and discharging as per our requirement. Bi-directional converter is used between the battery and the charger/load for efficient charging and discharging process [3]. The simulation circuit is shown in fig 4 below. Two 24 V battery packs are chosen and set to operate as lithium-ion battery chemistry. Every pack is connected to the discharging resistors through the Mosfets for cell balancing.

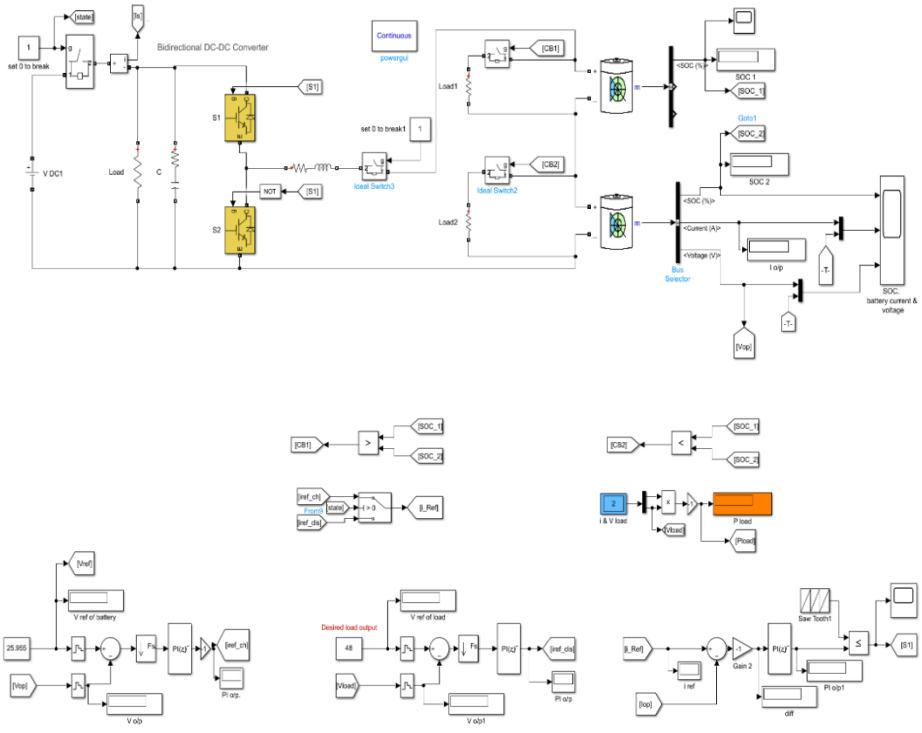

Fig 4: Simulink model for BMS.

7. RESULTS AND DISCUSSIONS

8.1.1 Hardware

The system designed for the battery management can perform the real-time monitoring of the Battery pack and each cell of pack for its voltage measurement, cell balancing, current and temperature monitoring. The BMS limits the battery pack from being over charged and discharged and make it to operate in the safe operating area. Fig 5 shows the voltage monitoring of each cell and current of the pack. The BMS system also indicates the remaining charge (SOC) of the battery by LED indicators.

0.5 mA -Current measured by the sense resistor in mA.

Note: A battery pack of 8 cells, 27V voltage is used for testing purpose.

Expressions

Expression	Type	Value	Address
(x)= Isense	float	5.06520092e-01	0xef84
(x)= V8	float	3.35074210e+00	0xefd8
(x)= V9	float	3.43617177e+00	0xefdc
(x)= V10	float	3.42667961e+00	0xefe0
(x)= V11	float	3.44566417e+00	0xefe4
(x)= V12	float	3.24632812e+00	0xefe8
(x)= V13	float	3.44566417e+00	0xefec
(x)= V14	float	3.44566417e+00	0xeff0
(x)= V15	float	3.42667961e+00	0xeff4
(x)= Vtotal	float	2.72235947e+01	0xef8c

Represents the voltage of each cell and Vtotal represents the Total pack voltage

Fig 5: ADC voltage reading of cells

How proposed method is different from the existing? – The BMS IC used in this work supports 16 series Li-ion cells and consume less power in its normal state and power down state when compared to other IC's. The IC provides the separate bits for increasing the gain of the parameters measured, so, the small values can be measured very accurately and increase the protection of the battery. It has built-in function to detect the short circuit and if short circuit is noticed, BMS IC will turn off the charging and discharging Mosfets without instruction from the MCU. This has become the independent operation for protection.

8.1.2 Simulation

Circuit designed in the MATLAB can perform cell Voltage monitoring, cell balancing function and current measurement function. Fig 6 shows the plot of the SOC decreasing and current consumed by the load.

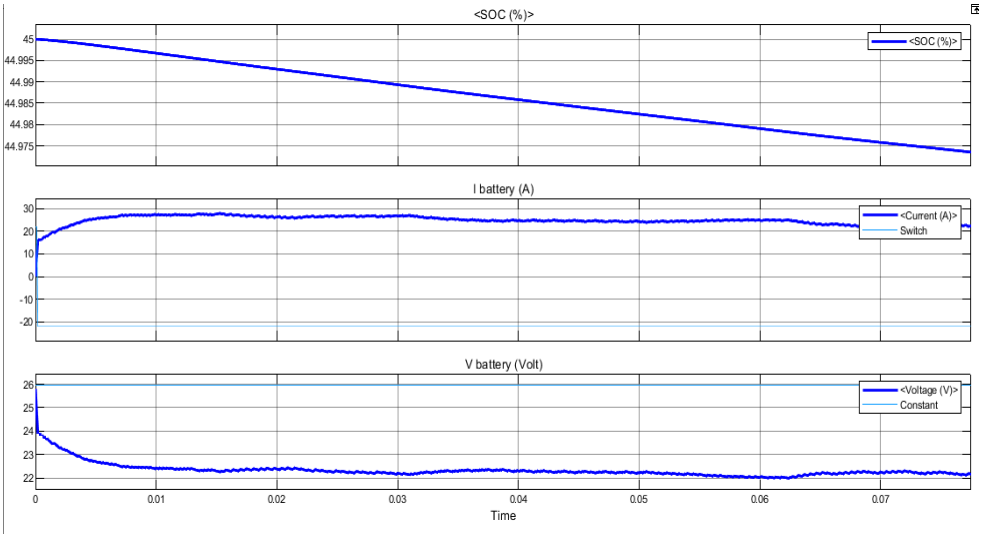

Fig 6: SOC, current and voltage of the battery.

The simulation is carried out with operational logic of BMS IC and the microcontroller and the hardware is carried out with large resistive load (compared with simulation) to limit the current drawn from the battery pack. The above figure shows the discharge waveform of the battery pack with current drawn up to 30A with slight sag in the voltage and when discharging is stopped, voltage comes to normal (voltage will be decreased over time, as it is in discharging state). The voltage sag of 2V is observed, as every source has current limitation, if current drawn exceeds that limit, supply voltage decreases to match the power delivery and when load is disconnected, voltage comes back to actual terminal voltage of the pack at that time after discharging.

It is observed that the hardware and simulation designed for 48 V battery management system performs the on demand basic operations of BMS efficiently and the parameters estimated in the hardware are also obtained from the simulation accurately.

8. CONCLUSION

In this work, Battery Management system used in EV applications is simulated and tested the hardware topology for functionalities like, operation and safety. In this research, our primary focus was to develop hardware to implement all the basic functionalities for a battery management system. The desired area of application is automotive sector and all the algorithms and designs were considered for the same. Ample literature survey was conducted initially to understand the requirements of a battery management system for EV's and based on the that information a basic BMS hardware was developed. The hardware and firmware prioritize better battery usage and thereby maintaining good battery health.

In the hardware section, the Analog Front End IC was integrated with various sections like a microcontroller, DC-DC converter, Charging and discharging FET's, Fuel gauge, temperature sensor and a SPI interface. Features like cell voltage and current monitoring, Cell balancing, Temperature monitoring and charging/discharging were controlled by firmware. The designed system can be configured for a 48V battery EV by considering the operating environment.

ACKNOWLEDGEMENT

I sincerely thank ROHM Semiconductor India for providing me the opportunity to utilise their labs and support me with their virtuosity in the subject. It has greatly assisted in the execution of this research.

9. REFERENCES

[1]. M. Brandl et al., "*Batteries and battery management systems for electric vehicles*" 2012 Design, Automation & Test in Europe Conference & Exhibition (DATE), 2012, pp. 971-976, doi: 10.1109/DATE.2012.6176637.

[2]. Yeqin Wang and Yixing Liu, "*Electronic control system design and test of pure electric vehicle battery management system*" 2011 Second International Conference on Mechanic Automation and Control Engineering, 2011, pp. 1289-1292, doi: 10.1109/MACE.2011.5987178.

[3]. A. Zhang, S. Song, C. Wang, J. Zhang, K. Wang and L. Li, "*Research of battery management system for integrated power supply*" 2017 Chinese Automation Congress (CAC), 2017, pp. 3178-3181, doi: 10.1109/CAC.2017.8243323.

[4]. Y. Xu, S. Jiang and T. X. Zhang, "*Research and design of lithium battery management system for electric bicycle based on Internet of things technology*" 2019 Chinese Automation Congress (CAC), 2019, pp. 1121-1125, doi: 10.1109/CAC48633.2019.8997319.

[5]. J. Xue, C. Yan, D. Wang, J. Wang, J. Wu and Z. Liao, "*Adaptive Dynamic Programming Method for Optimal Battery Management of Battery Electric Vehicle*" 2020 IEEE 9th Data Driven Control and Learning Systems Conference (DDCLS), 2020, pp. 65-68, doi: 10.1109/DDCLS49620.2020.9275259.

[6]. Adeepa. (2016). "*Electric Vehicle Battery Management System*". 10.13140/RG.2.2.24440.03847.

[7]. ROHM Semiconductor, "*General purpose 16-bit MCU*", ML62Q1367 datasheet, July. 2020.

[8]. ROHM Semiconductor, "16 Series Li-ion secondary battery pack protection, AFE IC", ML5238 datasheet, July. 2013.

[9]. Texas Instrument, Scalable Automotive HEV/EV 6s to 96s Lithium-Ion Cell Supervision Demonstrator Reference Design

Performance Analysis of Boost and Interleaved Boost Converter with a novel switching technique

Abhishek G A[1], R S Geetha[2]

[1]*M.Tech Student, Power Electronics, Department of EEE, B.M.S.C.E, Bengaluru, India.*
[2]*Professor, Department of EEE, B.M.S.C.E, Bengaluru, India.*

Email: abhishek.epe20@bmsce.ac.in

Abstract.

The Boost Converters are extremely used in today's world, especially in the high-power application such as household applications and automotive converters. Interleaved Converters are another topology of DC-DC converters. With the use of Interleaved Boost Converter, the size of the passive components of the circuit can be significantly reduced and thus voltage stress across the switches can be reduced. With increased number of phases, the stress on the switches and component size can be further reduced. In this paper, comparison of closed loop Conventional Boost Converter (CBC) and Interleaved Boost Converter (IBC) is carried out with a novel switching technique applied for the IBC.

Keywords: DC-DC Converter, Boost Converter, Interleaved Boost Converter, PI controller, Switching Technique.

1. INTRODUCTION

DC-DC Converters are more widely used converters in day-to-day applications. These converters are used in Automobile industry, in mobiles and laptop charging devices. DC-DC converters are those, which are used to get desired DC output with different DC-DC converter topologies such as Buck Converter, Boost Converter, Buck-Boost Converter etc.

In Conventional Boost, the output voltage rating depends upon the duty ratio of the switch. These are used in Hybrid Vehicles or Electric Vehicles and High-power applications. The duty ratio should be very high to provide desired output with large passive circuit components. This results in higher input current and output voltage ripple. With use of Interleaved Boost Converter, these problems can be reduced. Inductor and capacitor can be split into number of phases, which reduces the switching losses and size of the circuit components. With inductors connected in parallel, input current is shared between them and reduces the stress on switches.

Multiphase converter topologies that are used in high performance and low voltage applications have been increasing in recent years [1]. With the rise in the pollution and climate change, there is an increased demand for green energy. Hence, the need for Electric Vehicles is increasing, for which DC-DC converter are needed to step-up and step-down the energy from the battery and supply to the motors [2]. The Electric Vehicles can be classified as Battery Electric Vehicle (BEVs), Hybrid Electric Vehicles (HEVs), and Plug-in Electric Vehicles (PHEVs) [2].

Interleaved DC-DC Boost converters have gained prominence in modern automotive industry as attempts are being made to replace mechanical and hydraulic systems with their electrical counterparts [3]. As the electrical systems undergo technological revolution with power electronics as one of the driving forces, leaps have been made in terms of system efficiency, reliability and safety. The interleaved boost converter is a desirable DC-DC converter topology in applications that require less ripples in input current and output voltage when compared with that of a conventional boost converter. In this converter topology, the input current is shared between the two parallelly connected interleaved inductors [4]. In applications such as EV, HEV etc., the ratio of the output voltage to the input voltage, for a step-up DC-DC converter, could be as high as 6. Such a step-up ratio is obtained by the proper tuning of the duty ratio of the power semiconductor switch and, in effect, through an efficient power converter design. In the interleaved boost converter topology, the voltage across the switch and the on-state losses are reduced [5]. This is accomplished by collecting the energy leaked from the interleaved converter and storing it in the clamped capacitor. This stored energy is later discharged to the load by the clamping boost converter. In [6], the author discusses about the interleaved DC-DC converter for electric vehicle charging application. Here the adaptive neuro-fuzzy inference system (ANFIS) approach has been employed. Such an approach to provides better stability and system performance under transient operating conditions. Simulations and analysis of the same were also presented. In [7], a novel technique of soft-switching interleaved boost converter was discussed. This converter consists of two boost converters connected in parallel along with an auxiliary inductor. In this converter topology, the output voltage ripples are reduced by turning on both the active power switches at zero voltage. Multi-device structure topology reduces the input current ripples, output voltage ripples, and the size of the overall converter design. This topology employs interleaved control strategy and is found to yield better efficiency in relation to the other converter topologies. This performance of the interleaved converter is compared to the conventional boost converter in [8]. A novel power-factor corrected (PFC) boost converter that has two inductors interleaved is discussed in [9]. This converter when operated with duty ratio above 0.5, displays voltage-doubler characteristic.

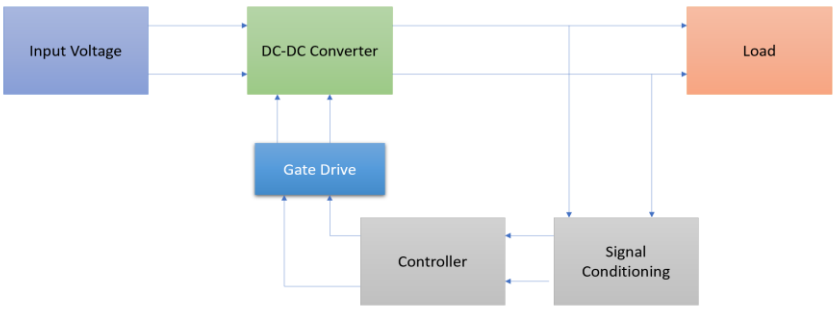

Figure 1: Block diagram of DC-DC Converter

Figure 1, is a generalized DC-DC Converter with closed loop controller to drive the gate of the switch to get desired outputs.

It has a signal conditioning block which senses the output voltage and input current for controlling the circuit.

The controller block has an outer voltage loop control that provides reference current for inner current loop control. Output voltage is sensed, and compared with the reference value and the error is given to a PI controller. Output from the PI controller is again compared with the input current, error is again sent through PI controller for the closed loop control.

Gate drive block is developed based on the proposed novel switching technique, that incorporates two sequence generators for generating the switching sequence which further will be explained in section III. The outputs from the sequence generator are compared with the PWM generator and are given to the MOSFET switches for controlling of circuit.

In this paper, performance, analysis of CBC and IBC is carried out using a new switching technique. The work carried out is presented as follows: Section I gives introduction for the work carried out in this paper. Section II describes the analysis and operation, design details of both the converter topologies. Section III describes the proposed switching technique for the Interleaved Boost Converter. Section IV has the simulation for converter topologies and results drawn from them. And the paper is concluded with a conclusion followed by references.

2. ANALYSIS AND OPERATION OF CONVENTIONAL AND INTERLEAVED BOOST CONVERTER

2.1. Operation of Boost Converter

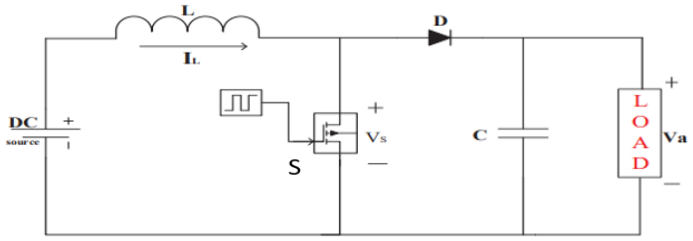

Figure 2: Boost Converter [2]

It consists of DC voltage source as input, inductor (L), diode (D), switch (S) and a capacitor (C). Based on the duty cycle value the voltage at the output can be changed.

When the switch(S) is closed, the diode is reverse biased and there is zero flow of current through the diode. The inductor voltage is equal to the input voltage [10].

When the switch(S) is opened, the diode is forward biased since the current of the inductor cannot change instantaneously, and thus diode provides a path for inductor current [10].

2.1.1. Design details of Boost Converter

The formulae used for the calculation of the circuit parameters of CBC are as follows [10]

$$D = 1 - \frac{Vs}{Vo} = 1 - \frac{10}{40} = 0.75 \quad (1)$$

When the switch is closed, the voltage across the inductor is,

$$V_l = V_s = L\frac{di}{dt} \quad \text{or} \quad \frac{d_{iL}}{dt} = \frac{Vs}{L} \tag{2}$$

The change in inductor current is given by,

$$\frac{\Delta i_L}{\Delta t} = \frac{\Delta i_L}{DT} = \frac{V_s}{L} \tag{3}$$

Solving for Δi_L for the switch closed,

$$(\Delta i_L)_{closed} = \frac{V_s DT}{L} \tag{4}$$

Solving for Δi_L for the switch open,

$$(\Delta i_L)_{open} = \frac{(V_s - V_o)(1-D)T}{L} \tag{5}$$

$$L = \frac{I_L D}{\Delta i_{Lf}} = \frac{5.33 * 0.75}{0.30 * 25000} = 0.5 \text{ mH} \tag{6}$$

Ripple voltage is given by,

$$\frac{\Delta V_o}{V_o} = \frac{D}{RCf} \tag{7}$$

And Capacitance is be given from the above equation as,

$$C = \frac{D}{R\left(\frac{\Delta V_o}{V_o}\right)f} = \frac{0.75}{30 * 0.01 * 25000} = 0.1\ mF$$

2.2. Operation of Interleaved Boost Converter

Figure 3 shows the schematic diagram of IBC

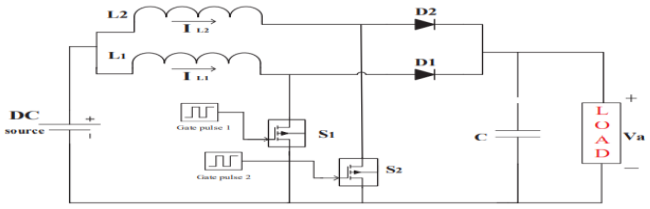

Figure 3: Interleaved Boost Converter [2]

In IBC, based on the number of phases the inductor is split and switches are used. The topology considered for the simulation is a two-phase IBC with equal inductance for each inductor.

Power Flow in Interleaved Boost Converter

The circuit is operated in four modes (M-1, M-2, M-3, M-4)

In M-1, switch S1 is ON and switch S2 is ON, thus both inductors will be conducting in this mode. Figure 4 shows the working of circuit in mode 1.

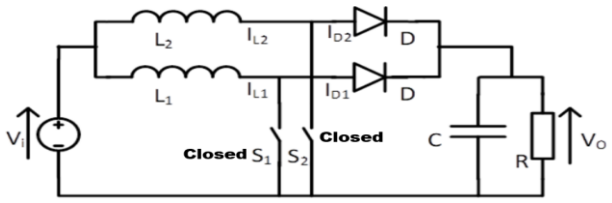

Figure 4:M-1[1]

Similarly, from Figure 4, In M-2, the switch S1 is ON and switch S2 is OFF, thus inductor L1 conducts during this period and S2 will be open circuit.

Similarly, from Figure 4, In M-3, switch S1 is ON and switch S2 is ON, working of mode 3 is same as M-1 conduction.

Similarly, from Figure 4, In M-4, the switch S1 is OFF and S2 is ON, thus the inductor L2 conducts during this period and S1 will be open circuit.

The switching table corresponding to the four modes of operation are shown in Table 1

Table 1: Switching Table

	M-1	M-2	M-3	M-4
S1	ON (1)	ON (1)	ON (1)	OFF (0)
S2	ON (1)	OFF (0)	ON (1)	ON (1)

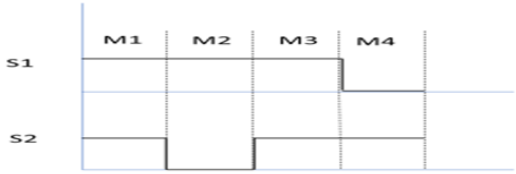

Figure 5: Switching Pulses for the two switches

Both the switches are ON for the 75% or 0.75 duty cycle of the entire cycle.

2.2.1. Design details of Interleaved Boost Converter

The formulae used for the calculation of the parameters of IBC are as follows [10]

The equations from 1 to 7 from section 2.1.1 is same for IBC

The inductor for Interleaved Boost Converter is given by,

Inductor value for IBC is given by,

$$\mathbf{L = \frac{V_s DT}{\Delta i_L} = \frac{V_s D}{\Delta i_L fn}} \quad \textbf{(8)}$$

Where, n is number of phases

$$\mathbf{L1{=}L2{=}\frac{5.33*0.75}{0.30*25000*2} = 0.25\ mH}$$

n= number of phases used in the IBC.

In this case n=2, as there are two phase Interleaved Boost Converter

Capacitor value is given by,

$$\mathbf{C = \frac{D}{R\left(\Delta V_o / V_o\right) fn} = \frac{0.75}{30*0.01*25000*2} = 0.05\ mF} \quad \textbf{(9)}$$

3. PROPOSED SWITCHING TECHNIQUE FOR INTERLEAVED BOOST CONVERTER

The proposed control technique is easy to implement as it has to generate 0 and 1 pulses at the given switching frequency, which can be generated using a microcontroller, which is very convenient compared to the conventional switching technique.

The block diagram to generate gate pulses using the novel switching technique is shown in Figure 6 for the closed loop IBC.

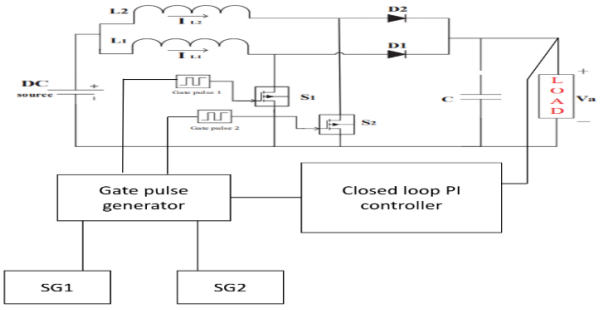

Figure 6: Block Diagram for Control Technique for closed loop Interleaved Boost Converter

The circuit involves two signal generators SG1 and SG2. The switching sequence for SG1 is considered as 1110 and that of SG2 is 1011 corresponding to 180^0 phase shift generated at 25 kHz frequency.

For the close loop control, PI controller is used for controlling output voltage and current. The output voltage and the reference voltage are compared and the error is given to the PI controller with P=1, I=7. The output of PI controller is compared with the input current and error is given as an input to another PI controller with P=1, I=100. From the second PI controller the signal is sent to the PWM generator, that converts the PI controller value to switching pulses i.e., 0 and 1. This PWM generator output is compared with the two signal generators and if the signal generator output is equal to the PWM generator output, then the signal is sent to the switch S1 and S2 respectively for switching of circuit.

The designed values of the circuit components for the CBC and IBC are shown in Table 2.

Table 2: Table of Specification

Parameter	Interleaved Boost Converter	Boost Converter
Input Voltage Range	10-22 V	8-18 V
V_s	10 V	10 V
V_o	35 V	35 V
I_o	1.16 A	1.12 A
L1	0.25 mH	0.5 mH
L2	0.25 mH	-
C	0.05 mF	0.1 mF
R	30 Ω	30 Ω
f	25 kHz	25 kHz

4. SIMULATION RESULTS

In this section, the simulation results of both the converter topologies are presented.

The CBC simulation is presented in Figure 7, closed loop control is carried out using the dual PI controller, one for outer voltage loop and other for inner current loop control. PI values for outer loop control is P=1, I=7. The PI controller values for inner loop is P=1, I=100.

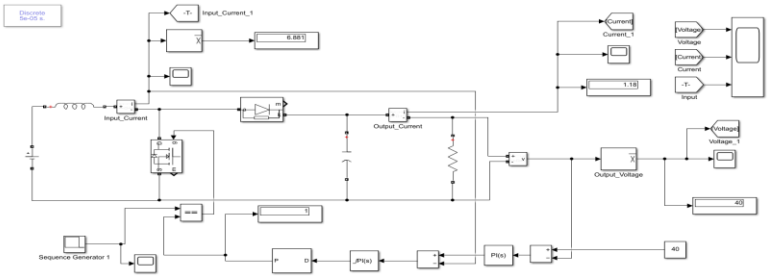

Figure 76: Simulink model of Conventional Boost Converter

The waveforms for CBC are given in Figure 8. The output voltage is at 35V, current has a mean value of 1.16A and mean value of input current 4.95A.

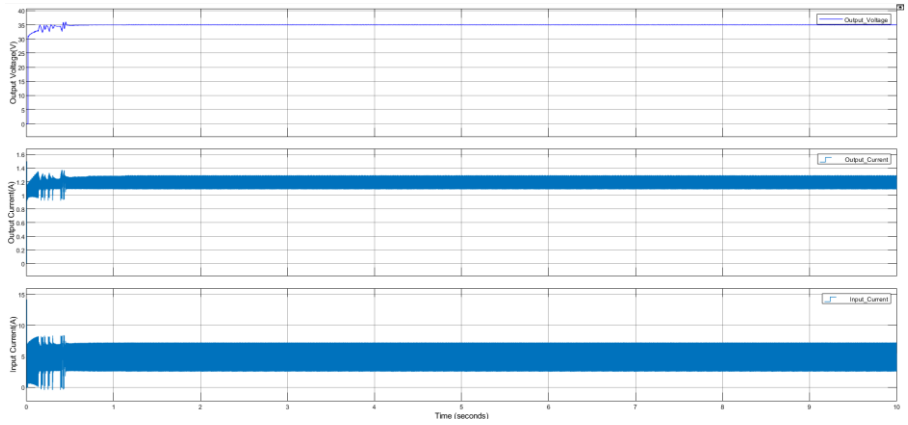

Figure 8: Waveforms of Boost Converter a) Output Voltage b) Output Current c) Input Current

Figure 10, is the IBC carried out in MATLAB Simulink with the parameter values mentioned in the table above.

The Interleaved Boost Converter simulation is presented in Figure 10, the closed loop control is done using dual PI controller, one for outer voltage loop and inner current loop. PI values for outer loop control is P=1, I=7. The PI controller values for inner loop is P=1, I=100.

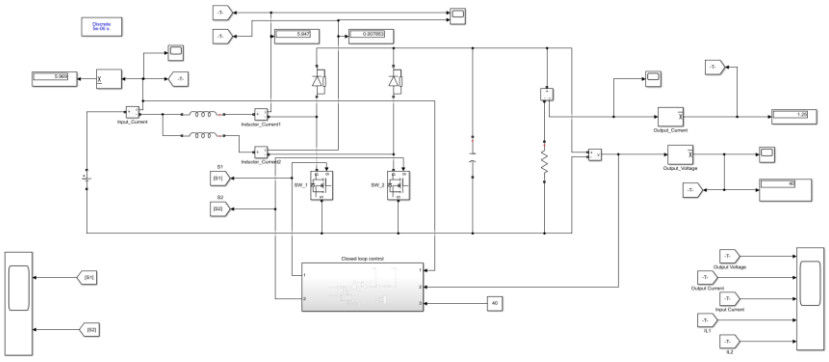

Figure 7: Simulation Model of Interleaved Boost Converter

The subsystem for the control loop of IBC is shown in Figure 10. The operation for the circuit is explained in section 3.

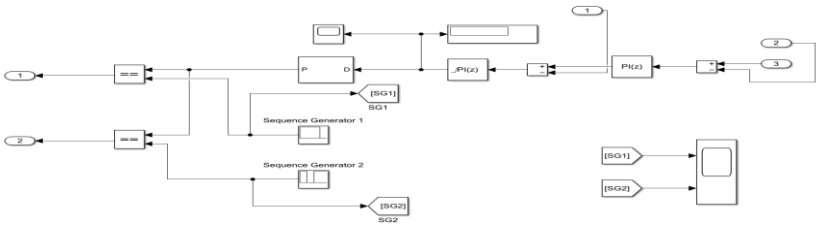

Figure 8: Novel switching technique for Interleaved Boost Converter

The waveforms for the IBC are shown in the Figure 11. The output voltage is at 35V, current has a mean value of 1.16A and mean value of input current 4.482A.

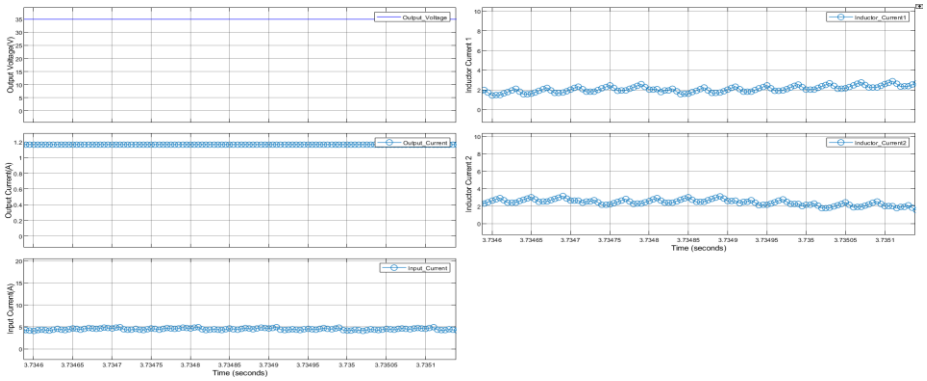

Figure 9: Waveforms of Interleaved Boost Converter a) Output Voltage b) Output Current c) Input Current d) Inductor Current 1 e) Inductor Current 2

The waveforms of switches for the IBC are shown in the Figure 12. Based on PI output and the input signal from the sequence generator are compared and the switches are controlled.

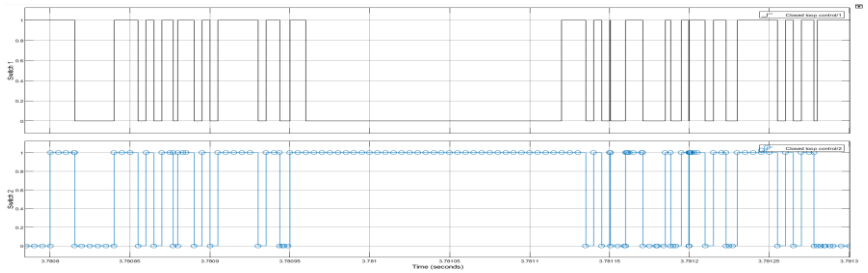

Figure 10: MOSFET switching waveforms a) S1 b) S2

The waveforms of sequence generators for the IBC are shown in the Figure 13. Both the sequence generators are ON for 75% duty cycle mention in section 2.2.

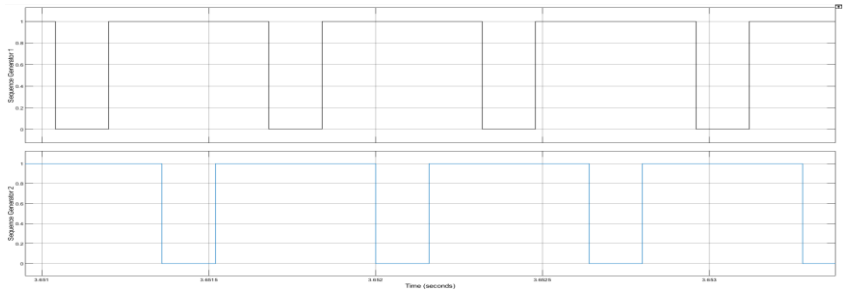

Figure 11: Sequence Generator waveforms a) SG1 b) SG2

5. COMPARISON OF BOOST CONVERTER AND INTERLEAVED BOOST CONVERTER

Results from the simulation of IBC and CBC are shown in Table 3.

Table 3: Simulation Results

Parameter	Boost Converter	Interleaved Boost Converter
V_{in}	10V	10V
V_{out}	35V	35V
ΔV	0.2V	0.05V
ΔI	0.2A	0.015A
$I_L(Mean)$	1.129A	1.167A
PI Controller	P=1, I=7 P=1, I=100	P=1, I=7 P=1, I=100

From the output waveforms it can be seen that stress on the MOSFET switches is been reduced due to the less current flowing through the switches, it is found that I^2R loses are less in IBC(0.5022W) compared to the CBC (2.4453W).

From Table 3, it can be seen that by using IBC the switching stress and size of the components. Thus, performance of IBC is better when compared to CBC, with IBC the input current ripple and output voltage ripple can be reduced significantly.

6. CONCLUSION

In this paper, a novel switching technique has been discussed to control the output voltage and input current of the Conventional Boost Converter and Interleaved Boost Converter. It is observed that, with the use of interleaved boost converters incorporating the proposed switching technique, the switching stress and size of the components is reduced when compared to the Convention Boost converter.

7. REFERENCES

1. https://ijisrt.com/wp-content/uploads/2018/03/Design-Modelling-and-Implementation-of-Interleaved-Boost-DC-DC-Converter.pdf
2. Modabbir and M. R. Khalid, "Design and Evaluation of IBC for EV Applications," 2021 International Conference on Intelligent Technologies (CONIT), 2021, pp. 1-7, doi: 10.1109/CONIT51480.2021.9498498.
3. D. M. Bellur and M. K. Kazimierczuk, "DC-DC converters for electric vehicle applications," 2007 Electrical Insulation Conference and Electrical Manufacturing Expo, 2007, pp. 286-293, doi: 10.1109/EEIC.2007.4562633.
4. A. Thiyagarajan, S. G. Praveen Kumar and A. Nandini, "Analysis and comparison of conventional and interleaved DC/DC boost converter," - ICCTET 2014, 2014, pp. 198-205, doi: 10.1109/ICCTET.2014.6966287.
5. S. m. Dwari and L. Parsa, "A Novel High Efficiency High Power Interleaved Coupled- Inductor Boost DC-DC Converter for Hybrid and Fuel Cell Electric Vehicle," 2007 IEEE Vehicle Power and Propulsion Conference, 2007, pp. 399-404, doi: 10.1109/VPPC.2007.4544159.
6. S. K. Ram et al., "Analysis of Interleaved DC-DC Converter using ANFIS Control for EV Charging Applications," 2021 6th International Conference on Inventive Computation Technologies (ICICT), 2021, pp. 374-378, doi: 10.1109/ICICT50816.2021.9358606.
7. Y. Hsieh, T. Hsueh and H. Yen, "An Interleaved Boost Converter With Zero-Voltage Transition," in IEEE Transactions on Power Electronics, vol. 24, no. 4, pp. 973-978, April2009, doi: 10.1109/TPEL.2008.2010397.
8. O. Hegazy, J. V. Mierlo and P. Lataire, "Analysis, Modeling, and Implementation of a Multidevice Interleaved DC/DC Converter for Fuel Cell Hybrid Electric Vehicles," in IEEE Transactions on Power Electronics, vol. 27, no. 11, pp. 4445-4458, Nov. 2012, doi:10.1109/TPEL.2012.2183148.
9. Y. Jang and M. M. Jovanovic, "Interleaved Boost Converter With Intrinsic Voltage- Doubler Characteristic for Universal-Line PFC Front End," in IEEE Transactions on Power Electronics, vol. 22, no. 4, pp. 1394-1401, July 2007, doi: 10.1109/TPEL.2007.900502.
10. Hart, Daniel W. Power electronics / Daniel W. Hart, Pearson Education, Inc

Selection and Contingency Analysis of EV Charging Station on 24-bus IEEE system

Surbhi Aggarwal; Amit Kumar Singh

National Institute of Technology Delhi, surbhi@nitdelhi.ac.in
National Institute of Technology Delhi, amitsingh@nitdelhi.ac.in

Abstract

In today's deregularized electricity grid, power system security has become a challenging task for power system engineers. Operational engineers must make reasonable efforts to address unnoticed contingency issues. As a result, contingency planning is essential to ensuring the safety and security of power systems. Performance Index is a contingency ranking mechanism that places the best performance index line first, followed by the remaining lines descendingly depending on the computed performance index. It aids in the establishment of adequate security measures for power systems. The paper uses Newton Raphson's (NR) technique for contingency ranking based on the Voltage Performance Index and the Active Power Performance Index. The 5MW charging stations are connected to the load bus lines as if they were real loads in the course. The suggested technique is evaluated on a 24-bus IEEE system with pre-installed Charging Stations.

Keywords. Contingency method, Newton Raphson method, Performance Index, Power system Security

1. INTRODUCTION

As the world's industrialization and population growth, as the standard of living rises, so does the power demand. This condition may result in a constrained transmission network[1]to keep up with demand and supply. Congestion Management [2]is one of the problems with the security and safety of the current deregulated power grid. The paper covers several congestion management options for a reorganized power system, as well as various essential issues and challenges for system stability and security. A power system is a multiplex network of various equipment and test case conditions. Breakdown to meet any test conditions or equipment failure can cause a loss of reliability, resulting in a power system outage [3], [4]. Some contingency scenarios may result in line overloads or bus voltage magnitude limit violations [5], [6]. Power system operators should rapidly identify such unfavorable situations for a more thorough analysis. Contingency analysis (CA) is a “preview” analysis tool. It is an online tool for operational engineers to analyze the consequence of future outages. The line outages' Performance Index (PI) is one of the contingency ranking methods. It starts with the best performance index line and progresses in descending order for all line outages based on the determined PI.

Reference [7] discusses the new congestion point, considering system limitations and the transmission system's physical limitations. Reliability, dynamic stability, transient stability, and node voltage limits are under the category of system limitation, whereas the equipment's thermal limits are considered under the system's physical limitation. For power system security, prediction of violation in bus voltages, and inline power flows, full CA has been presented in [8], [9]. References [10], [11] present radial basis function networks for the contingency evaluation of the power system. A fast-approximate method

is presented in [12] for solving the line and generator outages for the AC load flow program. The paper demonstrates that the approximate solution is more accurate than the basic NR load flow technique. In reference [13], a probabilistic PI method is used for a composite power system to perform the contingency ranking and selection. It shows that the second-level contingency is more accurate and better in computation time. A detailed survey on congestion management has been provided in [14], [15]covering the congestion management methods and the different congestion management issues in the electricity market. The various techniques of congestion management when upgrading from a conventional grid to a smart grid scenario are explained in reference [16]. Reference [17] discusses the different congestion management methods, especially for the distribution networks penetrated by many distributed energy resources. For the system to run safely, the system and physical limitations must be removed as soon as possible [18].

Also, various FACTS devices are used for congestion management in the transmission lines [19]– [21]. In [22], two new congestion techniques are introduced to identify the system's critical transmission lines. For the congestion management of the particular system, DGs and Energy Storage Systems (ESS) are acquainted with the system with the aid of power transfer distribution factors. Many optimization techniques are used for congestion management. The considerable penetration of renewable energy sources and their uncertain nature makes the grid network uncertain, and installing an ESS is suggested to deal with these uncertainties [23]. The Voltage Performance Index (PI_V) and Active Power Performance Index (PI_P) are utilized in this study to rate contingencies on the IEEE 24-bus system using the NR approach. In the study, 5MW charging stations are attached to load bus lines as real loads [24]. Adding real loads to the system will increase the number of losses. DGs are included in the system to compensate for the losses using the Weak Bus placement approach [25].

The total contributions and insights of our work are as follows: (1) Section 1 provides a review of existing surveys in the literature, illustrating the need for our study by examining recent publications and related papers for a better understanding; (2) a thorough review in section 2 of the contingency selection using the NR Load flow solution, detailing the PI_P and PI_V; (3) section 3 of the study covers the experimental section giving in all the minor and significant details about the 24-bus IEEE test system, as well as the voltage limits and the loading margin limits of the load lines in the test system; and (4) all of the experimental results and discussion with tabulated results and graphs are elaborated in section 4; (5) section 5 concludes the work .

2. CONTINGENCY SELECTION USING LOAD FLOW SOLUTION

CA is a “what if” computer software that evaluates, provides, and ranks the implications of any power system contingency unplanned outage condition. A contingency is when a device (such as a generator or transformer) or a small area of the power system fails (for example, a transmission line). For each existing problem defined in a power system, CA does a "power flow" study.

For example, a transmission line that was 85 percent loaded before the contingency event may now be loaded at 120 percent of its MVA rating following the contingency event. A load bus nominal voltage may also fall to 90% of its rated voltage due to the same contingency event. If there is a violation, the changes are noted and calculated according to the severity of the violations or overloads.

Because there are only 3MW charging stations available at the moment. However, as we move towards a green transportation industry, high-capacity charging stations will be required. The paper uses the PI for a 5MW charging station to calculate the IEEE 24-bus system's contingency rating. The PI_V and PI_P are used for the test system, and the overall PI is used to prioritize the contingencies in order of priority. Contingencies are sorted in decreasing order based on the total PI calculation findings, with the highest-valued contingency rated first, followed by the others. This assists in implementing the required safeguards to keep the system safe.

Active Power Performance Index (PI_P)
To measure the degree of line overloads, the Active Power Performance Index is used with the formula:

$$PI_P = \sum_{i=1}^{N_L} (W / 2n)(P_i / P_i^{max})^{2n} \quad (2.1)$$

$$P_i^{max} = (V_i * V_j) / X \quad (2.2)$$

Voltage Performance Index (PI_V)
To determine the outage of voltage magnitude limits, Voltage Performance Index is used with the formula:

$$PI_V = \sum_{i=1}^{N_B} (W / 2n) \left\{ \left(\left|V_i\right| - \left|V_i^{sp}\right| \right) / \Delta V_i^{\lim} \right\}^{2n} \quad (2.3)$$

The overall formula for the calculation of PI will be formulated as:

$$PI_{Total} = PI_P + PI_V \quad (2.4)$$

The flow chart for the calculation of PI and PI_{Total} is shown in figure 1. Depending on the importance of a line, contingency can be ranked. If it is not desired to overload a specific line, the weightage of that line is set to a high value.

3. EXPERIMENTAL SECTION

The flow chart in Figure 1 depicts the test system's step-by-step contingency evaluation. The 24-bus IEEE system used for the contingency evaluation is shown in Figure 2. The test system is comprised of 10 generator buses with 32 generating units ranging from 12MW to 400MW, 13 load buses linked by 38 lines, and one slack bus with a 100 MVA base.
The transmission system supports two voltage levels, 138kV and 230kV. Figure 2 depicts the 230kV system in the upper half, while the 138kV system is shown in the lower half, with 230/138kV transformer stations on buses 11, 12, and 24. To maintain rated voltage under transient conditions, two voltage correcting devices, a Synchronous Condenser and a Reactor, are coupled at bus 14 and bus 6, respectively.
The flow chart described in figure 1 was programmed in MATPOWER MATLAB Software. For every time a transmission line is weighted out of the system for the contingency calculation, the individual bus voltages and power flows are calculated using the NR load flow technique. For PI_V calculation, a margin of ±5% is kept for assigning

minimum and maximum voltage limits on the line, i.e., 0.95 pu and 1.05 pu, respectively. It is also possible that any line can become overloaded with the outage of any of the lines. That congested line scenario accounts for the calculation of the PI_P index. The above two PIs are used to calculate the line contingencies and are explained in the next section.

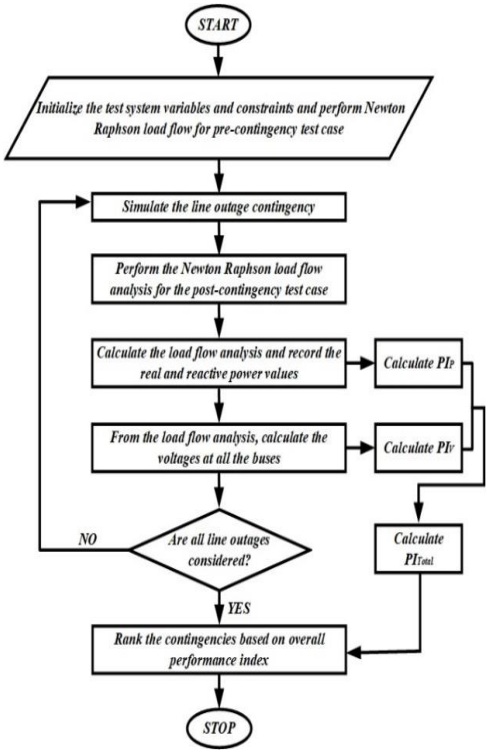

Figure 1: Flowchart for the work

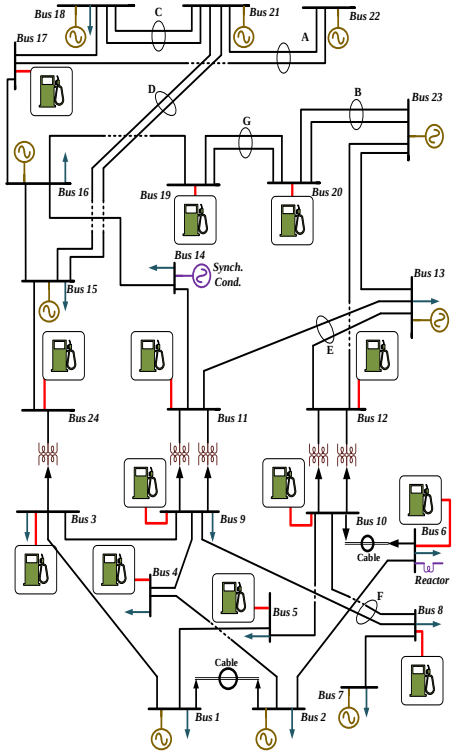

Figure 2: 24-bus Test System

4. RESULTS AND DISCUSSION

As depicted in figure 2, the system demonstrates the placement of 5MW charging stations at the load buses with NO DGs connected to the system. For the sake of simplicity, the charging stations are connected to the system as actual loads.

Section 3 of the report gives a quick overview of the IEEE 24-bus system. The pre-contingency analysis case is referred to as the base case CA. The NR analysis is employed for the study's post-contingency analysis. Because there are 13 load lines in the system, there are 13 charging stations [25], as illustrated in figure 2. The performance indexes, such as PI_P and PI_V, are also calculated with only one line outage at a time. Because the system has 38 lines, the pre-and post-contingency analysis is performed 38 times for PI calculation.

From the contingency analysis, it is calculated that neither of the bus or lines is over-rated or under-rated from its base MW value. So, table 1, Columns 2 & 3, illustrates the PI_P results and contingency ranking based on the pre-and post- contingency analysis

evaluation. It can be seen that the outage of line 15-24 results in the highest value of PI_P, and hence it is ranked first for the contingency evaluation. Also, the outage of line 17-18 results in the lowest PI_P value, and, accordingly, is ranked as the last in the contingency evaluation. The pre and post contingency analysis evaluation for the overall PI_V calculation is shown in Table 1, in columns 4 & 5, with the contingency ranking. It can be seen that the outage of line 6-10 results in the highest value of PI_V, and hence it is ranked first for the contingency evaluation. Also, the outage of line 17-18 results in the lowest PI_V value, and accordingly, is ranked as the last in the contingency evaluation.

Both PIs are summated, and ranking is based on the calculated overall PI value. Table 1, columns 6 & 7, displays the overall calculated PI values for the specific case where NO DG is connected to the system. Table 1 outlines the lines' overall contingency ranking, where the outage of line 6-10 is ranked first. It can be inferred from the study that the outage of line 6-10 is the most vulnerable in the system and should be given the highest priority in the cases of a blackout or worn-out situation. Also, outage of line 17-18 is ranked last, which means it is the least affected line in the system.

5. CONCLUSION

In the study, we use MATLAB MATPOWER software to complete the CA and ranking of IEEE 24-bus system adopting the NR Load Flow approach. As the list of potential contingency cases for the test system is so extensive, the strategy of contingency selection is essential, as it eliminates a substantial number of contingency instances and focuses on the most severe contingency scenario. Clearly, the interruption of line 6-10 will have the most impact, whereas line 17-18 would have the least.

Table 1: Overall Contingency Value and Ranking

Outage Line	Power_ PI Value	Power_ PI Ranking	Voltage_ PI Value	Voltage_ PI Ranking	Overall PI Value	Contingency Ranking
1-2	1.96	29	2.88	26	28.88	29
1-3	1.96	31	3.15	9	12.15	12
1-5	2.03	22	2.80	34	36.80	30
2-4	2.00	23	3.56	5	8.56	6
2-6	2.14	11	2.79	35	37.79	24
3-9	1.96	30	2.97	16	18.97	25
3-24	3.02	2	4.19	4	8.19	3
4-9	2.06928	18	2.938	19	21.938	22
5-10	1.96622	28	2.905	2	4.905	28
6-10	2.48980	4	25.8968	1	26.8968	**1**
7-8	2.30729	5	4.6058	3	7.6058	4
8-9	1.99482	24	2.8898	23	25.8898	27

8-10	1.98535	26	3.1206	11	14.1206	14
9-11	2.04979	20	3.1658	8	11.1658	10
9-12	2.12005	13	3.3774	7	10.3774	7
10-11	2.10579	15	2.9082	21	23.9082	21
10-12	2.20176	7	2.8608	32	34.8608	16
11-13	2.04224	21	2.9962	15	17.9962	18
11-14	2.06546	19	3.0302	13	16.0302	15
12-13	1.97000	27	2.9458	17	19.9458	26
12-23	2.29423	6	3.0066	14	17.0066	8
13-23	2.16385	8	2.9454	18	20.9454	13
14-16	2.77851	3	3.5072	6	9.5072	5
15-16	2.12328	12	2.924	20	22.924	17
15-21	2.14975	9	2.8644	30	32.8644	19
15-21	2.14975	10	2.8644	31	33.8644	20
15-24	3.07116	1	6.65	2	8.65	2
16-17	2.09841	16	3.1448	10	13.1448	9
16-19	2.08814	17	3.096	12	15.096	11
17-18	1.86229	38	2.7056	38	40.7056	**38**
17-22	2.11363	14	2.8678	29	31.8678	23
18-21	1.93179	36	2.8888	24	26.8888	34
18-21	1.93179	37	2.8888	25	27.8888	35
19-20	1.94961	34	2.872	27	29.872	32
19-20	1.94961	35	2.872	28	30.872	33
20-23	1.95714	32	2.7462	37	39.7462	36
20-23	1.95714	33	2.7462	36	38.7462	37
21-22	1.99239	25	2.8438	33	35.8438	31

6. REFERENCES

[1] Pillay, S. Prabhakar Karthikeyan, and D. P. Kothari, “Congestion management in power systems - A review,” International Journal of Electrical Power and Energy Systems, vol. 70, pp. 83–90, 2015, doi: 10.1016/j.ijepes.2015.01.022.

[2] A. Narain, S. K. Srivastava, and S. N. Singh, “Congestion management approaches in restructured power system: Key issues and challenges,” The Electricity Journal, vol. 33, no. 3, p. 106715, Apr. 2020, doi: 10.1016/j.tej.2020.106715.
[3] S. Nandini, P. Suganya, and Lakshmi. K.M, “Congestion Management in Transmission Lines Considering Demand Response and FACTS Devices,” Int J Innov Res Sci Eng Technol, vol. 3, pp. 682–688, 2014.
[4] V. K. Tumuluru and D. H. K. Tsang, “A Two-Stage Approach for Network Constrained Unit Commitment Problem With Demand Response,” IEEE Trans Smart Grid, vol. 9, no. 2, pp. 1175–1183, Mar. 2018, doi: 10.1109/TSG.2016.2580578.
[5] H.-M. Chung, C.-L. Su, and C.-K. Wen, “Dispatch of generation and demand side response in regional grids,” in 2015 IEEE 15th International Conference on Environment and Electrical Engineering (EEEIC), Jun. 2015, pp. 482–486. doi: 10.1109/EEEIC.2015.7165210.
[6] M. B. Nappu and A. Arief, “Network Losses-based Economic Redispatch for Optimal Energy Pricing in a Congested Power System,” Energy Procedia, vol. 100, pp. 311–314, Nov. 2016, doi: 10.1016/j.egypro.2016.10.183.
[7] H. Emami and J. A. Sadri, “Congestion management of transmission lines in the market environment,” International Research Journal of Applied and Basic Sciences, vol. 3, no. S, pp. 2572–2580, 2012, [Online]. Available: www.irjabs.com
[8] A. J. Wood, B. F. Wollenberg, and G. Sheble, “Power System Security,” in Power generation, operation, and control, 2013, pp. 296–349.
[9] B. Stott, O. Alsac, and A. J. Monticelli, “Security Analysis and Optimization.,” Proceedings of the IEEE, vol. 75, no. 12, pp. 1623–1644, 1987, doi: 10.1109/PROC.1987.13931.
[10] J. A. Refaee, M. Mohandes, and H. Maghrabi, “Radial basis function networks for contingency analysis of bulk power systems,” IEEE Transactions on Power Systems, vol. 14, no. 2, pp. 772–778, 1999, doi: 10.1109/59.761911.
[11] D. Devaraj, B. Yegnanarayana, and K. Ramar, “Radial basis function networks for fast contingency ranking,” International Journal of Electrical Power and Energy Systems, vol. 24, no. 5, pp. 387–393, 2002, doi: 10.1016/S0142-0615(01)00041-2.
[12] N. M. Peterson, W. F. Tinney, and B. Donald, “Iterative linear AC power flow solution for fast approximate outage studies,” IEEE Transactions on Power Apparatus and Systems, no. 5, pp. 2048–2056, 1972.
[13] A. M. Al-Shaalan, “Contingency selection and ranking for composite power system reliability evaluation,” Journal of King Saud University-Engineering Sciences, vol. 32, no. 2, pp. 141–147, 2020.
[14] N. I. Yusoff, A. A. M. Zin, and A. bin Khairuddin, “Congestion Management in Power System—A Review,” in 2017 3rd International Conference on Power Generation Systems and Renewable Energy Technologies (PGSRET), 2017, pp. 22–27. doi: 10.1007/978-981-15-7994-3_39.
[15] A. Kumar, S. C. Srivastava, and S. N. Singh, “Congestion management in competitive power market: A bibliographical survey,” Electric Power Systems Research, vol. 76, no. 1–3, pp. 153–164, 2005, doi: 10.1016/j.epsr.2005.05.001.
[16] S. Gumpu, B. Pamulaparthy, and A. Sharma, “Review of Congestion Management Methods from Conventional to Smart Grid Scenario,” International Journal of Emerging Electric Power Systems, vol. 20, no. 3, pp. 1–24, 2019, doi: 10.1515/ijeeps-2018-0265.
[17] S. Huang, Q. Wu, Z. Liu, and A. H. Nielsen, “Review of congestion management methods for distribution networks with high penetration of distributed energy resources,” in IEEE PES

Innovative Smart Grid Technologies Conference Europe, 2014, pp. 1–6. doi: 10.1109/ISGTEurope.2014.7028811.

[18] Y. Wang, Z. Sun, Z. Yan, L. Liang, F. Song, and Z. Niu, "Power transmission congestion management based on quasi-dynamic thermal rating," Processes, vol. 7, no. 5, p. 244, 2019, doi: 10.3390/pr7050244.

[19] K. Thekdi, V. Varnamiya, and D. Desai, "Congestion Management in Transmission Lines using FACTS Devices," International Journal of Engineering Research & Technology (IJERT), vol. 8, no. 1, pp. 17–21, 2019.

[20] T. T. Nguyen and F. Mohammadi, "Optimal placement of TCSC for congestion management and power loss reduction using multi-objective genetic algorithm," Sustainability, vol. 12, no. 7, pp. 1–15, 2020, doi: 10.3390/su12072813.

[21] N. Padmini, P. Choudekar, and M. Fatima, "Transmission congestion management of IEEE 24-Bus test system by optimal placement of TCSC," in 2018 2nd IEEE International Conference on Power Electronics, Intelligent Control and Energy Systems, ICPEICES 2018, 2018, pp. 44–49. doi: 10.1109/ICPEICES.2018.8897421.

[22] E. Dehnavi, F. Aminifar, and S. Afsharnia, "Congestion management through distributed generations and energy storage systems," International Transactions on Electrical Energy Systems, vol. 29, no. 6, pp. 1–12, 2019, doi: 10.1002/2050-7038.12018.

[23] V. K. Prajapati and V. Mahajan, "Reliability Assessment and Congestion Management of Power System with Energy Storage System and Uncertain Renewable Resources," Energy, 2020, [Online]. Available: https://doi.org/10.1016/j.scitotenv.2019.135907

[24] S. Aggarwal, M. Bajaj, and A. K. Singh, "Analysis of Electric Vehicle Charging Station Allocation in Deregulated Electric Power System," in 2020 IEEE 9th Power India International Conference (PIICON), Feb. 2020, pp. 1–6. doi: 10.1109/PIICON49524.2020.9113022.

[25] S. Aggarwal and A. K. Singh, "Impact analysis of electric vehicle charging station integration with distributed generators on power systems," International Journal of Circuit Theory and Applications, vol. 49, no. 6, pp. 1811–1827, Jun. 2021, doi: 10.1002/cta.2974.

Biographies

Ms. Surbhi Aggarwal received the bachelor's degree in Electrical and Electronics Engineering from UPTU in 2015, the master's degree in Power Systems from Thapar University in 2017, and currently pursuing the doctorate degree in Electric Vehicles from National Institute of Technology Delhi, respectively.

Dr Amit Kumar Singh received the bachelor's degree in Electrical and Electronics Engineering from UPTU in 2007, the master's degree in Power and Energy Systems Engineering from NIT Silchar in 2009, and doctorate degree in Electrical Engineering from IIT Patna, respectively. He is currently working as an Assistant Professor at the Department of Electrical and Electronics Engineering, NIT Delhi. His research areas include Power System Restructuring /Deregulation, Electricity Market, Distributed Generation, Renewable Energy, Security Analysis, Fault Detection, Operation and Control of Power Systems, Smart Energy Network.

Detection and classification of Array Faults in Photovoltaic System using Wavelet Packet Transform

M. Nivash[1], C. Kannan[1], S. Priyadharsini[1]and V. Saravanan[1]

[1]*Department of EEE, Arunai Engineering College, Tiruvannamalai*

nivas10194@gmail.com,kannanc305@gmail.com,priyamshanmugam@gmail.com, vsaranaec@yahoo.co.in

Abstract.

Due to nonlinear photovoltaic (PV) characteristics, working of maximum power point tracker, presence of the blocking diodes, and the low irradiance conditions prevents the operation of protection devices under fault conditions and leads to reduction of efficiency and even it may cause fire hazards. Additionally, the characteristics of photovoltaic (PV) array under certain partial shading conditions looks like fault characteristics and results in maloperation of the protection devices Thus, it is inevitable to design a fault detection algorithm for identifying and differentiating the faults and shading conditions to avoid false tripping of the protection system. To address the above problem, a fault detection method is developed by processing the available data of array voltage, current using wavelet packets. For analysing the array faults, a 4 x 4 PV system is considered and simulated by using MATLAB/Simulink. After observing the energy values for various faults with distinct %mismatch, shading and cloudy conditions, threshold values are determined for identifying the faults and partial shading condition.

Keywords. Photovoltaic (PV) Module, PV array Characteristics, Partial Shading, PV array Faults and wavelet packets.

1. INTRODUCTION

As per the REN21 report, globally the solar power generation is exponential increasing and has reached 720 GW [1] due to its easy installation, low maintenance and government subsidies. On the other side, PV systems are more vulnerable to various faults such as line to ground (LG) faults, line-line (LL), arc fault and mismatch faults. Among these, LL and LG faults induce massive fault currents and even it may create fire risks. One such fire hazard occurred in a 383kW PV array located at Bakersfield, California, in 2009 [2]. Furthermore, the Line-line faults and partial shading conditions exhibits similar operating characteristic [3]. Thus, it is necessary to detect and differentiate the LL faults and shading conditions. In the literature, to address this issue, various methods have been proposed using different techniques and some of them are reviewed as follows.

Line-line faults that occurs in Photovoltaic system and its impact are explained in and discussed the challenges in detecting the array faults such as active MPPT, non-linear

output characteristics of photovoltaic arrays, fault impedance, location of fault, faults with low percentage mismatch [7]. More importantly, the fault occurred in night and progress from night to day period. Such faults are not detected by the existing protection system even when the irradiation changes to high values. Comparison based techniques, an online fault identification of PV system approach in [9] have measured outputs and model-forecasted outputs the difference between these 2 outputs are taken as a fault, these approach cannot provide information of type and location of fault. In [10]a new monitoring technique of PV system is introduced. It can identify static and dynamic shadowing, accumulation of dust, aging. similarly, those no. of sensors are required which leads to increasing in complexity and cost.

Signal-processing based methods, this method is used for analysing, extracting features of faulted PV array parameters and it works on time domain reflectometry, under normal conditions there is no reflections and uniform impedance throughout transmission line. When fault is occurred delay of signal, waveform distortions show type and location of fault. A TDR based technique [11] is used for detecting, locating open circuit faults, LG faults and it is implemented to 1MW plant but inverter switches are reducing operational performance.

Machine-learning based techniques [12], for detection and location of short-circuit faults a artificial neural network model is introduced it is implemented to 3x2 PV array and it takes irradiation, temperature, voltage, current at maximum power as input and provides terminal voltage to each PV module it have huge computational burden. For detection and diagnosis short circuit, open circuit, degradation faults, partial shading a extreme learning technique is implemented [13], this technique is very fast and accurate but the performance of this model is mainly depends on PV module and it cannot generalise across different PV module and also it needs large labelled data.

Thus, this paper proposes an effective algorithm based on wavelets for detecting faults and also able to differentiate from the normal environment condition. The rest of the paper is explicated as follows- section II-PV system configuration –protection devices, array faults and shading condition, Section III- illustrated the P-V characteristics under various LL faults and partial shading conditions, Section IV- discussed about wavelets, algorithm for the detection of faults, and validation of the proposed method followed by conclusion in Section V.

2. DESCRIPTION OF PV SYSTEM CONFIGURATION, ARRAY FAULTS

A 1.6 kW, 4 x 4 series-parallel connected PV array configuration with protection devices like OCPD, GFPD and with blocking and bypass diodes is shown in Fig. 1. Various possible LL faults that are occurred in the PV array are illustrated in Fig. 1: F1 – Single module LL fault or 25%mismatch (out of 4 module one module shorted), F2 – Two module LL fault or 50%mismatch (out of 4 module two module shorted), F3 – Three module LL fault or 75%mismatch (out of 4 module three modules shorted). Percentage mismatch is calculated based on no. of modules shorted by total no. of modules in a string

of PV array. Another frequently occurring temporary fault known as shading, which occurs due to shadows of beside building, poles is shown in Fig. 1.

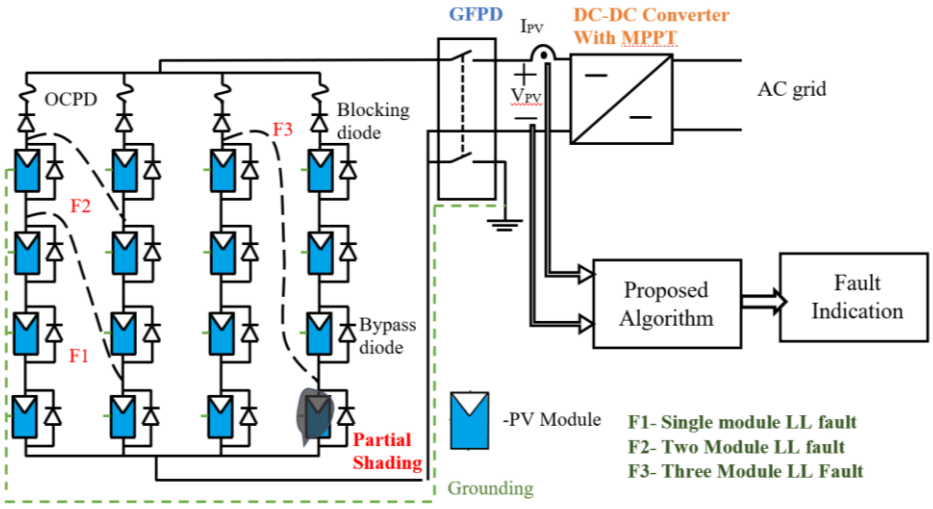

Fig. 2.1 4x4 PV System with protection device and proposed algorithm

3. SIMULATION RESULTS OF LL FAULTS AND SHADING CONDITIONS

3.1. Single Module LL Fault(F1)

Single module LL fault means one module is short circuited across 4 modules in the PV array it is also called as 25% mismatch. The single module LL fault(F1) as shown in Fig. 2.1 is simulated using MATLAB/Simulink and attained volage, current waveforms as shown in fig 3.1

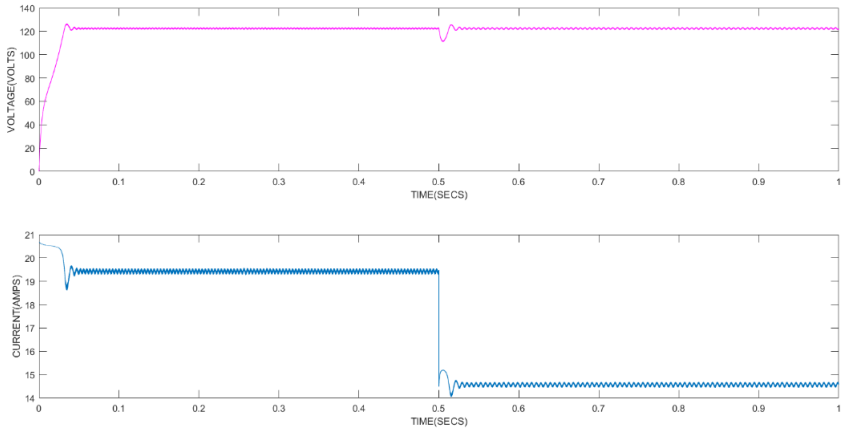

Fig 3.1 voltage, current waveforms of single module LL fault (F1)

3.2 Two Module LL Fault(F2):

Two module LL fault means two modules is short circuited across 4 modules in the PV array it is also called as 50% mismatch. The two module LL fault(F2) as shown in Fig 2.1 is simulated using MATLAB/Simulink and attained volage, current waveforms as shown in fig 3.2

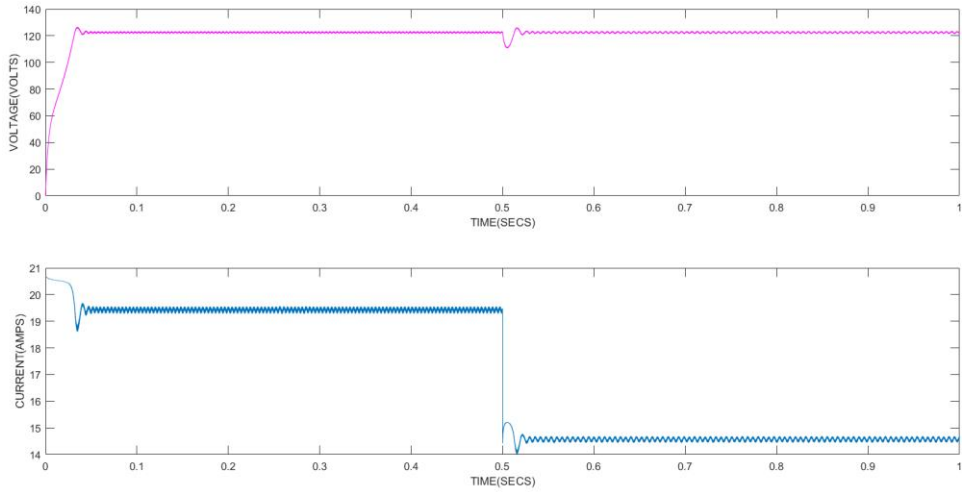

Fig 3.2 voltage, current waveforms of Two module LL fault (F2)

3.3 Three Module LL Fault(F3):

Three module LL fault means three modules is short circuited across 4 modules in the PV array it is also called as 75% mismatch. The three module LL fault(F3) as shown in fig 3.1 is simulated using MATLAB/Simulink and attained volage, current waveforms as shown in fig 3.3

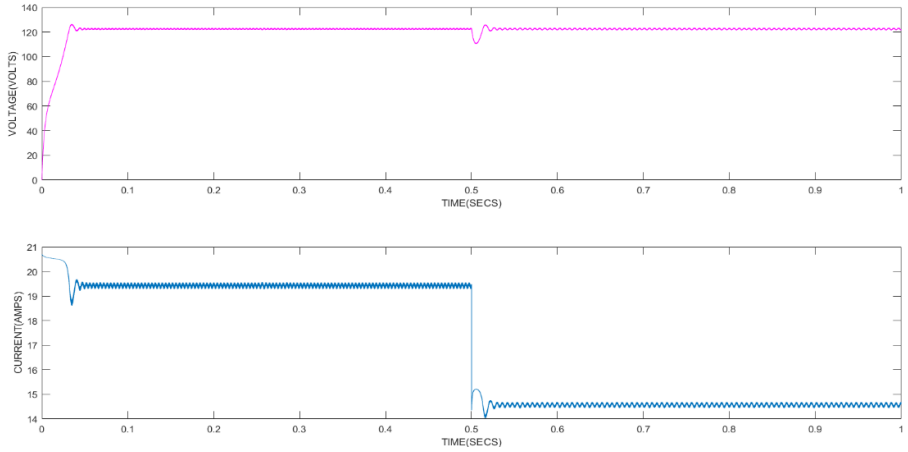

Fig 3.3 voltage, current waveforms of Three module LL fault (F3)

3.4 Partial Shading Condition:

It is classified into 2 types based on retain of shadow on PV panels

1. Static shading condition: It means area of shadow appeared on the PV panels is constant throughout a complete day.
2. Dynamic shading condition: It means area of shadow appeared on the PV panels is varied throughout a complete day.
3. The partial static shading condition is considered as shown in fig 3.1, it is simulated using MATLAB/Simulink and attained volage, current waveforms as shown in fig 3.4

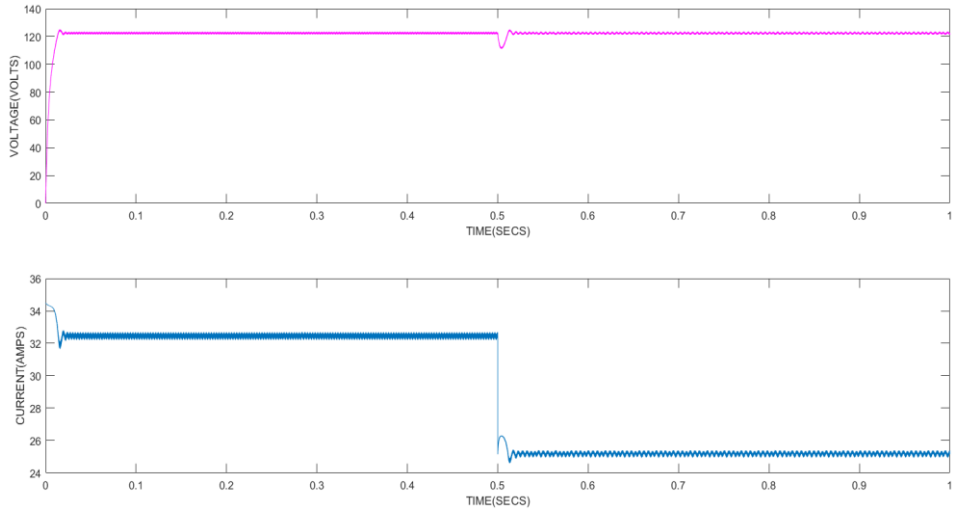

Fig 3.4 voltage, current waveforms of partial shading condition

By considering all the above graphs, it is concluded that both faults and partial shading condition have similar PV characteristics, for LL fault with > 25% age mismatch faults occurred within string the complete string is isolated and blocking diode opposes entering of reverse currents into the faulty string. The remaining strings supply power to load hence, from the above voltage and current waveforms it is concluded that at any of LL percentage mismatch faults the power delivered to the load is constant irrespective of type of faults.

4. FAULT DETECTION ALGORITHM BASED ON WAVELETS

During fault occurrences the PV parameters like fault voltages and fault currents are having abrupt changes in their waveforms, Fourier transform cannot represent abrupt changes in signal efficiently. The reason is Fourier transform shows data in sum of sine waves which cannot not localised in time or space. To accurately analyse signals that have abrupt changes a wavelet transform is used which is well localised in time and frequency.[14]

In CWT wavelet coefficients are calculated at each scale generates lot of data, requires more computation time and is overcome by sing DWT. However, DWT only

approximations are decomposed into N-level. In wavelet packet analysis, for more accuracy the approximations as well as the details are decomposed into N-level

4.1 Extracted Features of PV system:

The extracted features are obtained from voltage across PV array and current though the PV array.

1) Difference in voltage across PV array between 2 successive samples.

$$\Delta V = V_{PV}(i+1) - V_{PV}$$

2)Energy of array voltages (E_{av}), the energy is calculated by doing summating the squares of its wavelet packets coefficients.

$$E_{av} = \sum V^2_{WPC}(i)$$

V_{WPC} = wavelet packet coefficient of voltage across array

3)energy of change in impedance (E_{IMP})

$$E_{IMP} = \sum Z^2_{WPC}(i)$$

Z_{WPC} = wavelet packet coefficient of change in impedance Z(i)

$$\text{Where } Z(i) = \frac{V_{PV}(i+1) - V_{PV}}{I_{PV}(i+1) - I_{PV}}$$

i=sample number.

By Examining the ΔV and energy values, the threshold values are assumed which are used to detect faults and separates faults from partial shading condition. An algorithm is to be implemented in such a manner that it should consider threshold values and its inputs are only from voltage across PV array and current though the PV array. When any fault or partial shading condition is occurred based on threshold values the algorithm should check whether it is belong to fault or partial shading region and concludes as fault or partial shading.

4.2 Fault Detection Algorithm (FDA)

The algorithm can be explained as follows:

Step 1: Get the features E_{AV}, and E_{IMP} for every t_0 seconds (1 s). Set i = 1.

Step 2: If $E_{AV} < \varepsilon 1$ (or) $E_{IMP} > \varepsilon 4$, then go to step 4; otherwise, go to next step.

Step 3: If E_{AV} lies within the limits (ε2, ε3) (or) $E_{IMP} > \varepsilon 5$, then go to step 4; otherwise, go to step 5.

Step 4: “Fault occurred.” Go to step 7.

Step 5: “Fault has not occurred.” Go to the next step.

Step 6: If i < 1000, increment i by 1 and go to step 2; otherwise, go to step 1.

Step 7: Disconnect the PV array from the ac grid

4.3 Determination of threshold values

The threshold vales are determined by examining the energy values under various fault conditions at distinct irradiance values, partial shading conditions at one module, two module and cloudy conditions. The threshold values for identifying the LL faults are tabulated in Table 4.1

Table 4.1 Threshold values for E_{av} and E_{imp}

Variable	**Constant**	**Value**
E_{av}	ε_1	10,000
	ε_2	4000
	ε_3	5000
E_{imp}	γ_1	9000
	γ_2	$3x10^6$

4.4 Validation of the proposed method under 25% of mismatch fault

A one module fault LL fault is created and the corresponding energy values for the array voltage and impedance is computed by applying the wavelet packets and the corresponding energy values are plotted in Fig. 4.1(a) and Fig. 4.1(b) respectively. From the Fig. 4.1(a) and Fig. 4.2(b), it is clear that one of the energy condition (E_{imp} >9000) is satisfied and the fault is identified by the proposed algorithm.

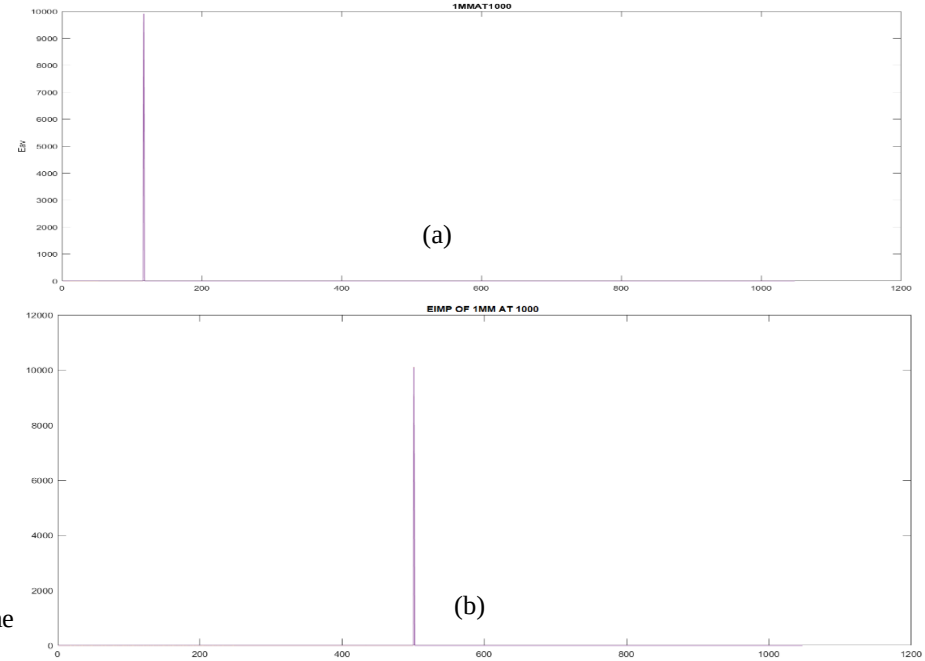

5.

same

Fig. 4.1.(a) E_{AV} for 25% mismatch at 1000 irradiation and (b) E_{IMP} for 25% mismatch at 1000 irradiation.

tracker, bypass and blocking diodes in PV system. While in the presence of blocking diodes in PV array, the severity of fault current depends on percentage mismatch.

To detect and differentiate array faults and partial shading an algorithm is need to be implemented by using wavelet packets. By applying wavelets to the input data, energy values were calculated for different case studies such as faults with discrete %mismatch at distinct irradiance values, cloudy conditions and shading conditions. After observing the energy values, threshold values are determined. Based on these energy threshold values, faults and partial shading conditions can be identified and differentiated. Most of faults can be detected by using this method.

6. REFERENCES

[1] "Renewables 2016 Global Status Report," 2016. [Online]. Available: http://www.ren21.net/wp-content/uploads/2016/06/GSR_2016_Full_Rep ort.pdf

[2] B. Brooks, "The Bakersfield fire: A lesson in ground-fault protection," Sol. Pro Mag., vol. 4, no. 2, pp. 62–70, Feb./Mar 2011.

[3] M. N. Akram and S. Lotfifard, "Modelling and health monitoring of dc side of photovoltaic array," IEEE Trans. Sustain. Energy, vol. 6, no. 4, pp. 1245–1253, Oct. 2015.

[4] R. Hariharan, M. Chakkarapani, and G. S. Ilango, "Challenges in the detection of line-line faults in PV arrays due to partial shading," in Proc. Int. Conf. Energy Efficient Technol. Sustain., Nagercoil, India, 2016, pp. 23–27.

[5] R. Hariharan, M. Chakkarapani, G. Saravana Ilango, and C. Nagamani, "A method to detect photovoltaic array faults and partial shading in PV systems," IEEE J. Photovoltaics, vol. 6, no. 5, pp. 1278–1285, Sep. 2016.

[6] U.S. National Electrical Code, "Article 690—Solar Photovoltaic Systems," 2011.

[7] Y. Zhao, J. F. de Palma, J. Mosesian, R. Lyons, and B. Lehman, "Line– line fault analysis and protection challenges in solar photovoltaic arrays," IEEE Trans. Ind. Electron., vol. 60, no. 9, pp. 3784–3795, Sep. 2013.

[8] Review and Performance Evaluation of Photovoltaic Array Fault Detection And Diagnosis Techniques, International Journal Oh Photoenergy Volume 2019.

[9] R. Platon, J. Martel, N. Woodruff, and T. Y. Chau, "Online fault detection in PV systems," IEEE Trans. Sustain. Energy, vol. 6, no. 4, pp. 1200–1207, Oct. 2015.

[10] B. Ando, S. Baglio, A. Pistorio, G. M. Tina, and C. Ventura, "Sentinella: smart monitoring of photovoltaic systems at panel level," IEEE Transactions on Instrumentation and Mea-surement, vol. 64, no. 8, pp. 2188–2199, 2015.

[11] L. Schirone, P. F. Califano, U. Moschella, and U. Rocca,"Fault finding in a 1 MW photovoltaic plant by reflectome-try," in Proceedings of 1994 IEEE 1st World Conference on Photovoltaic Energy Conversion - WCPEC (A Joint Confer-ence of PVSC, PVSEC and PSEC), Waikoloa, HI, USA, 1994.

[12] E. K. Syafaruddin and T. Hiyama, “Controlling of artificial neural network for fault diagnosis of photovoltaic array,” in 2011 16th International Conference on Intelligent System Applications to Power Systems, pp. 1–6, Hersonissos, Septem-ber 2011.

[13] Z. Chen, L. Wu, S. Cheng, P. Lin, Y. Wu, and W. Lin, “Intel-ligent fault diagnosis of photovoltaic arrays based on opti-mized kernel extreme learning machine and I-V characteristics,” Applied Energy, vol. 204, pp. 912–931, 2017.

[14] F. H. Magnago and A. Abur, “Fault location using wavelets,” IEEE Trans. Power Del., vol. 13, no. 4, pp. 1475–1480, Oct. 1998.

[15] P. K. Murthy, J. Amarnath, S. Kamakshiah, and B. P. Singh, “Wavelet transform approach for detection and location of faults in HVDC system,” in Proc. IEEE Region 10 3rd Int. Conf. Ind. Inf. Syst., Kharagpur, India, 2008.

[16] B. P. Kumar, G. S. Ilango, M. J. B. Reddy and N. Chilakapati, "Online Fault Detection and Diagnosis in Photovoltaic Systems Using Wavelet Packets," in IEEE Journal of Photovoltaics, vol. 8, no. 1, pp. 257-265, Jan. 2018, doi: 10.1109/JPHOTOV.2017.2770159.

EFFECT, ANALYSIS AND ASSESSMENT OF ELECTRICITY USAGE PATTERN IN AN EDUCATIONAL INSTITUTE DURING COVID-19 PANDEMIC

Shilpa Aralasurali Subramanya[1], A. N. Nagashree[2]

[1] *Research scholar, Dept. of Electrical Eng., B.M.S College of Eng., Bangalore, India*
[2] *Associate professor, Dept. of Electrical Eng., B.M.S College of Eng., Bangalore, India*

Abstract.

The COVID-19 pandemic has caused significant impacts on energy demand in India and many countries worldwide. It is important to understand the impact of emergencies such as pandemic on the electricity usage pattern so as to improve the energy planning and management. The main purpose of this paper is to demonstrate how the recent coronavirus pandemic affected energy consumption in an Indian educational institute. Two different situations of electricity usage patterns are considered: (i) Operation under normal period (non-COVID) (ii) Operation under pandemic period. A data-driven analysis was performed which utilized the measured electricity usage data in real buildings. The forecasting of post pandemic energy demand of the institute has been carried out using predictive models built in Python.

Keywords. COVID-19, Data driven analysis, Educational Institute, Forecasting, Load Modelling.

1. INTRODUCTION

Many countries worldwide have undertaken various measures to tackle the COVID-19 pandemic. Partial or full lockdown have been imposed on public places, commercial and industrial buildings. Building occupancy schedules have been changed into distance work. These radical changes have led to remarkable impacts on energy consumption and electricity usage pattern. This has led to the scope of understanding the sudden increase or decrease of energy consumption.

India imposed an initial lockdown in four successive phases over a span ninety-two days [1] to avoid the spread of COVID-19. Pandemic-driven restrictions changed people's way of life and their working habits. All the government and private educational institutes took many initiatives to avoid the spread of COVID-19[2]. These initiatives significantly changed the energy consumption of educational institutes [3][4][5]. In particular, the virtual class modality generated huge changes in the patterns of energy consumption at the institutional level. With the significant changes in the electricity consumption pattern, the accuracy of the load forecasting tool declined [6] and the demand forecasting has become more challenging ever [7]. Forecast can be improved with machine learning techniques which further helps in better calculation of the flexibility potential of buildings, grid etc. [8][9]. There are several techniques to effectively forecast the time series data out of which

the methods which gained significant attentions are classic Auto-Regressive Integrated Moving Average (ARIMA) model and deep learning based Long-Short Term Memory (LSTM) model [10][11].

In this paper, the electricity usage data in an educational institution has been considered. The analysis is made using real time data over a time period from Jan 2018 to Feb 2022. This includes pre-pandemic, pandemic and post-pandemic periods. The study was conducted not only to analyse changes in the energy usage under COVID-19 but also to forecasts the post pandemic energy demand with an objective to assess the future energy utilization in the educational institution. The forecasting has been carried out using predictive models ARIMA and LSTM in Python.

2. DATA COLLECTION OF THE EDUCATIONAL INSTITUTE

The educational building considered in this paper is located in Bengaluru, India. Power supply to the institute campus is supported by power from Bangalore Electricity Supply Company (BESCOM) Ltd. The diesel generator (DG) sets supporting this power supply are also available in the institute campus. Online UPS are installed to support the continuity of supply for few minutes during the change over from BESCOM to DG set. There are three numbers of step-down transformers (11kV/ 440V) of which two transformers TR1 and TR2 with 500kVA and TR3 with 2000kVA. The educational campus has high tension (HT) meter installation in the premises which records the dynamic energy consumption.

The data of six different building types under the institute is studied. The typical consumption under TR1, TR2 and TR3 are 21.2%, 20.6% and 58.2% respectively. The electricity demand of various building types under TR1, TR2 and TR3 is shown in the Figure 1.

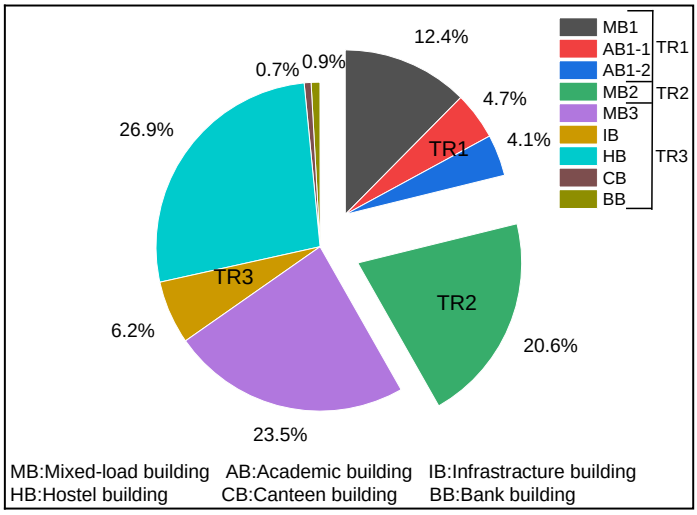

Figure 1. Typical electricity demand of various building types under educational institute

Academic building (AB) load constitutes combination of teaching, research, laboratory, library etc. Though mixed-load building (MB) i.e, MB1 and MB2 are dominated by loads similar to AB load type, they have been combined with other loads such as administration, data centre, cafeteria, cell tower etc. MB3 is much more diverse, complex and bulky load compared to rest of all other category of building load types. MB3 consists similar load to that of AB. In addition, MB3 also consists of heavy loads like air handling unit (AHU) of heating ventilation and air conditioning (HVAC) system, administration section, admission section, auditorium, sports complex, sewage treatment plant etc. Infrastructure building (IB) are chiller houses of HVAC system. The campus also has hostel building (HB), bank building (BB), canteen building (CB) where in energy consumption is substantial.

3. EDUCATIONAL BUILDING OPERATIONS UNDER DIFFERENT SITUATIONS

Two different situations of electricity usage patterns have been considered as follows:

3.1. Situation 1 - Electricity demand based on normal mode

Electricity use from 1st Mar 2018 to 29th Feb 2020 which comprises normal conditions without lockdown or other temporary disruption has been considered.

The electricity usage pattern of different building types under two situations is shown Figure 2. The individual building behaviour under two different situations are illustrated in Figure 3. In AB, MB, IB, CB and BB, there is a remarkable difference in electricity demand between daytime on weekdays and off-work hours, which is mainly caused by the different campus activities and attendance between the time slots. The electricity use was at minimum levels during weekend and off-work hours on weekdays, with the almost zero attendance.

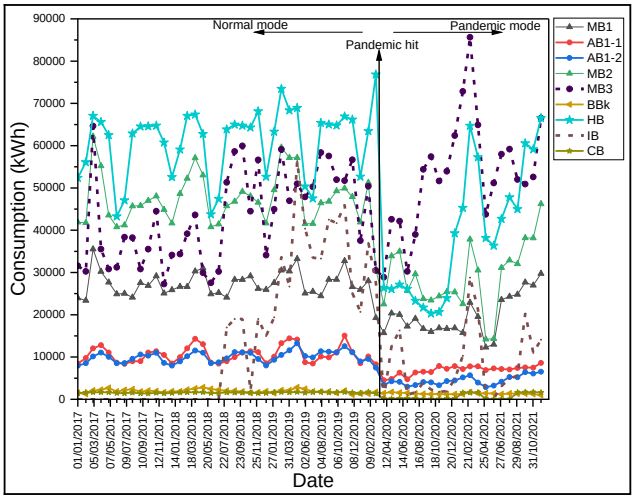

Figure 2. Electricity usage pattern of different building types during normal mode and pandemic mode

The electricity use pattern in HB is unlike the rest of building types. The HB load pattern can be compared to any residential load pattern. It generally has low demand during working hours and high demand when students are at hostel. IB are chiller houses of HVAC system, which use more energy in summer as shown in Figure 3(h). The IB demand has increased drastically during summer time i.e, in the month of May 2019.

3.2. Situation 2: Electricity demand based on pandemic operation mode

The decrease in the electricity usage due to pandemic which comprises the time period from Mar 2020 to Feb 2022 has been considered.

There were significant reductions in energy use during the COVID-19 pandemic in AB because of online teaching mode (Figure 3(a) and Figure 3(b)). similarly, MB1 and MB2 which were dominated by academic loads also showed significant drop (Figure 3(c) and Figure 3(f)). However, in MB3, the energy use change was insignificant due to certain mandatory loads such as HVAC systems. After COVID lockdown, the MB3 load increased drastically as offline activities started (Figure 3(i)).

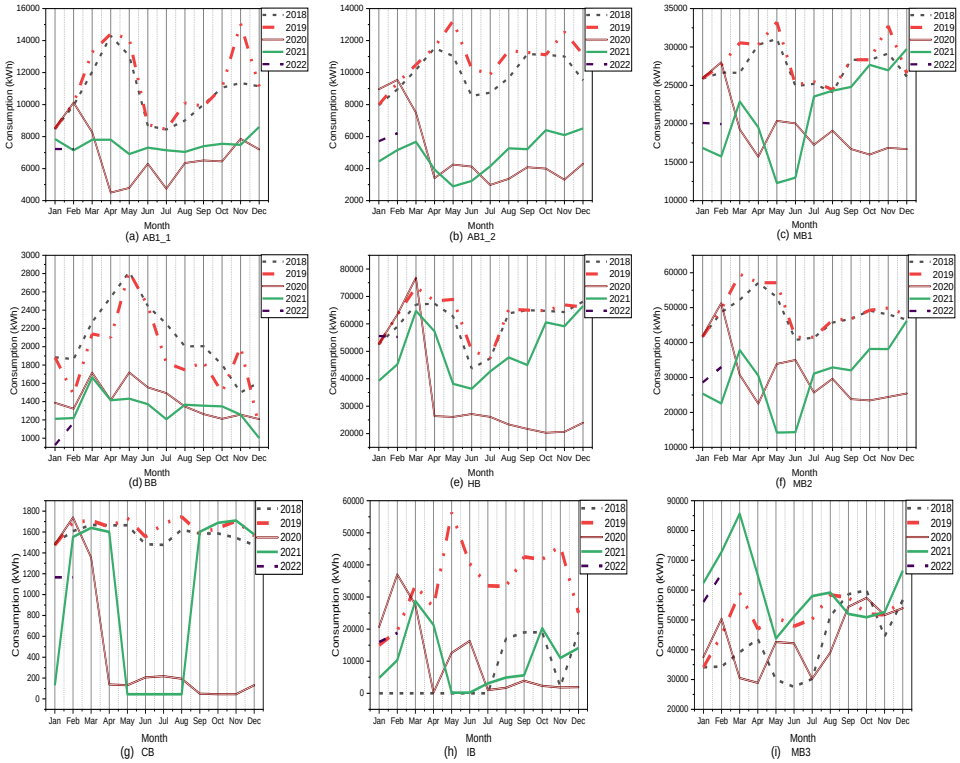

Figure 3. Behaviour of different building types during normal mode and pandemic mode

BB being the commercial establishment and open to public, the usage pattern has shown less deviation during pandemic and post pandemic period (Figure 3(d)). Due to the lesser number of students, there is a rapid decrease in the HB demand (Figure 3(e)). CB too is

severely affected during pandemic. Canteens were completely shut down to prevent people from gathering. Though canteens were kept open for very few months during loosing of lockdown restriction in the year 2020, later it was completely closed (Figure 3(g)).

AHU were kept under ON condition, however the chillers/IB were under off during most of the building working hours due to low occupancy. Therefore, the energy used by IB in situation 2 was considerably lower to that of situation 1, resulting in the energy use differences being more statistically significant (Figure 3(h)).

4. RESULTS AND DISCUSSION

Figure 4, Figure 5 and Figure 6 show the electricity usage pattern on monthly, daily and hourly basis. The trendlines show several features, summarized below:

The first phase of COVID-19 was reported during Mar 2020 due to which there was sudden drastic reduction in the energy consumption by the end of Mar 2020 and full month of Apr 2020, as the government of India undertook the decision of nationwide full lockdown which can be seen in Figure 4 as well as in Figures 6(c) and 6(d). The second wave started in the year 2021 with announcement of another complete lockdown in the month of May 2021 whose impact can be can be seen in Figure 6(e). It is interesting to observe that in the initial months of the year 2021 the electricity demand was increasing steadily day by day, whereas it started declining by the end of Apr 2021. The demand was low throughout months May and Jun 2021. Again, there was improvement from the month of Jul 2021 onwards.

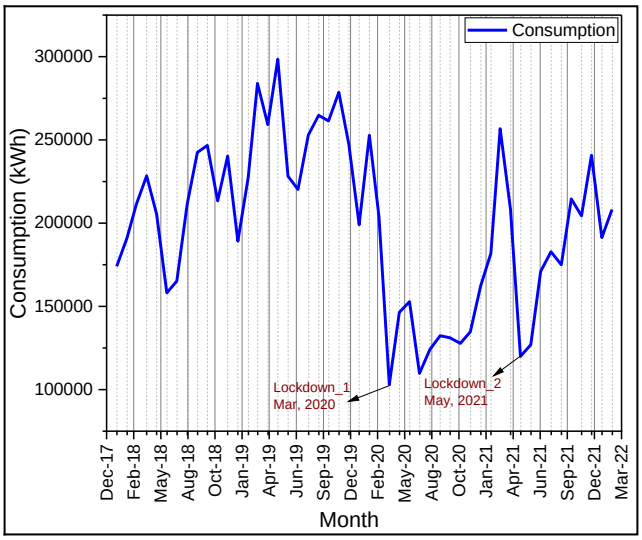

Figure 4. Monthly electricity demand of the educational institute from Jan 2018 to Feb 2022

Electricity demand for all the months in the year 2018 and 2019 were high and were declined only in the months Jan, Feb, Jun and Jul due to semester holidays. The energy

demand reduced significantly on daily basis during 2020 which can be seen in Figure 5. The demand dips were sharper and more instant both in 2020 as well as 2021 when there was complete lockdown, whereas they were curvy during other pandemic. This is because during complete lockdown some of the essential loads such as administration staff, research work, HVAC systems, canteen facility etc too were at halt. The electricity demand for lockdown months in the year 2020 were identical to 2019 weekend demand profiles. For the rest of the months in the year 2020 the demand profiles were extreme low and steady. Summary of the daily electrical demand variation is given in Table. 1.

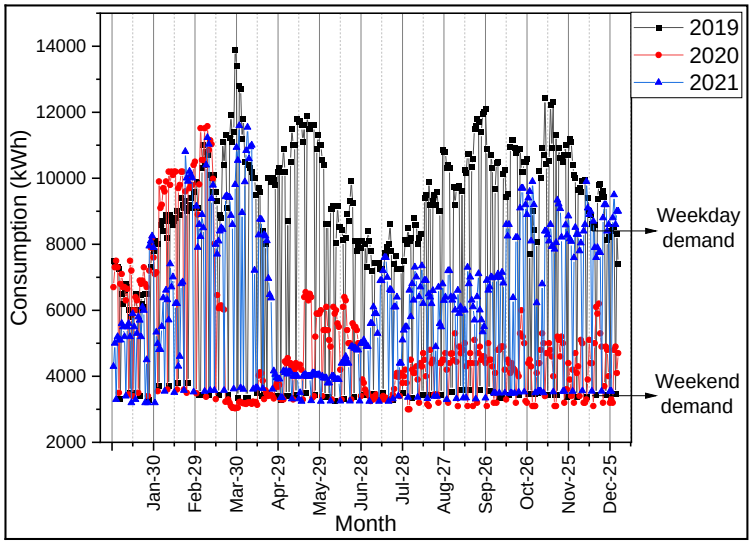

Figure 5. Daily electricity demand of the educational institute, which illustrates the impact of COVID-19

Table 1. SUMMARY OF THE DAILY ELECTRICAL DEMAND VARIATION

		Daily demand reduction in 2020 compared to 2019	Daily demand reduction in 2021 compared to 2019	Daily demand increase in 2021 compared to 2020
Weekday	Max demand	-16.71%	-16.58%	0.14%
	Min demand	-47.28%	-34.48%	24.75%
	Average demand	-43.42%	-27.64%	27.89%
Weekend	Max demand	-5.26%	-3.84%	1.5%
	Min demand	-8.08%	-1.96%	6.66%
	Average demand	-5.15%	-0.38%	5.02%

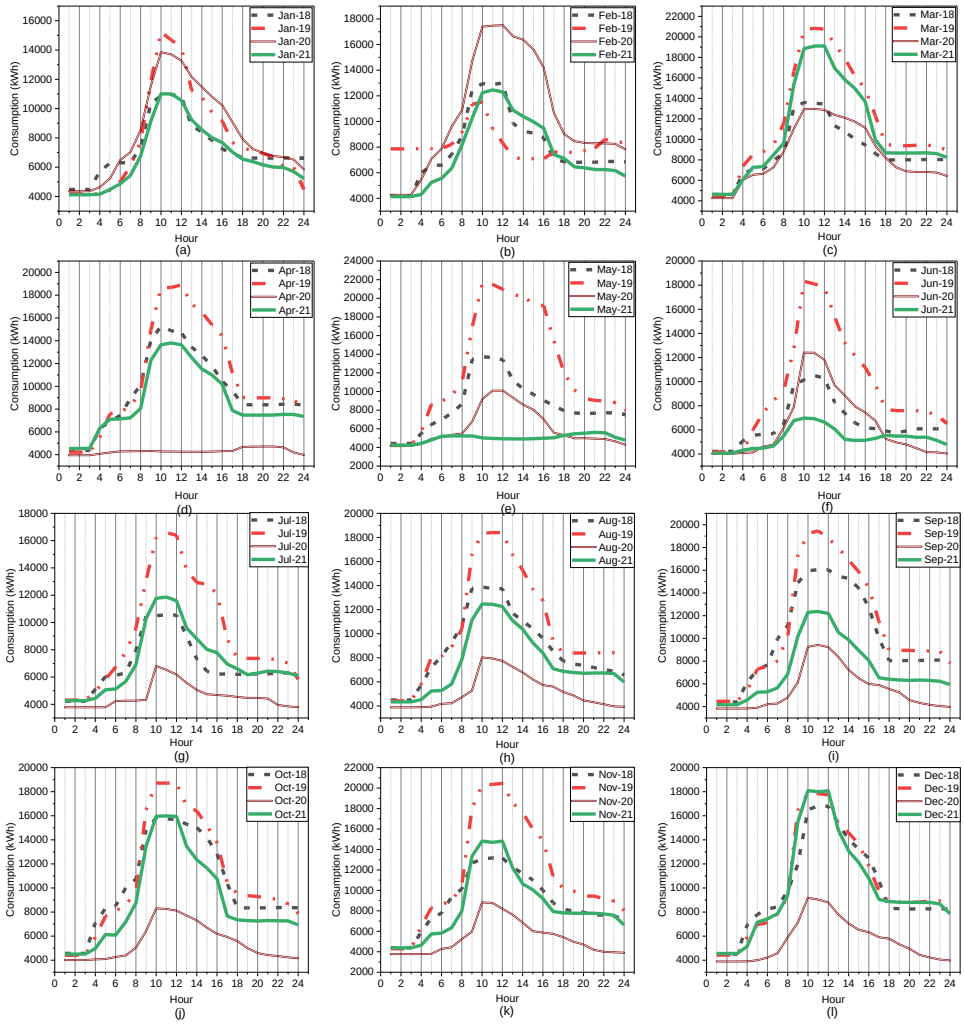

Figure 6. Hourly electricity demand of the educational instiute, which illustrates impact of impact of COVID-19

To further clarify the phenomena, the daily demand variation for the month of Mar and the first week of Apr for the years 2019, 2020 and 2020 are shown in Figure 7. The consumption profiles show how increasing lockdown measures caused a decrease in energy demand. In particular, from the second week of Mar 2020, a decrease in load was observed. Each box plot in Figure 7 shows the distribution of daily electrical demand. The median daily electrical demand of the institute was around 10300 kWh, 6000 kWh and 8500 kWh for the years 2019, 2020 and 2021 respectively and it was lowest for the year 2020 compared to other years. Furthermore, for the year 2020, the electrical demand values are approximately distributed between 3000 and 11500 kWh, which gives a wide range of possible electrical demand scenarios and illustrates the uncertainty in the demand during pandemic hit.

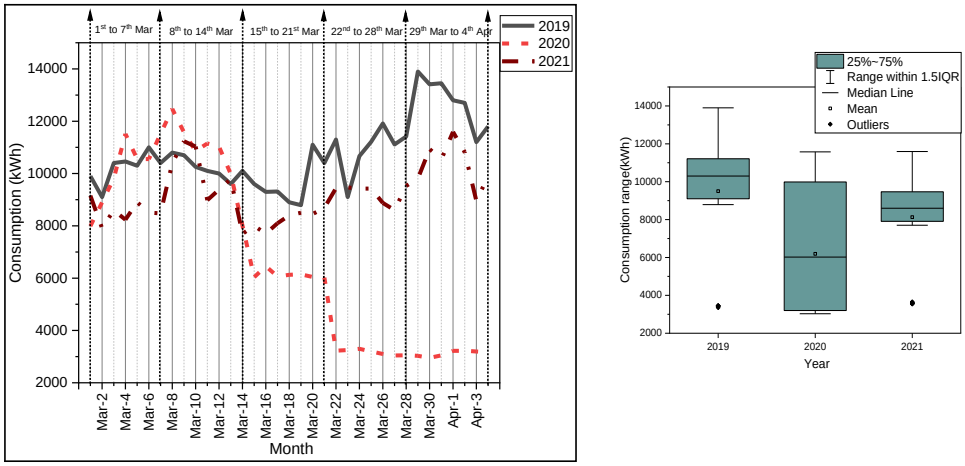

Figure 7. Five-week daily energy demand comparison and its descriptive statistics

Machine learning models were developed to assess the impact of COVID-19 and to forecast the post pandemic demand of the institute. In the modelling study, two different machine learning approaches were selected which includes ARIMA and LSTM. For determining the accuracy of the model, the current data is divided into two sets. They are training dataset (80% of the total data) and testing dataset (20% of the total data). Actual and predicted daily demand values are shown in Figure 8.

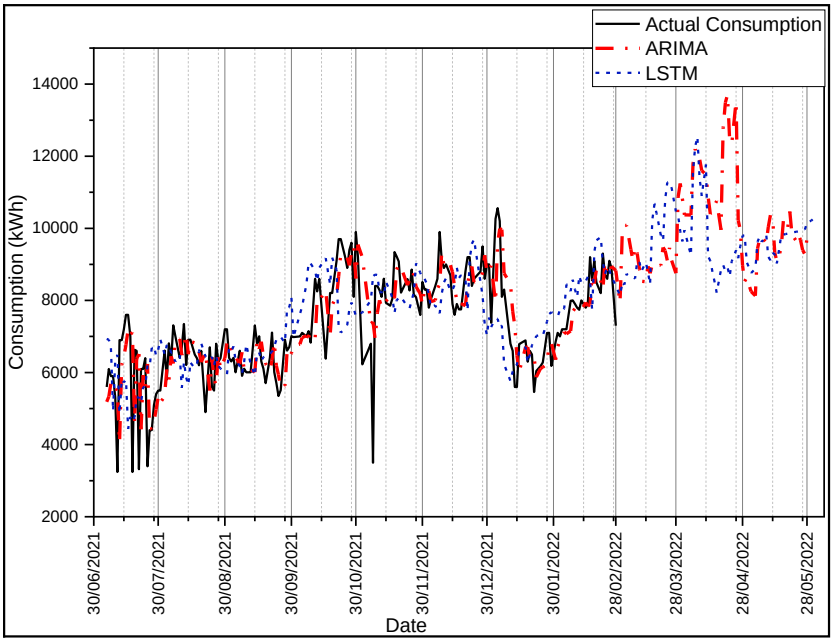

Figure 8 Daily electricity demand forecast

The last 3 months of the daily demand data were predicted and evaluated. When all the prediction values are evaluated, it can be said that the LSTM approach gave effective results compare to ARIMA. Prediction accuracy for ARIMA was 101.20 while the prediction accuracy for LSTM was 87.66.

5. CONCLUSION

COVID-19 has influenced the overall energy consumption of the educational institute. The overall energy consumption dropped by 43.42% in the year 2020 compared to its previous year 2019. However, the magnitude of impact varied from one category of building to another. In post covid condition the energy demand started increasing slowly which resulted in increase in the energy consumption by 23.48% in the year 2021 compared to its previous year 2020. LSTM technique is proved to be the most accurate approach for the data analysed in this study. However, the impact of the COVID-19 pandemic continues, and will have a long-term effect on stabilization of energy consumption of the educational institutes. Hence it is critical to study the future energy utilization and to forecast the energy usage pattens under various situations using various tools and techniques.

6. REFERENCES

[1] Subhadip Bhattacharya, Rangan Banerjee, Ariel Liebman, Roger Dargaville, 'Analysing the impact of lockdown due to the COVID-19 pandemic on the Indian electricity sector', International Journal of Electrical Power and Energy Systems, Elsevier, Feb., 2022

[2] Janmenjoy Nayak, Manohar Mishra, Bighnaraj Naik, Hanumanthu Swapnarekha, Korhan Cengiz, Vimal Shanmuganathan, 'An impact study of COVID-19 on six different industries:Automobile, energy and power, agriculture, education, traveland tourism and consumer electronics', Survey article, Wiley, Dec., 2020

[3] Xuechen Gui, Zhonghua Gou, Fan Zhang, Rongrong Yu, 'The impact of COVID-19 on higher education building energy use and implications for future education building energy studies',Energy & Buildings, Elsevier, Aug., 2021

[4] Yiyu Ding, Dmytro Ivanko, Guangyu Cao, Helge Bratteb, Natasa Nord, 'Analysis of electricity use and economic impacts for buildings with electric heating under lockdown conditions: examples for educational buildings and residential buildings in Norway', Sustainable Cities and Society, Elsevier, Aug., 2021

[5] Mehdi Chihib, Esther Salmeron-Manzano, Mimoun Chourak, Alberto-Jesus Perea-Moreno, Francisco Manzano-Agugliaro, 'Impact of the COVID-19 Pandemic on the Energy Use at the University of Almeria (Spain)', Sustainability, Article, MDPI, May, 2021

[6] Nima Safari, George Price, C.Y. Chung, 'Comprehensive assessment of COVID-19 impact on Saskatchewan power system operations', IET Generation, Transmission & Distribution, Wiley, Sep., 2020

[7] Ali Arjomandi-Nezhad, Amirhossein Ahmadi, Saman Taheri, Mahmud Fotuhi-Firuzabad, Moein Moeini-Aghtaie, Matti Lehtonen, 'Pandemic-Aware Day-Ahead Demand Forecasting Using Ensemble Learning', IEEE Access, Jan 2022

[8] Simona Vasilica Oprea, Adela Bara, Vlad Diaconita, Catalin Ceaparu, Anca Alexandra Ducman, 'Big Data Processing for Commercial Buildings and Assessing Flexibility in the Context of Citizen Energy Communities', IEEE Access, Dec., 2021

[9] Adnan Sozen, M. Mustafa İzgec, Ismail Kırbas, F. Sinasi Kazancıoglu, Azim Dogus Tuncer, 'Overview, modeling and forecasting the effects of COVID-19 pandemic on energy market and electricity demand: a case study on Turkey', Energy Sources, Part A: Recovery, Utilization, and Environmental Effects, Taylor & Francis, Apr.,2021

[10] Samir M. Shariff, 'Autoregressive Integrated Moving Average (ARIMA) and Long Short-Term Memory (LSTM) Network Models for Forecasting Energy Consumptions', European Journal of Electrical Engineering and Computer Science, Vol 6, Issue 3, May 2022

[11] Ashutosh Kumar Dubey, Abhishek Kumar, Vicente Garcia-Diaz, Arpit Kumar Sharma, Kishan Kanhaiya, 'Study and analysis of SARIMA and LSTM in forecasting time series data', Sustainable Energy Technologies and Assessments, Elsevier, Jul 2021

Design and Implementation of Forward-Boost Hybrid Converter for Solar Powered Electric Vehicle Charging Applications

Rakesh B*, Prakash D B

Department of EEE, B.M.S. College of Engineering, Bengaluru, India-560019

Email: rakesh.epe20@bmsce.ac.in

Abstract

Now a days, charging the Electric vehicle battery is the main concern. To make complete carbon free or emission less transportation, charging the battery using Non-Renewable energy will not suite well. For the development Environment and to withhold the sustainability of the society, we need to preserve the conventional energy resources and use the abundant energy called Renewable energy [1]. Integrating this with EV could be called as complete carbon free transportation. Though renewable energy such as Solar or wind is not stable or stagnant over the time, we could use an Energy storage system at the charging station end. By overcoming this unstable power generation from Solar panel, the designed converter has to feed constant Voltage and current to the energy storage. A well-within magnitude of power should be fed from the converter side. A simple kind of converter could only be used but over the large gain conditions, it results in lower conversion thus efficiency is decreased [2]. This paper will present an intelligent method for charging battery (energy storage) from Forward-Boost hybrid Converter. The gain factor was higher even at very low generation of solar power. A constant 200Volts and 20Ampere is achieved for charging the battery with the overall efficiency of nearly one hundred percent. This was simulated in MATLAB Simulink.

Keywords. EV-Electric vehicle, medium level voltage (level-2), Non-isolated Converter (Boost converter), Isolated Converter (Forward converter), PV-array, Li-ion battery, Environmentally friendly

1. INTRODUCTION

In this Era of revolutionary Technologies, Transportation domain is first in the segment. Having said that, electrifying them stands out from the rest. The very basic why to electrify them is to overcome Emission less transportation and Aid Carbon free, Pollution free, Noise free and Environmentally friendly Transportation [3]. There are many methods to generate this kind of Fuel globally. But, majority of them are Conventional energy generation method. By using the fuel which was produced from conventional method could only be segregated into Noise free and semi environmentally friendly transportation list but still comes under indirect way of carbon emission.

So, to be called Carbon free, Pollution free, Noise free and Full Environmentally friendly Transportation, the fuel has to generated from Non-Conventional energy sources. By integrating the Non-conventional energy produced into EV sector, will overcome the above non- environmentally friendly hurdle [4]. The very next hurdle is charging the battery of EV. Currently there are two types of charging implementations, one with

combination of Grid and Non-Conventional energy sources and other is Fully non-conventional way. The only advantage of Grid-Renewable combination is that, there is no requirement of Energy storing devices and the unusable power could be fed back to Grid, which helps in Power factor correction and balances the grid condition. The second, Trendy way is through Fully Renewable (Stand-alone) in which, it overcomes many disadvantages of Grid-Renewable combination and surplus generated power could be stored in the battery [5][6]. The main key element (Technically speaking) to charge the battery is Constant Voltage and Current across it. As we speak, the technology advancement increases the hassle of adopting to it. We all know that power generation through Non-Conventional sources like Solar, wind etc... will not be same at all time and its dependant on Solar Irradiance and Temperature mainly. This Solar Irradiance and Temperature will vary according to Season to season and weather to weather. Same goes with Wind, As the Atmospheric pressure changes with the distance (Pressure gradient) results in High Speed wind generation. During less pressure gradient, wind speed will be less and couldn't meet the generation requirement. So, the produced power from Solar or Wind won't be constant or same over the entire period. The necessary changes to get constant voltage and current can only be done at converter side and not at generation side most of the time. Since, the title deals with Solar powered, we'll be using Solar array or PV array as source of fuel generation to charge the battery [7]. As the converter is receiving input through PV array, the necessary changes have to be made at converter side. Be it in regulating the voltage levels or Amplifying or Attenuating it. Many DC-DC Converters are prominent in this segment for medium to high powered EV. Converter topology has to be chosen based on requirement. During very less power generation, the charging efficiency will decrease drastically in medium and High powered EV due to Converter performance limitation. There are many Chopper topologies available, be it Non-Isolated Chopper like Buck, Boost, Sepic, Cuk converters or Isolated Choppers like Flyback, Forward, Flyback-Forward, or even advanced converters like LLC Resonant or Series resonant DC-DC Converter [8]. The main hurdle is the random generation of power from PV array. Here in this paper, the level-2 voltages and current are been considered. During the peak time, the power generation will be more so at that time it's easy to boost up the voltage levels, so no doubt Boost Converter [9] [10] is most suitable due it its reliability, simple design and Implementation and cost wise. But the real problem comes while choosing the Proper converter which could not only boost up the voltage levels and also maintains the efficiency throughout off peak time. So, for this Forward converter is chosen because of instant conversion of voltage levels and no energy storage and normally way better when the required output current is on higher side. By considering all the parameter like components used, gain factor, overall efficiency, stress on the switches during operation, these two Topologies are best suitable.

In this paper, the hassle of Charging efficiency for medium and High powered EV is achieved nearly one hundred percent by proposing an Intelligent Forward-Boost Hybrid converter. The proposed converter is chosen so that one converter will overcome the performance limitation of the other and vice versa. The proposed converter is Design and Implemented for Medium Level (Level 2) which has voltage between 200-240Volts and current from 20-32Amperes. Here a Constant 200V & 20A is achieved to charge the Li-ion Battery. By this, losses at low power generation is minimised and switching stress of both the switches of converter is minimised thus improving converter life span.

2. BLOCK DIAGRAM OF PROPOSED MODEL:

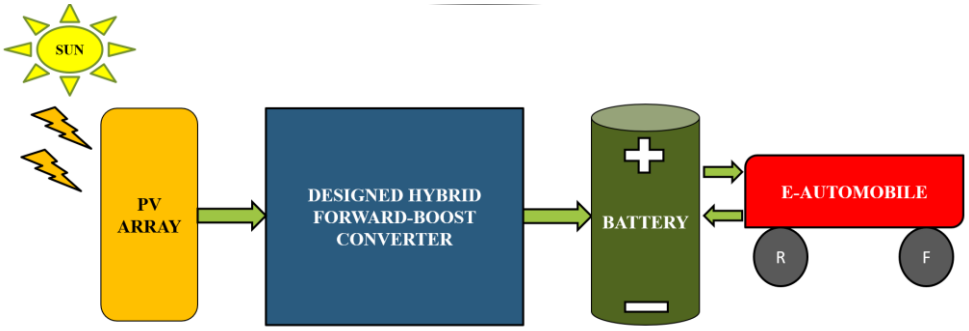

Figure 1: Block Diagram

The above figure gives an overall glimpse of the Proposed model. The radiation delivered from the sun will be captured by Solar Panel or an PV-Array. This intern will produce the massive amount of power in terms of voltage and current which completely depend on the Solar Irradiance and temperature on any particular day. Now, the generated power is completely not constant and varies depend on Irradiances and temperature. This is fed as an input to the Forward-Boost hybrid Converter, based upon the generated power, one of them is will carry the fuel to charge the battery while other won't. From this there will be constant DC voltage which is required for the battery to charge. Finally, the charged battery will be discharged or can also be charged (regenerative action) as the input fed into electric motor of the Automobile. The design and implementation concept of Forward-Boost converter is the heart of the model, along with PV-array, Battery. Here instead of Electric automobile, a simple Resistance load is considered to verify the charging and discharging period of the battery. The detailed flow flow-chart how exactly the flow (power flow) goes is discussed below.

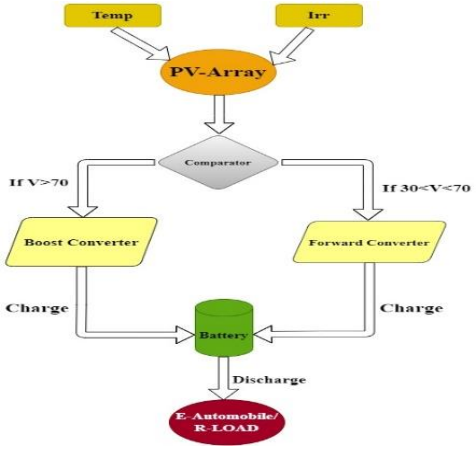

Figure 2: Flow chart of Proposed Model

3. METHODOLOGY:

3.1. Mode 1: Forward Converter =Activated, Boost Converter = De-activated

In this mode, Forward converter will be activated and Boost converter will be in off mode. This mode will be activated when the power generated from PV-array is anywhere in between 30V to 70V. For this a suitable design of Forward converter has been done with less switching loss and stress and greater efficiency. The switching frequency is high of 100kHz to reduce the compactness of the circuit by limiting the lesser values of Passive components like Inductor, capacitor and Resistor. A closed loop design is implemented to get the better results, accuracy and very less ripple while charging and dis-charging of battery through Isolated converter. (Forward converter)

3.2. Mode 2: Boost Converter = Activated, Forward Converter =De-activated

In this mode, Boost converter will be activated and Forward converter will be in off mode. This mode will be activated when the power generated from PV-array is above 70-80Volts. For this a suitable design of Boost converter has been done with less switching loss and stress and greater efficiency. The switching frequency is high of 100kHz to reduce the compactness of the circuit by limiting the lesser values of Passive components like Inductor, capacitor and Resistor. A closed loop design is implemented to get the better results, accuracy and very less ripple while charging and dis-charging of battery through Non-Isolated converter. (Boost converter)

3.3. Converter Design parameters:

3.3.1. Boost Converter:

$V_o = \frac{Vin}{(1-D)} \Rightarrow$ gives D, Duty ratio (1)

$L_{min} = \frac{\mathrm{D}(1-D)^2\mathrm{R}}{2f} \Rightarrow$L=1.25 L_{min} & C=$\frac{D}{Rf\left(\frac{\Delta Vo}{Vo}\right)} \Rightarrow$ C

gives L & C value for Continuous conduction of current (2)

3.3.2. Forward Converter:

$V_o = \mathrm{VinD}(\frac{\mathrm{N2}}{\mathrm{N1}}) \Rightarrow$D, Duty ratio (3)

By Assuming, 40% variation in Inductor Current

$iL_x = \frac{Vo}{R}$ (4)

$L_x = \frac{Vo(1-D)T}{\Delta iLx}$ & C =$\frac{(1-\mathrm{D})\,V_o}{8\Delta V_o\, L_x f^2}$ (5)

gives L & C value for Continuous conduction of current

Solving equations 1 to 5 and with some assumptions, converters parameter is designed.

Parameters	Forward Converter	Boost Converter
Input Voltage, Vin	30-70v	≥70v
Output Voltage, $Vout$	300v	300v
Output Current, Iout	20A	20A
Output ripple, $\frac{\Delta v_0 \cdot}{v_0}$	5%	5%
Frequency, f	100KHz	100KHz
Transformer ratio, N1:N2		1:10
Duty ratio, D	0.9-0.76%	42.85%
Inductor, L	2.76µH	$L_{x=}$0.4mH
Capacitor, C	15.µF	100µF
Load, R	10-15Ω	10-15Ω

The above table, represents the designed parameters which is implemented for Boost and Forward converters. Frequency of 100KHz is considered so that the size of the apparatus could be compact enough. All the Passive components designed are with respect to the continuous conduction mode of the current. The output ripple is will not be more than 5%.

At low power generation from PV-array, comparator will confirm whether the voltage generated is well within 30-70v, then Forward converter will be responsible for boosting up voltage to 300v. Later this voltage will be again stepped down from the switching actions and fed to the battery with constant 200v 20A rating. Similarly, when the comparator founds that voltage is above 70v, then boost converter will be responsible to produce 300v output voltage, this voltage is stepped down and fed into battery with constant 200v 20A rating in the designed MATLAB Simulink model and results were shown in section 4 & 5.

4. DESIGN & IMPLEMENTED MATLAB SIMULINK MODEL:

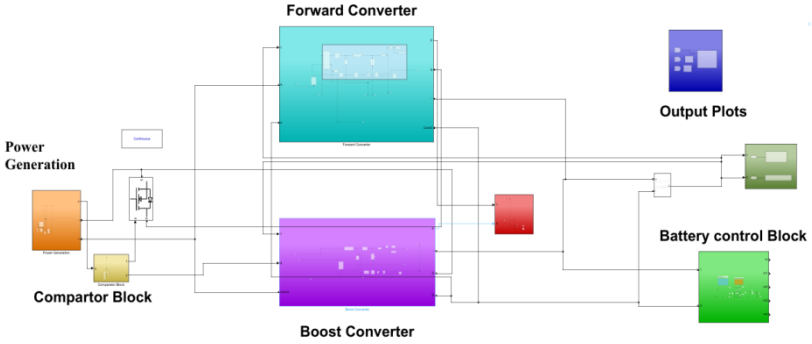

Figure 3: Forward-Boost Hybrid Converter

4.1. Battery Control Block:

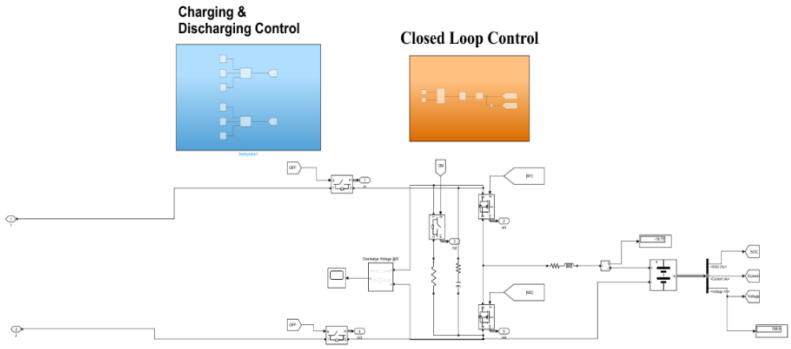

Figure 4: Battery Control Block

5. RESULTS:

5.1. Forward mode results:

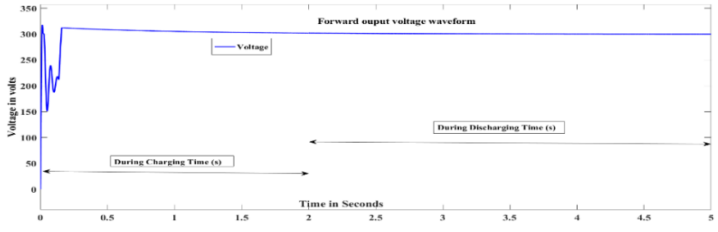

Figure 5: Forward Operated Output Voltage, 300V

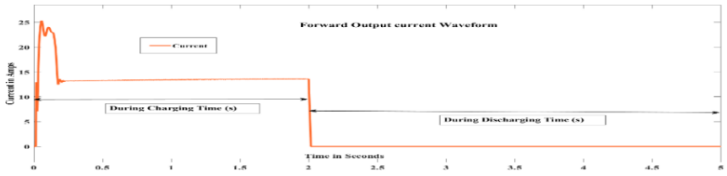

Figure 6: Forward Operated Output Current, $\boldsymbol{Iavg}$ =15-20A, 0-2s=Charging & 3-5s=Discharging

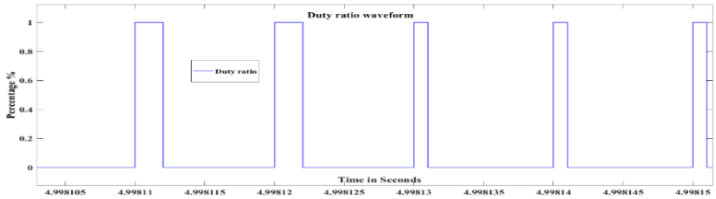

Figure 7: PID Generated Duty ratio during charging

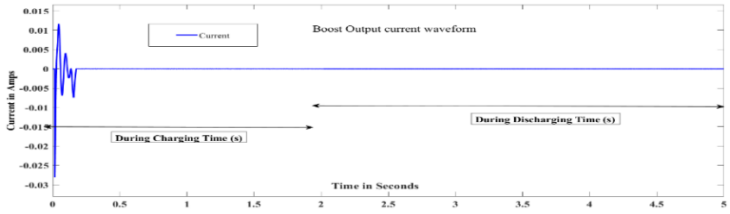

Figure 8: Boost Generated Current, 0A

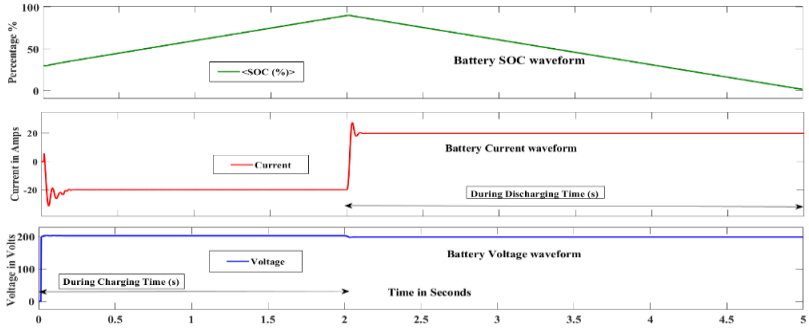

Figure 9: Battery Charging & Discharging Cycle, 0-2s=Charging & 3-5s=Discharging

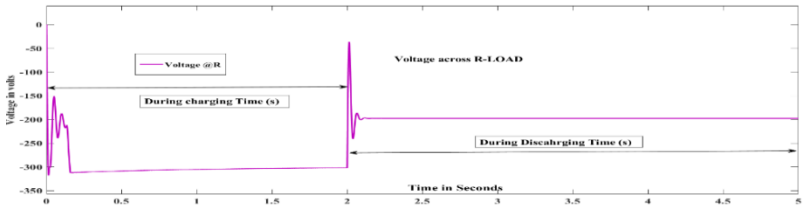

Figure 10:Output Voltage Across R-Load during charging=300v & discharging=200v

5.2. Boost mode results:

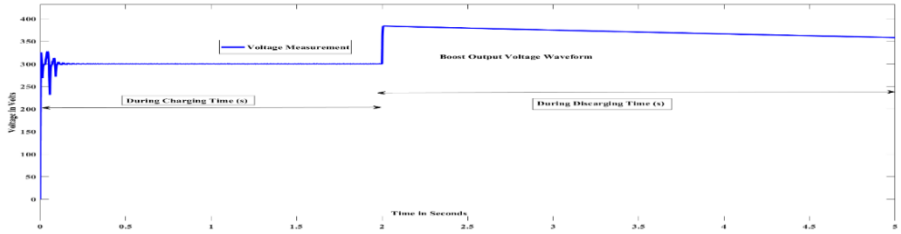

Figure 11: Boost Operated Output Voltage, 300V

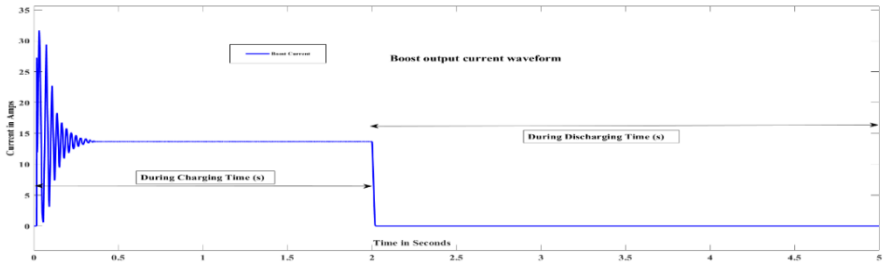

Figure 12: Boost Operated Output Current, $\boldsymbol{Iavg}$ =15-20A, 0-2s=Charging & 3-5s=Discharging

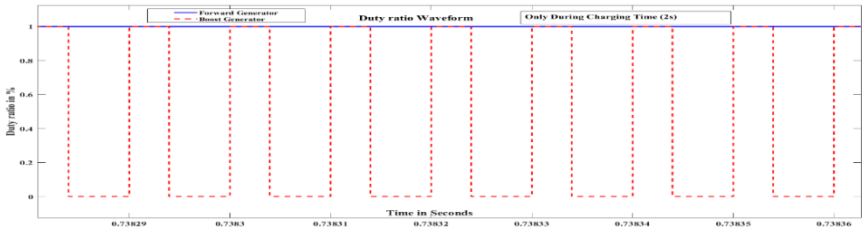

Figure 13: PID Generated Duty ratio during charging

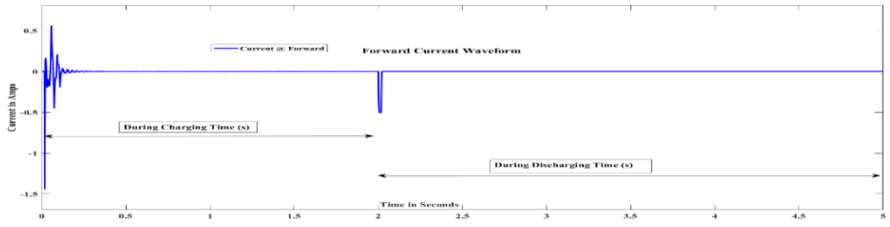

Figure 14: Forward Generated Current, 0A

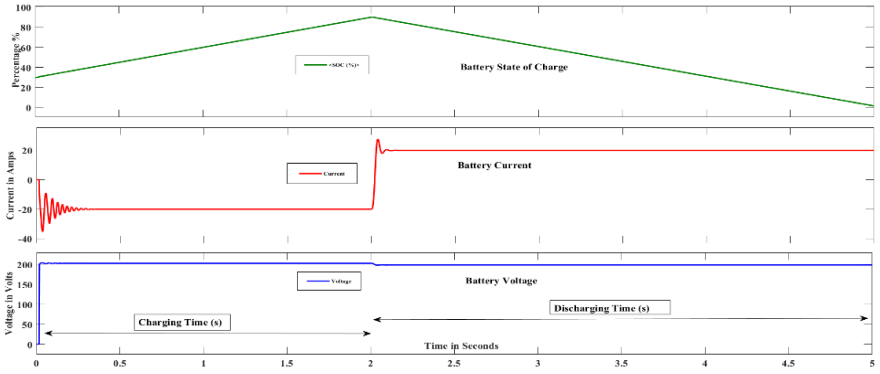

Figure 15: Battery Charging & Discharging Cycle, 0-2s=Charging & 3-5s=Discharging

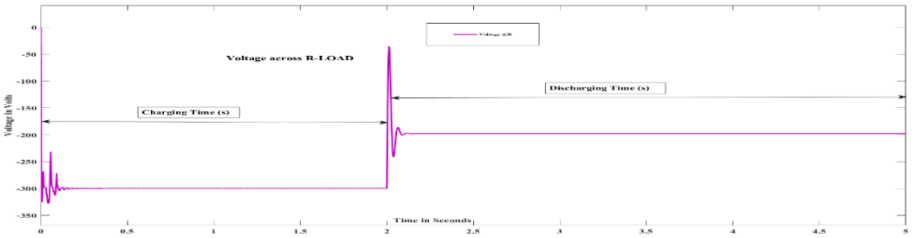

Figure 16: Output Voltage Across R-Load during charging=300v & discharging=200v

The Figure 5 & 11 shows the constant 300V during Charging & Discharging mode both from Forward and Boost converter. The figure 6 & 12 shows the 15-20A current during charging (0-2s) time and no current during discharging (3-5s) time in both the converters. Figure 7 & 13 represents the Duty ratio which is generated by PID controller in closed loop to trigger the Forward & Boost converter switches. The current across the other converter while one converter is feeding the load is shown in figure 8 & 14 respectively. This entire time, the voltage & current across the battery is 200V, 20A (both during charging & discharging) & Battery is charged till 90% of SOC in 2sec & discharges in 3sec from 90% to initial SOC value of 30% which could be seen in figure 9 & 15. Finally, the voltage across the R-load during charging (0-2s) is the voltage which is feeding the battery from converters that is 300V and while discharging time (3-5s) the voltage is found to be 200V which is fed from battery is shown in figure 10 & 16 respectively.

6. CONCLUSION:

By all means of experimentation, the best suitable Forward-Boost converter has been designed and implemented. The hassle of charging the battery with non-conventional energy sources is overcome. With this irrespective of power generated from PV-array a constant output producing of Hybrid converter is been implemented and verified in MATLAB Simulink. So, A Constant uninterrupted DC output voltage and Current of 200V, 20A is achieved to charge the Electric Vehicle Battery irrespective of Power generated from the PV-Array. When the voltage from the solar PV-array lies between 30V to 70V, forward converter is operational and Boost converter is in an idle state. On the other hand, when the input voltage from the solar PV-array is greater than 70V, Boost converter is operational and Forward converter is in an idle state. The Study, Analysis and Simulation of this hybrid converter topology has proven to be a reliable candidate for battery charging applications. By considering overall performance, we can say it's best suited for medium power EV charging applications, perfectly suitable for standalone solar powered charging stations for EV.

7. REFERENCES

[1] B. K et al., "Design and Simulation of Converters for HEV," 2022 International Conference on Electronics and Renewable Systems (ICEARS), 2022, pp. 436-439

[2] R. Rizzo and P. Tricoli, "Power Flow Control Strategy for Electric Vehicles with Renewable Energy Sources," 2006 IEEE International Power and Energy Conference, 2006.

[3] T. Ahmed et al., "Implementation of multi-input dual-output DC-DC boost converter using renewable energy for hybrid electric vehicle," 2015 2nd International Conference on Electrical Information and Communication Technologies (EICT), 2015, pp. 223-227

[4] A. A. Nilangekar and R. G. Kale, "Design and development of electric vehicle battery charging using MIMO boost converter," 2016 Online International Conference on Green Engineering and Technologies (IC-GET), 2016, pp. 1-6

[5] J. R. Babu, M. R. Nayak and B. Mangu, "Renewable Energy Applications and a Multi-Input DC-DC Converter for Hybrid Electric Vehicle Applications using Matlab/Simulink," 2021 Innovations in Power and Advanced Computing Technologies (i-PACT), 2021

[6] C. -G. Lee, J. -H. Kim and J. -H. Park, "Charge balancing PV System using charge-pumped flyback-boost-forward converter including differential power processor," 2016 IEEE 8th International Power Electronics and Motion Control Conference (IPEMC-ECCE)

[7] J. Chen, P. Shen and Y. Hwang, "A High-Efficiency Positive Buck–Boost Converter with Mode-Select Circuit and Feed-Forward Techniques," in IEEE Transactions on Power Electronics, vol. 28, no. 9, pp. 4240-4247, Sept. 2013

[8] S. Prabhakar and Febin Daya J L, "A comparative study on the performance of interleaved converters for EV battery charging," 2016 IEEE 6th International Conference on Power Systems (ICPS), 2016, pp. 1-6

[9] R. V. Muñoz, H. Renaudineau, S. Rivera and S. Kouro, "Evaluation of DC-DC buck-boost partial power converters for EV fast charging application," IECON 2021 – 47th Annual Conference of the IEEE Industrial Electronics Society, 2021, pp. 1-6

Investigation and Analysis of Real Time Transformer Oil Images at different Temperatures using Gabor Texture Features

Maheshan C M[1], H Prasanna Kumar[2]

[1]*Research scholar, Department of Electrical Engineering, VTU-RRC Mysuru.*
(Affiliated to VTU, Belagavi). Karnataka State, India
And
Associate Professor, Department of Electrical Engineering,
University Visvesvaraya College of Engineering, Bangalore University city campus,
K. R. Circle, Bengaluru-560 001.
maheshan.cm@gmail.com

[2] *Professor, Department of Electrical Engineering,*
University Visvesvaraya College of Engineering,
Bangalore University city campus, K. R. Circle, Bengaluru-560 001.
uvcehpk@gmail.com

Abstract.

A new technique in the investigation and analysis of real time transformer oil at different temperatures using Gabor image texture features is proposed in this paper. A numerical evaluation performed using Gabor filtering technique to characterize its textural properties of transformer oil test images. Transformer oil characteristics define the performance of power transferring equipment. An experiment conducted to capture test images at different temperatures. These images are enhanced using linear and nonlinear noise eliminating filters. The statistical features extracted for unused or normal as well as enhanced transformer oil image at different temperatures. The results of improved complex shock filtered images indicate the better recognition of significant textures of the test images since they are nearly equivalent to normal oil test images. The experimental results of texture features extracted from the Gabor filter realize a modern method in the analysis of real time transformer oil images operating under different temperatures.

Keywords: Transformer oil, image processing, Gabor filter, OSF, ICSF.

1. INTRODUCTION

Texture feature extraction is a process of evaluating as well as describing the feature characteristics of an image which numerically describes that texture image properties. Texture features are very helpful and have been used practically in image processing domain. Besides, the texture features can also differentiate between objects with similar colours and shapes [1-2]. Gabor filter is an efficient method to extract texture features from the images. Basically, Gabor filters are collection of wavelets. Each wavelet of the filter captures energy at a specific frequency along with a specific direction. Expanding a signal through this filter presents a localized frequency description, thus capturing local features of the signal. Thus the texture features can be extracted through this group of energy distributions [3-5].

Transformer is an important device which connects generation, transmission and distribution electrical power system. Its performance depends on the cooling as well as insulation efficiency of the working device. Transformer oil provides the insulation along with cooling for the internal parts of the transformer [6-7]. The characteristic electrical, chemical, thermal as well as physical properties of the transformer oil changes with the different operating temperatures in addition to loading conditions [8-10]. Digital image processing methods are used as latest technology to monitor the performance of the transformer instead of time consuming classical methods [11]. This paper proposes an image analysis technique to identify the Gabor texture features of a test image. Transformer oil images acquired through digital camera in specific combined with noise signal due to improper lighting levels in addition to as well movement of oil. The image preprocessing filters used to eliminate the noise in the test images.

In this paper, the weiner filter, Non-Local Means (NLM) filter, Original Shock Filter (OSF), Complex Shock Filter (CSF) and Improved Complex Shock Filters (ICSF) are used for image enhancement of transformer oil images at different temperatures [12-14]. The objective of this paper is to investigate the Gabor texture features of real time transformer oil images at different temperatures. An experiment was conducted to acquire the transformer oil images using digital camera at 30^0C, 60^0C, 90^0C and the maximum temperature limited to 120^0C [15]. The betterment of test images are achieved using image enhancement filters. Gabor texture features extracted from the original image as well as from the filtered transformer oil images.

2. MATERIALS AND METHODS

This section explains the data collection, method adopted to extract textures of test images. In this paper the test images are real time transformer oil images.

2.1. Data Collection

An experiment is conducted on transformer oil to capture the transformer oil images at different temperatures. In this paper the transformer oil images are captured at 30^0C, 60^0C, 90^0C as well as 120^0C temperatures. These images are enhanced with difference noise eliminating filters. The original images captured as well as filter image considered as test images. Typical test images are presented in figure 1[15].

Figure 1 Typical transformer oil test images captured at different temperatures [15]

2.2. Method

Gabor filter introduced by Gabor [16] and it is applied to extract features by analyzing the frequency domain of the image. Gabor filter is basically a Gaussian function modulated by complex sinusoidal of frequency and orientation. It has the ability to perform both in spatial and frequency domain and can be in any number of dimensions. These filters are more desirable since they provide the finer distinctions of the different textures [17-19]. Figure 2 demonstrates Gabor image texture feature extraction methodology of real time transformer oil images. The real impulse response of two dimensional Gabor filter given as in Equation (1).

$$h(x,y) = \frac{1}{2\pi\sigma_x\sigma_y} \equiv e^{-\frac{x^2}{2\sigma_x^2}-\frac{y^2}{2\sigma_y^2}} cos(2\pi\, u_0 x) \quad (1)$$

Where u_0 is radial frequency of Gabor function, σ_x and σ_y are constants of Gaussian envelope along x and y axis respectively. The Gabor wavelets or filters are generated to cover the two dimensional image planes with arbitrary orientations can be obtained as in equation (2) as

$$x' = x\cos\theta + y\sin\theta \;\text{ And }\; y' = -x\sin\theta + y\cos\theta \quad (2)$$

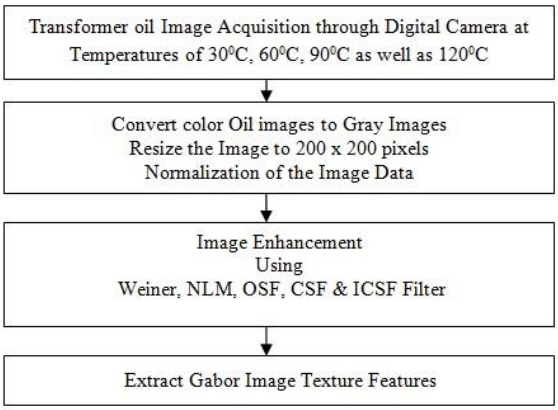

Figure 2. Gabor Image Texture Feature Extraction Methodology

3. RESULTS AND DISCUSSION

In this section, the numerical and graphical results of Gabor texture features of transformer oil test images are presented. The acquired transformer oil images at different temperatures are converted into gray images. The gray scale images are resized to 200 x 200 pixels. All images are enhanced through wiener, NLM, OSF, CSF and ICSF. The 25 Gabor image texture features were extracted from transformer oil (normal or unused / with metal nails / with metal nails and conductor coil) 30^0C, 60^0C, 90^0C and 120^0C images. In this paper, only 30^0C Gabor feature magnitude values listed in table 1 to table 3, but figure 3, 4 and 5 shows the Gabor texture features for all temperatures using Column plots.

Table 1 Gabor Texture features of Unused/Normal Transformer oil at 30^0 C

Sl. No.	Gabor Texture features	30^0 C N	30^0 C N- Weiner filter	30^0C N- NLM filter	30^0C N- OSF filter	30^0C N- CSF filter	30^0C N- ICSF filter
1	Gabor-1	459.16	459.13	460.97	459.16	459.20	459.35
2	Gabor-2	3.89	3.86	3.90	3.99	3.89	3.89
3	Gabor-3	9.41	9.35	9.37	9.46	9.37	9.36
4	Gabor-4	27.61	27.42	26.99	27.67	27.47	27.26
5	Gabor-5	352.10	352.16	353.46	352.10	352.12	352.22
6	Gabor-6	328.71	328.68	330.00	328.71	328.74	328.85
7	Gabor-7	29.96	29.95	30.08	29.97	29.97	29.98
8	Gabor-8	8.63	8.53	8.54	8.70	8.58	8.56
9	Gabor-9	35.37	35.26	35.10	35.40	35.30	35.22
10	Gabor-10	226.54	226.62	227.39	226.55	226.55	226.61
11	Gabor-11	378.05	378.01	379.53	378.04	378.08	378.20
12	Gabor-12	12.72	12.69	12.77	12.73	12.72	12.73
13	Gabor-13	9.28	9.06	8.99	9.41	9.16	9.11
14	Gabor-14	26.41	25.92	24.57	26.59	26.12	25.83
15	Gabor-15	304.15	304.22	305.31	304.14	304.17	304.27
16	Gabor-16	378.05	378.01	379.53	378.04	378.08	378.20
17	Gabor-17	12.72	12.69	12.77	12.73	12.72	12.73
18	Gabor-18	9.27	9.06	8.99	9.40	9.16	9.11
19	Gabor-19	26.38	25.88	24.58	26.54	26.09	25.80
20	Gabor-20	304.29	304.36	305.46	304.28	304.31	304.41
21	Gabor-21	328.71	328.68	330.00	328.71	328.74	328.85
22	Gabor-22	29.96	29.95	30.08	29.97	29.97	29.97
23	Gabor-23	8.63	8.53	8.54	8.69	8.57	8.55
24	Gabor-24	35.33	35.22	35.08	35.36	35.27	35.19
25	Gabor-25	226.70	226.78	227.55	226.70	226.71	226.77

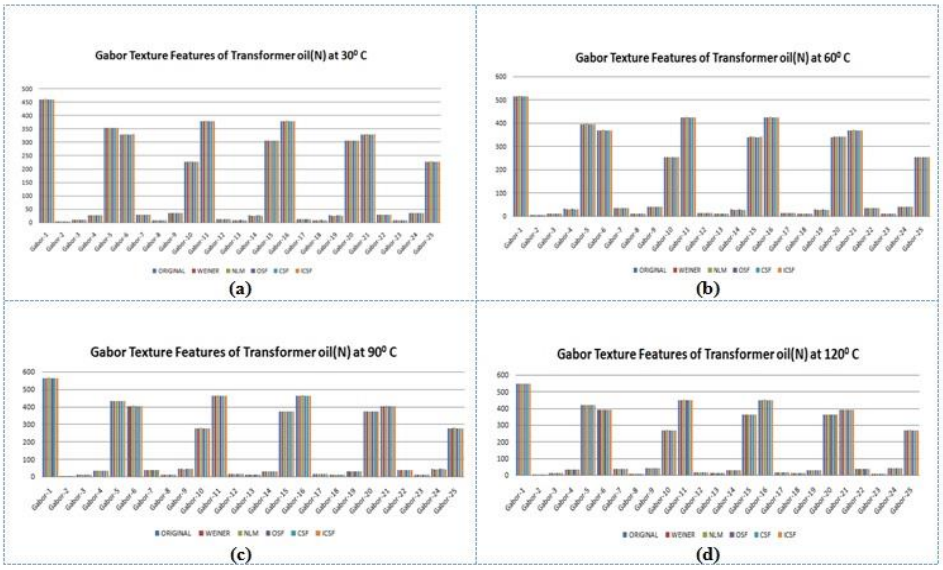

Figure 3 Column plot of Gabor Texture Features of Unused/Normal Transformer oil At (a) 30^0 C (b) 60^0 C (c) 90^0 C (d) 120^0

Table 2 Gabor Texture features of Transformer oil with metal nails at 30^0 C

Sl. No.	Gabor Texture features	30^0 C WM	30^0 C WM-Weiner filter	30^0C WM-NLM filter	30^0C WM-OSF filter	30^0C WM-CSF filter	30^0C WM-ICSF filter
1	Gabor-1	416.73	416.68	418.35	416.74	416.75	416.83
2	Gabor-2	3.50	3.47	3.51	3.60	3.50	3.50
3	Gabor-3	8.45	8.39	8.42	8.50	8.42	8.40
4	Gabor-4	24.72	24.55	24.11	24.80	24.59	24.39
5	Gabor-5	318.82	318.86	319.98	318.83	318.82	318.87
6	Gabor-6	298.32	298.28	299.48	298.33	298.33	298.39
7	Gabor-7	27.18	27.17	27.29	27.19	27.18	27.19
8	Gabor-8	7.75	7.68	7.70	7.81	7.71	7.70
9	Gabor-9	31.82	31.72	31.62	31.85	31.76	31.70
10	Gabor-10	204.96	205.03	205.66	204.98	204.96	204.98
11	Gabor-11	343.10	343.06	344.43	343.11	343.11	343.18
12	Gabor-12	11.54	11.52	11.59	11.55	11.54	11.55
13	Gabor-13	8.31	8.19	8.16	8.39	8.24	8.22
14	Gabor-14	24.40	23.90	22.46	24.50	24.07	23.74
15	Gabor-15	275.85	275.91	276.88	275.86	275.86	275.90
16	Gabor-16	343.10	343.06	344.43	343.11	343.11	343.18
17	Gabor-17	11.54	11.52	11.59	11.55	11.54	11.55
18	Gabor-18	8.31	8.19	8.16	8.39	8.24	8.22
19	Gabor-19	24.38	23.88	22.44	24.47	24.06	23.72
20	Gabor-20	275.98	276.04	277.00	275.98	275.98	276.03
21	Gabor-21	298.32	298.28	299.48	298.33	298.33	298.39
22	Gabor-22	27.18	27.17	27.29	27.19	27.18	27.19
23	Gabor-23	7.75	7.68	7.70	7.80	7.71	7.70
24	Gabor-24	31.81	31.71	31.61	31.84	31.75	31.69
25	Gabor-25	205.11	205.17	205.80	205.11	205.10	205.12

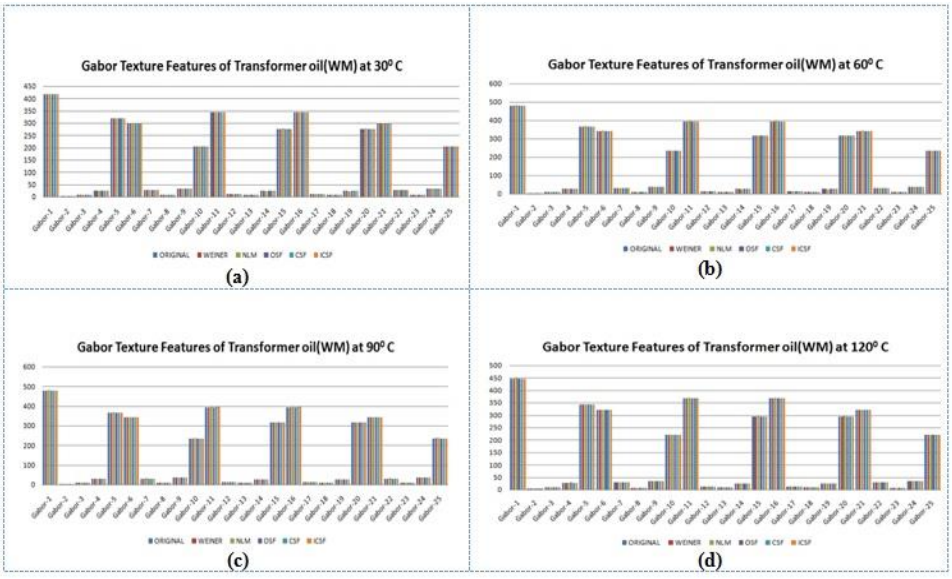

Figure 4 Column plot of Gabor Texture Features of Transformer oil with metal nails At (a) 30^0 C (b) 60^0 C (c) 90^0 C (d) 120^0 C

Table 3 Gabor Texture features of Transformer oil with metal nails and Conductor coil at 30^0 C

Sl. No.	Gabor Texture features	30^0 C WMC	30^0 C WMC-Weiner filter	30^0C WMC-NLM filter	30^0C WMC-OSF filter	30^0C WMC-CSF filter	30^0C WMC-ICSF filter
1	Gabor-1	579.31	579.28	581.59	579.33	579.35	579.47
2	Gabor-2	4.88	4.84	4.89	4.95	4.87	4.87
3	Gabor-3	11.83	11.72	11.72	11.89	11.76	11.72
4	Gabor-4	34.00	33.78	33.43	34.06	33.84	33.66
5	Gabor-5	443.59	443.65	445.30	443.61	443.62	443.69
6	Gabor-6	414.71	414.68	416.34	414.72	414.73	414.82
7	Gabor-7	37.77	37.76	37.92	37.78	37.77	37.78
8	Gabor-8	10.74	10.63	10.65	10.81	10.68	10.65
9	Gabor-9	43.81	43.72	43.72	43.84	43.76	43.71
10	Gabor-10	284.16	284.24	285.22	284.17	284.17	284.20
11	Gabor-11	476.97	476.94	478.84	476.99	477.00	477.10
12	Gabor-12	15.98	15.95	16.05	15.99	15.98	15.99
13	Gabor-13	11.18	11.06	11.08	11.26	11.12	11.08
14	Gabor-14	30.28	30.00	29.51	30.38	30.10	29.90
15	Gabor-15	381.46	381.54	382.91	381.48	381.48	381.55
16	Gabor-16	476.97	476.94	478.84	476.99	477.00	477.10
17	Gabor-17	15.98	15.95	16.05	15.99	15.98	15.99
18	Gabor-18	11.18	11.06	11.08	11.26	11.12	11.08
19	Gabor-19	30.22	29.95	29.50	30.31	30.05	29.84
20	Gabor-20	381.08	381.15	382.53	381.10	381.10	381.17
21	Gabor-21	414.71	414.68	416.34	414.72	414.73	414.82
22	Gabor-22	37.77	37.76	37.92	37.78	37.77	37.78
23	Gabor-23	10.74	10.63	10.65	10.80	10.68	10.64
24	Gabor-24	43.78	43.70	43.72	43.81	43.73	43.69
25	Gabor-25	283.60	283.67	284.65	283.61	283.60	283.64

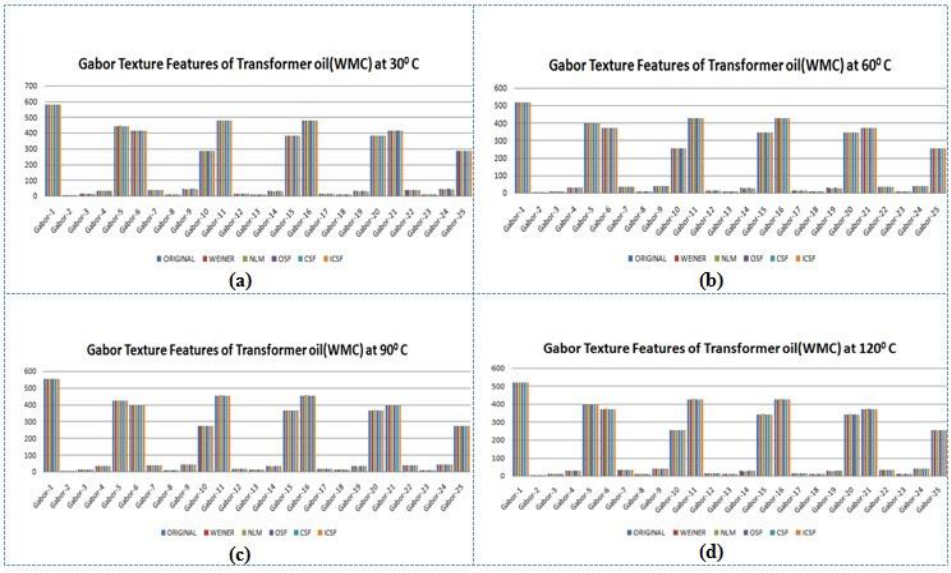

Figure 5 Column plot of Gabor Texture Features of Transformer oil with metal -nails and conductor coils at (a) 30^0 C (b) 60^0 C (c) 90^0 C (d) 120^0

Gabor texture features explore the spatial and frequency values in terms of magnitude. From tables and figures, it is observed that higher variations of the magnitude values with special frequency relation of Gabor image texture features. Gabor feature envelope controls the frequency magnitude of the image texture feature. For a very large feature envelope approaches a high magnitude, and for a very small feature envelope, the magnitude height stretches across the image.

4. CONCLUSIONS

This paper presents an effective method in the investigation and analysis of Gabor texture image features for real time transformer oil images acquired at 30^0C, 60^0C, 90^0C as well as 120^0C temperatures. This paper demonstrates numerical results of transformer oil for normal as well as enhanced images. Twenty five Gabor image texture features were evaluated for all the test images. The results indicate that the features evaluated were substantially identifying texture features. The ICSF filter texture features provide best results among all filters. This paper concludes that the Gabor texture features extracted through ICSF is best for further analysis of images. The extension of this study can be used for online or offline condition monitoring of transformer oil.

5. REFERENCES

[1] D. Zhang, M. M. Islam, G. Lu, and I. J. Sumana, "*Rotation Invariant Curvelet Features for Region Based Image Retrieval",* International Journal Computer Vision, Vol. 98(2), 2012. pp. 187-201. DOI:10.1007/s11263-011-0503-6

[2] A. Humeau-Heurtier, "*Texture Feature Extraction Methods: A Survey*", IEEE Access, Vol. 7, 2019. pp. 8975-9000. DOI: 10.1109/ACCESS.2018.2890743.

[3] Ajay Kumar and Grantham K. H. Pang., "Defect Detection in Textured Materials Using Gabor Filters", IEEE Transactions on Industry Applications, Vol. 38, 2002. pp. 425-439.

[4] J. Kamarainen, "*Gabor features in image analysis*", 3rd International Conference on Image Processing Theory, Tools and Applications (IPTA), 2012. pp. 13-14. DOI: 10.1109/IPTA.2012.6469502.

[5] Erwin et al., "*The Enhancement of Fingerprint Images using Gabor Filter*", ICONISCSE. IOP Publishing. IOP Conf. Series: Journal of Physics: Conf. Series 1196. 2019. pp. 1-6. DOI:10.1088/1742-6596/1196/1/012045.

[6] Waldemar Ziomek, “Transformer Electrical Insulation”, Editorial, IEEE Transactions on Dielectrics and Electrical Insulation, Vol. 19(6), 2012. pp.1841-42.

[7] Liao, R.J. Hao, J. Chen and G. Yang, “*Quantitative analysis of insulation condition of oil-paper insulation based on frequency domain spectroscopy*”, IEEE Transactions on Dielectrics and Electrical Insulation, Vol. 22(1), 2015. pp. 322-334. DOI:10.1109/TDEI.2012.6215085.

[8] Suwarno and Pasaribu RA., “*Thermal aging of mineral oil-paper composite insulation for high voltage transformer*”, Int J Electr Eng Inf., Vol. 8(4), 2016. pp. 820–835. DOI: 10.15676/ijeei.2016.8.4.9.

[9] R. Siva Sai, J. Rafi, S. Farook, NMG. Kumar, M. Parthasarathy and Ashok B. R., “*Degradation studies of electrical, physical and chemical properties of aged transformer oil”,* First International Conference on Advances in Physical Sciences and Materials. J. Phys.: Conf. Ser. 1706 012056. 2020. DOI:10.1088/1742-6596/1706/1/012056.

[10] Akshatha S Raj and C M Maheshan, “*Artificial bee colony algorithm based interpretation of dissolved gas analysis*”, 4th International Conference on Electrical, Electronics, Communication, Computer Technologies and Optimization Techniques (ICEECCOT), 2019. pp. 106 -110.

[11] C M Maheshan and Prasanna Kumar H, *“A Review of image Processing Applications in Fault Detection of Transformer Oil”,* International Journal of Research in Advent Technology. ICTTSTM, 2018. pp. 433-437.

[12] C M Maheshan and H Prasanna Kumar, “*Image enhancement of Transformer oil images using improved complex shock filter*” IIETA Instrumentation Mesure Metrologie, Vol. 18, issue 4, 2019. pp. 407-412.

[13] C M Maheshan and H Prasanna Kumar, “*Investigation and analysis of real time transformer oil Images using haralick texture features*”, Third International Conference on Multimedia Processing, Communication & Information Technology (MPCIT), 2020. pp. 45-50. DOI: 10.1109/MPCIT51588.2020.9350502.

[14] C M Maheshan and H Prasanna Kumar, “*Intensity-Based Feature Extraction of Real-Time Transformer Oil Images*”, Book chapter in Advances in VLSI, Signal Processing, Power Electronics, IoT, Communication and Embedded Systems, 2021. pp. 379 -396. DOI: 10.1007/978-981-16-0443-0_31.

[15] C M Maheshan and H Prasanna Kumar, “*Performance of image pre-processing filters for noise removal in transformer oil images at different temperatures*”, Research article. SN applied sciences, A Springer Nature Journal. 2:67, 2020.

[16] D. Gabor, “*Theory of Communication. Journal of the Institution of Electrical Engineers*”, Vol. 93(26), 1946. pp. 429-441.

[17] Tadic V, Kiraly Z, Odry P,Trpovski Z and Loncar-Turukalo T, "*Comparison of Gabor Filter Bank and Fuzzified Gabor Filter for License Plate Detection*", Acta Polytech., Hung., Vol.17, 2020; pp. 61–81.

[18] Luan S, Chen C, Zhang B, Han J and Liu J., "*Gabor Convolutional Networks*", IEEE Trans. Image Processing, Vol. 27, 2018. pp. 4357–4366.

[19] Allagwail S, Gedik O.S and Rahebi J, "*Face Recognition with Symmetrical Face Training Samples Based on Local Binary Patterns and the Gabor Filter*", Symmetry, 11, 2019. DOI:10.3390/sym11020157

Biographies

Maheshan C M received the BE and ME from Bangalore University in 1999 and 2003 respectively. He is pursuing his Ph.D. in Electrical Engineering from VTU, Belagavi. He is currently working as an Associate Professor at the Department of Electrical Engineering, UVCE, K.R.Circle, Bangalore University, Bengaluru-01. His research areas include Power systems engineering, Image Processing, and Control systems.

Dr. H. Prasanna Kumar received the BE from Karnataka University in 1997, M. Tech from Visvesvaraya Technological University (VTU) in 2005 and received his Ph.D. during 2015 at Anna University, Chennai. He is currently working as Professor in the Department of Electrical Engineering, University Visvesvaraya College Engineering (UVCE), Bangalore University, K.R. Circle, Bengaluru-01. His research interests cover Biomedical Image processing, Instrumentation and Process Control.

Modification of Electronic Warfare (EW) Suite on Jaguar Fighter Aircraft

Sujitha S[1], Deepa V B[2], Vishnupriya G[3], Sankeerthini [4], Saranya S[5]

[1]Associate Professor,[2] Assistant Professor, Department of Electrical & Electronics Engineering, New Horizon College of Engineering, Bangalore.

[3,4,5] Student, Department of Electrical & Electronics Engineering, New Horizon College of Engineering, Bangalore.

Abstract.

The performance of electronic reconnaissance equipment as a component of the Electronic intelligence (ELINT) and the Electronic Support Measure (ESM) systems is directly influenced by radar signal sorting, which is a critical mechanics in campaign prioritization .Regularities of signal sorting are significantly undermined as radar systems become more complicated, countermeasure measures in modern electronic warfare become harsher, and low-probability of intercept (LPI) develops. As a result, the outcomes of sorting radio signals based on five customary characteristics aren't particularly impressive. The basic restriction of signal filtering in ESM and ELINT systems is de inter leaving advanced radar signals, which is restricting the capability of ECM apparatus. As a result, we investigate the history and the magnitude of radar signal cataloguing in compound systems.

Keywords Electronic warfare, User-defined Database, Electronic Intelligent Database, Electronic Support Measures, Radar Emitter Signal Sorting

1. Introduction

This paper describes how to prosper a coalesce Electronic Warfare (EW) Suite for Jaguar Fighter Aircraft by combining multiple Line Replaceable Unit (LRUs) executing discrete EW operations into a sole Line Replaceable Modules (LRM) with the notion of smallermagnitude,mass,andenergy,higherextensibility,andgreaterenduranceforopenquality, which fosters communal, profitable off-the-shelf (COTS) conducts for communication and calculation resource advancement. A study of modern technology employed in electronic warfare systems is also carried out. Current electronic and optical technology in use in the detection, localization, processing, and identification of a set of signals are all steps in the detection, localization, processing, and identification of a set of signals, both active and passive countermeasures are two terms that are used interchangeably analyzed. Popular aredesignsandarrangementsinspiredbythe"marineworld."Intermsofefficacyanddependabilit y, as well as design and operational trade-offs. The following are the topics: classified according to the current classification of electronic warfare covers confusion reflectors which are intercepted by masking and misleading jammers. The special attributes of the Navy of Surface are discussed in addition to the burgeoning issue of Spectra-Optical Electronics Warfare. The Appendices are a collection of documents located in the book's back. An experiment with a circuit developed for signaling a list of missiles with recognition as well as a description of the recognition, is shown .Electronic and guidance characteristics are discussed.

Electronic warfare is typically defined as military activity that uses electromagnetic radiation to allow friendly forces to use their electronic or optical equipment while limiting or denying enemy usage of the electromagnetic spectrum. The most often utilized EW divisions are as follows:

a. Electronic support measure (ESM)

Although Signal Intelligence (SIGINT) is a planned fourth branch, it is often included in ESM.

Electronic Support Measures are designed to collect data that will be useful in the case of an electromagnetic battle. This data can be used individually for threat detection and warning or in tandem with ECM or ECCM. As a result, duties including searching for, intercepting, locating, and evaluating transmitted electromagnetic radiation are common in ESM. In a broader sense, these support measures include all forms of reconnaissance missions, including industrial reconnaissance.

b. Electronic Counter measures (ECM)

Electronic Countermeasures (ECM) is a branch of EW that deals with efforts made to diminish or avert an enemy's exploitation of electronic warfare. Electromagnetic Spectrum is put to good use. It's true. These acts may be carried out by force. They can try to trick orconfusetheenemybyapproachingclose.It'ssometimesusefultocategoriesECMasactivesorpassives.

c. Electronic Counter Counter measures (ECCM)

Electronic Counter-measures (ECM) is a component of electronic warfare that includes efforts to counter the enemy's ECM while ensuring that friendly soldiers can successfully use the electromagnetic spectrum.

Electronic warfare systems include radar, scanners, communications, weapons guidance and navigation. The existing literature, on the other hand, is mostly concerned with the dangers posed by radar. Even though all systems follow the same basic principles they each have their distinct traits.

In contrast to the radar situation, numerous components of communications, for example, should be fine-tuned:

- At the opposite extremities of the spectrum, the transmitter and receiver are located .As a result the transmission line is just one-way ,jammers and communicative ns transmitters compete on an equal basis, with both having an inverse square of distance dependence factor. The two-way path in the Radar Equation creates an inverse fourth power distance dependency factor, which is a considerable disadvantage at ordinary working ranges.
- Communication systems are now available in a far broader range of styles and sizes. A wide range of modulation schemes is not only feasible but also widely used. The typical pulsed mode is employed by a considerable percentage of radar systems now in operation. In addition, communications links might be found in almost any section of the spectrum, from low frequencies to infrared and optical wavelengths.
  Interm so femission time, communications lines are more flexible suggesting that transmission is more within the control of the operator and less dependent on external variables. Because of these qualities, communications EW is more complex and unpredictable than radar EW and the findings are more difficult to interpret.

2. LITERATURE REVIEW

[1] 'Electronic Warfare Self-Protection of Battlefield Helicopters: A Holistic View,' by Johnny Heikell .Applied Electronics Laboratory ,Helsinki University of Technology, Department of Electrical and Communications Engineering, 2005. Author Johnny Heikell has analyzed and commented on the features and limitations of helicopters, as well as the existing Electronic Warfare system on helicopters, as well as its conceptual model and methodology, in this journal. He has also conducted research and presented on threat systems, technologies, and counter measure advances.

[2] The Journal of the JAPCC, Edition 27 Autumn/Winter2018, Giuseppe S gamba, 'Transforming Joint Air and Space Power'. In his publication, pages 41-45, the author and Brigadier General, ITA AF, Assistant Director JAPCC surveyed and elaborated on North Atlantic Treaty Organization (NATO) operations and strategic view of Electro-magnetic System, scope, advantages, and over look on Electronic Warfare and Electromagnetic spectrum and environment.

[3] R. Pitchammal and S. Sarala, Defense Avionics Research Establishment, Bangalore, India, 'A Blue Print for the Future Electronic Warfare Suite Development.'2013.The writers of this article, R. Pitchammal, and S. Sarala, covered the Integrated Modular Avionics system and development considerations, as well as an examination of the existing Electronic Warfare Suite and IMA implementation for the construction of a unified EW Suite.

[4] 'Electronic Warfare' is a term used to describe the use of technology in combat. DEPARTMENT OF THE NAVY Headquarters the United States Marine Corps Warfighting Publication(MCWP)3-40.5 ,Electronic Warfare, Edward Hanlon Jr. Lieutenant General, USMC Commanding General Marine Corps Combat Development Command Quantico, Virginia, DEPARTMENT OF THE NAVY Headquarters the United States Marine Corps Warfighting Publication (MCWP) 3-40.5, Electronic Warfare, 2002.Author and Commanding General Edward Hanlon Jr. spoke about the development of electronic warfare and the technology used in naval operations, battlespace and function concerns, joint and multinational operations, and the Radio Battalion.

[5] 'Management Information Systems for Electronic Warfare Command and Decision Support,' University of KwaZulu-Natal Durban, South Africa, 2015. 5. Brett Van Niekerk and Christo Cloete, 'Management Information Systems for Electronic Warfare Command and Decision Support,' University of KwaZulu-Natal Durban, South Africa, 2015. The writers of this journal article explore the Electromagnetic Spectrum and its impact on modern society.

3. SEPECAT JAGUAR

The SEPECAT Jaguar was first developed in the 1960s by the Royal Air Force of the United Kingdom and the Air Force of France as part of their first significant joint military initiative, dubbed 'SEPECAT.' Jaguar was developed with two engines primarily for ground-attack or bomb-dropping missions .Jaguar's particular benefits are its ability to go great distances ,fly fast even at low altitudes, and carry a large load. Jaguar is also equipped with refueling probes ,allowing it to carry out any type of air refueling missionin any weather.

In July 1979, India purchased its first two Jaguar fighter aircraft from the British, and by1981, it had purchased 40 Jaguars for a total cost of one billion dollars. India was later granted permission to build 120 Jaguars at HAL under the name 'Shamsher.' HAL has produced 90 Jaguars to date, many of which are still in use. With its dual Adour Mk-

102engines, the Jaguar aircraft can reach speeds of up to 1,700 mph. DARIN-III upgrades are now being carried out in Jaguar aircraft ,with the first successful upgrade flight taking place in November 2012. The Aero India Exhibition in February 2019 featured new updated cockpit design features as well as advanced avionic technologies. HAL plans to upgrade 60Jaguarsto DARIN-III standards, with the EW Suite being the first to be upgraded.

4. ELECTROMAGNETIC SPECTRUMINEW SUITE

The control and exploitation of the Electromagnetic- Spectrum is the focus of Electronic-Warfare .All types of electromagnetic radiation ,including radio waves ,infrared, ultraviolet ,and gamma rays, as well as their frequencies and wavelengths, are included in the electromagnetic spectrum.

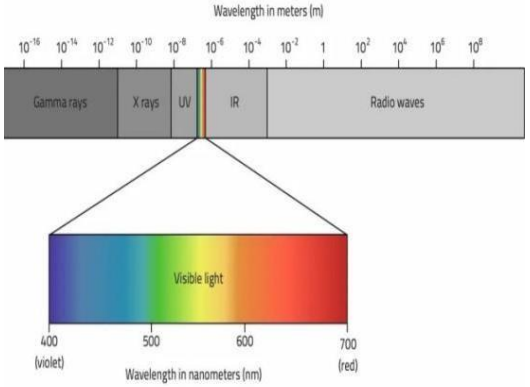

Fig.1 Electro magnetic Spectrum

This spectrum is used by the military, navy and airforce to detect and attack hostileorces. With today's technology and threat exposure, it's more important than ever to be able to distinguish friendly forces from enemy forces and successfully defend our aircraft .Electronic warfare employs the electromagnetic spectrum for IFF (Identification of Friend or Foe) via the Radar Warning Receiver to detect hostile aircraft and deploy counter measures such as chaff to mislead enemy radars. Electronic warfare aid sour forces by assisting our fighter aircraft in gaining control of the electromagnetic environment, which advantages our aircraft while diminishing adversary control. Controlling the electromagnetic environment in warfare is extremely helpful and vital and it is dependent on Electronic Warfare's successful exploitation of the Electromagnetic-Spectrum.

- ***PROBLEM STATEMENT***

A range of communication-navigation systems have been developed for aircraft. Fighter aircraft, on the other hand, are primarily built for military use and must be equipped with powerful defense and offensive capabilities. Aircraft, on the other hand, lack defense mechanisms to ensure their safety. A system must be able to successfully allow the aircraft to avoid hostile radar sorelude their missiles to give security to the aircraft.

- ***SOLUTION***

Hindustan Aeronautics Limited (HAL) fighter aircraft have been receiving a major upgrade as part of the DARIN-III Modern Avionics System program, which aims to provide advanced defense systems to the Indian Air Force (IAF) fighter aircraft. HAL is introducing the Counter Measure Dispensing System (CMDS) with different equipment's like as chaff, flares, and decoys to supply the combat aircraft with the capacity to escape missile launches and compromise enemy radars on all of their fighter aircraft and helicopters.

Electronic Warfare Suites had their origins in 1943 when the British aircraft Avro Lancaster was equipped with chaff capable of disorienting enemy radar systems. Since2013, SEPECAT Jaguar has been undergoing the DARIN-III upgrade and is now being upgraded to include the EWsuite. HAL Overhaul Division is implementing these improvements and upgrades, which involve hardware and software design, mechanical and electrical design, and requirements. The SEPECAT Jaguar EW suite has been delayed because of a paucity of essential components for this upgrade, but it is now being actively worked on as the Indian Air Force gets airframes from the British and French for the modifications. By 2038, it is predicted that all Jaguar aircraft in the Indian Air Force will have received improvements.

- ***METHODOLOGY***

A combat aircraft armed for EW, or demeaning the efficiency of opposing radar-radio electronics through radio jamming-deception techniques, is known as an electronic-warfare aircraft.

- The **Radar Warning Receiver (RWR)** gathers radar signals from the ground and the air and sends them to the aircraft cockpit's Cockpit Display System (CDS) or Smart Multifunction Display (SMD).

- The aircraft radar system detects any unidentified or foreign signal or object as seen by the **ELINT or Electronic Intelligence Database** and the **UDF or User-defined Database.**

- The threat is then analyzed by the aircraft defense system, and an **Electronic Counter Measure (ECM)** is undertaken. **CMDS (Counter Measure Dispensing System)** is fitted with 'Chaff and Flare' or other counter measures like jammers and transponders.

As a result of the actions done, hostile radar systems are confused. InFig.2 and 3 can see the block diagram of both RWR and CMDS. RWR and CMDS work hand in hand to form the EW system although they are two different systems independent of each other. RWR focuses on the threat detection and the CMDS works on preventive measures for protection against the threats detected.

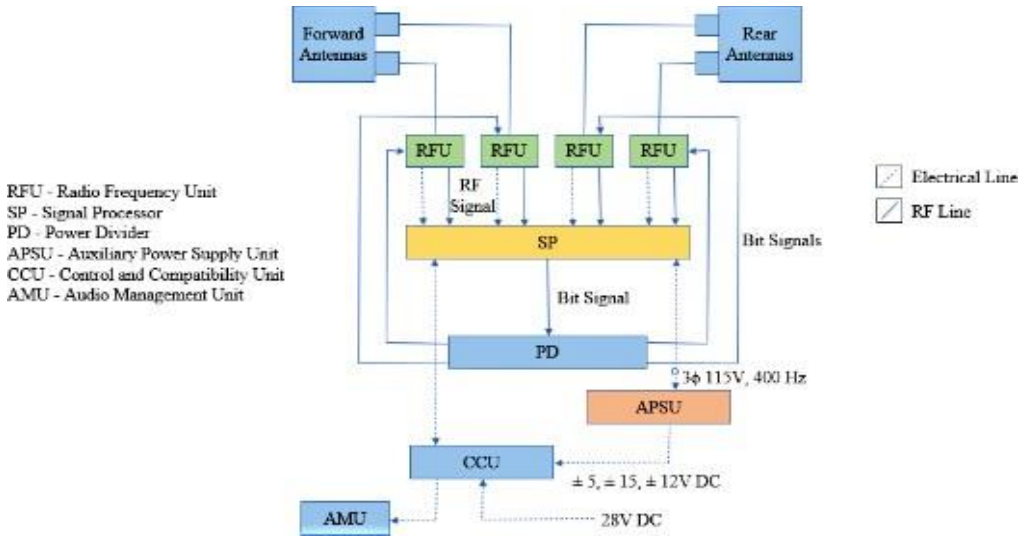

Fig.2 Block Layout of RWR

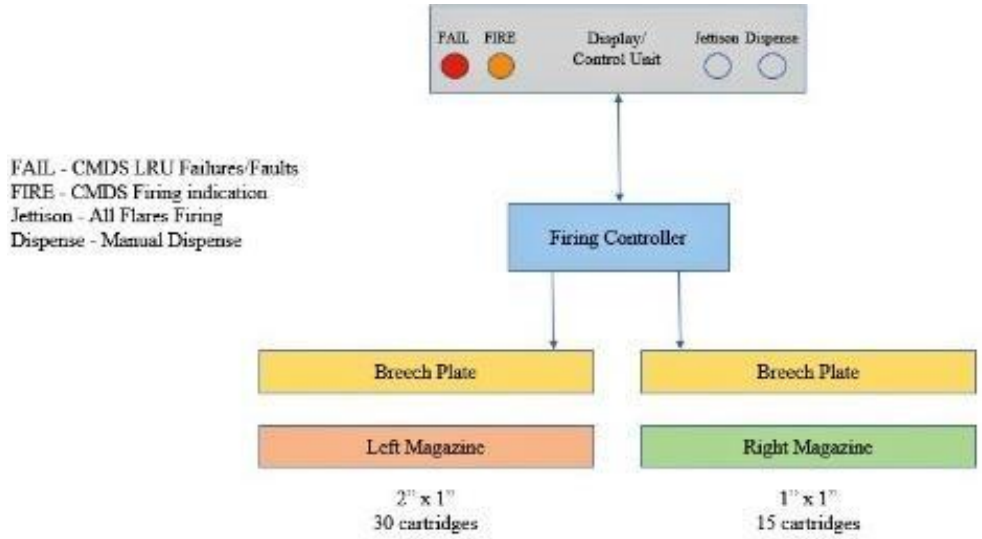

Fig.3 Block Layout of CMDS

5. BACKGROUND WORK

Procedures and technology that brought about the improvement of equipment able to electronically recognize and counter a weapon device, in addition to the improvement of counter-countermeasures, are called "electronic war." The electromagnetic spectrum has been controlled/utilized by the primary electronic protection systems that carry out digital conflict duties, and that they can be labeled into the subsequent classes:

- **Electronic-Support (ES)** offers the skill and hazard detection wished for a hit assault and conservation. The main goal is a diplomatic interference. Commanders can use it to look

for, become aware of, and stumble on both premeditated and accidental electromagnetic intensity assets.

- **Electronic-Attack (EA)** uses electromagnetic radiation to obstruct or degrade opposing forces' powerful utilization of the electromagnetic spectrum via jamming and deception. Deception is a huge part of electronic attacks.
- **Electronic-Protection (EP)** is a wide period that consists of everything from constructing jam-resistant systems to hardening equipment to with stand excessive-energy microwave assault to destroying foe jammers with anti-emission ammunitions.

The EW suite for each battle platform with complete EW potential includes the auxiliary-systemsindicatedinFigure4.

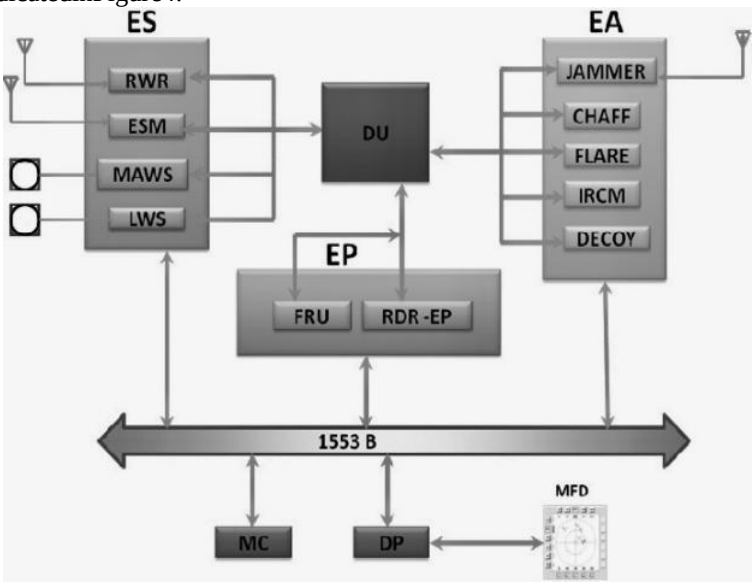

Fig.4 The architecture of the current EW suite.

MAWS (Missile-Approach Warning System) is an apathetic system which recognizes and follows an approaching missile's burning plume as it surfaces within a protective circle around the airplane (using just EM spectrum reception). The MAWS distinguishes between dangerous and safe missiles by examining ammunition paths.

The **Laser-Warning System (LWS)** is a static system that detects, tracks, and warns of adverse laser resources aiming at the platform (only EM spectrum reception).

A **jammer** is a lively device that makes noise and uses misleading jamming strategies to both reduce the automated monitoring abilities of chance structures and generate enough monitoring mistakes to impede a hit engagement.

Decoys - In the very last degrees of a conflict, towed decoys are deployed to spoil opposing missiles.

Chaff – Metal or metalized plastic ribbon-like debris thrown by using planes to hide or display other planes or motive monitoring radar to lose latch.

Flare is the most not unusual counter-measure for an IR missile that can discriminate among IR indication of the plane and IR indication of a historical past disturbance.

The energetic device **IRCM (infrared countermeasure)** can lessen the strength of IR hazard electronics. The primary is to lessen power degree to reduce the aircraft's warmth

signature intensity. This flare-rejection countermeasure system is referred to as a flare rejection unit (FRU).

RDR-EP (RADAR EP) is a Counter-Counter-Measure gadget that could guard radar receivers, avoid jamming, the most jamming signals and over power jamming alerts.

The general trend towards increasing the complexity of these EW systems have large implications for plane costs throughout the board, which includes improvement (range of the various device), upkeep (quantity of alternative gadget), evolution (system specificity, technology dependence), overall performance, and so on. To remedy this issue in the current EW suite concept, the progression is necessary.

MIL-STD 1553 is an avionics machine data bus protocol that defines the electric, useful, and mechanical components of serial facts- bus for navy avionics.

The Multi-function show, or MFD, is the cock pit display panel in which several avionic gadget functions can be finished in addition to other communique and navigation structures maintained and changed.

6. SOFTWARE

a. Keil u Vision

A microcontroller can be programmed using a number of software tools which is usually associated with the chip used or the programming board or the method of transfer of the code to the chip. For this project, Nuvoton manufacturer has a designated software tool for transfer of the code in HEX file format to the chip via the COM port of the CPU.

C or C++ code can be used for a microcontroller. We have used C code which can be compiled using any software tool. Keil u Vision is a software tool used for C or C++ programming especially for 8051 microcontroller applications. The programmed code once complied and verified of all errors must be converted to HEX file format and with the help of the Nuvoton ISP/ICP software tool, can be uploaded to the 8051-microcontroller chip W78E052DDG via the COM port.

b. RWR Display

The RWR display in real-time aircrafts or helicopters is represented or visualized as a group of varying diameter concentric circles along a mid-point defined as the aircraft itself. Any threat detected by the 4 antennas is displayed on the RWR on the 4 divided quadrants. This display can be represented in visual graphics C or MATLAB.

In MATLAB , we can construct antenna-based radars using Sensor Array Analyzer which serves as a sample for the real-life RWR system.

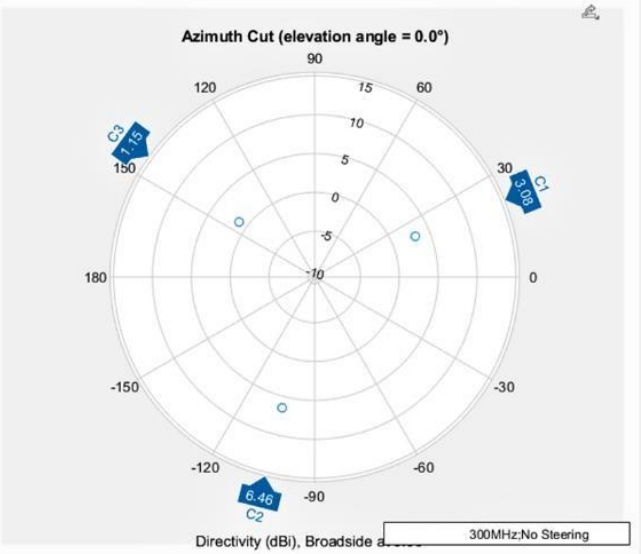

Fig.5 RWR MATLAB DISPLAY

7. CONCLUSION

Many attack mechanisms and equipment are created without considering the Electronic Warfare Suite. However, a relatively simple Radar Warning System in conjunction with a Counter Measures Dispensing System is extremely beneficial in not only degrading the energy are a and strategy but also in providing a secure battle environment for our military and naval aircraft and missions. While improved avionic systems focused on precision and dependability are being aggressively introduced, more improvements in EW systems are being worked on to improve and eliminate the limitations of this defense mechanism.

REFERENCES

[1] JohnnyHeikell, 'ELECTRONICWARFARESELF-PROTECTION OF BATTLEFIELD HELICOPTERS: A HOLISTIC VIEW' Helsinki University of Technology, Department of Electrical and Communications Engineering, Applied Electronics Laboratory, 2005.

[2] 'A Blue Print for the Future Electronic Warfare Suite Development 'by R.Pitchammaland S.Sarala, Defense Avionics Research Establishment, Bangalore,India,2013.

[3] Sujitha,S., Venkatesh, C. "Analysis of regulated PV fed switched reluctance motor drives using repression resistor converter.", "International Journal of Engineering and Technology, 2014, 6(3), pp. 1309–1313".

[4] Electronic Warfare' EDWARD HANLON, JR. Lieutenant General, U.S. Marine Corps Commanding General Marine Corps Combat Development Command Quantico,Virginia, DEPARTMENT OF THE NAVY Headquarters the United States Marine Corps Warfighting Publication(MCWP) 3-40.5, Electronic Warfare, 2002.

[5] Gopal M.K., Amirthavalli M. “Applying machine learning techniques to predict the maintainability of open source software”, International Journal of Engineering and Advanced Technology,2019.
[6] Sujitha, S., Vinoth Kumar, K., Vinodha, K., Josh, T.F., Venkatesh, B. “Experimental Setup of Smart E-Vehicle Charging Station using IOT Technology”. “2021 IEEE International Conference on Mobile Networks and Wireless Communications, ICMNWC 2021, 2021”.
[7] Sujitha, S., Vinoth Kumar, K., Shiva, R.V., Kulkarni, S., Ponnappa, M.M. “An implementation of soft computing approach of smart control for induction motor using ANFIS”, “4th International Conference on Smart Systems and Inventive Technology, ICSSIT 2022, 2022, pp. 1410–1413”.
[8] Naveen H., Chetan H., Kulkarni B., Mohanty S., Druva Kumar S., Sreerama ReddyG.M.”The effective transmission of acquired sensor data with FFT, DWT and DTCWT in different channel environment”,International Journal of Recent Technology and Engineering,2019.

SMART IRRIGATION SYSTEM USING AGRIBOT

Ahir Jay Satish[1], Gourav Kumar Patel[2], Pathak Krutarth Dhimant[3], Prajwal S C[4], Dipesh Kumar[5]

B.M.S. College of Engineering, Bengaluru, Karnataka, India[1, 2, 3, 4, 5]

jay.ee18@bmsce.ac.in[1], gouravk.ee18@bmsce.ac.in[2], krutarth.ee18@bmsce.ac.in[3] prajwal.ee18@bmsce.ac.in[4], 5dipeshkumar.eee@bmsce.ac.in[5]

Abstract

Traditional irrigation systems often waste a lot of water, without considering how many litres of water can be saved. Since water is directly irrigated to the land, plants under these conditions are subjected to high levels of stress and often have reduced appearance. The uncontrolled growth of the population is causing water management problems. The main reasons are that the population is growing rapidly, and automatic controls have not been able to keep up. There is worldwide water constraint where regulating shortage of water is becoming a critical problem. Such issues are typically observed in regions with a lack of water reserves and lesser economic development. Thus, the present paper provides a solution by designing a smart irrigation system based on Raspberry Pi 3 B+ to control a robot along with a moisture sensor. It also controls other sensors required to take care of the moisture content of land and to automate the irrigation process by turning on or off the pump using a relay without interference from the user.

Keywords. Smart irrigation system, irrigation automated robot, moisture sensing, irrigation control system, raspberry pi.

1. INTRODUCTION

Agriculture in the 21st Century is being digitally transformed quickly and products are being released in this domain as solutions for the latter problems. There is a rapid increase in the demand for food and agricultural stocks, cultivation process to improve yield, cost-effectiveness and quality of crops [1]-[2]. The agricultural products being produced with upcoming technologies like Internet of Things (IOT), Artificial Intelligence (AI) and Machine Learning (ML) [3]. Yield is a problem that needs to be solved, efficacious and increase production of land per unit area taken under deliberation. To overcome these problems, it is necessary to embrace new technologies. There are various benefits associated with the enactment of new technologies which include increased productivity, proper crop distribution, and crop pattern suggestion [4]. Moreover, proper utilization of resources such as automation and AI model are new solutions to technologies which create new types of fertilizers and manures [5].

2. AUTOMATIC PLANT WATERING SYSTEM USING PROTEUS

Watering is an important cultural practice in greenhouse operations, and it is one of the most labour-intensive tasks. Watering systems make it easier for plants to get water whenever required. The prime characteristic of watering is to understand the timing of water supply and quantity of water supply. The automatic plant watering system makes it easier for the gardener to work [6]-[7]. There are various types of automatic watering systems, including sprinkler systems, tube systems, and nozzle systems. This system uses an Arduino UNO board, which is equipped with an ATmega328 microcontroller. This type of irrigation system is designed to detect the moisture level of plants and provide water if necessary. It is generally utilized for caring plant of different sizes in the garden. The microcontroller has been programmed to irrigate the garden under the condition when moisture level in the land falls below 80%. This automation system was designed to help farmers. The system hopes that with this prototype, people will enjoy the joy of owning plants without the challenges associated with absence or forgetfulness.

2.1. Solution and methodology

Automation is the technology that allows a process to be carried out without the need for any specialized worker. The prime goal of this paper is to understand that how a worker can operate the automatic watering system with his own moderately available facility in a short duration and to assemble the required electronic as well as other components. Thus, an automatic watering system using various sensors has been developed and implemented in order to utilize it widely with profitable irrigation system. This system can be very helpful for human in their day to day work life, thereby minimizing their work time, hard work and cost. The present irrigation system employs relay, microcontroller, battery and DC motor along with the sensor technology. If the soil moisture level is low, the system will irrigate the plant. The ON / OFF switch will be based on the moisture level of the land. The proposed irrigation system can be easily monitored by a computer system. This computer system receives sensor readings and creates graphs to analyse the moisture level. Moreover, the present system can be automatically implemented for small-scale and large-scale gardens as well as green roofs, greenhouses and nurseries. It will save the cost, work time and reduce the loss of water. The automatic watering system will also assist the farmer by providing them with an alternate source of irrigation, solving irrigation planning problem.

Modelling of the automatic irrigation system when pump is ON and OFF is presented in Fig. 1 and Fig. 2 respectively. Working of this system is given in steps as follows:

- Change in moisture is simulated by changing resistance in potentiometer connected to the test pin of soil moisture sensor.
- Analog values are then calculated by Arduino
- After calculation, moisture percentage is displayed on the LCD display connected to the Arduino.
- There are two motors connected the Arduino: Watering motor, Tank motor
- If the moisture is less than 85% watering motor is turned ON.
- If moisture is more than 85% watering motor is turned OFF.

- When water level in tank is less than 65% tank motor is turned ON and when it is more than 65% tank motor is turned OFF.
- Whenever any of the two motor is turned ON or OFF alert message with moisture level is sent to the smartphone/cell phone.

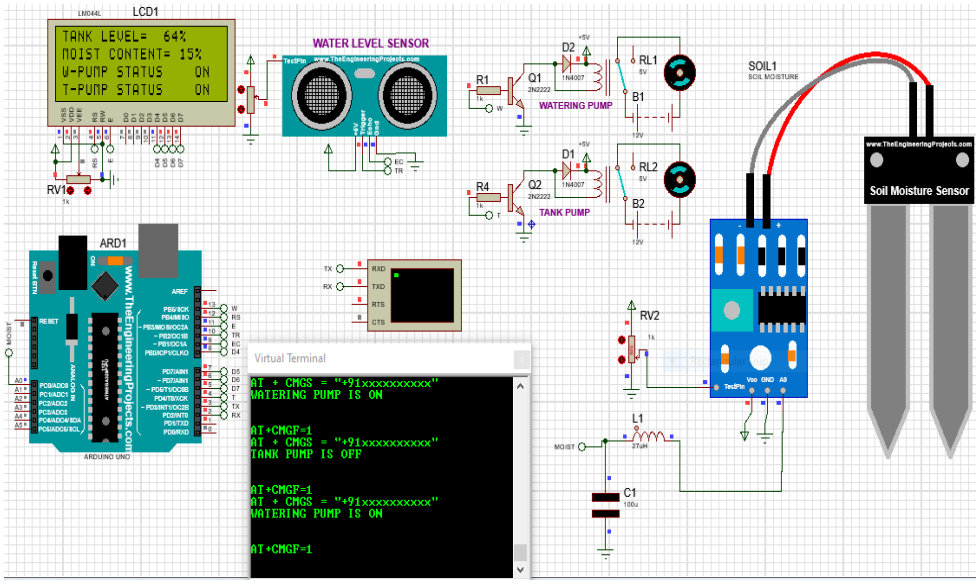

Fig. 1. Modelling the automatic irrigation system when pump is ON.

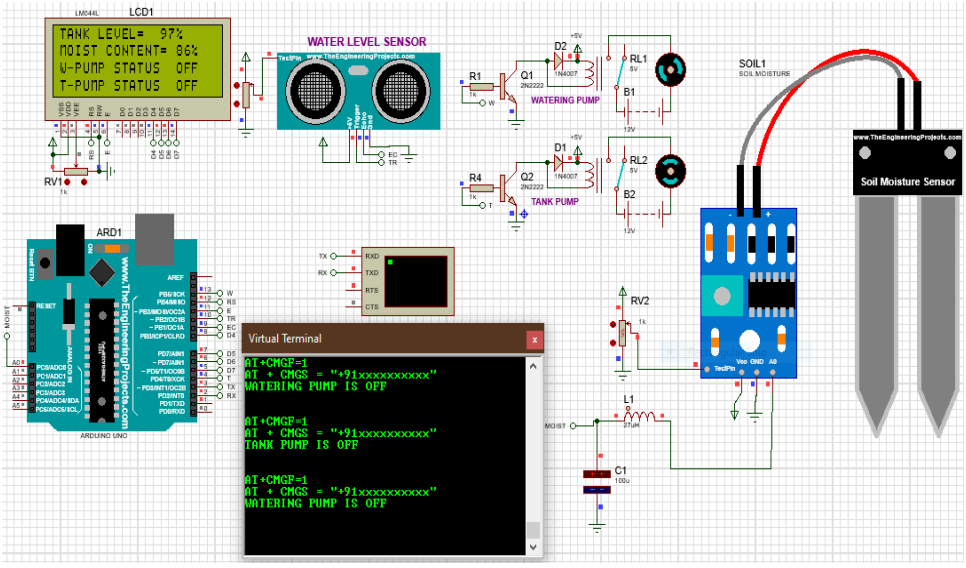

Fig. 2. Modelling the automatic irrigation system when pump is OFF.

3. IRRIGATION SYSTEM USING AGRIBOT

Water wastage is not of consideration in traditional irrigation systems. Water is irrigated directly into the land, plants undergoing increasing stress from variation in soil moisture, therefore plant appearances are reduced. Without proper control or automation of the control of this system, results in improper water control system. The major reason for these inhibitions is the growth of population which is increasing at an exponential rate.

Global water crisis is a problem that is emerging at present, thereby managing shortage of water has become a serious issue. This growth is prevalent in the countries in which there is scarcity of water and are economically backward, which is a very serious problem in the sector of agricultural sector. So, the present paper designed a smart irrigation system based on Raspberry Pi 3 B+ controlling a robot along with moisture sensor and other required sensors. It automate the process of watering and taking care of the moisture content in the soil by sensing the moisture level and turn ON/OFF the pump using relay without the involvement of worker.

3.1. Comparison of integration system with existing work

The automatic plant watering system in the previous project work presented a robot which can perform various irrigation tasks with the integration of Artificial Intelligence, Machine Learning, and Internet of Things. Sending and receiving data on the cloud and collecting these substantial data using sensors on-board, such as water level, soil moisture and obstacle detector sensors, overall building a smart agribot.

The problem with making a smart robot which incorporates the use of Artificial Intelligence, Machine Learning and Internet of Things is that the usage of RAM and processes will be very high and a microcontroller like Arduino is not designed to handle such heavy process and memory consuming tasks. Thus the better solution is to switch to the Raspberry Pi based automatic watering system.

The Raspberry Pi based proposed system overcomes the problem that was posed due to newer technologies and so it provides a really good solution. Hence a different and more passive approach has been incorporated, and the usage of a Raspberry Pi provides a wide range of utilities that one can use and provide a solution to our problem statement.

3.2. Proposed irrigation system

The present paper uses a Raspberry Pi 3 B+ since it has a very good selection of utilities in terms of using it for an Artificial Intelligence, Machine Learning, and Internet of Things Applications. The automatic irrigation system has been assembled on a synthetic chassis with a board, which can fit the processor and other required components. This system employs the following components: single shaft DC motors (4 Nos.), tires with treads (4 Nos.), battery pack (Li-ion), Micro-SD card, Wi-Fi module, moisture sensor and ultrasonic sensor. The software used for the system are Proteus software, Python, Octave, and Android App for Wi-Fi control.

The overall block diagram of the proposed irrigation system is shown in Fig. 3. The Raspberry Pi is programmed by using a Micro-SD card in which the program is encoded. The Wi-Fi module and the Battery Pack is connected to the Raspberry Pi via connectors. The four single-shaft DC motors are connected to a power supply via H-bridge connector. The Raspberry Pi controls the H-Bridge along with the input from the sensors and the Wi-

Fi module relays information from the Mobile App, which is used to control the latter. This therefore helps in the movement of automatic robot.

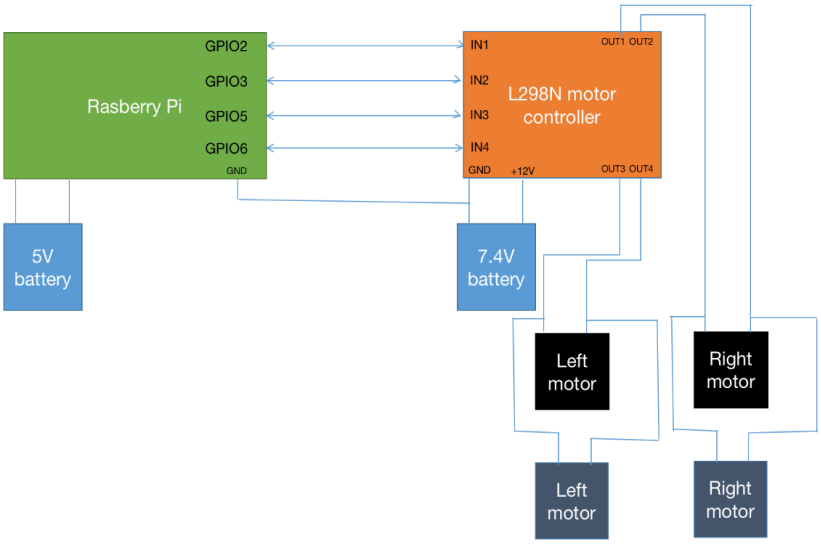

Fig. 3. Block diagram of the automatic irrigation system.

The working of the proposed automatic irrigation system is provided in steps as follows:

- The Battery powering both the Raspberry Pi and the motor driver are powered on and connected.
- The server receiving signal for controlling the Raspberry Pi and Motor Driver is started on a laptop.
- The mobile is connected to the laptop via Bluetooth and The Raspberry Pi is connected via the Wi-Fi module through wireless interface.
- Similarly, the moisture sensor is being actuated by lead screw mechanism along with a DC Motor with the help of a motor driver and the signal from the Raspberry Pi from the mobile phone.
- Also designed is a motor pump control using a node MCU which is again wirelessly controlled through cloud methods.
- The mobile provides signal to the Robot for movement or other instructions and the Raspberry Pi executes the same.
- Signals to run program on-board as well can be given.
- All the devices and sensors are further being programmed to be controlled solely via the Raspberry Pi without any external interface.
- This will establish an IOT network which will be completely automated.

4. RESULT AND DISCUSSION

The hardware model of automatic irrigation system is shown in Fig. 4 and the model used to measure soil moisture levels in dry and wet conditions is shown in Fig. 5. The robot consisted of the Raspberry Pi B+ Model and the other components such as the single-shaft motors, battery packs, H-bridge, WI-FI module, lead-screw mechanism, node MCU etc. A mobile app and an OS on the Raspberry Pi used as software and backend model for this project.

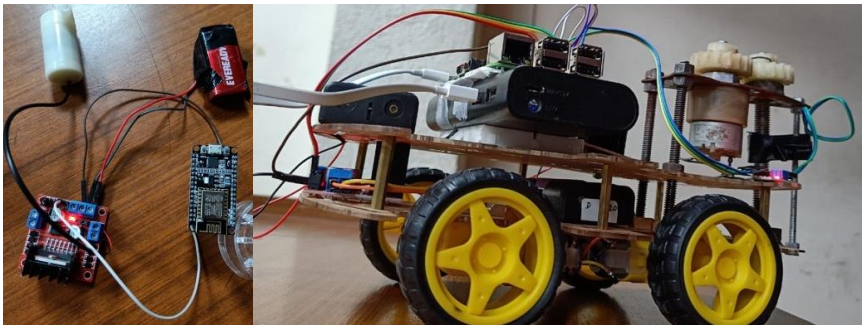

Fig. 4. Hardware model of automatic irrigation system.

The connections for the Robot were made on a breadboard using jumper wires along with all the above mentioned components. The Raspberry Pi B+ model was installed with an OS and connected to the mobile app through a laptop server. The commands were given to the Robot through wireless mode. The movement of the Robot was verified in Front, Back and Yaw Directions following which a lead-screw mechanism powering and mechanising the sensor to take readings of moisture level and send it to the cloud. Thus allowing the Robot to be used with Artificial Intelligence and Internet of Things.

Fig. 5. Hardware model used to measure soil moisture levels in dry and wet conditions.

Firstly the Arduino is connected with the moisture sensor fitted in a lead-screw mechanism driven by a 9 V DC Motor through a Motor Driver. The mechanism allows the sensor to enter the soil and sense the moisture content. These values are analog values, which are taken from the sensor and since the Pi does not have Analog to Digital converter, we have to make use of Arduino to take the input of the moisture value. Moisture values from the Arduino are sent to Raspberry Pi using serial communication. For collection of cloud data, an open source website called ThingSpeak.com has been used. There are two API keys that allow us to read or write data. Moisture values from the Raspberry Pi are sent to Thing-Speak could using the write key API. Then the data is stored on a channel in ThingSpeak.com. The module that is used to interface between cloud and the motor pumps is the ESP8266. The ESP8266 module reads API key and then it reads the relevant data from the cloud. The module will also compare moisture values received from the clouds with reference values to determine if the water has to be released through the pump control setup**.** If the value is high then the motor will be left turned OFF, otherwise if it is low then the motor is signalled to be turned ON. Data collected in database in wet and dry conditions through thingspeak.com is shown in Fig. 6.

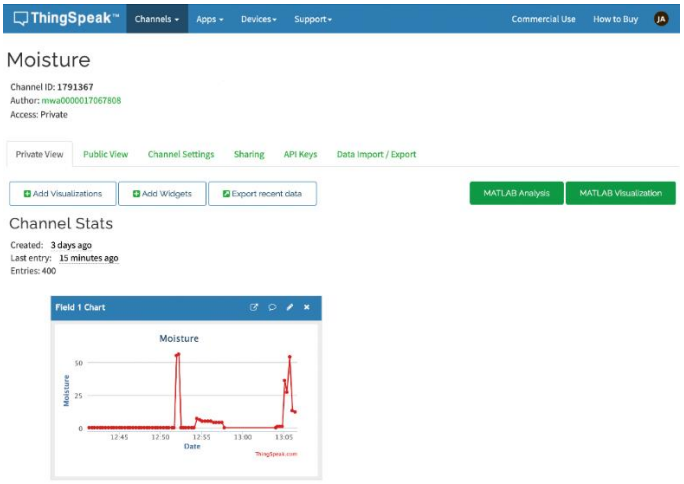

Fig. 6. Data collected in database in wet and dry conditions through thingspeak.com

5. CONCLUSIONS

An autonomous bot including the hardware and software models is designed in this paper. The agri-bot was used to measure various levels of moisture in the soil which is dry wet and semi-wet soil. The sensors and the robot were inserted in the explained mediums and relevant results discussed in the previous section were obtained. The website named thing-speak.com was used to obtain the data and provide insights on the results and values of moisture using API keys to read and write the same. Using this data, we can build a database for further analysis. Future scope for building AI algorithms based on this database model is possible. Different considerations were made to keep the model sustainable and green for the environment. Over all the work reached completion and plenty of improvements and additions are also being planned for the same.

6. REFERENCES

[1] Emiko Fukase, Will Martin, "Economic growth, convergence, and world food demand and supply", World Development, Volume 132, 2020.

[2] Adam M. Komarek, Shahnila Dunston, Dolapo Enahoro, H. Charles J. Godfray, Mario Herrero, Daniel Mason-D'Croz, Karl M. Rich, Peter Scarborough, Marco Springmann, Timothy B. Sulser, Keith Wiebe, Dirk Willenbockel, "Income, consumer preferences, and the future of livestock-derived food demand", Global Environmental Change, Volume 70, 2021.

[3] A. Subeesh, C.R. Mehta, "Automation and digitization of agriculture using artificial intelligence and internet of things", Artificial Intelligence in Agriculture, Volume 5, 2021, Pages 278-291.

[4] Victor Galaz, Miguel A. Centeno, Peter W. Callahan, Amar Causevic, Thayer Patterson, Irina Brass, Seth Baum, Darryl Farber, Joern Fischer, David Garcia, Timon McPhearson, Daniel Jimenez, Brian King, Paul Larcey, Karen Levy, "Artificial intelligence, systemic risks, and sustainability", Technology in Society, Volume 67, 2021.

[5] Jinha Jung, Murilo Maeda, Anjin Chang, Mahendra Bhandari, Akash Ashapure, Juan Landivar-Bowles, "The potential of remote sensing and artificial intelligence as tools to improve the resilience of agriculture production systems", Current Opinion in Biotechnology, Volume 70, 2021, Pages 15-22.

[6] Prabhakar Mishra, G.P. Khare, "Water controlling by soil moisture", Materials Today: Proceedings, 2021.

[7] Hari Kishan Kondaveeti, Nandeesh Kumar Kumaravelu, Sunny Dayal Vanambathina, Sudha Ellison Mathe, Suseela Vappangi, "A systematic literature review on prototyping with Arduino: Applications, challenges, advantages, and limitations", Computer Science Review, Volume 40, 2021.

Biographies

Ahir Jay Satish received the bachelor's degree in Electrical and Electronics Engineering from B.M.S. College of Engineering, Bengaluru, Karnataka, India in 2022.

Gourav Kumar Patel received the bachelor's degree in Electrical and Electronics Engineering from B.M.S. College of Engineering, Bengaluru, Karnataka, India in 2022.

Pathak Krutarth Dhimant received the bachelor's degree in Electrical and Electronics Engineering from B.M.S. College of Engineering, Bengaluru, Karnataka, India in 2022.

Prajwal S C received the bachelor's degree in Electrical and Electronics Engineering from B.M.S. College of Engineering, Bengaluru, Karnataka, India in 2022.

Dipesh Kumar received the B.E. in Electrical and Electronics Engineering from CSVTU Bhilai in 2010, the M.E. in Electrical Engineering from BIT Mesra, Ranchi in 2012, and the Ph.D in Electrical Engineering from IIT (ISM) Dhanbad in 2019, respectively. He is currently working as an Assistant Professor at the Department of Electrical and Electronics Engineering, B.M.S. College of Engineering, Bengaluru. His research areas include renewable energy, control system, power system, and artificial intelligence. He has been serving as a reviewer for many reputed journals.

Optimal Location and Sizing of FACTS Controllers in Transmission System Using Genetic Algorithm Under Contingency Condition

Tanuja K.S[1], Dr.Shankaralingappa C. Byalihal[2], Dr.Prakash.R[3]

[1]*Research Scholar, Department of Electrical and Electronics Engineering, Dr. Ambedkar Institute of Technology, Bengaluru, India*

[2]*Professor, Department of Electrical and Electronics Engineering, Dr. Ambedkar Institute of Technology, Bengaluru, India*

[3]*Professo& Head, Department of Electrical and Electronics Engineering, Acharya Institute of Technology, Bengaluru, India.*

Abstract.

With ever increasing power in the power systems optimal sizing and location of Flexible AC Transmission Systems is necessary to compensate these power dynamics. This paper presents optimal location of Flexible AC Transmission System's (FACTS) devices in a transmission system under N-1 contingency condition. Location of FACTS device is at the most contingent bus in the transmission system. Sizing, choice of different FACTS devices and location in a standard power system topology are exploited using Genetic Algorithm (GA). GA based optimization of sizing of single and multiple FACTS devices is carried out using simulation in MATLAB on IEEE 9 bus system. Results indicate effectiveness in fuel cost saving and loss minimization under contingency condition with optimal location of FACTS controllers. Placement of multiple FACTS devices using GA is found to be efficient.

Keywords. Genetic Algorithm, FACTS, N-1 Contingency, TCSC, SVC

1. INTRODUCTION

Contingency analysis being an important security analysis for power system, needs quick and effective counter measure. FACTS devices are capable of compensating these contingency conditions. FACTS devices include Static Synchronous Compensator (STATCOM), Thyristor Controlled Synchronous Compensator (TCSC), Static Var Compensator (SVC), Unified Power Flow Controller (UPFC) and are incorporated in the transmission system by optimizing the compensation using evolutionary computational algorithms [1]. GA is applied to optimize the MVAR injection in a IEEE 30 bus system [2]. Literature [3] discusses Particle Swarm Optimization (PSO) and GA. A new approach with Improved Teaching Learning Based Optimization (ITLBO) and Weight Improved Partial Swarm Optimization (WIPSO) estimating optimal location viz a viz parameter setting of UPFC and SVC are developed and implemented on IEEE 14 bus system [4]. Power system problems that include overloading and voltage limit violation is mitigated using Biogeography Based Optimization (BBO) [5] by optimal location of UPFC and Interline Power Flow Controller (IPFC) . Optimal location and the parameter setting of

UPFC under N-1 contingency criterion is optimized using “Artificial Algae Algorithm” (AAA) [6]. In [7], the total hourly generation cost of generator units is minimized to meet load demand and system losses using Real Coded GA and PSO methods. In [8], PSO and GA are used for the analysis of OPF. The Minimization of the average load-ability on all transmission lines is considered as the objective function. Mitigation of line overload problem during contingency by optimal placement of FACTS devices is developed monitoring both real power flow performance index(PI) and contingency severity index(CSI)[10].TCSC and UPFC are considered and modelled for steady-state analysis. After the location is determined, their type, their optimal settings and cost of installation are obtained by solving the optimization problem using GA. Optimal reallocation of generators is proposed in [11] for the management of contingency condition in the power system. Sizing is carried using Krill Herd Algorithm and optimal power flow is obtained in the presence of TCSC. The contingency analysis is performed using Rapid contingency ranking technique. A planning model to optimally allocate TCSCs in the transmission network under N -1 contingency is developed using the reformulation technique that linearizes the nonlinear power flow problem with constraints [12]. In [13], power system stability, minimum power loss with voltage stability is used as an index for optimal allocation of the controllers. First SVC is placed based on model analysis using GA in a power system. After placing the SVC based on minimum power loss with voltage stability index, the most appropriate location and size of SVC is found. PSO to find the optimal location of multi-type FACTS devices in a power system to alleviate the line over loads is developed [14]. The optimization is performed to locate different FACTS devices with their ratings with installation cost for single and multiple contingencies. TCSC, SVC and UPFC are considered and modelled for steady-state analysis to improve system security criteria for optimisation. The optimal location of TCSC is found in[15] by performance indices calculation to reduce overloading of each transmission line in normal case and under contingency condition. Review of various FACTS devices are discussed with its application in power system [16]. PSO is used to find optimal location and the optimal parameter settings of TCSC under single line contingency (N-1 contingency) [17]. Contingency analysis is performed to detect and rank the severest line faulted contingencies in a power system. Power system get restructured based on the market conditions. Optimal allocation of multiple FACTS in this restructured system with wind generator is developed that maximizes profit by minimizing device investment and operating cost under normal and contingency conditions [18]. Two reliable and efficient evolutionary-based methods named Shuffled Frog Leaping Algorithm (SFLA) and Grey Wolf Optimizer (GWO) to solve Optimal Power Flow (OPF) problem is developed [19]. Shunt and series compensation devices are integrated to be able to both regulate voltage and enhance line loadability in the transmission line [20].

2. SVC AND TCSC MODEL

Shunt and the series compensator is shown in Figure 1. The reactive power model is used for SVC is the shunt compensator. And reactance model is used for TCSC acting as the series compensator.

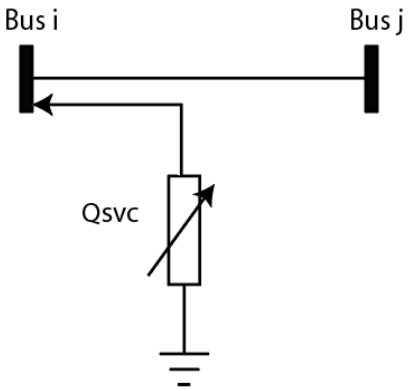

Figure 1(a) : SVC model

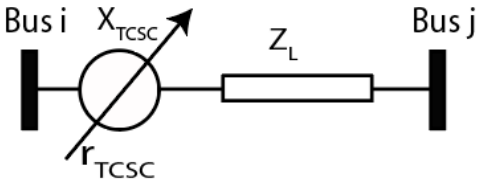

Figure 1(b): TCSC model

The value of reactance is the function of reactance of the line where the TCSC is placed. The impedance of the transmission line

$$Z_{ij} = Z_L + jX_{TCSC} \quad (1)$$

$$X_{TCSC} = r_{TCSC}X_L \quad (2)$$

Where

$$Z_L - transmission\ line\ impedance$$

$$X_{TCSC} - reatance\ of\ hte\ line\ where$$

$$TCSC\ is\ located$$

$$r_{TCSC} - compensation\ degree\ of$$

$$TCSC\ (Coefficient)$$

The FACTS device SVC is operated as both inductive and capacitive mode and control bus voltage by absorbing or injecting reactive power. A shunt variable susceptance added at both ends of the line for model the SVC. The injected reactive power at bus i is

$\Delta Q_{is} = Q_{svc}$ (3)

Q_{svc} – reative power injected by SVC in MVAR

$Q_{svc} - Q_{Min} \sim$ Qmax (4)

The constraint limit of the TCSC is,

$X_{TCSC} = X_{Lmin}\ to\ 0.7\ X_{Lmax}$ (5)

$Q_{svc} = Q_{svc\,min}\ to\ Q_{svc,max}$ (6)

Operational Cost Optimization Problem Formulation

The objective function is minimization of total fuel cost and is given in Equation 1.

$$Minimize\ F_{cost}(P_g) = \sum_{i=1}^{N_g} xP_{g_i}{}^2 + yP_{g_i} + z \quad (7)$$

Where P_{g_i} is power generated at 'ith' generator, $F_{cost}(P_g)$ is the total fuel cost, x, y, z are the cost coefficients.

$V_{i\,min} < V_i < V_{i\,max}$ (8)

$V_{i\,min}$ 0.9 p.u and $V_{i\,max}$ 1.1 p.u.

Impedance variation of TCSC is limited to 70% of the line impedance in capacitive and 20% inductive. Impedance range is represented in Equation (3).

$$X_{TCSC} = -0.8\ X_L \leq X_L \leq 0.2\ X_L \quad (9)$$

MVAR injection the SVC can apply in the line is limited to 100MVAR in both the directions meaning it can inject or absorb maximum of 100MVAR from and to the line.

$$Q_{svc} = -100MVAR \leq Q_{svc} \leq 20MVAR \quad (10)$$

Power balance Equation acting as the equality constraint is as given in Equation (11).

$P_{Load} + P_{Loss} - \sum_{i=1}^{N_g} P_{gi} = 0$ (11)

P_{Load} – Total Demand in entire power system.

P_{Loss} – total line loss in entire power system.

3. FACTS SIZING AND PLACEMENT

Generator and line outage condition is applied for the N-1 contingency condition. The power flow equation in a transmission line is

$$P = \frac{V_1 V_2}{X} sin\delta \quad (12)$$

GA flowchart used for the proposed implementation is given in Figure 2.

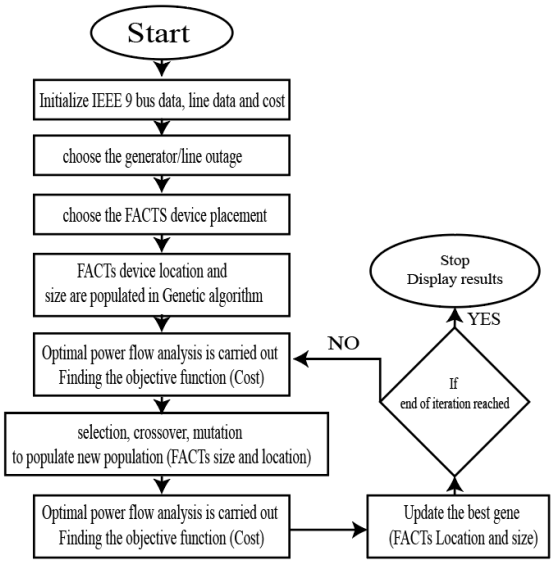

Figure 2: Overall implementation details of the optimization algorithm for outage mitigation

4. RESULTS AND DISCUSSIONS

MATLAB based simulation is carried out with different cases in the FACTS placement scenario. The table that would define all the cases is listed in Table 1.

Table1. Cases Used in the Proposed FACTS Sizing Algorithm

Cases	Load Flow Conditions
Case1	Without any FACTS Device; Without contingency; With Line Outage; With Generator Outage
Case2	SVC; Without contingency; With Line Outage; With Generator Outage
Case3	TCSC; Without contingency; With Line Outage; With Generator Outage
Case4	TCSC and SVC; Without contingency; With Line Outage; With Generator Outage

Network consists of 3 Generators, nine branches, 3 Transformers & 6 Transmission lines respectively.

The total cost of generation is determined by performing OPF without any FACTS controllers, without and with contingency condition (Line outage, generator outage) for the base case study (case-1). Seven different cases of individual and combined FACTS controllers (SVC and TCSC) are tested and for each case, total generation cost, total system loss and real power generation of generators are given in Table-5. Further, for each TCSC & SVC setting and for each case, optimal locations of FACTS controller with ratings and total power generation are given in Table-2. Results are discussed case wise.

Table 2: Generation Cost and Transmission Loss without Outage

CASE-1: In this case, without incorporating FACTS controllers & without outage gives the TSL is 3.80744 corresponding generation cost is 5309.486 $/hr. It is observed that under each line outage and Generator outage TSL will be quite high and corresponding generation cost increases. Hence it is decided to locate FACTS controllers based on the minimum Generation cost rather than minimum TSL.

CASE-2: a) Without outage: SVC located at bus 5 with 74.6237 MVAR gives better generation cost savings with 3.986 $/hr (34917.36 $/yr). The corresponding reduction in system loss is found to be 0.14334 MW. The results are tabulated in Table 2.

b) With line outage: It is observed that under line outage, each line outage gives more promising reduction in cost of generation. The corresponding system loss is also reduced. Location of SVC and its ratings shown in Table 3. For each line outage reduction in generation cost /hr., generation cost/year and corresponding reduction in system loss is tabulated shown in Table3.

Sl. No	Types of FACTS Controllers	TCSC Compensation Setting	Reduction in generation		Loss reduction in system
			Generation Cost in $/hr	Generation cost in $/yr	System Loss MW
1	SVC	--------	3.986	34917.36	0.14334
2	TCSC	50%	2.286	20025.36	0.05784
		70%	2.686	23529.36	0.07814
3	SVC & TCSC	50%	4.186	36669.36	0.12914
		70%	4.886	42801.36	0.22804

c) With Generator outage: It is also observed that under each generator outage except reference bus the cost of generation is reduced. The corresponding system loss also reduced. Location of SVC and its ratings shown in table 3. For each Generator outage reduction in generation cost /hr, generation cost/year and corresponding reduction in system loss is tabulated shown in Table 3.

CASE-3:a) Without outage: Location of TCSC in the line 9-4 is not varying irrespective of TCSC settings. Increase in TCSC compensation setting will reduce the generation cost and TSL. The transmission line 9-4 is found to be location of TCSC with 51.56 MVAR compensation settings gives optimal generation cost savings of 2.686 $/hr. The corresponding reduction in TSL is found to be 0.07814 MW

Table 3: Line outage & Generator outage with SVC

Sl. No	Line No.	Reduction in Generation		Loss reduction in system
		Generation Cost in $/hr	Generation cost in $/yr	System Loss MW
Line Outage				
1	Line-2	6.96	60969.6	0.37743
	Line-3	10.87	95221.2	0.3099
	Line-5	7.66	67101.6	0.34544
	Line-6	10.94	95834.4	0.49689

	Line-8	29.29	2,56,580	0.07688
	Line-9	28.22	247207.2	1.32221
Gen Outage				
2	Gen2	4.26	37317.6	0.10056
	Gen3	7.49	65612.4	0.22323

b) With line outage: It is observed that Location of TCSC varies in line 2 (line 4-5) with different compensation setting. TCSC with 8-9 and 9-4 are found to be more promising reduction in cost/hr and corresponding reduction in TSL are shown in Appendix III (Table -8). Compensation setting and location is tabulated in Table4.

c) With Generator outage: TCSC Location is same for different compensation setting. TCSC in line 9-4 gives better generation cost savings and also corresponding TSL reduction is shown in Table-4. Compensation setting and location is tabulated in Table4

CASE-4: **a) Without outage**: Location of TCSC varies with different compensation settings in the transmission line 9-4 for minimum compensation & 5-6 for Maximum compensation and no changes in the location of SVC. Location of TCSC in line 5-6 is found to be better generation cost savings of 4.886 $/hr. Corresponding reduction in TSL found to be 0.22804.

b) With line outage: It is observed that location of TCSC is changes in line 5 under different line outage, but the location of SVC is same for various compensation setting. In 70% (Maximum) compensation setting gives more promising reduction in generation cost/hr and reduction in system loss is tabulated in Table 5.

c) With Generator outage: Location of SVC in Generator outage is same, TCSC placement is not identical in case of Generator 3 outage of different TCSC compensation setting. In 70% (Maximum) compensation gives more promising reduction in cost/hr and corresponding reduction in loss is tabulated in Table 5.

The stochastic nature of the injected MVAr is exploited in the meta-heuristics methods to populate the different reactive power injection at different lines to find the optimal position that exhibits better overall losses of the complete bus system.

Table 4: Line outage & Generator outage with TCSC

Sl. No	Line No.	50% COMPENSATION			70% COMPENSATION		
		Reduction in generation		Loss reduction in system	Reduction in generation		Loss reduction in system
		Generation Cost in $/hr	Generation cost in $/yr	System Loss MW	Generation Cost in $/hr	Generation cost in $/yr	System Loss MW
Line Outage							
1	Line2	2.76	24177.6	0.10333	3.26	28557.6	0.15543
	Line3	5.97	52297.2	0.0386	6.47	56677.2	0.0935
	Line5	2.26	19797.6	0.10274	2.46	21549.6	0.12504
	Line6	4.54	39770.4	0.08679	5.04	44150.4	0.09769
	Line8	13.29	116420.4	0.01568	21.99	192632.4	0.44768
	Line9	25.12	220051.2	1.29321	32.02	280495.2	1.35441
Gen Outage							
2	Gen2	7.76	67977.6	0.19156	8.26	72357.6	0.19896
	Gen3	7.99	69992.4	0.25733	9.79	85760.4	0.30053

Table 5: Cost and Loss analysis with Line Outage SVC and TCSC

Sl. No	Line No.	50% COMPENSATION			70% COMPENSATION		
		Reduction in generation		Loss reduction in system	Reduction in generation		Loss reduction in system
		Generation Cost in $/hr	Generation cost in $/yr	System Loss MW	Generation Cost in $/hr	Generation cost in $/yr	System Loss MW
Line Outage							
1	Line-2	6.56	57465.6	0.31383	9.16	80241.6	0.39713
	Line-3	11.57	101353.2	0.2396	14.17	124129.2	0.5328
	Line-5	5.56	48705.6	0.15614	8.26	72357.6	0.28624
	Line-6	14.14	123866.4	0.56919	15.74	137882.4	0.61619
	Line-8	18.09	158468.4	0.45058	26.89	235556.4	0.76578
	Line-9	42.22	369847.2	1.77241	44.52	389995.2	2.00781
Gen Outage							
2	Gen2	9.96	87249.6	0.24146	10.16	89001.6	0.26296
	Gen3	13.19	115544.4	0.39163	14.29	125180.4	0.43913

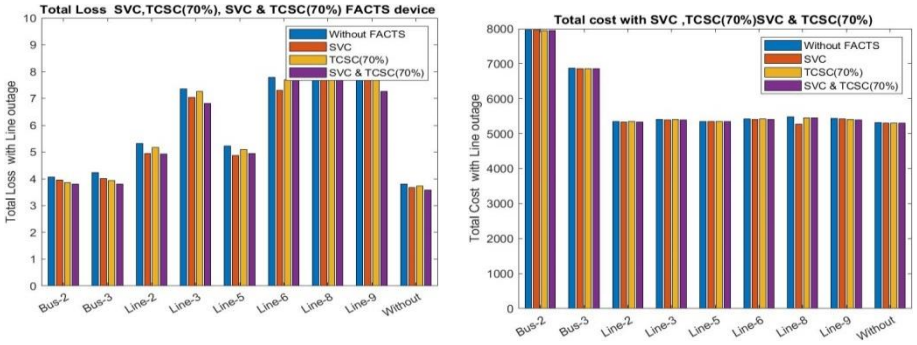

Figure3 : Reduction of total cost and losses in the 9-bus system with Facts controllers under contingency condition

It can be inferred that the SVC has performed better for the line outage conditions and at the same time TCSC has performed during the generator outage conditions. But while the combination of both TCSC and SVC is used the performance for both the outage condition is found to be better while individual FACTS Controllers are incorporated. The rare observation in the Table 3 &Table 4 is that the single TCSC and SVC has better performance even while compared to SVC & TCSC. It can be observed that the contingency while both the line outage and the generator outage occurs in the IEEE 9 bus system the total cost is observed to be reduced for SVC installation than the TCSC installation for the best possible setting of each of the FACTS devices. Total power generated (PG), total loss and the total cost /hr is tabulated for different configuration of SVC, TCSC and combined SVC and TCSC.

5. CONCLUSION:

The optimized placement of single and multiple FACTS devices in the standard IEEE 9 bus system is carried out. The overall fuel cost is reduced. The tradeoff is that the generation outage allows only lesser loss the cost of the generator outage is seen to be higher. The placement of multiple FACTS devices obtains the lesser overall cost and compared to the cost incurred when only single FACTS devices is installed. The overall optimization algorithm on the FACTS compensated contingency analysis is found to be satisfactory.

6. REFERENCES:

[1] Mithilesh Singh &Shubhrata Gupta, "Optimal Placement of Facts Devices in Power System for Power Quality Improvement", International Journal of Recent Technology and Engineering (IJRTE), Volume-7, Issue-6, March 2019.

[2] A. B.Bhattacharyya, B. S.K.Goswami, " OPTIMAL Placement of FACTS Devices by Genetic Algorithm for the Increased LoadAbility of a Power System", World Academy of Science, Engineering and TechnologyInternational Journal of Electrical and Computer EngineeringVol:5, No:3, 2011

[3] Dipesh Gaur and Lini Mathew, " Optimal placement of FACTS devices using optimization techniques: A review", IOP Conf. Series: Materials Science and Engineering 331 (2018) 012023

[4] H. Arul Devi, S. Padma, " Optimal Location and Parameter Setting of FACTS Devices based on WIPSO and ITLBO for Power System Security Enhancement under Single Contingency", International Journal of Engineering and Advanced Technology (IJEAT), Volume-6 Issue-6, August 2017.

[5] H. Arul Devi, S. Padma, "Power System Security Enhancement Using Optimal Placement and Parameter Setting of Multi-FACTS devices with BBO Algorithm, International Journal of Pure and Applied Mathematics Volume 118 No. 5 2018, 785-804

[6] Muhammad Zahidet.alm" New Approach for Optimal Location and Parameters Setting of UPFC for Enhancing Power SystemsStability under Contingency Analysis", Energies 2017, 10, 1738

[7] RenginIdil CABADAG1, BelginEmre TURKAY, " HEURISTIC METHODS TO SOLVE OPTIMAL POWER FLOW PROBLEM", R. I. CABADAG and B. E. TURKAY / IU-JEEE Vol. 13(2), (2013)

[8]SatyendraSingha, K.S. Vermab "Optimal Power Flow using Genetic Algorithm and Particle Swarm Optimization", IOSR Journal of Engineering (IOSRJEN), Vol. 2 Issue 1, Jan.2012, pp. 046-049

[9] A. LashkarAra, J. Aghaeib, M. Alaleh a, H. Barati a, "Contingency-based optimal placement of Optimal Unified PowerFlow Controller (OUPFC) in electrical energy transmission systems", ScientiaIranicaTransactions D: Computer Science & Engineering and Electrical Engineering

[10] Marouani Ismail1,*, GuesmiTawfik, HadjAbdallahHsen, " Optimal Location of Multi Type FACTS Devices for Multiple Contingencies Using Genetic Algorithms", International Journal of Energy Engineering 2012, 2(2): 29-35

[11] B. Sravana Kumar, M. Suryakalavathi, and G.V.Nagesh Kumar," Thyristor Controlled Series Compensator basedOptimal Reallocation of Generators for

Contingency Management", ECTI Transactions On Electrical Eng., Electronics, And Communications Vol.16, No.1 February 2018.
[12]Xiaohu Zhang and Kevin Tomsovic, " Optimal Investment on Series FACTS Device Considering Contingencies " arXiv:1703.10278v1 [math.OC] 30 Mar 2017
[13] Nagarajakumari CH1, K.ChandraSekhar, " Optimal Placement of SVC for the TransmissionCongestion Management" , Advanced Research in Electrical and Electronic Engineering, Volume 1, Number 5 (2014) pp. 54-58
[14] S. Sutha, and N. Kamaraj, " Optimal Location of Multi Type Facts Devices for Multiple Contingencies Using ParticleSwarm Optimization", International Journal of Electrical and Computer Engineering 3:13 2008
[15] ShrirangKulkarni ,T.N.Venkataraman, " Performance Improvement By Optimal LocationAnd Damping Of Oscillations In The Power System Using Tcsc", International Journal Of Current Engineering And Scientific Research (Ijcesr), Volume-2, Issue-9, 2015
[16] K.S.L. Lavanya1, P.Shobha Rani2, "A Review on Optimal Location and Parameter Settings of FACTS Devices in Power Systems Era:Models, Methods", International Journal for Modern Trends in Science and Technology Volume: 02, Issue No: 11, November 2016
[17] T.PavanKumar ,A.Lakshmi Devi, " OPTIMAL LOCATION AND PARAMETER SETTINGS OFTCSC UNDER SINGLE LINE CONTINGENCY USING PSO TECHNIQUE", IJAERS/Vol. I/ Issue I/October-December, 2011/30-34
[18] Elmitwally, A., Eladl, A., & Morrow, D. (2016). Long-Term Economic Model for Allocation of FACTS Devices inRestructured Power System Integrated Wind Generation. IET Generation, Transmission and Distribution, 10(1),19-30.
[19] Amr K. Khamees1, Ahmed El-Rafei1, N. M. Badra1, Almoataz Y. Abdelaziz2, " Solution of optimal power flow using evolutionary-based algorithms", International Journal ofEngineering, Science and TechnologyVol. 9, No. 1, 2017, pp. 55-68
[20] F. Solomonesc, C. Barbulescu, S. Kilyeni and A. Simo, "Optimal power flow computing GA applications," 2013 48th International Universities' Power Engineering Conference (UPEC), Dublin, 2013, pp. 1-6.

Design of Parameters of Buck Converter Integrated to a Hybrid DC Micro Grid using Genetic Algorithm

M N Suneetha and C Lakshminarayana
Department of Electrical and Electronics Engineering, B.M.S. College of Engineering, Bangalore

Abstract:
Buck converter transforms constant DC voltage into a variable DC voltage and gives out average output voltage less than the input voltage. Applications of Buck converter starts from few watts range such as consumer electronics like mobile charger, laptop charger to kilo watts range in electrical engineering like renewable energy sources, electric vehicles and DC micro grids. Buck converter considered for the study in this paper integrates wind power generation to a hybrid DC micro grid. When the wind generator output varies, input to Buck converter also varies. The inductance and capacitance values of the Buck converter are varied under the condition of variable input voltage; to maintain the average output voltage constant with reduced transients such as peak voltage, percentage ripple and settling time. To find the optimal values of inductance and capacitance under varying input voltage condition Genetic Algorithm is used. The proposed method is verified by simulating Buck converter and Genetic Algorithm in MATLAB/Simulink environment.

Keywords: Buck converter, Capacitance, Inductance, Genetic Algorithm

I. INTRODUCTION

Buck converter is a step down DC- DC transformer, it reduces the output voltage level to a desired value less than the input voltage without change in power, and therefore the output current of the Buck converter is always greater than the input current. The power rating of Buck converter varies from few Watts to KWs depending on the field of application. And some of the field of application of Buck converter are electronic gadgets like mobile and laptop charger, Electric vehicles, Renewable energy sources and DC micro grids. A Buck converter circuit consists of a main switch (a controllable power electronic device) such as power MOSFET or IGBT, auxiliary switch diode, energy storage elements like inductor and capacitor. A Buck converter operates in two modes, they are continuous current mode (CCM) and discontinuous current mode (DCM) and these two modes of operation depends on inductor value of the Buck converter circuit. The output voltage of the Buck converter depends on the ON time of the main switch, so the average output voltage can be maintained at the desired level by adjusting the duty ratio. Generally all converters are provided with at least one controller to maintain the output voltage constant. There are number of control techniques developed such as Sliding mode control [2], Model predictive control [1],[5], FPGA based control[4] to control the output voltage. Genetic Algorithm is used to obtain optimal values for the gain constants of PID controller [3] to control output voltage of Buck converter. But the performance of the controllers also depend on the parameters of the plant.

The Buck converter considered in this paper, is used to integrate wind generated power to a hybrid DC micro grid of voltage rating 110 volts. As the power output of

wind turbine depends on the wind speed and pitch angle, with variation of these parameters power output of turbine varies. In turn the output of the generator coupled to wind turbine also varies giving the power at varying voltage and this varying output voltage of generator is rectified and fed as input to the Buck converter.

Generally inductance and capacitance values are designed for constant value of input voltage, if the variation in the input voltage is around the designed value, then the Buck converter gives the acceptable performance. If there is large variation in the input voltage from the designed value then the performance of the Buck converter may be poor, like it may enter into DCM, increase in peak output voltage, increase in the ripple beyond the acceptable range. So to avoid such undesired performance an algorithm is proposed to find the optimal values for the inductance and capacitance based on Genetic Algorithm [11] to suit the variable input voltage.

Generally optimization techniques are used to obtain the optimal solution by finding the maximum or minimum value of the objective function. Genetic Algorithm is a random search method used to obtain optimal solution for a nonlinear equation and the solution is a numerical constant. But in this case the function to be optimized is transfer function of Buck converter which is a differential equation. And the solution is voltage and current waveforms which are functions of time. Therefore instead of optimizing the objective function, Buck converter with a PI controller is simulated with different pair of inductance and capacitance values for a particular value of input voltage. Noted down the peak values, percentage ripple and settling time for output voltage and inductor current for different pair of inductance and capacitance value starting from minimum to maximum values. This forms database for that particular input voltage, similarly database can be formed by simulating Buck converter for different input voltages with different set of inductance and capacitance values and stored. When the input voltage to the Buck converter varies, Genetic Algorithm finds the optimal values of the inductor and capacitor based on the specified limits of the required parameters. The paper is arranged in the following order, section I Introduction, section II Buck Converter, section III Genetic Algorithm, section IV Problem Formulation, section V Implementation, section VI Results and section VII Conclusion.

II. BUCK CONVERTER

A Buck converter converts constant DC input voltage into a variable DC voltage, and the average output voltage of the Buck converter is always less than the input voltage. This is achieved by switching operation of the main switch MOSFET Q. Figure .1 represents the circuit diagram of a Buck Converter. When the MOSFET is ‘ON’ (by applying gate pulse) current flows from source V_i through MOSFET Q, inductor L and through parallel connected capacitor and load resistor R and the diode is reverse biased acts as open circuit .During this period the output voltage is equal to voltage across capacitor V_c and current through inductor i_L increases from i_{Lmin} to i_{Lmax}. When the MOSFET is ‘OFF’ and acts as open circuit so the load is disconnected from the

supply. But the diode is forward biased and acts as freewheeling diode provides

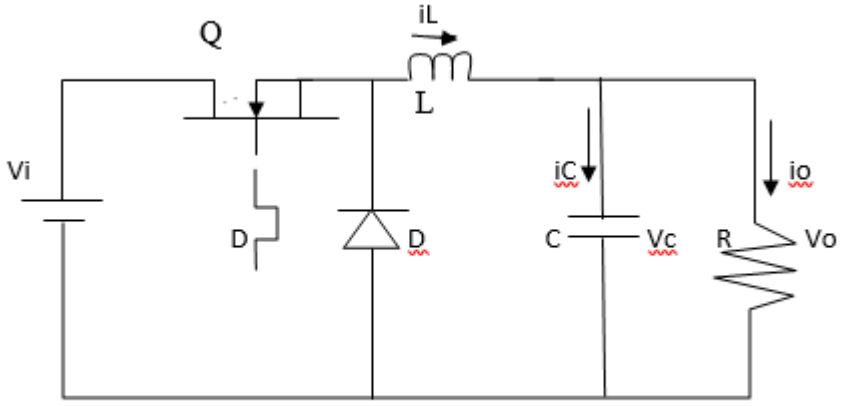

Figure.1 Buck Converter circuit

energy discharging path for the inductor and hence current through the inductor decreases from i_{Lmax} to i_{Lmin}. If the minimum current i_{Lmax} is less than zero then Buck converter enters into discontinuous current mode operation [9] [10]. Therefore selection of inductor value plays a vital role in the operation of Buck converter. The equations for calculating inductance and capacitance values are as follows; inductance,

$$L = \frac{V_o*(1-D)}{f_s*\Delta I_o} \quad (1)$$

Where

V_o – output voltage

D – duty ratio

$$D = \frac{V_o}{V_i} \quad (2)$$

Vi – input voltage

f_s - switching frequency

ΔI_o – ripple in the output current

capacitance,

$$C = \frac{\Delta I_o}{8*f_s*\Delta V_o} \quad (3)$$

ΔV_o – ripple in the output voltage.

III. GENETIC ALGORITHM

Genetic algorithm is a subset of Evolutionary computation inspired by theory of natural evolution proposed by Charles Darwin. This algorithm resembles natural selection process in which the appropriate individuals are nominated for reproduction to produce offspring for next generation. This process starts with a set of population, appropriate individuals are selected from this population to produce the off springs. These off springs have the inheritance of parent's characteristics and are part of the next generation. This process of finding the appropriate individuals keeps on iterating and at the end, appropriate individuals are obtained. This concept can be applied to a search problem to obtain best results. While applying this Genetic algorithm to optimization problem to obtain the best solution, phases have to be followed are;

Fitness function, Initialization of population, Selection, Reproduction, Crossover and Mutation.

The fitness function is a function of decision variables (individuals).The Genetic algorithm attempts to optimize the fitness function defined by the user. The fitness function examines and evaluates the 'fitness' of each potential solution. Initial population formed is a group of individuals. The fitness function is estimated using the members of the initial population. Based on the fitness of the individuals, the individuals which have higher fitness will be selected for next generation. These individuals then take part in reproduction to generate off springs. Then the off springs will be mutated randomly. This process will be repeated based on the accuracy requirement of the user [8].

In binary coded Genetic Algorithm the individuals are the binary strings [6],[7],[8].But in continuous Genetic Algorithm the individuals are real numbers. Estimation of the fitness function and selection process of chromosomes for reproduction of off springs remain the same as binary coded GA, but the crossover and mutation operations are carried out with minor modification.

The function f(x, y) to be optimized is a function of two decision variables x and y. Therefore the number of parameters Npar=2, and the chromosomes are of the form[x,y], size of the population is Np ,crossover percentage is Cp, mutation percentage is Mp,number of parents or off springs Nc and number of mutants is Nm. Therefore initial population is vectors of x and y with size Np and this population is randomly generated real numbers with minimum and maximum limits.

For the next generation to maintain the population size half of the fitting population from the existing population is retained through selection and other half of the population is obtained through selection and crossover. The probability of all the individuals for selection will be calculated, and individuals with higher value of probability will be selected as parents for production of next generation.

Mating of a pair creates two off springs, so Npar/2 parent chromosomes are required to produce appropriate number of off springs to obtain the desired population. In continuous Genetic Algorithm the chromosomes are real numbers so the crossover and mutation operations are to be conducted in a different way. Many methods are available for cross over operation. Here Haupt's method is used. Assume there are two parent chromosomes a=[xa, ya] and b=[xb,yb] ,select parameter y randomly as the point of crossover. Then introduce a new random value α between 0 and 1, and the y values of the offspring are ynew1= $(1-\alpha)ya+\alpha yb$ and ynew2=$(1-\alpha)yb+\alpha ya$ and the second parameter x is directly inherited from the each parent. So the off springs after the crossover are off spring1=[xa, ynew1] and offspring2=[xb,ynew2].

In mutation operation a new chromosome is created by introducing small diversity into a randomly selected chromosome. In GA, mutation introduces unpredictability in the results and hence the performance.

Data Base

Inductor L and capacitor C values are designed for the Buck converter at different input voltages. Buck converter is simulated with PI controller for a range of L and C values at each input voltage. From the waveforms of output voltage and current through inductor, peak value, percentage ripple and settling time for each set of L and

C values at a particular input voltage are measured. And the data base of measured parameters is formed.

IV. PROBLEM FORMULATION

The objective is to obtain the optimal values for Buck converter inductance L_{bu} and capacitance C_{bu} which give desired output voltage and inductor current with minimum transients like reduced peak values, percentage ripple and settling time. And subjected to constraints $L_{bumin} < L_{bu} < L_{bumax}$ and$C_{bumin} < C_{bu} < C_{bumax}$,$L_{bu}, C_{bu}$ parameter values to be adjusted, $L_{bumin}, C_{bumin}, L_{bumax}, C_{bumax}$ are boundary values of the components. Generally, Genetic algorithm is applied to solve the problem having the optimization function as a function of decision variables and the solution is a numerical value, but in case of Buck converter the output wave form cannot be represented by a single number because of its characteristics. Therefore the output of the Buck converter is represented by the parameters such as average value, peak value, percentage ripple and settling time. The inductance $L_{bu}$and capacitance C_{bu} pair which give the desired values of the said parameters is the solution for the problem. And instead of simulating Buck converter for each pair of L_{bu} and C_{bu} values inside Genetic algorithm, it is simulated offline in advance and the parameters are stored in the database for a range of L_{bu} and C_{bu} starting from designed minimum values.

Procedure for obtaining the optimum values of the inductor and capacitor using Genetic Algorithm.

1. Specify Vin, peak value, percentage ripple and the settling time for the output voltage and inductor current

2. Initial population is created randomly, to represent the decision variables L_{bu} and C_{bu} with the constraints.

3. The randomly created values and database values of inductor and capacitor are compared for computing the Least Square Index L_{ind} .Inductance and Capacitance values which give minimum value of L_{ind} are found out by the following equation

$$L_{ind} = index\left[min\ i = 1 \ldots N\ \sqrt{\left\{\frac{L_{bui} - L^*_{bu}}{L_{bumax}}\right\}^2 + \left\{\frac{C_{bui} - C^*_{bu}}{C_{bumax}}\right\}^2}\right] \qquad (4)$$

Where L_{bu} and C_{bu} are the values of decision variables from the database

L^*_{bu} and C^*_{bu} are values created by Genetic Algorithm

L_{bumax} and C_{bumax} are possible maximum values of decision variables.

4. For this pair of inductance L_{bu} and capacitance C_{bu} values corresponding peak value, percentage ripple and settling time of the output voltage and inductor current have to be tested to verify whether they are within the limits.

5. If the database values of the above said parameters of the output voltage and inductor current are within the limits the algorithm terminates.

6. If the optimal values for the decision variables are not found with the existing population, mutation and crossover operations are to be executed.

7. Crossover operation produces new population for L_{bu} and C_{bu}.

8. With the second generation population, fitness function L_{ind} is calculated.

9. Mutation operation is executed on any one set of randomly selected decision variables.

10. With the mutated pair of L_{bu} and C_{bu}values fitness function L_{ind} is calculated.

11. Out of the Selection, Crossover and Mutation operations, the best pair of decision variables L_{bu} and C_{bu} which give best values of the desired parameters is chosen for the design of the Buck converter.

V. IMPLEMENTATION

Following parameters are used for the simulation of Buck Converter.

Parameter	Value
Vi - input voltage	200 volts,400 volts,600 volts
Vo - output voltage	110 volts
fs - switching frequency	50 kilo hertz
R- Load resistance	8.06 ohms
Lmin - minimum value of inductance	2 milli Henry
Lmax - maximum value of inductance	6 milli Henry
Cmin - minimum value of capacitance	2 micro Farad
Cmax – maximum value of capacitance	6 micro Farad

Following parameters are used for Genetic algorithm

Parameter	Value
Npar – number of parameters	2
Np – size of the population	50
Cp – crossover percentage	0.7
Mp – mutation percentage	0.2
Itr – number of iterations	1
Lmin - minimum value of inductance	2 milli Henry
Lmax - maximum value of inductance	6 milli Henry
Cmin - minimum value of capacitance	2 micro Farad
Cmax – maximum value of capacitance	6 micro Farad

VI. RESULTS

The following output voltage and inductor current waveforms are obtained after simulating Buck Converter for different input voltages.

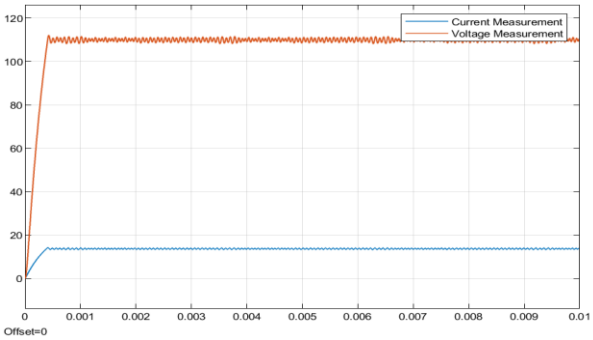

Figure.2 Vin=200 volts,L=4mH,C=2.5milli F

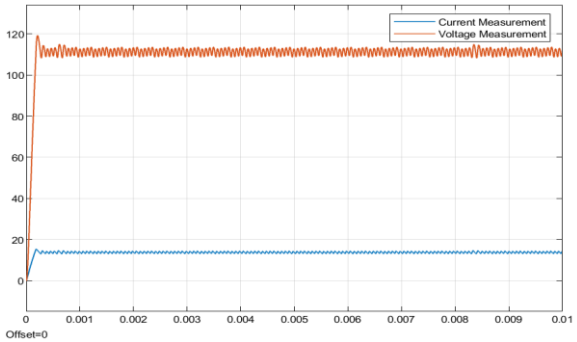

Figure.3 Vin=400 volts,L=6mH,C=5.5 micro F

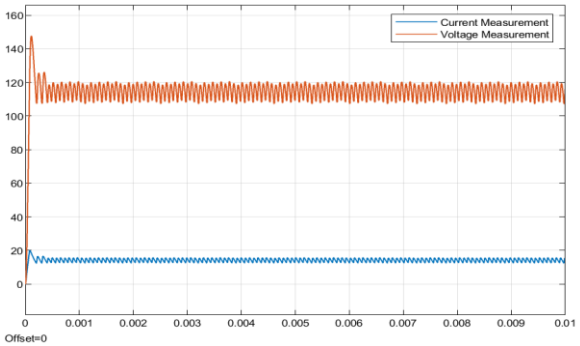

Figure.4 Vi= 600 volts,L=4 mH, C=2.5 micro F

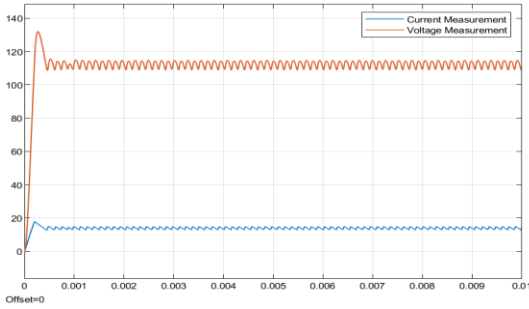

Figure.5 Vi= 600 volts,L=6mH,C=5.5microF

Table .1 Database values obtained after simulation of Buck converter at Vi=200 volts for different set of inductance and capacitance values.

L in milli H	C in micro F	Vp in volts	Ip in amps	Voltage ripple	Current ripple	Voltage settling time	Current settling time
5	4	140	15.2	2%	20%	0.0003 s	0.0003 s
4.5	4	142	15.8	2%	20%	0.0003 s	0.0003 s
4	4	146	16.2	2%	20%	0.0003 s	0.0003 s
3.5	4	150	17	2%	20%	0.0003 s	0.0003 s
3	4	158	18	2%	20%	0.0003 s	0.0003 s
2.5	4	164	20	2%	36%	0.0003 s	0.0003 s
2.0	4	164	20	2%	36%0	0.0003 s	0.0003 s
6	4	135	15	1%	<20%	0.0006 s	0.0006 s
6	6	144	16.2	1%	<20%	0.0008 s	0.0008 s
6	5.5	146	16.2	<1%	<20%	0.0008 s	0.0008 s
6	5	140	16.2	<1%	<20%	0.0008 s	0.0008 s
6	4.5	138	16.2	<1%	<20%	0.0008 s	0.0008 s
6	4	132	16.2	<1%	<20%	0.0008 s	0.0008 s
6	3.5	128	15.2	1.5%	20%	0.0008 s	0.0008 s
6	3	128	15.2	1.5	20%	0.0008 s	0.0008 s
6	2.5	126	15	1%	22%	0.0008 s	0.0008 s
6	2	124	15	1%	24%	0.0008 s	0.0008 s

From figures 2, 3, 4 and 5 it is observed that the inductance and capacitance pair which give best performance for 200 volts input will not give the same performance for the input of 400 volts. This variation in performance for input of 600 volts is shown in figure. 4 indicates increased peak values and percentage ripple. Figure .5 shows improved performance for different pair of inductance and capacitor values.

For the specifications of Vp< 130 volts, Ip<16 Amps, voltage ripple=20% and current ripple=2%, the Genetic Algorithm gave the optimal values of inductance and capacitance as 5.342 milli Henry and 3.428 micro Farad respectively. And the nearest inductance and capacitance values are 6 milli Henry and 3.5 micro Farad respectively from the data base table 1, the Buck converter inductance and capacitance values can be adjusted to these values to obtain the desired performance.

VII. CONCLUSION

A DC - DC Buck Converter is designed and simulated in MATLAB/Simulink environment at input voltage of 200 volts, 400 volts and 600 volts respectively to obtain 110 volts output. The Buck converter gives 110 volts output for the range of input from 200 volts to 600 volts with PI controller, but with increase in input voltage the performance i.e. the quality of the output reduces in the form of increased peak and percentage ripple of both output voltage and inductor current. By changing the values of inductance and capacitance peak values and percentage ripple of the output voltage and inductor current can be reduced. The optimal values of inductance and capacitance

which give better performance at the increased input voltage are obtained by Genetic Algorithm. Since mathematical model of a Buck Converter is a differential equation, it is not possible to obtain solution for the optimization function directly. Hence in this paper Genetic Algorithm is used to find the optimal values of the variables which gives the desired performance with the help of a stored database.

REFERENCES

1. Tobias Geyer, Georgios Papafotiou , and Manfred Morari ," Hybrid Model Predictive Control of the Step-Down DC-DC Converter," European Commission research projects IST2001-33520 Control and Computation (CC) *andand FP6-IST-511368 Hybrid Control (HYCON)*

2. Khalifa Al-Hosani , Andrey Malinin and Vadim I. Utkin , "Sliding Mode PID Control of Buck Converter, " *Proceedings of the European Control Conference 2009* • Budapest, Hungary, August 23–26, 2009

3. M Dinesh, K R Bhaskaran and J Baskaran , "Design ,Control and Simulation of Buck converter using PID Controller and Reference Regulator Technique, *" International Journal on Recent Technologies in Mechanical and Electrical Engineering*"(IJRMEE) October 2015,Vol 2,Issue 10 pp 58-62.

4. Ling Lv , Changyuan Chang , Zhiqi Zhou , and Yubo Yuan, " An FPGA-Based Modified Adaptive PID Controller for DC/DC Buck Converters,"*Journal of Power Electronics*, March 2015,Vol.15,No.2,pp.346-355.

5. Yahya DANAYİYEN, İsmail Hakkı ALTAŞ, Erdinç ŞAHİN," MODEL PREDICTIVE CONTROL OF A DC-DC BUCK CONVERTER," *Innovations on Intelligent Systems and Applications Symposium (ASYU)2016*, Sigma J Eng &Nat Sci 8(2), 2017, pp 91-97

6. S. Sumathi • L. Ashok Kumar • P. Surekha , "Solar PV and Wind Energy Conversion Systems, An Introduction to Theory, Modelling with MATLAB/SIMULINK, and the Role of Soft Computing Techniques", ISSN 1865-3529 ISSN 1865-3537 (electronic) Green Energy and Technology ISBN 978-3-.19-14940-0 ISBN 978-3-319-14941-7 (eBook).Springer .

7. S N Sivanandam and S N Deepa, "Introduction to Genetic Algorithms",ISBN 978-3-540-73189-4 Springer ,2008.

8. Jenna Carr, "An Introduction to Genetic Algorithms",May 16,2014

9. Muhammad H. Rashid "POWER ELECTRONICS CIRCUITS,DEVICES,AND

APPLICATIONS", second Edition, PHI publications.

10. Mohan, Undeland, Robbins,"Power Electronics Converters Applications and Design",Media Enhanced Third Edition, JOHN WILEY&SONS,INC.

11. P. Suresh,D.Kirubakaran, "POWER LOSS OPTIMIZATION OF BOOST CONVERTOR USING GENETIC ALGORITHM", *International Journal of Scientific & Engineering Research*, Volume 5, Issue 4, April-2014 112 ISSN 2229-5518 IJSER © 2014 http://www.ijser.org .

Design, Simulation of a SEPIC and CUK Converter For Solar Powered Electric Vehicle Battery Charging

Ankush K M[1], Venkatesh Boddapati[2]

[1, 2], Power Electronics, Department of EEE, B.M.S.C.E, Bengaluru, India.

Email: ankush.epe20@bmsce.ac.in

Abstract.

This work focuses on the design comparison and implementation of a Sepic converter and Cuk converter for the solar powered battery charging application. The proposed converter is designed and realized for the given specification using suitable equations. In this project design and comprehensive analysis is carried out for both Sepic converter and Cuk converter with same power rating and operating frequency. Detailed comparison is carried out in terms of battery charging and discharging with constant voltage and current using MATLAB/SIMULINK software.

Index: Sepic converter, Cuk converter, Battery, Charging, Discharging

1. INTRODUCTION

The solar PV array is widely used in both urban and rural areas to generate the electric power from sun. The output power from solar panel is varying and it can be utilized effectively by step up or step down to the required voltage and current for electric vehicle battery charging application.[1,2] PV based solar power has many advantages because it does not require fuel, less noise, low in maintenance, clean and green energy source [3,5]. The output voltage is varying depending on irradiance. Higher the irradiance, greater the output current and the power generation. In this work, PI controller is used for closed loop controller [4]. The two controllers are used like current controller and voltage controller. Using Sepic converter circuit we can control the voltage using PI controller and from current control circuit we can control the current using PI controller [5-8].

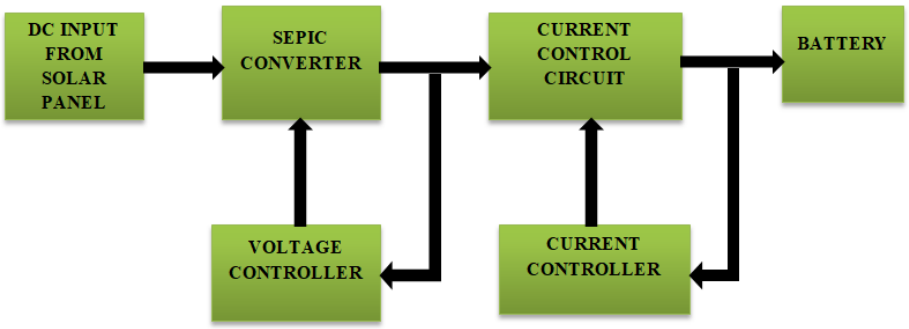

Figure 1.1: Block Diagram for the proposed Sepic converter

The Figure 1.1 shows the block diagram representation for the proposed converter along with the voltage and current controller [1]. From the P V panel solar energy converted into

electrical energy. A DC Source from P V Array as an input to the sepic converter. The output of the Sepic converter is connected to current control circuit and output of the current control circuit is connected to the battery [9-13]. The main aim is to battery charging application the output current and voltage should be maintained constant to charge or discharge of the battery.

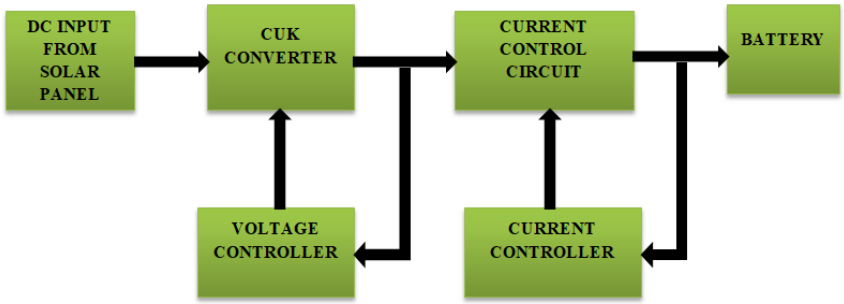

Figure 1.2: Block Diagram for the proposed Sepic converter

The Figure 1.2 shows the block diagram representation for the proposed DC-DC Cuk converter along with the voltage and current controller. A DC Source from P V Array as an input to the Cuk converter. The output of the Cuk converter is connected to current control circuit and output of the current control circuit is connected to the battery. If there is any variation in the output current and voltage, it is sensed by varying duty cycle. Thus output voltage and current is maintained constant. Compare to cuk converter major advantages of Sepic converter is that provide low input current ripple and reduce the harmonics and it also provide lesser electrical stress and higher converter efficiency.

In this paper, Design Simulation Comparative Study and Implementation of Sepic and Cuk converter for solar Powered Electric Vehicle Battery Charging Application. The work carried out is presented as follows: Section 1 gives introduction for the work carried out in this paper. Section 2 describes the analysis and operation, design details of the Sepic and Cuk converter. Section 3 describes the simulation results and comparison of Sepic and Cuk converter. And the paper is concluded with the conclusion and followed by references.

2 OPERATION AND DESIGN PROCEDURE

1.1. Sepic Converter Circuit Diagram

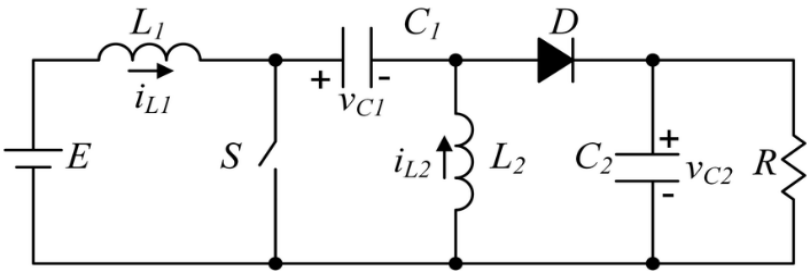

Figure 2.1: Circuit Diagram for the Sepic Converter

The DC-DC Converter is shown in Figure 2.1 works under two modes of operation which are switch S is closed and open. All DC-DC Converters operates simultaneously on and off

of a switch generally with a high frequency pulse for a Sepic converter Inductor-1 is charged by the solar panel as input voltage and Inductor-2 is charged by Capacitor-1, if the Diode is off output is maintained constant by Capacitor-2 or output of the Sepic controlled by the duty cycle of the control switch for the closed loop.

2.1.1 Design details of Sepic converter and Cuk converter

Duty cycle calculation

$$D = \frac{V_{out}+V_d}{V_{in}+V_{out}+V_d} \quad \textbf{(1)}$$

$$D_{max} = \frac{40 + 0.5}{25 + 40 + 0.5} = 0.6183 = 61.8\%$$

$$D_{min} = \frac{40 + 0.5}{50 + 40 + 0.5} = 0.447 = 44.7\%$$

Inductor selection

$$L = \frac{V_{in}\times D}{F\times \Delta I_0} \quad \textbf{(2)}$$

$$L = \frac{25 \times 0.6183}{50 \times 10^3 \times 0.5} = 618.3 \times 10^{-6} H$$

Capacitor selection

$$C = \frac{D\times V_{out}}{R\times \Delta V_o \times F} \quad \textbf{(3)}$$

$$C = \frac{0.6183 \times 40}{5 \times 0.5 \times 50 \times 10^3} = 197.85 \times 10^{-6} F$$

Table 1: Specification of Sepic converter and Cuk converter

Parameter	Valve
V_{in}	25-50V
V_{out}	40V
f	50kHz
Dmin	0.447
Dmax	0.618
L1, L2	618.3µH
C1, C2	197.85µF

Abbreviations:

V_{in}: Input voltage
V_{out}: Output Voltage
Dmin: Minimum Duty Cycle
Dmax: Maximum Duty Cycle
F: Switching frequency
ΔV_o: Voltage Ripple
C: Capacitance
ΔI_0: Current Ripple
L: Inductance

1.2. Cuk Converter Circuit Diagram

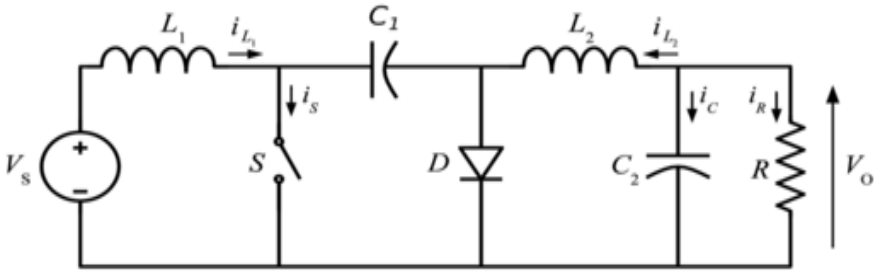

Figure 2.2: Circuit Diagram for the Cuk converter

The DC-DC Converter is shown in Figure 2.2 the cuk converter is a like a buck boost converter with inverted output voltage with lower and higher valve of input voltage from solar panel. In Cuk converter consists of a total six components L1, L2, C1, C2, Diode and the Mosfet Switch. When Switch is on source will charge the inductor that flow of current is observed from L1 to the Mosfet and buck to source and inductor L1 get charged and small amount of voltage in capacitor C1.When Switch is off and inductor L1 is dissipated the stored energy by reversing the positive the flow of current path when the switch is open is inductor L1 to capacitor C1 and diode and return to the source and disadvantages of using Cuk converter is high stress across the switch and inverted output voltage and capacitor is off large size.

Table2: Battery specification

Battery	Lithium ion
Charging voltage	25V
Charging Current	5A
Discharging Voltage	25V
Discharging Current	5A
Initial SOC	45%
Battery response Time	1S
Rated capacity	5Ah

2. SIMULATION RESULTS AND COMPARISON OF SEPIC AND CUK CONVERTERS

3.1 DC-DC Sepic Converter Mat lab Simulation.

To compare both sepic converter and cuk converter same specifications are considered and the simulation model is built in Mat lab / simulation software. The simulation circuit for sepic converter and across battery constant voltage and constant current waveforms. Li-Ion battery of 25V, Initial state of charge (SOC) of the battery is considered to be 45% and rated capacity of 5Ah.

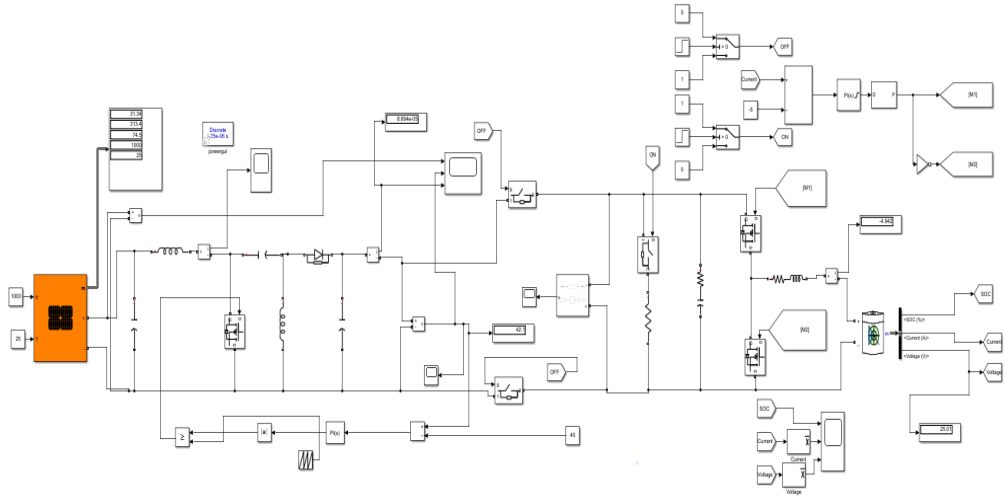

Figure 3.1: Sepic converter with current control circuit

The Figure 3.1 depicts the simulation circuit for Sepic converter. Constant DC Output voltage and current of 25V and 5A is achieved to charge and discharge of the battery of electric vehicle irrespective of power generated from the P V array.

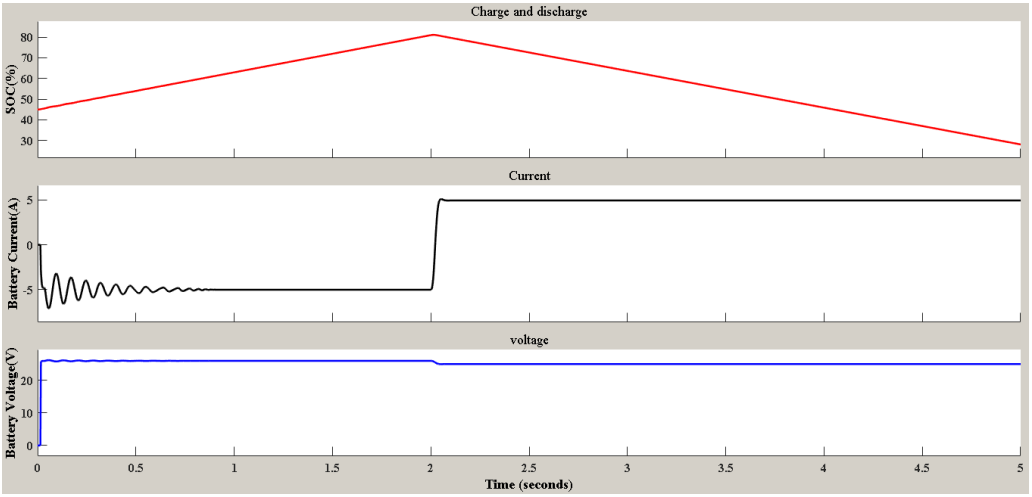

Figure 3.2: State of charge, Output voltage, Output current across the battery

The Figure 3.2 depicts the graph for State of charge, battery current and voltage with 2sec Battery will charge and 3 Sec battery will Discharge with Maintain the constant voltage of24V and constant current of 5A across the Battery using sepic converter.

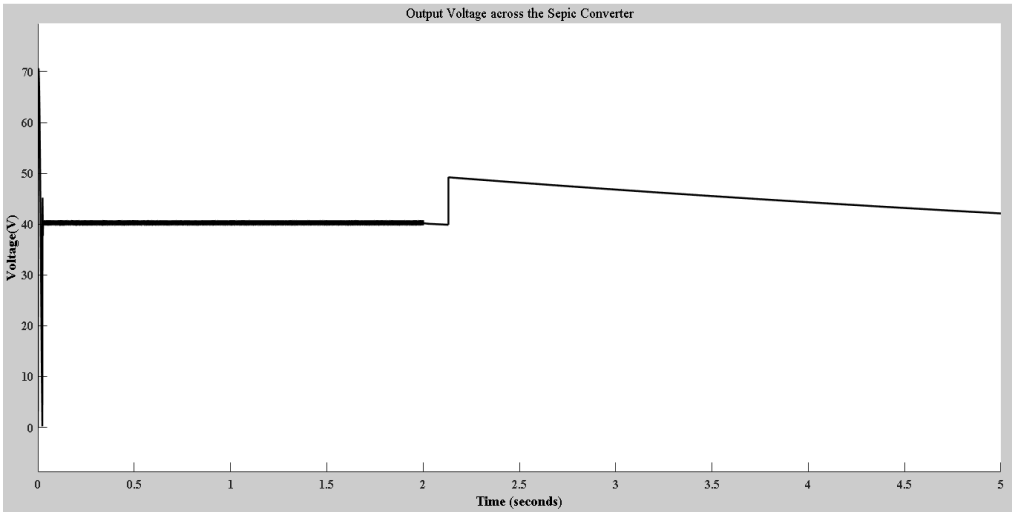

Figure 3.3: Output voltage across the sepic converter

The Figure 3.3 depicts the graph for Output voltage across the Sepic converter in which variation in input voltage the output voltage remains constant with less voltage fluctuation.

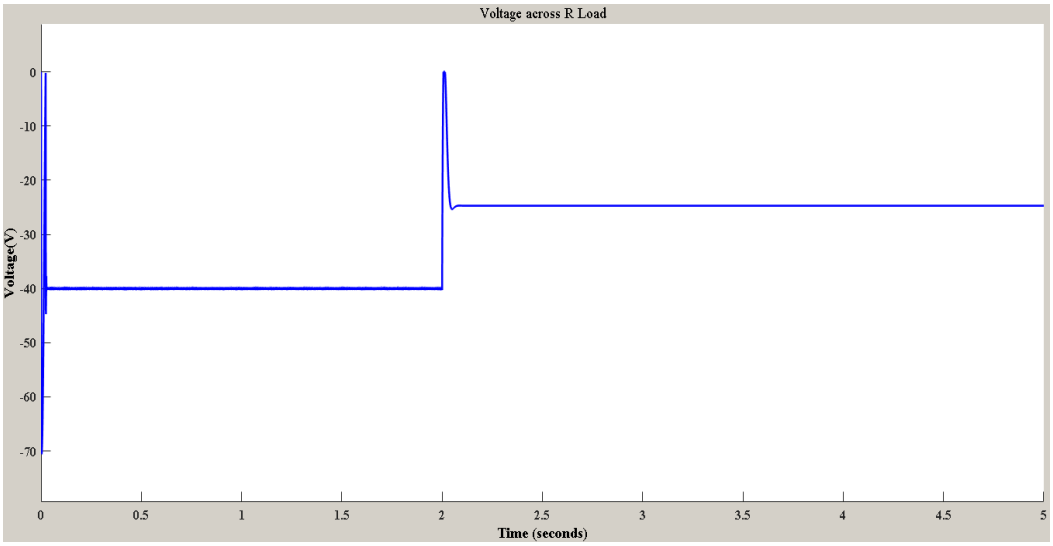

Figure 3.4: Charging and discharging Output voltage across the R load

The Figure 3.4 depicts the graph of Charging and discharging Output voltage across the R load, when charging voltage should be 40V and when Discharging Voltage should be 24V.

3.2 DC-DC Cuk Converter Mat lab Simulation.

The Figure 3.5 depicts the simulation circuit for Cuk converter and across battery constant voltage and constant current waveforms. Li-Ion battery of 25V, Initial state of charge (SOC) of the battery is considered to be 45% and rated capacity of 5Ah.

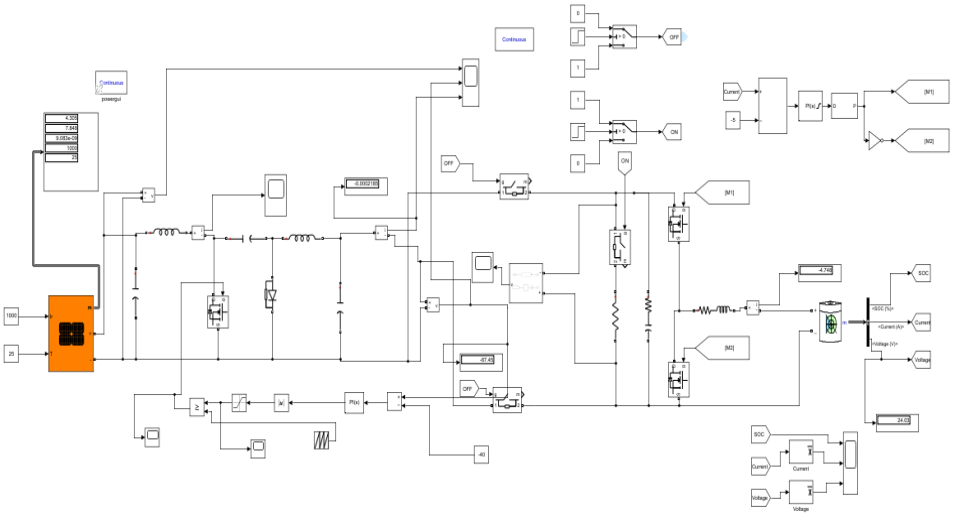

Figure 3.5: Sepic converter with current control circuit

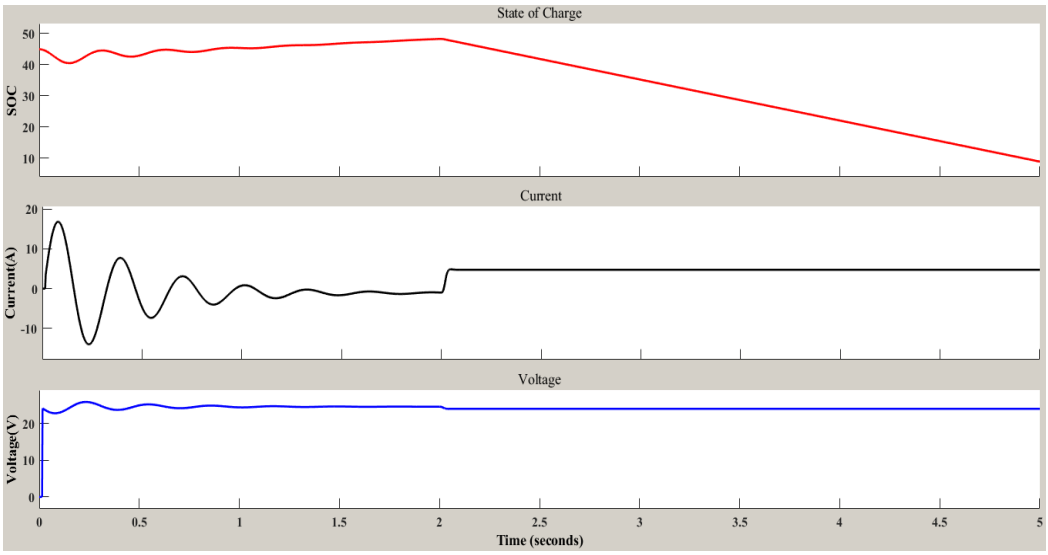

Figure 3.6: State of charge, Output voltage, Output current across the battery

The Figure 3.6 depicts the graph for State of charge, battery current and voltage with 2min Battery will charge and 3min battery will Discharge with Maintain the constant voltage of 24V and constant current of 5A across the Battery using Cuk converter.

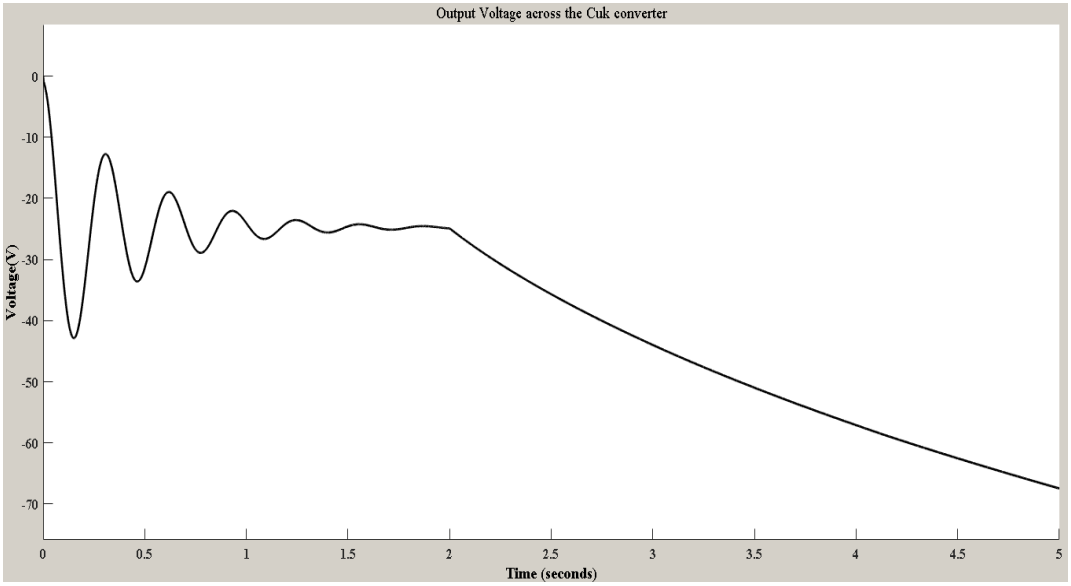

Figure 3.7: Output voltage across R Load of the Cuk converter

The Figure 3.7 depicts the graph of Charging and discharging Output voltage across the R load of the cuk converter as more ripple voltage compare to Sepic converter.

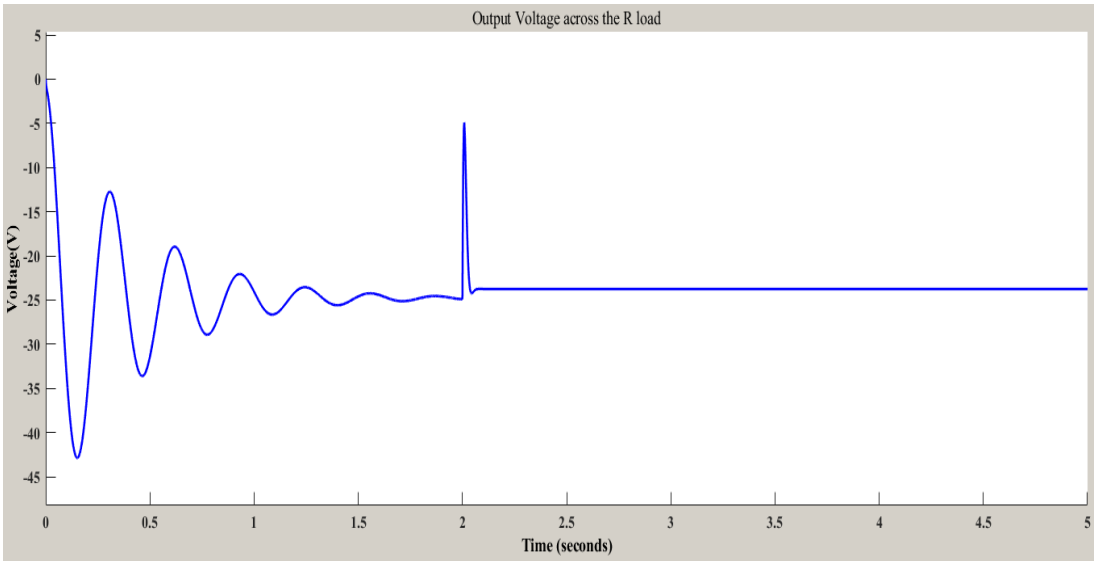

Figure 3.8: Charging and discharging Output voltage across the R load

The Figure 3.8 depicts the graph of Charging and discharging Output voltage across the R load, when charging voltage should be 40V and when Discharging Voltage should be 24V.

Table 3 the comparison between Sepic and cuk converter

SL.NO	TOPOLOGY	PARAMETERS			
		Input Voltage from Solar panel (V)	Output Voltage of sepic converter (V)	Output Voltage across the Battery(V)	Output Current across the Battery(V)
1	SEPIC CONVERTER	31.34	40.02	25.02	4.9
		39.64	39.73	25.12	5.2
		47.19	40.12	24.89	5.23
		55.39	40.16	25.10	5.26
2	CUK CONVERTER	31.34	-41.02	25.10	5.6
		39.64	-42.12	26.12	5.9
		47.19	-40.04	24.01	5.25
		55.39	-40.39	26.10	4.98

Finally two converters such as Sepic and Cuk converter are simulated in Mat lab simulation software. By varying the input voltage from solar panel by changing Parallel strings and Series-connected modules per string in PV array. The performance parameters such as output voltage across the converter, output voltage and current across the battery obtained for sepic and cuk converter, due to less output voltage ripple in sepic converter, non-inverted output voltage, less total harmonics, less electrical stress and hence given higher efficiency in sepic converter compared with cuk converter.

3. CONCLUSION

The Sepic DC-DC Converter and Cuk DC-DC Converter for Solar powered electric vehicle battery charging application is designed and simulated using MATLAB Simulink software. Simulation model also provided a closed loop control for sepic and a cuk converter which maintains a constant 24V output voltage and constant 5A output current across the battery. The comparison of sepic converter and cuk converter with the same specification in terms of switching frequency, charge, and discharge of the battery is carried out. Further, from the simulation results it is found that sepic converter has less fluctuation in output voltage and current across the battery when charging and discharging.

4. REFERENCES

[1] M. Karuppiah, P. Dinesh Kumar, “Design an Electric Vehicle Charger Based SEPIC Topology with PI Controller”. 2020 IEEE 19th Workshop on Control and Modeling for Power Electronics (COMPEL), 2020

[2] Venkatesh Boddapati, and S. Arul Daniel, Design and Feasibility Analysis of Hybrid Energy-Based Electric Vehicle Charging Station, Distributed Generation & Alternative Energy Journal, Vol. 37(1), 41–72. Doi: 10.13052/dgaej2156-3306.3713

[3] H. Suryoatmojo, I. Dilianto, Suwito, R. Mardiyanto, E. Setijadi and D.C. Riawan, "Design and Analysis of High Gain Modified SEPIC Converter for Photovoltaic Applications" 2020 IEEE 8th International Power Electronics and Motion Control Conference (IPEMC-ECCE Asia).

[4] Venkatesh Boddapati, Avinash Sree Ram Nandikatti, S. Arul Daniel: Design and feasibility analysis of a solar PV array installation during the construction of high-rise residential buildings. Journal of Energy Systems, DOI: 10.30521/jes.811978.

[5] P.Srinivasa, K.kamalapathi, N.Laxman, "Design and Simulation of BUCK-BOOST Type Dual Input DC-DC Converter for Battery Charging Application in Electric Vehicle." 2021 IEEE Applied Power Electronics Conference and Exposition - APEC 2021

[6] Azrita binti Alias, Maaspaliza binti Azri, "A Modified PID Controller of SEPIC Converter for Excellent Dynamic Performance" 2016 IEEE Transactions on Power Electronics,

[7] Platon, S. Oprea, A. Florescu and S. G. Rosu, "Simple and Digital Implementation of PI Controller Used in Voltage-Mode Control," 2018 10th International Conference on Electronics, Computers and Artificial Intelligence (ECAI), 2018

[8] Vivek Kumar, Yogesh, Praveen Kumar, "Charging of Electric Vehicles Battery Using Bidirectional Converter." 2020 IEEE Applied Power Electronics Conference and Exposition - APEC 2020

[9] Karthikeyan and R. Guptat "Closed-loop control of isolated dual active bridge converter using dual phase shift modulation" 2018 IEEE 8th International Power Electronics and Motion Control Conference (IPEMC-ECCE Asia),

[10] .M. Ishigaki, J. Shin and E. M. Dede, "A Novel Soft Switching Sepic DC–DC Converter Using Magnetic and Capacitive Hybrid Power Transfer," in IEEE Transactions on Power Electronics, vol. 32, no. 9, pp. 6961-6970, Sept. 2017.

[11] R. Gautam, O.P. Mahela, Suresh Singh, "A Double Input SMV Controlled DC/DC Buck-Boost Converter for Solar PV /Wind Energy Sources" Recent Advances and Innovations in Engineering (ICRAIE), May 09-11, 2014, Jaipur,

[12] Venkata Suresh Babu, Melimi Ravi Kumar, Venkatesh Boddapati, Design and control of a DC microgrid by using a modern predictive controller, 45, 2207–2215. Design and Feasibility Analysis of a Solar PV 815

[13] Venkatesh Boddapati, S. Arul Daniel, Performance analysis and investigations of grid-connected Solar Power Park in Kurnool, South India, Energy for Sustainable Development, 55, 161–169.

Design, Modelling and Simulation of Traditional DC - DC Boost Converter and Interleaved DC - DC Boost Converter

Abhay P Badnur*, Laksh C*, Shrayan Karkun*, Nishanth Madhava Navada*, Divya S*

**Department of Electrical and Electronics Engineering, B.M.S. College of Engineering*

Abstract

A DC-DC converter is an electrical circuit that employs switching techniques to convert a DC voltage input to the desired magnitude, which could be greater or lower, by momentarily holding input energy and then releasing it at a different voltage to the output. A DC-DC boost converter is a power converter that increases the magnitude of voltage from its input to its output. Boost converter finds many applications in battery power systems, photovoltaic systems, consumer electronics etc. A traditional DC-DC boost converter contains two semiconductors (a diode and a switch) and an energy storage element (inductor). Filters constructed from capacitors are added to the converter's output to reduce voltage ripple (load-side filters). This topology has certain limitations, therefore interleaving is a recommended approach for high-performance applications because it creates a harmonic circuit design by paralleling two or more identical converters. When compared to a traditional boost converter, the interleaved DC-DC boost converter (IBC) has higher efficiency, reduced size, and increased reliability. This work presents the design, development and modelling of the Traditional DC-DC boost converter and the Interleaved DC-DC boost converter (IBC) and compares their performance by simulating the mathematical models and circuits of the two converters using MATLAB/SIMULINK.

Keywords. Traditional Boost Converter, Interleaved Boost Converter, Current ripple, Voltage ripple, Continuous Conduction Mode, Efficiency.

1. INTRODUCTION

Batteries are frequently employed in energy storage systems to balance out power fluctuations between the generation and consumption of renewable energy sources. A step-up DC-DC converter is essential in applications requiring high dc voltage because battery voltage is often low and varies widely [2][7]. All modern systems require power converters that can deliver regulated voltages from a steady power source. The advantages of a simple circuit architecture and straightforward operation have led to a widespread use of the traditional boost converter for step-up applications[1][9]. However the Traditional DC-DC Boost Converter has quite a few limitations which include considerably high voltage and current ripples and a reduced output efficiency when compared to other topologies of the boost converter.[6] This paper proposes an interleaved converter with the intention of addressing the aforementioned issues and offering a superior solution. The method of interleaving, also known as multi phasing, is helpful for reducing the size of filter components, minimising the ripple in the input current, and it also has an impact on the converter's efficiency[4][8]. The optimal selection of the number of phases and the switching frequency results in a better efficient converter operation [3][5].

2. DC-DC BOOST CONVERTER

A boost converter is a device that boosts the output voltage in relation to the input voltage. The traditional DC-DC boost converter circuit is shown in Figure 2.1. It is a switching power converter that alternates between ON and OFF states on a regular basis. An input voltage source V_{in}, an inductor L, a diode D, a controlled semiconductor switch S that can be a MOSFET, an IGBT, or a BJT, an output capacitor C_{out} , and a load resistance R_{load} constitute a simple boost converter circuit. There are two modes of operation - Continuous Conduction Mode (CCM) and Discontinuous Conduction Mode (DCM), which can be implemented for the boost converter. These modes can be computed by duty ratio and also be determined by the current inductor value. This work focuses on the continuous conduction mode (CCM) of the boost converter only.

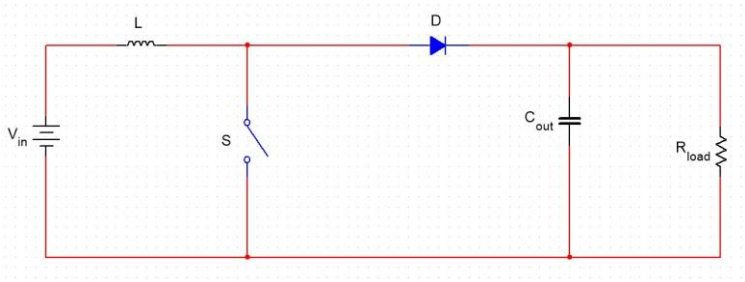

Figure 2.1. Traditional DC-DC Boost Converter Circuit Diagram

A traditional DC - DC boost converter has two modes of operation. **In the first mode** shown in Figure 2.2, the switch S is closed thus forming a path of least resistance for the current to flow. The inductor receives energy supplied from the input source, resulting in linear growth of current flowing in the inductor.

$$V_L = V_{in} \tag{2.1}$$

$$L\frac{diL}{dt} = V_{in} \tag{2.2}$$

$di_L = \Delta i_L$; $dt = DT$ when the switch is closed.

$$(\Delta i_L)_{closed} = \frac{Vin*D*T}{L} \tag{2.3}$$

Where D is duty cycle ($\frac{ton}{T}$), i_L and V_L are the inductor current and voltage respectively, T is the duration of a single switching cycle ($t_{on} + t_{off}$) and V_{in} is the input voltage.

In the second mode shown in Figure 2.3, the switch is opened and the stored energy in the inductor discharges through the diode (turned on), supplying the energy to the output capacitor and charges it to a voltage higher than the input voltage.

$$V_L = V_{in} - V_o \tag{2.4}$$

$$L\frac{diL}{dt} = V_{in} - V_o \tag{2.5}$$

$$(\Delta i_L)_{open} = \frac{(Vin - Vo)*(1-D)*T}{L} \tag{2.6}$$

At steady state operation:

$$V_o = \frac{Vin}{1-D} \tag{2.7}$$

where V_o is output voltage (V).

We can infer from the above equations 2.4 to 2.7 that the output voltage exceeds that of the input when the switch remains open (OFF). In order to obtain a more precise estimation of power for an ideal lossless converter, we can consider:

Input power = Output power

$$V_{in} I_{in} = \frac{Vo^2}{R} \tag{2.8}$$

Where R_{load} is the resistance considered as load.

The average value of inductor can be expressed as:

$$I_L = \frac{Vin}{(1-D)^2*R} \tag{2.9}$$

The maximum and minimum inductor currents are calculated using the mean value and current ripples. The maximum current that can flow in the inductor is given by:

$$I_{max} = I_L + \frac{\Delta iL}{2} = \frac{Vin}{(1-D)^2*R} + \frac{Vin*D*T}{L} \tag{2.10}$$

The minimum current of the inductor is given as:

$$I_{min} = I_L - \frac{\Delta iL}{2} = \frac{Vin}{(1-D)^2*R} - \frac{Vin*D*T}{L} \tag{2.11}$$

In the above equation 2.11, the inductor current has been calculated such that the converter operates in continuous conduction mode, i.e., current is always positive. For I_{min} to be positive, this is a required condition. Therefore,the boundary between continuous and discontinuous inductor current is given by the equation,

$$I_{min} = 0 = \frac{Vin}{(1-D)^2 * R} - \frac{Vin * D * T}{I_L} \quad (2.12)$$

From the above equation 2.12, we can obtain the least inductance value of the inductor in traditional DC-DC boost converters.

$$L_{min} = \frac{D*(1-D)^2*R}{2f} \quad (2.13)$$

where f is switching frequency (in kHz), I_{in} is input current (A), I_L is inductor current (A) and L_{min} is minimum value of inductor (H).

The L_{min} value calculated serves as a reference point and the selected inductor will have a slightly larger inductance value to ensure that the circuit operates in continuous conduction mode. It is beneficial to describe L in terms of a desired Δi_L.

$$L = \frac{Vin*D*T}{\Delta iL} = \frac{Vin*D}{\Delta iL.f} \quad (2.14)$$

The ripple factor (r) and the minimum capacitor value for continuous conduction mode is given as,

$$|\Delta Q| = \left(\frac{Vo}{R}\right) DT = C\Delta V_o \quad (2.15)$$

$$r = \frac{\Delta Vo}{Vo} = \frac{D}{RCf} \quad (2.16)$$

$$C_{min} = \frac{D}{R\left(\frac{\Delta Vo}{Vo}\right)f} \quad (2.17)$$

where ΔVo is change in output voltage (V), ΔQ is change in charge stored in the capacitor (C), r is ripple factor (%) and C_{min} is minimum capacitor value (F).

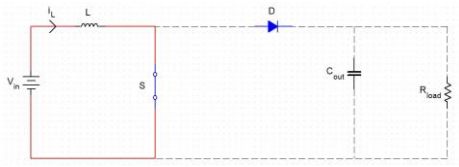

Figure 2.2. Mode-1 operation of Traditional DC-DC boost converter

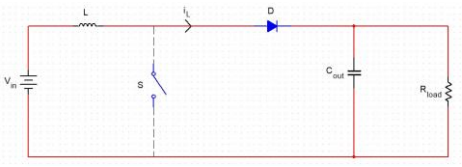

Figure 2.3. Mode-2 operation of Traditional DC-DC boost converter

2.1. Design of DC-DC Boost Converter

The design of the converter is done such that an output of 48 volts is obtained by supplying 12 volts to the circuit. The following parameters are considered while designing the traditional DC - DC Boost Converter: Inductor of 93.37 µH, Capacitor of 417 µF, Switching frequency of

100kHz, Voltage ripple of 2%, current ripple of 20% and output resistance of 48 Ω.

3. INTERLEAVED DC-DC BOOST CONVERTER

Two phase IBC comprises two identical Traditional boost converters in parallel with 180° phase delay and operating at the same frequency and duty cycles. Due to the parallel connection, the current is divided and I^2R losses are minimised and current stress is decreased. The interleaved DC-DC boost converter circuit is shown in Figure 3.1.

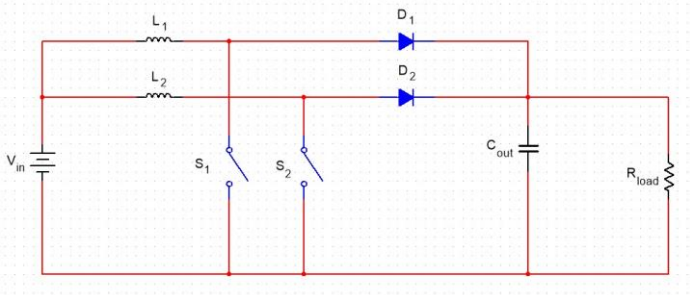

Figure 3.1. Interleaved DC-DC Boost Converter Circuit Diagram

IBC has four modes of operation. **In the first mode** shown in Figure 3.2, both the switches are closed. Thus the diodes are reverse biased (turned off). The current flowing in both the inductors builds up linearly and the energy is stored in the inductors.

$$V_{L1} = V_{in} \quad (3.1)$$

$$V_{L2} = V_{in} \quad (3.2)$$

where,

$V_{L1} = L_1\frac{di1}{dt}$ and $V_{L2} = L_2\frac{di2}{dt}$ (i_1 = current in Inductor 1 and i_2 = current in Inductor 2)

In the second mode shown in Figure 3.3, switch S_1 is closed and switch S_2 is opened. Diode D_1 is reverse biased (turned off) and the diode D_2 is forward biased (turned on). Current flowing in the first inductor increases as the supply is providing energy to that inductor. At the same time, the second inductor provides the load with energy resulting in lowering in the inductor current.

$$V_{L1} = V_{in} \quad (3.3)$$

$$V_{L2} = V_{in} - V_o \quad (3.4)$$

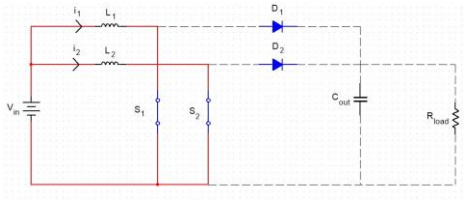

Figure 3.2. Mode-1 operation of IBC

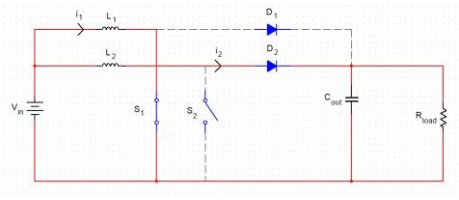

Figure 3.3. Mode-2 operation of IBC

In the third mode shown in Figure 3.4, switch S_1 is opened and switch S_2 is closed. Diode D_1 is forward biased (turned on) and the diode D_2 is reverse biased (turned off). The first inductor discharges current and thereby supplies energy to the load, leading to the decrease in inductor current. Simultaneously, the input source supplies the second inductor with energy causing the current flowing in that inductor to increase.

$$V_{L1} = V_{in} - V_o \quad (3.5)$$

$$V_{L2} = V_{in} \quad (3.6)$$

In the fourth mode shown in Figure 3.5, both switches are opened. Both the diodes are forward biased (turned on). This mode involves both inductors discharging and supplying the load with the energy and as a result both inductor currents decrease.

$$V_{L1} = V_{in} - V_o \quad (3.7)$$

$$\frac{di1}{dt} = \frac{di2}{dt} = \frac{Vin - Vo}{L} \quad (3.8)$$

It can be seen that, for the steady state operation of a boost converter:

$$V_o = \frac{Vin}{(1-D)} \quad (3.9)$$

For interleaved configuration and Continuous Conduction mode, L_1 and L_2 need to be selected such that:

$$L_{1min} = L_{2min} = \frac{Vin * D * T}{2 * \Delta iL} \quad (3.10)$$

where L_{1min} and L_{2min} are the minimum values of Inductors L_1 and L_2. Capacitor value is given by,

$$C_{min} = \frac{D}{R * (\frac{\Delta Vo}{Vo}) * f} \quad (3.11)$$

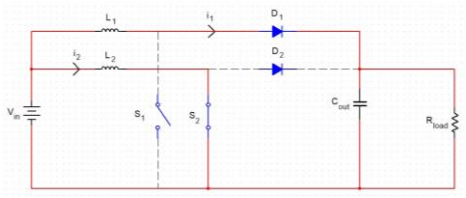

Figure 3.4. Mode-3 operation of IBC

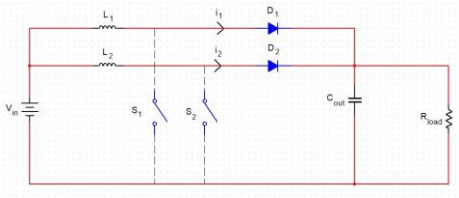

Figure 3.5. Mode-4 operation of IBC

3.1. Design of Interleaved DC-DC Boost Converter

The converter is designed to step-up a 12V input voltage to a 48V output voltage. Both inductor values used in IBC are equal. The following parameters are considered for the design of IBC: Inductors of 46.69 µH, Capacitor of 417 µF, Switching frequency of 100kHz, Voltage ripple of 2%, current ripple of 20% and output resistance of 48 Ω.

4. SIMULATION AND RESULTS

The simulation is done for the mathematical model developed for the Traditional DC-DC boost converter and the interleaved DC-DC boost converter and the circuits of the same in both open loop and closed loop configurations. The models and circuits of the simulations are developed on MATLAB/SIMULINK, version R2021a.

4.1. Mathematical Modelling

The Mathematical models of two different topologies of the DC-DC Boost converter are developed. These models are designed based on the design equations mentioned under Section 2 and Section 3 of the paper.

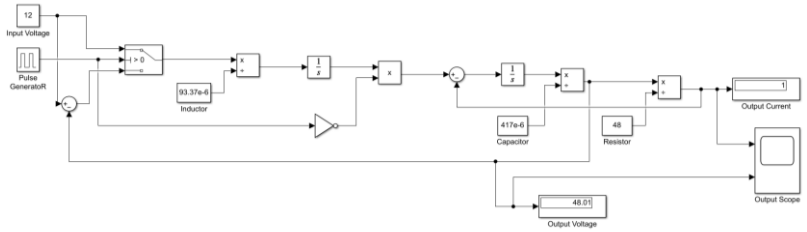

Figure 4.1 Mathematical model of Traditional DC-DC Boost Converter

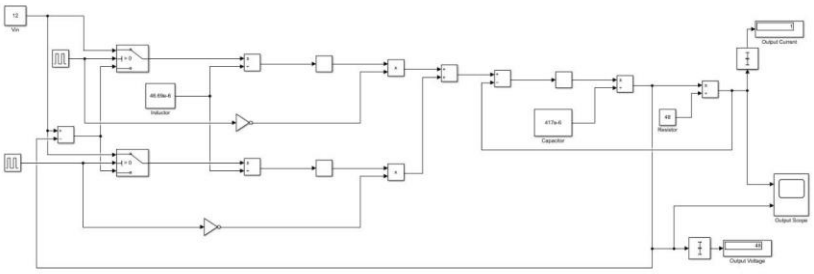

Figure 4.2 Mathematical model of Interleaved DC-DC Boost Converter

On simulation of the mathematical model we find that an output of 48V is obtained for the input of 12V with the following design parameters of the converter: Inductor of 93.37 µH (for Traditional Boost converter), Inductors of 46.69 µH (for IBC), Capacitor of 417 µF, Switching frequency of 100kHz, Duty cycle of 75%, Voltage ripple of 2%, current ripple of 20% and output resistance of 48 Ω.

4.2. Circuit Simulation

The input DC voltages vary from 9V to 12V. The results are shown by stepping up the voltage from 12V to 48V. The switching frequency of all switching elements is set at 100kHz. The main waveforms are shown with the horizontal axis and vertical axis depicting time and voltage/current respectively. The design parameters used in the simulation are the same as used for the mathematical modelling of the two converters as mentioned in section 4.1.

4.2.1. Traditional DC-DC Boost Converter

Figure 4.3 shows the simulated circuit for Traditional DC - DC Boost Converter without PI controller and Figure 4.4 depicts the obtained main waveforms for the output current is 1A, the output voltage is 48V and the input voltage is 12V.

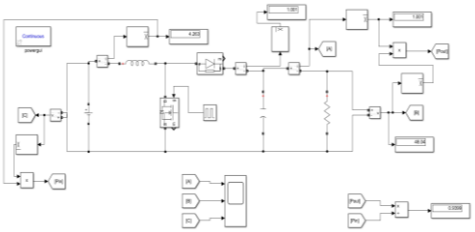

Figure 4.3 MATLAB/SIMULINK model of Traditional DC - DC Boost Converter

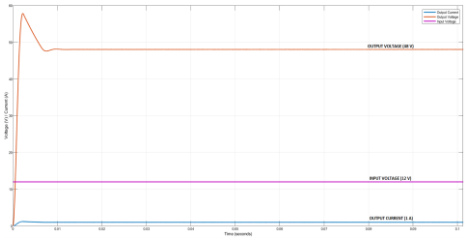

Figure 4.4 Simulation waveforms of output current (Blue), output voltage (Orange) and input voltage (Purple)

Figure 4.5 shows the simulated circuit for Traditional DC - DC boost converter with PI controller having values of P and I as 6 and 500 respectively and Figure 4.6 shows the obtained main waveforms for the output current is 1A , the output voltage is 48V, and the input voltage is varied in steps from 9V to 12V.

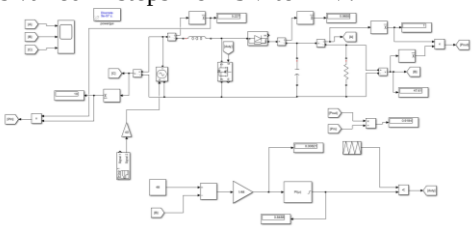

Figure 4.5 MATLAB/SIMULINK model of Traditional DC - DC Boost Converter (closed loop control)

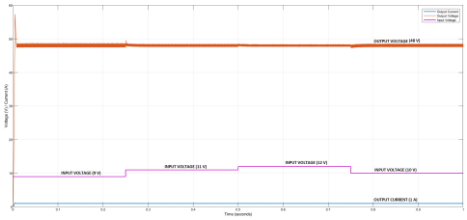

Figure 4.6 Simulation waveforms of output current (Blue), output voltage (Orange) and input voltage (Purple)

4.2.2. Interleaved DC-DC Boost Converter

Figure 4.7 shows the simulated circuit for Interleaved DC - DC Boost Converter without PI controller and Figure 4.8 shows the obtained main waveforms for the output current is 1A, the output voltage is 48V and the input voltage is 12V.

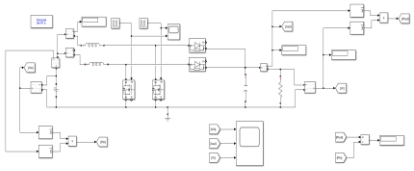

Figure 4.7 MATLAB/SIMULINK model of IBC

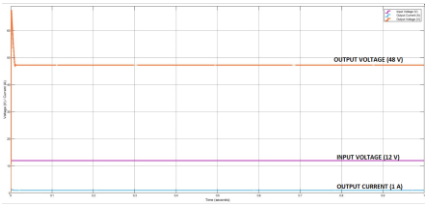

Figure 4.8 Simulation waveforms of output current (Blue), output voltage (Orange) and input voltage (Purple)

Figure 4.9 shows the simulated circuit for Interleaved DC - DC Boost Converter with PI controller having values of P and I as 6 and 1000 respectively and Figure 4.10 shows the obtained main waveforms for the output current is 1A , the output voltage is 48V, and the input voltage is varied in steps from 9V to 12V.

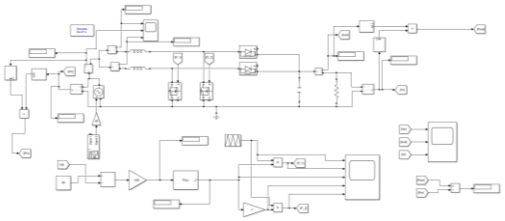

Figure 4.9 MATLAB/SIMULINK model of IBC (closed loop control)

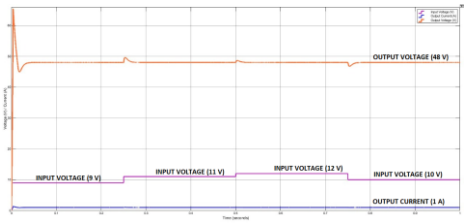

Figure 4.10 Simulation waveforms of output current (Blue), output voltage (Orange) and input voltage (Purple)

4.2.3. Current Ripple and Voltage Ripple

From Figure 4.11 and Figure 4.12 the values obtained for current ripple and voltage ripple of traditional DC - DC boost converter (closed loop control) is 20mA and 1.2V respectively.

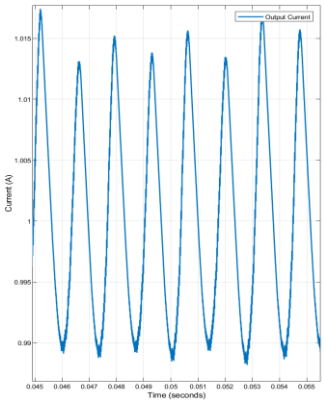

Figure 4.11 Current ripple in Traditional Boost Converter (closed loop control)

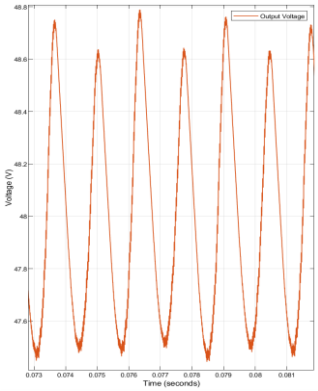

Figure 4.12 Voltage ripple in Traditional Boost Converter (closed loop control

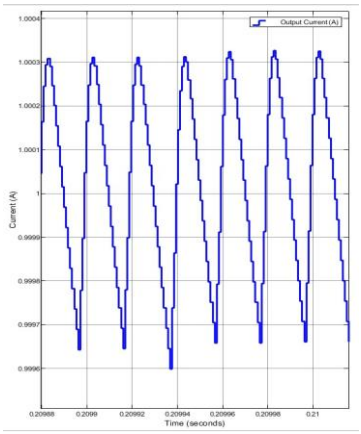

Figure 4.13 Current ripple in IBC (closed loop control)

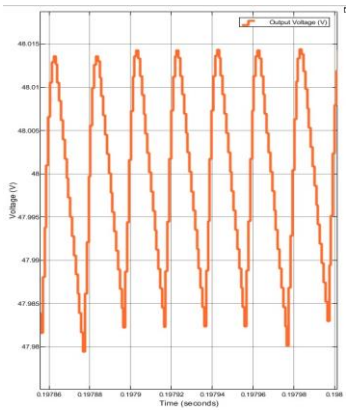

Figure 4.14 Voltage ripple in IBC (closed loop control**)**

From Figure 4.13 and Figure 4.14 the values obtained for current ripple and voltage ripple of Interleaved DC - DC Boost Converter (closed loop control) is 1mA and 30mV respectively.

For the given specification of stepping up the input voltage of 12V to an output voltage of 48V, it is observed that Interleaved DC - DC Boost Converter has better efficiency and lower current and voltage ripple content compared to Traditional DC - DC Boost Converter.

Table 1 shows the comparison of the simulation results of Traditional DC-DC Boost Converter and Interleaved DC-DC Boost Converter.

Table 1: Comparison of Traditional Boost Converter and Interleaved Boost Converter

Parameters	Traditional DC-DC Boost Converter	Interleaved DC-DC Boost Converter
Duty cycle	0.761	0.7575
Percentage Efficiency (open loop)	93.99%	94.43%
Percentage Efficiency (closed loop)	91.84%	93.42%
Output Current Ripple	20 mA	1 mA
Output Voltage Ripple	1.2 V	30 mV

5. CONCLUSION

Comparative analysis between the Traditional DC - DC Boost Converter and the interleaved DC - DC boost converter is performed only for continuous conduction mode (CCM). Both the converters were designed along with their mathematical models and simulated on MATLAB/SIMULINK to step up input voltage of 12V to an output voltage of 48V. Through the simulation results, IBC has reduced current and voltage ripple as a result IBC has better efficiency compared to the Traditional DC - DC Boost Converter. The input currents to inductor 1 and 2 are phase shifted by about 50%, the ripples produced by one inductor nullifies/reduces the ripples produced by the other. The same is the reason for the reduction of voltage ripples at the output of the IBC. Therefore, IBC is a more reliable topology than Traditional DC - DC Boost Converter. Finally, the results of the simulation points to IBC being implemented as a hardware model in the future.

6. REFERENCES

[1] Faraj, Karrar S. & Farhood, Jasim, “Analysis and Comparison of DC-DC Boost Converter and Interleaved DC-DC Boost Converter, International Journal of Engineering and Technology", pp. 622-635, 2020.

[2] Yong-Nong Chang, Hung-Liang Cheng, Hau-Chen Yen, Chien-Hsuan Chang, Wei-Di Huang, “An Interleaved DC/DC Converter with Soft-switching Characteristic and high Step-up Ratio, Applied Sciences”, 2020

[3] Divya M, Guruswamy K, “Design, Modelling and Implementation of Interleaved Boost DC-DC Converter”, International Journal of Innovative Science and Research Technology, Volume 3, Issue 2, pp. 709-721, February 2018.

[4] Shamsun Nahar, M. Bashir Uddin, “Analysis the performance of Interleaved boost converter, 4th International conference on Electrical Engineering and Information & Communication Technology”, 2018

[5] K. Latha Shenoy, C.Gurudas Nayak, Rajashekar P Mandi, “Design and Implementation of Interleaved Boost Converter”, International Journal of Engineering and Technology (IJET), Vol. 9, pp. 496-502, 2017.

[6] Anupa Ann Alex, Muhsina P Hameed, K V Mohamed Shabeeb, Nayana J, “Comparison Of DC-DC Boost Converters Using SIMULINK, IOSR Journal of Electrical and Electronics Engineering (IOSR-JEEE)”, 2017

[7] Boualem Salhi, Hassan El Fadil, Tarek Ahmed-Ali, Eric Magarotto, Fouad Giri. Adaptive Output Feedback Control of Interleaved Parallel Boost Converters Associated with Fuel Cell. *Electric Power Components and Systems*, Taylor & Francis, 2015, Renewable Energy Devices and Systems – Research Frede Blaabjerg, 43 (8-10), pp.1141-1158.

[8] Rashmi B Kananthoor and Bharathi A Rao, "INTERLEAVED BOOST CONVERTER," International Journal of Electrical and Electronic Engineering & Telecommunications, Vol. 1, No. 1, pp. 305-310, March 2015.

[9] Alireza Khosroshahi, Mehdi Abapour, Mehran Sabahi, "Reliability Evaluation of Conventional and Interleaved DC-DC Boost Converters, IEEE Transactions on Power Electronics", 2014

Biographies

Abhay P Badnur is currently pursuing his B.E. degree in Electrical and Electronics Engineering from B.M.S. College of Engineering, Bengaluru.

Laksh C is currently pursuing his B.E. degree in Electrical and Electronics Engineering from B.M.S. College of Engineering, Bengaluru.

Shrayan Karkun is currently pursuing his B.E. degree in Electrical and Electronics Engineering from B.M.S. College of Engineering, Bengaluru.

Nishanth Madhava Navada is currently pursuing his B.E. degree in Electrical and Electronics Engineering from B.M.S. College of Engineering, Bengaluru.

Prof. Divya S is working as an Assistant Professor in the Department of Electrical and Electronics Engineering, B.M.S College of Engineering, Bengaluru. Her areas of interest include Renewable Energy, DC Micro-grids, and Electric Vehicles.

Design and Implementation of Triple Output Flyback Converter with Current Mode Control for Space Applications

Shamanth Y[1], Usha A[1], Pradeep S[2], Nagaraju T K[2], B K Singh[2], Vinod Chippalkatti[2]

[1]*Department of EEE, BMSCE, Bengaluru, India*

[2]*Centum Electronics Ltd. Bengaluru, India*

Email: Shamanth.epe20@bmsce.ac.in

Abstract

This paper focuses on the design and implementation of triple output Flyback converter having built-in protection circuits to improve the reliability of the converter. The proposed converter is designed and realized with primary side current mode control technique using UC1846 PWM IC for faster response. The converter operates at a switching frequency of 200 kHz. Further, at the secondary side, Low Dropout Regulators (LDO) are employed for post regulation to achieve better, line, load and cross regulations. The experimental results of the converter producing triple outputs of 3.8 V/1 A, 5.6 V/0.5 A and 7.3 V/1 A from an input voltage that ranges from 26 V to 45 V and having an efficiency greater than 65% at full load are successfully obtained and hardware circuit implemented in this work.

Keywords. Flyback converter, post regulators, line and load regulations, current mode control.

1. INTRODUCTION

Switched Mode Power supplies have gained more popularity than the linear regulators because of its advantages like compact size, efficiency, reliability and ability to buck and boost the input voltage. Among the SMPS topologies, flyback topology is more commonly used for low to medium power application where isolation between input and output is required. Unlike Forward converters, Flyback converters does not require output filter for low current applications, which reduces the complexity, component count and space, which in turn greatly reduces the cost [1]. Hence flyback topology is selected here for multiple output requirement.

PWM technique is necessary to cope with the change in input voltage and output load. Hence to maintain a constant regulated output voltage, the duty of the main MOSFET is varied with constant switching frequency [2]. In this paper, UC1846 current mode controlled PWM IC is used [3]. Current mode control technique has advantages like faster transient response, simple compensation design and pulse to pulse current limiting ability. Multiple output converters with this control technique have poor load and cross regulation [4]. Hence to achieve tight line, load and cross regulation, Low Dropout Regulators (LDO) are used for post regulation at each output.

A wide range of operating temperature is necessary for any DC-DC converter to be able to use for space application for higher reliability purpose. Hence the proposed converter is

realised with components capable of operation at -55°C to 125°C range to achieve the requirement of -40 °C to +75 °C.

2. OPERATION AND DESIGN PROCEDURE

2.1. Converter Specification

- Input voltage range : 26 V to 45 V
- Switching Frequency : 200 kHz
- Output Parameters : +3.8 V/1 A, +5.6 V/0.5 A, +7.3 V/1 A
- Load regulation : ±1% (10% -100%load)
- Line regulation : ±1%
- Cross regulation : ±2%
- Ripple : <20mVpk-pk
- Operating Temperature : -40 °C to +75 °C
- Efficiency (100% load) : ≥65%

2.2. Converter Operation

The block diagram for the proposed 14W converter is illustrated in Figure 2.1 along with PWM controller, LDO regulators and protection circuits. The proposed converter operation is similar to that of a typical flyback converter. The flyback transformer acts as a choke i.e., when the MOSFET switch is ON, energy is stored in the primary winding of the power transformer and load is fed by the output capacitor. When the switch is OFF, the stored energy in the transformer is transferred to the secondary side and output capacitor replenish its charges and feeds the load.

The input voltage is applied through EMI filter which eliminates the common mode and differential mode noise. The start-up circuit provides the voltage to turn on the UC1846 PWM IC at the beginning and once the converter is completely turned on, bias voltage which is greater than start-up voltage will take over the start-up circuit. Here current sense resistor is used to measure the primary side current which is fed to UC1846 IC and is compared with the feedback error signal from the bias voltage feedback to generate PWM signals to drive the main MOSFET switch.

The switching frequency of the converter is accordingly adjusted by tuning the R_T and C_T of the PWM IC. The outputs at the secondary side are rectified and also filtered using Schottky diode and output capacitors respectively to generate the required RAW voltages. These RAW voltages are fed to respective post regulators, LDO's in order to obtain the regulated output of 3.8 V/1 A, 5.6 V/0.5 A and 7.3 V/1 A at the output stage. All protection circuits are of latch type and in case of any failure or abnormal conditions, shutdown pin of the PWM IC is latched to turn off the converter. Further, converter will not turn on unless the input is recycled.

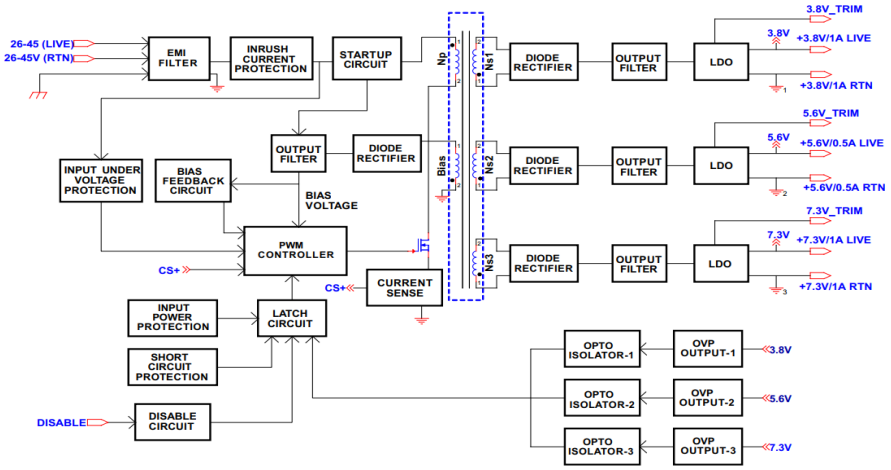

Figure 2.1. Block diagram of the proposed converter

3. DESIGN AND COMPONENT SELECTION

The design of the converter includes transformer design and core selection, controller design, MOSFET selection, output diode selection and also LDO regulator selection [5, 6].

Abbreviations:

$V_{in(min)}$	: Minimum input voltage	f_s	: Switching frequency
$V_{in(max)}$	: Maximum input voltage	E_{ff}	: Estimated efficiency
$V_{out(n)}$	: Output voltage for the nth output	K_w	: Window factor
V_D	: Diode voltage drop	J	: Current density
P_{in}	: Input Power	B_m	: Maximum flux density
P_{out}	: Output Power	A_p	: Area product of the core
D_{max}	: Maximum Duty	A_c	: Cross sectional area of the core
$I_{out(n)}$	: Output current for the nth output	A_W	: Window area of the core
$V_{ds(max)}$	: Maximum voltage stress of the MOSFET	N_p	: Number of turns for primary side
$T_{ratio(n)}$	: Transformer turns ratio for the nth output	$N_{s(n)}$	: Number of turns for the nth output
I_{pp}	: Input peak primary current	I_{srms}	: Secondary RMS current

I_{prms} : Primary RMS current

I_{dsp} : Maximum peak current of MOSFET

V_{RO} : Output voltage reflected to the primary

L_p : Transformer primary side inductance

3.1. Transformer design

The power transformer of the converter is designed using Area product (Ap) method [7].

Peak primary winding current is calculated by, $I_{PP} = \frac{2P_{out}}{D_{\max} V_{in(\min)}}$ (1)

Primary RMS current is calculated by, $I_{prms} = I_{pp}\sqrt{\frac{D_{\max}}{3}}$ (2)

Secondary RMS current is calculated by, $I_{srms(n)} = \frac{2}{\sqrt{3}}\left(\frac{I_{out(n)}}{\sqrt{1-D_{\max}}}\right)$ (3)

The primary inductance is calculated by, $L_p = \frac{(V_{in(\min)} D_{\max})^2}{2 * P_{in} f_s k_{rf}}$ (4)

Where, k_{rf} = Ripple factor = 0.3 (k_{rf} =1 for DCM operation and k_{rf} = 0.25 to 0.5 for CCM operation)

Area product formula is given by, $A_p = \frac{P_{out}\left(\frac{1}{E_{ff}}\sqrt{\frac{4D_{\max}\alpha}{3}} + \sqrt{\frac{4(1-D_{\max})\alpha}{3}}\right)}{K_w J B_m f_s}$ in mm^4 (5)

Where, Bm=0.18 $Tesla$, J= 4 A/mm^2, Kw=0.3, and α= 0.75

A core with area product greater than the calculated value is selected. Selected Toroidal core is: **CO55121-A2** with A_L value of 35nH /1000T.

Core area,A_C=19.2mm^2 and window area, A_W = 71.3mm^2

Area product for the selected core, $A_p = A_C A_W$ = 1369mm^4 (6)

Number of primary turns is given by, $N_p = \frac{L_p I_{PP}}{B_m A_c 10^{-6}}$ (7)

Turns ratio of each output is calculated by, $T_{ratio(n)} = \frac{(V_{out(n)} + V_D)(1-D_{\max})}{V_{in(\min)} D_{\max}}$ (8)

Number of secondary turns is calculated by, $N_{s(n)} = T_{ratio(n)} N_p$ (9)

3.2. MOSFET selection

The main MOSFET should be able to withstand the stress due to voltage spike by leakage inductance of the transformer, reflected voltage from the secondary and the maximum input voltage.

The reflected voltage on the MOSFET, $V_{RO} = \frac{D_{\max}}{(1-D_{\max})} V_{in(\min)}$ (10)

Maximum voltage stress on the MOSFET is calculated by the equation,

$$V_{ds(max)} = V_{in(\max)} + V_{RO} \quad (11)$$

The selected MOSFET is **BUY25CS12J** N-channel, V_{DS}= 250V, I_D= 12.4A, $R_{DS\ on}$= 0.13Ω

3.3. Output Diode selection

The voltage drop across the diode directly affects the efficiency of the converter. Schottky diodes are preferred as output diodes.

Reflected current is calculated by, $I_{s_{refelected(n)}} = \frac{(1-D_{\max})}{D_{\max}} * \frac{I_{dsp}}{\left(\frac{N_{s(n)}}{N_p}\right)}$ (12)

Reflected voltage is calculated by,

$$V_{s_{refelected(n)}} = \left(V_{out(n)} + V_D\right) + \left(\frac{N_{s(n)}}{N_p} V_{in(\max)}\right) \quad (13)$$

3.4. Current mode control

In conventional secondary side current mode control, the output voltage and current are measured and fed to respective error amplifiers. Output from the error amplifier is then applied to the PWM controller through an opto-coupler to generate PWM signal. This method has its drawbacks like complexity, increase in components count and space in PCB. Hence in this work, primary side current mode control is implemented where bias voltage from a separate bias winding provided in the converter which is used to power the PWM IC and other sub circuits, is also used as feedback to PWM controller [8, 9]. The primary current is measured indirectly by measuring the voltage drop across the current sense resistor which is in series with the source terminal of the main MOSFET switch.

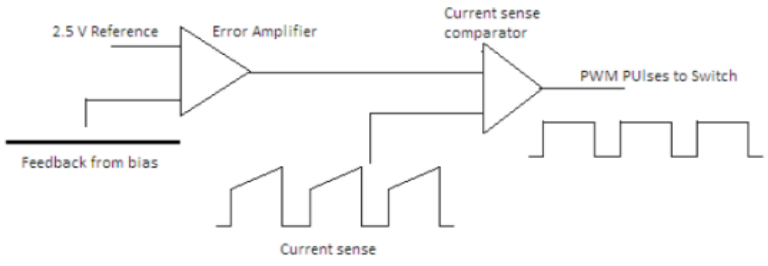

Figure 3.1. Current mode control scheme implemented in the converter

The sensed primary current produces ramp signal to the PWM controller which is then compared with the error amplifier output as demonstrated in Figure 3.1 to generate PWM signal for the required duty cycle to maintain constant output voltage. The UC1846 IC has

all the specific features having additional under voltage protection, current limiting and shutdown circuits.

3.5. LDO regulator

The Low Dropout Regulator comprises of an error amplifier and a series pass transistor (BJT/MOSFET). The main advantage of an LDO over a linear regulator is the varying dropout voltage. Drop out voltage is the minimum voltage difference between input and output to maintain regulation. Depending upon the change in input voltage and load, the error amplifier output varies the gate terminal of the series pass element. When the input voltage approaches the output voltage, error amplifier decreases/ increases the gate to source voltage V_{GS} for PMOS/NMOS series pass elements respectively, in order to reduce $R_{DS\ ON}$ to maintain regulation [10]. In this work, UC1834 IC is employed as post regulators along with external series pass device [11].

4. PROTECTION CIRCUITS

4.1. Under Voltage Protection (UVP)

The schematic for under voltage protection is presented in Figure 4.1. Resistor divider is used to set the UVP threshold voltage and is compared with the reference value. The threshold would always be higher than the reference value for 26V-45V input range. Once the input reduces below 22V, threshold is less than the reference and comparator output become high to latch the shutdown pin of PWM IC. The converter is turned on if input voltage is regained to 24V.

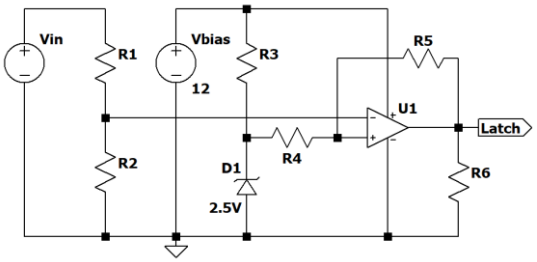

Figure 4.1 UVP circuit

4.2. Over Voltage Protection (OVP)

The schematic for output over voltage protection of one of the output terminals is presented in Figure 4.2. The comparator U1 continuously monitors the output voltage, when any of the three outputs increases beyond 125% of the nominal value, the output of U1 becomes high and through the opto-isolator drives the latch circuit to shut down the converter. Similarly, same OVP circuits are connected at each output terminals.

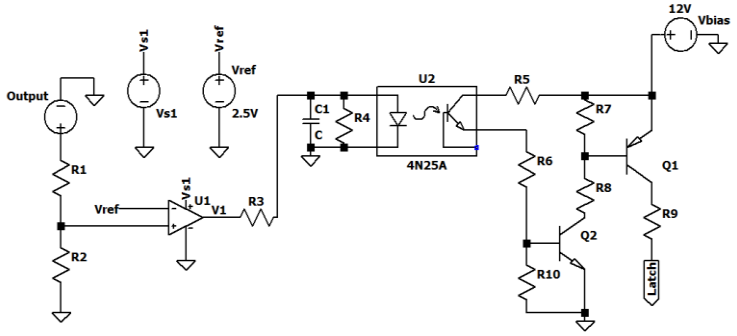

Figure 4.2 OVP circuit

5. HARDWARE IMPLEMENTATION AND RESULTS

The designed converter is effectively tested for an input voltage that ranges from 26V to 45V for different load conditions. Efficiency, line regulation, load regulation, cross regulation and ripple voltages are tabulated and presented in the following tables; TABLE I – V.

TABLE I. EFFICIENCY AT FULL LOAD

Input Voltage (V)	Input Current (A)	Output 1 (+3.8 V)	Output 2 (+5.6 V)	Output 3 (+7.3 V)	Efficiency (%)
26	0.7962	3.817	5.59	7.279	67.1
37	0.5685	3.817	5.59	7.28	66.04
45	0.4745	3.8174	5.591	7.28	65.06

Line regulation is calculated as follows,

$$\%\ Line\ regulation = \left(\frac{V_{out}\ at\ 26V - V_{out}\ at\ 45V}{V_{out}\ at\ 37V}\right) X\ 100 \quad (14)$$

TABLE II. LINE REGULTAION AT DIFFERENT LOADS

Load Condition	Line Regulation%		
	Output 1 (+3.8 V)	Output 2 (+5.6 V)	Output 3 (+7.3 V)
10% Load	0.00	0.00	0.00
50% Load	0.01	0.00	0.01
100% Load	0.01	0.02	0.01

Load regulation is calculated as follows,

$$\%\ Load\ regulation = \left(\frac{V_{out}\ at\ 10\%\ load - V_{out}\ at\ 100\%\ load}{V_{out}\ at\ 100\%\ load}\right) X\ 100 \quad (15)$$

TABLE III. LOAD REGULTAION FROM 10% LOAD TO 100% LOAD

Input Voltage (V)	Load Regulation%		
	Output 1 (+3.8 V)	Output 2 (+5.6 V)	Output 3 (+7.3 V)
26	0.50	0.34	0.48
37	0.49	0.34	0.46
45	0.48	0.32	0.46

Cross regulation is measured by keeping the measuring output at full load and other outputs at 10% load.

$$\%\ Cross\ regulation = \left(\frac{Measured\ output\ at\ 100\%\ load\ with\ remaining\ outputs\ at\ 10\%\ load - Measured\ output\ at\ 100\%\ load\ with\ remaining\ outputs\ at\ 100\%\ load}{Measured\ output\ at\ 100\%\ load\ with\ remaining\ outputs\ at\ 10\%\ load}\right) X\ 100 \quad (16)$$

TABLE IV. CROSS REGULATION AT DIFFERENT VOLTAGE

Input Voltage (V)	Cross Regulation%		
	Output 1 (+3.8 V)	Output 2 (+5.6 V)	Output 3 (+7.3 V)
26	0.02	0.02	0.01
37	0.01	0.02	0.01
45	0.01	0.02	-0.01

TABLE V. RIPPLE VOLTAGE AT FULL LOAD

Input Voltage (V)	Ripple voltage (mV)		
	Output 1 (+3.8 V)	Output 2 (+5.6 V)	Output 3 (+7.3 V)
26	3.20	4.20	5.20
37	3.60	3.60	4.20
45	3.80	4.20	6.00

Hardware setup for the designed converter is illustrated in Figure 5.1. The gate and drain voltages of the MOSFET is presented in Figures 5.2 and ripple voltages at 37V input with full load is presented in Figures 5.3. It is observed from the Figure 5.3 that Output voltage ripple value at different output terminals is within the specifications of the converter at 37V with full load.

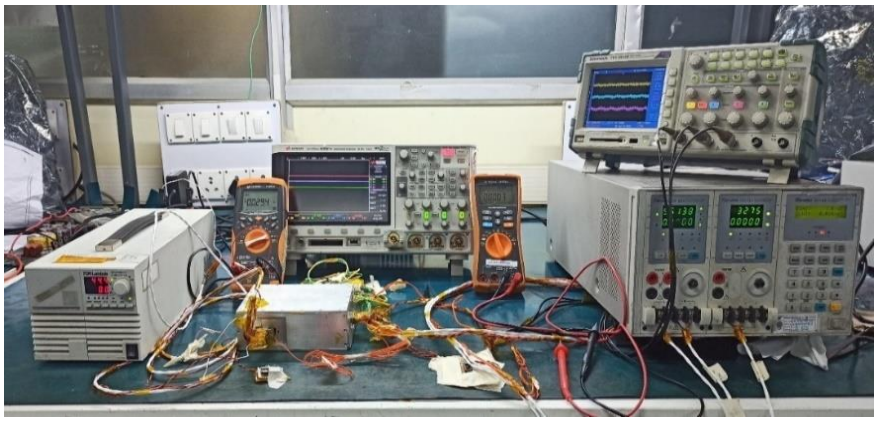

Figure 5.1. Hardware setup for the Converter with electronic load

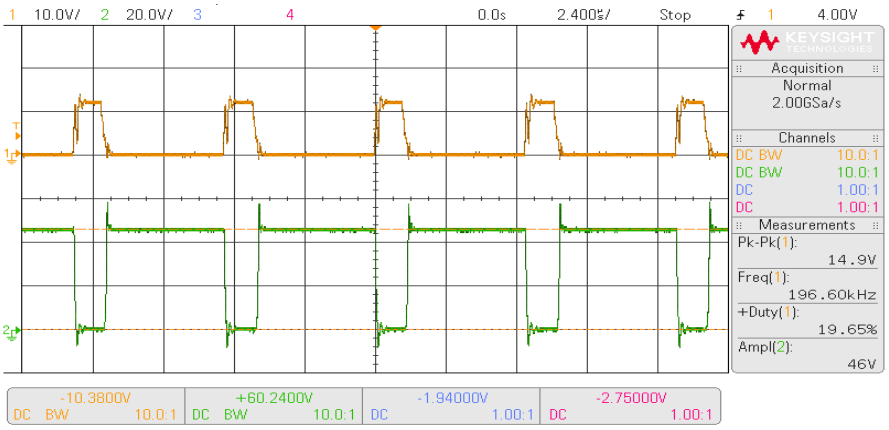

Figure 5.2. V_{GS} and V_{DS} at 37V with full load

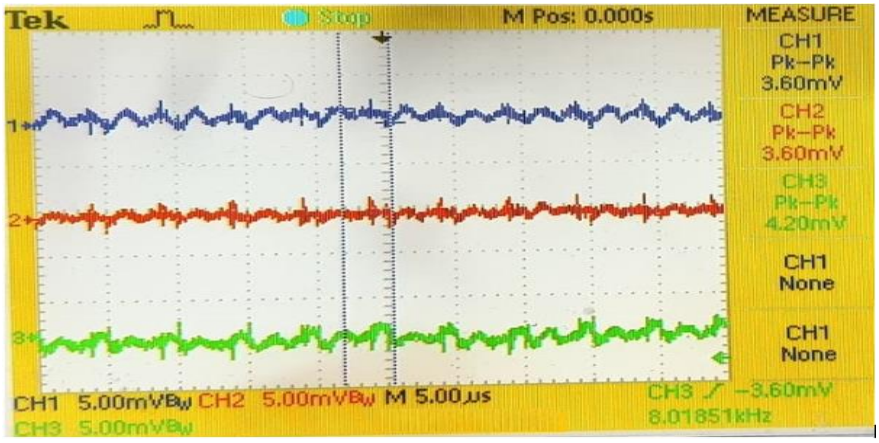

Output 1 Output 2 Output 3

Figure 5.3. Output voltage ripple at 37V with full load

6. CONCLUSION

The triple output Flyback converter having primary side current mode control with post regulators is designed, analysed, implemented and tested for wide input voltage that ranges from 26V to 45V for all the load conditions. The converter is tested for extreme conditions: -40 °C to +75 °C temperature range. Further, designed value of the efficiency for the converter is effectively obtained around 65% at full load. The line, load and cross regulation results are presented and are found within the required specifications.

Acknowledgement

Authors are grateful to the Management, BMS Educational Trust, B.M.S College of Engineering. Authors sincerely thank Centum Electronics Ltd for giving an opportunity to carry out this work at CENTUM, Bengaluru and also for their continuous support in the successful hardware implementation.

7. REFERENCES

[1] A.I. Pressman, “Switching Power Supply Design”, McGraw Hill, 1991.73.

[2] Daniel Hart, “Power Electronics”, McGraw Hill, 2011.

[3] Datasheet Texas Instruments, “UC1846-EP Current Mode PWM controller” SGLS329–MAY 2006

[4] Design Note, DN-62, “Switching Power Supply Topology Voltage Mode vs. Current Mode”, Unitrode Corporation, June 1994

[5] C. G. Satyaraddi, A. Usha, A. Bhat, P. K. Praveen, B. K. Singh and V. Chippalktti, "Design and Implementation of Multiple Output Interleaved Flyback Converter with Post Regulators," 2019 IEEE International Conference on Electrical, Computer and Communication Technologies (ICECCT), 2019, pp. 1-6, doi: 10.1109/ICECCT.2019.8869418.

[6] P. Kumar R., K. E. Rayees, B. K. Singh and V. S. Chippalkatti, "Multiple Pulsed Output DC-DC converter with Current mode control technique And Post Regulators," 2018 International Conference on Control, Power, Communication and Computing Technologies (ICCPCCT), 2018, pp. 34-39, doi: 10.1109/ICCPCCT.2018.8574268.

[7] L Umanand, S R Bhat, “Design of Magnetic components for Switched Mode Power Converters”

[8] T. T. Vu, S. O'Driscoll and J. V. Ringwood, "Primary-side sensing for a flyback converter in both continuous and discontinuous conduction mode," IET Irish Signals and Systems Conference (ISSC 2012), 2012, pp. 1-6, doi: 10.1049/ic.2012.0195.

[9] R. Nalepa, N. Barry and P. Meaney, "Primary side control circuit of a flyback converter," APEC 2001. Sixteenth Annual IEEE Applied Power Electronics Conference and Exposition (Cat. No.01CH37181), 2001, pp. 542-547 vol.1, doi: 10.1109/APEC.2001.911699.

[10] Michael Day, “Understanding Low Drop Out (LDO) Regulators” Texas Instruments Portable Power Design Seminar, 2006

[11] Datasheet Texas Instruments “UC1834 High Efficiency Linear Regulator”

Review of State of Health Monitoring Techniques inBattery Management System

R Sivapriyan, Sushmitha S V, C V Mohan, S Lavanraj
Department of EEE, Sir MVIT, Karnataka, India. sivapriyan@gmail.com PRTI (OPC) Pvt. Ltd, Karnataka, India. sushmithasv390@gmail.com Department of EEE, Sir MVIT, Karnataka, India. eeecvm@gmail.com PRTI (OPC) Pvt. Ltd, Karnataka, India. lavanraj.s@gmai.com

Abstract.

As in recent trends, the Electric Vehicles are tremendously growing and major research works are found in Battery Management System. This paper comprehensively analysis about the State Of Health (SOH) and its methodologies in applications of Battery Management System (BMS). Various algorithms along with the flowchart have been briefly discussed. The comparative analyses along with the various methodologies are included in the table for reference. The SOH monitoring and controlling applications in lithium-ion batteries and fuel cells are considered and discussed as regarding main topics. The model-based methods along with the real time applications with input and output features has briefed in general with a comparison. The algorithms with real time application in Machine Learning and AI techniques has given a highlight and its applications in real time examples are briefed. Thus, this paper briefs about BMS and discharge methods of the battery of the SOH techniques and highlights upon various algorithms which is used as model-based methods in Battery management system as well as SOH techniques.

Keywords. Battery Management System, State of Health, Experimental Method Analysis, Machine Learning, Model Based Methods.

1. INTRODUCTION

Nowadays, Electric vehicles are a trending technology in various applications, and one of its applications is used in Battery Management Systems (BMS). BMS monitors and protects the battery by considering its safe operation area such as Overvoltage/under voltage, Overpressure, over temperature/under temperature [1]. Also, to prevent the current leakage where battery cell is charged by an intelligent battery pack and makes use of rechargeable battery which has to be managed in an electronic or power storage system by considering available data for calculating and monitoring it in the environment and is efficiently used in the EV applications [2]. BMS consists of many cells stacked together within a smart battery pack to release the cell's energy to meet the load demand. Stability plays a significant role in the whole Battery Management System, where users can monitor each cell individually by authenticating and reporting the data [3]. There are many IC's available in BMS. It includes some functional blocks to keep track of all voltage balance,

monitor temperature and the energy recovery in electric vehicle systems, and sometimes the state of the battery can also be monitored by considering the state of the machine for simplicity purposes as shown in Fig.1.1. By considering standard parameters like SOC (State Of Charge) [4][5], SOH (state of health) [6], SOP (state of power), and SOS (state of safety), BMS computation can be determined [7].

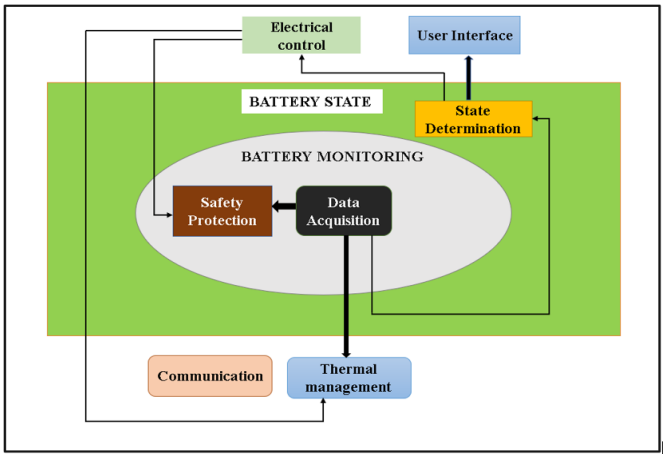

Figure 1.1 Battery Management System[8]

It can track the total number of cycles and energy consumed per kWh for the total operating time [9]. BMS also uses wireless kWh for the total operating time [9]. BMS also uses wireless communications for communicating with the hardware when it comes to internal purposes at the basic level of the cell.

When it comes to the external purpose, the hardware level will be high, making use of PCs, laptops, etc. For internal communication, BMS restricts with bulk number of cells [9]. When it comes to modular architecture with an increasing number of nodes, hardware combination cannot be used as it is limited, and cost plays a major role as cell price comes into existence which is comparable.

The protection of BMS is also important, so we can include a relay that acts as a protective switch by detecting faults when the battery's SOA crosses its limit. The balancing part of the BMS is handled by the balancers where energy is shuffled and also by passive regulators by connecting charged cells of an increasing number to the load side, and the major task is to maintain voltage at the same level for cells where the battery is composed, to prevent overcharging thus the battery's capacity can be maximized. Thus, BMS (Battery management system) plays a major role in electric and hybrid vehicles such as electric cars and lithium-ion batteries [10].

In electric train traction batteries, BMS is used to manage the high power and large battery packs. Some BMS applications are also found in Garbage compressors, Industrial machines, Hoists, Cranes, Robots, Forklifts, etc.

2. STATE OF HEALTH

SOH stands for the State of Health, and it is a battery condition to estimate the charge in smart battery packs by considering some of the Safe Operating Area (SOA) and aging limitations at the same time for monitoring the battery conditions for electric vehicle applications [11] as shown in Figure 2.1.

By considering ideal parameters, when manufacturing SOH's battery condition is 100 percent and due to some aging process, the battery's performance will decrease [12]. It is calculated by considering the ratio of capacitance, impedance to its initial rating.

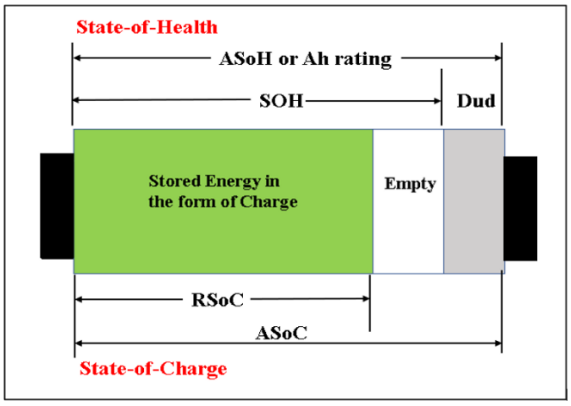

Figure 2.1 State of Health[13]

Nowadays, Lithium-ion batteries are used in SOH's battery for reliability purposes. A detailed analysis has been carried out to check for safety measures in power storage or energy storage requirements.

Currently, the study has been carried out in self-discharge rate, Number of operating cycles, power capability to ensure battery monitoring system by considering internal impedance, resistance, and capacitance aspects.

Some of the health features (HFs) for SOH battery estimation are the physical parameters to characterize the battery capacity, Electrochemical models with some degradation mechanisms.

The factors affecting the behaviour of the battery in SOH's batteries are dealt with by some of the algorithms and Artificial Neural Networks (ANNs) techniques by considering the capacity loss in the cycling behaviour of the power periodically [14]. The response of the voltage will be varied by considering the rate of current at different SOH parameters.

The battery parameters like SOC and SOH are the approaches used in various battery system methods such as Kalman Filter, Enhanced Coulomb Counting, and voltage methods in applications of Electric and Hybrid vehicles, HVDC, and photovoltaic applications systems [15].

3. SOH TECHNIQUES

As the Electric Vehicle Technology is tremendously growing in past few years, the Battery Management System (BMS) acts as a central coordinating system or main control system so as to provide reliability, efficiency, stability and safe use of battery by considering some standard parameters like State of Charge (SOC), State of Health (SOH), State of Power (SOP)[16][17].

SOC is used to collect the energy being consumed by battery and storage specifications of the battery. SOP is used for determining the power required for the battery and the flowchart of SOH Monitoring is shown in Figure 3.1.

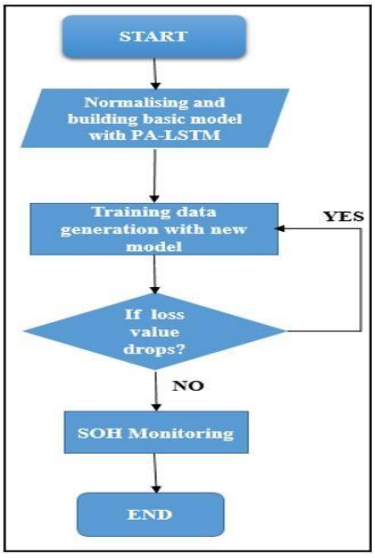

Figure 3.1. Flow Chart of SOH Monitoring[18]

SOH is a battery condition to estimate the charge and to detect degradation level of the battery in real-time automotive applications.

The Battery performance can be analyzed by SOH in HEV and AI applications [19] and discusses about the distribution of energy and how to improve their self-discharge rate, consumption of energy during their lifetime. So, some of the standard methods/techniques are used for SOH's battery estimation by considering internal resistance of the battery, battery's impedance, state of machine, state of discharge [20] and its capacity [21].

The SOH Battery estimation methods can be divided into 3 methods which include Experimental methods, Model-Based methods and Machine Learning methods. From the standard methods, machine learning technology can be implemented and it includes some of the techniques such as Support Vector Regression, Neural Network, Fuzzy logic and other standard algorithms.

In Experimental methods, some techniques include Impedance measurement, ICA/DVA, Internal resistance measurement, Capacity level etc. and these methods are usually conducted in laboratories.

Some Model Based methods include Adaptive filtering such as Kalman Filters, EKF, UKF, RLS, MAFFRLS, Electrochemical models and Enhanced Coulomb counting methods etc. SOH's battery uses PA-LSTM algorithm for monitoring accuracy of battery and also by updating the learning mechanism where data obtained from the experimental results are close to real time data model dynamically and can further be used in approach of Lithium-ion batteries.

4. VARIOUS METHODS OF SOH TECHNIQUES

In SOH Battery estimation, there are 3 types of methods namely Experimental technique, Machine learning methods and Model Based methods as shown in Figure 4.1.

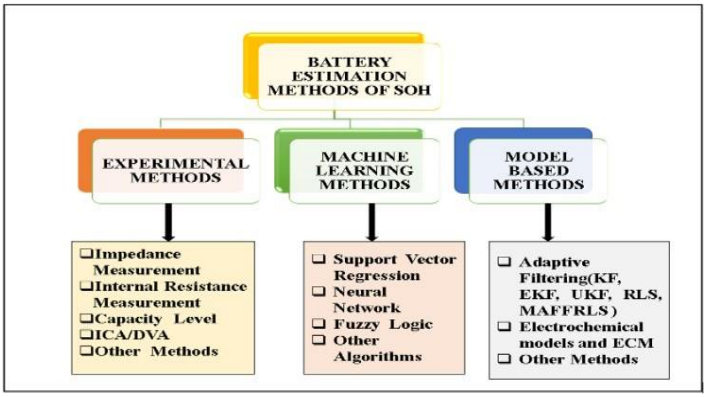

Figure 4.1 Battery SOH Estimation Methods[22]

5. EXPERIMENTAL METHOD ANALYSIS OF BATTERY SOH ESTIMATION

Usually, these Experimental methods are often time consuming and preferable equipment's have to be used in specific to meet the criteria or requirements, so these methods are usually performed in laboratories. The aging behaviour of the battery can be determined using these methods by collecting raw data measurements and understanding the behaviour of these collected data. Some of the techniques used in Experimental methods are discussed below:

• Impedance Measurement of the Battery:

The major technique which is used frequently to measure the impedance of the battery is Electrochemical Impedance Spectroscopy (EIS) which dealt with energy storage and conversion and it acts as a SOH indicator of battery. This technique is conducted as a function of frequency as a sinusoidal AC current is applied and output voltage response is calculated. Meanwhile, it is a non-destructive method and it is found that impedance of the battery is directly proportional to the aging phenomena.

The EIS method discusses about the super capacitor, cycling effect and energy storage in real-time applications of EV and major advantage is the accuracy which can be calculated efficiently in the aging phenomenon of the battery [23].

• Internal Resistance Measurement of the Battery:

In this technique, by applying AC sinusoidal current the voltage drops and current pulse is the most frequently used method to deter- mine the Internal Resistance which is based on the principle of Ohm's Law and acts as a SOH indicator.

By considering the parameters like aging and degradation whose impact decreases the resistance values with SOH battery conditions. With the help of Joule's law, loss of energy in Battery is evaluated by considering the impacting parameters. The main advantage of this method is the accuracy in domains of evaluating battery's internal resistance in different environmental working conditions and widely used in laboratories but is often a time-consuming process.

• Capacity Level:

In this technique, battery charging capacity is evaluated and energy stored in a battery is evaluated by a capacitor and it is inversely proportional to the aging phenomenon of the battery [24]. Here, time is the major factor to decide number of charging/discharging cycles based on the output voltage under different working conditions of the temperature for different levels of degradation by experimentally evaluating the capacity fading level in Lithium-ion battery applications [25].

• ICA/DVA and Other Methods:

ICA and DVA stands for Incremental Capacity Analysis and Differential Voltage Analysis respectively. These methods have to be done experimentally by testing battery SOH which is time consuming and these parameters vary with aging of the battery. By using some of the destructive methods such as X-ray Diffraction, state of the battery and machine can be determined from inside and estimation can be changed feasibly with modification of specific working conditions [26].

6. MACHINE LEARNING METHOD ANALYSIS

This method is basically a combination of both standard methods which include Experimental and Model Based methods. To estimate battery SOH some data has to be gathered using machine learning algorithms in process of learning to setup the standard algorithms [27].

• Support Vector Regression (SVR):

In this technique, training data is to be evaluated which requires a controller of high performance to manage the energy and taking into consideration real time data and experimentally to determine the online SOH indicator using Electrochemical Impedance Spectroscopy (EIS) technique. This SVR algorithm is also used to estimate RUL (Remaining Useful Life) of the battery and its applications in Fuel cells, e-Bikes, Hybrid Electric vehicles etc.

• Fuzzy Logic:

This technique is used for nonlinear systems and is the most commonly used machine learning method along with EIS technique to evaluate the training data to be accurate

which often uses Gaussian Algorithm process [28] to estimate the battery SOH in Lithium-ion batteries along with WLTC profiles [29].

• Neural Networks:

It is the most frequently used machine learning algorithm and it takes less data for computational analysis combining with EIS measurements and results are found to be more accurate with ample amount of data received than the Fuzzy Logic.

The main disadvantage of this method is difficulties faced in complex as well as nonlinear systems and also it requires a controller of high performance.

• Other Methods:

Some algorithms such as Gaussian algorithm makes use of training data to track accuracy of SOH battery in Lead Acid Batteries as well as Lithium-ion batteries.

Back Propagation Neural Network (BPNN) is the algorithm to trace the battery parameters like Internal Impedance, Resistance and to track the energy level and tolerance was found to be less.

Particle-filter based algorithm is used extensively for different vehicle applications and its accuracy on estimation of battery SOH and requirement of training data is found to be less for computational purpose in machine learning process.

RLS (Recursive Least Square) algorithm and LSTM-NN (Long Short-Term Memory Neural Network) are also used which are trending research topics and has to be tested experimentally for better accuracy of the SOH battery indicator.

7. MODEL BASED SOH BATTERY ESTIMATION ANALYSIS

In the research for evaluating the Battery SOH and real time feasibility, model-based methods have come into existence with filtering and standard indicators to determine battery capacity, impedance, energy level [30] etc. Some of the techniques are:

• Kalman Filters:

In order to evaluate the SOH battery parameters, an adaptive filtering algorithm is used in real time to consider the ECM (Equivalent Circuit Models). The advantage of these filters are some nonlinear systems as well as complex system battery state and parameters can be evaluated using Kalman Filters (KF), Extended Kalman Filters (EKF), Unscented Kalman Filter (UKF), Dual Kalman Filters etc.

• Electrochemical methods:

Differential equations of nonlinear systems as well as complex systems can be evaluated accurately and these models are found to be complex in tracing the battery's parameters and behaviour. It uses recursive parameter [31] for identification purpose and to predict online SOH indicator and capacity effects in SOC battery. For accurate results the battery behaviour can be predicted using ECM techniques where they have less complexity equations.

The main drawback of this method is the difficulty level of the equations and complexity of the algorithm to trace behaviour of SOH battery parameters like internal resistance and diffusion time of the battery.

• Other Methods:

Observers are also used in Model Based SOH estimation methods due to its robustness against error margin and diffusion time parameter for variations in temperature [32]. Least Square Based Filters is widely used one of the algorithms for testing the battery states in the OCV (Open Circuit Voltage) along with RLS algorithm for testing the high performance of a battery model.

MAFFRLS (Multi Adaptive Forgetting Factors RLS) is also used along with PSO (Particle Swam Optimization) algorithms for better efficiency and accurate results in temperature and time variations of dataset in Battery models.

8. COMPARATIVE ANALYSIS

In Support Vector Regression (SVR) method, the quality and quantity are entirely based upon the data used in the training and uses a controller when there is a need of high performance to control the training data. Compared to the other methods, the results obtained in the SVR is of accurate and applicable for any systems. The main advantage of SVR is as the system results obtained are of accurate and hence the system is stable and efficient. It can also be used to solve the regression problems. The main disadvantage of using SVR algorithm is that it is difficult for humans to understand the code and it takes long training time. In Feed Forward Neural Network (FNN) Algorithm, mathematical relationships are used for the algorithm with some input features to dynamics of battery such that SOH Estimation can be done in an accurate manner and rule used in FNN is of back propagation learning. The equations used in FNN are of mapping function where some function can be almost approximated to other functions. The main advantages of using FNN are the computation required to analyze the mathematical relations is less, so this type of algorithm is beneficial.

As large equations are being used, overfitting problem exists as to store the data of large number of parameters. In Recurrent Neural Network (RNN) Algorithm, the main input to be considered are current, temperature, voltage and output used to determine the application of SOH in functions of temperature in BMS applications [33]. The main advantage of using RNN Algorithm is information can also be easily stored in functions of time which is easy task and memory requirement is less. The pixel quality is effective and time series can be easily predicted. The disadvantage of this RNN algorithm is to train the RNN task and sometimes long sequences such as tanh function cannot be processed easily and gradient problems usually occur for this type of algorithm. In case of Particle Swarm Optimization (PSO) Algorithm the principle is based on the latest technology and its applications are still being in research for Electric Vehicles and Plug-in hybrid Electric vehicles. It makes use of Swarm Intelligence where parameters control can be done using simple concept and efficiency of computation compared to other algorithms is found to be extremely good and effective. This PSO algorithm can be easily implemented for different and various systems so that the over fitting problem can be overcome by this algorithm.

The main disadvantage of this algorithm is that it provides solution of some techniques which is of low quality and each time when the program is updated, memory updating has to be done which is time consuming and tedious process or task.

Table 1 COMPARISON OF EXPERIMENTAL BASED METHODS.

Methods	**Advantages**	**Disadvantages**
Internal Resistance measurements [34]	• Simple to implement and direct method to under-stand. • Less complexity and high level of accuracy.	• Estimation through online cannot be made. • Time consuming and tedious task.
Internal Impedance Measurements	• High accuracy and simplicity. • Reliable and degradation of the battery methods can be easily understood.	• Battery degradation and discharges is difficult to analyze.
ICA/DVA and Capacity Level [35]	• This technique is much faster than other methods. • It is fast to analyze and provides high level of accuracy.	• Sometimes this method is not reliable and feasible. • Operating conditions of the battery is difficult to analyze when fully charged.

Table 2 COMPARISON OF MODEL BASED METHODS.

Methods	**Advantages**	**Disadvantages**
Kalman FilterBased (KF) methods	• Simple to understand and accurate to interpret theoutput • It is bounded to errors	• For advanced systems and versions system is complex. • A controller of high performance is required and not valid for nonlinear systems [39].
Electrochemical models	• High accuracy and reliable • The battery degradation phenomenon can be understood and predicted easily.	• The computational level of high-performance con- troller is required [40]. • Structure of the battery is difficult to analyze.
Least Square Based methods	• This Technique is much precise and robust than other techniques. • The structure is easy to analyze.	• The model is mostly concentrated on accuracy and high-level performance controller is required [41].

Table 3 COMPARISON OF MACHINE LEARNING BASED METHODS [36].

Parameters	**Support Vector Regression Algorithm**	**Feed Forward Neural Network Algorithm**	**Recurrent neural network (RNN) Algorithm**	**Particle Swarm Optimization (PSO) Algorithm [37]**
INPUT	I(t), V(t), T(t)	I(t), V(t), T(t)	I(t), T(t), SOC(t), R/C(t)	I(t), V(t), T(t)
OUTPUT	SOH(t)	SOH(t)	SOH(t)	SOH(t)
FUNCTION	Regression and Classification Hyperplane Equation	Supervised Learning, Sigmoid function, Mapping of function to approximate value	Non-Linear, Auto-Regressive Network, Time Series Based Function	Swarm Intelligence, Randomized, Population Based Optimization Method
EQUATION	y=wx+b(Hyperplane) Condition: $-a > y-wx+b < a$	f(x)=yf(x) for all (x,y)	Current state equation: $h_t=f(h_{t-1}, x_t)$ Output equation: $y_t=W_{hy}h_t$ Activation Function: $h_t=\tanh(W_{hh}h_{t-1}+W_{xh}x_t)$	$x_i^{k+1}= x_i^{k}+ v_i^{k+1}$
ADVANTAGES	• Overfitting can be prevented as it has good regularization capabilities. • Using Kernel function, it handles non-linear data efficiently • Stable and Efficient. • Can be used to solve both classification and regression.	• Easy to setup. • Less computation. • Complex and Non- linear systems can be analyzed.	• Easy information is stored accordingly with time. • It is good for effective pixel extension. • Helps in prediction of time series.	• Simple concept. • Easy implementation. • Robustness to control parameters • High computational Efficiency.

LIMITATIONS	• The difficult task is to choose an appropriate Kernel function. • For large datasets, it takes long training time [38]. • It is difficult to understand the algorithm or models of SVR for humans.	• There exists Vanishing and Exploding Gradient problem. • Large model size. • There exists Overfitting of large number of parameters.	• Gradient Vanishing and problems are exploding. • It is difficult to train an RNN task. • As tanh function is used for activation function, it cannot process long sequences.	• Low convergence rate in iterative process. • Memory updating required and falls under local search. • Low quality solution.

Table 4 COMPARISON OF SOH ESTIMATION METHODS.

Methods	Advantages	Disadvantages
Experimental Based methods	• Simple to understand and accuracy is more. • Computational level is low	• Time consuming. • The measurements and the equipment to be used should be specific [42].
Machine Learning methods	• High accuracy and reliable compared to other two methods. • Easy to implement and process can be carried out easily.	• The computational level is difficult to understand and depends more on the training data [43]. • Sometimes the algorithms are difficult to under- stand for humans.
Model Basedmethods	• A simple structure is required to analyze the training data and easy to implement. • Accuracy level is high and robust estimation of battery parameters can be done.	• The model is mostly concentrated on accuracy levels of training data and pre-experimental setup is required. • The development process of the battery is time consuming and rely more on computational time.

9. CONCLUSION

As Electric vehicles are tremendously growing in recent technologies, BMS (Battery Management System) plays an important role in monitoring and controlling the various applications of Battery. This paper briefs about the different computational efficiency and the current technologies used in BMS. With respect to SOH, various techniques have been implemented for better performance. The objective, uncertainties, accuracy and efficiency has been discussed in this paper. Regarding SOH techniques, various algorithms have been used along with recent technologies of Machine Learning. It discusses about different algorithm advantages, limitations, standard equations along with the technology being implemented with a comparison structure. In brief, BMS and its applications, SOH with its techniques, Intelligent Algorithms have been highlighted in terms of input and output features. This paper has highlighted the real time applications with respect to EV and HEV with Lithium-ion batteries, Fuel cells, Lead acid batteries etc. Some model-based methods using different algorithms and techniques for the SOH estimation methods are key concerns. Overall, battery parameters with respect to EV model accuracy, adaptability, compatibility with best estimation methods for real time identifications and their applications summarized in a brief manner.

10. REFERENCES

[1] Lipu, MS Hossain, M. A. Hannan, Tahia F. Karim, Aini Hussain, Mohamad HM Saad, Afida Ayob, Md Sazal Miah, and TM Indra Mahlia. ”Intelligent algorithms and control strategies for battery management system in electric vehicles: Progress, challenges and future outlook.” Journal of Cleaner Production (2021): 126044.

[2] Sreedhar, R., and K. Karunanithi. ”Design, simulation analysis of universal battery management system for EV applications.” Materials Today: Proceedings (2021).

[3] Gabbar, Hossam A., Ahmed M. Othman, and Muhammad R. Abdussami. ”Review of Battery Management Systems (BMS) Development and Industrial Standards.” Technologies 9, no. 2 (2021): 28.

[4] Naguib, Mina, Phillip Kollmeyer, and Ali Emadi. ”Lithium-Ion Battery Pack Robust State of Charge Estimation, Cell Inconsistency, and Balancing.” IEEE Access 9 (2021): 50570-50582.

[5] Chandran, Venkatesan, Chandrashekhar K Patil, Alagar Karthick, Dharmaraj Ganeshaperumal, Robbi Rahim, and Aritra Ghosh. "State of charge estimation of lithium-ion battery for electric vehicles using machine learning algorithms." World Electric Vehicle Journal 12, no. 1 (2021): 38

[6] Singirikonda, Srinivas, and Y. P. Obulesu. ”Advanced SOC and SOH Estimation Methods for EV Batteries—A Review.” Advances in Automation, Signal Processing, Instrumentation, and Control (2021): 1963-1977.

[7] Laadjal, Khaled, and Antonio J. Marques Cardoso. ”A review of supercapacitors modelling, SoH, and SoE estimation methods: Issues and challenges.” International Journal of Energy Research 45, no. 13 (2021): 18424-18440

[8] ”Battery Management System (BMS) for Electric Vehicles.” Circuit Digest. December 05, 2018. Accessed November 30 , 2021. https://circuitdigest.com/article/battery-management-system-bms-for- electric-vehicles.

[9] Anselma, Pier Giuseppe, Phillip Kollmeyer, Jeremy Lempert, Ziyu Zhao, Giovanni Belingardi, and Ali Emadi. ”Battery state-of-health sensitive energy management of hybrid electric vehicles: Lifetime prediction and ageing experimental validation.” Applied Energy 285 (2021): 116440.

[10] Vichard, Lo¨ıc, Alexandre Ravey, Pascal Venet, Fabien Harel, Serge Pelissier, and Daniel Hissel. ”A method to estimate battery SOH indica- tors based on vehicle operating data only.” Energy 225 (2021): 120235.

[11] Lin, Jiayuan, Xinhua Liu, Shen Li, Cheng Zhang, and Shichun Yang. ”A review on recent progress, challenges and perspective of battery thermal management system.” International Journal of Heat and Mass Transfer 167 (2021): 120834.

[12] Kalaf, Omer, Davut Solyali, Mohammed Asmael, Qasim Zeeshan, Babak Safaei, and Alyaseh Askir. ”Experimental and simulation study of liquid coolant battery thermal management system for electric vehicles: A review.” International Journal of Energy Research 45, no. 5 (2021): 6495- 6517.

[13] Selvabharathi, D., and N. Muruganantham. ”Battery health and performance monitoring system: A closer look at state of health (SoH) assessment methods of a lead-acid battery.” Indonesian Journal of Electrical Engineering and Computer Science 18, no. 1 (2020): 261-267.

[14] Yue, Q. L., C. X. He, H. R. Jiang, M. C. Wu, and T. S. Zhao. ”A hybrid battery thermal management system for electric vehicles under dynamic working conditions.” International Journal of Heat and Mass Transfer 164 (2021): 120528.

[15] Hashemi, Seyed Reza, Ajay Mohan Mahajan, and Siamak Farhad. ”Online estimation of battery model parameters and state of health in electric and hybrid aircraft application.” Energy 229 (2021): 120699.

[16] Lee, Jeong, Jun-Mo Kim, Junsin Yi, and Chung-Yuen Won. ”Battery management system algorithm for energy storage systems considering battery efficiency.” Electronics 10, no. 15 (2021): 1859.

[17] Saraswathi, RJ Vijaya, and V. Vasan Prabhu. ”Battery Safety Enhancement in Electric Vehicles—A Review Paper.” Emerging Solutions for e- Mobility and Smart Grids (2021): 175-183.

[18] Qu, Jiantao, Feng Liu, Yuxiang Ma, and Jiaming Fan. ”A neural-network-based method for RUL prediction and SOH monitoring of lithium-ion battery.” IEEE access 7 (2019): 87178-87191.

[19] Sivaraman, P., and C. Sharmeela. ”IoT-Based Battery Management System for Hybrid Electric Vehicle.” Artificial Intelligent Techniques for Electric and Hybrid Electric Vehicles (2020): 1-16.

[20] Deng, Zhongwei, Xiaosong Hu, Xianke Lin, Le Xu, Yunhong Che, and Lin Hu. ”General discharge voltage information enabled health evaluation for lithium-ion batteries.” IEEE/ASME Transactions on Mechatronics (2020).

[21] Kilic, Ensar, Ramazan Bayindir, and Samet Ayik. ”Real-Time Monitoring with Labview of the Battery Management System and the Estimated Electric Vehicle Battery SoH.” In Sixth International Conference on Intelligent Computing and Applications, pp. 565-576. Springer, Singapore,2021.

[22] Noura, Nassim, Loïc Boulon, and Samir Jemeï. "A review of battery state of health estimation methods: Hybrid electric vehicle challenges." World Electric Vehicle Journal 11, no. 4 (2020): 66.

[23] Locorotondo, Edoardo, Vincenzo Cultrera, Luca Pugi, Lorenzo Berzi, Marco Pierini, and Giovanni Lutzemberger. ”Development of a battery real-time state of health diagnosis based on fast impedance measurements.” Journal of Energy Storage 38 (2021): 102566.

[24] Kaur, Kirandeep, Akhil Garg, Xujian Cui, Surinder Singh, and Bijaya Ketan Panigrahi. ”Deep learning networks for capacity estimation for monitoring SOH of Li-ion batteries for electric vehicles.” International Journal of Energy Research 45, no. 2 (2021): 3113-3128.

[25] She, Chengqi, Lei Zhang, Zhengpo Wang, Fengchun Sun, Peng Liu, and Chunbao Song. ”Battery State of Health Estimation Based on Incremental Capacity Analysis Method: Synthesizing from Cell-Level Test to Real- World Application.” IEEE Journal of Emerging and Selected Topics in Power Electronics (2021).

[26] Wang, Xueyuan, Xuezhe Wei, Jiangong Zhu, Haifeng Dai, Yuejiu Zheng, Xiaoming Xu, and Qijun Chen. ”A review of modeling, acquisition, and application of lithium-ion battery impedance for onboard battery management.” ETransportation 7 (2021): 100093.

[27] Oji, Tsuyoshi, Yanglin Zhou, Song Ci, Feiyu Kang, Xi Chen, and Xiulan Liu. ”Data-Driven Methods for Battery SOH Estimation: Survey and a Critical Analysis.” IEEE Access 9 (2021): 126903-126916.

[28] Li, Xiaoyu, Changgui Yuan, Xiaohui Li, and Zhenpo Wang. ”State of health estimation for Li-Ion battery using incremental capacity analysis and Gaussian process regression.” Energy 190 (2020): 116467.

[29] Jianfang, Jia, Wang Keke, Pang Xiaoqiong, Shi Yuanhao, Wen Jie, and Zeng Jianchao. ”Multi-Scale Prediction of RUL and SOH for Lithium- Ion Batteries Based on WNN-UPF Combined Model.” Chinese Journal of Electronics 30, no. 1 (2021): 26-35.

[30] Mc Carthy, Kieran, Hemtej Gullapalli, and Tadhg Kennedy. ”Online state of health estimation of Li-ion polymer batteries using real time impedance measurements.” Applied Energy (2021): 118210.

[31] Ungurean, Lucian, Mihai V. Micea, and Gabriel Carstoiu. ”Online state of health prediction method for lithium-ion batteries, based on gated recurrent unit neural networks.” International journal of energy research 44, no. 8 (2020): 6767-6777.

[32] Khaleghi, Sahar, Yousef Firouz, Maitane Berecibar, Joeri Van Mierlo, and Peter Van Den Bossche. ”Ensemble gradient boosted tree for SoH estimation based on diagnostic features.” Energies 13, no. 5 (2020): 1262.

[33] Eddahech, Akram, Olivier Briat, Nicolas Bertrand, Jean-Yves Deletage, and Jean-Michel Vinassa. ”Behavior and state-of-health monitoring of Li-ion batteries using impedance spectroscopy and recurrent neural net- works.” International Journal of Electrical Power and Energy Systems 42, no. 1 (2012): 487-494

[34] Qaisar, Saeed Mian. ”Li-Ion Battery SoH Estimation Based on the Event-Driven Sampling of Cell Voltage.” In 2020 2nd International Conference on Computer and Information Sciences (ICCIS), pp. 1-4. IEEE, 2020

[35] Roy, Sourov, and Faisal Khan. ”Detection of degraded/aged cell in a li-ion battery pack using spread spectrum time domain reflectometry (SSTDR).” In 2020 IEEE Applied Power Electronics Conference and Exposition (APEC), pp. 1483-1488. IEEE, 2020.

[36] Vidal, Carlos, Pawel Malysz, Phillip Kollmeyer, and Ali Emadi. "Machine learning applied to electrified vehicle battery state of charge and state of health estimation: State-of-the-art." IEEE Access 8 (2020): 52796-52814.

[37] Pan, Dawei, Hengfeng Li, and Yuchen Song. "A Comparative Study of Particle Filters and its Variants in Lithium-ion Battery SOH Estimation." In 2020 International Conference on Sensing, Measurement and Data Analytics in the era of Artificial Intelligence (ICSMD), pp. 198-203. IEEE, 2020.

[38] Li, Weihan, Monika Rentemeister, Julia Badeda, Dominik Jöst, Dominik Schulte, and Dirk Uwe Sauer. "Digital twin for battery systems: Cloud battery management system with online state-of-charge and state-of-health estimation." Journal of energy storage 30 (2020): 101557.

[39] Park, Seongyun, Jeongho Ahn, Taewoo Kang, Sungbeak Park, Youngmi Kim, Inho Cho, and Jonghoon Kim. "Review of state-of-the-art battery state estimation technologies for battery management systems of stationary energy storage systems." Journal of Power Electronics (2020): 1-15.

[40] Wang, Yujie, Jiaqiang Tian, Zhendong Sun, Li Wang, Ruilong Xu, Mince Li, and Zonghai Chen. "A comprehensive review of battery modelling and state estimation approaches for advanced battery management systems." Renewable and Sustainable Energy Reviews 131 (2020): 110015.

[41] Gou, Bin, Yan Xu, and Xue Feng. "State-of-health estimation and remaining-useful-life prediction for lithium-ion battery using a hybrid data-driven method." IEEE Transactions on Vehicular Technology 69, no. 10 (2020): 10854-10867.

[42] Sauer, Dirk Uwe Sauer, Hendrik Zappen Zappen, Marcus Knips Knips, Hannes Nordmann Nordmann, Markus Lelie Lelie, Thomas Braun Braun, and Florian Ringbeck Ringbeck. "Battery Management System Hardware Concepts: An Overview." (2018).

[43] Yang, Ruixin, Rui Xiong, Hongwen He, Hao Mu, and Chun Wang. "A novel method on estimating the degradation and state of charge of lithium-ion batteries used for electrical vehicles." Applied Energy 207 (2017): 336-345.

Design and Simulation of Back to Back Converter for Bifurcated Winding Induction Generator

Manoj Kumar S[1], Prema V[2]

[1] *M-Tech student, Department of EEE, BMSCE, Bengaluru, India*

[2]*Associate professor, Department of EEE, BMSCE, Bengaluru, India*

Email: manoj.epe20@bmsce.ac.in

Abstract.

WECS (wind energy conversion system) is the system which converts wind velocity into other forms of energy. Induction generator is the machine used to convert wind energy into electrical energy. Novel BWIG machine has various advantages over convention type of induction generator such as it can easily connected to the grid, can work in standalone condition, easy controllability, three phase operation. This paper focuses on design and simulation of Back to Back converter for controlling frequency and output voltage of Bifurcated Winding Induction Generation (BWIG) machine. Back to Back converter is a combination of Front end converter (FEC) and Back end converter (BEC). Front end converter maintains harmonic free input current with unity power factor at supply end, Back end converter maintain constant output voltage.

Keywords. WECS, BWIG, front end converter, backend converter, and Phase lock loop.

1. INTRODUCTION

Bifurcated Winding Induction (BWIG) machine is the novel type of induction machine used to convert wind velocity into Electrical energy. It is important to generate low cost, efficient and environmental friendly power. To reach these criteria we can go for non-conventional type of power generation like hydro power, tidal power, wind power etc. Wind is the most abundantly available source, Induction generator is the machine used to convert velocity of wind speed into electrical energy. The limitation of this energy conversion is that the velocity is variable in nature, the output which is function of input is also variable which cannot be connected to the load or gird. BWIG machine which uses wind power and convert it into electrical energy. Advantage of this machine is that it provides constant frequency and constant output voltage for a given constant excitation voltage. But it is very important to maintain a constant value voltage at the output to make it easy to connect to the grid/load. This control is done with the help of back to back converter.

Back to Back converter is a cascaded connection of FEC and BEC. These converters use power semiconductor devices as a switches, and the pulses are given to these switches by a proper technique to have control over the output voltage.

Three phase voltage source PWM rectifier has two loops voltage loop and current loop, voltage loop resist disturbances and current loop provides high power factor [1], Space

vector modulation technique for improvement of power quality in front end converter has better output voltage of 15.5% greater than sinusoidal pulse width modulation and the number of the switches also reduced by 30% also % threshold harmonic distortion of 3.59% [2], for bulk application there will be increased harmonics and lower power factor, using IGBT as a switch it facilitate bidirectional power flow and reduces the nonlinear characteristics it also provide unity power factor under steady state and transient state condition, reduces % THD, reliable output voltage will be possible even if any one of the converter fails [3] , using hybrid AC-DC converter power quality can be increased for low and medium power application, where current injection method using zig zag transformer also reduces third harmonic disadvantage of this method is size is more [4], using unipolar switch has advantages over using bipolar switches the advantages are – reduction in ripple by half , frequency is doubled and the filter size is reduced [5],Discontinues pulse width modulation reduces electromagnetic interferences (EMI) but critical to improve power density [6] , closed loop converter with space vector pulse width modulation provide UPF and reduced %THD [7].

In this work, Design and simulation of back-to-back converter is carried out in MATLAB, due to non-availability of BWIG machine, 3 phase voltage source is used instead of BWIG.

This paper includes block diagram, circuit diagram of back-to-back to converter which has FEC and BEC their filter design, MATLAB simulation of back-to-back circuit is carried, and their result are observed. This is for the BWIG machine which is novel machine which reduces requirements of hardware such as need of cycloconverter because machine itself act as frequency follower.

2. BACK-TO-BACK CONVERTER

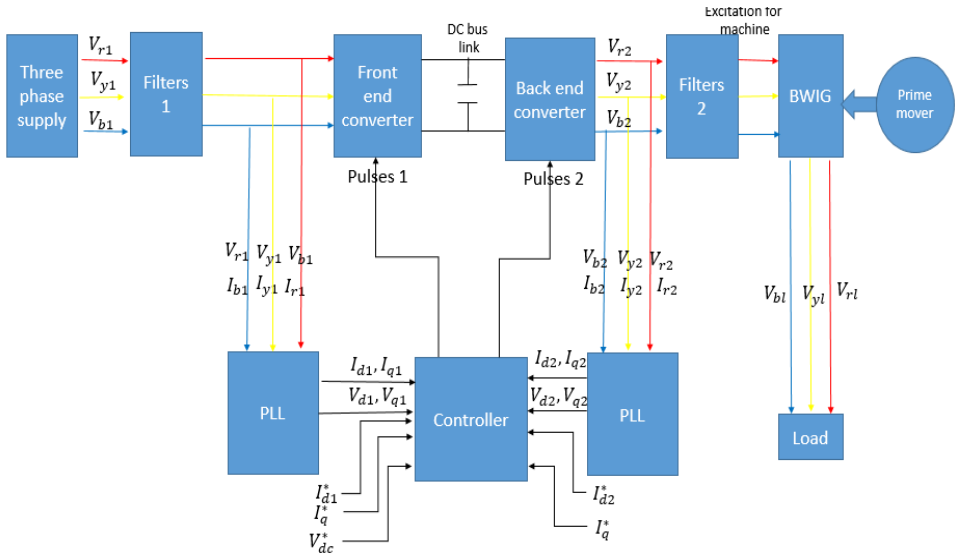

Figure 2.1. Block diagram representation

2.1. Components of back-to-back converter

The key components of back to back converter consist of

1. Front end converter (FEC)
2. Back end converter (BEC)

FEC and BEC are connected back-to-back through a DC link capacitor so it is called back to back converter. FEC is used to maintain constant DC voltage at DC bus link and to reduce harmonic of drawn current. BEC are used to maintain constant output voltage which are made available for excitation for BWIG machine. Figure 2.1 shows the block diagram representation of the work where the 3-phase supply is passed through filters LC filters to reduce harmonics and filtered signal is passed to FEC which converter AC to DC the voltage at DC link is maintained constant through PI controller. The DC link voltage is used as an input for BEC converter which convert available DC voltage at DC link to AC voltage filters are used and designed to reduce harmonics and it is used in phase lock loop (PLL) and controller design to give pulses for the switch to have a controlled output. The switch used in the work is IGBT because it has to support bidirectional power flow when the BWIG machine generates high power.

Phase lock loop is an important technique used, where it locks active and reactive power and provide reference. The output of these active and reactive values are used for controller design. Sinusoidal pulse width modulation is the technique used to generate pulses – it compares sinusoidal wave with triangular wave and pulses are generated and it is used as gate input for the IGBT switches.

Figure 2.2 shows the electrical circuit representation for FEC and BEC.

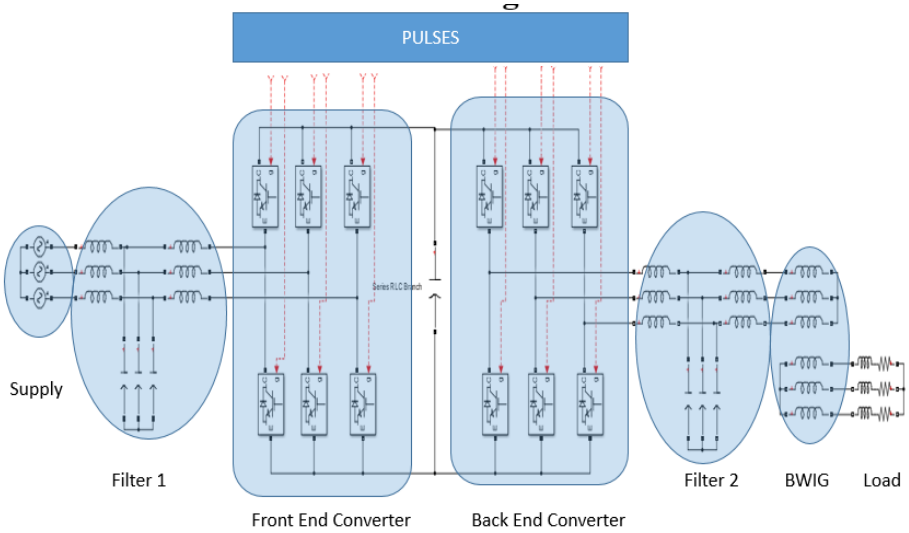

Figure 2.2. Circuit representation of back-to-back converter

3. FILTER DESIGN

3.1. Filter design

LC filters are used to reduce harmonics in the circuit.

- V_{in}= 415 V , V_{dc}=800 V, P = 100 KVA, f= 50 Hz, Switch Frequency, f_{sw}= 10 kHz
- Resonance Frequency, $f_{res} = \frac{f_{sw}}{10}$ = 1000 Hz.
- $I_{gsw} = 0.03\%\ and\ V_{gsw} = 0.9\%\ V_g$
- Current = $\frac{P}{3*V_g}$ = 144.92 A
- Capacitor = $\frac{0.05(p_g)}{v^2(2\pi f)}$
- Capacitor = $\frac{0.05*(\frac{100*10^3}{3})}{230^2*2*pi*f} = 100$ µF
- Inductance = $\frac{1}{w_{sw}(\frac{I_{gsw}}{V_{isw}})(1-\frac{w_{sw}^2}{w_{res}^2})}$ = 76.68 µH
- $L_{1min} = L_{2min} = \frac{76.68}{2}$ = 38.35 µH
- $L_{Max} = \frac{0.2*V_g}{2*pi*f*I}$ = 1 mH.
- $L_{1Max} = L_{2Max} = \frac{1mH}{2}$ = 500 µH

3.2. Design of control loop

3.2.1. Voltage Control Loop

- Capacitor , C = 100 µF
- Capacitor internal resistance, r = 20 mΩ
- T =200µS
- $K_p = \frac{3*c}{T}$ = 1.5
- $K_i = \frac{3*r}{T}$ = 300

3.2.2. Current Control Loop

- Capacitor, L_{1max} = 500 µs
- Capacitor internal resistance, r = 20 mΩ
- $K_p = \frac{3*L1}{T}$ = 10
- $K_i = \frac{3*r}{T}$ = 400

4. SIMULATION MODEL

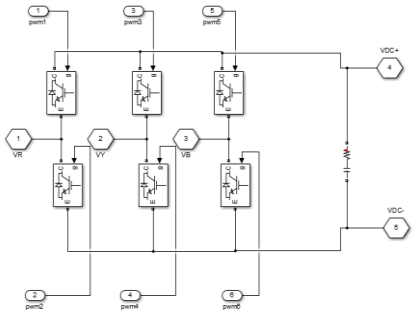

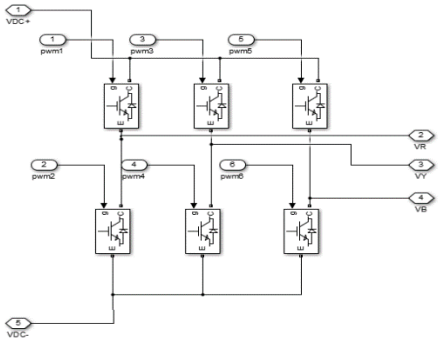

Figure 4.1. Active front end converter

Figure 4.2. Active back-end converter

Figure 4.1 shows Simulink model for FEC. In which it is shown that there are three legs in the bridge. Each leg has two switches, and the supply is given to each leg assumed to be V_R, V_Y, V_B. The pulses as pwm1, pwm2, pwm3, pwm4, pwm5, pwm6 which are controlled by controller and the output is taken out and it is named $V_{DC+,}$ $V_{DC-.}$

Figure 4.2 shows Simulink model circuit for active inverter (back end converter). In which it is shown that there are three legs in the bridge. Each leg has two switches and the supply across leg is given as $V_{DC+,}$ V_{DC-}. The pulses named as pwm1, pwm2, pwm3, pwm4, pwm5, pwm6 which are controlled by the controller and the output is taken out and it is named as V_R, V_Y, V_B.

These two converters are connected through DC link

4.1. Front end MATLAB simulation circuit

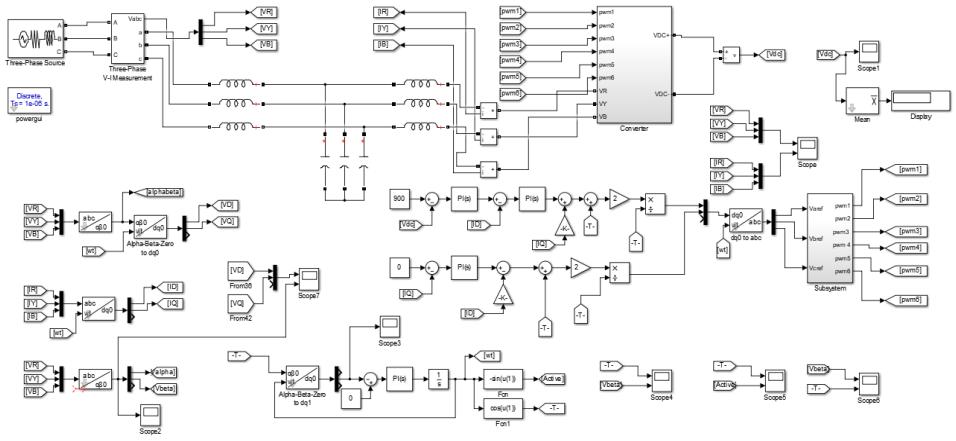

Figure 4.3. Front end converter

4.2. Back-end converter

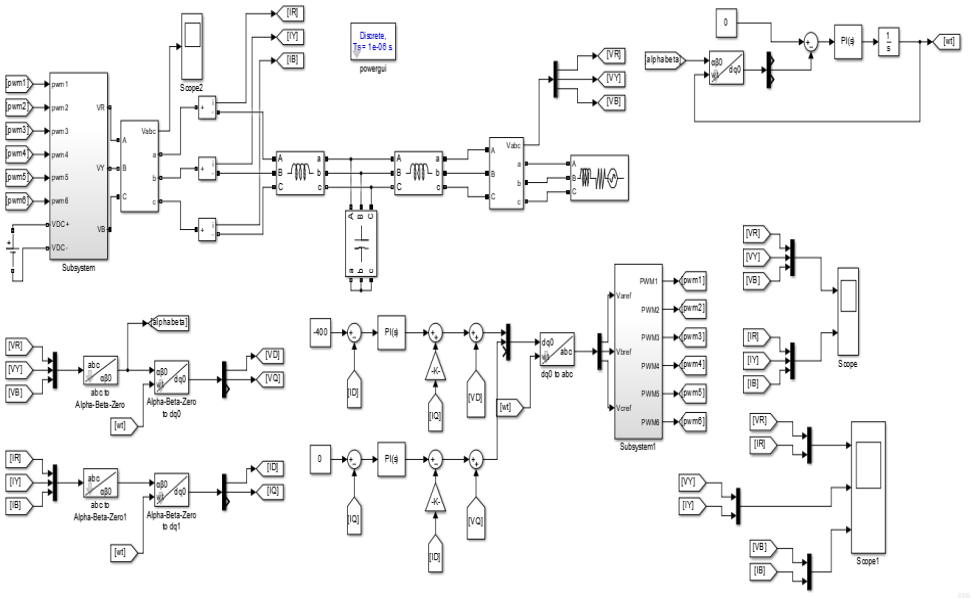

Figure 4.4. Back-end converter

4.3. Back-to-back converter

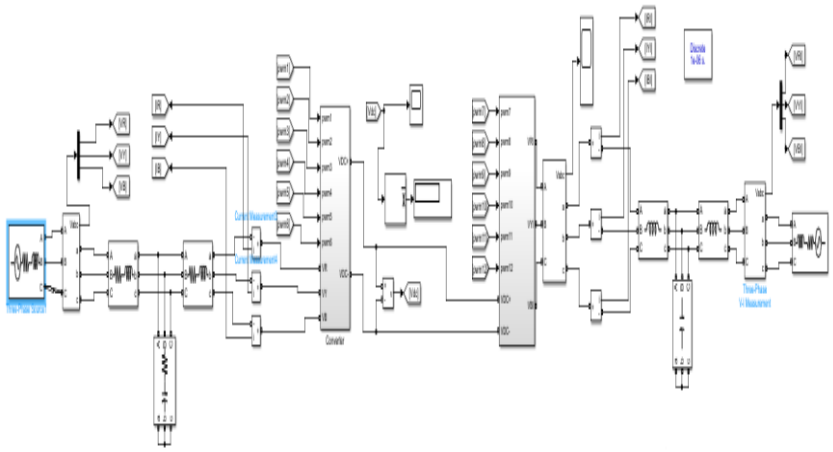

Figure 4.5. Back-to-back converter

Figure 4.3 shows the MATLAB circuit for active end converter. The 3-phase voltage is fed into converter through LC filter which reduces harmonics into the rectifier circuit. PI controller is used to produce controlled pulse signal to the switches which is a function of DC link voltage. Figure 4.4 shows the MATLAB circuit for back-end converter. Here the volage is fed from DC voltage to the inverter circuit, provide filter to reduce harmonics, PI controller is used to produce controlled pulse signal to the inverter switches. Figure 4.5 shows the Back-to-Back converter where output of a rectifier is used as input of inverter input circuit.

5. RESULT AND DISCUSSION

Purpose of Front-End Converter is to maintain distortion free constant DC voltage at Bus link and figure 5.1 shows that the output voltage showing constant DC voltage of 800V which is considered as reference voltage at voltage loop.

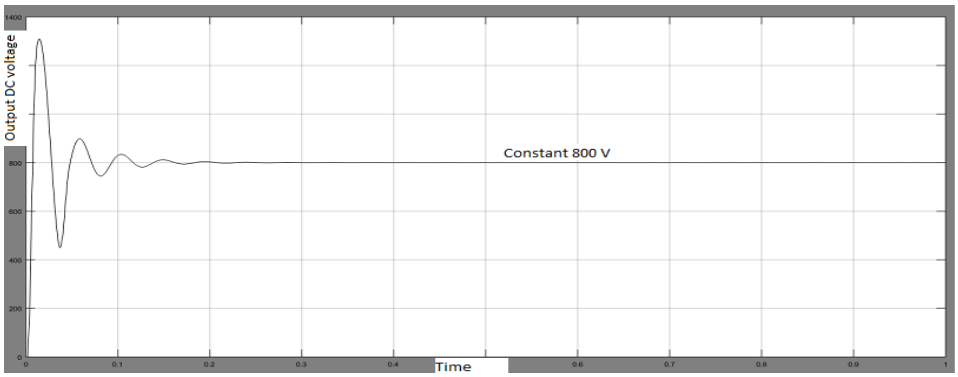

Figure 5.1. DC link voltage

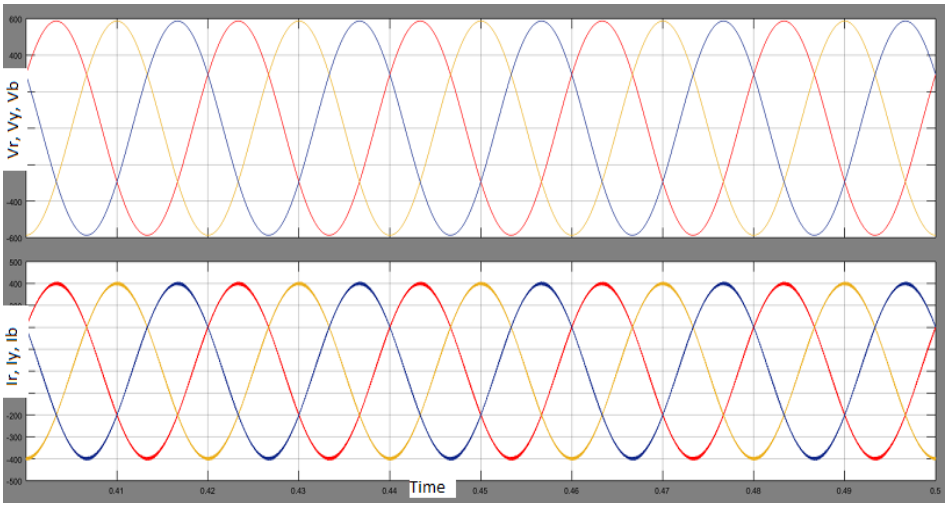

Figure 5.2. Output voltage of back-end converter

Figure 5.2 shows the output voltage (upper) and current drawn (lower) waveforms, and it is showing voltage and current are in phase. Therefore, active power at the excitation is available.

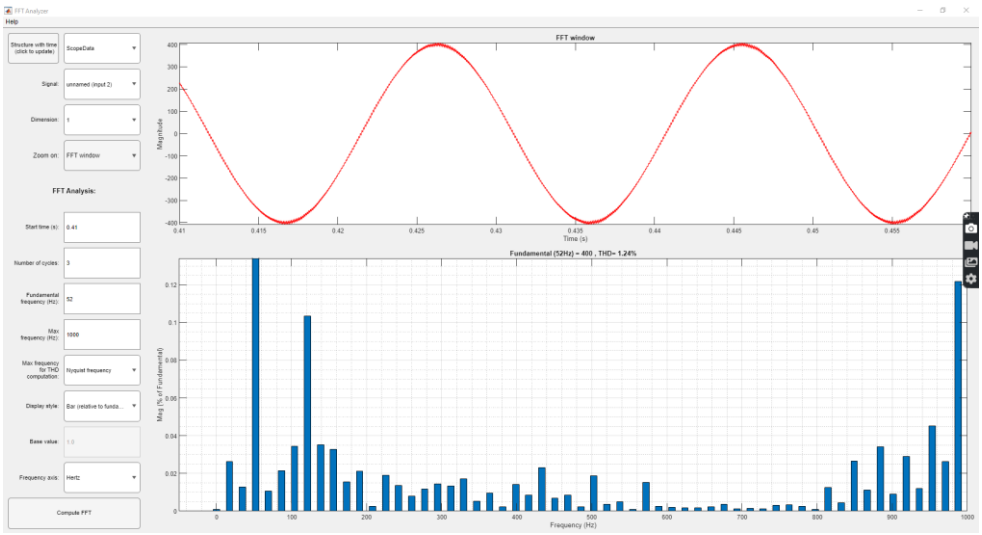

Figure 5.3. % THD

Figure 5.3 shows % Total Harmonic Distortion of 0.9% .Similarly, simulation carried out for input frequency of 48, 50, 52 Hz, the output voltage found to be constant having frequency same as the input frequency.

6. CONCLUSION

Back-to-Back End converter is designed and simulated using MATLAB. By proper design and PWM control- distortion free voltage is obtained to BWIG along with controlled constant voltage is fed to DC link. Therefore, Front End Converter able to maintain constant voltage at DC link. When BWIG generates a power there will be a power reversal into the converter and disturbs the DC voltage at DC link which is undesirable which effects excitation voltage to the BWIG machine. Proper design and PWM control can overcome this disadvantage. And provide an active power supply to the BWIG machine which is desirable for any electrical equipment. Therefore, Back End Converter able to give proper sinusoidal and active power to the Machine. Therefore, combined Back-to-Back Converter was able to provide a distortion free sinusoidal supply with Active power to the BWIG machine.

7. REFERENCES

[1] Ke-Xin, Wei, and Wang Shui-Ming. "Modeling and simulation of three-phase voltage source PWM rectifier." 2008 International Conference on Advanced Computer Theory and Engineering. IEEE, 2008.

[2] Chang, Hung-Chun, and Chang-Ming Liaw. "On the front-end converter and its control for a batterypowered switched-reluctance motor drive." IEEE transactions on power electronics 23, no. 4 (2008):2143-2156

[3] Mathew, Renju, Neha Agarwal, Manisha Shah, and P. N. Tekwani. "Design, modelling and simulation of three-phase front-end converter for unity power factor and reduced harmonics in line current." In 2013 Nirma University International Conference on Engineering (NUiCONE), pp. 1-6. IEEE, 2013

[4] Selarka, Viraj, et al. "Close loop control of three phase Active Front End Converter using SVPWM technique." *2016 International Conference on Electrical Power and Energy Systems (ICEPES)*. IEEE, 2016.

[5] Selarka, Viraj, Prem Shah, Divyesh J. Vaghela, and Manisha T. Shah. "Close loop control of three phase Active Front End Converter using SVPWM technique." In 2016 International Conference on Electrical Power and Energy Systems (ICEPES), pp. 339-344. IEEE, 2016..

[6] Kalpana, R., Bhim Singh, and G. Bhuvaneswari. "Power quality improvement in front-end hybrid AC-DC converter based on current injection technique." In 2017 IEEE Transportation Electrification Conference (ITEC-India), pp. 1-5. IEEE, 2017.

[7] Zhang, Zhe, et al. "Optimized digital implementation of carrier-based randomized discontinuous PWM technique for active front end (AFE) drives." *2019 IEEE Energy Conversion Congress and Exposition (ECCE)*. IEEE, 2019

[8] Batra, Rupanshi. "Operation and Control of Single Phase Front End Converter." In 2020 First IEEE International Conference on Measurement, Instrumentation, Control and Automation (ICMICA), pp. 1-6. IEEE, 2020.

[9] Hamid, Nurul Farhana Abdul, Muhammad Alleef Abd Jalil, and Nor Syafiqah Syahirah Mohamed. "Design and simulation of single phase inverter using SPWM unipolar technique." In Journal of Physics:Conference Series, vol. 1432, no. 1, p. 012021. IOP Publishing, 2020.

Biographies

Manoj Kumar S received the bachelor's degree in Electrical and Electronics from Visveshvaraya Technological University in 2010, pursuing master's degree in power electronics from Visvesvaraya Technological University in 2020-2022 , He is currently doing Mtech in BMSCE.

Dr. PREMA V (Senior Member, IEEE) was born in Thiruvananthapuram, Kerala, India, in 1979. She received the B.Tech. degree in electrical engineering and power electronics from Calicut University, in 2001, and the M.Tech. degree in electrical engineering and power electronics and the Ph.D. degree in electrical engineering from Visvesvaraya Technological University, in 2005 and 2018, respectively. She has 17 years of teaching and industry experience. She is currently working as an Associate Professor with the B.M.S. College of Engineering, Bengaluru. She has authored more than 40 articles in various journals and conferences. Her research interests include renewable energy, forecasting, and power electronics.